Identification of *MYC*-dependent therapeutic vulnerabilities for targeting Group 3 medulloblastoma

Gemma Llargués Sistac

A thesis submitted in part requirement for the degree of Doctor of Philosophy

Translational and Clinical Research Institute

Newcastle University Centre for Cancer

Newcastle-Upon-Tyne

January 2020

Declaration

I certify that no part of the material documented in this thesis has previously been submitted for a degree or other qualification in this or any other university. I declare that this thesis represents my own unaided work, carried out by myself, except where it is acknowledged otherwise in the thesis text.

Gemma Llargués Sistac

January 2020

Acknowledgments

I would like to thank my supervisor Professor Steven Clifford and Dr. Daniel Williamson for giving me the opportunity to work on such an amazing project and their support throughout it. I would also like to thank all the members and friends of the Paediatric Brain tumour group and the Herschel, who have not only made me a better scientist, but a better person throughout this journey. In particular, I would like to thank our technicians Jemma Castle and Marie Claire Buttigieg for contributing in the completion of the data presented in this thesis.

I would sincerely like to thank Dr. Janet Lindsey and Dr. Matthew Selby for they unconditional support and guidance throughout these years, even when they were gone. I most definitely would have not been able to achieve what I have without their guidance. My most sincere gratitude goes to Dr. Florence Burté, for always being there for me throughout the hardest times of the PhD, for her endless encouragement and never ever doubt my scientific skills.

I would especially like to thank my friends Nefeli, Maggie and Emma, a blessing to have shared this journey with such brilliant minds and wonderful persons. I would have not come this far without them.

Above all, I would like to thank my parents, who have given me everything and continue to do so. This is an achievement of us all.

My final gratitude goes to Skye. I wish you could see what you have achieved. Thank you, it will not be in vain.

Dedication

To Skye,

for a closer loom to the moon.

Abstract

Introduction

Group 3 medulloblastoma (MB_{Group3}) is a highly aggressive tumour characterised by *MYC* amplification and elevated expression (17% of MB_{Group3}). *MYC* amplification confers a dismal prognosis, and there is an urgent unmet need for novel therapeutic approaches. The identification and targeting of *MYC*'s biological dependencies thus represent a promising strategy to treat *MYC*-driven MB_{Group3} tumours.

Methods

Three independent *MYC*-regulable isogenic MB_{Group3} cell lines, in which *MYC* expression can be directly regulated by shRNA, were used to characterise *MYC*-dependency in these novel models of MB_{Group3} tumours. The lines were used to investigate the role of *MYC* in drug resistance and sensitivity by characterising the *MYC*-dependent response to a panel of cancer therapeutics and small molecule inhibitors, to identify drugs whose efficacy is *MYC*-dependent, or which synergise with *MYC* knockdown. Three indirect *MYC*-targeting strategies (targeting *MYC* transcription and *MYC* mRNA translation) were assessed using candidate drugs, alongside undertaking a high-throughput compound screen (HTCS) (>500 inhibitors) using the models.

Results

Data from the *MYC*-dependent lines was used to identify *MYC*-dependent differences in drug-sensitivity between *MYC*-overexpressing and *MYC*-knockdown cell lines after inhibition of specific proteins. This approach identified several specific druggable dependencies (e.g. cell cycle regulators, DNA-damage response controllers, mitotic control machinery) with potential for the development of treatments against MB_{Group3}. Integration of drug-sensitivity results with data on *MYC* transcriptional (by RNA-seq) and biological (by whole-genome CRISPR screening) dependencies in the models, identified BRD4, PLK1, CHK1 and AURK as specific molecular targets. Subsequent validation of target inhibition revealed *MYC*-dependent effects, associated with downregulation of *MYC* and target-dependent pathways, across MB_{Group3} models.

Conclusions

These findings support the development of PLK1, CHK and AURK inhibition as therapeutic approaches against *MYC*-dependent MB_{Group3}. Future work is now essential to validate our findings *in vivo*, to support the design of future clinical trials.

Table of contents

List of figures

List of tables

Abbreviations

Abbreviation	Definition
µl	micro litre
µM	Micromolar
AML	acute myeloid leukaemia
AT/RT	atypical teratoid/rhabdoid tumours
AURK	aurora kinase
BET	bromodomain and extraterminal
CDK	cyclin-dependent kinase
CDK9	cyclin-dependent kinase 9
CHK1	Checkpoint kinase 1
CLA	classic
CNS	central nervous system
CRISPR	whole-genome CRISPR screen
CRUK	Cancer Reaserch UK
CSF	craniospanial fluid
CTA	CellTiter 96 AQueous One
CTG	CellTiter-Glo
D/N	desmoplastic/nodular
DDR	DNA damage response
DMEM	Dulbecco's Modified Eagle's Medium
DMSO	Dimethyl sulfoxide
DN	desmoplastic nodular
DNA	dexorinonucleic acid
DNMT	DNA methyltransferase
DOX	doxycycline
EGFR	Epidermal growth factor receptor
ERK	Extracellular Signal-regulated Kinase
FACS	Fluorescent activated cell sorting
FCS	Foetal calf serum
g	gram
GSEA	Gene set enrichment analysis

GTR	gross-total ressection
GTR	gross total resection
Gy	Greu
h	hours
HDAC	histone deacetylase
HFRRT	hyperfractionated radiotherapy
HTCS	high-throughput compound screening
HTS	high-throughput screening
IC50	half maximal inhibitory concentration
LCA	large-cell/anaplastic
MB	medulloblastoma
MBEN	medulloblastoma with extensive nodularity
MBGroup3	medulloblastoma group 3
MBGroup4	medulloblastoma group 4 subgroup
MBSHH	medulloblastoma SHH subgroup
MBWNT	medulloblastoma WNT subgroup
min	minutes
ml	mililitre
mTOR	mammalian target of rapamycin
MYC2	MYC2 shRNA construct
MYC3	MYC3 shRNA construct
NB	neuroblastoma
nM	nanomolar
NS	non-silencing
OS	overall survival
PBS	Phosphate-buffered saline
PCR	polymerase chain reaction
PI	propidium iodide
PI3K	phosphatidylinositol 3-kinase
PLK	polo-like kinase
PNET	primitive neuroectodermal tumours
P-TEFb	positive transcription elongation factor b

p-value	Calculated value of probability
RLU	relative luminescence units
RNAi	RNA interference
RNAi	ribonucleic acid
SHH	sonic hedgehog
shRNA	Short Haipirin RNA
siRNA	Small interfering RNA
SNP	Single nucleotide polymorphism
STR	subtotal resection
Tet	tetracycline
TopoI	topoisomerase I
w/v	weight to volume ratio
Wes	simple western assay
WHO	World health organisation
WT	wild type
xg	Relative centrifugal force

Chapter 1. Introduction

1.1 Cancer

Cancer is a group of genetic diseases characterised by uncontrolled cell proliferation, leading to the accumulation of fast-growing abnormal cells with the ability to invade surrounding tissues, and disseminate throughout the body. Cancer is a complex disease that involves progressive dynamic changes in cells' genome to progressively acquire the mechanisms that will direct their transformation from normal human cells into malignant derivatives (Hanahan and Weinberg, 2000).

Tumour development and progression requires the acquisition of specific cellular capabilities, including sustained proliferative signalling, evasion of growth suppressors, cell death resistance, replicative immortality, induction of angiogenesis, activation of invasion and metastatic mechanisms, deregulation of cellular energetics and the ability to bypass the immune system (Figure 1)(Hanahan and Weinberg, 2000). Acquisition of these multiple hallmarks is dependent on the acquisition of a succession of genetic alterations that affect genes involved in the biological processes mentioned above, which is promoted by genomic instability and a tumour-promoting microenvironment (Hanahan and Weinberg, 2000, Hanahan and Weinberg, 2011).

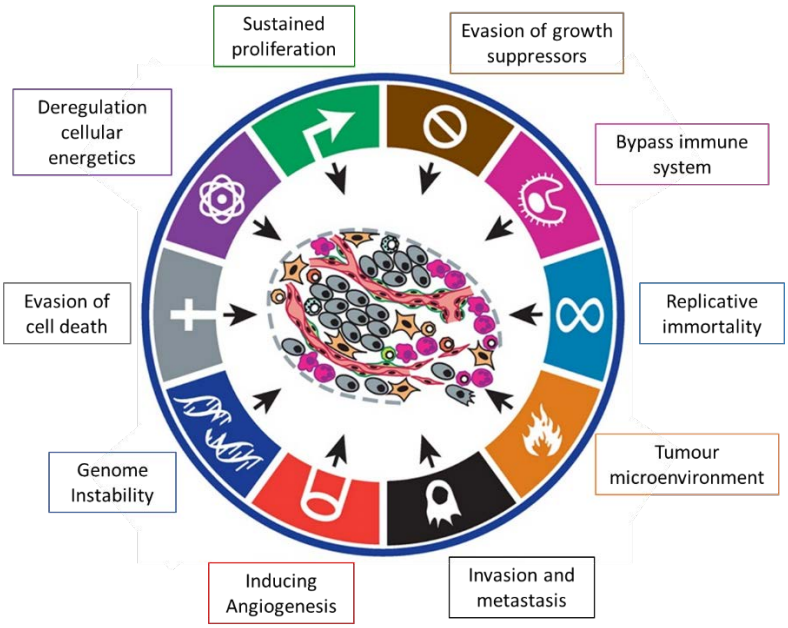

Figure 1.1. Hallmarks of cancer. Illustrative representation of the 12 hallmarks of cancer as described by Hanahan and Weinberg (2011)(Adapted from Hanahan and Weinberg, 2011).

Despite great efforts and advances over the last ten years to understand this complex disease, cancer is still one of the biggest health problems worldwide, and one of the greatest challenges faced by science and medicine. Over the last ten years, cancer incidence rates have increased by 20% in the United Kingdom, with a yearly average of 364,000 new cancer cases in the UK (CRUK, 2016). Despite the diversity and disparity of cancer types, breast, prostate, lung and bowel cancers account for 53% of all cancers diagnosed (Figure 1.2).

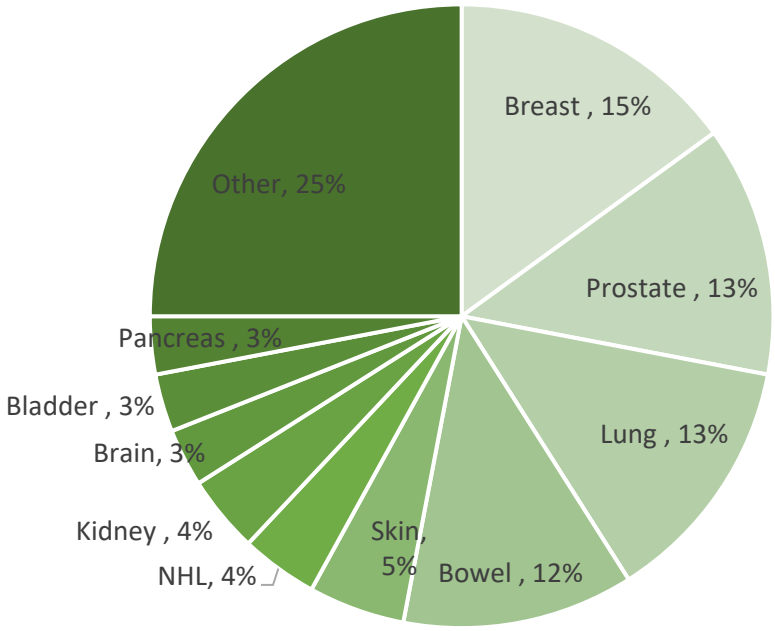

Figure 1.2. Incidence (%) of most common cancer in the United Kingdom. NHL, Non-hodgkin's lymphoma. (CRUK, 2016).

1.2 Paediatric cancer

Paediatric cancer is rare (an average of 1900 new cases per year in the United Kingdom), accounting for less than 1% of all new cancer diagnosis (CRUK, 2016). Recent decades have seen cancer incidence rates among children and adolescents increase, whilst death rates have experienced an overall reduction of 63%, as a result of major advances in cancer diagnosis and treatments (Hudson *et al.*, 2015).

Leukaemia, central nervous system (CNS) tumours, and lymphomas are the most common types of cancer diagnosed in children, accounting for more than two thirds of all paediatric cancers (Figure 1.3). Despite ranking second in terms of incidence, brain, CNS, and intracranial tumours are the most frequent cause of death amongst children (CRUK, 2016).

Despite all the progress made, current therapy causes long-term sequelae and related toxicities (Calaminus et al., 2007). The substantial progress on survival rates for the majority of childhood cancers indicates the need for continued advances and research to find effective treatments to further reduce childhood cancer mortality and the treatment-related toxicities that accompany it (Landier et al., 2015).

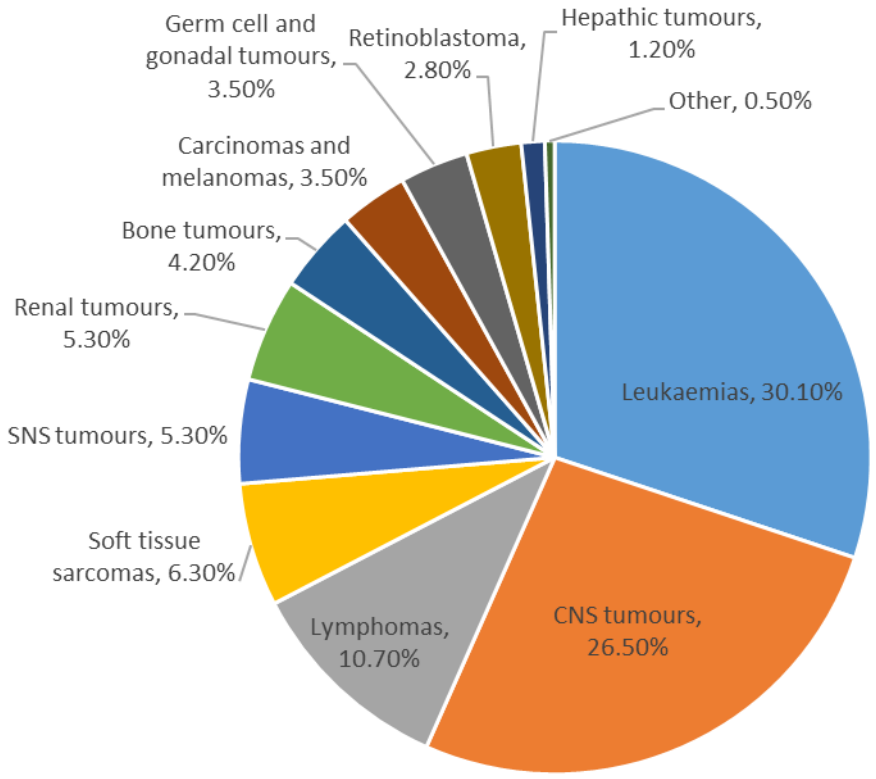

Figure 1.3. Incidence (%) rates of childhood cancers in the United Kingdom. NHL, Non-hodgkin's lymphoma. (CRUK, 2016).

1.2.1 Tumours of the CNS

The most commonly diagnosed type of CNS tumours are gliomas. Gliomas arise in the glial cells of either the brain or the spine, of which astrocytomas are the most frequent subtypes.

Embryonal tumours account for approximately 19% of all childhood brain cases, and are the second most frequent form of malignant tumours. This group includes atypical teratoid/rhabdoid tumours (AT/RT), primitive neuroectodermal tumours of the central nervous system (CNS-PNETs) and medulloblastoma (MB). Embryonal CNS tumours are extremely aggressive tumours and are associated with higher mortality rates and long-term side effects for the survivors. They are the most common form of malignant brain tumour, of which MB is the most frequent type.

1.3 Medulloblastoma

Tumours of the central nervous system (CNS) and brain are the second most common solid malignancies diagnosed in children, comprising 25-30% of childhood cancer diagnoses (Ward et al., 2014)(Figure 1.4). Medulloblastomas are the most frequent malignant brain tumours (WHO grade IV), accounting for 10% of all paediatric deaths from cancer (Pizer and Clifford, 2009)

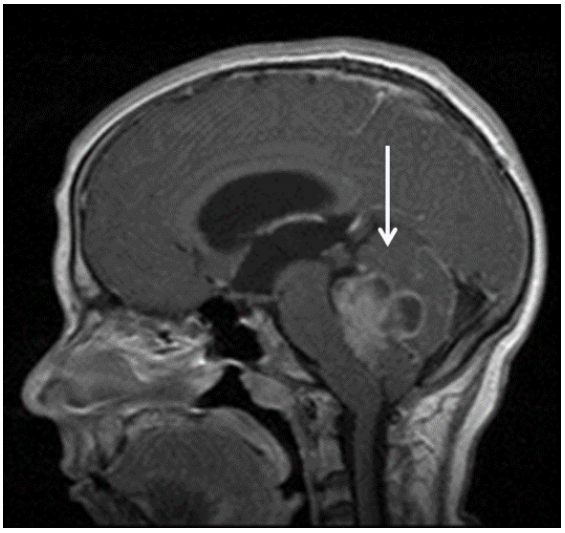

Figure 1.4. MRI of a medulloblstoma. Sagittal view of a cranial MRI image of a patient with medulloblatoma, indicated by the arrow. Image provided by Prof. Simon Bailey (PBTG, Newcastle).

MB defines a heterogeneous group of intracranial embryonal tumours, with a male to female predominance (1.8:1) and a peak incidence at 4-7 years of age. However, they can occur at any age from infants to elderly patients, although they are far more rare in adulthood. MB commonly arise in the cerebellum in the posterior fossa of the cranium, and are characterised by a tendency to disseminate (~35% of cases at diagnosis) commonly via cerebrospinal fluid (CSF) pathways (Smoll and Drummond, 2012, Pizer and Clifford, 2008).

Insights into MB biology, based on histopathological features and molecular signatures have enabled the sub-classification of this heterogeneous disease and now inform treatment strategies. However, despite huge advances in understanding the disease biology, over 30% of MB patients will experience disease recurrence, from which current survival rates are under 10% (Ramaswamy et al., 2016).

1.3.2 Diagnosis and staging

The diagnosis of MB is based on clinical symptoms, magnetic resonance imaging (MRI) of the brain and a lumbar puncture of CSF cytology, to assess the presence of primary tumour and metastasis (Northcott et al., 2019).

Patients with MB usually present with symptoms that are a direct effect of the tumour localisation in the brain, with obstruction of CSF and increased intracranial pressure (Pizer and Clifford, 2008). Some of these symptoms include vomiting, headaches, speech and optical disturbances, and ataxia.

Clinical staging of the disease involves MRI of the brain and CSF cytology at the time of diagnosis. Staging of MB uses the modified Chang's classification (Chang et al., 1969) to determine the metastatic state of the disease, which ranges from M0 to M4 (Table 1.1).

Metastatic stage	Definition
M0	no evidence of metastasis
M1	presence of tumour cells in CSF
M2	Intracranial metastasis
M3	spinal metastasis
M4	metastasis outside the CNS

Table 1.1. Metastatic staging of Medulloblstoma. Adapted from Chang *et al*., 1969.

Current protocols for clinical trials and patient management group patients into two main risk categories, standard and high risk, in order to adjust treatment according to the extent of the disease.

Standard-risk children are those over the age of 3, with no evidence of metastatic spread at diagnosis, with complete or almost-total tumour resection. High-risk patients are those presenting any of the above risk factors, thus requiring intensified therapy, including higher doses of chemotherapy, hyperfractionated radiotherapy (HFRRT) and stem cell rescue (Table 1.2) (Ellison, 2010, Ramaswamy et al., 2016). All children under 3 years of age are now classified as high-risk as they do much worse after treatment.

Incorporation of risk stratification schemes in the clinical setting based on disease risk has underpinned a dramatic improvement in survival rates in the last three decades, where around 80% of standard risk patients survive over 5 years, and between 60-65% of those with high-risk features (Juraschka and Taylor, 2019).

Parameters	Standard Risk Group	High Risk Group
Age	Patients older than 3 years of age	Patients younger than 3 years of age
Extent of previous surgical resection	<1.5 cm^2 residual tumour after resection	Subtotal resection or >1.5 cm^2 residual tumour after resection
Tumour stage	M0 stage confirmed by MRI and CSF sampling	M1-M3 stage or presence of leptomeningeal seeding

Table 1.2. Parameters used to risk stratify children with medulloblastoma.

1.3.3 Prognostic factors

Before the identification of MB subgroups, patient risk stratification was based on metastatic stage (Chang's classification), age at diagnosis, histological variant and extent of resection to divide patients into high- and standard-risk schemes for treatment adjustment.

The molecular characterisation of MB allowed the incorporation of subgroup and molecular characteristics to the clinicopathological variants to stratify the disease to adjust therapeutic regimes according to patients' prognosis.

This features are currently being used in the risk stratification schemes for the pan-European PNET5 and the United States clinical trial for medulloblastoma (Pizer and Clifford, 2009, Gottardo et al., 2014, Ramaswamy et al., 2016). Current disease stratification factors used in ongoing clinical trials are summarised in Table 1.3.

	2013		2014	2017
	SJMB12		SIOP-PNET5-MB	SIOP-PNET5-MB SIOP-HR-MB
	WNT and SHH	non-WNT/non-SHH		
High Risk	M+ R+ *MYC/MYCN* amplification	M+ R+ MYC/MYCN amplification	M+ R+ LCA pathology *MYC/MYCN* amplification	M+ R+ LCA pathology *MYC/MYCN* amplification MB_{SHH}/*TP53* mutation MB_{WNT} with HR features
Standard Risk	MB_{WNT} and MB_{SHH} M0 GTR/NTR	M0 GTR/NTR no LCA histology no MYC/MYCN gain	Non-MB_{WNT} Negative for all HR features	Non-MB_{WNT} Negative for all HR features MB_{WNT} >16 years without HR features MB_{WNT} <16 years with HR features
Favourable Risk	MB_{WNT} only M0 GTR/NTR Classic histology Monosomy 6 no *MYC/MYCN* amplification	M0 GTR/NTR no LCA histology no MYC/MYCN gain or amplification	MB_{WNT} < 16 years Negative for all HR features	MB_{WNT} < 16 years Negative for all HR features

Table 1.3. Pathological and clinical biomarkers used for clinical trials. M+, metastatic disease; R+, subtotal resection; LCA, large-cell/anaplastic histology; MB_{WNT}, WNT medulloblastoma; MB_{SHH}, SHH medulloblastoma; SIOP, International Society of Paediatric Oncology; HR, high-risk; PNET, primitive neuro ectodermal tumours.

1.3.4 Histological subtypes

Accurate MB diagnosis can be difficult since the posterior fossa is a common location for other types of tumours to arise, which can present with similar features to MB. Therefore, integrated histopathological and molecular analysis alongside brain imaging is essential for MB diagnosis.

According to the 2016 World Health Organization (WHO) classification of tumours of the CNS, MB comprises four main biological subtypes: classic (CLA), desmoplastic/nodular (DN), medulloblastoma with extensive nodularity (MBEN) and large-cell/anaplastic (LCA, a combined category)(Figure 1.5)(Villa et al., 2018, Gilbertson and Ellison, 2008, Ellison, 2010).

Classic MB is the most common histological subtype, present in 70% of all cases; LCA and DN/MBEN each represent between 10-15% of patients. Distribution of histological variants varies depending on age and partially correlates with the molecular subgroups, which can often be used as prognostic factors to risk stratify the disease (Gajjar and Robinson, 2014).

In the WHO classification 2016, an adaptation was made to jointly diagnose large-cell and anaplastic medulloblastomas as large-cell/anaplastic (LCA) medulloblastomas, since both rare entities showed mixed cellular composition and were difficult to differentiate from one another (Pietsch and Haberler, 2016). LCA histology can be found in all subgroups, and it is indicative of aggressive tumours with the ability to metastasise. LCA is used as prognostic marker to identify patients with high-risk disease.

On the other hand, DN/MBEN histology is linked to a much more favourable prognosis in infant patients (<3 years of age) when compared to CLA and LCA histology (Ellison, 2010).

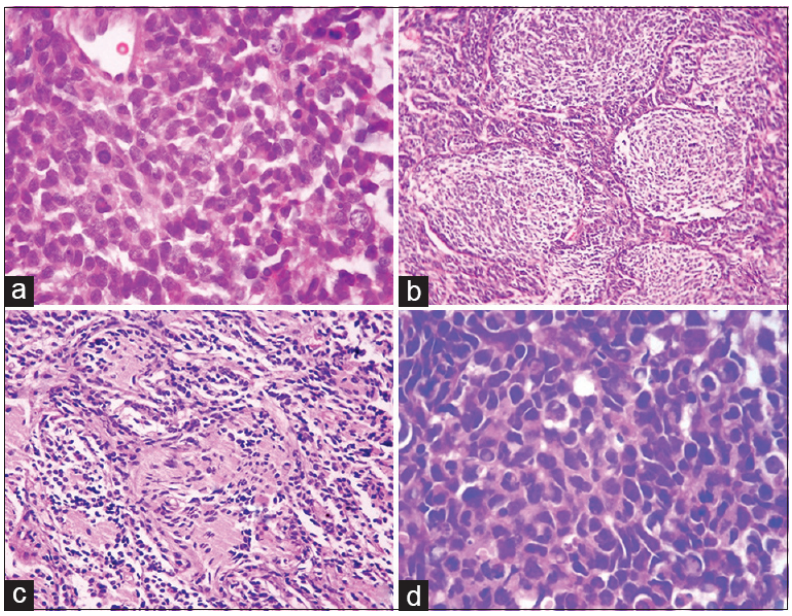

Figure 1.5. Histological subtypes of medulloblastoma. Microscopy images showing the different histological features that MBs present. a) Classic MB is characterised by packed cells surrounded by very little cytoplasm, with high mitotic and apoptotic activity. b) DN MB are characterised by the variable presence of nodules (N) of differentiated neurocytic cells. Among the nodules desmoplastic internodular (IN) regions are interspersed. c) MBEN MB are characterised by large and irregular areas of nodules with internodular desmoplasia in sparse. d) LCA MB are characterised by nuclear pleomorphism accompanied by cell wrapping and frequent mitotic and apoptotic figures. Abbreviations: DN, desmoplastic nodular; LCA, large cell/anaplastic; MBEN, medulloblastoma with extensive nodularity. Scale x20. (Adapted from Gupta, 2017)

1.3.5 Treatment of Medulloblastoma

The past 20 years have seen significant improvements in MB risk stratification that have led to overall increased survival rates up to 80% with little to no change in the treatment protocol of standard care established for MB (Juraschka and Taylor, 2019). Generally, therapy is based on a multimodal treatment that consists of surgical resection and radiotherapy followed by chemotherapy. Depending on the presence of risk factors at diagnosis the intensity of adjuvant therapy varies (Gandola et al., 2009, Packer et al., 2006, Lannering et al., 2012, von Bueren et al., 2016).

With this approach, the estimated 5-year overall survival is around 80% for non-infants, without metastasis, and gross total resection (GTR) of the tumour, and 60% for children presenting metastasis at diagnosis and/or subtotal resection (STR)(where a residual portion of the tumour, >1.5cm^2, is left). Survival estimates have remained stable for the last couple of decades (Oyharcabal-Bourden et al., 2005, Packer et al., 2006, Gajjar et al., 2006, Lannering et al., 2012, von Bueren et al., 2016).

1.3.5.1 Surgery

Surgical resection of the tumour is an essential part of MB treatment. The main objectives of surgery are to achieve a total gross resection of the primary tumour and to re-establish CSF circulation before administration of radio- and chemotherapy (Gerber, 2014). The importance of the extent of tumour resection remains a prognostic factor in the molecular era, where GTR or near-total resection (NTR; residual portion of the tumour is <1.5cm^2) are consistently associated with better prognosis, compared to STR (Gerber et al., 2014, Thompson et al., 2016, Albright et al., 1996).

The prognostic significance of subtotal resection, however, remains controversial. Recent studies have reported similar prognosis for patients that have GTR or NTR, which leaves the surgeons to weigh the potential of leaving residual tumour in order to avoid extensive neurological damage (Thompson et al., 2018, Schreiber et al., 2017, Gajjar et al., 1996).

Aside from primary tumour removal, an important goal of surgery is to provide tissue for histological and molecular analysis, which is essential for risk stratification of the disease and treatment planning (Rutkowski et al., 2018, Mack and Northcott, 2017, Juraschka and Taylor, 2019).

1.3.5.2 Radiotherapy

After neurosurgery, patients are given a localised boost of radiation to the site of the primary tumour in the posterior fossa to prevent MB spread in the CSF (Ivanov et al., 2016). Craniospinal irradiation (CSI) dose is risk stratified. For standard risk patients, a CSI dose of 23.4Gy is given in 13 fractions followed by administration of a tumour bed boost of 54-55.8Gy. High-risk patients are irradiated with CSI doses of 36Gy, followed by a tumour bed boost to 55-55.8Gy (Gajjar et al., 2006, Thomas and Noël, 2019, Ivanov et al., 2016).

Considering that the brains of younger patients are in a stage of rapid development, radiation has major consequences for infants and children, it is therefore not recommended in patients <3 years of age, but either reduction or omission of radiotherapy have failed to increase patient outcomes (Ashley et al., 2012).

Despite widespread side effects, radiation prolongs survival of patients with MB, which clearly implies the need to effectively risk-classify patients in order to lower radiation dosages in

those patients with lower risk of dissemination and tumour recurrence. Current studies are investigating alternative ways of delivering radiation treatment, such as modulation of radiation intensity or use of proton beams, to minimise exposure of normal tissue and avoid overexposure (Mulhern et al., 2005, St Clair et al., 2004, Vatner et al., 2018, Yock et al., 2016, Deutsch et al., 1996).

In this regard, the Phase III clinical trial ACNS0331 conducted by the Children's Oncology Group was designed to test whether a 5.4Gy reduction in the CSI dose (total of 18Gy) and boost volume resulted in differential overall or event-free survival rates. Administration of 18Gy radiation dose with an in-field boost from posterior fossa to tumour bed did not change event free survival or overall survival of patients, whereas a reduction of CSI dose resulted in inferior survival rates and increased risk of recurrence (Michalski et al., 2016).

1.3.5.3 Adjuvant Chemotherapy

Chemotherapy is the second adjuvant in MB treatment, established to increase survival and reduce the intensity of radiation by using chemotherapeutic agents (Deutsch et al., 1996, Evans et al., 1990). The most widely used chemotherapeutic agents are cisplatin, carboplatin, vincristine, cyclophosphamide, and lomustine (Packer et al., 2013, Dhall et al., 2008, Taylor et al., 2003).

The optimal chemotherapeutic regime, as per multi-drug regime and number of cycles administrated, has yet not been strictly defined, it remains highly variable between clinical trials, which makes the systematic assessment of combinatorial therapy effects hard to determine and improve for those patients categorised as high-risk. Nonetheless, the primary goal of current chemotherapy regimens are to deliver the minimum required dose with the least toxic agents possible for maximal disease control (Northcott et al., 2019).

MB has always been considered sensitive to chemotherapeutic agents, and standard-risk patients under this adjuvant treatment have been reported to have increased event-free survival. Drugs listed and dosages are well established in this population of MB patients, but adverse side effects are still prevalent. To advance the effectiveness of adjuvant chemotherapy regimes in MB, exploration of new and conventional chemotherapeutic agents in accordance to molecular subtypes might dictate better responsiveness to therapy with fewer or reduced side effects, and improve the management of the disease (Gajjar et al., 2006, Packer et al., 2006, Sirachainan et al., 2011, Martirosian and Neman, 2019).

1.3.5.4 Treatment side effects

The effectiveness of the multimodal treatment comes at the expense of long-term sequelae and side effects that have a tremendous effect on survivors' quality of life. Many MB survivors experience long term neurocognitive impairments that worsen over time, with a direct effect on intelligence quotient (Frange et al., 2009, Edelstein et al., 2011, Ribi et al., 2005).

Several studies performed over the years have established the importance of radiation therapy volume and age at treatment on intelligence quotient (IQ). Despite the use of lower CSI doses for standard-risk patients, radiation is still severely detrimental to younger patients (<8.8 years), where several studies have reported up to 12 and 14-point IQ deficit for patients treated with radiation in comparison to those who did not receive it. Also, lower IQ points after cranial irradiation was seen in younger patients in comparison to those who were older at treatment (>8.8 years)(Palmer et al., 2003, Palmer et al., 2007, Gottardo and Gajjar, 2006).

Resection in itself can be problematic and the main cause of neurological deficits, with cerebellar mutism syndrome occurring in approximately 25% of patients. As a result of radiation and adjuvant chemotherapy patients develop neuroendocrine disorders, orthopaedic impairments, gonadal alterations, hormonal dysfunctions, along with the development of secondary malignancies (Law et al., 2012, Kennedy et al., 2014, Chevignard et al., 2017, Camara-Costa et al., 2014).

These long-term side effects reflect the clear need to keep improving therapy stratification in an attempt to reduce treatment side effects in standard-risk patients, to increase survival in high-risk disease, and to move forward to use novel targeted agents that could reduce the toxicity of current chemotherapeutic regimes.

1.3.6 Cancer predisposition syndromes

The association observed between numerous hereditary cancer predisposition syndromes and MB was the first step towards insights into the molecular biology of MB. The development of MB brain tumours in patients with Gorlin syndrome (*PTCH1* mutations – SHH signalling pathway), Turcot syndrome (*APC* mutations – WNT signalling pathway) and Li-Fraumeni syndrome (*TP53* mutations), led early research studies to focus on understanding how these signalling pathways were disrupted in these syndromes and their association with MB tumourigenesis (Smith et al., 2014, Brugières et al., 2012, Taylor et al., 2002, Kool et al., 2014).

Comprehensive genetic predisposition studies have linked germline mutations in *APC* (Turcot syndrome), *PTCH1* (Gorlin syndrome), *SUFU* and *TP53* (Li-Fraumeni) to be primary risk factors for the development of MB (Figure 1.6). Waszak *et al.*, associated the presence of biallelic mutations or heterozygous mutations in *BRACA2* and *PALB2*¸ observed in 1% and <1% of all MB cases respectively, with increased risk of MB in patients with germline predisposition mutations (Waszak et al., 2018, Twigg et al., 2016, Vladoiu et al., 2019). Previous studies have found a 5% risk of medulloblastoma in Gorlin syndrome. In 2014, Smith *et al.* provided evidence that *SUFU* mutations can cause classical Gorlin syndrome, and that those presenting with *SUFU* mutations have 20x higher risk (33%) of developing medulloblastoma than those with *PTCH1* mutations (<2%)(Smith et al., 2014).

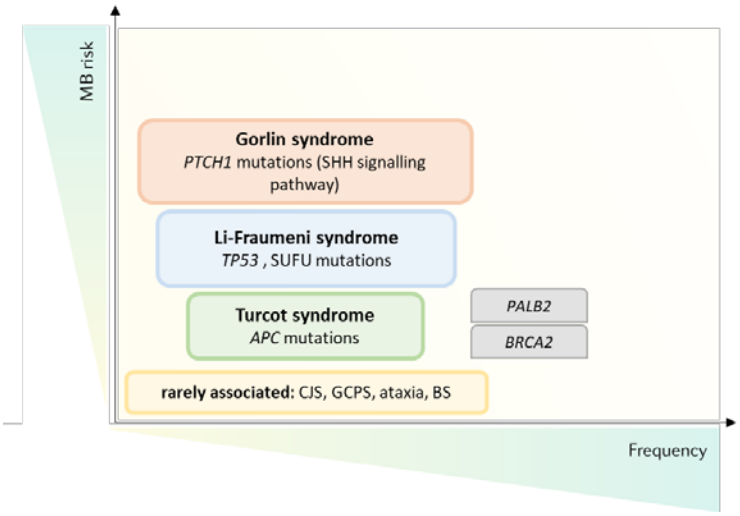

Figure 1.6. Medulloblastoma genetic predisposition. Germline mutations in six genes have been associated with increased risk of MB, which are *TP53* (Li-Fraumeni syndrome), *APC* (Turcot syndrome; familial adenomatous polyposis syndrome), *PTCH1* (Gorlin syndrome), *SUFU*, *TP53* (Li-Fraumeni), PALB2 and BRCA2 (Fanconi anemia). Other syndromes associated with increased risk of MB in rare cases include Curry-Jones syndrome (CJS; *SMO* mutations), Greig cephalopolysyndactyly syndrome (GCPS; *GLI3* mutations), ataxia telangiectasia (*ATM* mutations) and Bloom syndrome (BS; *BLM* mutations) (Adapted from Northcott, et al., 2019)

1.3.7 Molecular subgroups

Advances in molecular genetics and epigenetics has enabled the molecular profiling of tumours, which has shed light on heterogeneous MB biology, and has become the standard methodology for subgroup determination and sub-classification within each subgroup. In 2012, a consensus was reached based on transcriptomic and methylomic data, describing that MB comprises four different molecular subgroups: Wnt (MB_{WNT}), Shh (MB_{SHH}), Group 3 (MB_{Group3}) and Group 4 (MB_{Group4}), each of them associated with distinct prognosis, molecular alterations, and demographics (Northcott et al., 2012b, Kool et al., 2012, Taylor et al., 2012, Schwalbe et al., 2013).

In 2016, the WHO classification of tumours of the central nervous system officially adopted these four molecular subgroups, and since then further refinement of the subgroups has been possible allowing the determination of substructures within each subgroup (Northcott et al., 2017, Schwalbe et al., 2017, Cavalli et al., 2017).

The four distinct molecular subgroups present substantial biological and survival differences (Figure 1.7), which is still present within the sub-classification of each subgroup.

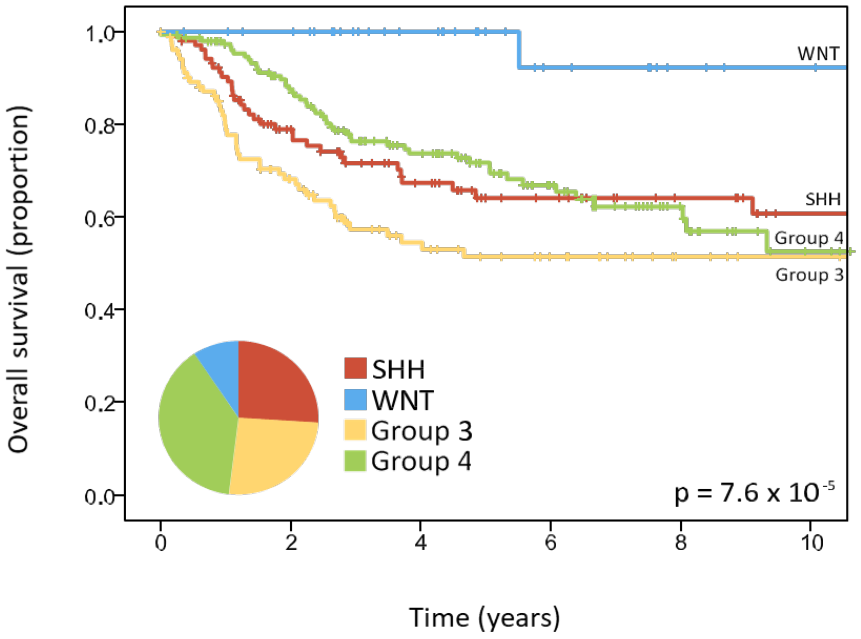

Figure 1.7. Overall survival of patients with MB. Kaplan-Meier plot of overall survival in MB, according to molecular subgroup. MB_{WNT} (WNT; blue), MB_{SHH} (red; SHH), MB_{Group3} (yellow; Group 3), MB_{Group4} (green; Group 4). The pie chart represents the proportion of MBs in each subgroup (PBTG, Newcastle, UK)

1.3.7.1 WNT subgroup

MB_{WNT} is the least common subgroup, accounting for approximately 10% of all MB cases. MB_{WNT} predominantly affects older children but can occur at all ages, with a peak incidence between 6-13 years of age and usually presenting with classic histology (Taylor et al., 2012).

Tumours that fall in this category are characterised by loss of chromosome 6 (80-85% of patients) and hyper-activation of the WNT signalling pathway. Over 85% of MB_{WNT} tumours harbour a point mutation in exon 3 of the gene encoding for β-catenin, *CTNNB1*, leading to the constitutive activation of the WNT signalling pathway (Northcott et al., 2012b, Northcott et al., 2017, Juraschka and Taylor, 2019). Aberrant activation of the WNT pathway causes β-catenin stabilisation and consequent nuclear accumulation, which triggers the transcription of pro-tumourigenic genes, including *MYC* and cyclin D1, promoting proliferation.

Recent studies have shown that the majority of MB_{WNT} tumours that lack *CTNNB1* mutations correspond to patients with germline *APC* mutations (Waszak et al., 2018). Other recurrent genetic alterations include mutations in *DDX3X* (36%), *SMARCA4* (19%), *TP53* (14%), *CSNK2B* (14%), *PIK3CA* (11%), and *EPHA7* (8%)(Figure 1.8)(Jones et al., 2012, Northcott et al., 2017, Pugh et al., 2012, Robinson et al., 2012) .

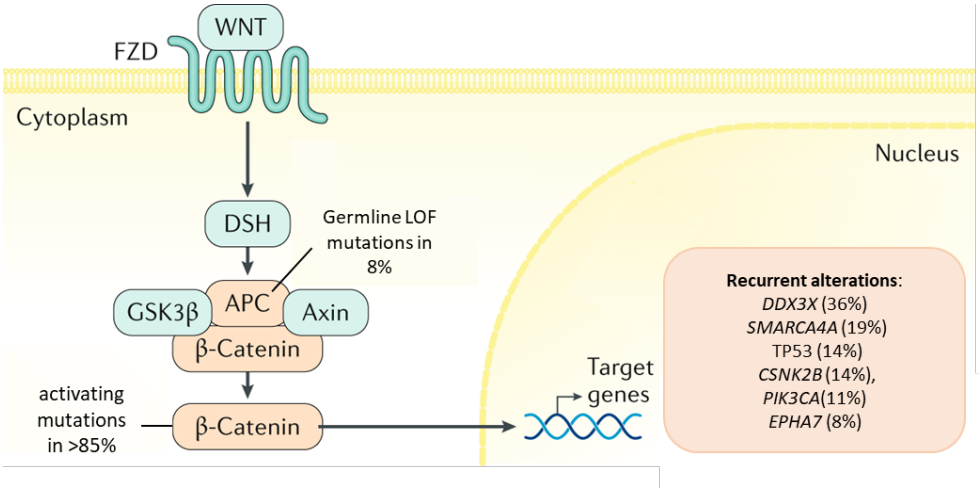

Figure 1.8. WNT subgroup. MB_{WNT} are characterised by alterations in genes involved in the canonical wingless (WNT) signalling pathway. Upon binding of Wnt protein to its receptor Frizzled (FZD), dishevelled (DSH) is activated which prevents the degradation of β-catenin through the disruption of the protein complex APC/AXIN/GSK3β. β-catenin is translocated to the nucleus and activates the expression of downstream target genes, including *MYC* and cyclin D1. When the pathway is inactive, β-catenin is phosphorylated and bound to the APC/AXIN/GSK3β protein complex, which mediates its proteasomal degradation. The percentage values denote the proportion of patients of MB_{WNT} who have the genetic mutation. LOF, loss-of-function (Adapted from Northcott, et al., 2019)

MB_{WNT} confers the best prognosis of all subgroups, with a much lower metastatic spread and with survival rates at five years above 95% in patients under 16 years of age. The association of <16 years of age and favourable prognosis was not seen in the SJMB12 study performed by St. Jude Children's Research Hospital, with 100% survival for all WNT patients.

The high overall survival (OS) of patients with MB_{WNT} includes those patients presenting high risk factors like LCA phenotype or *TP53* mutations (summarised in Figure 1.9) (Kool et al., 2012, Taylor et al., 2012, Lindsey et al., 2011).

Current multicentre clinical trials for MB have incorporated subgroup and risk features to stratify patients in order to adjust therapy intensity according to their biomarkers, in an attempt to reduce treatment toxicity and long-term side effects (NCT02724579; NCT02066220; NCT01878617)(Pizer and Clifford, 2009). Currently, only the SJMB12 trial enrols high-risk patients on a biologically informed basis, and there are no open trials for high-risk non-infants in Europe (Ramaswamy et al., 2016).

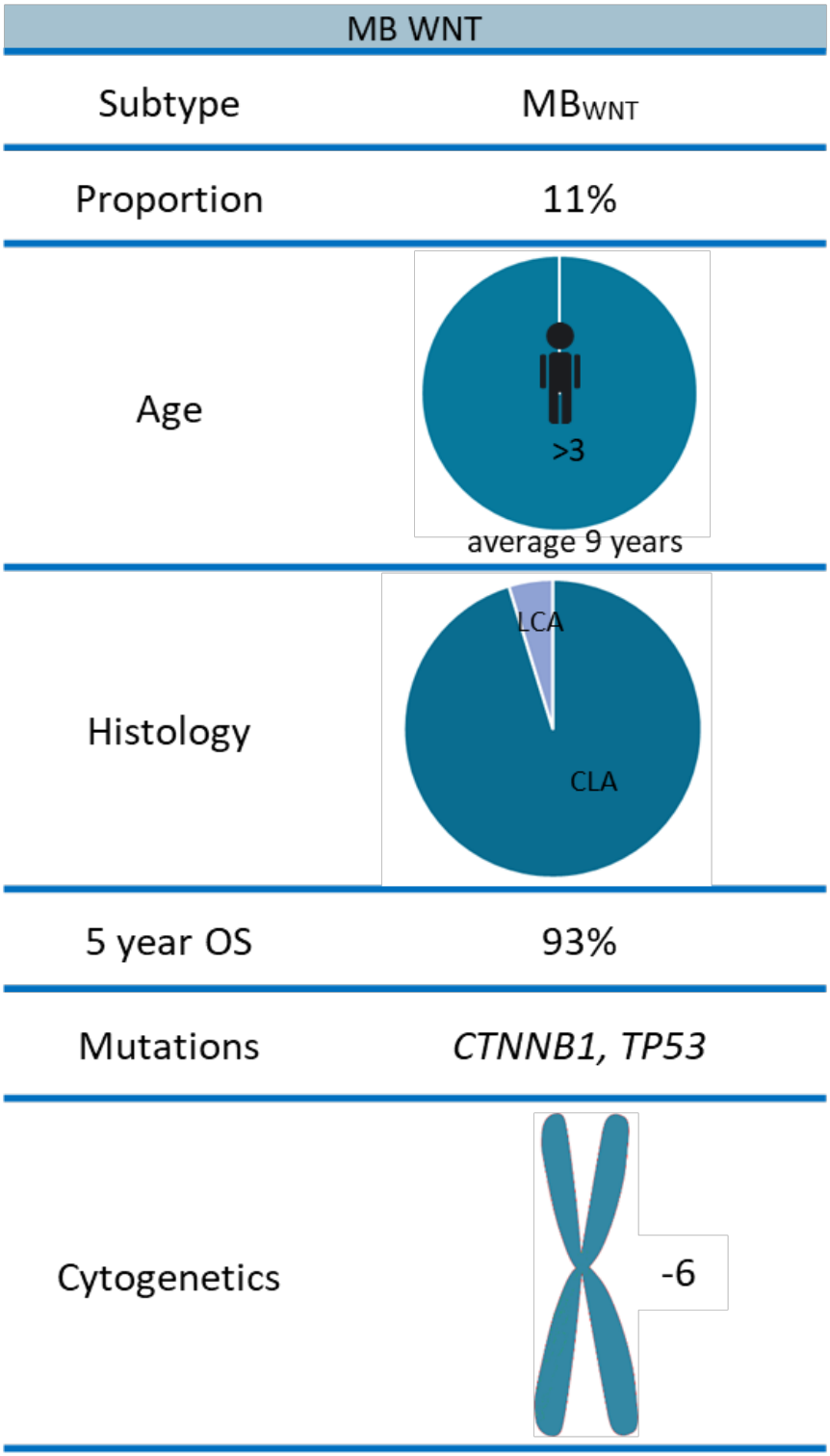

Figure 1.9. Summary of the main clinical and molecular features of WNT subgroup. Values for the proportion of cases, age, histology 5-year overall survival (OS), frequent mutations and cytogenetics of MB_{WNT}. CLA, classic histology; LCA, large-cell/anaplastic histology; DN, desmoplastic nodular histology (Adapted from Schwalbe et al., 2017)

1.3.7.2 SHH subgroup

MB_{SHH} accounts for approximately 30% of MB cases, and together with MB_{WNT}, are the best defined and understood subgroups. MB_{SHH} tumours are very heterogeneous diseases in terms of pathology, response to therapy, and outcome.

MB_{SHH} often present with nodular/desmoplastic histology, with all MBEN cases belonging exclusively to this subtype. MB_{SHH} affects males and females equally, with a bimodal age distribution, occurring most commonly in infants less than 3 years of age and in patients greater than 16 years old (Summarised in Figure 1.11).

The subgroup is characterised by alterations in genes involved in the SHH signalling pathway. Common alterations found within MB_{SHH} subgroup are mutations in *PTCH1* (43%), *SUFU* (10%), and *SMO* (9%), and amplifications of *GLI1* or *GLI2* (9%), and *MYCN* (7%) (Figure 1.10). Most adult SHH cases present mutations at the *TERT* promoter region (39%). Another frequently observed alteration is the mutation of *TP53*, occurring in 9.4% of MB_{SHH}, which confer an extremely poor prognosis (Northcott et al., 2012b, Juraschka and Taylor, 2019, Lindsey et al., 2014, Zhukova et al., 2013). In a very few cases MB_{SHH} patients have metastatic spread at diagnosis and in general have an intermediate prognosis. Despite OS rates around 70%, patients with either *GLI2* amplifications, chromosome 14 loss, 10q deletions, *MYCN* amplifications and particularly those with *TP53* mutations have a poor prognosis and overall survival of 41% (Pezzolo et al., 2011, Pugh et al., 2012, Zhukova et al., 2014).

Four different subtypes have so far been described within MB_{SHH} (SHHα, SHHβ, SHHγ and SHHδ)(Cavalli et al., 2017). SHHα has the worst prognosis, which primarily presents with *GLI2* and *MYCN* amplifications, and mutations in *TP53*. SHHβ and SHHγ are both infant subtypes, with distinct biology and outcome. SHHβ are generally metastatic and harbour multiple focal amplifications and focal *PTEN* deletions, whereas SHHγ are associated with MBEN histology and fewer copy number alterations, which have better outcomes than SHHβ. Lastly, the SHHδ subtype affects mainly adults and is characterised by *TERT* promoter mutations (Cavalli et al., 2017, Schwalbe et al., 2017).

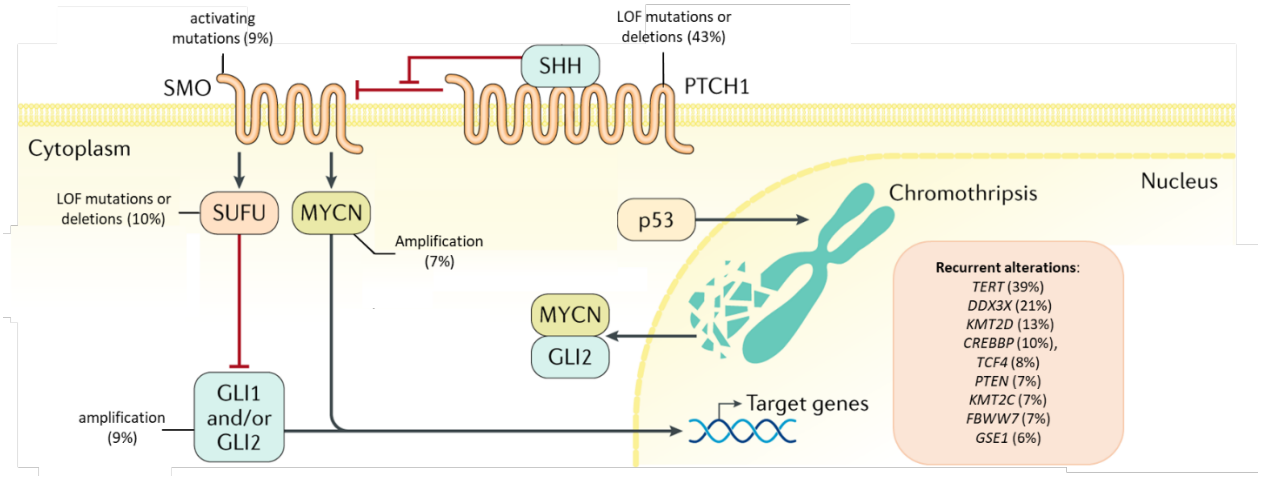

Figure 1.10. SHH subgroup. MB_{SHH} are characterised by alterations in genes involved in the sonic hedgehog (SHH) signalling pathway. When inactive, Ptch receptors (PTCH1) prevent the translocation of smoothened receptors (SMO) to the cilium, which mediates the activation of SUFU, who binds to GLI1 and GLI2 transcription factors in the cytoplasm preventing their translocation to the nucleus, mediating their degradation. Upon binding of SHH to PTCH1, PTCH1 ceases to repress SMO, liberating SUFU from binding the Gli proteins, which can then translocate to the nucleus and activate the transcription of target genes. The percentage values denote the proportion of patients of MB_{WNT} who have the genetic mutation. LOF, loss-of-function (adapted from Northcott, et al., 2019).

Most advances in targeted therapies have been made in the MB_{SHH} subgroup, where inhibitors of the SHH signalling pathway are in phase I/II clinical trials (Romer and Curran, 2005, Gajjar et al., 2013). Importantly, resistance to treatment has emerged after exposures to *SMO* inhibitors, which has led to the targeting of CK2 instead (downstream target of *SMO* in the SHH pathway) for durable remission. A phase I/II trial is recruiting patients with recurrent MB_{SHH} to test the efficacy of the CK2 inhibitor CX-4945 (NCT03904862)(Purzner et al., 2018).

MB SHH		
Subtype	MB $_{SHH\text{-}Child}$	MB $_{SHH\text{-}Infant}$
Proportion	9%	16%
Age	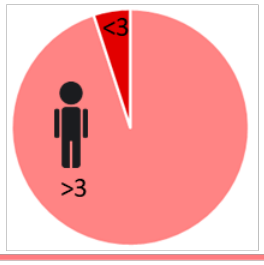	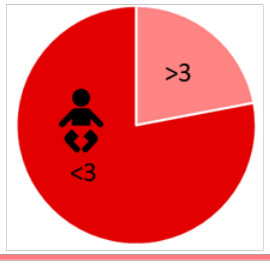
Histology	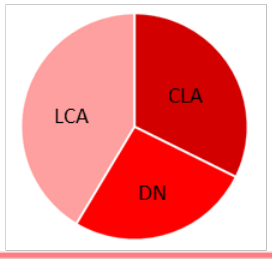	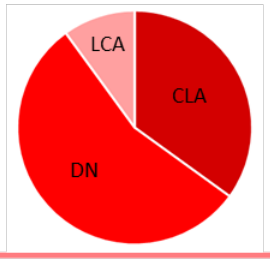
5 year OS	58%	62%
Mutations	*TP53, TP53* germline, *TERT, SUFU, PTCH1*	*SUFU, PTCH1*
Cytogenetics	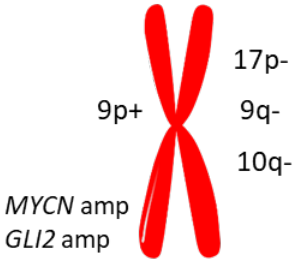	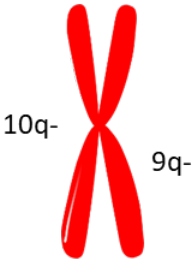

Figure 1.11. Summary of the main clinical and molecular features of SHH subgroup. Values for the proportion of cases, age, histology 5-year overall survival (OS), frequent mutations and cytogenetics of MB_{SHH}. CLA, classic histology; LCA, large-cell/anaplastic histology; DN, desmoplastic nodular histology (Adapted from Schwalbe et al., 2017)

1.3.7.3 Group 3 subgroup

MB_{Group3} comprise 25% of MBs and carry the worst prognosis of all subgroups, with overall survival at 5 years less than 60%. MB_{Group3} affect mostly infants and children, with a 2:1 male to female predominance. Tumours within this subgroup exhibit LCA or classic histology and are characterised by metastatic disease at diagnosis (47%)(Taylor et al., 2012, Jones et al., 2012, Northcott et al., 2012a).

Despite having the poorest prognosis, unlike SHH and WNT subgroups, a common driver pathway has not yet been identified, and it is the most poorly understood in regards to its biology. MB_{Group3} present unstable genomes, but the most common recurring alteration is the amplification or over-expression of the c-*MYC* oncogene (c-*MYC* is hereafter referred to as *MYC*), accounting for 17% of MB_{Group3} cases. Clifford and colleagues have shown that the gravest prognosis in infant MB_{Group3} is defined by the amplification of *MYC* (copy number ≥5; ~91% of patients) with patients with this aberration succumbing to disease within 1 year (PBTG, unpublished)(Taylor et al., 2012, Northcott et al., 2012b).

MB_{Group3} exhibit tetraploidy, and present several copy number alterations, the most recurrent being the loss of chromosomes 17p (~40-45%), 8, 10q and 16q; and gain of chromosomes 1q, 7, and 18. Chromothripsis is a form of genome structural variation that frequently occurs in *MYC*-amplified MB_{Group3}. Upregulation *GFI1* and *GFI1B* has been seen in around 15-20% of MB cases as a consequence of structural variations placing the coding sequences of both genes next to super-enhancers, instigating their activity ('enhancer hijacking')(Northcott et al., 2014, Northcott et al., 2017, Jones et al., 2012, Taylor et al., 2012, Northcott et al., 2012b, Lee et al., 2019).

Somatic mutations are less common in this subgroup, events occurring in only 5% of patients. Only 4 genes are recurrently mutated: *SMARCA4*, *KBTBD4*, *CTDNEP1* and *KMT2D*. The amplification of the *OTX2* (2%) and *MYCN* (5%) can also be seen in a small subset of these tumours.

Like in the other subgroups, several MB_{Group3} subtypes have been proposed. In 2017, Schwalbe *et al*., using DNA methylation data, divided MB_{Group3} into a high-risk and a low-risk subtype, with *MYC* amplification/overexpression and LCA histology being high-risk features associated with shorter progression free survival (summarised in Figure 1.12)(Schwalbe et al., 2017, Northcott et al., 2019).

MB Group 3		
Subtype	$MB_{Group3-LR}$	$MB_{Group3-HR}$
Proportion	12%	16%
Age	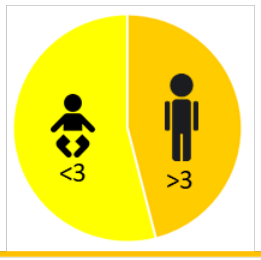	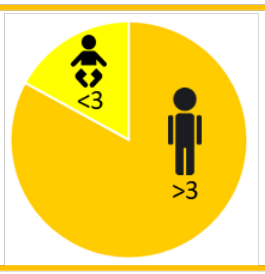
Histology	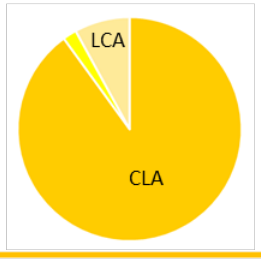	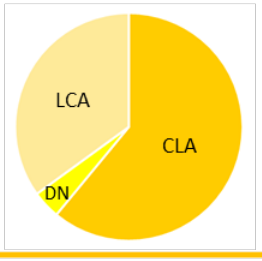
5 year OS	69%	37%
Mutations	-	*GFI1*
Cytogenetics	+7 +14 +18  -4 -8 -10 -11 -13 -15 -16 -21	+5 +8 +13 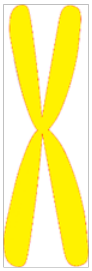 i17q 16q- *MYC* amp

Figure 1.12. Summary of the main clinical and molecular features of Group 3 subgroup. Values for the proportion of cases, age, histology 5-year overall survival (OS), frequent mutations and cytogenetics of MB_{Group3}. CLA, classic histology; LCA, large-cell/anaplastic histology; DN, desmoplastic nodular histology (adapted from Schwalbe et al., 2017)

1.3.7.4 Group 4 subgroup

MB_{Group4} is the most common subgroup, comprising ~ 40% of all MB diagnosis. MB_{Group4} can occur at all ages, but is less common in infants, affecting males more frequently (3:1 ratio). Despite frequently presenting with CLA histology and metastasis at diagnosis (35-40% of cases), patients with MB_{Group4} have an intermediate prognosis (Taylor et al., 2012, Northcott et al., 2012b).

Similarly to MB_{Group3}, the underlying molecular mechanism of this subgroup is poorly understood. Gene-level somatic mutations are rare (6-9% of cases), occurring more commonly in *KDM6A*, *ZMYM3*, *KTM2C* and *KBTBD4*, genes encoding for chromatin modifying proteins.

Common genomic aberrations involve the amplification of *MYCN*, *OTX2* and *CDK6* (all comprising 6% of cases), and enhancer-hijacking-mediated overexpression of *GFI1* and *GFI1B* (5-10%), and PRMD6 (17%)(Figure 1.13). MB_{Group4} can also present with large chromosomal alterations, especially gains of chromosome 7 and 17q, and the loss of chromosome 8, 11 and 17p (Northcott et al., 2012b, Northcott et al., 2017, Taylor et al., 2012, Kool et al., 2012).

As with MB_{Group3}, the MB_{Group4} subgroup was further subdivided into two subtypes, low- and high-risk. Features conferring high-risk status are metastatic disease and gain of chromosome 7; whereas, in a MB_{Group4} specific context *MYCN* amplification and LCA histology did not confer a poorer prognosis (Summarised in Figure 1.14)(Schwalbe et al., 2017).

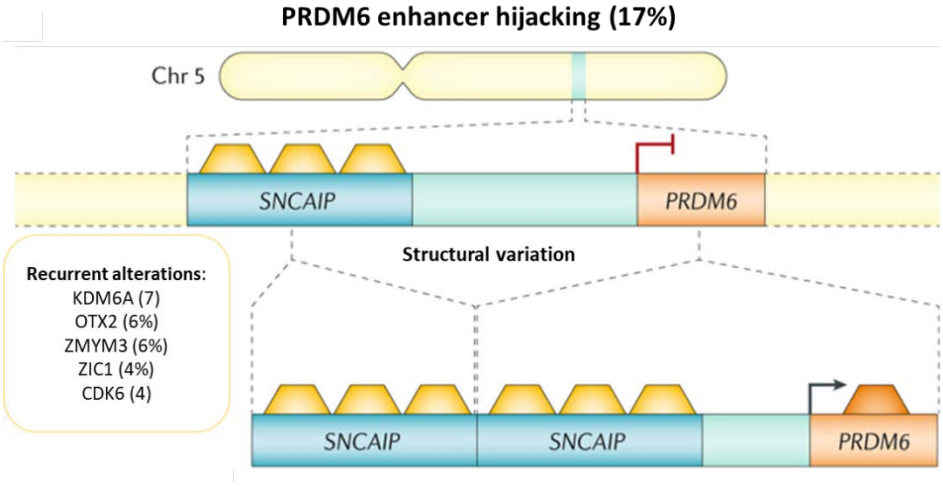

Figure 1.13. Main molecular characteristics of Group 4 subgroup. MB_{Group4} tumours present little single gene mutations, with overexpression of PRDM6 as a consequence of its translocation downstream SNCAIP, promoting its overexpression. The percentage values denote the proportion of patients of MB_{Group4} who have the genetic mutation (adapted from Northcott et al., 2019)

MB Group 4		
Subtype	$MB_{Group4\text{-}LR}$	$MB_{Group4\text{-}HR}$
Proportion	18%	21%
Age	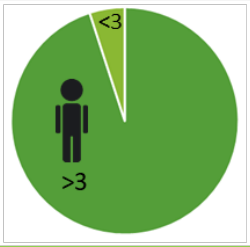	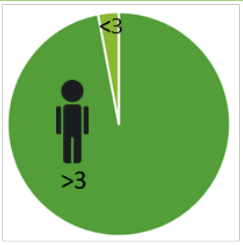
Histology	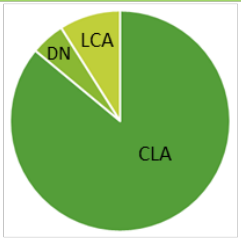	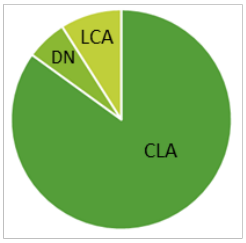
5 year OS	80%	69%
Mutations	-	-
Cytogenetics		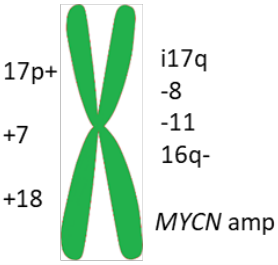

Figure 1.14. Summary of the main clinical and molecular features of Group 4 subgroup. Values for the proportion of cases, age, histology 5-year overall survival (OS), frequent mutations and cytogenetics of MB_{Group4}. CLA, classic histology; LCA, large-cell/anaplastic histology; DN, desmoplastic nodular histology (Adapted from Schwalbe et al., 2017).

1.4 *MYC*

he *MYC* family of oncogenes consists of *c-MYC, MYCN* and *MYCL*, which encode c-Myc, N-Myc and L-Myc (Nesbit et al., 1999). This family of genes are multifunctional transcription factors with helix-loop-helix leucine zipper motifs that regulate the expression of up to 15% of the entire genome (Fernandez et al., 2003, Conacci-Sorrell et al., 2014). MYC proteins act as transcription amplifiers of effectors involved in multiple cellular processes, including cell-cycle progression, metabolism, ribosome biogenesis and protein synthesis (Figure 1.15). The major involvement of *MYC* in controlling such fundamental biological processes requires its strict regulation at the expression and functional level (Tansey, 2014).

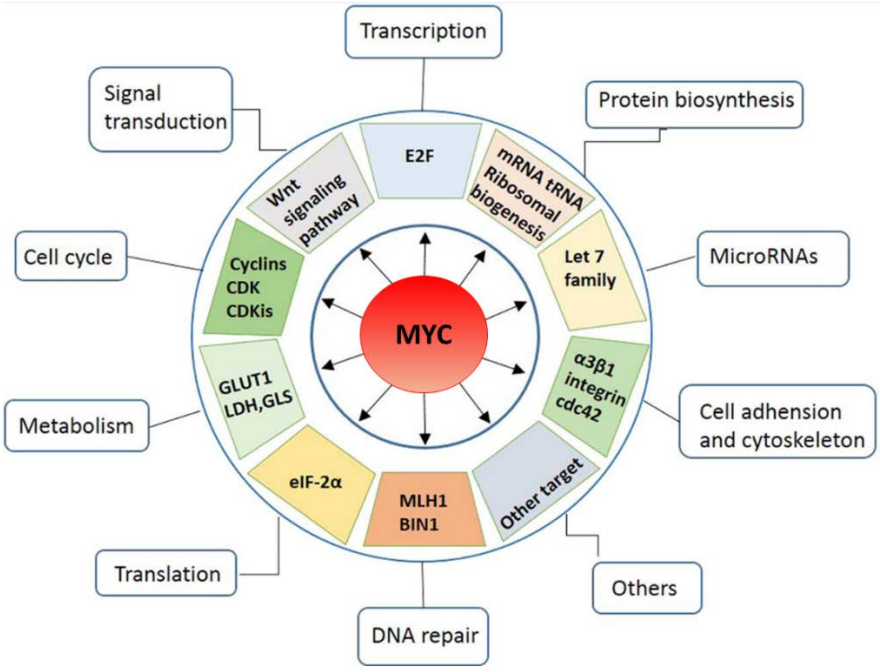

Figure 1.15. Cellular processes regulated by *MYC*.As a transcription factor, *MYC* regulates the expression of genes whose effectors are involved in a broad range of cellular functions, including cell cycle progression, metabolism, and protein biosynthesis. Adapted from Chen et al., 2018.

1.4.1 MYC structure

MYC is situated on human chromosome 8q24, and comprises three exons, with one of them being non-coding. The two coding exons translate into three different isoforms; the one starting at a canonical AUG codon in exon 2 (size 64kDa) is the most studied one, referred to as *MYC* (Hann et al., 1994). MYC proteins are characterised by a highly conserved N-terminal region, containing a transactivation domain comprised of two MYC boxes (I and II), essential for DNA-binding and MYC's role as a transcriptional regulator (Ryan and Birnie, 1996). At the C-terminal region lies the basic-helix-loop-helix leucine zipper (bHLHZ), required for binding to specific DNA sequences (enhancer boxes; E-Box) (Figure 1.16)(Dang, 1999).

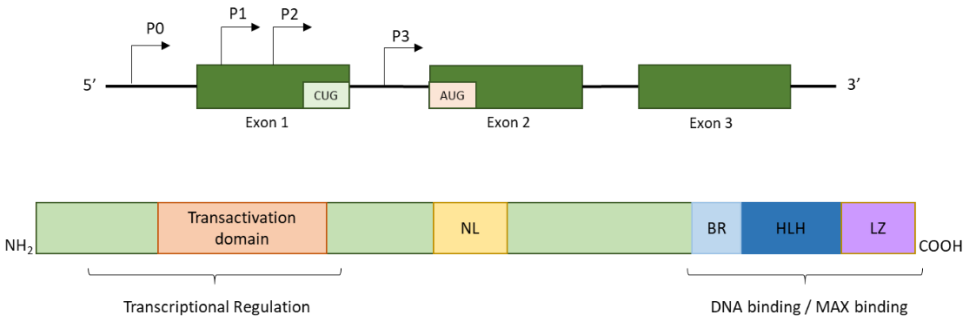

Figure 1.16. *MYC* structure and functional domains of human *MYC*. Schematic representation of *MYC* gene and the structure of its resultant protein products. The sites of the gene's promoters are indicated as P0, P1, P2 and P3. The initiation sites for the translation of the two MYC isoforms are shown as codons of the initial amino acids (CUG; AUG); NL, nuclear localization; BR, basic region; HLH, helix-loop-helix; LZ, leucine zipper. Adapted from *(Ryan and Birnie, 1996).*

1.4.2 Transcriptional control of MYC

MYC regulates transcription of its target gene by dimerization with its protein partner MAX. Interaction with MAX is done through the common BR-HLH-LZ motif, which enables the formation of a MYC/MAX complex with the ability to bind to the conserved DNA sequence (CACGTG) found in E-box elements of target genes. Upon recognition and binding to these specific sequences, MYC/MAX heterodimer recruits a chromatin remodelling complex (TRRAP, GCN5, TIP60 and TIP48) that allows the stimulation of gene expression (Adhikary and Eilers, 2005, Pelengaris et al., 2002, Chen et al., 2018b). Alternatively, repression of transcription can also occur upon binding with MIZ1 (Figure 1.17). Activation of *MYC* expression upon mitogenic stimuli recruits Miz1 to interact with the MYC/MAX heterodimer to repress transcription of MYC target genes. The ratio of Myc and Miz1 bound to E-boxes of gene promoters guide the direction of the transcription response (Vo et al., 2016)(Figure 1.16).

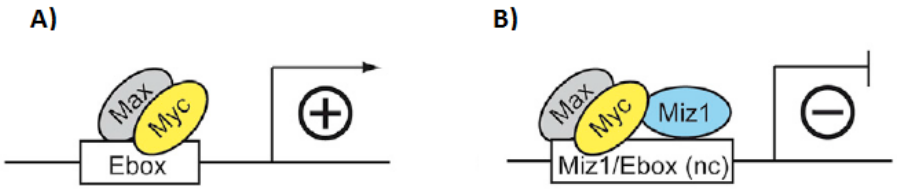

Figure 1.17. Interaction of MYC with MAX and MIZ1 to promote/repress genes expression. Schematic of the MYC-MAX-MIZ1 interactions to stimulate/repress gene expression. A) Formation of the heterodimer MYC/MAX complex promotes gene expression (+) upon binding to Enhancer box regions (E-box). B) When Miz1 is recruited to E-boxes with the MYC/MAX heterodimer, *MYC* represses gene transcription (Adapted from Vo et al., 2016)

In addition, MAX can also form complexes with the bHLHZ-Mad family proteins, Mga and Mnt, which bind to E-box consensus sequences and repress transcription through the recruitment of histone deacetylase complexes (Grandori et al., 2000). Cellular differentiation and growth arrest has been associated with increased expression of Mad protein, suggesting their function as tumour suppressor proteins. To date, Mxi-1 (Mad2) protein is the only Mad family member with evidence of tumour suppressor capabilities (Boxer and Dang, 2001).

1.4.3 MYC protein stability

It is not surprising, given the importance of *MYC* as a transcriptional regulator able to determine cell fate (proliferation and apoptosis), that sophisticated mechanisms are in place to ensure proper levels of *MYC* expression, at the transcriptional (initiation and elongation), post-transcriptional (mRNA stability) and translational level (protein stability)(Sears, 2004).

MYC protein stability is regulated by several post-translational modifications, which include phosphorylation, acetylation, glycosylation and ubiquitination. MYC-stability is mediated by its phosphorylation at two specific residues within the N-terminal region, Threonine 58 (T58) and Serine 62 (S62), upon mitogenic activation of the Ras-dependent signalling cascade (Adhikary and Eilers, 2005). Activation of Ras results in the *ERK*-mediated phosphorylation of MYC at S62, which increases MYC protein stability. By contrast, phosphorylation of the MYC Thr58 site by GSK-3β through the PI3K/AKT signalling pathway destabilises MYC and facilities the de-phosphorylation of MYC at Ser62. Phosphorylation of the T58 residue is recognised by the E3 ubiquitin ligase SCF^{fbw7}, which stimulates the Ub-dependent proteasomal degradation of MYC (Figure 1.18). Therefore, MYC stability is granted by the Ras-dependent inhibition of GSK-3β, preventing MYC phosphorylation at T58 and its concomitant proteasomal degradation (Tansey, 2014, Sears, 2004, Vervoorts et al., 2006).

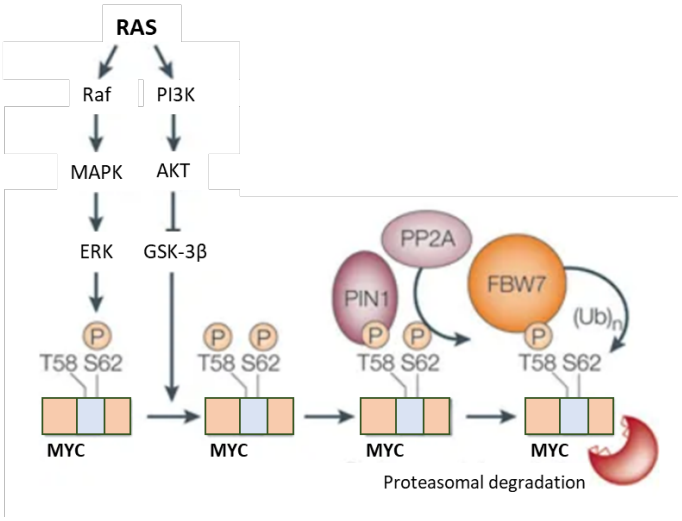

Figure 1.18. Transcriptional regulation of *MYC*.MYC protein stability is regulated by its phosphorylation at Serine 62 (S62) and Threonine 58 (T58) of its conserved N-terminal domain, by the Ras-dependent signalling cascade. Following mitogen stimulation, Ras is activated, which stabilises MYC through its phosphorylation at S62 through the MAPK/ERK pathway and phosphorylation at T58 by inhibition of GSK-3β through the PI3K/AKT signalling pathway. Phosphorylation of MYC at T58 is recognised by the prolyl isomerase (PIN1), which enables the removal of the phosphate residue at S62 by the phosphatase-2A (PP2A). MYC phosphorylation at T58 is recognised by the ubiquitin ligase SCF^{fbw7}, which marks MYC for proteasomal degradation (adapted from Adhikary and Eilers, 2005).

1.4.4 Biological functions of MYC

1.4.4.1 Cell cycle and proliferation

One of the key biological functions of *MYC* is its ability to promote and regulate cell-cycle progression. Upon mitogenic stimuli, MYC proteins have the capacity to activate and repress genes involved in the process, expediting the entry of both G_1 and G_2 phases of the cell cycle, speeding cells' cycling rate whilst reducing their requirements for growth factors to sustain it (Pelengaris et al., 2002, Tansey, 2014).This is most likely due to the ability of *MYC* to directly upregulate gene expression of cyclin-dependent kinases (cyclin D2, D3, E1, E2, CDC25A, E2F1 and E2F2) and downregulate those involved in cell cycle arrest (p15, p21, p27) (Dominguez-Sola and Gautier, 2014).

1.4.4.2 Apoptosis

It is now widely acknowledged that programmed cell death by apoptosis is a natural impediment during neoplastic transformation. Over the past decade much effort has been spent on unravelling *MYC*-driven apoptosis mechanisms to convert oncogenic levels of MYC from pro-survival to pro-apoptotic (McMahon, 2014).

Oncogenes like *MYC* activate the apoptotic signalling pathway in a cell-specific context in the absence of appropriate survival signals (Figure 1.19). *MYC* can induce apoptosis by affecting the transcription of downstream effectors of the apoptotic pathway, causing an imbalance between pro-apoptotic and anti-apoptotic proteins (Tansey, 2014, Pelengaris et al., 2002). *MYC* can regulate the expression of members of the BH3-only category of Bcl-2 family proteins, stimulating the expression of Bim (Bcl2 antagonist) whilst inhibiting the expression of the pro-apoptotic proteins Bcl-2 and Bcl-X_L (Eischen et al., 2001, Pelengaris et al., 2002). Bim promotes the release of cytochrome c from the mitochondria causing the induction of apoptosis by associating with apoptotic protease-activating factor 1 (APAF1) protein to create the apoptosome, which activates the downstream caspase-dependent effectors cascade (Figure 1.19)(Pelengaris et al., 2002).

Nonetheless, the ARF-MDM2-p53 axis is the most common pathway by which *MYC* induces apoptosis. Upregulation of expression of the tumour suppressor ARF leads to the destabilisation and inactivation of the ubiquitin ligase MDM2, which targets p53 for degradation. Induction of p53 leads to the activation of its broad tumour suppressive apoptotic response (Soucie et al., 2001, Tansey, 2014). The importance of the ARF/p53 pathway to combat the tumorigenic capacity of *MYC* is reflected by the frequent loss of the tumour suppressor p53 in human cancers (Phesse et al., 2014).

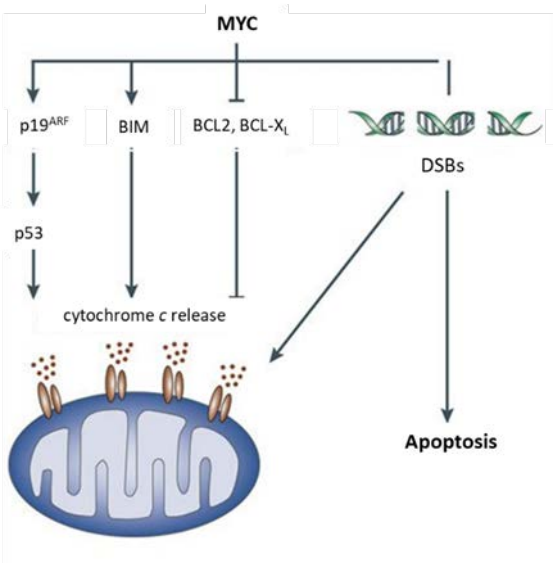

Figure 1.19. Pathways associated with *MYC* induced apoptosis. *MYC* can induce apoptosis through several pathways. *MYC* can stabilise p53 through the induction of $p19^{ARF}$. Alternatively, *MYC* can directly regulate the expression of the pro-apoptotic BH3-only protein BIM, whilst blocking the expression of anti-apoptotic proteins BCL2 and BCL-X_L, which both lead to the release of cytochrome c from the mitochondria. Another mechanism by which *MYC* potentially induces apoptosis is through its ability to induce genomic instability - DNA damage (DNA double-strand breaks (DSBs)(Adapted from Adhikary and Eilers, 2005).

1.4.4.3 Differentiation

Normal tissues constrain cell growth by driving cell differentiation, which is an irreversible post-mitotic state. Inhibition of cell differentiation was one of the first *MYC* activities to be described (Leon et al., 2009). *MYC*-dependent cell cycle progression is generally incompatible with terminal differentiation; suppression of *MYC* expression has been shown to trigger negative growth inhibitory signals that are essential to exit the cell cycle and undergo differentiation (Oster et al., 2002). Moreover, severe downregulation of *MYC* and its transcriptional partner MAX is seen in cells under terminal differentiation (Meyer and Penn, 2008).

Several studies have established the importance of the MYC-MAX-Mad network in regulating cell proliferation and differentiation (Grandori et al., 2000). MAD protein members MAD1, MXI1, MAD3, and MAD4 have been linked to terminal differentiation and inhibition of cell cycle progression by antagonising MYC-MAX function as transcriptional activators. MAX-MAD heterodimers repress transcription by recruiting class I histone deacetylases to target gene promoters, thereby decreasing the accessibility of activator factors to the DNA (Amati et al., 2001, Pelengaris et al., 2002).

1.4.4.4 Genomic instability

Neoplastic transformation occurs with the progressive acquisition of changes in the genome, conferring upon them selective advantages that lead to their clonal expansion. Under normal circumstances, a complex array of DNA monitoring and repair is in place in order to maintain genomic integrity, preventing mutation events occurring (Hanahan and Weinberg, 2000).

The main mechanism by which *MYC* causes genomic instability is by promoting replication stress (Felsher and Bishop, 1999). *MYC* promotes the rapid turnover of cells by activating the transcription of genes involved in cell cycle progression and DNA synthesis, which is in need of a rapid replication process. Upregulation of *MYC* expression coupled with the loss of tumour suppressor genes like *TP53*, prevents cells from sensing DNA damage and its consequent repair (Dominguez-Sola and Gautier, 2014, Mazouzi et al., 2014). *MYC* activation allows cells to bypass the checkpoint controls of the cell cycle, allowing the aberrant replication and survival of cells with genetic load, which confer a selective advantage to normal cells (Oster et al., 2002, Kumari et al., 2017)

Alternatively, *MYC* can promote genetic instability by inducing DNA damage through the accumulation of reactive oxygen species (ROS)(Vafa et al., 2002). Upregulated *MYC* expression leads to elevated cellular metabolic activity and mitochondrial biogenesis that causes an increase in ROS, which leads to DNA oxidative damage (Rohban and Campaner, 2015).

1.5 *MYC* deregulation in cancer

MYC has the ability to regulate most of the cellular processes in the body. It is no surprise, that under normal circumstances, *MYC* expression is stringently controlled to ensure cellular homeostasis. Deregulation of the strict regulatory control of *MYC* activity can provide the basis to acquire the fundamental traits needed for neoplastic transformation (Dang, 2012).

In cancer, *MYC* is the most frequently deregulated oncogene, partly due to the fact that unlike other oncoproteins such as Ras, its coding sequence does not need to be changed in order to unleash its oncogenic potential (Grotzer et al., 2009). In fact, most human cancers show increased *MYC* expression, which is correlated with tumour aggressiveness (Vita and Henriksson, 2006). Although point mutation and c-*MYC* locus rearrangements have been reported, mostly in Burkitt's lymphoma, their prevalence is low in other cancers (Schmitz et al., 2014).

MYC deregulation in cancer cells can occur through a series of direct and indirect mechanisms. *MYC* activation can occur through the direct regulation of the cellular mechanisms that maintain *MYC*-expression control, or through the activation of upstream signalling cascades that enhance MYC stability (Oster et al., 2002). The most common mechanism to acquire constitutive overexpression of *MYC* is through gene amplification, which can take the form of small or large focal amplifications, or in the form of double-minute chromosomes, as an extrachromosomal gene amplification (Vita and Henriksson, 2006).

An additional documented process that can result in oncogene amplification is chromothripsis (Figure 1.20). Chromothripsis occurs when cells fail to properly segregate chromosomes during mitosis, causing chromosomes to break into multiple fragments causing the accumulation of damaged DNA in the cell. When this occurs, the generation of DNA double-strand breaks triggers the DNA damage response as an attempt to re-join the fragmented chromosomal pieces, primarily through the non-homologous end-joining (NHEJ) repair mechanism (Rode et al., 2016, Holland and Cleveland, 2012). Through the repair process, chromosomes can be randomly joined together, losing those pieces that cannot bind a centromere during cell division, whilst some chromosomal fragments might fuse together generating a derivative chromosome called a double-minute (Dmin) (Alseraye et al., 2009, Koltsova et al., 2019). Dmin containing oncogenes that confer a selective advantage amongst normal cells, are retained and readily amplified by the cell (Rode et al., 2016).

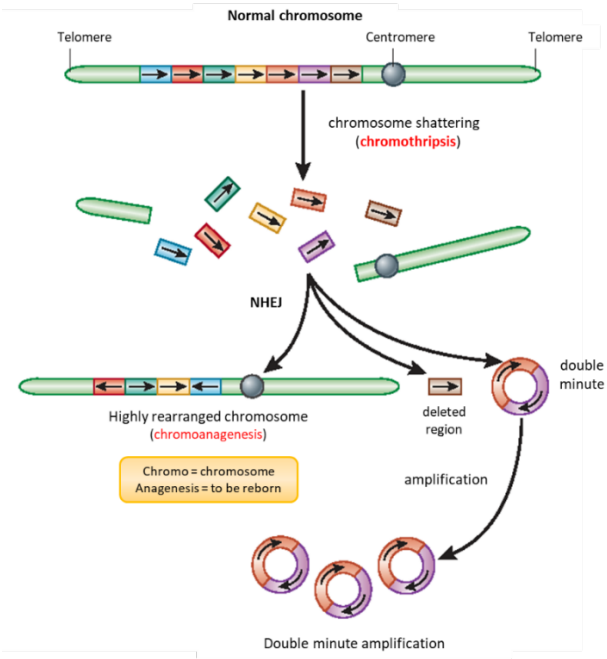

Figure 1.20.Chromothripsis as a mechanism of gene amplification. The shattering of chromosomes are rearranged and stuck back together through the non-homologous end-joining repair mechanism, leading to chromosomes with complex rearrangements. Fragments that are not reincorporated can be either lost or ends fused together to form circular, derivative chromosomes (double minute; Dmin). Dmin harbouring oncogenes are frequently amplified resulting in increased copy number of DNA fragments on these chromosomes. (Adapted from Holland and Cleveland, 2012)

Sustained high levels of *MYC* have a dramatic impact on cell proliferation, growth, metabolism, DNA replication, cell cycle progression, cell differentiation, and metastasis. The genomic instability caused by *MYC* accelerates the multistep tumorigenic process by facilitating the acquisition of the set of genetic changes required to maintain the hallmarks of malignancy (Gabay et al., 2014). Despite being the most commonly activated oncogene implicated in the pathogenesis of human cancers, upregulation of *MYC* expression alone is incapable of driving neoplastic transformation (Gabay et al., 2014). This has led to increased interest in elucidating the biological context-specific role of *MYC* in tumorigenesis, and its complex interacting network of genes to identify those who synergise with *MYC* to promote malignant transformation (Meyer and Penn, 2008).

It is well established that enhanced expression of MYC proteins contribute to almost every aspect of tumour biology, hence its involvement in most human cancers. The entire MYC family of oncoproteins has been found to be overexpressed in a diverse set of neoplastic malignancies, including blood, skin, breast, colon, and brain, becoming a representative malignant signature for each type (Nesbit et al., 1999). The fact that MYC depletion causes growth arrest and tumour regression supports the feasibility of *MYC* targeting as a new therapeutic strategy for most, if not all, oncological diseases (Wang et al., 2008).

1.6 Role of *MYC* in Medulloblastoma

Childhood medulloblastomas are extremely heterogeneous. Highly aggressive MB tumours frequently harbour *MYC* or *MYCN* amplification and/or expression. *MYC* and *MYCN* amplifications have been correlated with poor clinical outcomes and are currently accepted as adverse prognostic factors in MB (Kool et al., 2012, Ryan et al., 2012).

However, MYC proteins relate differently to each medulloblastoma subgroup, accentuating the importance of considering the molecular subgrouping of the disease for patient risk-stratification, and the need to clarify the relationship of *MYC* to MB prognosis.

1.6.5 MYC *in MB_{WNT} subgroup*

Paediatric patients with MB_{WNT} have a favourable prognosis, with >95% survival at 5 years. This is despite the frequent occurrence of *TP53* mutations in this group, and elevated expression of *MYC* (poor prognostic markers)(Roussel and Robinson, 2013). Noteworthily, amplification of the *MYC* family of oncogenes almost never occur in MB_{WNT}. In this subgroup, elevated expression of MYC proteins occurs as a direct consequence of the constitutive activation of the WNT signalling pathway, in which *MYC* is a downstream target, and thus a marker of enhanced WNT pathway activity. Therefore, the high levels of *MYC* expression in a subgroup with an excellent prognosis further confirms the notion that *MYC* expression alone is a poor prognosticator (Northcott et al., 2019).

1.6.6 MYC *in MB_{SHH} subgroup*

There is substantial biological heterogeneity within MB_{SHH}. *MYCN* and *MYCL1* are found to be uniformly highly expressed in this subgroup, whilst *MYC* amplification is very rare in this group. Activation of the SHH signalling pathway promotes the expression and stabilisation of *MYCN*, which leads to its elevated expression. Moreover, *MYCN* amplifications are frequently observed in MB_{SHH}, specifically in older children and adolescents (SHHα subtype), and are predictive of prognosis. Amplification of *MYCN* is commonly coupled with *TP53* mutations and LCA histology, high-risk features conveying poor prognosis and significantly worse outcome (Juraschka and Taylor, 2019, Northcott et al., 2019, Roussel and Robinson, 2013).

1.6.7 MYC *in* MB_{Group3} *subgroup*

MYC is more intricately linked to MB_{Group3} than any other subgroup, becoming its defining feature. *MYC* is significantly more highly expressed compared to MB_{SHH} and MB_{Group4} (similar levels to MB_{WNT}), but its aberrant amplification occurs at a much higher frequency. *MYCN* amplifications are less common in MB_{Group3}, and occur in a mutually exclusive fashion to the amplification of *MYC*, suggesting overlapping functions in a subgroup-specific manner (Roussel and Robinson, 2013). Recent MB subgroup subclassification divides MB_{Group3} into high-risk and a low-risk subtypes, in which the high-risk subgroup is associated with *MYC* amplification or overexpression (Figure 1.12).

1.6.8 MYC *in* MB_{Group4} *subgroup*

As in Group 3 tumours, *MYCN* amplification is a recurrent alteration in MB_{Group4}. Group 4 tumours generally present lower expression of the genes *MYC* and *MYCN* when compared to the other MB subgroups. Contrary to MB_{Group3}, MB_{Group4} patients with *MYCN* amplification are subclassified as low-risk and its amplification does not correlate with decreased survival rates (Swartling et al., 2010).

1.7 Role of *MYC* and *TP53* in Medulloblastoma

Medulloblastoma is a very heterogeneous entity and most of its molecular features need to be studied in the context of subgroup specificity. A particular example has been the role of the tumour suppressor gene *TP53* in the oncogenesis of MB (Ramaswamy et al., 2016), which has been widely scrutinised in the recent years.

p53 is one of the most important molecules involved in the pathogenesis of cancers. Tumour suppression by *TP53* occurs via both transcription-dependent and a transcription-independent manner (Stiewe, 2007). Transcription-dependent activities occur in the nucleus by which p53 regulates transcription of genes involved in the cell cycle, apoptosis, DNA repair, transcription, and metabolism. Transcription-independent activities induce apoptosis and autophagy in the cytoplasm (Ho et al., 2005, Yu et al., 2019). In response to cellular stress, activation of p53 mediates the upregulation of genes involved in apoptosis, cell-cycle arrest and senescence (Riley et al., 2008). Therefore, mutations in *TP53* and dysregulation of the pathway are important in the pathogenesis of many human cancers, including MB.

It has been hypothesised that *MYC* acts co-ordinately and tightly with p53 to mediate responses to stresses, where p53 levels accumulate whilst *MYC* levels are reduced, and vice-versa. Synchronised up and downregulation of *MYC* and *TP53* determine whether the cells will undergo apoptosis or senesce, and important cell fate in cancer and tumourigenesis (Ramaswamy et al., 2016).

TP53 has different roles in medulloblastoma, and the prognostic value of somatic mutations in this tumour suppressor gene is subgroup dependent. Patients with WNT tumours harbouring somatic *TP53* mutations have an excellent prognosis, whereas the prognosis of patients with SHH tumours with *TP53* mutations is dismal (Zhukova et al., 2013). Children with SHHα subtype constitute a high-risk group of patients and have the worst prognosis. This subtype primarily presents with *GLI2* and *MYCN* amplifications, and mutations in *TP53*, and its associated with treatment failures and relapse after radiotherapy (Doussouki et al., 2019)

On the other hand, *TP53* mutations are rarely observed in patients with MB_{Group3} and MB_{Group4} tumours, but they can be observed at relapse, and are usually associated with *MYC* amplification (Hill et al., 2015, Kool et al., 2014) . Although mutations are not frequent, these two subgroups usually present with the loss of one copy of *TP53* as a result of the deletion of chromosome 17p.

1.8 Study of *MYC* in MB_{Group3} context

Despite the aggressive treatment, over the past two decades survival rates for paediatric patients with MB have not increased. Subgroups with dismal prognosis, namely those with SHH with *TP53* mutations and Group 3 with *MYC* amplification, respond poorly to therapy, usually relapse and are essentially incurable. Therefore, the best opportunity to cure MB is by improving frontline therapy efficacy. To increase cure rates, it is of crucial importance to develop new targeted therapy strategies and combinational approaches with current chemotherapeutic agents for high-risk MB patients.

Despite this, MB_{Group3} driver pathways have not yet been identified, *MYC* oncogene amplification or overexpression is the most common recurring alteration (accounting for 17% of MB_{Group3} cases), and it is a high-risk factor for this subgroup (Figure 1.21) (Kool et al., 2012, Ryan et al., 2012). There is an urgent need to better understand the biology of Group 3 MB disease and to elucidate *MYC*'s role in its pathogenesis and aggressiveness, in order to translate this knowledge into the development of new treatment strategies to improve survival rates of children with these tumours.

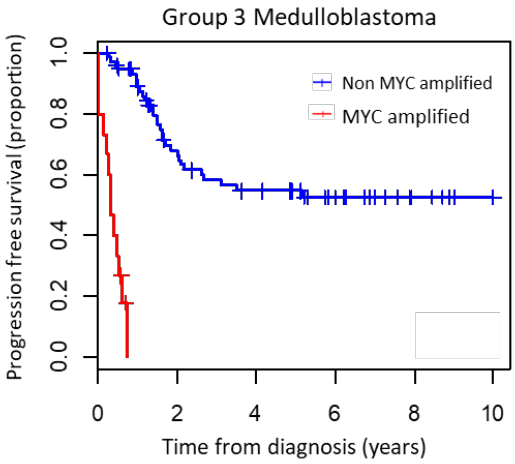

Figure 1.21. Prognosis of *MYC* amplification in Group 3 medulloblastoma. Kaplan-Meier survival comparing the progression free survival of children with Group 3 medulloblastoma with and without *MYC* amplification. Image kindly provided by Dr. Janet Lindsey

1.9 Therapeutic strategies to target *MYC*

In principle, *MYC*-driven cancers could be targeted by affecting *MYC* at the molecular level or by targeting some of the unique properties that *MYC* confers upon cancer cells for the maintenance of the malignant phenotype (Tansey, 2014).

Despite the undisputable therapeutic opportunity that *MYC* offers, *MYC* inhibitors have yet to become clinically available. For a long time, *MYC* was thought to be undruggable; the main reason being *MYC's* global implication in cells gene regulation, which its complete inhibition could cause severe toxicity and adverse side effects to normal tissues. MYCs structure as a transcription factor is another major challenge, due to its lack of an enzymatic active site that could be efficiently targeted by small molecule inhibitors (McKeown and Bradner, 2014). In addition, its nuclear localisation, which makes it harder to reach than membrane or cytoplasmic molecular targets, and the fact that the *MYC* family includes three different proteins with redundancy in some of their function, has posed a challenge in delivering a specific and efficient *MYC* inhibitor (Beaulieu et al., 2019, Whitfield et al., 2017). The technical difficulties with targeting *MYC* directly created the need to develop alternative strategies to inhibit its action, which explain the broad range of indirect targeting strategies developed over the years (Figure 1.22).

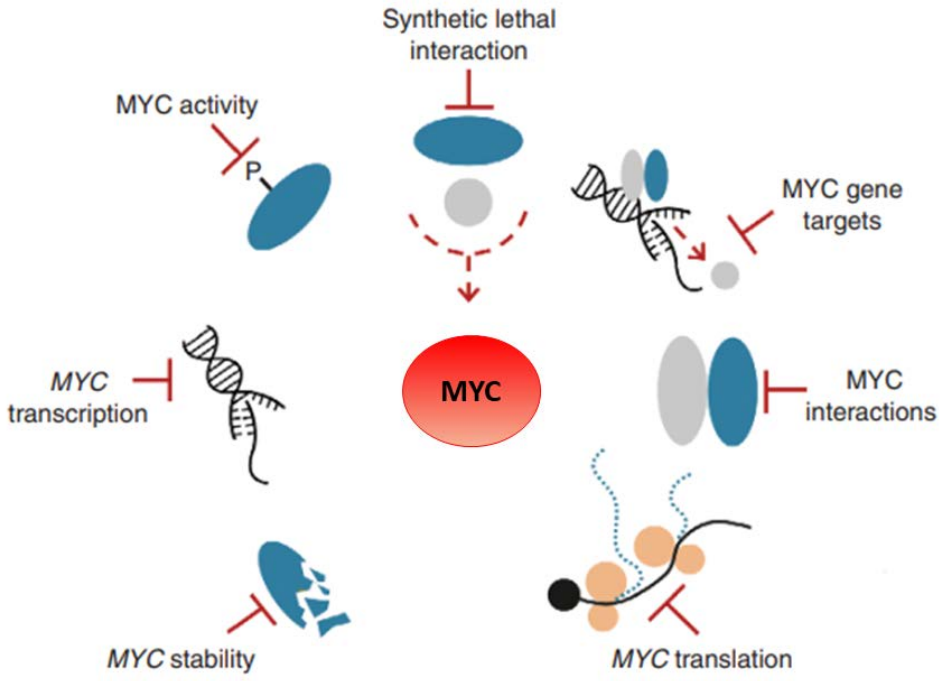

Figure 1.22. *MYC*-targeting strategies. Schematic representation of current strategies to target *MYC* activity (Adapted from Castell and Larsson, 2015).

1.9.1 Direct targeting of MYC

A great number of researchers have been addressing these difficulties in recent years, and have shown the feasibility of developing small molecules that can directly bind to and inhibit *MYC* activity (Han et al., 2019a). Strategies aiming to directly inhibit *MYC* focus on interfering with its production (promoter accessibility and/or recruitment of transcription factors) or function (preventing its interaction with MAX, or binding to DNA).

1.9.1.1 G-quadruplex stabilisers

G-quadruplex are secondary guanine-rich structures formed in nucleic acids, which reside upstream of transcriptional start sites, inhibiting expression. The NHIII(1) region of the *MYC* promoter forms G-quadruplexes. Small molecule ligands can be used to specifically stabilise G-quadruplex structures on *MYC* promoters to supress *MYC* expression at the mRNA and protein levels (Whitfield et al., 2017) (Allen-Petersen and Sears, 2019). The small molecule compounds GQC-05, CZ1, IZCZ-3 and DC-34 have been seen to stabilise *MYC* G-quadruplex and repress *MYC* expression (Calabrese et al., 2018, Das et al., 2018). So far, CX-3543 is the only G-quadruplex stabiliser that has reached clinical trials (Chen et al., 2014).

1.9.1.2 MYC/MAX disruption

Most inhibitors developed for the direct targeting of *MYC* expression have focused on disrupting MYC/MAX dimerization, or their interaction with E-box motifs to reduce *MYC* expression (Shalaby and Grotzer, 2016). MYC's bHLHZ domain is essential for *MYC* dimerization with its partner MAX and subsequent binding to E-box sequences in gene promoters to activate transcription of target genes. Several peptide mimetic compounds have so far been developed, and despite being highly selective, most of them display low potency and off-target effects, lacking *in vivo* efficacy (Mo and Henriksson, 2006, Kiessling et al., 2006).

Recently it has been reported that a new MYC/MAX inhibitor, MYCMI-6, binds directly within the conserved bHLHZ domain and disrupts the formation of the MYC/MAX complex at a low micromolar range. Its utilisation in *in vivo* studies of *MYCN* amplified neuroblastoma cell lines significantly reduced proliferation whilst inducing apoptosis. Treatment with MYCMI-6 did not cause MYC protein degradation (Castell et al., 2018).

Another promising compound found to stabilise MAX/MAX homodimers and decrease MYC protein levels is KI-MS2-008. Struntz *et al* demonstrated the efficacy of the compound in perturbing the *MYC*-driven transcriptional program, exhibiting preliminary *in vivo* efficacy by reducing tumour volume in hepatocellular carcinoma murine models (Struntz et al., 2019).

1.9.1.3 OmoMyc

The therapeutic promise of using peptide compounds to directly disrupt *MYC* activity has led to the optimisation and development of compounds for better clinical applicability. Great advances have been made with the compounds Omomyc, a dominant negative molecule consisting of the *MYC* dimerisation domain with four mutations in the *MYC* leucine zipper, which prevents its binding to all *MYC* family member promoters. Omomyc has the ability to form dimers with MYC, preventing MYC/MAX association and binding to E-box for transcriptional activation, supressing *MYC*-dependent transcription (Savino et al., 2011) (Soucek et al., 2002, Soucek et al., 2004, Jung et al., 2017).

More recently, the use of purified Omomoyc protein was proven to penetrate cell membranes and effectively interfere with *MYC* transcriptional activity, in glioma and non–small cell lung cancer *in vitro* and *in vivo* models (Wang et al., 2019a, Beaulieu et al., 2019)

There is great promise for small molecule peptides that directly interact with *MYC* and disrupt its transcriptional activity. Results published so far are encouraging researchers to further optimise these compounds for clinical application of *MYC*-targeted peptides (Figure 1.23).

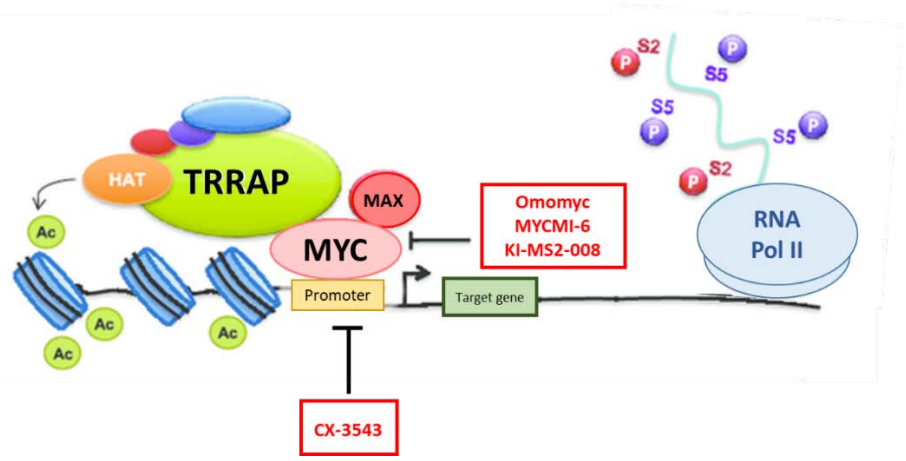

Figure 1.23. Direct targeting of *MYC*. *MYC* activity can be directly disrupted by interfering with the accessibility of transcription factors to its promoter (e.g. CX-3543 small molecule inhibitor) or by disrupting MYC/MAX dimerization to inhibit translation of *MYC*-target genes (e.g. Omomyc, MYCMI-6, KI-MS2-008 inhibitors)(adapted from Posternak et al., 2016).

1.9.2 Indirect targeting of MYC

The evident challenge that direct *MYC* targeting has presented, has led to many researchers taking indirect approaches to target *MYC* transcriptional regulation in *MYC*-driven cancers. Indirect approaches have focused on targeting *MYC* transcriptional regulation, or modulating its stability and activity (Figure 1.24)(Whitfield et al., 2017).

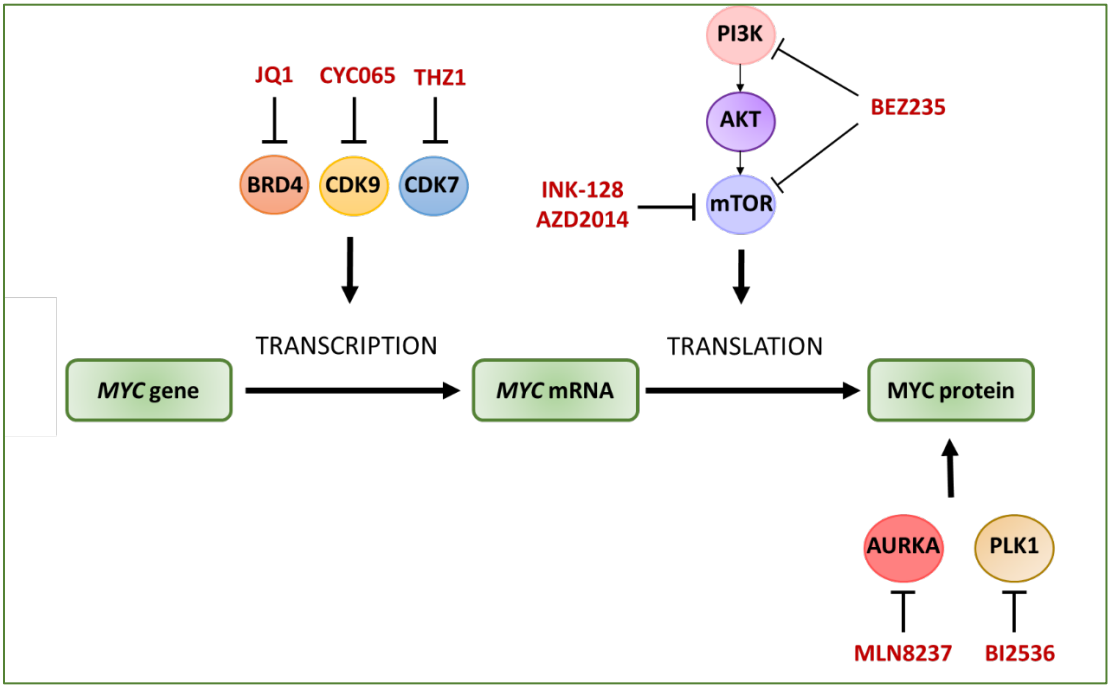

Figure 1.24. Indirect targeting of *MYC*. *MYC* activity can be indirectly disrupted by affecting its transcription, translation and protein stability. *MYC* expression at the transcriptional level can be inhibited by the use of BRD4, CDK7 and CDK9 small molecule compounds. Translation of MYC mRNA can be downregulated by inhibiting the PI3K/AKT/mTOR signalling pathway using BEZ235, INK-128 and AZD2014 small molecule compounds. *MYC* inhibition at the post-translational level can be achieved by affecting MYC protein stability with AURKA and PLK1 inhibitors (e.g. MLN8237, BI2536)(adapted from Chen et al., 2018).

1.9.2.1 Targeting MYC *transcription*

MYC transcription requires local and global epigenetic changes that control the ability of the transcriptional machinery to interact with promoters and enhancers of genes to be transcribed (You and Han, 2014). Disruption of epigenetic modifications has become a strategy of great interest to reduce *MYC* expression and activity.

Inhibitors of histone deacetylases, histone methyltransferases, histone demethylases, bromodomain, and extra-terminal motif (BET) bromodomain inhibitors have shown efficacy against *MYC* (Allen-Petersen and Sears, 2019).

1.9.2.1.1 BET bromodomain inhibition

MYC/MAX dimerisation and consequent binding to E-boxes of target gene promoters initiates the organisation of histone acetyl transferases, which promote accessible chromatin for the transcriptional machinery to interact with gene promoters.

Bromodomain proteins function as chromatin readers by recognising acetylated lysine residues on N-terminal tails of histones of active promoter regions, usually associated with an open chromatin state and therefore transcriptional activation. The bromodomain and extra-terminal domain (BET) family of proteins is composed of four members: BRD2, BRD3, BRD4, and BRDT, which exclusively recognise histone acetylation motifs. Interaction with acetylated residues enables the assembly of chromatin complexes and transcription activators at specific promoter sites of genes (Florence and Faller, 2001, Choi et al., 2016, Barone et al., 2013, Sakaguchi et al., 2018).

It is well established that through the recruitment of the multiprotein complex positive transcription elongation factor b (P-TEFb), BRD4 regulates gene transcription. P-TEFb is a cyclin dependent kinase with catalytic (CDK9) and regulatory (CDKT) subunits, and it is constituted by several other polypeptides. BRD4 has a high affinity for binding to CDK9 contained within P-TEFb. Upon interaction, P-TEFb is recruited to promoters to activate RNA polymerase II (pol II) through phosphorylation at serine 2 at the carboxyl-terminal domain, resulting in transcriptional elongation (Chen et al., 2018b, Henssen et al., 2013, Stathis and Bertoni, 2018, Florence and Faller, 2001, Sims et al., 2004).

BRD4 regulates *MYC* transcription through interaction with the heterodimers MYC/MAX and recruitment of P-TEFb on *MYC* enhancer and super-enhancer regions to promote transcriptional activation (Rahl and Young, 2014, Fowler et al., 2011, Levens, 2008, Yang et al., 2005).

BET bromodomain inhibitors have shown potent anti-tumorigenic effects in multiple *MYC*-driven models, in both *in vitro* and *in vivo* studies, displaying potent downregulation of *MYC* transcriptional programs. The small molecule inhibitor JQ1 (BRD4 inhibitor) is the most studied BET inhibitor, which preferentially decreases *MYC* transcription by preventing the binding of BRD4 to acetylated histones within the *MYC* promoters and enhancers (Figure 1.25) (Allen-Petersen and Sears, 2019).

There are more than 15 different BET inhibitors under current clinical assessment. However, most of them have shown limited clinical response. Current studies suggest that BET inhibitors lack power as single agents, but in combination with other drugs like kinase inhibitors, could potentially achieve more durable responses in the clinic (Gerlach et al., 2018, Bolin et al., 2018).

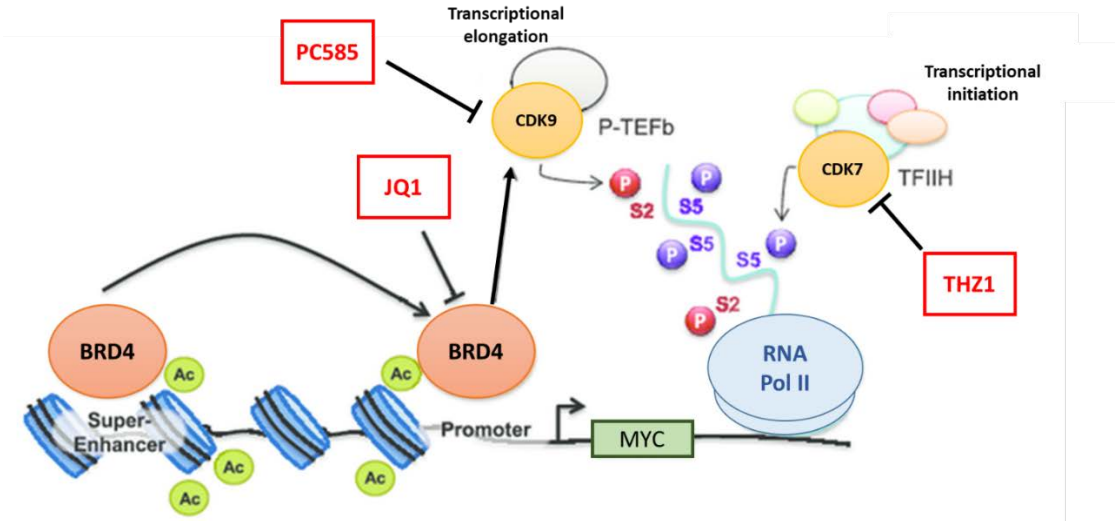

Figure 1.25. Indirect targeting of *MYC* through BET bromodomain inhibition.*MYC* activity can be indirectly disrupted by affecting its transcription. *MYC* expression at the transcriptional level can be inhibited by the use of BRD4, CDK7 and CDK9 small molecule compounds (e.g. JQ1, PC585 and THZ1)(adapted from Chen et al., 2018).

1.9.2.1.2 Inhibition of cyclin dependent kinases 7 and 9

For MYC target genes to be transcribed, the multiprotein complex P-TEFb has to be recruited at gene promoters to phosphorylate RNA polymerase II and to initiate transcription.

The cyclin dependent kinase 7 is part of the transcription factor II Human (TFIIH) protein complex. TFIIH is a component of the RNA Pol II preinitiation complex (PIC) assembled in gene promoters to aid RNA pol II travel to the promoters of those genes to be transcribed (Vannini and Cramer, 2012). CDK7, as part of its catalytic subunit, together with its cofactor cyclin H, phosphorylates the C-terminal domain of the RNA polymerase II at Ser5 to initiate transcription (Whittaker et al., 2017).

Pol II pause release is stimulated through P-TEFb recruitment to promoters, which activates the polymerase through phosphorylation at Ser2 of its CTD domain. As explained above, CDK9 is the catalytic subunit of P-TEFb, and becomes active upon phosphorylation by different kinases, one of them being CDK7 (Mbonye et al., 2018).

Numerous studies have demonstrated that inhibition of CDK7/9 results in a global reduction of *MYC* transcriptional programs. The use of THZ1 (CDK7 inhibitor) and PC585 (CDK9 inhibitor) on *MYC*-driven models of blood, lung and brain cancers showed potent anti-tumour effects, encouraging the pursuit of its targeting as a potential cancer treatment (Chipumuro et al., 2014) (Garcia-Cuellar et al., 2014, Brisard et al., 2018). Despite the *MYC*-downregulatory effect of CDK7/9 inhibition, *in vivo* studies have raised awareness of the global effect on cell cycle and proliferation that the suppression of the activity of these kinases for extended periods of time can have (Ganuza et al., 2012, Posternak and Cole, 2016).

1.9.2.2 Targeting MYC *translation*

Another plausible approach to repress *MYC* activity is by blocking its translation. Once transcribed, MYC mRNA is exported to the cytoplasm under the direct control of mitogenic signals, and this process is coordinated by the eIF4F complex.

The complex is formed by the eukaryotic initiation factors eIF4E, eIF4A and eIF4G, and recruits ribosomes to the 5'-cap of mRNA to initiate mRNA translation. Some mRNAs, like MYC, have an internal ribosomal entry site (IRES) at the 5' end of the sequence, allowing the mRNA to be translated by both mechanisms (Castell and Larsson, 2015).

The family of proteins 4E-BPs are negative regulators of translation, interfering with the assembly of the eIF4F complex by binding to eIF4E. Phosphorylation of 4E-BPs by mTORC1 inactivates the inhibitors allowing the formation of the eIF4F complex and subsequent initiation of translation (Roux and Topisirovic, 2018).

The central role of mTOR in mediating the translation of MYC mRNA has fuelled the development of small molecule compounds targeting mTOR complexes to downregulate *MYC*, with a large number of them being approved for clinical use. However, studies have shown that mTOR inhibition alone fails to inhibit *MYC* expression due to the activation of feedback loops that increase the expression of growth factor receptors and activate the MAPK signalling pathway, which consequently upregulates MYC mRNA expression (Carneiro et al., 2015, Yang et al., 2019).

In this regard, recent studies using the small molecule inhibitor CUDC-907, with dual targeting of PI3K and HDAC, resulted in the reduction of *MYC* transcription which translated into the inhibition of tumour growth in several *MYC*-dependent murine models (Sun et al., 2017). Its efficacy is currently being studied as part of Phase II clinical trials of patents with *MYC* alterations. Another dual-functioning compound showing great anti-tumour effects in *MYCN* amplified Neuroblastoma is SF2523, which targets PI3K and BRD4. SF2523 showed reduced toxicities compared to the individual inhibition of its main targets (Andrews et al., 2017). The potent effect of dual function compounds on *MYC* expression highlights the importance of combinational therapies to further develop strategies to treat *MYC*-dependent tumours.

1.9.2.3 Targeting MYC protein Stability

Regulation of MYC protein is a complex process. Even after synthesis, the protein itself is under complex control and it is subject to several post-translational modifications to establish particular states of *MYC* activity (Tansey, 2014).

1.9.2.3.1 Ubiquitin-dependent degradation

The ubiquitination of MYC plays a crucial role in its control. As mentioned in section 1.4.3, phosphorylation of *MYC* at Threonine 58 site acts as a tag for SCF^{fbw7} ubiquitin ligase to ubiquitinate *MYC* and stimulate its proteasomal degradation (Welcker et al., 2004). USP28, USP7, and USP36 are some of the deubiquitinases that counteract SCF^{fbw7} and help stabilise MYC protein (Wang et al., 2018).

Numerous studies have proposed the use of inhibitors targeting deubiquitinating enzymes to increase MYC turnover (Chen et al., 2019). P22077, a small molecule inhibitor of USP7, supressed growth of *MYCN*-amplified neuroblastoma murine models (Tavana et al., 2016, Fan et al., 2013).

1.9.2.3.2 Aurora Kinase A

Aurora Kinase A, apart from its role in cell cycle progression, is involved in the stabilisation of MYCN protein. Recent studies have shown that AURKA binds to MYCN forming a protective complex that prevents the MYCN SCF^{fbw7}-mediated proteasomal degradation. *In vitro* and *in vivo* studies using the AURKA inhibitor MLN8237 (Alisertib) have demonstrated correlation between aurora A and *MYCN* expression levels, whereby inhibition of *AURKA* disrupts the complex formed by MYCN and AURKA, triggering MYCN degradation (Richards et al., 2016, Li et al., 2018). MLN8237 is currently being evaluated in multiple late phase clinical trials. These studies support the use of *AURKA* inhibitors as potential destabilisers of *MYC*.

1.9.2.3.3 Polo-like kinase 1

The polo-like kinases (PLK) family of proteins are kinases involved in the control of many biological processes, and have an essential role in mitosis and maintenance of genome stability. PLK1 is the best characterised *PLK* family member, due to its involvement in the regulation of multiple steps of the mitotic process (Strebhardt, 2010).

Like AURKA, apart from being a downstream regulator of *MYC* expression signatures, it has been demonstrated that PLK1 also affects MYC stabilisation. Phosphorylation of SCF^{fbw7} by PLK1 triggers its auto-polyubiquitination and consequent degradation, inhibiting MYCN-SCF^{fbw7} mediated degradation. Inhibition Fbw7 stabilises MYCN, which in turn directly promotes PLK1 transcription, constituting a positive feedback loop resulting in tumour proliferation (Sato et al., 2015, Xiao et al., 2016).

The use of PLK1 inhibitors in models of *MYCN*-amplified neuroblastoma and small cell lung carcinomas, such as BI6727 or BI2536, consistently reduced *MYCN* expression and induced apoptosis of *MYC*-overexpressing cell lines. Recent studies have revealed synergy between PLK1 inhibition and BCL2 antagonism, validating the PLK1-SCF^{fbw7}-MYC interconnected signalling as a potential therapeutic strategy for *MYC*-dependent cancers (Ren et al., 2018).

1.9.2.4 Targeting by synthetic lethality

Advances in genome screening have intensified indirect approaches to target *MYC*-dependent tumours by synthetic lethality. It is well established that cancer cells develop a prime dependency on their overexpressed oncogene for the maintenance of the malignant phenotype and their survival (Weinstein and Joe, 2008). Indeed, downregulation of *MYC* in *MYC*-overexpressing cell lines results in tumour regression (Pei et al., 2012, Li et al., 2014b). Utilisation of whole genome screens has enabled the identification of pathways supporting oncogenic *MYC* transcriptional signalling that could be exploited to treat *MYC*-dependent cancers.

Several studies have highlighted the dependency of *MYC* overexpressing cell lines on the expression of CDKs. Pharmacological inhibition of CDK2, CDK1 and CDK9 has been shown to selectively target *MYC* overexpressing cell lines (Whitfield et al., 2017). The CDK1 inhibitor purvalanol A greatly induced apoptosis in *MYC*-dependent hepatoblastoma and lymphoma murine models, through the upregulation of pro- and anti-apoptotic molecules (Kang et al., 2014, Campaner et al., 2010).

MYC deregulation increases cell replication, causing a state of replicative stress in the cell, promoting genome instability. CHK1 plays an important role in cell cycle progression and DNA damage control, which *MYC*-overexpressing tumours with rapid cell turnover are in need of for their survival. Indeed, pharmacological inhibition of CHK1 significantly increases genome instability and massive cell death in *MYC*-dependent models (Figure 1.26)(Murga et al., 2011).

Many *MYC*-synthetic genes identified are involved in cell metabolism. The need of *MYC*-dependent cancer cells for constant and proper metabolic support for cell growth and proliferation has led to the targeting of various metabolic enzymes like Glutaminase or LDHA, to inhibit tumour growth (Xiao et al., 2015, Chen et al., 2018b, Hsieh and Dang, 2016). CB-839, a selective glutaminase inhibitor, is currently under investigation for tumours with *MYC* upregulation (Grinde et al., 2019).

Various other targets have been identified in *MYC* synthetic studies, some of them being PIM kinases, RNA polymerases or Aurora kinases. Recently, SUMOylation enzymes have been linked to essential roles in *MYC*-driven tumourigenesis (Chen et al., 2018b).

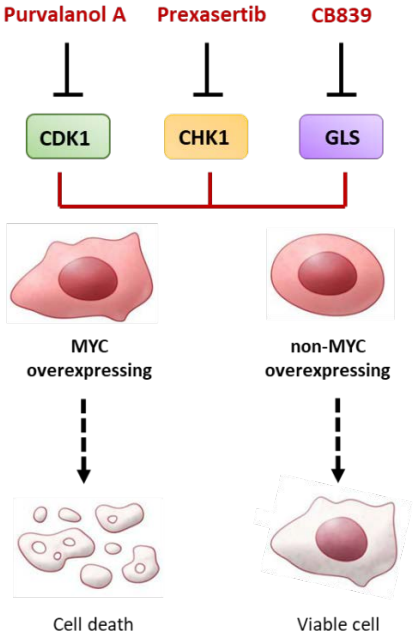

Figure 1.26. Example of strategies to target *MYC*-dependent tumours by synthetic lethality. *CDK1* (cell cycle), *CHK1* (DNA-repair mechanisms) and *GLS* (cells metabolism) are essential genes for the survival of *MYC*-overexpressing cancerous cells. Pharmacological inhibition of *CDK1*, *CHK1* and *GLS* specifically sensitises cells overexpressing *MYC* to apoptosis (synthetic lethal) over those expressing normal levels of *MYC*. (Adapted from Chen *et al.*, 2018).

1.10 Proposed *MYC*-targeting strategies for MB_{Group3}

The expanding wealth of molecular data on MB, has allowed a thorough understanding of the molecular changes that characterise each subgroup, paving the way for targeted therapeutic strategies.

Of all subgroups, MB_{Group3} have the worst outcome and yet its molecular pathway of origin is still undefined, with few driver gene alterations identified in MB_{Group3} tumorigenesis. Despite only accounting for 17% of MB_{Group3} cases, the amplification and/or overexpression of *MYC* has been associated with poor clinical outcome, becoming the defining feature of this subgroup (Northcott et al., 2012b, Pizer and Clifford, 2009).

The fact that *MYC* suppression causes tumour regression in *MYC*-driven murine MB models and its association with highly aggressive tumours, indicate that *MYC* plays a key role in MB_{Group3} tumour development. This has led research to focus on developing strategies to disrupt *MYC* function in this specific cellular context (Pei et al., 2012, Roussel and Robinson, 2013).

The incorporation of molecular and histopathological features for disease stratification has enabled small adjustments to the conventional MB therapy to reduce related toxicities. Current clinical studies are stratifying patients on the basis of molecular subgroups, which has enabled incorporation of *SMO* inhibitors for MB_{SHH} patients and reduced treatment intensity of MB_{WNT} patients presenting with low-risk features (NCT01878617)(Northcott et al., 2019). Unfortunately, no major changes have proceeded to enhance outcomes for, or palliate, MB_{Group3} patients. However, the SJMB12 study is currently investigating the effect and tolerability of adding cycles of combined gemcitabine and pemetrexed to the conventional treatment of MB_{Group3} and MB_{Group4} patients with high-risk features (Morfouace et al., 2014).

Results from pre-clinical studies are pointing to the combined use of HDAC and PI3K inhibitors (Figure 1.27), compounds with dual activity on PI3K-*BRD4*, *CHK* inhibitors with current cytotoxic chemotherapeutic agents, *CDK* inhibitors alone or in combination with cytotoxic agents, or targeting *GFI1* and *GF1B* overexpression to treat patients with MB_{Group3}, but nothing has yet been translated to the clinic (Prince et al., 2016, Pei et al., 2016, Cook Sangar et al., 2017, Faria et al., 2015, Lee et al., 2019, Song et al., 2019, Eckerdt et al., 2019, Juraschka and Taylor, 2019).

Despite the vast knowledge and current understanding of *MYC* and its involvement in cancer development, there has been no systematic assessment of anti-*MYC* strategies in *MYC*-dependent medulloblastoma models. The current lack of innovative treatments for patients with MB_{Group3} requires further efforts be placed in the development of new combinational therapeutic strategies to establish and specifically target essential *MYC*-dependent vulnerabilities in MB_{Group3}.

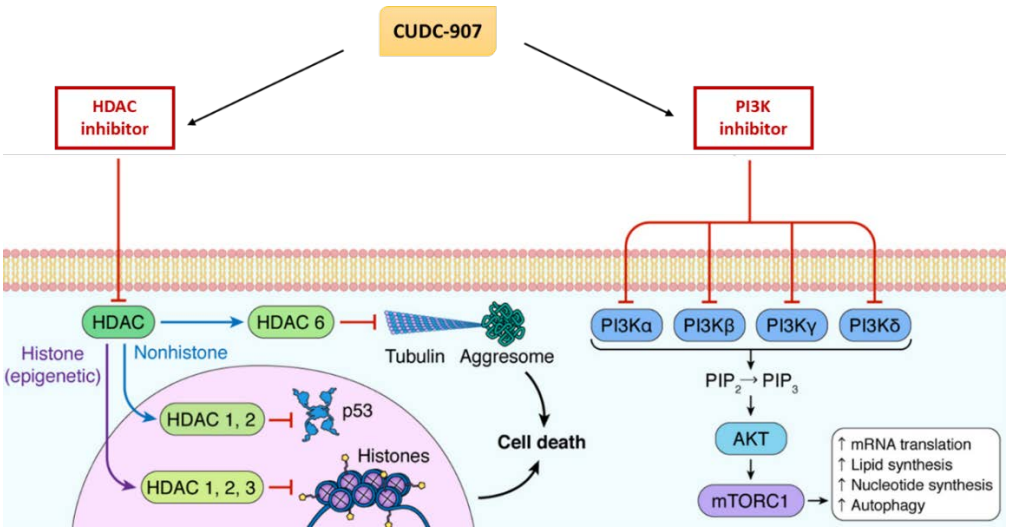

Figure 1.27. HDAC and PI3K inhibition as potential strategy to target MBGroup3 tumours. Dual Inhibition of HDAC and PI3K using the CUDC-907 compound has been shown to downregulate *MYC* expression, and it has been proposed as a potential therapeutic strategy to target *MYC*-driven MB_{Group3} tumours. The figure highlights the signalling pathways affected by the compound (adapted from Allen-Petersen et al., 2019).

1.10.1 Isogenic MYC *regulable* MB_{Group3} *cell lines*

One way to study the underlying pathophysiology of MB biology is using cell-lines derived from MB patients. The use of established MB cell lines can certainly help gain a better understanding of the molecular and genetic mechanisms of those MB tumours that confer the worst prognosis and are resistant to treatment, like MB_{Group3}.

For the large number of established MB cell lines there is little diversity regarding genetic features, and most cell lines modelling MB_{Group3} harbour *MYC* amplifications (Xu et al., 2015, Clifford et al., 2006, Ivanov et al., 2016). To explore specific *MYC*-dependent biology and its potential for therapeutic targeting in a MB_{Group3} context, the Paediatric Brain Tumour Group at Newcastle University has established three *MYC*-regulable isogenic cell lines (using D425, D283 and HDMB03 as hosts) in which *MYC* expression can be directly regulated experimentally (Dr. Shanel Swartz, PhD thesis).

To the current day, this is the first time that regulable models of *MYC* in Group 3 medulloblastoma are described. The utilisation of cell lines facilitates their manipulation to make regulable models of specific genes, which would result extremely challenging in patient derived xenografts (PDX) and genetically engineered mouse (GEM) models. The use of *MYC*-regulable Group 3 medulloblastoma cell lines will allow the investigation of the *MYC*-dependency of this subgroup of tumours.

1.10.1.1 Tet-inducible shRNA system for MYC knock down

Short Haipirin RNA (shRNA) is one of the most used and well established techniques for efficient and stable knockdown of gene expression. shRNA techniques have long been used to study gene function by inducing temporary knockdown of genes that are essential for cell survival, where its knock out would otherwise be lethal (Frank et al., 2017).

Selection of cell models was performed according to their *MYC* expression levels (Table 1.4). MB cell line subgroup was assigned using primary MB methylation data (process described in Dr. Shanel Swartz PhD thesis). D425 and HDMB03 harbour *MYC* amplification, which leads to increased mRNA expression and subsequent protein translation. On the other hand, D283 is a *MYC*-gained cell line containing an extra copy of the *MYC* gene (Dr. Shanel Swartz, PhD thesis).

Cell lines	Subgroup	TP53	MYC
D283	Group 3	WT	Gain
D425	Group 3	Mutant	Amplified
HDMB03	Group 3	WT	Amplified

Table 1.4. Genetic characteristics of medulloblstoma cell lines. Summary of *MYC* and *TP53* status of the medulloblastoma cell lines selected for the study. WT, wild type.

The cell lines were transduced with an inducible shRNA system (pLKO-Tet-On-Puro vector) to temporarily control and modulate *MYC* oncogene expression by the administration of doxycycline (DOX)(inducing agent) to the culture media. The lentiviral vector pLKO-Tet-On-Puro contains all the necessary components of a TeT inducible shRNA expression system in the host cells (Wiederschain et al., 2009)(www.addgene.org).

The pLKO vector contains a TetOperator (TetO) located in the H1 promoter (Figure 27), containing two Tet responsive elements (TRE) flanking a TATA box, which regulates the expression of the shRNA. The Tet repressor (TetR) is located downstream of the constitutive polymerase II hPGK promoter. Between the TetR and puromycin selection cassette, an IRES was inserted to allow simultaneous expression of both proteins (Wiederschain et al., 2009).

In the absence of the inducer DOX, the expression of the shRNA is blocked by the continued expression of TetR, which binds to TRE in the H1 promoter containing TetO, allowing intrinsic levels of *MYC* expression within the host cell. The addition of DOX to the culture media triggers the transcription of the shRNA construct by displacing TetR from the promoter, therefore targeting MYC mRNA expression inducing *MYC* gene knockdown (Figure 1.28)(Wiederschain et al., 2009).

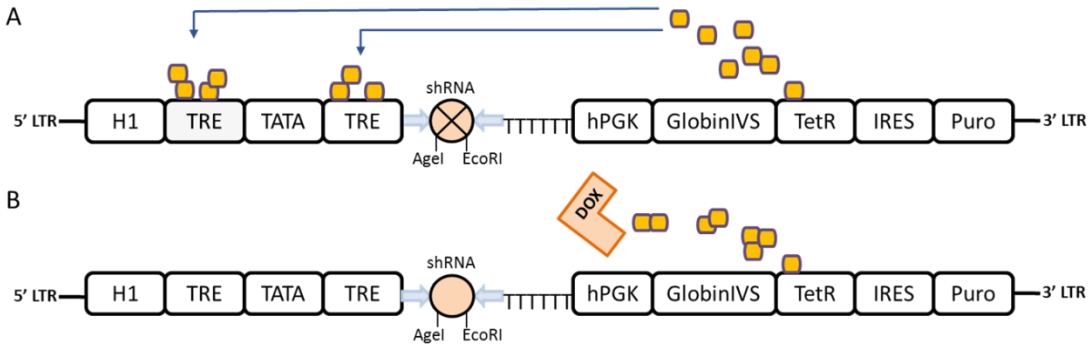

Figure 1.28. Tet-ON doxycycline inducible shRNA expression system. Mechanism of transcriptional control of TeT inducible shRNA expression system. The pLKO-Tet-On vector contains all the necessary elements for lentiviral insertion and inducible expression of shRNA in target cells. In the absence of inducer, the Tet repressor protein (TerR) blocks shRNA expression by binding to the Tet Response Element (TRE) at the H1 promoter. The system is activated by the addition of doxycycline, which binds to TerR and stimulates transcription of the shRNA, which targets specific mRNA for degradation (Adapted from Wiederschain et al., 2009).

Each isogenic cell line generated has two experimental constructs targeting two different MYC sequences, called MYC2 and MYC3 (expressing shRNA to silence *MYC*), and a control construct (NS) expressing a non-silencing shRNA. Both experimental shRNAs target different positions of the third exon of *MYC* (Dr. Shanel Swartz, PhD thesis).

The use of cells transfected with a non-targeting shRNA allows the use of the same pool of cells as controls, including studying the possible side effects of the insertion of the lentiviral vector, and of doxycycline addition.

The generation of stable isogenic cell lines with a DOX-inducible system for *MYC* knockdown brings the opportunity for direct investigation of the nature and extent of *MYC's* involvement in MB_{Group3} pathogenesis, and its dependency. The use of these models could allow the identification of key pathways for the survival of *MYC*-overexpressing cells, and to identify and develop novel therapeutic strategies to bring into the clinic, providing a systematic and promising strategy to understand the best way to treat *MYC*-driven cancers.

1.11 Summary and aims

Over the last few years tremendous advances have been made in understanding the molecular underpinnings of MB, becoming one of the best molecularly characterised cancers. The discovery of specific genetic features that characterise each subgroup are already being translated directly into the clinic, for more precise treatment approaches that aim to keep improving survival of patients whilst reducing the extremely toxic side effects of current standard treatment (Northcott et al., 2019, Allen-Petersen and Sears, 2019).

One of the greatest challenges remains in translating this wealth of molecular data into effective novel treatments for the high-risk patients with MB_{Group3}. *MYC* amplification and/or overexpression is the hallmark of MB_{Group3}, and its key association with MB_{Group3} tumour development makes it a promising target to specifically treat patients with this subgroup of tumours (Northcott et al., 2012b, Pizer and Clifford, 2009, Pei et al., 2012, Roussel and Robinson, 2013). It is crucial to better understand the biological role of this prognostic marker in a subgroup specific context to better inform and design therapeutic regimens that would improve clinical outcomes and survival for high-risk patients.

The major objective of this project is to gain a better understating of *MYC*'s role in MB_{Group3} pathogenesis, and to identify potential *MYC*-dependent targets for the development of new therapeutic strategies to treat high-risk MB_{Group3} patients.

1. The project aims to directly investigate the nature and extent of *MYC*'s involvement and dependency in MB_{Group3} pathogenesis, using the newly generated *MYC*-regulable isogenic cell lines.
    - Validation of the effectiveness of *MYC* knockdown achieved with the inducible shRNA system, and establishment of any *MYC*-dependent phenotypes, will be performed to establish the suitability of the isogenic models as new tools to study *MYC*-dependent biology within human MB_{Group3}.

2. The project will then focus on using the novel *MYC*-regulable isogenic cell lines to investigate the role of *MYC* amplification/gain in drug resistance and sensitivity; to identify drugs which show (i) greater efficacy in *MYC* expressing cells and (ii) potential synthetic lethal interactions following *MYC* knockdown, which have potential for targeting *MYC*-dependent MB_{Group3}.

- Candidate drugs (drugs chosen based on their published efficacy in *MYC* models, mechanism of action, pharmacological properties and potential for clinical use in the near future) targeting signalling pathways associated with *MYC*, will be tested in a *MYC*-dependent manner using the newly generated models.

3. Alongside looking at candidate drugs, the project will take an unbiased approach by undertaking a high-throughput drug library screen on the isogenic cell-based models, to identify *MYC*-dependent therapies which could potentially be used to treat this subgroup of highly lethal paediatric tumours.
   - The *MYC*-modulable models will be exposed to hundreds of compounds to look for *MYC*-dependent drug-sensitivity effects. Integrative analysis of screen results with data on transcriptional and genetic MB dependencies will be used to identify compounds to specifically target *MYC* in *MYC*-driven MB_{Group3} cell lines.

4. Prioritised candidates will be validated individually by assessing their effects in *MYC* amplified/regulable MB cell lines, alongside non-amplified MB_{SHH} models. *MYC*-dependent effects of inhibitors will be investigated, including impact on cell proliferation, apoptosis, cell cycle, and target and downstream pathway expression. Together, this data will be used to prioritise candidates suitable for progression to *in vivo* testing.

Chapter 2. Materials and Methods

2.1 Materials

2.1.1 Laboratory equipment

Instrument	Manufacturer
2720 Thermal Cycler	Applied Biosystems
Attune NxT flow cytometer	ThermoFisher Scientific
Benchtop centrifuge 5424	Epppendorf
Cell Irradiator	Gulmay Medical Ltd
Centrifuge 5415 R	Epppendorf
Centrifuge 5804R (tissue culture use)	Eppendorf
CO_2 incubator (MCO-230AICUV-PE)	Panasonic
Countess II FL Automated Cell Counter	ThermoFisher Scientific
FLUOstar Omega plate reader	BMG Labtech
Heraeus Multifuge 3S Plus	ThermoFisher Scientific
Microcentrifuge technico Mini	Labnet
Microlab STAR platform	Hamilton
Mr Frosty	Nalgene
Multidrop Combi Reagent Dispenser	ThermoFisher Scientific
NanoDrop ND-1000 spectrophotometer	ThermoFisher Scientific
Nebauer-improved haemocytometer	Marienfeld-Superior
StoragePod	Roylan Developments
VICTOR Multilabel Plate Reader	PerkinElmer
ViiA 7	Applied Biosystems
Wes	Protein Simple

Table 2.1. List of equipment

2.1.2 Materials for tissue culture

Tissue Culture	Supplier
Cell bind 96 well plate (3340)	Corning
clear 384 well plate (3701)	Corning
Countess Cell Counting Chamber Slides	ThermoFisher Scientific
ErgoOne Multi-Channel Pipettes	StarLab
ErgoOne Single-Channel Pipettes	StarLab
MACS SmartStrainers	Miltenyibiotec
Nebauer-improved haemocytometer	Marienfeld-Superior
Olympus CKX53 microscope	Life Science
TEVOS FL Cell Imaging System	ThermoFisher Scientific
white 384 well plate (3570)	Corning
white 96 well plate (3917)	Corning

Table 2.2. Materials used for tissue culture equipment

2.1.3 Chemicals and reagents

Item	Supplier
0.4% trypan blue	BIO-RAD
0.45µm filter	Merck-Millipore
Agarose	Bioline
BCA protein assay kit	ThermoFisher Scientific
Caspase3/7-Glo	Promega
CellTiter AQueous One Solution	Promega
CellTiter-Glo	Promega
Corning Tissue culture flasks (T25, T75, T150)	Sigma-Aldrich
Cryovials	ThermoFisher Scientific
Doxycycline hyclate	Sigma-Aldrich
Dymethyl Sulfoxide (DMSO)	Cell signaling
Eppendorf LoBind microcentrifuge tubes	Sigma-Aldrich
Gibco foetal calf serum	ThermoFisher Scientific
Halt Protease inhibitor Cocktail (100X)	ThermoFisher Scientific
High capacity cDNA reverse transcription kit	Applied Biosystems
L-Glutamine	Sigma Aldrich
Lobind microfuge tubes	VWR
MEM Non- Essential Amino Acids Solution (100x)	ThermoFisher Scientific
Microfuge tubes	Eppendorf
Nuclease-Free water	Ambion
Platinum SYBR Green Super Mix UDG	Applied Biosystems
PowerUp SYBR Green Master Mix	ThermoFisher Scientific
Propidium iodide	Sigma-Aldrich
Puromycin Dihydrochloride (10µg/ml)	ThermoFisher Scientific
QIAshredder	QIAGEN
RIPA buffer (10X)	Sigma-Aldrich
RNase A, DNase and protease-free (10mg/ml)	ThermoFisher Scientific
RNeasy mini Kit	Qiagen
Tet System Approved FBS	Takara
Triton (100X)	Sigma-Aldrich
Trypsin-EDTA solution (10X)	Sigma-Aldrich

Table 2.3. List of general chemicals and reagents

2.1.4 RT-qPCR primers

Gene	Forward primer (5' to 3')	Reverse primer (5' to 3')
MYC	TGAGGAGACACCGCCCAC	CAACATCGATTTCTTCCTCA
TBP	GTATTAACAGGTGCTAAAGTCAG	TTTTCAAATGCTTCATAAATTTCTGC

Table 2.4. Primers for RT-qPCR.

2.1.5 Small molecule compounds

Compound	Alternative name	Target	Vendor
(+)-JQ1		BRD4	Selleckchem
Adavosertib	MK-1775	Wee1	Selleckchem
Alisertib	MLN8237	AURKA	Selleckchem
AZD7762		CHK1	Selleckchem
BI2536		PLK1	Selleckchem
CYC065		CDK9	Cyclacel Pharmaceuticals
Milciclib	PHA-848125	CDK2	Selleckchem
Prexasertib	LY2606368	CHK1/2	Selleckchem
Sapanisertib	INK128	mTORC1/2	Selleckchem
SN38		DNA topoisomerase I	Selleckchem
Vistusertib	AZD2014	mTORC1/2	Selleckchem
YM155	Sepantronium Bromide	BIRC5	Selleckchem

Table 2.5. List of small molecule inhibitors.

2.1.6 Antibodies

Target	species	Manufacturer
GAPDH	rabbit	Cell Signaling
CHK1	rabbit	Abcam
pCHK1	rabbit	Cell Signaling
PI3 Kinase p110α	rabbit	Cell Signaling
Phospho-4E-BP1 (Thr37/46)	rabbit	Cell Signaling
Phospho-S6 Ribosomal Protein (Ser235/236)	rabbit	Cell Signaling
Phospho-MEK1/2 (Ser217/221)	rabbit	Cell Signaling
PARP	rabbit	Cell Signaling
Cleaved PARP (Asp214)	rabbit	Cell Signaling
Aurora A/AIK	rabbit	Cell Signaling
Phospho-Aurora A(Thr288)/AuroraB	rabbit	Cell Signaling
CDK2	rabbit	Cell Signaling
PLK1	rabbit	Cell Signaling
Phospho-cdc25 (Ser216)	rabbit	Cell Signaling
c-MYC	rabbit	Cell Signaling
mTOR	rabbit	Cell Signaling
MCL-1	rabbit	Cell Signaling
Phospho-GSK-3β (Ser9)	rabbit	Cell Signaling

Table 2.6. List of antibodies used for protein detection with Wes.

2.1.7 Software

Software	Owner/Developer
Attune NxT flow cytometer (version 2.7)	ThermoFisher Scientific
FlowJo (version 10)	FlowJo
GENESys (version 1.5.1.0)	SYNGENE
Primer3	ELIXIR - European research infrastructure for biological information
R (version 3.5.0)	The R Foundation for Statistical Computing
R studio (version 1.1.453)	JJ Allaire
QuantStudio Real-Time PCR System	ThermoFisher Scientific
Compass	Protein Simple
Prism8	GraphPad

Table 2.7. List of software used for data analysis

2.2 Cell culture

2.2.1 Cell line models

Several Group 3 and SHH medulloblastoma cell line models were used in this study. D283Med, D425Med, D458Med, HDMB03 were used to model MB_{Group3} tumour biology. DAOY and UW228.2 cell lines were used as MB_{SHH} models. A list with information on the cell lines, their growth and tumour characteristics can be seen in Table 2.9.

The isogenic *MYC*-regulable cell lines used D425, D283 and HDMB03 as hosts. Table 2.8 shows the genetic characteristics of the isogenic models.

Cell lines	Subgroup	*TP53*	*MYC*
D283	Group 3	WT	Gain
D425	Group 3	Mutant	Amplified
HDMB03	Group 3	WT	Amplified

Table 2.8. Genetic characteristics of medulloblstoma cell lines. Summary of *MYC* and *P53* status of the medulloblastoma cell lines selected for the study. WT, wild type.

2.2.2 Cell culture maintenance

Cell lines used in this study were grown in the appropriate media (specified in Table 2.10) and incubated at 37°C with humidified atmosphere of 5% CO_2. Cells were passaged when reaching 70-80% confluence.

In general, cell suspensions were collected and remaining adherent cells washed with phosphate buffered saline (PBS) and detached from the flask surface using 1x trypsin-EDTA. Trypsin was neutralised with a 2:1 ratio of concordant fresh culture media. Cell suspension was then centrifuged at 700*xg* for 5 minutes, supernatant removed and cell pellet re-suspended. An appropriate volume of cell suspension was transferred to new flasks containing fresh pre-warmed growth medium.

Cell cultures were tested monthly for the presence of mycoplasma.

				Growth characteristics		Patient Characteristics		Tumour characteristics
Cell line	**Subgroup**	**Source**	**Date published**	**Growth**	**Doubling time**	**age at diagnosis**	**sex**	**Line derived from**
DAOY	SHH	American Type Culture Collection (Manassas, VA, USA)	1985	adherent	48 hours	4 years	Male	Primary tumour (pre-treatment)
D283Med	Group 3	American Type Culture Collection (Manassas, VA, USA)	1985	semi-adherent	52.55 hours	6 years	Male	Metastases from ascites and pertoneal implant (post-radiotherapy)
D425Med	Group 3	Dr. D. Bigner (Duke University, Durham, NS, USA)	1991	semi-adherent	62 hours	6 years	Male	Primary tumour at diagnosis
D458Med	Group 3	Dr. D. Bigner (Duke University, Durham, NS, USA)	1991	semi-adherent	83 hours	6 years	Male	Metastases at relapse
UW228.2	SHH	Dr. J. Silber (Univeristy of Washington, Seattle, WA, USA).	1995	adherent	25.2 hours	9 years	Female	Primary tumour (pre-treatment)
HDMB03	Group 3	Hedwig E. Deubzer (German Cancer Research Cemter (DKFZ))	2012	semi-adherent	72-96 hours	3 years	Male	Primary tumour (pre-treatment)

Table 2.9. Information of primary MB cell lines used in this study.

Media	Cell line	Composition of media
Dulbecco's Modified Eagle's Medium High glucose (DMEM – D6171 – Sigma Aldrich)	Isogenic D425Med Isogenic D283Med	1% L-Glutamine 1µg/ml puromycin 10% Tet-free foetal bovine serum DMEM
Dulbecco's Modified Eagle's Medium High glucose (DMEM – D6171 – Sigma Aldrich)	D425 Med D283 Med D458 Med DAOY UW2281	1% L-Glutamine 10% foetal bovine serum DMEM
RPMI-1640 (R5886 – Sigma-Aldrich)	Isogenic HDMB03	1% L-Glutamine 1% Non-essential amino acids 1µg/ml puromycin 10% Tet-free foetal bovine serum RPMI 1640
RPMI-1640 (R5886 – Sigma-Aldrich)	HDMB03	1% L-Glutamine 1% Non-essential amino acids 10% foetal bovine serum RPMI 1640

Table 2.10. Media used for culturing cell lines.

2.2.3 Cell counting

Cell density and viability was determined using the Countess Automated Cell Counter or a haemocytometer following trypan blue (BIO-RAD) staining. Trypan blue staining allows the counting of viable cells under the microscope, as they remain unstained whilst non-viable cells absorb the dye and become blue.

An aliquot of the cell suspension was mixed with 0.4% Trypan blue in a 1:1 ratio, and 10µl of the mixture loaded to a chamber of the haemocytometer or countess slide. For manual counting, a percentage of viable cells was calculated by counting the number of unstained cells in the 4 corner counting quadrants.

$$\text{total cells/ml} = \frac{\text{n}^{\text{o}}\text{cells counted x dilution factor}}{\text{n}^{\text{o}}\text{ squares counted x } 10^4}$$

2.2.4 Cell collection

For cell pellet collection, suspension cells were transferred to a 1.5ml Eppendorf tube and centrifuged at maximum speed for 2 minutes. The media was aspirated and cell pellet washed twice with ice-cold PBS. After the second wash, the tube containing only the cell pellet was stored at -80ºC for future use.

2.2.5 Cell line cryopreservation and thawing

Freezing media was made with 80% foetal bovine serum and 20% sterile DMSO. A suitable number of cells was centrifuged for 5 minutes at 250*xg*, supernatant aspirated and cell pellet resuspended in ice-cold FBS followed by the addition of the same amount of ice-cold freezing media. Cells were transferred into pre-labelled cryovials, left on ice for a few minutes before being transferred to a room temperature Mr. Frosty, and stored at -80ºC. The freezing container Mr. Frosty helps preserve cell viability by providing a gradual freezing rate of the vials (1ºC/min). For long-term storage, frozen cryovials were stored in a -150ºC freezer.

To recover cell lines, cryovials were placed in a 37ºC water bath, and only when there was a small amount of ice remaining, vials were left on ice to completely thaw. Cell suspensions were then transferred to a Falcon tube and 5ml of appropriate pre-warmed media was added, dropwise, to ensure the slowly diffusion of DMSO from the cells. Cell suspension was gently mixed and transferred to a new flask with an appropriate amount of media, and left in the incubator overnight. After 48h, media was replaced to avoid possible toxic effects of the remaining DMSO in the media. For the isogenic cell lines, the media was changed to the one containing 1µg/ml of puromycin 72h after cell thaw.

2.3 General Laboratory techniques

2.3.1 Doxycycline treatment

Doxycycline (DOX) is a tetracycline antibiotic used as inducer for pLKO-Tet-On shRNA expression system. DOX is stable in culture medium for 48h. In this study, DOX was added to cell culture at a final concentration of 1mg per ml for shRNA *MYC* knockdown.

2.3.2 Proliferation Assay

To assess the proliferative characteristics of the cells, cells were plated into either 384 or 96 well plates at the appropriate cell density (dependent on cell lines and type of experiment), and left in the incubator at 37°C for the desired amount of time. Cells bearing the MYC and NS shRNAs were pre-treated with DOX 24h before plating. DOX was then refreshed when seeding. For experimentations longer than 72h, DOX was refreshed accordingly to ensure continued *MYC* knockdown.

Cell proliferation was assayed at the appropriate time with either CellTiter 96 AQueous One (CTA) for colorimetric assay or CellTiter-Glo (CTG) for luminescence assay. For the colorimetric assessment of cell proliferation, CTA reagent was added to the cells followed by 2h incubation at 37°C. After incubation, absorbance of each well was measured with FLUOstar Omega plate reader (BMG Labtech) at 490nm. For the luminescence assay, plates were left to equilibrate at room temperature before adding CTG reagent. Plates were left on a rocker for 10min at room temperature. The luminescence signal was then read using the Omega microplate reader.

The optical density (OD) or relative luminescence units (RLU) were used as indicator of cell survival. The untreated control was used to normalise values obtained from treated cells. Data was analysed using Graphpad Prism version 8.

2.3.3 Protein extraction

Eppendorf tubes containing the cell pellets were left to defrost on ice. The appropriate amount of cold RIPA buffer (used at 10X) was added to the cell pellet (approximately 250µl per $5x10^6$ cells), and the mixture pipetted up and down to suspend the pellet until dissolved. The solution was supplemented with Halt protease inhibitor cocktail (100X), used at 1X concentration. Eppendorfs containing the solution were left on ice for 15min and cells sheared using a Bioruptor Plus sonication device (Diagenode), for 3 cycles of 10 seconds on / 10 seconds off with 50% pulse. After sonication, samples were centrifuged at 112*xg* for 15min at 4ºC. Total amount of protein was quantified right after centrifugation or samples were left at -80ºC for future use.

2.3.4 Protein Quantification

Pierce BCA Protein Assay Kit (ThermoFisher Scientific) was used for quantification of total protein according to manufacturer's instructions. Briefly, protein concentrations were determined with reference to standards of diluted concentrations of bovine serum albumin (BSA) protein, based on a standard curve. Dilution of standards were prepared according to the manufacturer's protocol. Between 1-5µl of sample and 25µl of each standard were pipetted into a 96-well plate, followed by the addition of 200µl of working solution reagent, made up at a 50:1 ratio of the kits reagents A:B. The plate was mixed for 30 seconds on a plate shaker and incubated for 30 minutes at 37°C. After incubation, the plate was cooled to room temperature and the absorbance measured using the FLUOstar Omega microplate reader (490nm) (BMG Labtech). The protein concentration of each sample was then determined using the standard curve created with blank-corrected 562nm measurements for each BSA standard.

2.3.5 Protein detection and analysis

2.3.5.1 Simple Western Assay (Wes)

Simple Western Assay (Wes) was used to identify and analyse proteins of interest. Wes (https://www.proteinsimple.com/wes.html) is a capillary electrophoresis-based western blot that offers automated steps equivalent to traditional western blots. Samples are processed in capillary columns were they are separated based on size and identified as they pass through a separation and stacking matrix. Proteins are immobilised onto the capillary wall by photo-activated cross-linkage. The washing step removes the matrix and target proteins are then identified using a primary antibody immunoprobed with a horseradish peroxide (HRP)-conjugated secondary antibody. Similar to traditional western blotting, the resultant chemiluminescent signal generated by the HRP-catalysed reaction visualises the protein of interest. The resultant signals are automatically detected, quantified and converted to electropherograms and gel-like images by the Compass software.

Protein and reagent preparation for the Wes assay were conducted according to manufacturer's protocol (ProteinSimple).

2.3.6 Cell Irradiation

To study the effect of *MYC* on radioresistance, exponentially growing *MYC*-regulable cells were induced with and without DOX for *MYC* knockdown. 24h after DOX induction, an appropriate number of cells was seeded onto 96 well plates and allowed to recover for 24h. Cells in each plate were irradiated using a D3300 X-Ray system (Gulmay Medical Ltd., Surrey, UK). Cell lines underwent single doses of irradiation of either 2, 5, 10, 15 or 50Gy. Control plates received no irradiation. D425 NS was used as negative control to compare to those D425 cells bearing a *MYC*-knockdown construct being exposed to DOX treatment.

After irradiation, plates were incubated at 37°C and cell viability assessed at 72h using the colorimetric CellTiter 96 AQueous One reagent. Absorbance of each well was read with a FLUOstar Omega microplate reader (BMG Labtech) and data analysed with Prism8 (GraphPad).

2.3.7 Drug testing

2.3.7.1 Drug handling

Drugs were diluted in dimethyl sulfoxide (DMSO) to a final concentration of 10mM and stored at -80°C. Before treatment, all drugs were freshly diluted in media to the desired working concentration.

2.3.7.2 Drug sensitivity assay

To assess the effect of the inhibitors on cell proliferation, cells were seeded in plates 24h prior to treatment. Drugs were added to the cells at the final required concentration and left in the incubator for the required time of exposure. For data normalisation, cells were grown with equivalent volumes of DMSO-containing media without drug. At the end of each treatment, CTG or CTA was added to the plate and read as previously described. The effect of drugs on cell viability was determined by comparing growth results of untreated cells.

2.3.7.3 Time pulse cell viability assay

To assess the effect of CYC065 inhibitor on the cell cycle and its overall effect on cell viability, cells were seeded in cell bind 96 well plates 24h prior to treatment for cells to recover. For *MYC*-silencing, cells were pre-induced with DOX 24h before seeding to start drug treatment when maximum *MYC* knockdown was achieved. Cells were exposed to decreased concentrations of CYC065, 1:3 serial dilutions from 100µM to 0.03µM, for 1h, 2h, 4h and 8h. For data normalisation, cells grown with serial dilutions of DMSO served as controls.

After the specified time of exposure, drug-containing media from the plates was removed and refreshed with drug-free media. Cells were left in the incubator to grow for 72h, at which point cell viability was assessed with CTG. Data was analysed with Prism and presented as percentage of viable cells compared to the untreated control for each respective construct and cell line.

2.3.7.4 Protein analysis for time pulse assays

To assess the effect of CYC065 at the protein level, cells were seeded in cell bind 6 well plates 24h prior to drug treatment to allow recovery. For *MYC*-silencing, cells were pre-induced with DOX 24h before seeding to ensure drug treatment started when *MYC* was completely knocked down. Cells were exposed to 1x, 2x and 4x the IC_{50} of CYC065, for 1h, 2h and 8h. For data normalisation, cells grown with an equal volume of DMSO were used as controls.

After the specified times of exposure, cell pellets were collected and washed two times with ice-cold PBS and stored at -80°C until required. Protein analysis and quantification was done with Wes.

2.3.7.5 Determination of half-maximal inhibitory concentration (IC_{50})

IC_{50} are a measure of a drug's efficiency that indicate the quantity of drug needed to inhibit a biological process by half. To assess the effect of the inhibitors on cell growth, cells were seeded in either 96 or 384 well plates 24 hours prior to treatment with a titration (10 fold dilutions from 10pM-10µM) of the drugs. For data normalisation, cells were grown with equivalent volumes of DMSO-containing media. At 72h, cell proliferation was measured.

Values were analysed and growth curves created with Prism8 (GraphPad) using the log(inhibitor) vs. normalized response curve [Y=100/(1+10^((X-LogIC50)))]. Each experiment was performed in triplicate and repeated independently at least three times.

2.3.7.6 Rescue assays

To confirm reduced cell viability caused by treatment with the inhibitors, appropriate numbers of cells, previously grown in the presence and absence of DOX for *MYC* knockdown, were seeded in cell bind 96 well plates and left overnight in the incubator to recover. Drugs were added to the plates the following day, to the desired final concentration. At day 5 post treatment, media-containing drug was removed from plates using a multi-channel pipette and replaced with drug-free media. Cell viability was assessed with CellTiter-Glo (CTG) at 3, 5, 10 and 14 days following initial drug exposure. Relative luminescence units (RLU) were used as an indicator of cell survival (metabolically active cells). Luminescence readings were analysed using Prism8 (Graphpad).

2.3.8 High-throughput compound screen

The liquid handling of the small molecule inhibitor high-throughput screen was done using a Microlab STAR robotic platform (Hamilton), with the exception of cell seeding. Compounds were stored in 100% DMSO as 10mM stocks, and further diluted in DMSO to obtain a final concentration in each well of the 384-well plate of 0.5nM, 1nM, 5nM, 10nM, 100nM, 500nM, 1000nM or 0.5nM, 5nM, 50nM and 500nM, depending on the compound library (Library content described in Chapter 5, Appendix 5.1, Appendix 5.2 and Appendix 5.3). Final DMSO concentration in all wells was 0.2% (v/v). Inhibitors were stored in a StoragePod, (Roylan Developments) under nitrogen atmosphere. Compounds on the screen were assessed in triplicate on separate plates to avoid plate to plate variations.

48h prior to drugging, doxycycline (DOX) was added to flasks containing cell lines for *MYC* knockdown (cell lines cloned with NS shRNA constructs included). The day before the screen 1000-2000 cells in 25µl of media were seeded in a 384-well assay plate using a Multi-Drop combi. To ensure single cell suspensions, cells were passed through 30µm MACS cell strainers when diluting to the appropriate number and volume required. Plates were then left in the incubator for 24h to recover. After the incubation time, compounds were freshly diluted in the Microlab STAR platform (Hamilton) (to the final titration explained above) and 25µl of the aliquoted drugs were added to the plates. Cells were cultured in the presence of the inhibitors for five days. After treatment, cell viability was assessed using CellTiter-Glo (CTG), by adding 20µl to the media. After 10 minutes of gentle incubation on a shaker, luminescence signal was captured using a Victor X-light plate reader.

An untreated control (no compound or DMSO) alongside positive and negative controls 50% DMSO only or camptothecin) were included on every assay plate for data normalisation. Signal from each well was normalised to the median of the negative controls (software analysis as described by Witkiewicz et al., 2016)(Witkiewicz et al., 2016).

2.3.9 Gene expression quantification

2.3.9.1 RNA extraction

RNA was extracted from frozen pellets using the QIAGEN RNeasy Mini Kit. To lyse the cells, samples were resuspended in 300µl of RLT buffer and transferred to a QIAshredder column. After a 2min centrifugation at 20000xg, the resultant elution was homogenised with 300µl of 70% ethanol and transferred to a RNeasy column, which was then centrifuged for 30sec at 8000xg. Sequential washings with 700µl RW1 and 500µl RPE buffer, followed by 15s centrifugation at 8000xg after each step, were performed to remove contaminants from RNA bound in the columns. 30µl of RNAse-free water was used to elute the RNA from the RNeasy columns. The final RNA concentration was immediately quantified using a nanospectrophotometer, which provided with the 260/280 ratio to assess the quality of the RNA extracted. RNA was then stored at -80°C until required.

2.3.9.2 cDNA synthesis

The high capacity cDNA reverse transcription kit (Applied Biosystems) was used to synthesise cDNA from extracted RNA. Following the manufacture's protocol, up to 5.8µl of sample was mixed with 4µl of reaction mix and 1µl of reverse transcriptase, and made up to a total volume of 20µl with nuclease-free water, to produce 50ng/µl of cDNA. After the reverse transcription, cDNA was stored at -20°C.

2.3.9.3 Quantitative reverse transcription PCR (RT-qPCR)

To quantify mRNA expression of genes of interest, PowerUp SYBR Green Master Mix kit (Applied Biosystems) was used to amplify cDNA synthesised from samples RNA. The use of the SYBR green dye enables the quantification of DNA as it intercalates between DNA bases of double-stranded DNA, emitting fluorescent signal upon excitation. Resultant fluorescence is used as a measure of total DNA amplified. Primers for our target genes (summarised in table 2.4) were designed using Primer3Plus software.

A volume of 4µl of cDNA at a final concentration of 1ng/µl, was mixed with the reverse and forward primers alongside the SYBR master mix and the water. Components of the master mix are described in Table 2.11.

Component	Volume
SYBR Green Mix	5.1µl
Forward primer (10µM)	0.2µl
Reverse primer (10µM)	0.2µl
Sample	4µl
Nuclease-free H_2O	0.5µl

Table 2.11. Components of the SYBR Green assay for RT-qPCR

Total volumes of 10µl reactions were run in triplicate on 384-well plates in a ViiA7 machine using *TBP* as internal control (reference gene). RT-qPCR cycling conditions used can be seen in Table 2.12.

Condition		Temperature (°C)	Time
Hold stage	step 1	50	2 min
	step 2	95	10 min
PCR stage (40 cycles)	step 1	95	15 sec
	step 2	60	1 min
Melt Curve stage	step 1	95	15 sec
	step 2	60	1 min
	step 3	95	15 sec

Table 2.12. Thermal cycling conditions for RT-qPCR SYBR assay

Data produced was analysed with QuantStudio Real-Time PCR System (Applied Biosystems), and the comparative Ct method was used, which assumes uniform amplification efficiency of 100% across samples. The housekeeping gene was used to normalise the expression of each gene of interest, yielding a ΔCt value, which was then used to compare the non-drug treated control and the experimental sample. The resultant ΔΔCt value was then linearised to obtain relative mRNA expression.

Differential gene expression was calculated as follows:

$$\Delta Ct = (Ct_{\text{target gene}} - Ct_{\text{reference gene}})$$

$$\Delta\Delta Ct = (\Delta Ct_{\text{target gene}} - \Delta Ct_{\text{reference gene}})$$

$$\text{Fold change expression} = 2^{-\Delta\Delta Ct}$$

2.3.10 Flow cytometry

Flow cytometry analysis was used to assess cell cycle phases of cells of interest. Samples were harvested, washed twice with ice cold PBS and fixed by adding drop wise cold 70% ethanol while vortexing. Cells were kept at 4°C until required.

For cell cycle analysis, samples were spun at 850*xg* in a 4°C centrifuge for 5min. Ethanol was carefully aspirated to minimise cell loss. Cell pellet was resuspended in 0.5ml of PBS. Cells were treated with 50µl of 100µg/ml RNase A (pre-heated at 100°C for 10 mins) to ensure only DNA content of cells was stained. To lyse and stain the cells, 250µl of 1:10 mix of Propidium iodide (PI) and triton (100X) was added to each sample. Cells were analysed using the Attune NxT Flow Cytometer (ThermoFisher Scientific) and data was processed and cell cycle distribution verified using FlowJo software. Percentage of cells in each cell cycle phase was calculated relative to total phases.

Chapter 3. *MYC*-dependent models of *MYC*-amplified Group 3 medulloblastoma

3.1 Introduction

MYC's involvement in MB_{Group3} pathogenesis is well established (Chapter 1). As explained in Chapter 1, the *MYC* oncogene family members are super-transcription factors that have the ability to regulate 15% of the entire genome. Downstream effects of *MYC* involve key biological functions like cell proliferation, differentiation and survival, being of crucial importance to tightly regulate its expression. Several studies have demonstrated that inactivation of *MYC* can translate into an anti-tumorigenic effect. Tumour addiction to *MYC* thus offers a therapeutic window to target oncological diseases (Dang et al., 2006, Hutter et al., 2017).

Despite several attempts to target *MYC* directly, single drug development has proven to be challenging and no drugs for its direct targeting are clinically available yet. Indirect targeting of *MYC* has been widely investigated over the last decade, making it clear that therapeutic strategies aiming to alter MYC abundance or disrupt key *MYC* functions are going to be required in order to target the effects of this master cell regulator (Vita and Henriksson, 2006, Shalaby and Grotzer, 2016).

A few studies using small interference RNA (siRNA) strategies (von Bueren et al., 2009, Ćwiek et al., 2015) have been done in MB_{Group3} to try and elucidate *MYC*´s role in MB tumour biology and identify druggable genetic dependencies, but none have yet explored it in a context-specific *MYC*-dependent manner. To specifically explore the role of *MYC* in MB_{Group3}, the Paediatric Brain Tumour Group (PBTG) at Newcastle University has established three *MYC*-regulable MB_{Group3} cell lines, using D425, D283 and HDMB03 as hosts, where *MYC* can be silenced through the DOX-induced expression of shRNA. *MYC* knockdown is achieved by the addition of DOX to the media, which triggers the expression of the shRNA construct transduced into the cells knocking down *MYC* expression. The expression vector system is described in Chapter 2.

The host cell lines used inherently express different levels of *MYC*. D425 and HDMB03 have *MYC* amplification, whereas D283 has gained an extra copy of the *MYC* gene. Each set of isogenic cell lines generated have two experimental constructs targeting two different *MYC* sequences, called MYC2 and MYC3 (expressing shRNA to silence *MYC*), and a non-silencing control construct (NS) expressing a non-silencing shRNA (Dr. Swartz, PhD thesis)(constructs and shRNA system is explained in Chapter 2).

The generation of stable isogenic cell lines with a DOX-inducible system for *MYC* knockdown brings the opportunity for direct investigation of the nature and extent of *MYC's* involvement in MB_{Group3} pathogenesis, and its dependency. The use of these models could allow the identification of key pathways for the survival of *MYC*-overexpressing cells, and to identify and develop novel therapeutic strategies to bring into the clinic, which is a promising strategy to understand the best way to treat *MYC*-driven cancers.

3.2 Aims

To the present day, this is the first time that *MYC*-regulable MB_{Group3} cell models have been generated. The aim of this chapter is to validate the effectiveness of *MYC* knockdown achieved with the inducible shRNA system, and to independently characterise phenotypic changes associated with *MYC* knockdown in these three sets of isogenic cell lines. Corroboration of achievement of *MYC*-silencing by the shRNA system, and *MYC*-dependent cancer phenotypes, will establish the suitability of these models as new tools to study the *MYC*-dependent biology within human MB_{Group3} as a basis for the investigational approaches described in following chapters.

3.3 Validation of DOX-inducible *MYC*-regulable MB_{Group3} cell lines

3.3.1 Validation of MYC *knockdown at the protein level*

The modelling principle on which this thesis is based is the ability to experimentally regulate *MYC* expression in MB_{Group3} cell lines. Therefore, prior to experimentation, testing the reproducibility of *MYC* knockdown by doxycycline (DOX) in each host cell line was necessary.

The DOX concentration selected for experimentation was based on previous optimisation work done in the PBTG (Dr. Swartz, PhD thesis), where it was established that 1µg/ml was the minimum dose required to achieve maximum *MYC* knockdown with minimal effects on MYC expression caused by DOX alone in control cells. Therefore, it was decided to start validation experiments with a concentration of a 1µg/ml to determine if each shRNA targeting *MYC* could knock it down at the chosen concentration in each host cell line.

Initial experiments to determine the time course of *MYC* knockdown over 96h were only carried out in D425. To confirm *MYC* knockdown at the protein level, D425 cells bearing the NS, MYC2 and MYC3 constructs were cultured in the presence and absence of DOX (1µg/ml) (Figure 3.1) and harvested at different time points (24, 48, 72, 96h).The NS construct was used as a negative control for the function of the shRNA and to determine the specific effects of the silencing constructs on the cell lines.

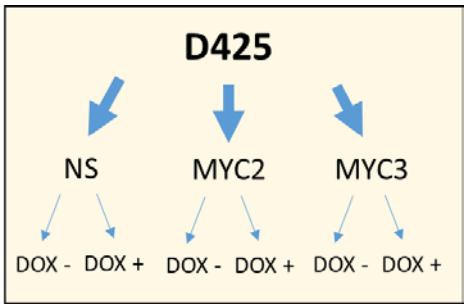

Figure 3.1. Overview of the isogenic working system. Schematic representation of the isogenic shRNA model system. The D425 MB_{Group3} cell line has been transduced with a non-silencing (NS), MYC2 and MYC3 shRNA construct for silencing *MYC* expression. Expression of the shRNA system and the consequent silencing of *MYC* is triggered by the addition of doxycycline (DOX+) to the media. Constructs need to be grown separately to avoid mixing. For DOX-treated conditions, cells from the same passage are grown in parallel with and without doxycycline in the media.

Cell lysates from DOX-treated cells were collected, protein quantified and protein detected with a simple western Assay (Wes) as described in Chapter 2.

Protein quantification of D425 with Wes validated that maximum *MYC* knockdown was achieved at 72h by the MYC2 and MYC3 constructs (Figure 3.2), showing no significant differences in MYC protein levels at later time points (MYC2 p=0.787; MYC3 p=0.525), thus confirming prolonged *MYC* knockdown throughout the time course of DOX induction. Treatment of D425 NS with DOX did not have an effect on the cells or in MYC protein expression levels. Time course experiments of DOX induction independently validated the concentration of DOX previously determined to use to achieve maximum *MYC* knockdown (1µg/ml), and the time at which this is achieved (72h).

Considering maximum *MYC* knockdown was achieved at 72h, validation of *MYC* knockdown in D283 and HDMB03 was only performed at this single time point.

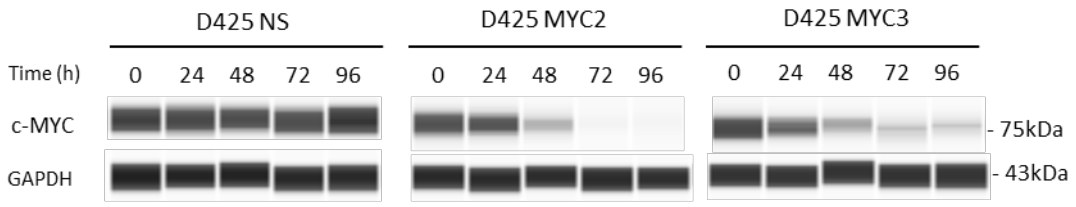

Figure 3.2. Time course of *MYC* knockdown in D425 MB_{Group3} cell line.Simple western assay (Wes) of MYC protein levels (~75kDa) expressed by D425 cells transduced with the NS, MYC2 and MYC3 shRNA constructs, cultured in the presence of doxycycline (DOX) for 96h. Protein levels were assessed at 0, 24, 48, 72 and 96h. D425 NS was used as a non-targeting control for shRNA. DOX-induced MYC knockdown was achieved at 72h in the MYC2 and MYC3 construct. GAPDH (~40kDa) was used as internal loading control

3.1.1.1 Establishment of the level of MYC knockdown achieved

Next, D425, D283 and HDMB03 isogenic cell lines cloned with the NS, MYC2 and MYC3 constructs were cultured with DOX for 72h to induce the expression of the shRNA constructs for *MYC* knockdown. Un-treated cells were used as controls for each construct. For data normalisation, MYC protein levels were normalised to the expression levels of *GAPDH*.

After DOX treatment, no changes in MYC protein expression levels were seen for any of the NS controls when cultured in the presence and absence of DOX. In the presence of DOX, a decrease in MYC protein levels was seen in MYC2 and MYC3 constructs across cell lines when compared to their correspondent un-treated controls (Figure 3.3). Triggering the expression of D425 MYC2 and MYC3 shRNA caused a reduction in MYC protein levels of 73% for MYC2 and 60% for MYC3 (% of the average of two replicates), when compared to their respective DOX-untreated control, in both cases statistically significant (p=0.0081; p=0.042, respectively). Similarly, D283 MYC2 and MYC3 shRNA significantly reduced MYC protein expression by 72.1% and 65.3%, respectively (p=0.014; p=0.023). Treatment with DOX also triggered the expression of HDMB03 MYC2 and MYC3 shRNA constructs, reducing MYC protein levels by 51.6% in MYC2, and 37% in MYC3 (only significant in MYC2, p=0.012), when compared to their untreated counterparts (Figure 3.3). Results from all 3 cell lines indicate that the MYC2 shRNA construct is the most efficient in knocking down *MYC* expression, achieving an average of 65% *MYC* knockdown across cell lines.

In summary, *MYC* knockdown at the protein level was successfully reproduced with the addition of the established doxycycline concentration (1µg/ml) to the media. DOX triggered the expression of the MYC2 and MYC3 shRNA constructs across cell lines, achieving a reduction of MYC protein levels of 65% on average. These experimental conditions were taken forward for use in further experimentation.

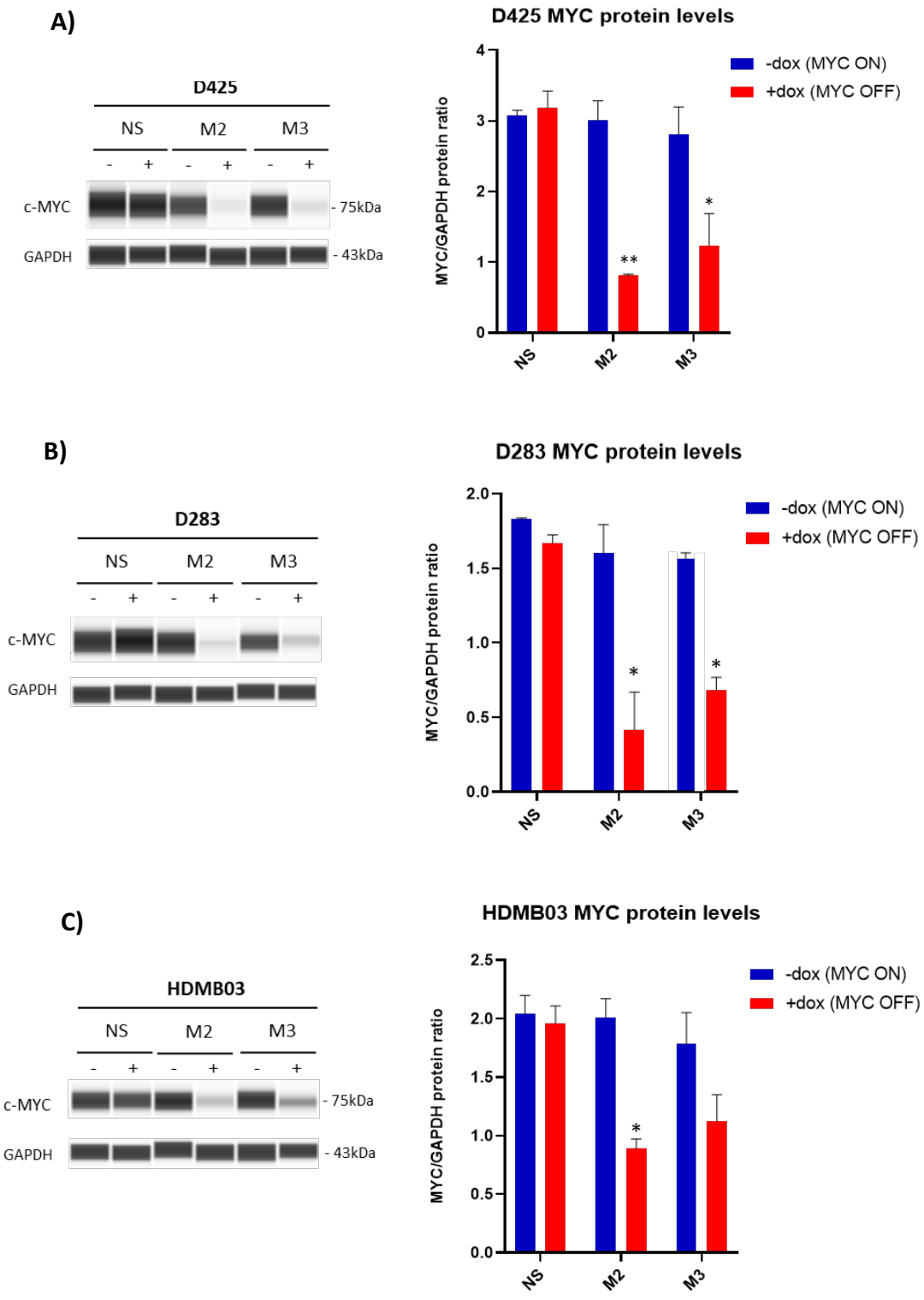

Figure 3.3. Validation of MYC knockdown at the protein level by inducible shRNA constructs in D425, D283 and HDMB03 MB cells. D425, D283 and HDMB03 cell lines cloned with the NS, MYC2 (M2) and MYC3 (M3) constructs, were cultured for 72h in the presence (+DOX) and absence (-DOX) of doxycycline for *MYC* knockdown. Cells were harvested at 72h, protein extracted and protein levels analysed with Wes. The image shows automated western blots and densitometry analysis of MYC protein expression in A)D425, B)D283 and C)HDMB03. GAPDH was used as internal loading control. MYC protein expression was normalised to GAPDH protein expression levels. Graphs show the comparison of MYC protein levels between *MYC* overexpressing cell lines (blue: -dox; MYC ON) and those with *MYC* knockdown (red: +dox; MYC OFF). Densitometry results are shown as means ± SEM of two independent experiments and the significance determined by paired student's t-test (significance denoted by *$p \leq 0.05$, ** $p \leq 0.01$)

3.3.2 Validation of MYC knockdown at the RNA level

Following confirmation of shRNA-mediated silencing of MYC protein expression, we sought to examine if *MYC* knockdown was also observed at the mRNA level.

D425 and D283 isogenic cell lines were grown in the presence of DOX for DOX-inducible *MYC* knockdown, harvested at 3 and 7 days after DOX induction and RNA extracted for quantification of mRNA expression by quantitative real-time PCR.

DOX-induced *MYC* knockdown was also identified at the mRNA level. No differences in MYC mRNA levels were observed for the NS constructs, consistent with results at the protein expression level. Both targeting shRNA constructs caused a significant decrease in MYC mRNA expression with 3 days of DOX treatment in both cell lines.

In D425, after 3 days, *MYC* knockdown caused a significant reduction of MYC mRNA expression in MYC2 and MYC3 cells when compared to the DOX-untreated control (day 0). A decrease of 60% in MYC2 and 19% in MYC3 was observed within 3 days of DOX treatment (MYC2 p=0.0004; MYC3 p=0.007). A further decrease in MYC mRNA expression was seen with prolonged treatment with DOX (day 7) when compared to un-induced counterparts, by 74% and 47% in MYC2 and MYC3 respectively (MYC2 p=0.0017; MYC3 p=0.0025) (Figure 3.5, A).

Triggering of shRNA expression in D283 MYC2 and MYC3 also caused a significant decrease in MYC mRNA levels when compared to the control, of 41% and 19% respectively for both constructs (MYC2 p=0.011; MYC3 p=0.03). MYC mRNA levels were further reduced when exposed to DOX for 7 days (relative to control), by 57% in MYC2 and 39% in MYC3 (MYC2 p=0.023; MYC3 p=0.01) (Figure 3.4, B).

The same effect was seen in HDMB03 cell line. *MYC* knockdown caused a significant decrease in MYC mRNA levels after 3 days of DOX exposure, for both constructs (MYC2 p=0.0293; MYC3 p=0.0113). A further decrease in MYC mRNA levels were seen after 7 days of DOX exposure, by 48.4% in MYC2 and 27.7% in MYC3, only significant for MYC2 construct (MYC2 p=0.0131; MYC3 p=0.0542).

Overall, *MYC*-knockdown was also seen at the mRNA level in both sets of isogenic cell line models. DOX-induced *MYC* knockdown caused a decreased in MYC mRNA expression levels after 3 days of exposure to DOX. Prolonged induction with doxycycline further significantly reduced *MYC* levels in both D425 and D283.

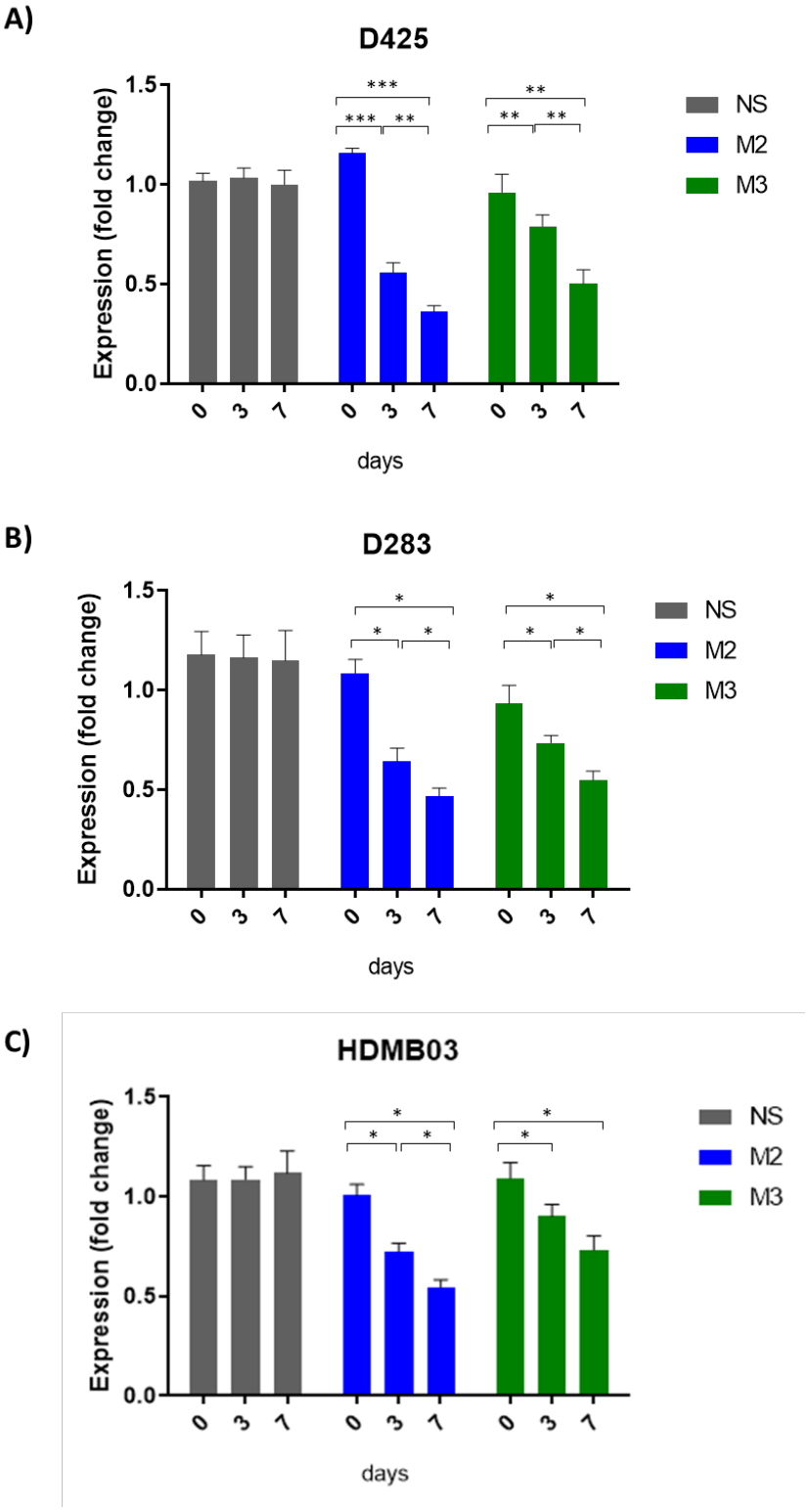

Figure 3.4. Validation of *MYC* knockdown at the mRNA level by inducible shRNA constructs in D425, D283 and HDMB03 MB cells. RT-qPCR result showing MYC mRNA expression levels of the NS, MYC2 (M2) and MYC3(M3) constructs in A) D425, B) D283 and C)HDMB03 cells. Isogenic cell lines were cultured in the presence of DOX for 3 and 7 days. Changes in MYC mRNA expression levels are compared to the untreated control (no DOX) for each construct (day 0). Data represents the mean (±SEM) of triplicates. Expression fold change was calculated relative to TBP expression (control gene). Statistical significance determined by students t-test (statistically significant; *$p \leq 0.05$, ***$p \leq 0.001$, ****$p \leq 0.0001$).

3.4 Effect of *MYC* knockdown on cell proliferation

The proliferative consequences of knocking down *MYC* by shRNA was assessed next, in order to determine whether the cell lines retained their addiction to the oncogene.

To study the proliferative effect of *MYC* knockdown, cell growth of D425, D283 and HDMB03 cell lines following reduction of *MYC* expression was studied. Cell proliferation was assessed using CellTiter-Glo (CTG) assay, as described in Chapter 2, every 24h for 6 consecutive days. Luminescence measurements, as an estimation of cell number, were used to generate growth curves. Growth curves generated for each construct of each cell line were compared according to *MYC*-expression levels (Figure 3.5, 3.6 and 3.7).

A significant decrease in cell proliferation was seen across all cell lines following *MYC* knockdown. *MYC*-silencing significantly reduced MYC2 and MYC3 cells proliferation by 72h when compared to their counterparts not exposed to DOX (i.e. expressing high levels of *MYC*), in all three host cell lines. DOX itself did not have a reproducible effect on cell proliferation, (NS shRNA cells). The effect of *MYC* knockdown was consistent in D425, D283 and HDMB03. Statistical significance of the comparisons performed are summarised in Table 3.1.

Cell lines selected for use in this study were thus characterised by their addiction to *MYC* and *MYC*-dependent growth.

A)

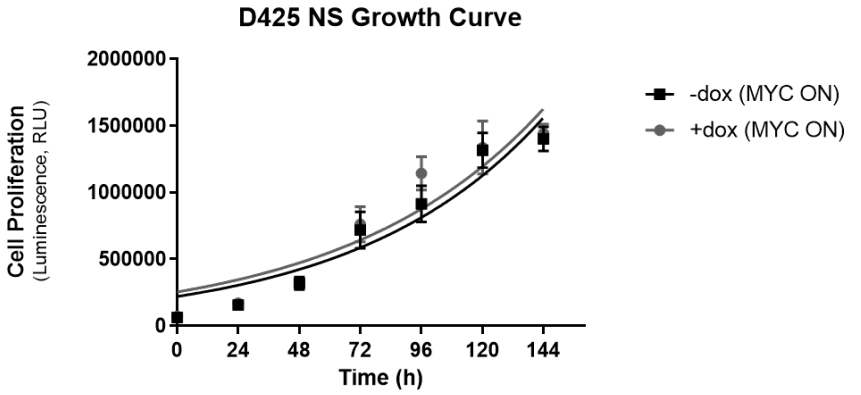

B)

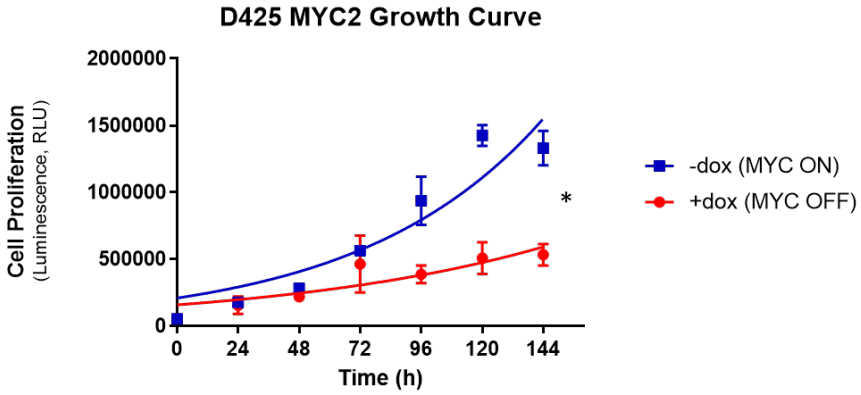

C)

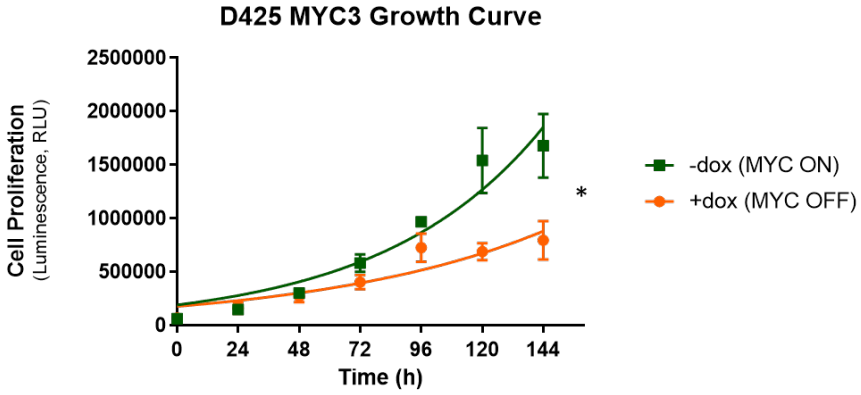

D)

Exponential Growth	D425					
Best-fit values	NS -dox	NS +dox	MYC2 -dox	MYC2 +dox	MYC3 -dox	MYC3 +dox
Doubling Time	50.89	50.01	49.71	73.23	49.27	65.51

Figure 3.5. Growth curves of *MYC*-amplified D425 cells following *MYC* knockdown. Growth curves of D425 NS, MYC2 and MYC3 cell lines grown in the absence (-DOX) and presence (+DOX) of DOX for *MYC* knockdown. Cell proliferation was assessed with CTG every 24h for a total of 6 days. Cell proliferation is presented as relative luminescence units (RLU). A) Growth curve of D425 NS cells in the absence (-dox; MYC ON) and presence (+dox; MYC OFF) of DOX. No difference in proliferation was observed between conditions. B) & C) Growth curves of D425 MYC2 and MYC3 cells in the absence (-dox; MYC ON) and presence (+dox; MYC OFF) of DOX. *MYC* knockdown (+DOX) caused a significant decrease in MYC2 and MYC3 proliferation across cell lines. D) Summary of doubling times for D425 cells following *MYC* knockdown. Results are shown as means (±SEM) of at least three individual experiments. Significance was determined by ratio paired student's t-test (*$p \leq 0.05$)

A)

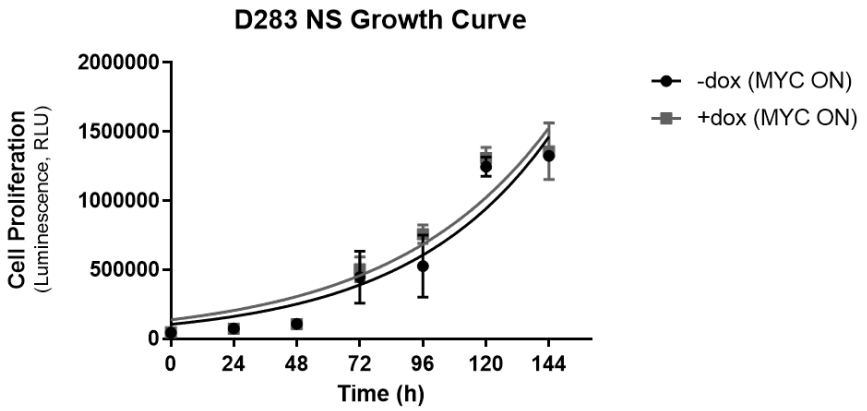

B)

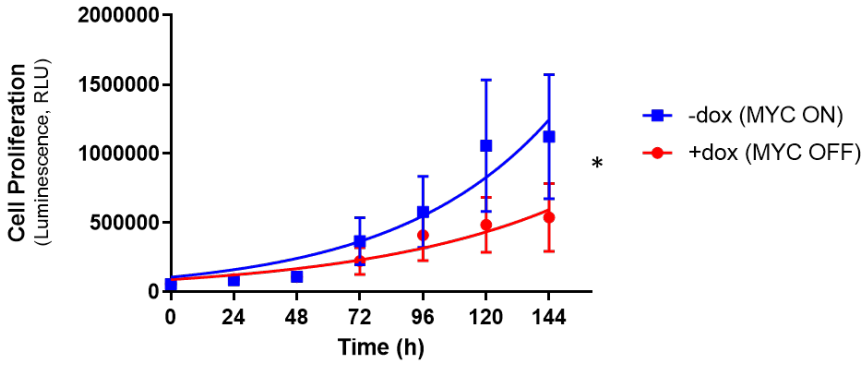

C)

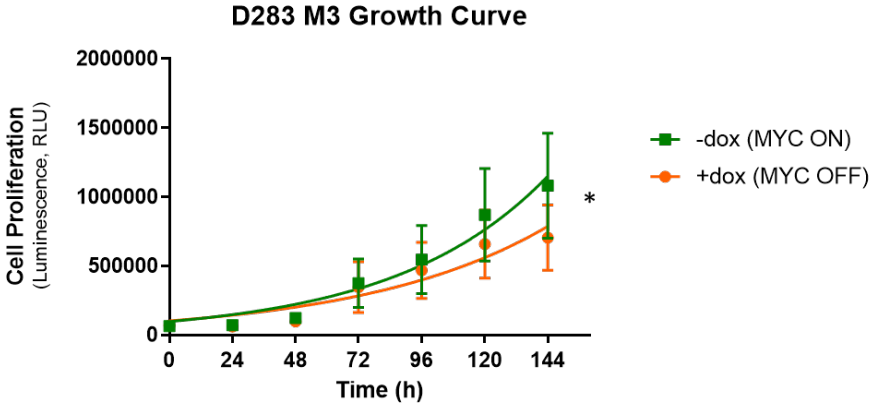

D)

Exponential Growth	D283					
Best-fit values	NS -dox	NS +dox	MYC2 -dox	MYC2 +dox	MYC3 -dox	MYC3 +dox
Doubling Time	37.77	41.37	40.74	52.98	40.44	48.88

Figure 3.6. Growth curves of *MYC*-amplified D283 cells following *MYC* knockdown Growth curves of D283 NS, MYC2 and MYC3 cell lines grown in the absence (-DOX) and presence (+DOX) of DOX for *MYC* knockdown. Cell proliferation was assessed with CTG every 24h for a total of 6 days. Cell proliferation is presented as relative luminescence units (RLU). A) Growth curve of D283 NS cells in the absence (-dox; MYC ON) and presence (+dox; MYC OFF) of DOX. No difference in proliferation was observed between conditions. B), C) Growth curves of D283 MYC2 and MYC3 cells in the absence (-dox; MYC ON) and presence (+dox; MYC OFF) of DOX. *MYC* knockdown (+DOX) caused a significant decrease in MYC2 and MYC3 proliferation across cell lines. D) Summary of doubling times for D283 cells following *MYC* knockdown. Results are shown as means (± SEM) of at least three individual experiments. Significance was determined by ratio paired student's t-test (*$p \leq 0.05$)

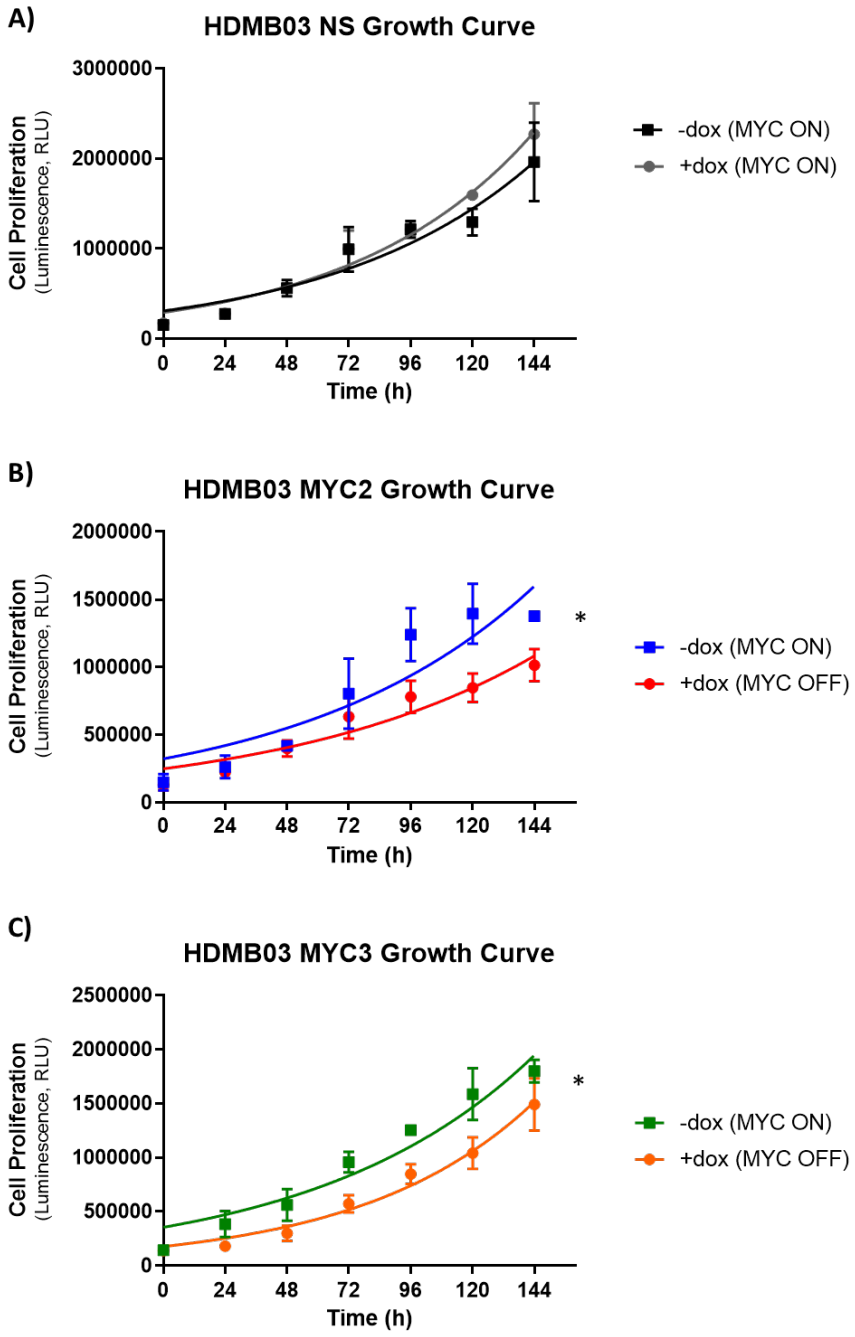

D)

Exponential Growth	HDMB03					
Best-fit values	NS -dox	NS +dox	MYC2 -dox	MYC2 +dox	MYC3 -dox	MYC3 +dox
Doubling Time	57.48	53.95	46.3	70.02	52.89	55.49

Figure 3.7. Growth curves of *MYC*-amplified HDMB03 cells following *MYC* knockdown. Growth curves of HDMB03 NS, MYC2 and MYC3 cell lines grown in the absence (-DOX) and presence (+DOX) of DOX for *MYC* knockdown. Cell proliferation was assessed with CTG every 24h for a total of 6 days. Cell proliferation is presented as relative luminescence units (RLU). A) Growth curve of HDMB03 NS cells in the absence (-dox; MYC ON) and presence (+dox; MYC OFF) of DOX. No difference in proliferation was observed between conditions. B), C) Growth curves of HDMB03 MYC2 and MYC3 cells in the absence (-dox; MYC ON) and presence (+dox; MYC OFF) of DOX. *MYC* knockdown (+DOX) caused a significant decrease in MYC2 and MYC3 proliferation across cell lines. D) Summary of doubling times for HDMB03 cells following *MYC* knockdown. Results are shown as means (± SEM) of at least three individual experiment. Significance was determined by ratio paired student's t-test (*$p \leq 0.05$).

CELL PROLIFERATION COMPARISON			
	D425		
Ratio paired t-test	**NS -DOX vs NS +DOX**	**MYC2 -DOX vs MYC2 +DOX**	**MYC3 -DOX vs MYC3 +DOX**
P value	0.1245	0.0024	0.0154
95% confidence interval	0.9912 to 1.058	0.3814 to 0.9103	0.5381 to 0.9973
	D283		
Ratio paired t-test	**NS -DOX vs NS +DOX**	**MYC2 -DOX vs MYC2 +DOX**	**MYC3 -DOX vs MYC3 +DOX**
P value	0.6743	0.0352	0.0486
95% confidence interval	0.9590 to 1.062	0.5745 to 0.8423	0.6127 to 0.9265
	HDMB03		
Ratio paired t-test	**NS -DOX vs NS +DOX**	**MYC2 -DOX vs MYC2 +DOX**	**MYC3 -DOX vs MYC3 +DOX**
P value	0.6290	0.0208	0.0501
95% confidence interval	0.9966 to 1.100	0.6197 to 0.9444	0.6328 to 0.8937

Table 3.1. Evaluation of cell proliferation according to *MYC* expression levels. Growth of NS, MYC2 and MYC3 D425, D283 and HDMB03 cell lines grown in the presence (+DOX) and absence (-DOX) of doxycycline were compared to assess differences in cell proliferation according to *MYC*-expression levels. Table summarises the statistical analysis of the growth comparison of cells with *MYC* knockdown (+DOX) compared to their untreated counterparts (-DOX). Significance was determined by ratio paired student's t-test. Data represents the mean (±SEM) of triplicates of at least three biological repeats..

3.5 Effect of *MYC* knockdown on the cell cycle

In order to understand the mechanism by which cell growth was reduced upon *MYC* knockdown, flow cytometry-based cell cycle analysis was performed for every variant of D425, D283 and HDMB03. Following the same methodology, cells grown in the presence and absence of DOX were harvested for cell cycle analysis at 72h. Staining of DNA content was performed using propidium iodide (PI) and analysed using the Attune NxT Flow Cytometer (ThermoFisher Scientific), as described in Chapter 2.

Cell cycle analysis identified no significant differences in cell cycle distribution for D425, D283 and HDMB03 cloned with the control NS construct. *MYC* silencing with shRNA caused an increase in cell numbers in G_1 phase and a decrease in the number of cells in the S phase of the cell cycle when compared to controls (no DOX); these changes in cell cycle distribution seen across all host cell lines.

In D425, *MYC* knockdown caused a significant increase in cells in G_1 phase for both MYC2 and MYC3 cells, when compared to cells overexpressing *MYC* (MYC2 p=0.0164; MYC3 p=0.0094). This increase of cell numbers in G_1 was accompanied by a significant decrease in cells in S phase for both constructs (MYC2 p=0.0411; MYC3 p=0.0209)(Figure 3.8).

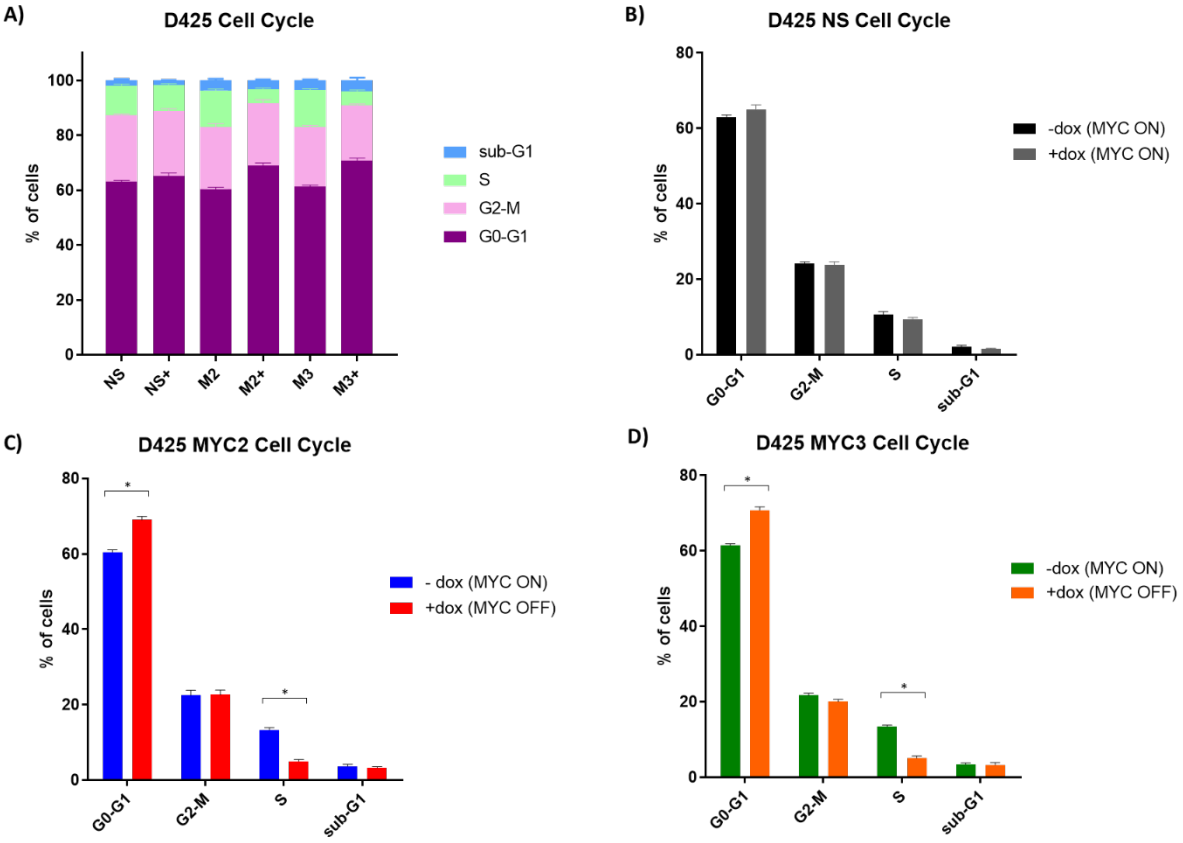

Figure 3.8. Cell cycle distribution of D425 MB cell line upon *MYC* knockdown. Cell cycle distribution of D425 NS, MYC2 and MYC3, grown in the presence (+DOX) and absence (-DOX) of DOX for *MYC* knockdown. A) Percentage of D425 NS, MYC2 (M2) and MYC3 (M3) cells at G_0-G_1, G_2-M, S, and sub-G_1 phases of the cell cycle. Graphs B), C) and D) show the percentage of cells in each phase of the cell cycle, for NS, MYC2 and MYC3 respectively. B)No significant changes were seen in the cell cycle distribution of D425 NS. C) *MYC* knockdown (red: +dox) caused a significant increase in the number of cells in G_0-G_1 phase and a significant decrease of cells in S phase in MYC2 cells when compared to controls cultured with no DOX (blue: -dox). D) *MYC* knockdown (orange: +dox) caused a significant increase in the number of cells in G_0-G_1 phase and a significant decrease of cells in S phase in MYC3 cells when compared to controls cultured with no DOX (green: -dox). Results are shown as means ± SEM of three individual experiments, and significance determined by paired students t-test (*$p \leq 0.05$).

For D283, despite a noticeable increase in cells on the G_1 phase of the cell cycle upon *MYC* knockdown, it was only significant for MYC2 (p=0.0210). Nevertheless, a significant decrease in the number of cells in the S phase of the cell cycle was seen for both MYC2 and MYC3 (MYC2 p=0.0241; MYC3 p=0.0271)(Figure 3.9).

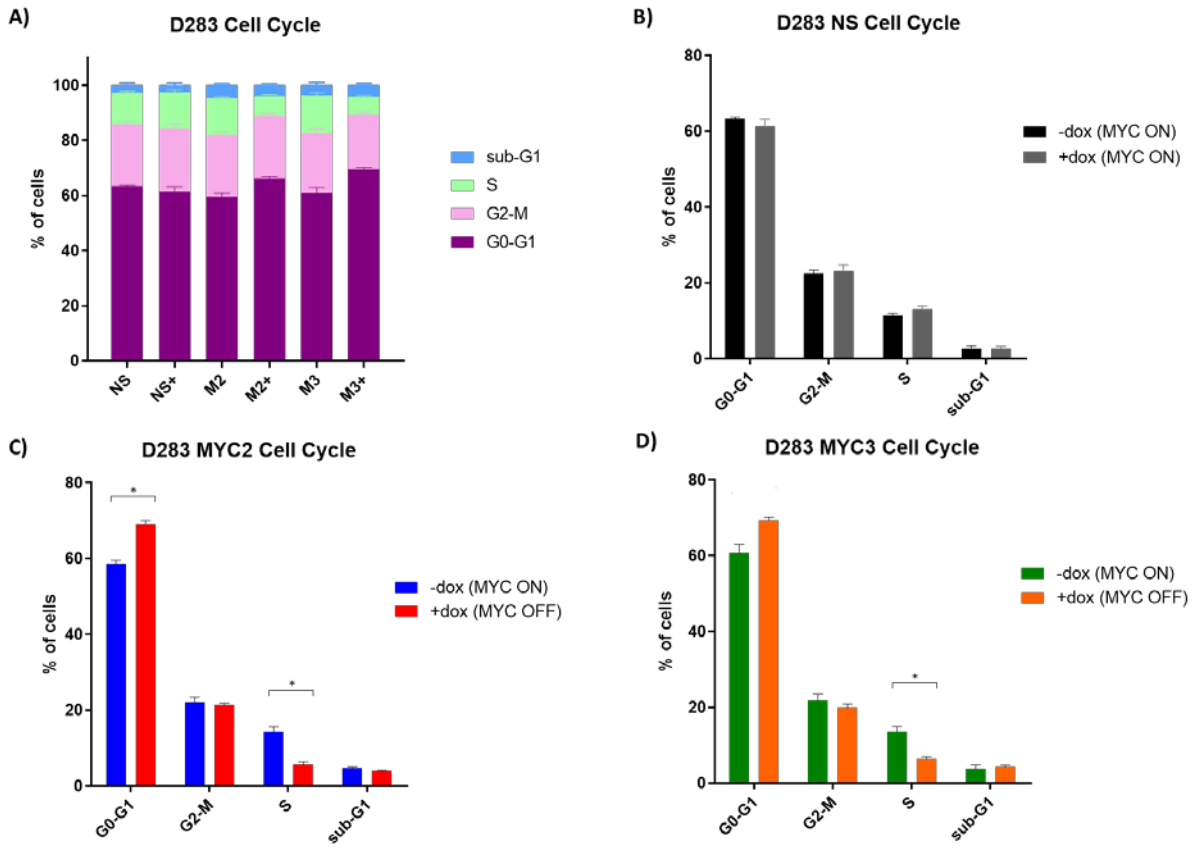

Figure 3.9. Cell cycle distribution of D283 MB cell line upon *MYC* knockdown. Cell cycle distribution of D283 NS, MYC2 and MYC3, grown in the presence (+DOX) and absence (-DOX) of DOX for *MYC* knockdown. A) Percentage of D283 NS, MYC2 (M2) and MYC3 (M3) cells at G_0-G_1, G_2-M, S, and sub-G_1 phases of the cell cycle. Graphs B), C) and D)show the percentage of cells in each phase of the cell cycle, for NS, MYC2 and MYC3 respectively. B)No significant changes were seen in the cell cycle distribution of D283 NS. C) *MYC* knockdown (red: +dox) caused a significant increase in the number of cells in G_0-G_1 phase and a significant decrease of cells in S phase in MYC2 cells when compared to controls cultured with no DOX (blue: -dox). D)*MYC* knockdown (orange: +dox) caused a significant increase in the number of cells in G_0-G_1 phase and a significant decrease of cells in S phase in MYC3 cells when compared to controls cultured with no DOX (green: -dox). Results are shown as means ± SEM of three individual experiments, and significance determined by paired students t-test (*p≤0.05).

Although the same pattern was seen in HDMB03, differences in cell cycle distribution of MYC2 and MYC3 were non-significant. Only the comparison of cell numbers of MYC2 cells in S phase of the cell cycle resulted to be statistically significant (p=0.0428) (Figure 3.10).

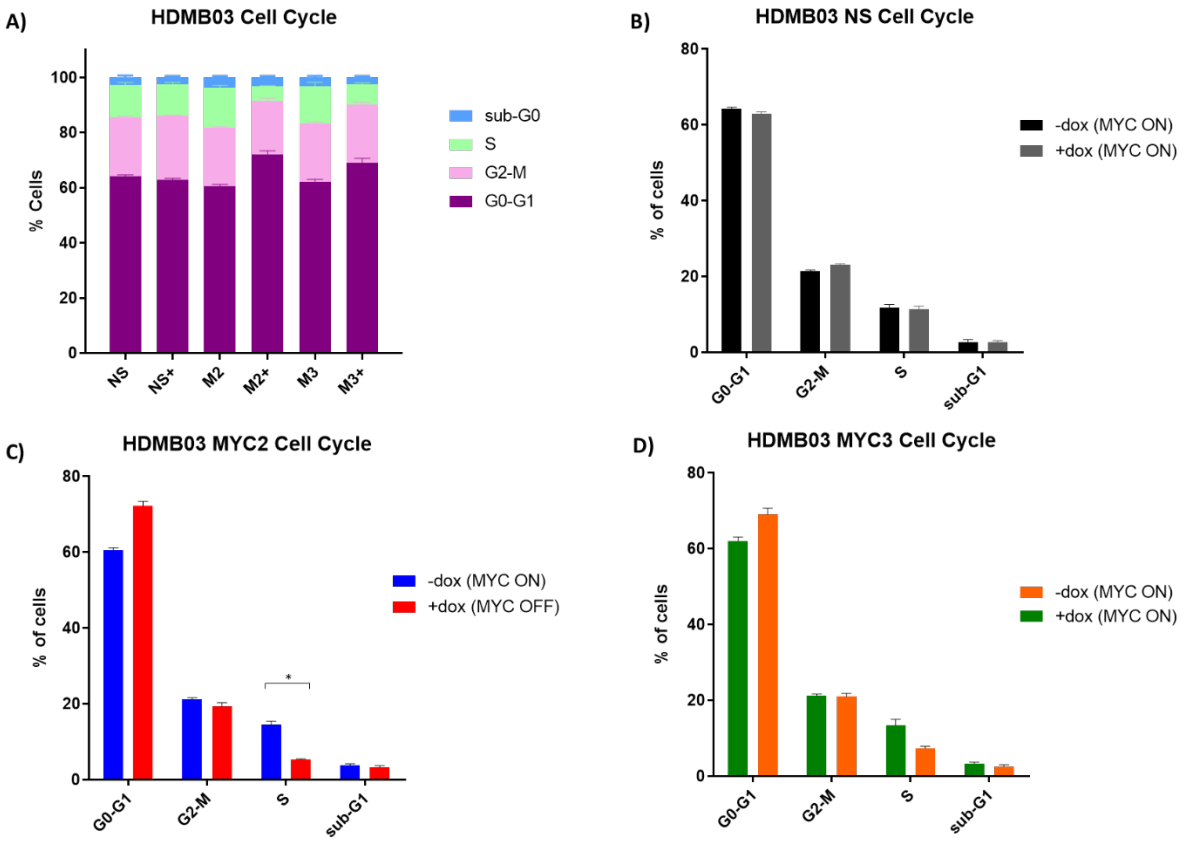

Figure 3.10. Cell cycle distribution of HDMB03 MB cell line upon *MYC* knockdown.Cell cycle distribution of HDMB03 NS, MYC2 and MYC3, grown in the presence (+DOX) and absence (-DOX) of DOX for *MYC* knockdown. A) Percentage of HDMB03 NS, MYC2 (M2) and MYC3 (M3) cells at G_0-G_1, G_2-M, S, and sub-G_1 phases of the cell cycle. Graphs B), C) and D) show the percentage of cells in each phase of the cell cycle, for NS, MYC2 and MYC3 respectively. B) No significant changes were seen in the cell cycle distribution of HDMB03 NS. C) *MYC* knockdown (red: +dox) caused an increase in the number of cells in G_0-G_1 phase (not significant) and a significant decrease of cells in S phase in MYC2 cells when compared to controls cultured with no DOX (blue: -dox). D)*MYC* knockdown (orange: +dox) caused an increase in the number of cells in G_0-G_1 phase and a decrease of cells in S phase in MYC3 cells when compared to controls cultured with no DOX (green: -dox)(not significant). Results are shown as means ± SEM of three individual experiments, and significance determined by paired students t-test (*p≤0.05).

3.6 Effect of *MYC* knockdown on apoptosis

To gain a better understanding of the mechanism by which *MYC* knockdown was reducing cell growth rates, apoptosis assays using the Caspase-Glo 3/7 reagent were performed D425 and D283 to study the effect of *MYC* silencing on apoptosis in a time-dependent manner (methods described in Chapter 2). Since HDMB03 apoptotic levels had already been established by Dr. Shanel Swartz as part of her PhD thesis, the effect of *MYC* knockdown on apoptosis was only investigated in D425 and D283 isogenic cell lines (Dr. Shanel Swartz, PhD thesis).

Caspase 3/7 activity was assessed in D425 and D283 transduced with NS, MYC2 and MYC3 shRNA after 72h of DOX treatment (apoptosis levels at all time points can be seen in Appendix 3.1). Non-treated cells for each construct were used as control for comparison. NS cells were used as internal control to account for possible effects of DOX treatment.

MYC knockdown in D425 MYC2 and MYC3 caused a significant decrease in apoptosis at 72h of DOX induction when compared to the corresponding untreated control (0h) (MYC2 $p<0.0001$; MYC3 $p=0.0001$). No significant changes in apoptotic markers were seen for D425 MYC2 cells expressing high levels of *MYC* (no DOX) between 0 and 72h. Following *MYC* knockdown, a significant decrease in apoptosis was seen in MYC2 cells when compared to the levels of apoptosis at 0h (Figure 3.11, A). A slight increase in apoptosis was seen in D425 MYC3 expressing high levels of *MYC* when compared the correspondent control (0h), however, this did not reach statistical significance. In D425 NS, apoptosis seemed to decline in a time dependent manner. Despite the slight decrease detected, changes observed were not statistically significant (Figure 3.11, A).

A significant decrease in apoptosis was also observed in D283 MYC2 and MYC3 cells following *MYC* silencing with shRNA at 72h, when compared to their correspondent control counterparts (0h) (MYC2 $p=0.0006$; MYC3 $p=0.0214$) (Figure 3.11, B). 72h after DOX-induction, a less marked but consistent increase in apoptosis was seen at 72h in MYC2 and MYC3 cells when expressing high levels of *MYC* (no DOX) in comparison to 0h (not statistically significant). No significant changes in apoptotic signal were seen in D283 NS, between both time points (Figure 3.11, B).

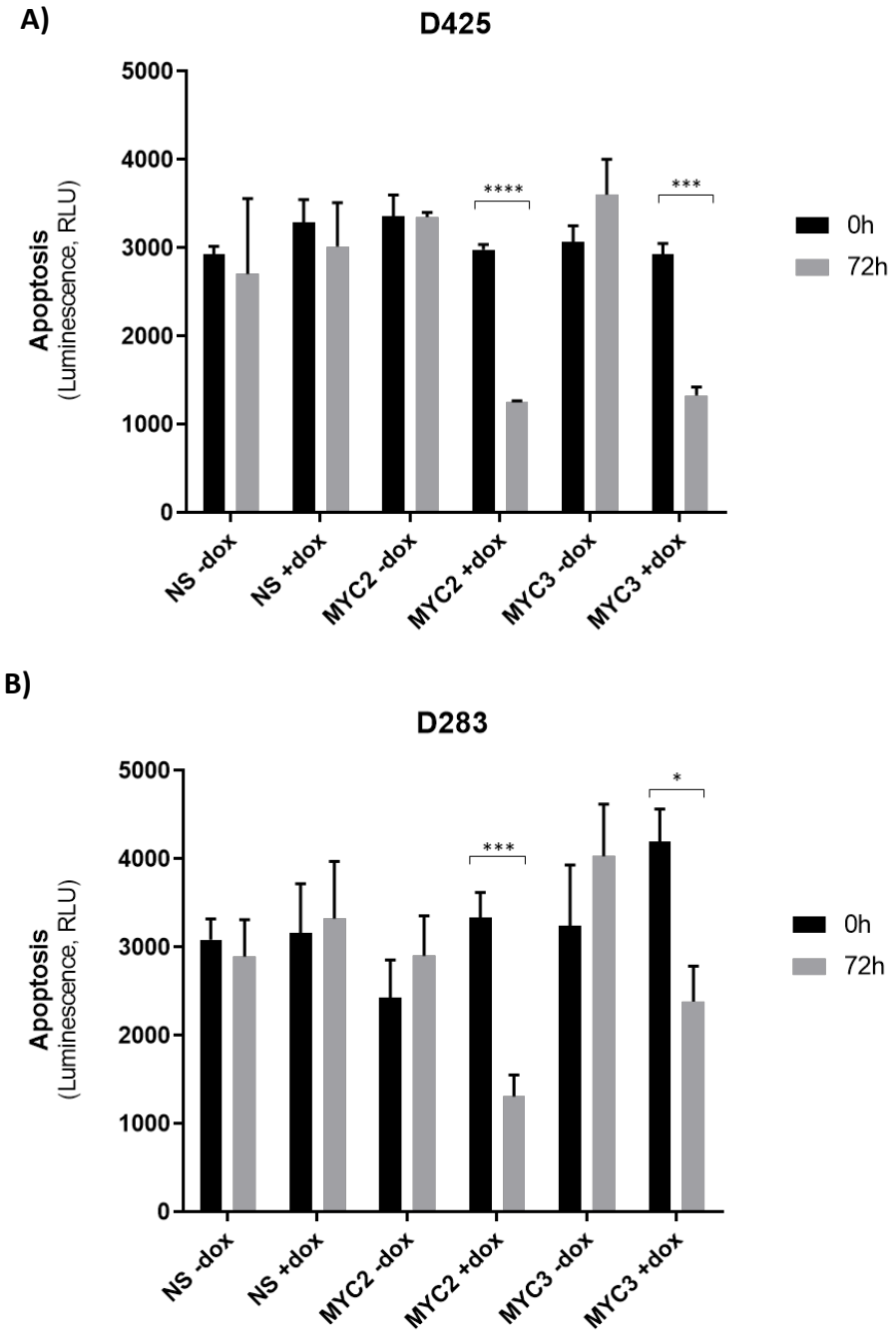

Figure 3.11.Effect of *MYC* knockdown on apoptosis in D425 and D283 regulable MB_{Group3} cell lines.Time dependent effect of *MYC* knockdown on apoptosis A) D425 and B) D283 *MYC*-regulable cell lines. Cells cloned with NS, MYC2 and MYC3 constructs were cultured with DOX for 72h (+DOX). Un-treated cells (-dox) were used as controls for each construct. A) At 72h, *MYC* knockdown (+dox) caused a significant decrease in apoptosis in D425 MYC2 and MYC3 cells. B) A significant decrease in apoptosis was observed following *MYC* knockdown in D283 MYC2 and MYC3 cells for both cell lines. Results are shown as means ±SEM of three individual experiments, values expressed as luminescence unit (RLU).

3.7 Effect of radiation on *MYC*-driven cell lines

Radiation plays a pivotal role in MB treatment (Ashley et al., 2012, Bloom, 1982). Patients with MB_{Group3} tumours respond poorly to treatment and those with *MYC* overexpression or amplification are associated with a significantly worse outcome (Schwalbe et al., 2017). Bueren *et al.* analysed how *MYC* expression determined the response of MB cell lines to radio- and chemotherapy. They studied the response of DAOY and UW228 (MB_{SHH}) cell lines engineered to express different levels of MYC mRNA to irradiation (2Gy, 5Gy or 10Gy). They found that higher levels of *MYC* expression sensitise MB cell lines to radiation treatment (von Bueren et al., 2011).

To study if similar effects are observed in a Group 3 background and further characterise phenotypes in our models, D425 cells cloned with the NS, MYC2 and MYC3 regulable-constructs were induced with DOX to knockdown *MYC* and exposed to ionising radiation (IR). Preliminary experiments with IR were only performed in D425.

3.7.1 MYC sensitises D425 MB cells to radiation

To examine whether MB_{Group3} sensitivity to radiation was *MYC*-dependent, radio-sensitivity assays were performed on D425 *MYC*-regulable cell line.

D425 NS, MYC2 and MYC3 cells were induced with DOX 48h before IR treatment to ensure maximum MYC knockdown when irradiating. DOX was refreshed before seeding to maintain *MYC* knockdown throughout the experiment. Cells in each plate were irradiated with single doses of either 2, 5, 10, 15 or 50Gy (described in Chapter 2). Control plates received no irradiation. D425 NS were used as negative control to compare to those D425 cells bearing also a construct and being exposed to DOX treatment. Cell viability was assessed 72h after irradiation as described in Chapter 2, and data normalised to DOX untreated controls.

A reduction in cell viability was observed after treatment with different concentrations of IR, which was more markedly pronounced in cells expressing high levels of *MYC* than in cells with *MYC* knockdown. 72h after IR treatment, no differences in cell viability between D425 NS cells treated with and without DOX were seen (Figure 3.12, A), showing that DOX treatment has a minimum effect on cell viability (p=0.7633). *MYC* knockdown reduced MCY2 and MYC3 cells susceptibility to IR when compared to cells expressing high levels of *MYC*, difference only significant in D425 MYC2 (MYC2 p=0.0488; MYC3 p=0.1031) (Figure 3.12, B and C). IR of 10Gy reduced MYC2 and MYC3 cells viability by 44.88% and 41.55% respectively, compared to a reduction of only 13.3% and 19.3% following *MYC* knockdown.

Overall, D425 cells expressing high levels of *MYC* were found to be more susceptible to IR, causing a decrease in cell viability in a dose-dependent manner. *MYC* knockdown increased resistance to IR, displaying higher cell viability after treatment.

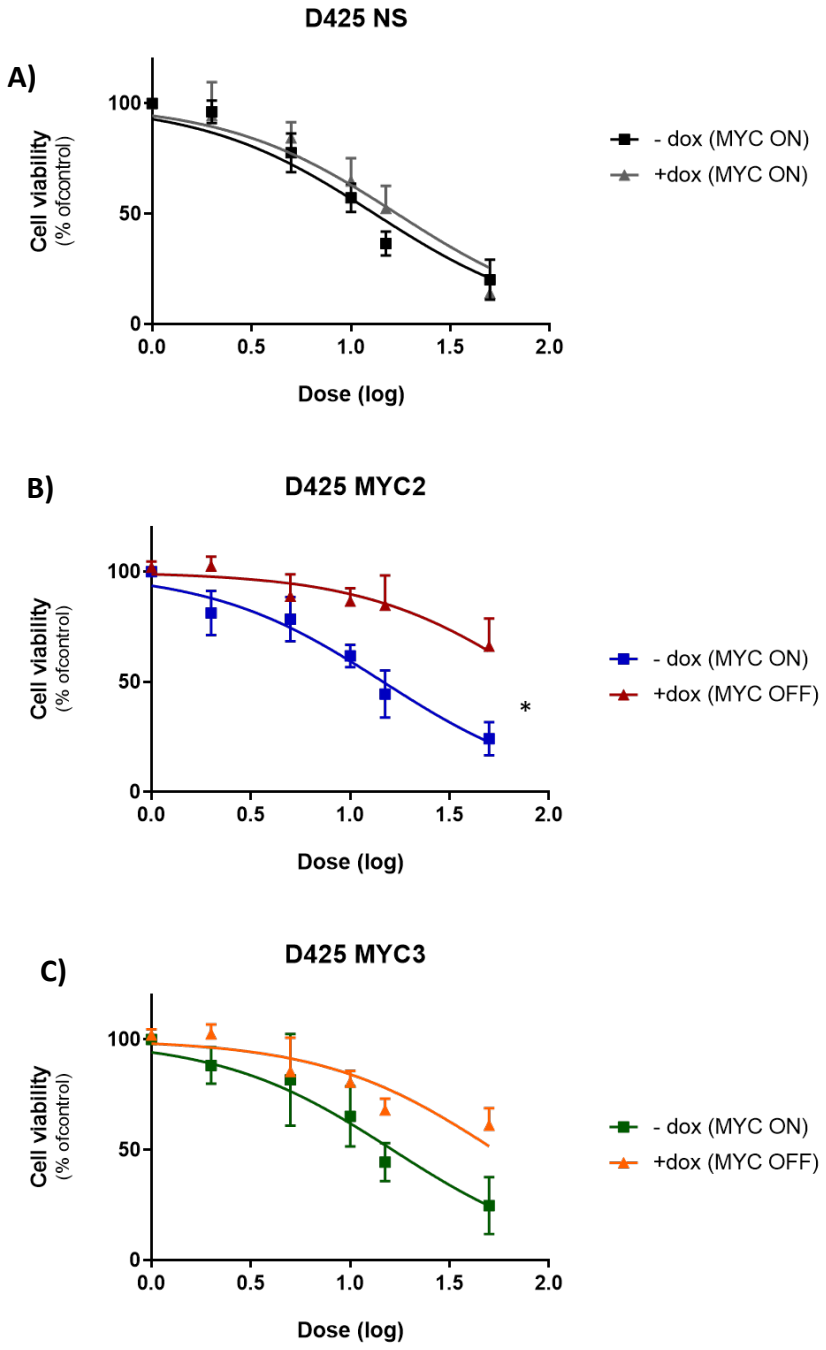

Figure 3.12. Radiation sensitivity of D425 NS, MYC2 and MYC3 cells. Dose-response curves of D425 NS, MCY2 and MYC3 cells response to single doses of ionising radiation (2, 5, 10, 15, 50Gy) after 72h post-treatment. A) Dose response curve of D425 NS in the absence (-dox; MYC ON) and presence (+dox; MYC OFF) of DOX. No differences in cell viability were seen after IR treatment when treated with and without DOX. B) Dose response curve of D425 MYC2 in the absence (-dox; MYC ON) and presence (+dox; MYC OFF) of DOX. Cell viability of *MYC* overexpressing cells (-dox; MYC ON) was significantly reduced after IR treatment, compared to cells with *MYC* knockdown (+dox; MYC OFF). C) Dose response curve of D425 MYC3 in the absence (-dox; MYC ON) and presence (+dox; MYC OFF) of DOX. Expression of high levels of *MYC* caused a decrease in cell viability after IR treatment compared to cells with *MYC* knockdown (+dox; MYC OFF), did not reach statistical significance. Curves are presented as log(concentration) vs response. Data is shown as percentage of the mean (±SEM) of three independent experiments. Statistical significance determined by paired students t-test (*$p \leq 0.05$).

3.8 Discussion

To study the role of *MYC* within MB_{Group3}, the Paediatric Brain Tumour Group generated three isogenic cell lines in which *MYC* expression can be directly regulated with the expression of shRNA. The use of *MYC*-regulable MB_{Group3} cell lines could give better insight on the direct role of *MYC* in MB_{Group3} biology and to enable the identification of targetable genetic pathways cooperating with *MYC* to promote tumorigenesis for the development of new therapeutic approaches.

Since the project is based on the inducible knockdown of *MYC* in MB_{Group3} cell lines, this chapter establishes and validates the *MYC*-dependent phenotypes of these *MYC*-regulable models. Automated Western blot analysis was performed to validate the induction of *MYC* knockdown in cells exposed to DOX, which showed the expected effective *MYC* knockdown at 72 hours and its prolonged effect at longer time exposures. Reproducibility of *MYC* knockdown was seen across all cell lines; D425, D283 and HDMB03. Knockdown of *MYC* at the protein level was also observed and validated at the mRNA level.

To assess the proliferative consequences of knocking down *MYC* by shRNA, and determine if the cell lines retained their addiction to *MYC* and *MYC*-dependent phenotypes, cell growth of D425, D283 and HDMB03 cell lines following reduction of *MYC* expression was studied. Knockdown of *MYC* caused a significant decrease in cells proliferation when compared to cells expressing *MYC*, and a decrease in apoptotic markers. Results concur with previous studies showing the involvement of *MYC* in cell proliferation and *MYC*-dependency of *MYC*-amplified MB (Felsher, 2010, Swartling et al., 2010).

MYC is a master regulator of key components of cell cycle progression, controlling proliferation and apoptosis. *MYC* is one of the most robust agents regulating programmed cell death through various mechanisms. *MYC* causes genome instability that triggers a signalling cascade that culminates in the expression of pro-apoptotic genes such as *BAX, PUMA* and *NOXA* (Luoto et al., 2010, Vousden and Lane, 2007).

MYC addicted cells present a rapid cell turnover, which consequently have higher rates of cell death when compared to those having *MYC* knockdown. The higher doubling time of cells expressing high levels of *MYC* could explain the increase in apoptotic markers seen in MB_{Group3} cell lines at 72h. Under normal circumstances, MB_{Group3} cells grow rapidly and after a few days in culture, the increased cell confluence affects cells ability to grow and the apoptotic response is triggered to limit unchecked cell growth. These results coincide with historical findings of cells presenting both a high mitotic index and a significant fraction of apoptotic cells (Topham and Taylor, 2013, McMahon, 2014). 72-96h after *MYC* knockdown, cell growth starts to slow down and plateau, associated with G_0/G_1 arrest and reduced apoptosis.

Reduction of *MYC* expression levels could be inhibiting *MYC*-induced apoptosis by arresting cell growth at G_1 phase of the cell cycle, suggesting that cells are entering a senescent phase instead of going to an apoptotic state. Alongside arrest at G_1 phase of the cell cycle upon *MYC* knockdown, previous studies on the cell lines have shown an increase in the expression of the gene Cyclin Dependent Kinase Inhibitor 1A (*CDKN1A*)(Dr. Swartz, PhD thesis). The protein encoded by *CDKN1A*, p21, binds and inhibits CDKs blocking cell cycle progression. Inhibition of the gene encoding for this particular protein has been found to be frequently supressed in *MYCN* amplified tumours like Neuroblastoma (Westermann et al., 2008, Ryl et al., 2017).

Results presented coincide with a preceding study done on MB_{Group3} cell lines, where *MYC* knockdown by siRNA resulted in inhibition of cell proliferation and reduction of apoptosis (von Bueren et al., 2009). Moreover, in conformance with the literature, these results indicate that reduction in *MYC* expression levels results in a G_1 cell cycle arrest, leaving cells in a metabolically activate state but without being actively growing (Florea et al., 2013, Schorl and Sedivy, 2003, Garcia-Gutierrez et al., 2019, Ćwiek et al., 2015).

As mentioned before, *MYC* has the ability to control both proliferation and apoptosis. Under cellular stress, such as exposure to radiation, apoptosis can be induced by *MYC* deregulation. The important implication of radiation in MB therapy has led several studies to investigate how *MYC* alters cells response to radiation in *MYC*-driven cancers (Bucci et al., 2005, von Bueren et al., 2009, von Bueren et al., 2011, Rieken et al., 2015).

To further investigate the models, cells were treated with radiation to simulate treatment of MB_{Group3} patients. A decrease in radiation-sensitivity was seen upon *MYC* knockdown, in comparison to D425 with higher levels of *MYC*. The findings are supported by studies showing that *MYC* is necessary for damaged-induced apoptosis. *MYC* triggers replication stress and

increased genomic instability, sensitising cancer cells overexpressing *MYC* to radiation (Dobbelstein and Sorensen, 2015, Taylor et al., 1997).

MBs are strikingly sensitive to DNA-damaging therapies. Higher levels of *MYC* expression have been found to sensitise MB cell lines to radiation treatment (von Bueren et al., 2011). But highly aggressive MB tumours, like Group 3 and SHHα, are associated with therapeutic failure and short patient survival, which often present with combined *TP53*-*MYC* defects.

MYC and *TP53* modulate each other's activity, since they are involved in many of the same cellular processes, therefore affecting similar targets. Loss of p53 function prevents the transcriptional repression of *MYC*, which potentiates *MYC*-induced oncogenesis by decreasing tumour cell apoptosis and increasing cells proliferative rate (Ho et al., 2005). This could explain the faster growth of D425 cell line (*TP53* mutant) in comparison to D283 and HDMB03 growth (*TP53* wild type).

It is important to consider the mutational status of *TP53* of our cell models when conducting experiments. The ability of p53 to promote apoptosis and cell cycle arrest is of extreme importance for its tumour suppression function. A halt of cell proliferation to allow time for the repair of damaged DNA is fundamental to avoid increased mutational load and genomic instability (Crowther et al., 2016). Studies on MB have shown that p53 function in triggering the apoptotic pathway is essential for treatment effectiveness, which could be the reason why patients with combined *MYC*-*TP53* alterations respond poorly to treatment, since loss of p53 has been seen to result in a reduction of treatment-induced apoptosis in medulloblastoma cell lines (Rausch et al., 2012, Ivanov et al., 2016). In this regard, D425's response to radiotherapy might differ from the D283 and HDMB03 response (both have functional *TP53*). Sensitivity to irradiation should be studied in the other cell lines to better understand the interplay of *MYC* and *TP53* in response to current therapeutic regimens. Moreover, the role of the tumour suppressor gene *TP53* and the burden of its mutational status should be taken into consideration when performing future experiments testing small molecule inhibitors, as cells sensitivity might differ.

Through the establishment of the knockdown system in our models, we have established that downregulation of *MYC* expression triggers cell cycle arrest at G_0/G_1 over apoptosis. A possible explanation why *MYC*-dependent tumours are nonresponsive to treatment could be that decreased *MYC* expression in *MYC*-dependent MB_{Group3} tumours leads to the production of

quiescent cells with the ability to survive the aggressive nature of MB treatment (radiation and DNA-damaging agents), re-emerging again after its administration. Therefore, it is pivotal that therapeutic strategies targeting this subgroup of tumours aim at molecular dependencies that sensitise *MYC*-overexpressing cells to the induction of apoptosis, rather than solely downregulating *MYC* expression.

Taken together, the *MYC* knockdown effect on cell proliferation further reinforces the notion of the reliance of MB_{Group3} on *MYC* to sustain rapid cell turnover for tumour growth and the reality of *MYC* oncogenic addiction in MB_{Group3} (Swartling et al., 2010).

Despite seeing consistent effects in achieving *MYC* knockdown at the protein and mRNA level, MYC2 construct achieved better knockdown on *MYC* expression across cell lines when compared to the one achieved with MYC3 construct. This could be due to differences in the targeted position within the third exon of *MYC* of both constructs. Efficiency of MYC3 constructs ability to achieve *MYC* knockdown could partially mask *MYC*-dependent effects, so should be taken into consideration when analysing results of future experiments.

Sensitisation of *MYC*-overexpressing MB_{Group3} cells to ionising radiation further exemplifies the appropriateness of using the newly generated *MYC*-regulable cell lines as models to study *MYC's* dependent biology and therapeutic response in MB_{Group3}.

3.9 Appendix

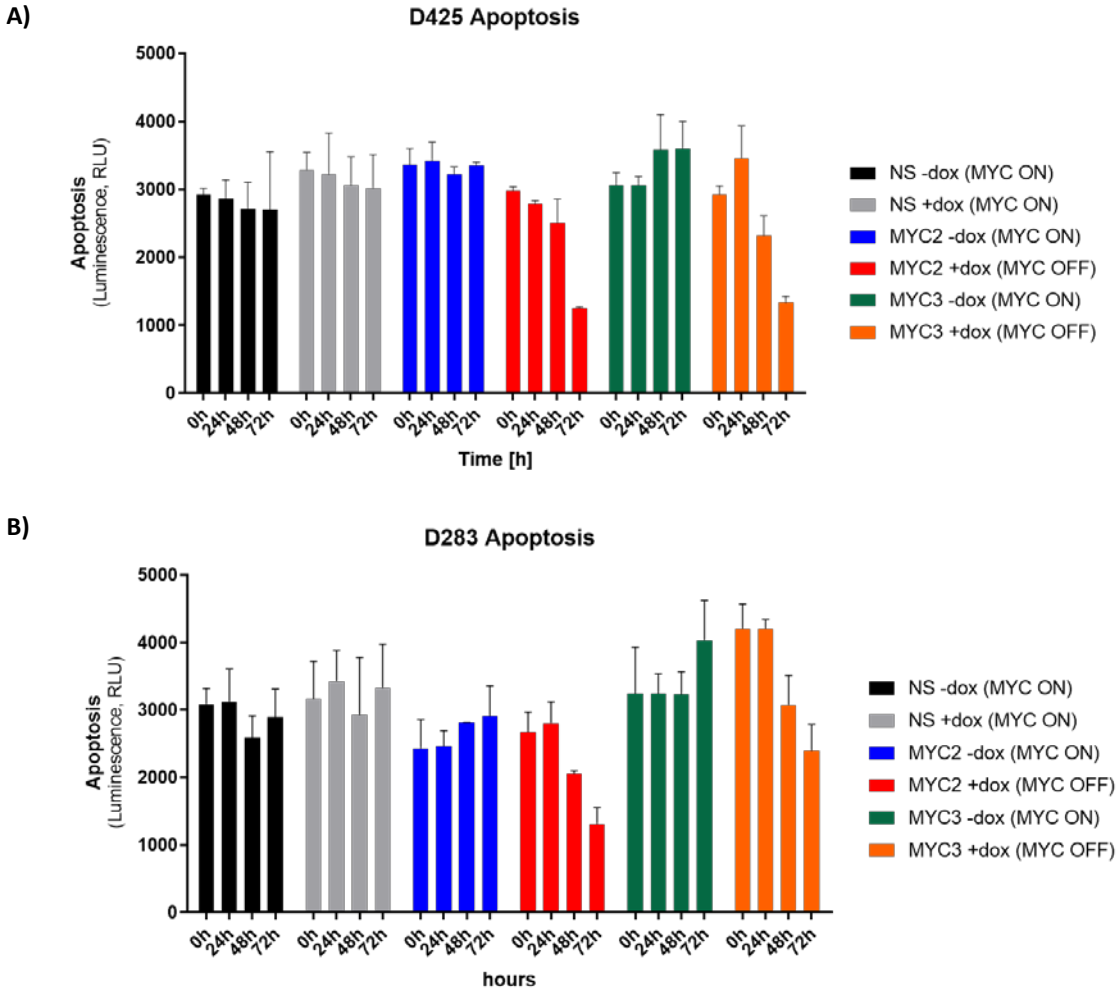

Appendix 3.1. Effect of *MYC* knockdown on apoptosis in MB_{Group3} cell lines. Time dependent effect of *MYC* knockdown on caspase 3/7 activity in two MB cell lines A) D425 and B) D283. *MYC* knockdown caused a decrease in apoptotic markers. In the presence of high levels of *MYC*, levels of caspase 3/7 increase throughout time. The results are shown as means ± SEM of three individual experiments, values expressed as luminescence unit (RLU) Significance determined by unpaired students t-test (*$p \leq 0.05$).

Chapter 4. *MYC*-targeting strategies in Group 3 medulloblastoma

4.1 Introduction

Overexpression and amplification of *MYC* family genes is commonly observed in MB, with each subgroup having different expression levels of *c-MYC* and *N-MYC* (Chapter 1). MB_{Group3} is characterised by *MYC* amplifications (~17%) and overexpression, which is linked to aggressive biological behaviour and reduced patient survival (Jones et al., 2012). *MYC* offers an ideal therapeutic target for this specific subgroup of tumours, to help improve survival rates. Despite numerous attempts over recent decades to develop drugs targeting *MYC* directly, none have yet been developed clinically. Efforts have been directed at therapeutic strategies targeting *MYC* indirectly, by compromising its transcription, translation, protein stability and its dependence on downstream pathways (Chapter 1)(Shalaby and Grotzer, 2016, Chen et al., 2018b).

4.1.1 Targeting MYC mRNA translation through the PI3K/Akt/mTOR signalling pathway

The phosphoinositide-3-kinase (PI3K)/Akt signalling pathway is one of the most important intracellular signalling cascades for cell regulation, as it controls survival, growth, metabolism, motility and cellular angiogenesis (Porta et al., 2014). This signalling cascade is aberrantly altered in various cancers, including MB. Independent of subgroup type, numerous alterations involving the PI3K/AKT signalling have been reported in MB, which is fundamental for its proliferation, maintenance and metastasis (Baryawno et al., 2010, Hartmann et al., 2006, Eckerdt et al., 2019). Genetic and epigenetic abnormalities affecting components of this signalling pathway are frequent events in cancer; including copy number gain and amplification of growth factor receptors (*EGFR*), or loss-of-function mutations of the *PTEN* tumour suppressor gene (Chalhoub and Baker, 2009). These alterations lead to aberrant activation of the pathway, which is correlated with high-risk subgroups and tumour resistance, making it a good candidate for new therapeutic approaches (Blom et al., 2010, Rogers et al., 2017).

As *MYC* is considered directly undruggable, interfering with the phosphorylation and activation of appropriate kinases within the PI3K/mTOR pathway to affect MYC protein stability has been exploited as an alternative strategy. Several mTOR/PI3K inhibitors used in neuroblastoma murine models have been shown to successfully destabilise MYCN (Cage et al., 2015). Inhibition of PI3K has been shown to promote apoptosis and morphological changes in DAOY MB cell lines (Frasson et al., 2015). Its inhibition, in combination with inhibition of hedgehog (HH), increased sensitivity of *MYC*-driven MB_{Group3} cell lines to cisplatin treatment (Aldaregia et al., 2018, Chaturvedi et al., 2018).

Additionally, gene expression profiling of our inducible isogenic models of *MYC*-driven MB_{Group3} before and after *MYC* silencing was used to identify differences in gene networks and pathways following *MYC* silencing. RNAseq results and subsequent analysis revealed that *MYC* knockdown caused the downregulation of genes involved in cell cycle progression at G_2/M phase and mTORC1 signalling pathway (Figure 4.1)(Dr. Swartz, PhD thesis).

The assessment of mTOR inhibition in a *MYC*-dependent manner using the *MYC*-regulable isogenic cell lines will allow us to investigate the relationship between mTOR and *MYC*, and the potential of using inhibitors targeting components of the PI3K signalling pathway to therapeutically exploit the *MYC*-dependency of MB_{Group3}.

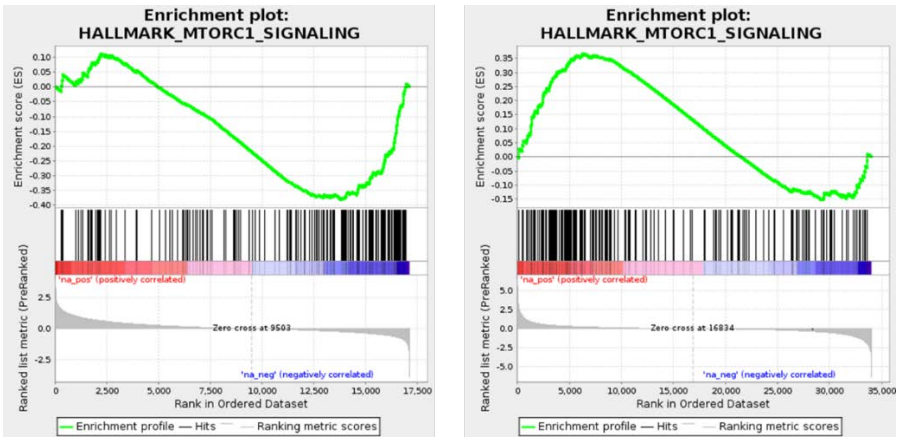

Figure 4.1. GSEA enrichment plot of mTORC1 signalling upon MYC knockdown.GSEA enrichment plot of MTORC1 signalling, showing a negatively enriched plot in MYC knockdown (A) and positively enriched in MB_{Group3} primary tumours (B). The enrichment score (ES) indicates the extent of which a gene is represented within the ranked gene list. The leading edge subsets indicates genes that contribute most to the enrichment score within the gene set, and is represented by the vertical lines. The ranked list metric shows the value of the ranking metric moving down the list of ranked genes, going from positive to negative. Data kindly provided by Dr.Shanel Swartz (PBTG)..

4.1.2 Targeting MYC *transcription through* BRD4 *inhibition*

Bromodomain (BRD) proteins are epigenetic modifiers that exclusively recognise and interact with histone acetylation motifs enabling the assembly of chromatin complexes and transcriptional activators at specific promoter sites of genes (Donati et al., 2018). As explained in Chapter 1, BRD4 regulates *MYC* transcription through interaction with the heterodimers MYC/MAX and recruitment of P-TEFb on *MYC* enhancer and superenhancer regions to promote transcriptional activation (Rahl and Young, 2014, Fowler et al., 2011, Levens, 2008, Yang et al., 2005).

Inhibition of the BET bromodomain by JQ1 has been proven to greatly diminish *MYC* expression and downregulate *MYC*/*MYCN*-associated transcriptional activity in several cancers. Various studies have used this strategy in *MYC*-driven cancers like MB and NB, where not only a decrease in the expression of *MYC*-associated proteins was observed, but treatment with JQ1 also significantly reduced cell proliferation, inducing apoptosis and senescence (Henssen et al., 2013, Bandopadhayay et al., 2014, Puissant et al., 2013, Venkataraman et al., 2014, Delmore et al., 2011).

With the aim to explore the potential therapeutic effect of targeting *MYC* transcription in a MB_{Group3} subgroup and *MYC*-dependent context, JQ1 was used on our isogenic models to assess the possibility of *MYC* downregulation through BET inhibition. Assessment of the effect of *MYC* modulation will enable the comparison to the effect inhibiting BRD4 has on *MYC* expression in MB_{Group3} cells, to assess this strategy as a therapeutic opportunity for *MYC*-driven medulloblastomas.

4.1.3 Targeting MYC transcription through CDK9 *inhibition*

In recent years, the use of gene silencing techniques has enabled the identification of components of the *MYC*-interactome, and the targeting of those pathways have emerged as an alternative therapeutic strategy to target *MYC*-oncogenic-signalling (Cermelli et al., 2014). *CDK9* has been found in several studies of different cancers as a key component for *MYC* expression, and its targeting opens a new therapeutic window to affect cells capabilities of proliferation and survival (Ma et al., 2019, Wang et al., 2019b, Kinoshita et al., 2018, Li et al., 2019, Wang et al., 2019c).

As previously stated, CDK9 is the catalytic subunit of the P-TEFb complex, which is essential to control the expression of *MYC*. Upon phosphorylation, CDK9 becomes active and phosphorylates the C-terminal domain of RNA Pol II, a hallmark of transcriptional pause-release and transcriptional elongation of most protein coding genes (Rahl and Young, 2014). Inability of CDK9 to phosphorylate RNA Pol II blocks transcriptional elongation, supressing the transcription of genes related to cell cycle and the synthesis of anti-apoptotic proteins (including MCL1), thereby sensitising cancerous cells to apoptotic stimuli. Overall, BRD4 recruitment of P-TEFb in the *MYC* promoter region is key for allowing transcription and concomitant *MYC*-effector genes (Wang et al., 2019c, Lu et al., 2015, Wang and Fischer, 2008).

CYC065 is a highly selective second-generation inhibitor of CDK2 and CDK9, with oral and intravenous availability. Mechanistically, CYC065 binds to cyclins 2 and 9 preventing the occurrence of their dependent cell cycle regulation and gene transcription mechanisms. CDK9/2 inhibition leads to apoptosis induction through the downregulation of genes involved in DNA repair and survival pathways (Saladino et al., 2015, Chen et al., 2018c). CDK9 inhibition by CYC065 successfully downregulated *MYCN* expression and caused tumour regression in NB cell models and xenografts (Poon et al., Childhood Cancer Meeting 2016, Abs. 1-19).

The sensitivity of the compound displayed in cell models of other *MYC*-driven tumours highlights the therapeutic potential of CYC065 in downregulating *c-MYC* expression in *MYC*-dependent MB_{Group3}.

4.2 Aims

The use of the regulable D425, D283 and HDMB03 cell lines, developed and validated in Chapter 2, provides the opportunity to study the effects of *MYC* overexpression in MB_{Group3} and its potential for therapeutic targeting.

The aim of this Chapter is to investigate the role of *MYC* amplification or gain in drug resistance and sensitivity in MB_{Group3} using the *MYC*-regulable isogenic cell lines. The potential of pharmacologically manipulating *MYC*-dependent signalling pathways to treat high-risk patients with MB_{Group3} will be assessed by undertaking two indirect pharmacological anti-*MYC* strategies (targeting *MYC* transcription through BRD4 and CDK9 inhibition, and *MYC* mRNA translation through mTOR inhibition). Candidate drugs targeting signalling pathways associated with *MYC* will be assessed in a *MYC*-dependent manner to investigate the therapeutic potential of exploiting the *MYC*-dependency of MB_{Group3} tumours as a therapeutic strategy to treat *MYC*-driven cancers.

Results from this Chapter will prove the specific *MYC*-downregulatory effect of mTOR, BRD4 and CDK9, previously shown to downregulate *MYC* transcriptional signature in other *MYC*-driven cancers, and undercover its potential use in combinatorial approaches for patients in this specific MB subgroup.

.

4.3 Targeting *MYC* translation

4.3.1 Effect of mTOR inhibition on cell viability in MB_{Group3} cell lines

Several studies have already reported the connection between the mTOR signalling pathway and *MYC* driven cancers. From previous studies, our group has RNAseq data available for all isogenic cell lines with *MYC* modulated by shRNA, and primary MB tumour expression data from samples of known subgroups and known *MYC* status. mTOR signalling pathway was shown to be downregulated by *MYC*, when expression data of primary tumours was compared to the RNAseq data of isogenic cell lines with *MYC* knockdown.

To further explore the interplay between MYC protein regulation and the PI3K signalling pathway in context of MB_{Group3}, two small molecule compounds, INK128 (Sapanisertib) and AZD2014 (Vistusertib), that act as ATP-competitive inhibitors of mTOR were used on the isogenic models. Both drugs are potent selective mTORC1/2 inhibitors which act in an ATP-dependent manner, and are highly selective toward several isoforms of PI3K.

Only the D425 isogenic cell line was used in preliminary experimentation to examine if the inhibitors had an effect on *MYC* expression. Growth-inhibitory assays were performed in order to determine the dose of drug required to give half-maximal response (IC_{50}) over 72h. D425 NS, D425 MYC2 and D425 MYC3 were treated with a 10-fold dilution series of these drugs for 72h, and cell viability was measured with CellTiter-Glo (CTG) at 72h, as explained in Chapter 2. Values obtained were analysed with Prism8.

In the presence of high levels of *MYC* expression, D425 MYC2 and D425 MYC3 presented a similar cellular sensitivity to INK128 when compared to the non-silencing control. Significant differences in growth inhibition were seen when *MYC* was knocked down, where D425 MYC2 and D425 MYC3 appeared to be less sensitive to INK128 (Students t-test, p=0.0005; p=0.03, respectively)(Figure 4.2).

Similarly, in the presence of high levels of *MYC* expression, cells bearing both MYC2 and MYC3 constructs presented a similar response to AZD2014 when compared to the NS control. Cell sensitivity to the inhibitor changed when *MYC* was knocked down in the presence of DOX, where MYC2 and MYC3 cell lines displayed decreased sensitivity to the drug (Figure 4.3). The inhibitor caused greater growth-inhibitory effect in the presence of high levels of *MYC* compared to the knockdown state, only reaching statistical significance in D425 MYC2, not MYC3 (p=0.035, p=0.104, respectively).

A)

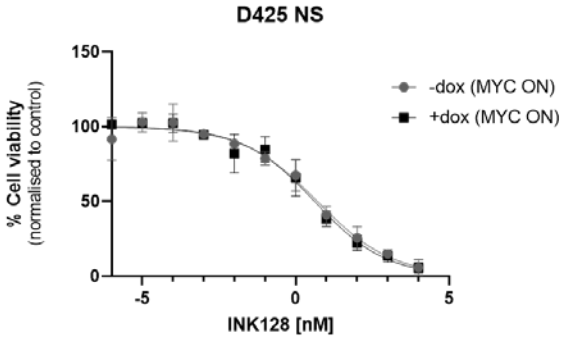

B)

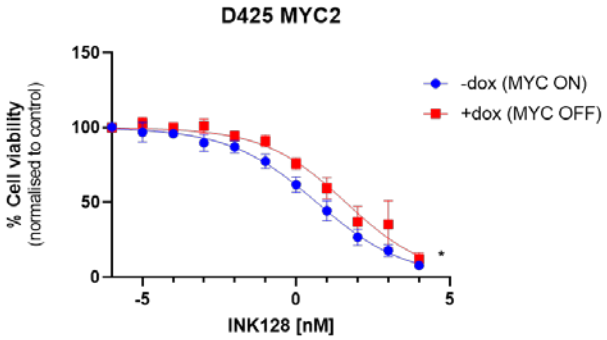

C)

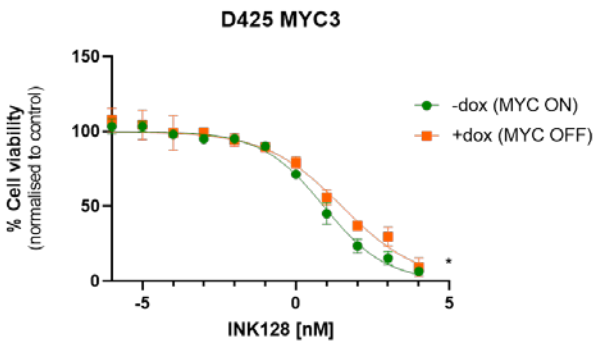

D)

D425

	INK128					
	NS -dox (MYC ON)	**NS +dox** (MYC ON)	**MYC2 -dox** (MYC ON)	**MYC2 +dox** (MYC OFF)	**MYC3 -dox** (MYC ON)	**MYC3 +dox** (MYC OFF)
IC50 (nM)	5.078	4.130	4.687	41.24	8.075	31.26
P value	0.2243		0.0055		0.0313	
SD of log(ratios)	0.03097		0.08919		0.09816	
SEM of log(ratios)	0.009338		0.02689		0.02960	

Figure 4.2. Growth-inhibitory curves of D425 in response to the mTOR inhibitor INK128. Growth-inhibitory curves of A)D425 NS, B)D425 MYC2 and C)D425 MYC3 isogenic MB_{Group3} cells treated with the mTOR inhibitor INK128. Cells were cultured in the presence (+dox; MYC OFF) and absence (-dox; MYC ON) of doxycycline for *MYC* knockdown. Values are shown as percentage of cell viability in three independent experiments relative to untreated cells, along with the fitting curve. The curve is presented as log(concentration) vs response. The growth inhibitory effect of the drug on *MYC*-overexpressing cell lines versus MYC knockdown was compared by paired student's t-test (statistical significance denoted by *; *p<0.05). D)Table summarising the half maximal inhibitory concentration (IC50) calculated from dose response curves. Significant differences between cells expressing high (-dox: MYC ON) and low (+dox: MYC OFF) levels of *MYC* was calculated with a ratio paired student's t-test (p-value). *P*-value is shown with the SD and SEM.

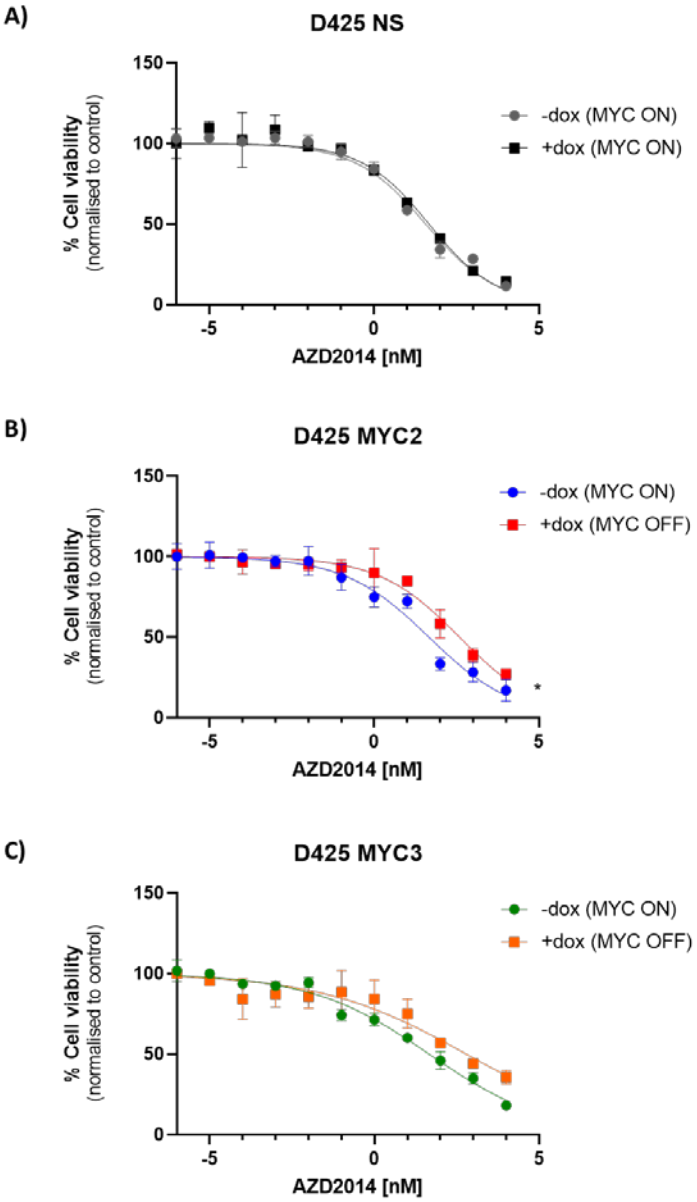

D)

D425

	AZD2014					
	NS -dox (MYC ON)	**NS +dox** (MYC ON)	**MYC2 -dox** (MYC ON)	**MYC2 +dox** (MYC OFF)	**MYC3 -dox** (MYC ON)	**MYC3 +dox** (MYC OFF)
IC50 (nM)	37.17	46.65	45.83	388.9	46.05	623.2
P value	0.6041		0.0354		0.1044	
SD of log(ratios)	0.05820		0.09115		0.09870	
SEM of log(ratios)	0.01755		0.02748		0.02976	

Figure 4.3. Growth-inhibitory curves of D425 to the mTOR inhibitor AZD2014. Growth-inhibitory curves of A)D425 NS, B)D425 MYC2 and C)D425 MYC3 isogenic MB_{Group3} cells treated with the mTOR inhibitor AZD2014. Cells were cultured in the presence (+dox; MYC OFF) and absence (-dox; MYC ON) of doxycycline for *MYC* knockdown. Values are shown as percentage of cell viability in three independent experiments relative to untreated cells, along with the fitting curve. The curve is presented as log(concentration) vs response. The growth inhibitory effect of the drug on *MYC*-overexpressing cell lines versus *MYC* knockdown was compared by paired student's t-test (statistical significance denoted by *; *p<0.05). D)Table summarising the half maximal inhibitory concentration (IC_{50}) calculated from the dose response curves. Significant differences between cells expressing high (-dox: MYC ON) and low (+dox: MYC OFF) levels of *MYC* was calculated with a ratio paired student's t-test (p-value). P-value is shown with the SD and SEM.

To validate the IC_{50}, D425 was exposed for 72h to 10 and 50nM of each drug to study its effect on cell viability. To compare the effect of the inhibitors on cell viability, cells which were not exposed to these compounds were used as controls. Cells bearing the NS construct were used as internal control to account for changes due to the shRNA constructs, and DOX-treated to normalise the effect of DOX on the cell line. As expected, no significant differences were seen in cell proliferation between D425 cells cloned with the NS, MYC2 and MYC3 shRNA constructs under normal growth conditions (*MYC* expressing)(Figure 4.4, A).

D425 exhibited a high sensitivity to mTOR inhibition by INK128. In the presence of high levels of *MYC* (*MYC* expression levels established in Chapter 3), D425 MYC2 and MYC3 exhibited a significant decrease in cell proliferation when exposed to 10nM of INK128 (p<0.0001 for both constructs) when compared to the untreated control. Further reduction in cell viability was observed when dosed with 50nM when compared to the un-treated controls. Following *MYC* knockdown, exposure to 10nM and 50nM of INK128 further reduced D425 NS, D425 MYC2 and D425 MYC3 cell viability although it was not as clear compared to *MYC*-overexpressing cells (Figure 4.4, B and C).

The same effect on D425 cell viability was observed when treated with AZD2014 (Figure 4.5). In this case, D425 MYC2 and D425 MYC3 cells with MYC knockdown showed no significant differences in cell viability when treated with 10nM and 50nM of the inhibitor when compared to the untreated control. Only cells overexpressing *MYC* showed a statistically significant decrease in cell viability upon treatment. *MYC* knockdown caused increased resistance to inhibition of mTOR.

In summary, mTOR inhibition by INK128 and AZD2014 had a *MYC*-dependent drug-sensitivity effect on D425. Inhibition of mTOR resulted in differential drug sensitivity between *MYC*-overexpressing and *MYC*-knockdown cell lines, where higher levels of *MYC* sensitised the cells to these compounds.

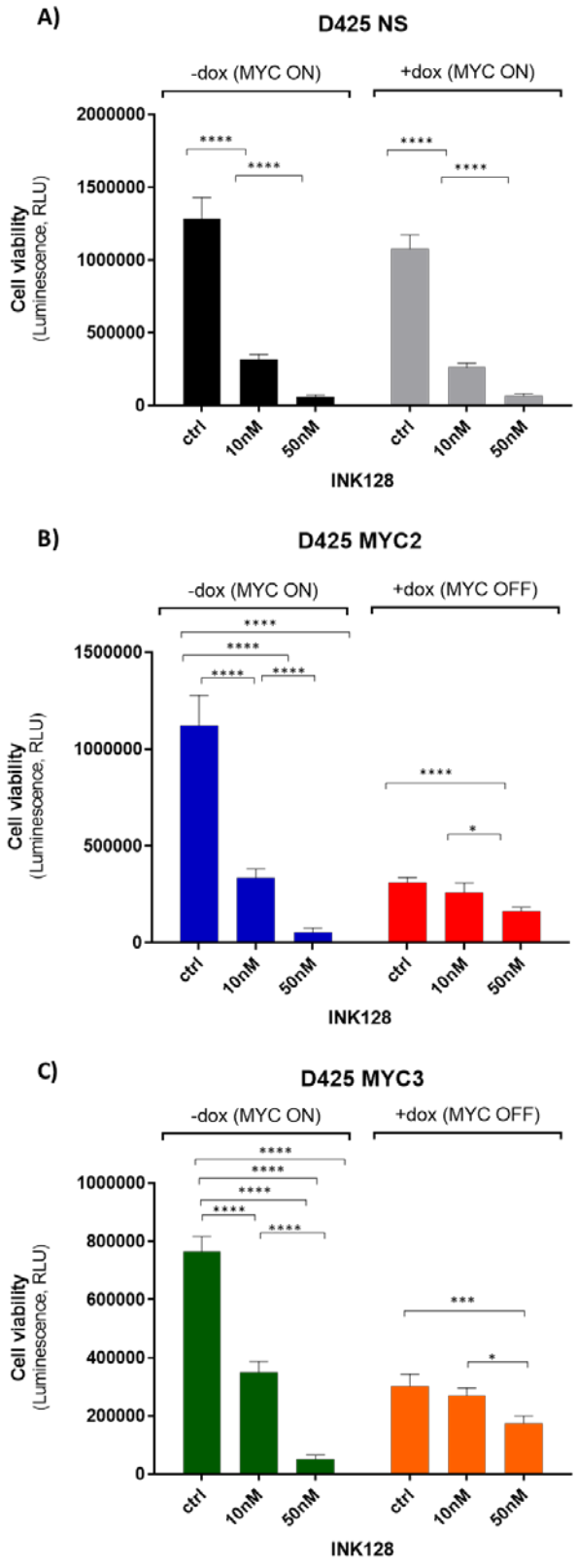

Figure 4.4.D425 viability in response to AZD2014 inhibitor. Graphs show INK128 effect on viability of A)D425 NS, B)D425 MYC2 and C)D425 MYC3, in the presence (-dox; MYC ON) and absence (+dox; MYC OFF) of high levels of *MYC* expression. Cells were exposed to 10nM and 50nM of mTOR inhibitor. Data is shown as means (±SEM) of three independent experiments. Statistical significance determined by students t-test (statistical significance denoted by *; *$p \leq 0.05$; ***$p \leq 0.001$; ****$p \leq 0.0001$).

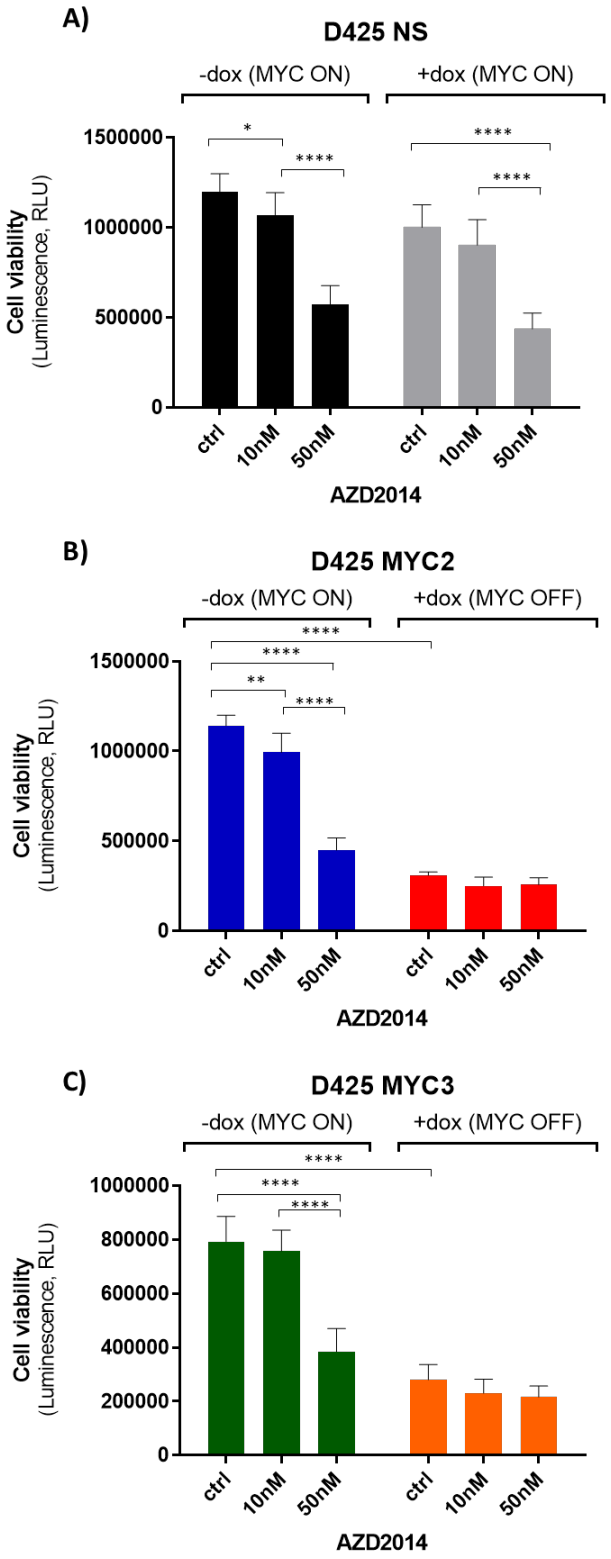

Figure 4.5. D425 viability in response to AZD2014 inhibitor. Graphs show AZD2014 effect on viability of A)D425 NS, B)D425 MYC2 and C)D425 MYC3, in the presence (-dox; MYC ON) and absence (+dox; MYC OFF) of high levels of *MYC* expression. Cells were exposed to 10nM and 50nM of the mTOR inhibitor. Data is shown as means (±SEM) of three independent experiments. Statistical significance determined by students t-test (statistical significance denoted by *; *$p \leq 0.05$; ***$p \leq 0.001$; ****$p \leq 0.0001$).

4.3.2 Effect of AZD2014 and INK128 at the protein level

After testing the *MYC*-dependent growth-inhibitory effect of the inhibitors, the next objective was to examine if mTOR inhibition caused downregulation of MYC protein expression. To evaluate this effect at the protein level, considering the short half-life of MYC, cells were treated with 10nM of each inhibitor for 15, 30, 60 and 120min. After drug exposure, cells were harvested and protein was extracted to perform a simple western assay (Wes; ProteinSimple) for protein quantification, as explained in Chapter 2.

Despite exhibiting a growth-inhibitory *MYC*-dependent effect, none of the drugs had a direct downregulatory effect on MYC protein levels (Figure 4.6 and 4.7). When quantified, MYC protein levels were increased after drug incubation. The use of mTOR inhibitors led to a slight reduction in MYC protein at early time points with a subsequent increase at later exposures, where a rapid upregulation of MYC protein was seen after only 1h.

An increase in MYC protein levels was seen with shorter exposures (15-30min) of both inhibitors following *MYC* knockdown. After 1 hour of drug exposure, protein levels of MYC were reduced on average by 22% in both D425 MYC2 and D425 MYC3 after treatment with INK128, when compared to the untreated control. Similarly a reduction of 35%, was observed in D425 MYC2 and D425 MYC3 when exposed to AZD2014 (Figure 4.7). Downregulation of MYC protein levels was only seen in cells with *MYC* knockdown and at later time points, which indicates a synergistic effect of the inhibitor with *MYC* knockdown.

Alongside the quantification of MYC protein levels, downstream effectors of the mTOR signalling pathway were analysed. INK128 caused a time-dependent decrease in phosphorylation of the kinase S6 at Ser2356/236, a direct downstream target of mTOR. This indicates that the inhibitor efficiently inhibited mTORC1, thus affecting the subsequent phosphorylation of the downstream effector, S6. The decrease in the phosphorylated form of S6 was not associated with *MYC* expression levels (not *MYC*-dependent).

Variable levels of PI3 kinase p110α (PI3K110α) protein were seen after treatment with 10nM of INK128 for all constructs and conditions, as seen in Figure 4.6. INK128 is supposed to inhibit the phosphorylation of PI3K110α, through the suppression of mTOR. The inconsistency in the levels of pPI3K110α across constructs was observed in two different biological repeats, which indicate that the concentration of inhibitor used for the experiment may not have been sufficient to inhibit its phosphorylation.

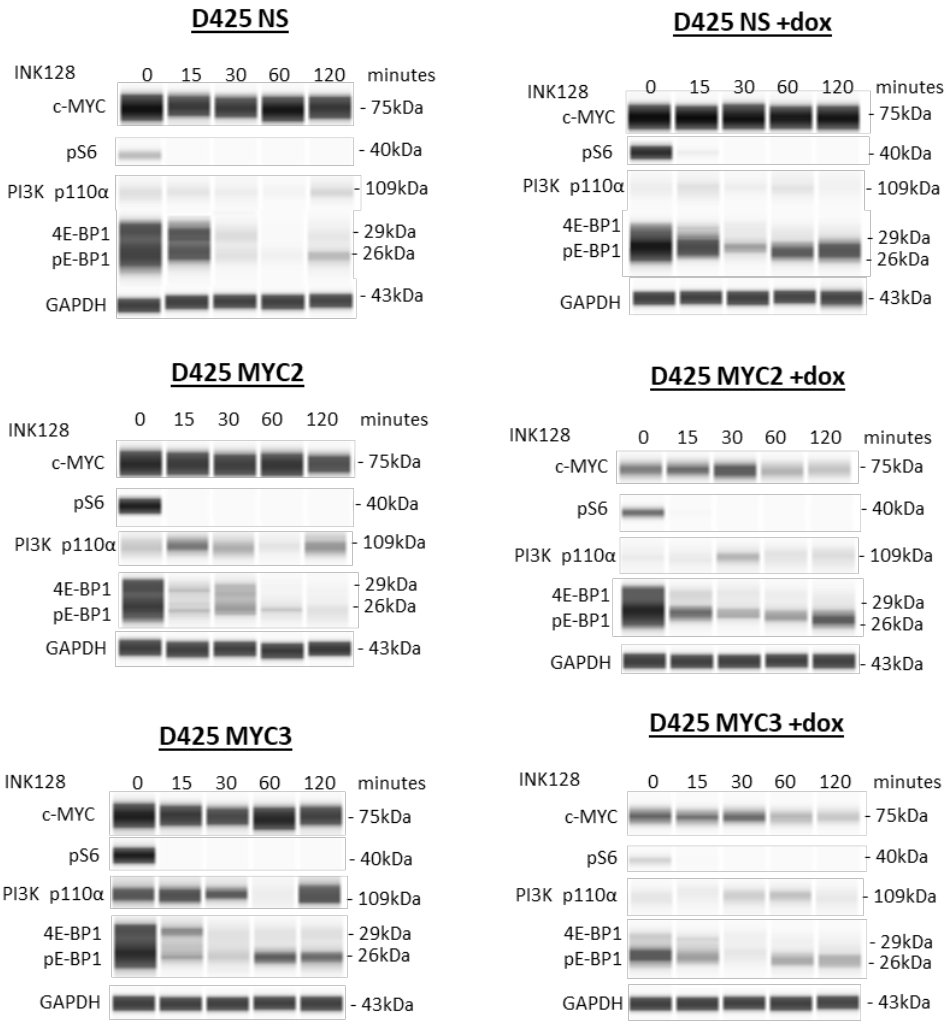

Figure 4.6. Effect of INK128 inhibitor at the protein level. Automated Western Blot (WES) analysis of c-MYC expression after treatment with INK128 inhibitor. D425 NS, MYC2 and D425 MYC3, with and without *MYC*-silencing by DOX (+), were treated with 10nM of the inhibitor for 15min, 30min, 60min and 120min. At each time point, MYC protein expression levels were examined alongside downstream effectors of the mTOR signalling pathway (pS6, PI3K p110α , p4E-BP1). Protein levels of GAPDH were used as internal control. The same effect of IN128 on downstream effectors of the mTOR signalling pathway was seen in two independent experiments.

The same time-dependent downregulation of pS6 across D425 constructs with and without *MYC* knockdown was also observed after exposure to AZD2014 in two biological repeats. A reduction in total protein levels of mTOR was seen at later time points following *MYC* knockdown (Figure 4.7). No change in total protein levels of mTOR was observed in D425 cells overexpressing *MYC*.

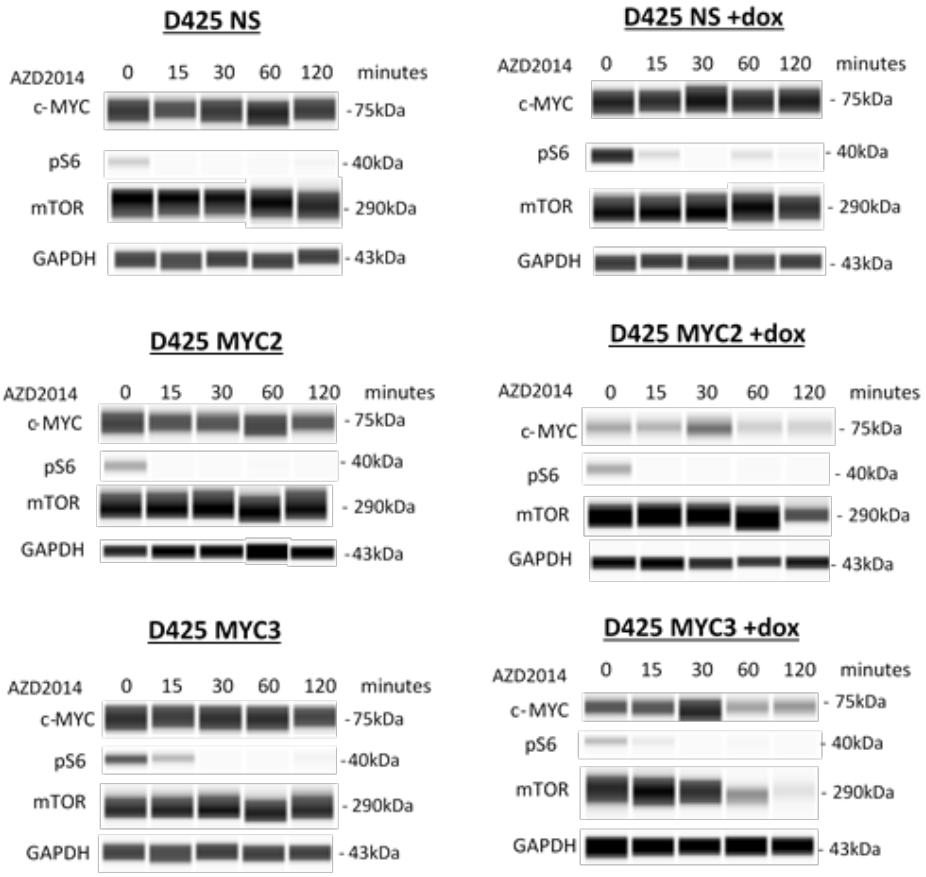

Figure 4.7. Effect of AZD2014 inhibitor at the protein level. Automated Western Blot (Wes) analysis of c-*MYC* expression after treatment with AZD2014 inhibitor. D425 NS, D425 MYC2 and D425 MYC3, with and without *MYC*-silencing by DOX (+), were treated with 10nM of the inhibitor for 15min, 30min, 60min and 120min. MYC protein expression levels were examined alongside downstream effectors of the mTOR signalling pathway (pS6, mTOR) at each time point. Protein levels of GAPDH were used as internal control.

In summary, mTOR inhibition with AZD2014 and INK128 had no clear effects on MYC protein expression. A slight reduction of MYC protein was observed at shorter exposure times (0-

30min) followed by an increase after incubation of over 1h was seen across D425 constructs. The same trend was seen using either AZD2014 or INK128. The opposite effect was seen when *MYC* was knocked down, where MYC protein levels increased during the first 30min of incubation and further increased at later time points.

Despite the slight additive effect of the inhibitors with *MYC* knockdown, further studies using these inhibitors were not pursued since no clear effects on MYC protein expression were observed. The main purpose of this study was to find a compound that had a clear effect on *MYC* expression which could be used as a therapeutic strategy to target *MYC*-driven MB_{Group3} tumours. Therefore, other targeting strategies were explored instead of attempting to elucidate the effect of mTOR signalling in controlling *MYC* translation in MB_{Group3} cell lines, discussed in the following section of this Chapter.

4.4 Targeting *MYC* transcription

4.4.1 BRD4 inhibition

4.4.1.1 Effect of BRD4 inhibition in MB_{Group3} cells viability

To explore the effect of BRD4 inhibition in MB_{Group3} cell lines, *MYC*-regulable D425 and D283 were chosen for analysis. The use of a *MYC* amplified and a *MYC* gained cell line (described in

Chapter 2 and 3) will enable a better understanding of the effect of JQ1 treatment in the presence of different levels of *MYC* expression in the context of MB_{Group3}.

Cells sensitivity to pharmacological inhibition of BRD4 with JQ1 was examined in growth inhibition studies. D425 and D283 isogenic cell lines induced with DOX prior to experimentation were treated with 10-fold dilutions of JQ1 for 72h (methodology described in Chapter 2). Cell viability after treatment was measured using CTG and resultant luminescence values analysed with Prism8 to generate a dose-response inhibition curve to calculate the IC_{50}.

Treatment with JQ1 caused a *MYC*-dependent growth-inhibitory effect on the D425 cell line (Figure 4.8). D425 NS, D425 MYC2 and D425 MYC3 cells overexpressing *MYC* exhibited higher sensitivity to the inhibitors when compared to cell lines with *MYC* knockdown. Exposure to JQ1 caused a significant reduction in D425 MYC2 and D425 MYC3 cells viability (p=0.01, p=0.02, respectively) when compared to their controls with reduced *MYC* expression. Summary table with IC_{50} values can be seen in Figure 4.8, G).

BRD4 inhibition by JQ1 selectively inhibited the growth of D283 cells expressing higher levels of *MYC* compared to those with *MYC* knockdown by shRNA. A significant reduction in D283 MYC2 and D283 MYC3 cell viability was observed when compared to their counterparts with *MYC* silenced (p=0.0049, p=0.0313, respectively)(Figure 4.8, A, B, C). Therefore, *MYC* knockdown caused a decrease in cell sensitivity to the JQ1.

No differences in growth inhibition were seen for the NS construct of cell lines, when grown in the presence and absence of DOX (D425 NS p=0.0685; D283 NS p=0.1773)

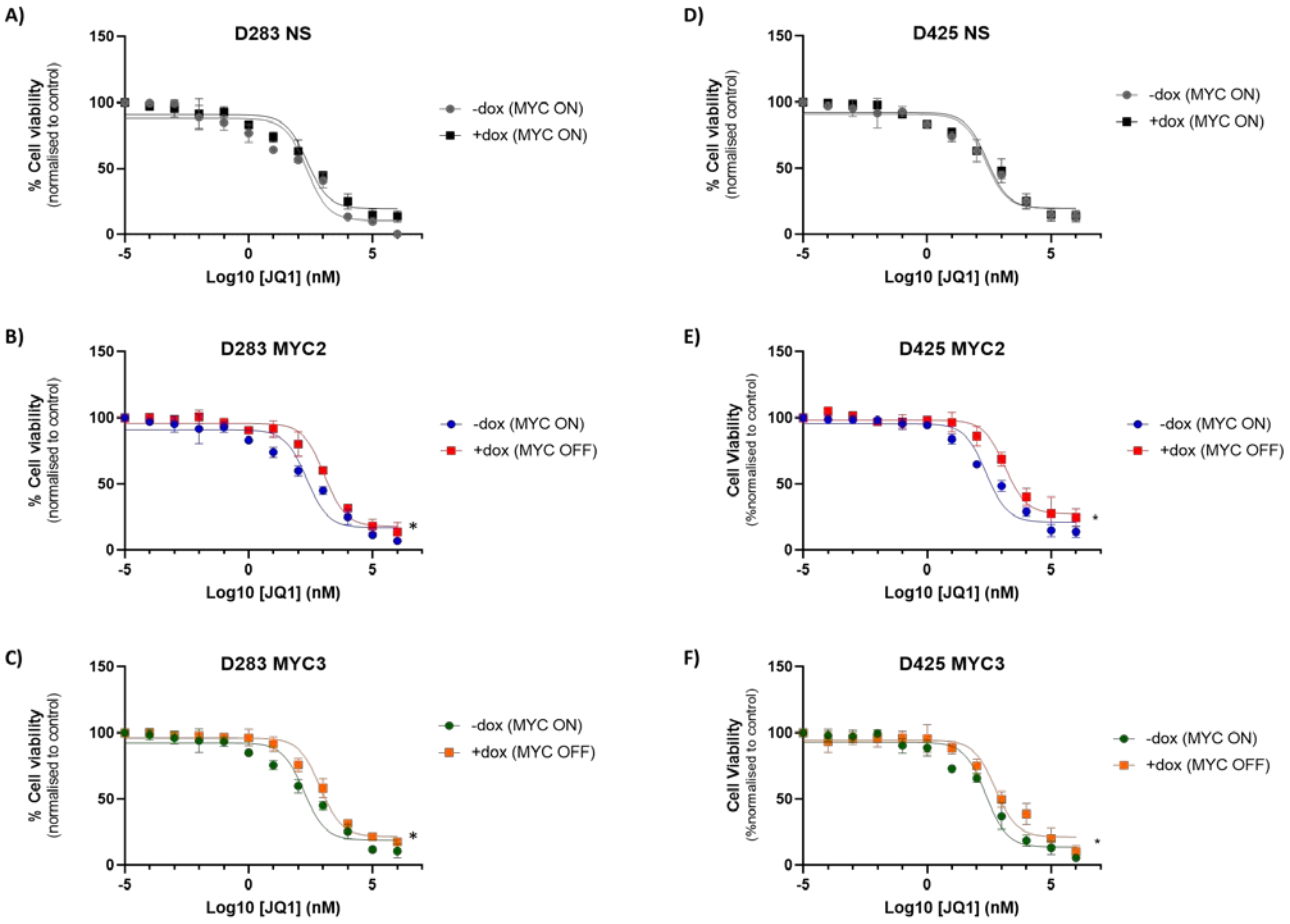

G)

D283

	JQ1					
	NS -dox (MYC ON)	NS +dox (MYC ON)	MYC2 -dox (MYC ON)	MYC2 +dox (MYC OFF)	MYC3 -dox (MYC ON)	MYC3 +dox (MYC OFF)
IC50 (nM)	224.2	230.5	220.9	1132	171.6	779.4
P-value	0.1773		0.0049		0.0313	
SD of log(ratios)	0.4466		0.08729		0.08407	
SEM of log(ratios)	0.1289		0.02520		0.02427	

D425

	JQ1					
	NS -dox (MYC ON)	NS +dox (MYC ON)	MYC2 -dox (MYC ON)	MYC2 +dox (MYC OFF)	MYC3 -dox (MYC ON)	MYC3 +dox (MYC OFF)
IC50 (nM)	230.5	261.7	237.1	1377	233.1	559.9
P-value	0.0685		0.0101		0.0214	
SD of log(ratios)	0.01291		0.09832		0.1129	
SEM of log(ratios)	0.003726		0.02838		0.03259	

Figure 4.8. Growth-inhibitory curves of D283 and D425 to JQ1 inhibitor. Dose-response inhibition curves of D283 (A)NS, B)MYC2, C)MYC3) and D425 (D)NS, E)MYC2, F)MYC3) MB_{Group3} cell lines treated with JQ1 (BRD4 inhibitor) for 72 hours, in the absence (-dox; MYC ON) and presence (+dox; MYC OFF) of DOX. Cells were exposed to 10-fold dilutions of the drug for 72 hours to determine the IC_{50} concentration (nM). Cell viability was measured with CellTiter-Glo (CTG). Results are shown as a percentage of cell viability of three independent experiments relative to cells grown in the presence of DMSO. Values obtained were analysed with Prism8 to generate a dose-response inhibition curve fitting a non-linear regression model. Curve is presented as log concentration versus response. Significance was determined by paired student's t-test (*p<0.05) G)Table summarising the half maximal inhibitory concentration (IC_{50}) of each cell lines calculated from the dose response curves. Significant differences between cells expressing high (-dox: MYC ON) and low (+dox: MYC OFF) levels of *MYC* was calculated with a ratio paired student's t-test (p-value). *P*-value is shown with the SD and SEM.

To further explore differences in response to JQ1 following *MYC* knockdown by shRNA, D425 and D283 were treated with different JQ1 concentrations around the IC_{50} range (10nM, 50nM, 100nM, 150nM, 200nM, 250nM, 300nM, 350nM). Cell viability after 72h of drug exposure was analysed for comparison.

Cell line with *MYC* overexpression appeared to be more sensitive to JQ1 treatment compared to cells with *MYC* knockdown. No differences in cell viability were seen for the NS constructs cultured in the presence and absence of DOX in response to JQ1 treatment. DOX did not affect responsiveness to the inhibitor, showing the expected 50% reduction of cells' proliferation by 200-250nM doses. The viability of cells with *MYC* knockdown was not affected by JQ1 treatment for these concentrations.

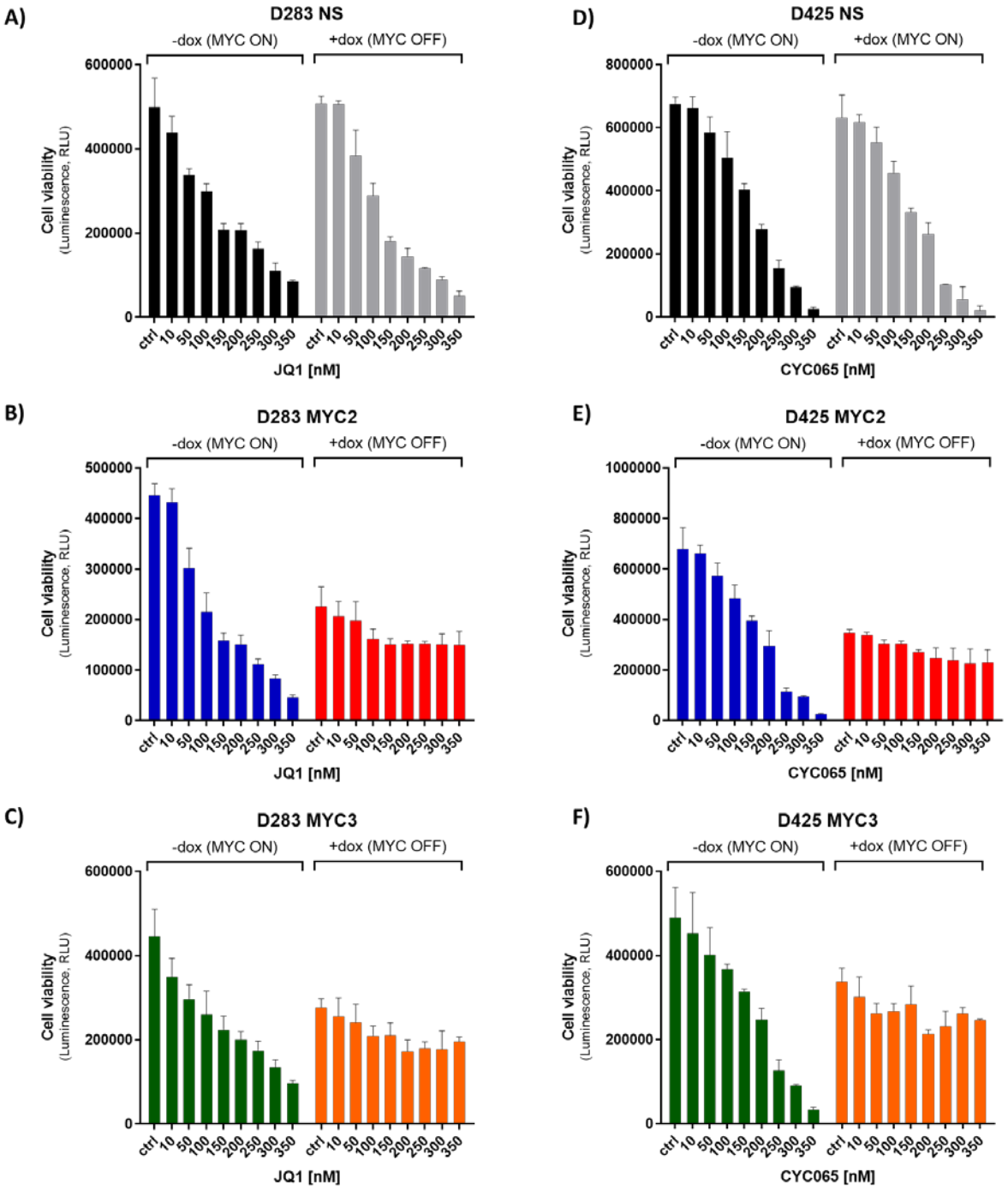

Figure 4.9. Effect of BRD4 inhibition on D425 and D283 viability. Cell viability of D283 (A)NS, B)MYC2, C)MYC3) and D425 (D)NS, E)MYC2, F)MYC3) after JQ1 treatment. Cells were cultured in the absence (-dox; MYC ON) and presence (+dox; MYC OFF) of doxycycline (DOX) for MYC knockdown. Cells were treated with 10nM, 50 nM, 100nM, 150nM, 200nM, 250nM, 300nM and 350nM of JQ1 for 72 hours. Cell viability was assessed with CTG. Untreated cells (no drug) were used for each condition (+/-DOX) as controls (ctrl). Data was blank-corrected to DMSO-containing wells. Data is presented as the mean (±SEM) of three independent experiments.

4.4.1.2 Effect of JQ1 treatment on D425 and D283 apoptosis

To gain a better understanding of the mechanism by which JQ1 was compromising cell viability, apoptosis assays were performed on D425 and D283 cloned with the MYC2 shRNA constructs, expressing high levels of *MYC* and with *MYC* knockdown.

Caspase 3/7 activity was assessed in D425 and D283 MYC2 cells (methodology explained in Chapter 2), overexpressing *MYC* and with *MYC* knockdown, after treatment with 0.2 µM and 0.5µM of JQ1 (Figure 10). Although no major differences were seen in overall signals, JQ1 treatment resulted in a significant increase in apoptosis in D425 MYC2 and D283 MYC2 when compared to the untreated counterpart of each cell line (p<0.0001 for both). A significant increase in apoptosis was seen when 0.2µM and 0.5µM treatments were compared only for D425 MYC2 (p=0.0064). Consistent with the growth inhibition results, BRD4 inhibition did not induce apoptosis in cells with *MYC* knockdown. JQ1 treatment caused increased apoptosis in cells overexpressing *MYC* compared with *MYC* knockdown (Figure 4.10).

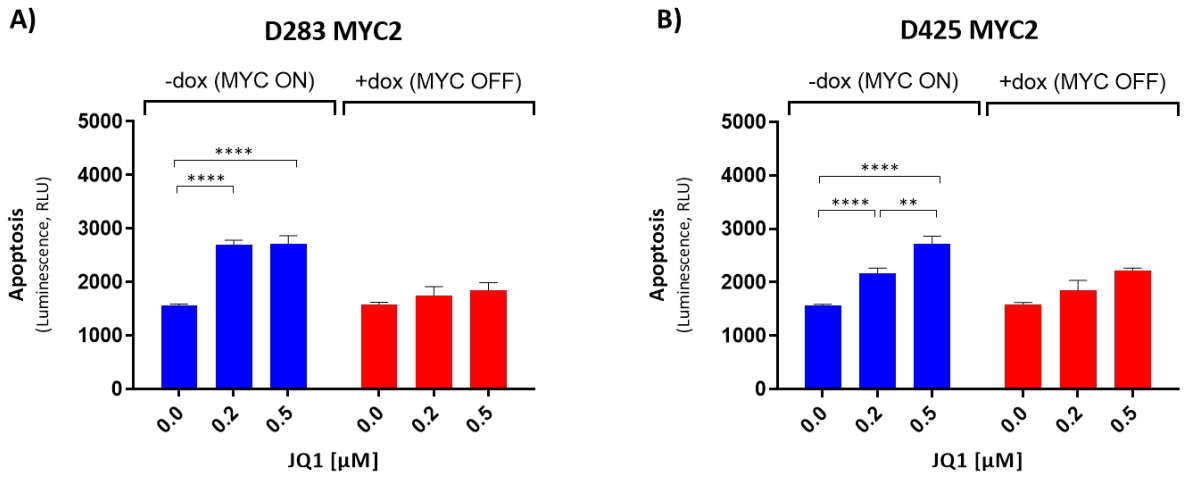

Figure 4.10. Effect of the JQ1 inhibitor on apoptosis in D425 and D283 cell models. Measurement of luminescent signal from the apoptotic executors caspase 3/7 in A)D425 MYC2 and B)D283 MYC2 after JQ1 treatment, in the absence (-dox; MYC ON) and presence (+dox; MYC OFF) of doxycycline for MYC knockdown. Cells were treated with 0.2µM and 0.5µM of JQ1 for 72h. Data is shown as means ±SEM of three independent experiments. Statistical significance determined by unpaired students t-test (**p≤0.01, ***p≤0.001, ****p≤0.0001).

4.4.1.3 Effect of BRD4 inhibition on MYC protein levels

The effect of JQ1 treatment on MYC and related proteins was then examined. D425 and D283 cell lines cloned with MYC2 and MYC3 shRNA constructs were treated with a range of concentrations of JQ1 (0.1µM, 0.2µM, 0.4µM, 1µM and 2µM) to test whether *MYC* expression was affected by BRD4 inhibition (Figure 4.11).

JQ1 treatment reduced MYC protein levels in the D425 and D283 cell lines in a dose-dependent manner. Quantification analysis of D425 MYC protein levels with automated western blot revealed a reduction of MYC protein by 50% with 0.2µM, 0.4µM and 1µM of inhibitor. At the highest concentration (1µM), *MYC* expression was reduced by 80%.

Although MYC protein levels were reduced following JQ1 treatment in D425 when the expression of shRNA was induced by DOX, the combinatory effect of JQ1 with *MYC* knockdown did not further reduce MYC protein levels to the same extent as observed by JQ1 treatment alone in *MYC* overexpressing cells. Interestingly, JQ1 treatment did not contribute to a decrease in MYC protein levels following knockdown (Figure 4.11, A). Treatment within the nM range only reduced protein levels by 20%, compared to a 65% reduction on MYC protein levels at the micromolar range. Overall, JQ1 had a greater effect in reducing MYC protein levels when cells were over-expressing *MYC* than in a *MYC* knockdown state.

A similar dose-dependent downregulation of *MYC* was seen in the D283 isogenic cell line. JQ1 inhibitor reduced MYC protein levels in a dose dependent manner, irrespective of *MYC* expression levels (*MYC*-overexpressing/*MYC* knockdown) (Figure 4.11, B). Protein quantification analysis with Wes after treatment with 0.2µM of JQ1 revealed a reduction in MYC protein levels by 65% in MYC2 and 58% in MYC3 cells which were each overexpressing *MYC*. Following *MYC* knockdown, BRD4 inhibition only downregulated MYC protein levels when treated at the highest dose.

Reduction in MYC protein was seen alongside a dose-dependent increase of levels of the anti-apoptotic protein MCL1, and a decrease in levels of total PARP for both cell lines. These effects were seen across cell lines and constructs, regardless of *MYC* expression levels.

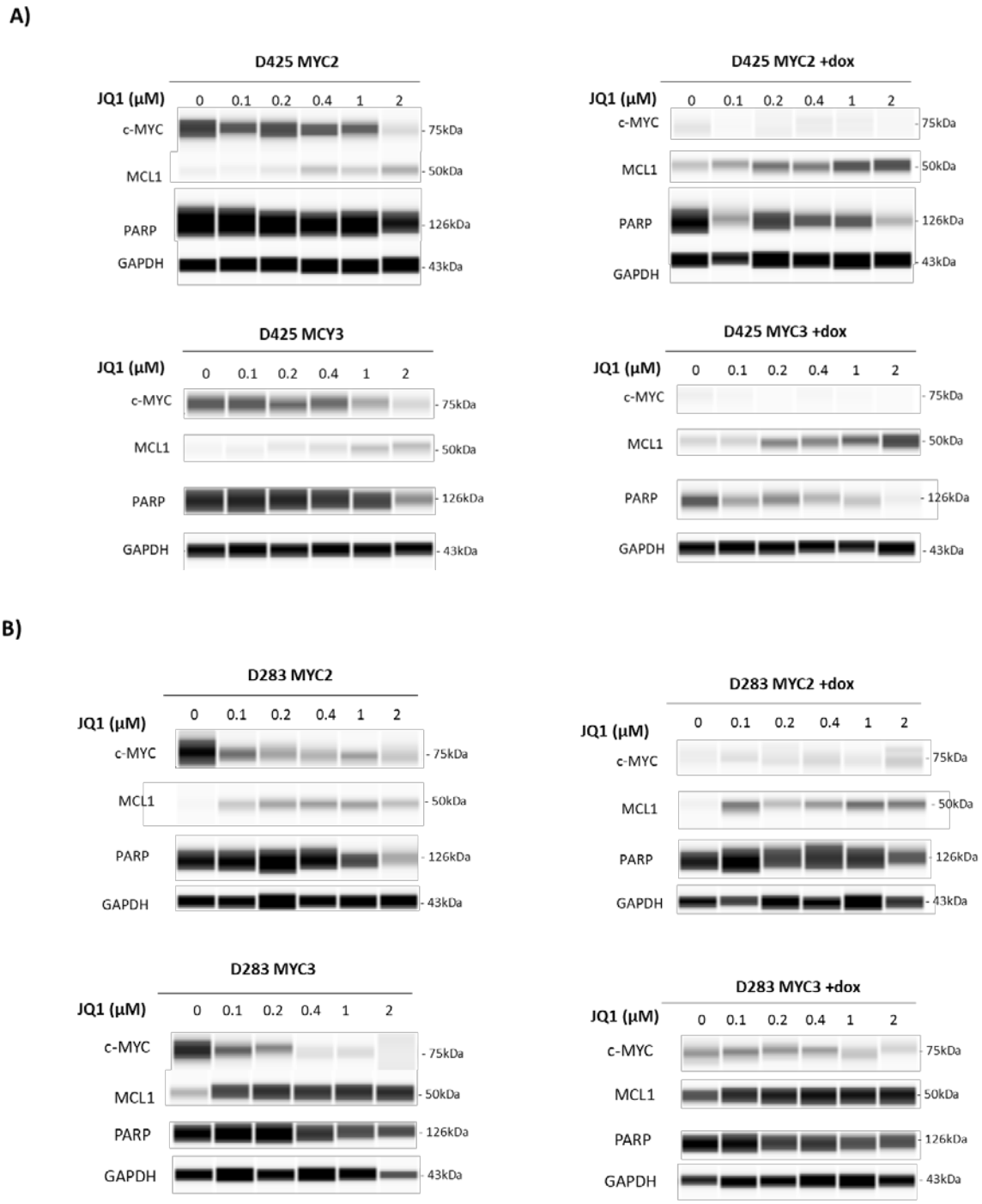

Figure 4.11. Effect of JQ1 inhibitor on D425 and D283 at the protein level. Automated Western Blot analysis of MYC protein levels express by A)D425 and B)D283 after 72 hours treatment with JQ1 inhibitor. D425 and D283 MYC2 and MYC3, with and without *MYC*-silencing by doxycycline (DOX), were treated with 0.1μM, 0.2μM, 0.4μM, 1μM and 2μM of the inhibitor for 72 hours. MYC protein levels were analysed alongside protein levels of the anti-apoptotic markers MCL1 and PARP. Protein levels of GAPDH were used as internal control. Protein quantification was performed in two independent biological experiments.

4.4.1.4 Effect of BRD4 inhibition in gene expression of D425 and D283

To see if the downregulation of MYC protein expression was correlated with a decrease in *MYC* expression at the mRNA level, expression of *MYC* in D425 MYC2 and D283 MYC3 was studied following JQ1 treatment (Figure 4.12). MYC mRNA expression of D425 MYC2 and D283 MYC2 cell lines decreased with JQ1 treatment (by 38.6% and 29.3%, respectively), although the reduction was not as profound as the reduction which was achieved by shRNA knockdown. Combination of JQ1 and DOX-induced *MYC* silencing resulted in a greater reduction of MYC mRNA expression for both D425 and D283 cell lines, 61.2% and 70.7% (data from Jemma Castle, MRes Project).

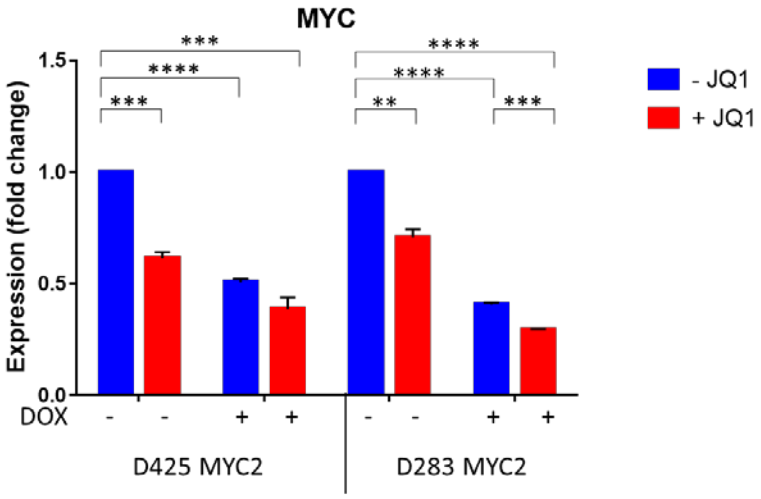

Figure 4.12. Effect of JQ1 inhibitor on *MYC* expression levels in D425 and D283 MYC2.Analysis of changes in MYC mRNA expression levels by RT-qPCR of D425 and D283 in response to treatment with JQ1. Cells cultured with (+) and without (-) DOX for *MYC* knockdown were treated with JQ1 for comparison. Expression fold change was calculated relative to the control cells with no DOX and no JQ1 of the respective cell line. Data represents the mean (±SEM) of triplicates of two biological repeats. Expression fold change was calculated relative to TBP expression (control gene). Significance is denoted by *$p \leq 0.05$, **$p \leq 0.01$, ***$p \leq 0.001$, ****$p \leq 0.0001$). Data kindly provided by Jemma Castle (MRes)

4.4.2 Cyclin-dependent kinase 9 inhibition

4.4.2.1 Effect of CDK9 inhibition on D425 and D283 cell viability

As previously shown, targeting *MYC* transcription through BRD4 inhibition with JQ1 resulted in the downregulation of MYC protein expression in our regulable models. Following the same indirect strategy, CYC065 (CDK9 inhibitor) was tested on D425 and D283 to compare which anti-*MYC* targeting strategy was more effective in downregulating *MYC* in our MB_{Group3} cell lines.

The growth inhibitory effect of pharmacological CDK9 inhibition was examined in D425 and D283 isogenic cell lines, transduced with NS, MYC2 and MYC3 shRNA constructs. Cells were induced with DOX prior to experimentation for maximum *MYC* knockdown, and treated with 10-fold dilutions of CYC065 to determine the IC_{50}, as described in Chapter 2. Cell viability was measured at 72h using CTG and resultant luminescence values analysed with Prism8 to generate a dose-response inhibition curves (Chapter 2).

MB_{Group3} cell lines overexpressing *MYC* exhibited higher sensitivity to CYC065, when compared to those with *MYC* knockdown (Figure 4.13). A *MYC*-dependent growth inhibitory effect was seen in both D425 and D283. CDK9 inhibition caused a significant reduction in viability of D425 and D283 cells expressing high-levels of *MYC* when compared to those with *MYC* knockdown by shRNA (D425 MYC2 p=0.0109; D425 MYC3 p=0.0206; D283 MYC2 p=0.0109; D283 MYC3 p=0.0259). No differences in growth inhibition were seen for cell lines cloned with the NS shRNA construct when grown in the presence and absence of DOX (D425 NS p=0.3172; D283 NS p=0.3237).

D283 NS, D283 MYC2 and D283 MYC3 cells gave similar IC_{50} values of around 200nM (Figure 4.13, G). Cell sensitivity to the inhibitor decreased when *MYC* was knocked down, increasing IC_{50} values to around 1 and 5µM when compared to the control. Similar IC_{50} values were seen for all constructs of D425, with values around 120nM. *MYC* knockdown by DOX caused an increase in resistance to the inhibitor, increasing the IC_{50} value to the micromolar range. When IC_{50} values were compared for both cell lines as a measure of sensitivity to the inhibitor, D425 appeared to be more sensitive to the CDK9 inhibitor (Figure 4.13, G).

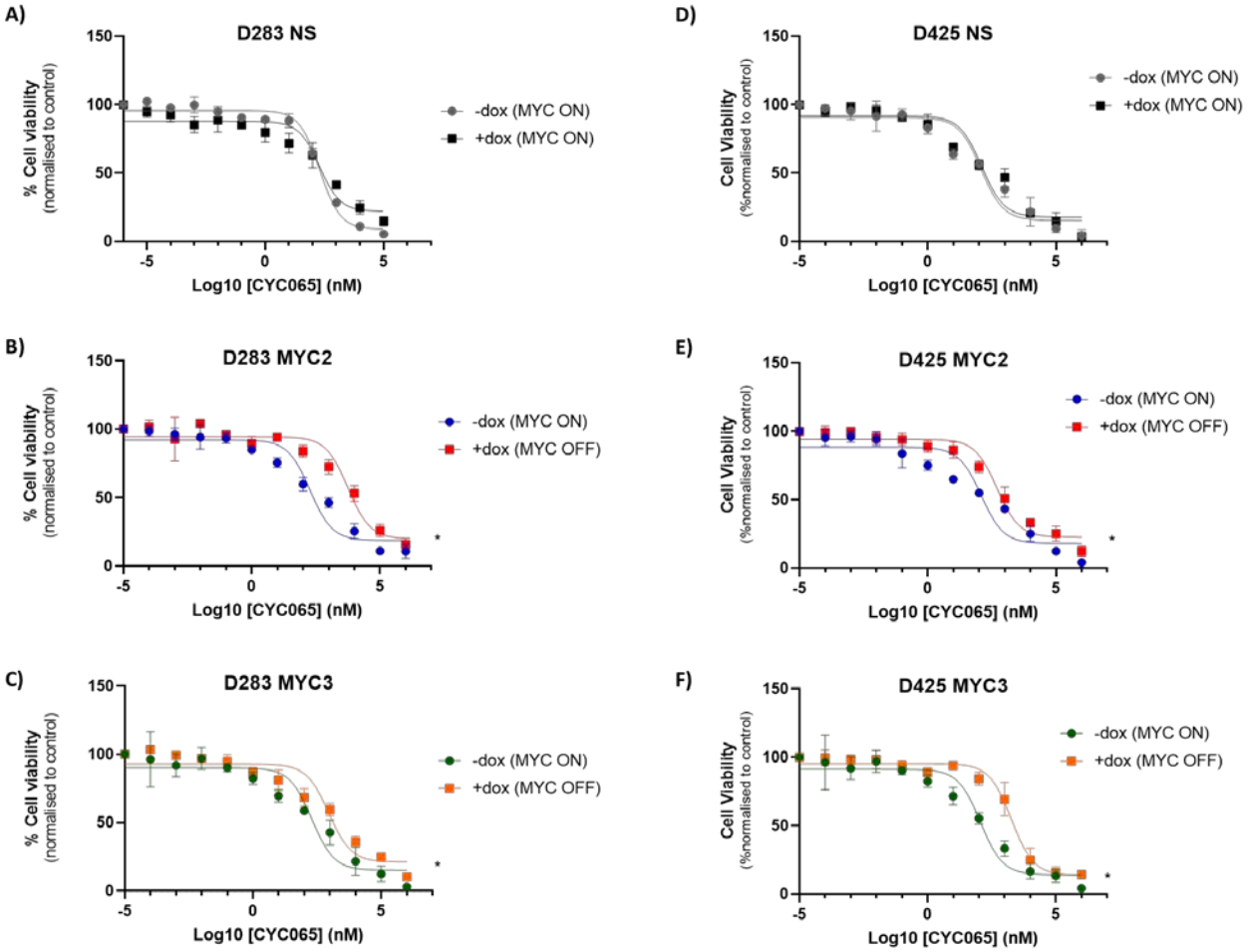

G)

D283

	CYC065					
	NS -dox (MYC ON)	NS +dox (MYC ON)	MYC2 -dox (MYC ON)	MYC2 +dox (MYC OFF)	MYC3 -dox (MYC ON)	MYC3 +dox (MYC OFF)
IC50 (nM)	199.3	195.4	187.5	5627	198.6	906.6
P-value	0.3172		0.0109		0.0259	
SD of log(ratios)	0.1744		0.1297		0.1622	
SEM of log(ratios)	0.05035		0.03743		0.04682	

D425

	CYC065					
	NS -dox (MYC ON)	NS +dox (MYC ON)	MYC2 -dox (MYC ON)	MYC2 +dox (MYC OFF)	MYC3 -dox (MYC ON)	MYC3 +dox (MYC OFF)
IC50 (nM)	119.1	128.1	121.4	499.7	115.1	1871
P-value	0.3237		0.0170		0.0206	
SD of log(ratios)	0.06623		0.1440		0.1594	
SEM of log(ratios)	0.01912		0.04156		0.04602	

Figure 4.13. Growth-inhibitory curves of D283 and D425 to CYC065 inhibitor. Dose-response inhibition curves of D283 (A)NS, B)MYC2, C)MYC3) and D425 (D)NS, E)MYC2, F)MYC3) MB_{Group3} cell lines treated with CYC065 (CDK9 inhibitor) for 72h, in the absence (-dox; MYC ON) and presence (+dox; MYC OFF) of DOX. Cells were exposed to 10-fold dilutions of the drug for 72h to determine the IC_{50} (nM). Cell viability was measured with CellTiter-Glo (CTG). Results are shown as percentage of cell viability of three independent experiments relative to cells grown in the presence of DMSO. Values obtained were analysed with Prism8 to generate a dose-response inhibition curve that fits a non-linear regression model. Curve is presented as log(concentration) vs response. The significance was determined by paired student's t-test (*p<0.05) G)Table summarising the half maximal inhibitory concentration (IC_{50}) of each cell line calculated from the dose response curves. Significant differences between cells expressing high (-dox: MYC ON) and low (+dox: MYC OFF) levels of *MYC* was calculated with a ratio paired student's t-test (p-Value). p-value is shown with the SD and SEM.

Considering that CDK9 is a short-lived protein with a half-life of 4-7h depending on the cell type (Hellvard et al., 2016), D425 and D283 MYC2 were incubated with CYC065 for shorter time periods to observe direct effects of CDK9 on cell viability (Garriga et al., 2003). After each time point, the drug was removed, and the media was refreshed. Cell viability was assessed after 72h to allow cells to recover and enable a complete round of cell division if cells remained viable.

CYC065 showed good efficacy in MB_{Group3}. D283 and D425 were extremely sensitive to CDK9 inhibition, significantly reducing cell viability with an exposure of 8h with CYC065 (Figure 4.14).

Comparison of cell viability at each time point after drug exposure was statistically significant, showing a reduction in cell viability in a time dependent manner. When *MYC* was knocked down in D425, a clear difference in sensitivity to the inhibitor was only observed after 8h of exposure when compared to MYC2 control, where lower levels of *MYC* expression were associated with resistance to the inhibitor in D425 cells. The same trend was seen for D283. D283 MYC2 cells cultured in the presence of DOX exhibited greater resistance to the inhibitor, showing major differences at the longest exposure time (Figure 4.14).

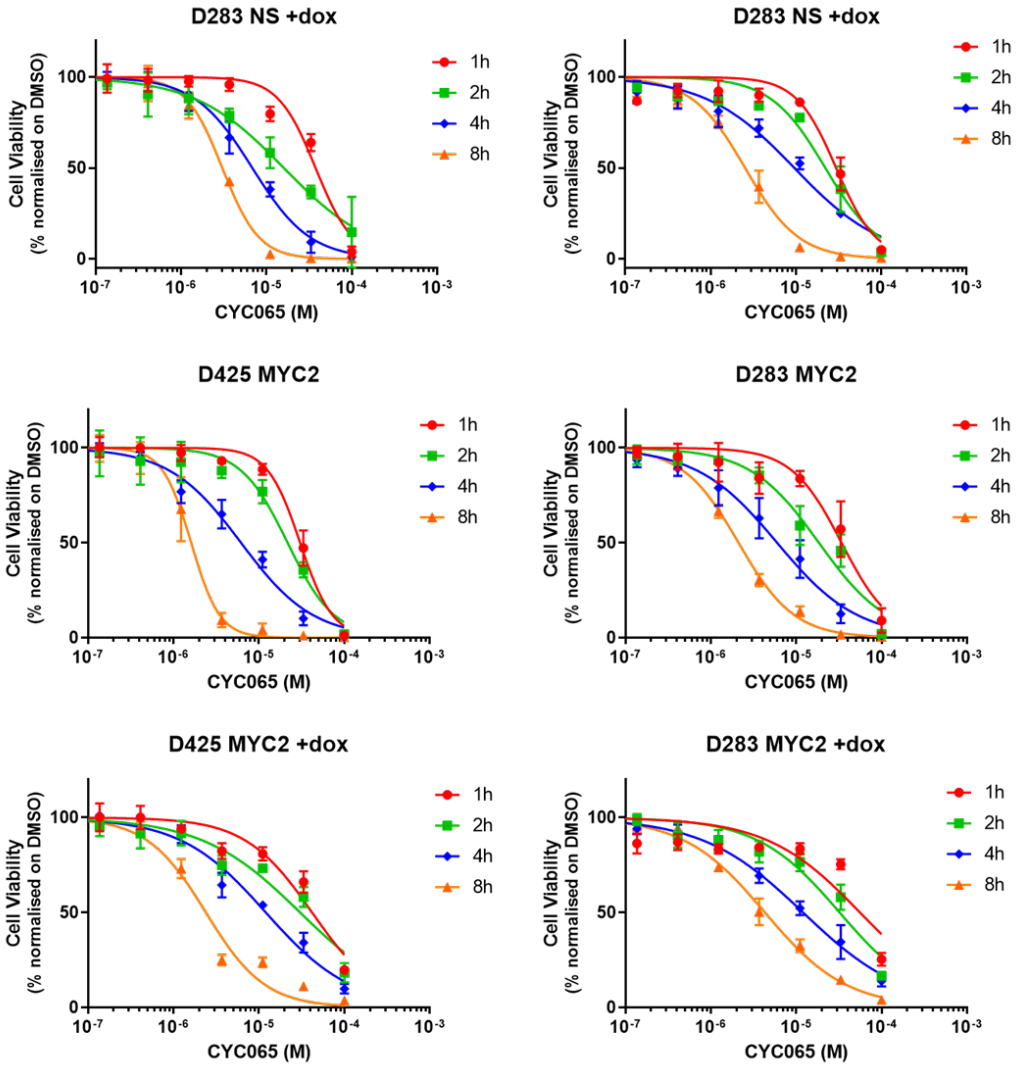

Figure 4.14. Effect of CDK9/2 inhibition on D425 and D283 cell viability. Dose-response curves of D425 and D283 MB_{Group3} cell lines treated with CYC065 (CDK9 inhibitor) for 1h, 2h, 4h, and 8h, in the presence and absence of DOX for *MYC* silencing. Cells were exposed to decreased 1:3 serial dilution concentrations of CYC065 (from 100µM to 0.03µM). Cell viability was measured with CTG. Values are shown as percentage of cell viability of three biological repeats of three independent experiments relative to cells grown in the presence of DMSO. Values obtained were analysed with Prism to generate a dose-response inhibition curve fitting a non-linear regression model. Curve is presented as log(concentration) vs response.

4.4.2.2 Effect of CDK9 inhibition on D425 and D283 apoptosis

To assess whether CYC065 was compromising cell viability through the induction of apoptosis, the caspase-Glo 3/7 assay was performed on D425 MYC2 and D283 MYC2 after treatment with 0.2µM and 0.5µM of CYC065 as described in Chapter 2. The apoptotic signals of cells with *MYC* knockdown were also measured for comparison.

Inhibition of CDK9 caused a significant increase in apoptosis (p<0.0001), in both conditions with and without *MYC* knockdown (Figure 4.15). Similar levels of apoptosis were seen between D425 and D283. Treating *MYC* expressing cells with CYC065 resulted in a significant increase in cell apoptosis of around 6-fold and 10-fold when compared to the untreated controls. When *MYC* was silenced, apoptosis was significantly increased by around 2-fold and 4-fold for both cell lines. When compared, the increase in apoptosis seen in both cell lines after CYC065 treatment was significantly different between cells overexpressing *MYC* and with *MYC* knockdown (p<0.0001)(Figure 4.15).

Results indicate that *MYC*-driven MB_{Group3} cell lines are sensitive to CDK9 inhibition in a *MYC*-dependent manner, where CYC065 preferentially targets *MYC*-overexpressing cell lines, compromising their viability through the induction of cell apoptosis.

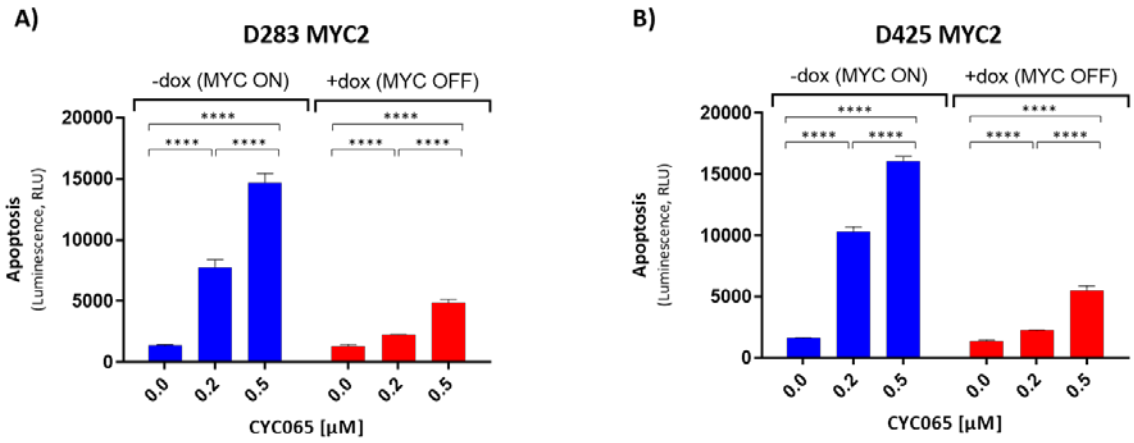

Figure 4.15. Effect of CYC065 inhibitor on D283 and D425 apoptosis. Measurement of apoptotic executors caspase 3/7 on D425 and D283 after JQ1 treatment, in the presence and absence (+; MYC knockdown) of high levels of *MYC* expression. Cells were treated with 0.2µM and 0.5µM of CYC065 for 72h. Data is shown as means ±SEM of three independent experiments. Statistical significance determined by unpaired students t-test (****p≤0.0001).

4.4.2.3 Effect of CYC065 treatment on D425 and D283 at the protein level

The effect of CDK9 inhibition at the protein level was examined to identify if decrease in cell viability was associated with alteration of *MYC* expression. D425 and D283 cells with the NS and MYC2 construct were exposed to 1x, 2x and 4x the IC_{50} of CYC065, for 1 hour, 2 hours and 8 hours, as explained in Chapter 2.

When analysed at the protein level with Wes, CYC065 successfully reduced MYC protein expression in a time and dose-dependent manner (Figure 4.16). CDK9 inhibition by CYC065 caused a rapid downregulation of *MYC* expression in both cell lines, which was accentuated with longer exposures and higher doses of the inhibitor. Densitometry analysis showed that, with only 2h of exposure, CYC065 caused a reduction in MYC protein expression of almost 50% with 4x$IC_{50,}$ when compared to untreated control. Treatment with IC_{50} concentration reduced MYC protein by 40% after 2h and 4h, reaching 55% reduction in just 8h of exposure.

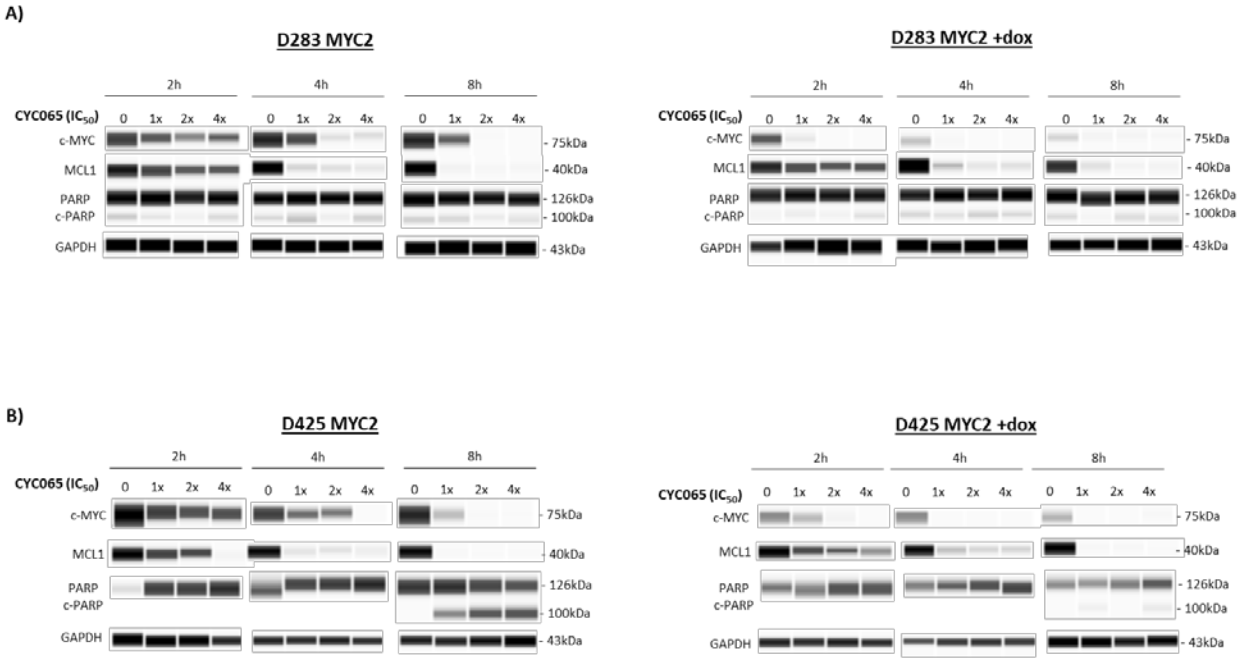

Figure 4.16. Effect of CYC065 inhibitor on D425 and D283 at the protein level. Automated Western Blot analysis of MYC protein levels expressed by A)D283 and B)D425 after 72h treatment with JQ1 inhibitor. D425 MYC2 and D283 MYC2, with and without *MYC*-silencing by doxycycline (DOX), were treated with 0.1μM, 0.2μM, 0.4μM, 1μM and 2μM of the inhibitor for 72 hours. MYC protein expression levels were examined alongside protein levels of the anti-apoptotic markers MCL1 and PARP After treatment. Protein levels of GAPDH were used as internal control. Protein quantification was performed in two independent biological experiments.

The combination of CYC065 and *MYC*-silencing with doxycycline had an additive effect and caused a further reduction of MYC in both cell lines (Figure 4.16). Protein quantification with Wes revealed a reduction in MYC protein levels of D283 by 50% with only 2h of exposure to the drug, abrogating MYC protein levels completely with time and dose. CYC065 had a similar effect on D425 MYC2. Protein was reduced around 55% with exposures to IC_{50} for 2h. The largest reduction in MYC protein levels was observed in D425 with *MYC* knockdown after CYC065 treatment (Figure 4.16, B).

As expected CDK9/2 inhibition by CY065 induced a rapid downregulation of MCL1 protein levels. An upregulation of PARP protein was also induced in a time and dose dependent manner. Both proteins were seen to be up and downregulated in the same way when *MYC* was knocked down.

4.4.2.4 Effect of CDK9 inhibition by CYC065 on D425 and D283 gene expression

To see if the downregulation of MYC protein expression was correlated with a decrease in *MYC* expression at the mRNA level, expression of *MYC* in D425 MYC2 and D283 MYC3 was studied following CYC065 treatment.

A *MYC*-dependent reduction of MYC mRNA expression levels was seen after treatment with CYC065 in D425 and D283 (Figure 4.17). CDK9 inhibition significantly decreased MYC mRNA expression of D425 and D283 MYC2 cell lines overexpressing *MYC*, by 49.22% and 57% respectively, when compared to untreated cells (D425 MYC2 p=0.0002; D283 MYC2 p=0.0003). Following *MYC* knockdown, CYC065 had no significant effect on MYC mRNA expression in either cell lines (p=0.1495 and p=0.566, for D425 and D283, respectively)(data from Jemma Castle, MRes Project).

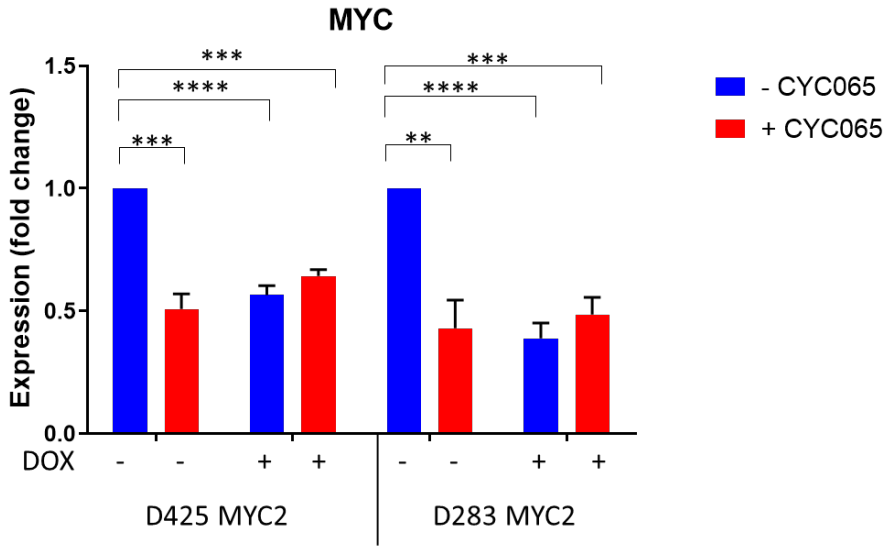

Figure 4.17. Effect of CYC065 inhibitor on *MYC* expression levels in D425 and D283 MYC2. Analysis of changes in MYC mRNA expression levels by RT-qPCR of D425 and D283 in response to treatment with CYC065. Cells cultured with (+) and without (-) DOX for *MYC* knockdown were treated with CYC065 for comparison. Expression fold change was calculated relative to the control cells with no DOX and no CYC065 of the respective cell line. Data represents the mean (±SEM) of triplicates of two biological repeats. Expression fold change was calculated relative to TBP expression (control gene). Significance is denoted by *p≤0.05, **p≤0.01, ***p≤0.001, ****p≤0.0001). Data kindly provided by Jemma Castle (MRes).

4.5 Discussion

4.5.1 MYC *sensitises* MB_{Group3} *cell lines to mTOR inhibition*

The PI3K/AKT/mTOR signalling pathway has a key role in controlling and regulating cellular maintenance. It is well established that this signalling cascade is aberrantly altered in various cancers, including MB. Independent of subgroup type, numerous alterations involving the PI3K/AKT signalling have been reported in MB, which is fundamental for MB proliferation, maintenance and metastasis. Its aberrant activation is usually associated with high-risk subgroups and tumour resistance, making it an ideal target for new therapeutic approaches (Baryawno et al., 2010, Hartmann et al., 2006, Eckerdt et al., 2019).

Previous studies have shown the effectiveness of targeting this signalling pathway in MB using mTOR inhibitors. Moreover, inhibiting the PI3K/AKT/mTOR pathway with small molecule inhibitors has been shown to destabilise MYC and MYCN proteins. As mTOR is a downstream target of *MYC* upregulation, it is a good candidate for therapeutic targeting (Pei et al., 2016, Cage et al., 2015, Buonamici et al., 2010).

The potential effect of mTORC1/2 inhibition using INK128 and AZD2014 against *MYC*-driven MB cells was examined in this study. D425 MB_{Group3} cells showed different sensitivities to mTOR inhibition following *MYC* knockdown. D425 MYC2 treated with DOX for *MYC* knockdown showed greater resistance to the mTOR inhibitors when compared to both the NS control and untreated D425 MYC2 expressing *MYC*. In contrast, D425 MYC3 showed a trend of decreased sensitivity following *MYC* knockdown, but this was not statistically significant. In general, D425 cells expressing high levels of *MYC* exhibited greater sensitivity to INK128 and AZD2014 than cells with *MYC* knockdown, showing a clear *MYC*-dependent sensitivity to mTOR inhibition.

Despite *MYC*-dependent sensitivity to mTOR inhibitors, treatment with INK128 and AD2014 did not cause downregulation of MYC protein levels. In fact, re-expression of *MYC* was observed after 1-2 hours of drug exposure. Although no effects were seen on MYC protein levels, a *MYC*-independent reduction in S6 phosphorylation was observed, indicating the efficacy of the inhibitors. A *MYC*-dependent reduction of total levels of mTOR was seen in cell lines with *MYC* knockdown at later time points after treatment with AZD2014. The results indicate that mTOR inhibition might be additive to *MYC*-knockdown.

The PI3K/AKT/mTOR signalling pathway involves crosstalk nodes with other pathways, numerous feedback loops and compensatory pathways. The complexity of the network brings many opportunities for cancerous cells to circumvent PI3K inhibition, limiting its therapeutic efficacy (Yang et al., 2019). It has been reported that the interaction between mTORC1 and S6K, mediates potent negative feedback loops that affect upstream signalling of several tyrosine kinases (TRKs) and insulin receptors in addition to promoting growth signalling in normal and cancerous cells. mTORC1 inhibitors cause compensatory activation of the PI3K and AKT nodes when supressing the feedback loops, causing enhanced activation of upstream signalling of pro-oncogenic and survival pathways (MEK/ERK), thus opposing the anti-proliferative effects of the inhibitors (Rozengurt et al., 2014, Guri and Hall, 2016).

Several studies exposing different cancer types to selective mTOR inhibitors have shown them to induce over activation of ERK, a kinase member of the Ras-Raf-ERK signal transduction cascade. Ras is an oncogene that plays a pivotal role in cell growth. Ras activation stimulates the effector kinases MEK and ERK that activate key transcription factors for mitogenesis. This compensatory mechanism could explain the rebound in MYC expression after drug treatment with mTOR inhibitors, a way cells have to circumvent PI3K inhibition and promote MYC transcription (Mendoza et al., 2011, Asati et al., 2016).

Evidence shows that PI3K/mTOR inhibition increases *MYC* expression through activation of the NOTCH signalling pathway. Muellner *et al*. showed a reduction in Bez-235 inhibitor efficacy (dual PI3K/mTOR inhibitor) through activation of NOTCH-*MYC* signalling (Shepherd et al., 2013, Muellner et al., 2011, Dey et al., 2015). These studies offer another explanation of an alternative mechanism by which *MYC*-driven MB_{Group3} cell lines could upregulate *MYC* expression when downstream effectors of the PI3K signalling pathway are affected, to maintain high levels of *MYC* expression.

Although the use of AZD2014 and INK128 did not have a direct effect on *MYC* expression in *MYC*-driven MB_{Group3} cell lines, further investigation at the mRNA and protein level should include more time points and varied concentrations to properly evaluate the effect of mTOR inhibition. Gene expression alterations are dynamic and therefore time-dependent, making experimental approaches often challenging to capture in detail this time-dependent biological process. In this regard, some changes in gene expression might have been missed, since only short time periods were considered as a preliminarily approach to investigate the effect these inhibitors had on *MYC* expression.

Downstream effectors of the apoptotic signalling pathway should also be studied to understand the mechanism by which AZD2014 and INK128 reduced the viability of D425 cells. In summary, mTOR inhibition did not result in downregulation of *MYC* expression, and due to time constraints, mTOR inhibition in MB_{Group3} cell lines was not pursued, and alternative drugs and signalling pathways were investigated.

4.5.2 BRD4 inhibition decreases MYC *expression*

The BET family of proteins has become a promising target for epigenetic therapy. Involvement of BRD4 in regulating *MYC* expression and the transcription of *MYC*-targeted genes has been seen as a promising new anti-cancer therapeutic approach to use on *MYC*-driven cancers.

JQ1 has previously been shown to reduce *MYC* expression and downregulate *MYC*-associated transcriptional activity in MB and NB *MYC*-driven cancers (Henssen et al., 2013, Bandopadhayay et al., 2019, Bandopadhayay et al., 2014, Venkataraman et al., 2014). Currently, this is the first study assessing the efficacy of JQ1 and *MYC* dependency in Group 3 medulloblastoma.

In accordance to these published studies, treatment with JQ1 did destabilise *MYC* and caused a reduction in its expression, both at the protein and mRNA level in a *MYC*-dependent manner in our regulable models. JQ1 treatment caused a *MYC*-dependent growth-inhibitory effect on the MB regulable models, where a significant difference between the IC_{50} concentrations was seen when compared cells overexpressing *MYC* with its *MYC*-silenced counterparts.

Reduction of *MYC* expression levels through BRD4 inhibition caused a reduction in cell proliferation. Interference with *MYC* translation through JQ1 treatment seemed to cause a similar effect to *MYC*-silencing with doxycycline, reducing cellular proliferation but without inducing cell death. This correlates with small differences seen in expression of the apoptosis executors caspase 3 and 7 following treatment with JQ1. Results are in accordance with other studies reporting the involvement of BRD4 in regulating cancer cell proliferation through induction of cellular senescence (Dong et al., 2018).

JQ1 treatment upregulated the expression of *MCL1*, resulting in an increase in MCL1 protein levels after JQ1 treatment. JQ1-induced upregulation of the anti-apoptotic protein *MCL1* has been previously linked to resistance to JQ1. BRD4 has a role in non-homologous end joining

(NHEJ) DNA damage repair. Inhibition of BRD4 with JQ1 has been shown to increase DNA damage by inhibiting DNA repair.

Increased levels of MCL1 trigger anti-apoptotic signalling pathways, arresting cell cycle progression to prevent cells sustaining DNA damage from replicating (Fujise et al., 2000, Zhang et al., 2018b). The decrease seen in the expression levels of PARP, a protein involved in DNA repair, indicates that increased MCL1 levels might occur to ensure cells bearing damaged DNA do not replicate. This could explain the maintenance of some viable cells following JQ1 treatment, as after 72h 50% of the cells were still viable at the highest tested concentration of the inhibitor.

Stability of MCL1 is tightly regulated through phosphorylation and ubiquitination by various oncogenic signalling pathways, including the MAPK pathway. These oncogenic signalling cascades promote rapid increase of MCL1 to promote cell survival and escape the apoptotic signal (Williams and Cook, 2015, Basu and Sridharan, 2017). These studies are in agreement with the upregulation of the RNA expression of genes involved in the MAPK signalling pathway seen in the regulable models, which could explain the increase in levels of MCL1 protein after JQ1 treatment.

Further study of drug response should include the analysis of cell cycle and gene expression of genes involved in the apoptotic and senescence-signalling pathway, to better determine the mechanism by which JQ1 reduced proliferation and cell viability in MB_{Group3}.

JQ1 development offered a new therapeutic strategy to treat cancer through targeting the transcription of critical oncogenes driving tumorigenic processes. The mechanism of action of JQ1 has been key to establish proof of principle of BET inhibition as a target strategy for many human cancers. However, the short half-life of the compound has made it challenging to identify an effective dosage range *in vivo* without going above physiologic safety levels. In fact, clinical JQ1-related toxicities have already been reported and its exact mechanism of toxicity is still unknown, it may be due to its broad target spectrum across the BET family members (Bakshi et al., 2018, Stathis and Bertoni, 2018).

The pharmacokinetic and pharmacodynamic properties and molecule structure of JQ1 has become a model for the development of new drugs with increased bioavailability and reduced neurocognitive related toxicities. Many BET inhibitors (like OTX015 and I-BET76) have been approved for clinical studies, but unfortunately initial evaluation has reported toxic side

effects associated with treatment in various different cancers (Piha-Paul et al., 2019, Blum et al., 2018, Aftimos et al., 2017, Hottinger et al., 2016, Amorim et al., 2016, Patnaik et al., 2018)

Current literature and the results of this study indicate that BET inhibition is a promising anticancer strategy to compromise *MYC* expression in *MYC*-driven tumours. Administration of BET inhibitors alone may not be sufficient to kill *MYC*-driven MB cell lines, as attenuation of *MYC* expression does not trigger the apoptotic pathway, but a combination of BET inhibitors and compounds affecting the expression of anti-apoptotic proteins could be a good strategy to induce cell death in MB (Miller et al., 2019).

4.5.3 CDK9 inhibition results in inhibition of MYC *transcription*

MYC is a potent oncogenic driver, and its overexpression induces the upregulation of gene transcription, protein translation and DNA replication, resulting in aberrant cell proliferation that gives a competitive advantage. In recent years, much effort has been directed in developing strategies to target *MYC* function indirectly. Targeting *MYC* transcription through BRD4 inhibition has shown great promise. The use of BET inhibitors has demonstrated great potential in supressing *MYC* transcriptional activity, and overall good anti-tumour properties. JQ1 treatment on MB_{Group3} isogenic models successfully reduced *MYC* expression both at the mRNA and protein level. However, despite JQ1's great efficacy, the use of pan-BRD inhibitors has been shown to be toxic in pre-clinical models (Alqahtani et al., 2019), and its lack of selectivity against *MYC* transcription is still a concern.

Published data indicates that recruitment of the P-TEFb complex to the *MYC* promoter region by BRD4 is essential to control *MYC* expression. CDK9 is the catalytic subunit of the P-TEFb, which is tempting to speculate that direct inhibition of P-TEFb through CDK9 inhibition would produce a similar or greater effect in inhibiting *MYC* transcription, which would in turn induce growth arrest in MYC addicted cell lines (Lu et al., 2015, Blake et al., 2019). Therefore, efficacy of CDK9 inhibition in disrupting *MYC*-dependent transcription was explored in MB_{Group3} as an alternative therapeutic approach to target *MYC* transcription. The CDK9 inhibitor CYC065 (Cyclacel), was chosen for the study because of its great potential seen in NB (Chen et al., 2018b, Hashiguchi et al., 2019).

MYC-expressing MB_{Group3} cell lines demonstrated enhanced susceptibility to CYC065. Treatment with CYC065 caused a reduction in cell counts alongside reduced viability. The role

of CDK9 as a global regulator of gene transcription, and its particular role in regulating *MYC* expression directly, may explain why its inhibition caused a reduction in D425 and D283 proliferative capacity.

CDK9 has been shown to be an intermediary involved in MYC phosphorylation at Ser62, an important contributor to subsequent MYC degradation and apoptosis, which could explain the decreased in cell viability seen in *MYC* over-expressing MB_{Group3} cell lines (Hashiguchi et al., 2019).

MYC expression levels positively correlated with sensitivity to the CDK9 inhibitor CYC065. *MYC*-overexpressing D425 and D283 were more sensitive to CDK9 inhibition when compared to its *MYC*-silenced counterparts. Although not as pronounced, differences between cell line sensitivities were observed, with D425 being more sensitive to CDK9 inhibition. Differences in CYC065 sensitivity may be explained by differences in intrinsic levels of *MYC* expression. D425 is a *MYC* over-expressing cell line, whereas D283 has only gained one additional copy of *MYC* (Chapter 1, section 1.7.1.1), the difference in overall *MYC* expression levels might affect response to treatment with CYC065.

CDK9 regulates both *MYC* transcription and MYC protein stability in a *MYC*-dependent manner. As expected, its inhibition resulted in downregulation of *MYC* at the mRNA and protein level. CYC065 successfully reduced protein expression levels of MYC and MCL1, oncogenic drivers whose transcription is directly regulated by *CDK9*. Downregulation of MYC and MCL1 protein expression with CYC065 was greater in D425 than in D283. As mentioned, overall expression levels of *MYC* could explain differences in the efficiency by which MYC protein levels were downregulated after *CDK9* inhibition. Higher levels of *MYC* expression in D425 would translate into more transcription of *MYC* target genes in comparison to D283.

Inhibition of CDK9 by CYC065 shows great promise as a new therapeutic strategy to target *MYC*-dependent MB_{Group3} tumours. CYC065 significantly reduced *MYC* expression both at the protein level, reducing proliferation and cell viability in D425 and D283 MB_{Group3} cell lines in a *MYC*-dependent way. Further studies involving cell cycle analysis and apoptotic assays should be pursued to elucidate the mechanism by which the inhibitor is affecting cell viability.

All things considered, the results of this Chapter provide a degree of validation to use CDK9 inhibition as a therapeutic strategy to downregulate *MYC* transcription in *MYC*-dependent tumours, in an attempt to compromise cell growth and survival.

4.5.4 Summary

This chapter outlines the pursuit of two different pharmacological strategies to indirectly target *MYC* in two *MYC*-regulable MB_{Group3} cell lines. The use of the isogenic models enabled the testing of candidate drugs targeting *MYC*-associated signalling pathways in a *MYC*-dependent manner.

Despite *MYC* being a downstream effector of the PI3K/AKT/mTOR signalling pathway, mTOR inhibition did not downregulate *MYC* expression. The rebound of *MYC* expression following inhibition has been linked to acquired resistance to PI3K inhibitors. The complexity of underlying compensatory feedback loops that malignant cells use to circumvent the effect of PI3K inhibition, necessitates deeper understanding to overcome drug resistance. Until the underlying mechanism of the signalling pathway is well established in a tissue-specific context, it is clear that single-agent targeting of this signalling cascade is not the best approach to treat *MYC*-dependent MB_{Group3} tumours. Combinational approaches would be better options to treat MB to increase treatment efficacy and reduce treatment resistance (Yang et al., 2019, Vora et al., 2014).

Targeting *MYC* transcription holds the promise for a better strategy to directly downregulate *MYC* expression. MB_{Group3} cell lines are specifically sensitive to CDK9 and BRD4 inhibition in a *MYC*-dependent fashion, and have shown great efficacy in destabilising MYC protein levels, decreasing cell proliferation and inducing apoptosis. When compared, CYC065 had a greater effect in reducing MYC protein levels than JQ1.

Despite CDK9 inhibition causing a general reduction in expression of most human genes, the induction of *MYC* expression upon prolonged pharmacological inhibition of CDK9 has been previously reported (Lu et al., 2015). BRD4 recruits P-TEFb at the *MYC* enhancer and superenhancer regions to promote its transcription. It has been found that binding between BRD4 and P-TEFb protects CDK9 from drug inhibition, which would explain the induction of *MYC* expression to maintain the transcription of key genes for cell survival and to compensate for the loss of CDK9 (Lu et al., 2015).

Work presented in this chapter identifies MB_{Group3} *MYC*-overexpressing cell lines to be more sensitive to the candidate inhibitors. As shown in Chapter 3, *MYC* knockdown downregulates cell cycle and proliferation, which could mask the effect of the inhibitors. To discern whether the sensitives to the inhibitors identified are *MYC*-dependent or a consequence of reduced

cell turnover, the recapitulation of the experiments using alternative non-*MYC* amplified MB_{Group3} cell lines or MB_{Group3} lines expressing lower levels of *MYC* would be key to understand the contribution of *MYC* overexpression to the drug sensitivity observed. Testing of the inhibitors on alternative MB_{Group3} cell lines would be key to differentiate *MYC*-dependent sensitivities from those susceptibilities identified as a direct result from downregulation of cell proliferation upon *MYC*-knockdown.

Results presented in this chapter, indicate that targeting of BRD4 and CDK9, alone or in combination, is a potential therapeutic strategy to treat *MYC* overexpressing MB_{Group3} tumours. The potential of simultaneous inhibition of BRD4 and CDK9 should be further explored to inhibit *MYC* expression, induce growth arrest and apoptosis in MB_{Group3}.

Chapter 5. Chemosensitivity profiling of Group 3 medulloblastoma cell lines

5.1 Introduction

High-throughput genomic and proteomic methods have had a huge impact on our understanding of cancer biology, paving the way for major improvements in cancer therapeutics. Integration of 'omic' data sets have aided in the identification of targetable molecular mechanisms altered in a particular cancer, with the aim of developing new therapeutic approaches to increase survival rates and reduce adverse effects of current standard therapy (Hajare et al., 2013).

The need for major improvements in personalised medicine has driven the acceleration of the process of identifying new antitumoural drugs for translational research. Combination of bioinformatics, combinatorial chemistry and automation of cell-based assays has created a more effective platform to accelerate the drug discovery process (Entzeroth et al., 2009).

An important drug discovery methodology is compound screening, which is the process of assaying the effect of chemical compounds on biological models of interest and measuring phenotypic effects such as growth. The establishment of laboratory robots and automated machinery has facilitated the emergence of high-throughput screening (HTS) approaches, whereby large numbers of compounds can be assayed in a very time- and cost-efficient manner (Xia and Wong, 2012, Shukla, 2016).

Availability of a compound library is a prerequisite for HTS. Chemical libraries can vary from being broad (with a huge variety of small molecules with diverse targeting) to more specific (tailored to a family of related targets). Usually, a compound library is chosen to be as diverse as possible to assay for potential effects without pre-conceived assumptions (Szymanski et al., 2012).

HTS, performed by means of automated miniaturised cell-based assays, enables the evaluation of hundreds of potential drug targets at a time by functionally assessing their efficacy in biological models of interest. In this regard, cell-based phenotypic screening is usually used in academic research to compare the effect of several compounds on cell proliferation (Hughes et al., 2011).

The application of HTS technologies has required the parallel development of informatic systems in order to analyse and interpret the large amounts of data generated. Computational analysis of data generated through HTS has facilitated its integration with other platforms, allowing the connection of basic research with preclinical and clinical data providing new avenues for cancer treatment (Szymanski et al., 2012).

Whilst working on the candidate drug list described in Chapter 4, the opportunity to run a high throughput compound screen (HTCS) as part of a collaborative project (INSTINCT) with the Institute of Cancer Research (ICR) London arose.

Although, there has been some progress in the development of small molecule inhibitors targeting the SHH pathway of potential utility in MB_{SHH}, no major breakthroughs have been made in the treatment of MB_{Group3}. As the genetic changes between our isogenic models is limited to *MYC*, performing a HTCS presented the opportunity to observe *MYC*-dependent drug sensitivity effects (i.e. differences in drug sensitivity according to the level of *MYC* expression)(Postel-Vinay et al., 2013). Exposing our *MYC*-regulable models to hundreds of inhibitors offered the opportunity to identify inhibitors that have a greater effect in the presence of *MYC* expression and those which have an additive effect following *MYC*-silencing with shRNA. Integration of results from the screen with data on transcriptional and biological MB dependencies will help the identification of targetable cellular mechanisms to optimise strategies to selectively treat *MYC*-amplified MB_{Group3}.

5.2 Aims

This chapter aims to use the *MYC* silencing isogenic models described in chapters 1 and 3 to investigate the *MYC* dependency of the response to a large panel of small molecule inhibitors, to identify drugs which target both *MYC* and which synergise with *MYC* knockdown. Identification of drugs with a greater effect on proliferation of *MYC*-overexpressing cells potentially target *MYC* or *MYC*-associated processes, whereas greater sensitivity following *MYC* knockdown may indicate a synergistic effect with *MYC*.

5.3 Results

5.3.1 High throughput drug sensitivity screening on MYC*-dependent* MB_{Group3} *cell lines*

The compound libraries used at the ICR (icr.ac.uk) for screening contain a diverse assortment of small molecule inhibitors that are either already established for cancer treatment or are in late stages of clinical development. The list of compounds of each library can be found in tables 5.1, 5.2 and 5.3 of the Appendix (Postel-Vinay et al., 2013)(Holme et al., 2018)(Campbell et al., 2016, Menon et al., 2019).

This is of great use when assessing paediatric cancers, since most drugs are not made available for children until tested in adults. Therefore, the advantage of using a compound library with inhibitors already approved for the clinic is that any promising drugs discovered have a realistic chance of being directly translated into an early phase clinical trial for children (Holme et al., 2018).

Additionally, a large variety of cell models of different cancers have already been screened with the libraries at the ICR (Chong et al., 2018, Campbell et al., 2016)(Holme et al., 2018), and this provides a valuable resource to compare our *MYC* amplified medulloblastoma cell lines with, potentially highlighting compounds which show increased efficacy either specifically in medulloblastoma cells or more broadly in all *MYC* amplified cancer types.

To maximise the possibility to find positive and reproducible 'hits' (compounds which have a differential effect on *MYC* expressing compared to *MYC* downregulated cells, or vice versa), all three isogenic *MYC*-regulable cell lines were subjected to high-throughput chemosensitivity screening of three different compound libraries consisting of nearly 600 small molecule inhibitors. Library 11-12 contained 80 compounds, each one of them tested at 8 different concentrations (0.5, 1, 5, 10, 50, 100, 500, 1000nM). Library 13 contained a wider range of compounds, 397, but only tested at 4 concentrations (0.5, 5, 50 and 500nM). Library 14 involved 120 compounds tested individually at 8 different concentrations (0.5, 1, 5, 10, 50, 100, 500, 1000nM)(Figure 5.1).

Each MB_{Group3} cell line, with and without *MYC* knockdown, was subjected to each compound library for the identification of differences in sensitivity according to their *MYC* expression levels.

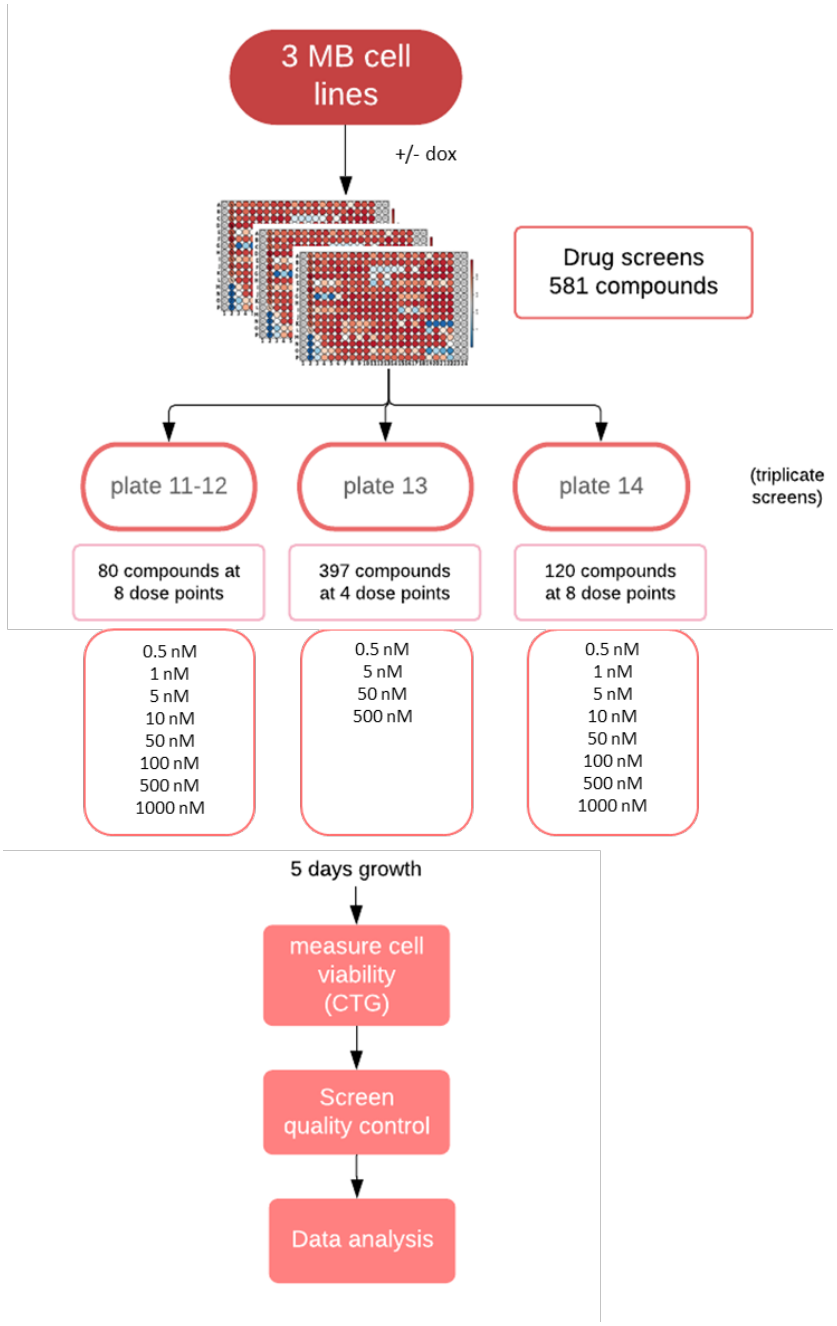

Figure 5.1. High throughput drug screening overview. Schematic summary of high throughout small compound chemosensitivity screen. D425, D283 and HDMB03 MB_{Group3} cell lines were seeded in 384 well plates and exposed to 3 compound libraries (plate 11-12, plate 13 and plate 14) for five days. Each one of the 80 compounds on library 11-12 were tested at 8 different concentrations (0.5, 1, 5, 10, 50, 100, 500, 1000nM), the 397 contained in library 13 were tested at 4 concentrations (0.5, 5, 50 and 500), and the 120 on library 14 at 8 different concentrations (0.5, 1, 5, 10, 50, 100, 500, 1000nM).Cells were pre-treated with DOX 48h prior to drugging. Cell viability was estimated with CellTiter-Glo (CTG) reagent. Data was processed through the ICR database, and quality controls for each screen determined to compile data for hit identification and further analysis. Each experiment was performed in triplicate.

Is it worth to point out that our working system adds an extra degree of complexity to the standardised performance of a regular HTCS. Considering each cell line, shRNA constructs and doxycycline treatment conditions, compound libraries 11-12, 13 and 14 were performed at least 18 times (Figure 5.2).

It was decided to run the screen on all conditions to enable reproducibility of drug sensitivity data to be assessed, and to increase robustness of the results found, since no other MB cell lines had been previously screened with this specific library of compounds.

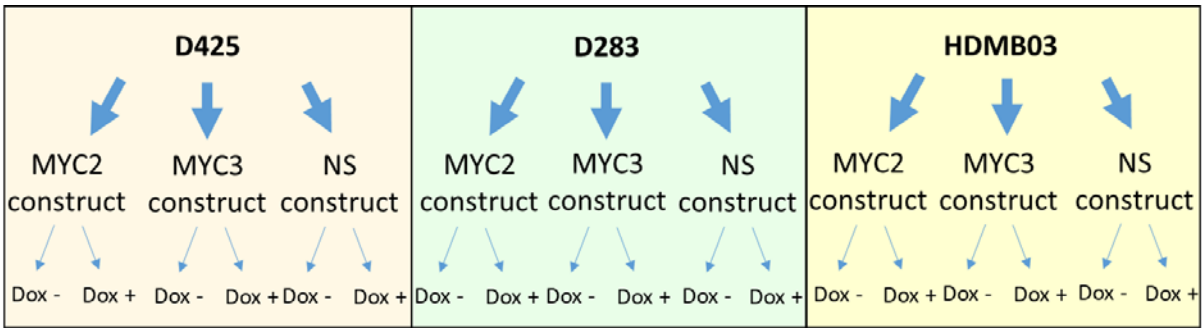

Figure 5.2. Complexity of the isogenic working system. Schematic representation of the isogenic model system. Each D425, D283 and HDMB03 MB_{Group3} cell line has cloned a non-silencing (NS), MYC2 and MYC3 shRNA construct for silencing *MYC* expression. Expression of the shRNA system and the consequent silencing of *MYC* is triggered by the addition of doxycycline (DOX +) to the media. Constructs need to be grown separately to avoid mixing. For DOX treated conditions, cells from the same passage are grown in parallel with and without doxycycline in the media.

5.3.1.1 Optimisation of drug screening

Screening of cell sensitivity to small molecule inhibitors is performed in 384 well plates. Cell lines in each well are exposed to a single-dose concentration of the compounds and left to grow for five consecutive days. Compounds in the screen are assessed in triplicate on separate plates to avoid plate to plate variations. An untreated control (no compound or DMSO) alongside positive and negative controls (50% DMSO only or camptothecin) are included on every assay plate for data normalisation. Residual viability is estimated with CellTiter-Glo (CTG). Signal from each well is normalised to the median of the negative controls (DMSO treated)(for more detail, see Chapter 2).

Maximum *MYC* knockdown is achieved 72h after DOX induction. With this under consideration, ideally cell lines would have to be pre-induced with DOX 24h prior to seeding, to ensure maximum efficacy of shRNA when the inhibitors hit their specific target.

To ensure that results seen are only representative of cell lines' sensitivity to the drugs, prior optimisation of HTCS conditions were performed to determine such factors as the seeding density and the length of the pre-treatment with DOX to ensure *MYC* was knocked down prior to the screen.

Firstly, the cell density recommended in the screen (500 cells/well) was assessed by growing cell lines cloned with each construct on 384 well plates for five days. Fast growing cell lines like D425 and HDMB03 reached cell confluence of around 85% by day 5, whilst D283 only around 60%. Having a lower doubling time, cell density of D283 was chosen to be 1000 cells/well to ensure all cell lines were in optimal growing conditions when exposed to the inhibitors.

The ability of the cells to maintain *MYC* knockdown for 5 days without refreshing the media with DOX, conditions which the cells would undergo during the screening, was further assessed to ensure *MYC*-silencing was maintained throughout the duration of the experiment. Due to time constraints, D425 was chosen to validate conditions for HTCS and taken as reference for the rest of the cell lines.

For *MYC* knockdown, NS, MYC2 and MYC3 shRNA constructs were cultured in the presence of DOX 24 hours prior to seeding. NS, MYC2 and MYC3 cultured in the presence and absence of DOX, were seeded and then cultured in media without puromycin, with puromycin, grown without puromycin and media refreshed, grown with puromycin and media refreshed with DOX (Figure 5.3). After 5 days cells were harvested and protein extracted to analyse MYC protein expression levels with Wes after being cultured in each condition (Chapter 2).

Wes quantification of MYC protein levels showed no major differences between conditions. *MYC* knockdown was maintained throughout the 5 days the experiment lasted. Furthermore, no major differences in MYC protein expression was seen between cells grown in the presence of DOX, with and without having DOX refreshed (Figure 5.3).

Results showed that puromycin did not causes differences in *MYC* expression and therefore it was decided that the best condition to run the HTCS under was to use puromycin free media when seeding cells into 384-well plates, and to refresh the *MYC* knockdown cells (which had been cultured in DOX 24 hours prior to seeding) with DOX at the time of plating avoiding further disturbance to the cells after addition of the compound library.

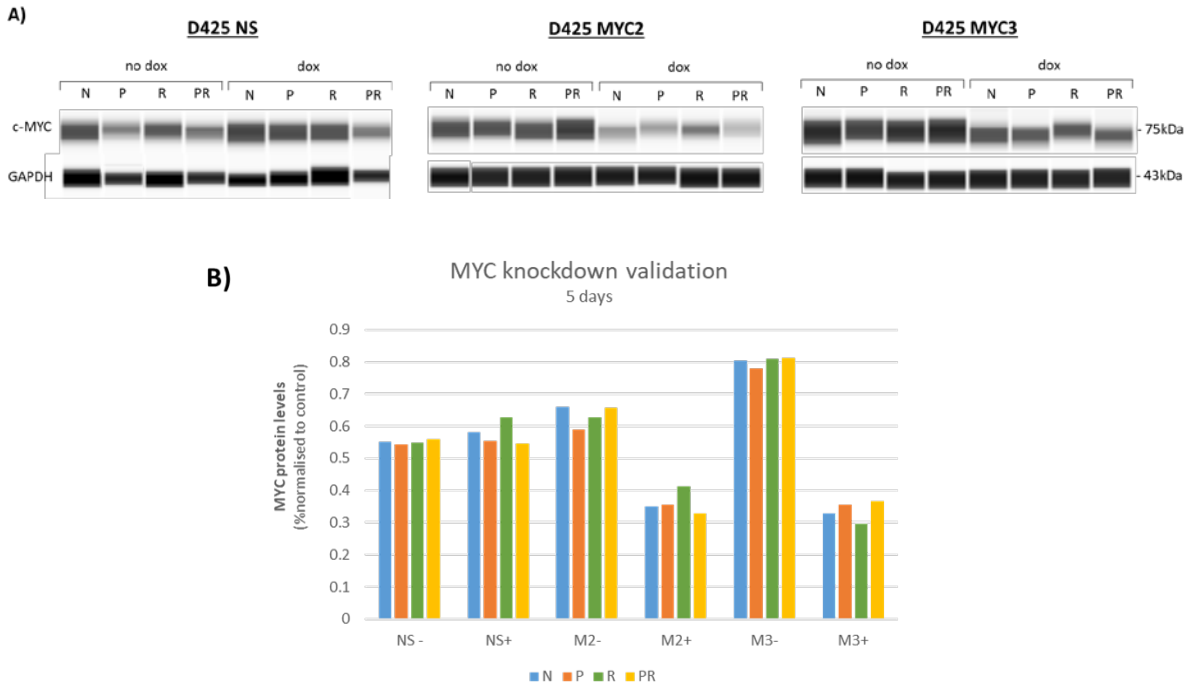

Figure 5.3. *MYC* knockdown validation for high throughput drug screening. A)Automated Western Blot image of c-MYC protein levels to optimise *MYC* knockdown conditions for HTCS. D425 NS, MYC2 and MYC3 shRNA constructs were cultured in the presence(dox) and absence(no dox) of DOX for *MYC* knockdown. Each condition was cultured without puromycin (N), with puromycin (P), grown without puromycin and media refreshed (R), grown with puromycin and media refreshed (PR), to check differences in expression of MYC protein. Cells were harvested and protein extracted after 5 days of culturing. GAPDH was used as internal control. B) Wes quantification analysis of MYC protein expression levels of each construct grown in a particular condition (N, P, R or PR). Data is shown as % of MYC protein expression normalised to protein levels of GAPDH expression.

5.3.1.2 Small molecule drug screen overview

To reach the maximum drug diversity without prejudice on the molecular mechanism of the drug, D425, D283 and HDMB03 were exposed to all three compound libraries available, which encompass a total of 581 drugs targeting a broad range of key signalling pathways in tumour biology.

HTCS at the ICR uses a 384-well screening approach where the process of liquid handling of inhibitor dilutions is done automatically in a Microlab STAR platform (Hamilton)(Methodology explained in Chapter 2). All three constructs of each *MYC* isogenic cell line, cultured in the presence and absence of DOX for *MYC* knockdown, were seeded in 384 well plates and exposed to a single-dose concentration per well of each inhibitor contained in each compound library (11-12, 13 and 14)(Figure 5.4). After a period of 5 days, cell viability was assessed with CTG reagent as explained in Chapter 2. NS, MYC2 and MYC3 shRNA constructs of each cell line were screened in triplicate, and data from replicate screens were combined in the final analysis (Campbell et al., 2016).

Luminescence measurements of cell viability from each compound library were processed through the ICR database (The Institute Cancer Research, London), producing an experiment report for preliminary evaluation of the results (described in Chapter 2). Prior to assessment of drug sensitivity effects in *MYC*-amplified MB_{Group3}, quality control (QC) values generated for each screen were checked to ensure the quality of the data produced.

Two measures were used as quality control metrics for replicate cell line samples: replicate reproducibility and a measure of overall distribution of the logged normalised luminescence values for the compounds (Cowley et al., 2014). The processing of the data through the ICR database calculates the Pearson correlation between all replicate samples, and a threshold of 75^{th} percentile of the correlation of all non-replicate pairs (0.6795) is used to fail individual replicate samples. The database uses the GenePattern module 'ReplicatesQC' to run these metrics and identify replicate samples to be removed (Campbell et al., 2018). Compound screen replicates are expected to be strongly correlated, therefore, pairs of replicates with correlation coefficient less than 0.7 were then rejected.

A further quality control parameter is the Z-prime (Z) value for each screen. Z scores provide a measure of the separation of the positive and negative control compounds included in the screen, and so can be considered an estimate of how much it is possible for the individual cell-treated wells to vary in Z-scores. Larger Z values indicate better screens. Screens with Z scores ≥0.5 are considered excellent. Those with Z values ≤0 are considered unusable and should be rejected and the experiments repeated. Only screens that passed the threshold of ≥0.3 were used for further analysis.

Data from reports not passing QC test, which meant screens with median Z scores ≤0.3, or presenting median correlation coefficients ≤0.7 between replicates, were excluded for further analysis and the screen repeated (Menon et al., 2019).

Plate	Replicate	Channel	Filename	Status	Replicate dynamic range	Average dynamic range	Repeatability standard deviation	Spearman rank correlation (min - max)
1	1	1	P1.txt	✓	7.23	7.31	0.18	0.79 - 0.91
1	2	1	P3.txt	✓	7.3	7.31	0.18	0.79 - 0.91
1	3	1	P5.txt	✓	7.4	7.31	0.18	0.79 - 0.91
2	1	1	P2.txt	✓	7.44	7.53	0.2	0.88 - 0.94
2	2	1	P4.txt	✓	7.55	7.53	0.2	0.88 - 0.94
2	3	1	P6.txt	✓	7.6	7.53	0.2	0.88 - 0.94

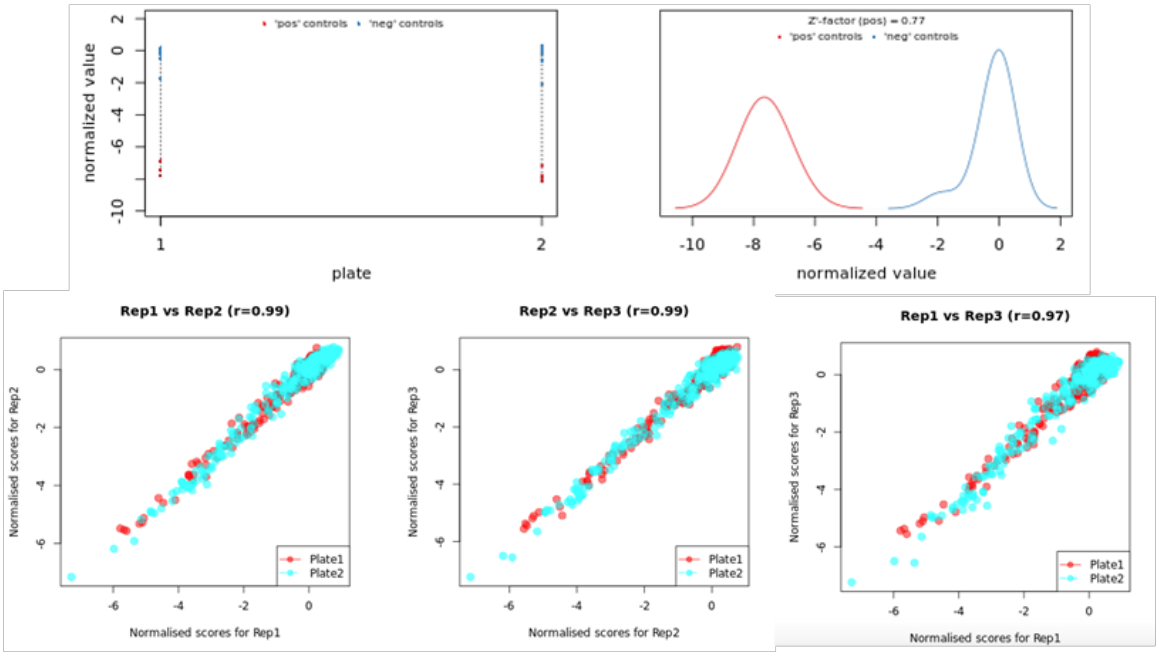

Figure 5.4. Results report from high-throughput compound screening. Example of an overview of a report produced by the processing of the luminescence readings through the in-house ICR data base. A) The report presents information about the replicate/average dynamic range, repeatability standard variation and calculation of the spearman rank correlation of replicates. B) visual representation of the dynamic range of each individual screen estimated with the Z score. C) Scatterplots showing correlation between replicates.

5.3.1.2.1 High-throughput compound screen results

With the processed luminescence readings, percentage of control (POC) survival values were generated, by normalising the raw CTG readings from each plate to the median signal of the negative controls (cells not exposed to small molecule inhibitors, DMSO only). Results were expressed as a proportion of viable (metabolically active) cells relative to the DMSO control (as an example, 0.5 indicates that cell numbers were reduced by 50% relative to the DMSO only control).

To better assess if drug sensitivity effects differed according to *MYC* expression levels (whether *MYC* knockdown by shRNA or not), screen analysis was focused only on data from D425, D283 and HDMB03 MYC2 constructs. Although drug sensitivity effects were consistent between MYC2 and MYC3 constructs, they were less pronounced in the MYC3 construct therefore in order not to generate false negatives we thought it was more appropriate to focus on results seen on MYC2 since it is the most efficient construct in knocking down *MYC* expression levels (see Chapter 3). Cells cloned with the NS shRNA construct were used as a negative control for the function of the shRNA and to determine the specific effects of the silencing constructs on the cell lines. Data from NS cell lines can be used to assess reproducibility of the data, to ensure the response to the drug was similar, if not the same, to those cloned with the MYC2 construct expressing high-levels of *MYC*.

5.3.1.3 Analysis of screen results

Remaining surviving fractions of cells after exposure to the compounds was scrutinised for candidate hit identification.

The diversity of compounds tested translated into a varied range of effects on the isogenic models. A few inhibitors displayed inconsistent effects across the dosing range, where surviving fractions increased and decreased regardless of increased concentrations of the inhibitor. Some compounds only had a growth inhibitory effect on one of the cell lines, others significantly reduced cell growth of 2 of the cell lines, and the rest had a consistent growth inhibitory effect across D425, D283 and HDMB03. The diversity of effects seen in the screen is exemplified in Figure 5.5.

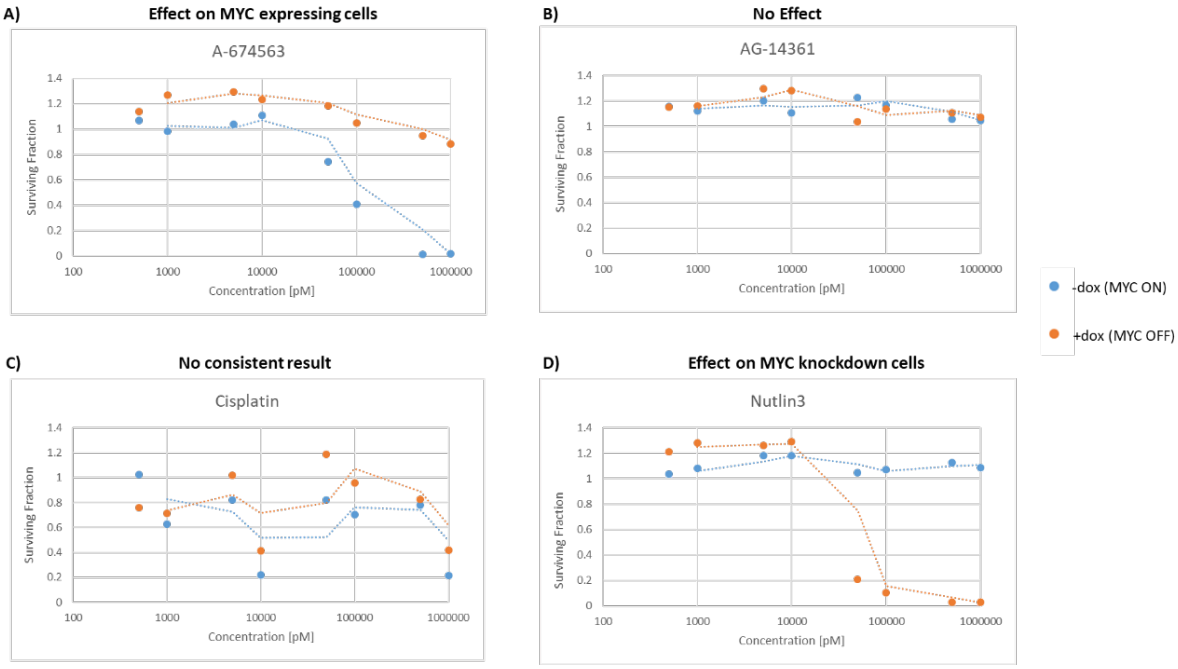

Figure 5.5. Examples of differential effects on isogenic cell line viability. Example of dose-response curves from surviving fractions of D425 MYC2 cells after drug exposures. Compounds tested on the screen elicited different effects on the cell lines; being specifically effective on *MYC* overexpressing A) or *MYC* knockdown cell lines D), not having a growth-inhibitory effect B), or showed inconsistent results C). Graphs show the different responses of D425 MYC2 expressing *MYC* [blue; -dox(MYC ON)] and with *MYC* knockdown [orange; +dox(MYC OFF)].

Compounds that had an inconsistent growth-inhibitory dose-dependent effect were generally excluded from the dataset. Only those inhibitors that were contained in all three compound libraries and therefore repeatedly tested trice across compound libraries were considered for revision. If the dose-dependent growth-inhibitory effect was only inconsistent in 1 out of the 3 libraries, the effect of the compound seen on that plate was removed, and only the effect on the other 2 libraries was considered. That particular compound was left for further analysis and the specific inconsistent effect observed in that one plate considered a mechanical discrepancy during robotic handling. Compounds presenting an inconsistent effect in 2 or 3 compound libraries were discarded and not considered for further analysis.

Of 581 inhibitors tested across the 3 compound libraries, 95 drugs were repeated in different plates, leaving a total of 457 unique small molecule inhibitors. We then sought to perform a one-on-one analysis approach of the 457 compounds, plotting dose-response curves to establish IC_{50}. Utilisation of the calculated IC_{50} to discern compound effectiveness was problematic. Despite some compounds causing a significant growth inhibitory effect across cell lines, a more resistant proportion of cells at high concentrations was seen for some of the constructs, translating into misleading results with each cell line having the same IC_{50} value when there was a clear difference in the proportion of surviving cells (Figure 5.6, A, B).

On the other hand, some inhibitors had no growth-inhibitory effect on one arm of the experiment. The inability of the compounds to cause 50% growth inhibition prevented the calculation of the IC_{50} concentration. The same problem was seen for those compounds to which the cell lines were extremely sensitive. Inhibitors causing equal decrease of surviving cell fraction in both *MYC* expressing and *MYC* downregulated arms increased the error margins when trying to fit a nonlinear regression curve with Prism, resulting in ambiguous IC_{50} results (Figure 5.6, C).

To ease the automation process with a Microlab star platform (Hamilton), inhibitors contained in the compound libraries are all screened in the same concentration range, which does not account for the optimal concentration range for each individual compound. Not considering the pharmacokinetic properties of each particular compound translated into some of them not killing 50% of cells at the highest dose, indicating that the range used in the screen was not the correct one to determine the IC_{50} on our cell lines. In this regard, compounds of Library 13 were only tested at 4 different concentrations, resulting in some cases in error margin too large to calculate an IC_{50} reliably.

Considering all these variables that could impair the analysis, we decided that it was optimal not to directly use the IC_{50} values calculated from the surviving fractions of cells from the screen. To ensure to most accurate identification of compounds of interest, the remaining surviving fraction of cells at every concentration was considered to establish the growth inhibitory effect the compounds had on the cell lines. A threshold of 50% growth inhibition was chosen to deem compounds to have an effect, and therefore be ‘effective’, to truly capture differences in drug sensitivity.

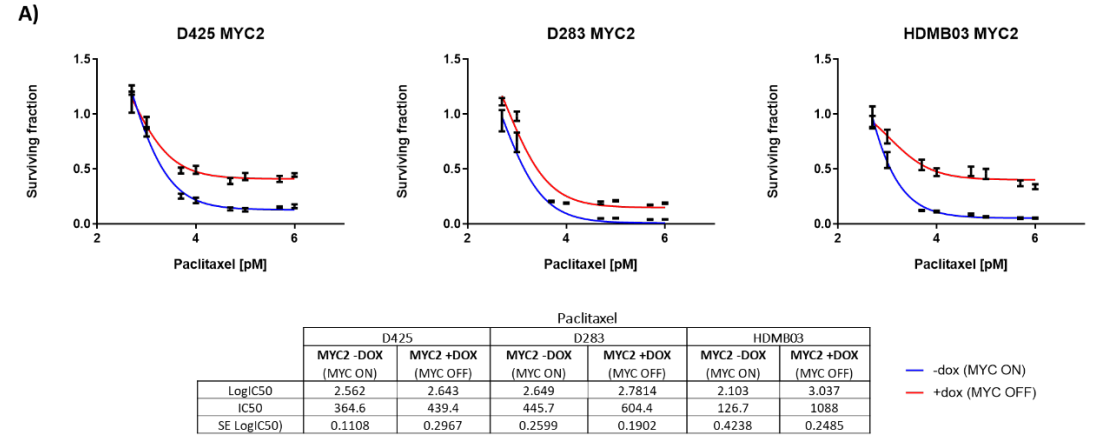

Paclitaxel

	D425		D283		HDMB03	
	MYC2 -DOX (MYC ON)	MYC2 +DOX (MYC OFF)	MYC2 -DOX (MYC ON)	MYC2 +DOX (MYC OFF)	MYC2 -DOX (MYC ON)	MYC2 +DOX (MYC OFF)
LogIC50	2.562	2.643	2.649	2.7814	2.103	3.037
IC50	364.6	439.4	445.7	604.4	126.7	1088
SE LogIC50)	0.1108	0.2967	0.2599	0.1902	0.4238	0.2485

-dox (MYC ON)
+dox (MYC OFF)

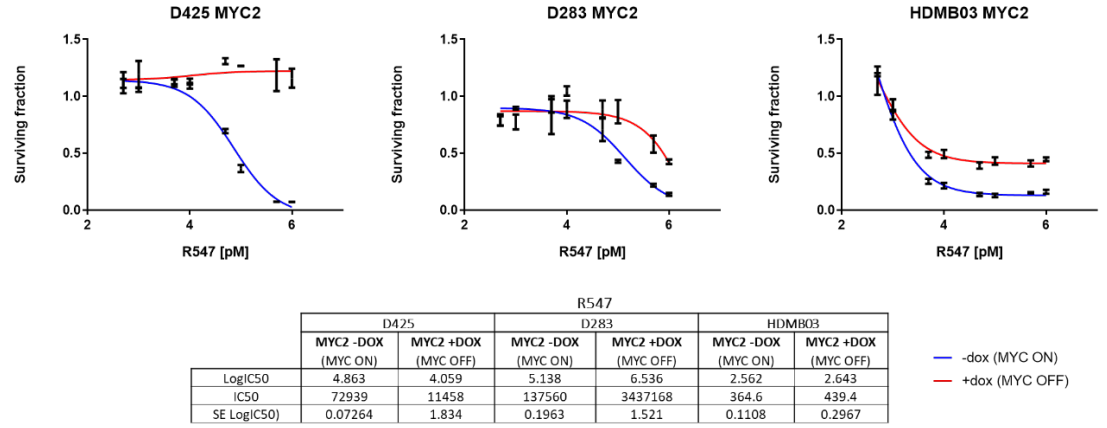

R547

	D425		D283		HDMB03	
	MYC2 -DOX (MYC ON)	MYC2 +DOX (MYC OFF)	MYC2 -DOX (MYC ON)	MYC2 +DOX (MYC OFF)	MYC2 -DOX (MYC ON)	MYC2 +DOX (MYC OFF)
LogIC50	4.863	4.059	5.138	6.536	2.562	2.643
IC50	72939	11458	137560	3437168	364.6	439.4
SE LogIC50)	0.07264	1.834	0.1963	1.521	0.1108	0.2967

-dox (MYC ON)
+dox (MYC OFF)

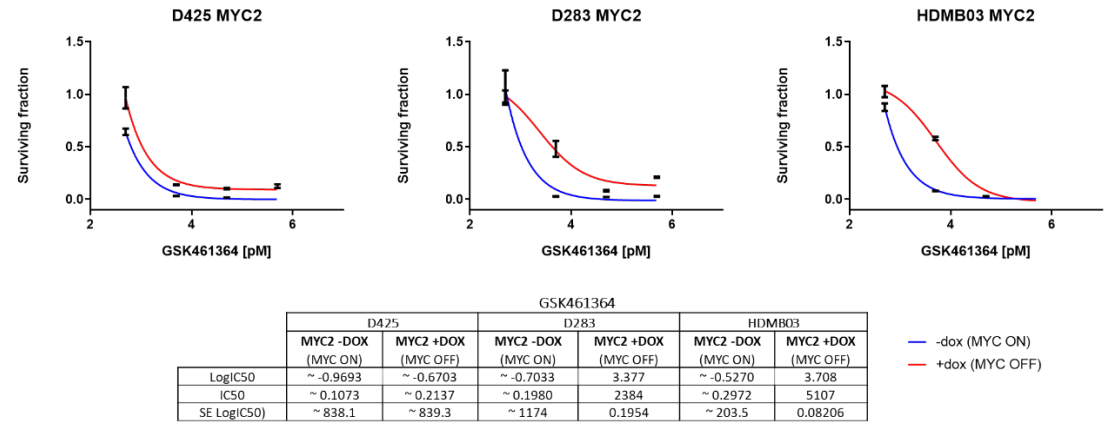

GSK461364

	D425		D283		HDMB03	
	MYC2 -DOX (MYC ON)	MYC2 +DOX (MYC OFF)	MYC2 -DOX (MYC ON)	MYC2 +DOX (MYC OFF)	MYC2 -DOX (MYC ON)	MYC2 +DOX (MYC OFF)
LogIC50	~ -0.9693	~ -0.6703	~ -0.7033	3.377	~ -0.5270	3.708
IC50	~ 0.1073	~ 0.2137	~ 0.1980	2384	~ 0.2972	5107
SE LogIC50)	~ 838.1	~ 839.3	~ 1174	0.1954	~ 203.5	0.08206

-dox (MYC ON)
+dox (MYC OFF)

Figure 5.6. Examples of misleading results from direct IC_{50} calculation. Dose-response curves of surviving fractions of D425, D283 and HDMB03 MYC2 cells after drug exposures from the screen. The graphs show the different growth inhibitory effect of A) Paclitaxel, B) R547 and C) GSK-461364 on *MYC*-overexpressing (blue; -dox [MYC ON]) and *MYC* silenced (red; +dox [MYC OFF]) cells. A) A resistant proportion of cells was seen after treatment with Paclitaxel at higher doses, but IC_{50} calculated between arms was the same, not reflecting the true difference between sensitivity. B) Treatment with R547 did inhibit the growth of D425 cells with *MYC* knockdown, nonetheless, a higher IC_{50} was calculated for the *MYC* expressing arm. C) Exposure to GSK-461364 caused an equal drop in surviving fractions of *MYC*-expressing and *MYC*-knockdown cells, which increased the error margins in Prism, preventing the calculation of reliable IC_{50}. Curve is presented as log(concentration) vs response.

Among all 457 drugs tested, 76.1% of compounds elicited low or no effect across cell lines (growth inhibition <50%). A total of 137 compounds displayed 50% growth inhibition at at least one concentration across D425, D283 and HDMB03 (Figure 5.7).

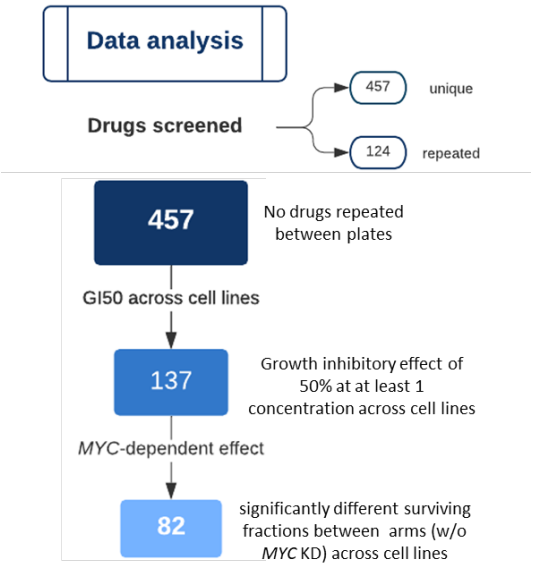

Figure 5.7. High throughput drug screen data analysis. Schematic summary of hit identification process from the high-throughput small compound chemosensitivity screen. Normalised data from D425, D283 and HDMB03 MYC2 MB_{Group3} cell lines was processed and filtered to identify drugs that presented a *MYC*-dependent effect, by causing differences in growth between cell lines overexpressing *MYC* and with *MYC* knockdown. Data from MYC2 constructs of each cell line was considered for hit identification.

Drugs contained in the compound libraries are annotated with information regarding their main target or their inhibitory mechanism of action, which was used to classify the inhibitors identified. The MB cell lines displayed particular sensitivity to compounds targeting the 20S core particle of the proteasome (3/3 20S proteasome inhibitors screened), polo-like kinases (4/4 PLK inhibitors screened), WEE1 (3/3 WEE1 inhibitors screened), β-tubulin for microtubule formation (11/12 β-tubulin inhibitors screened) and aurora kinases (10/11 AURK inhibitors screened)(Figure 5.8).

With the objective to identify inhibitors that could be used against *MYC*-dependent tumours, we focused the analysis on finding differential drug sensitivity effects depending on *MYC* expression levels. *MYC*-dependent effects were identified by pairing POC scores of normalised triplicate data of each construct according to the presence and absence of DOX in the media. Significant differences between *MYC* expressing and *MYC* silenced cells were established with student's t-test ($p \leq 0.05$).

From those compounds identified to cause cell growth inhibition of 50% across the isogenic MB lines, 82 compounds displayed a significant difference between the surviving fractions of *MYC* expressing and *MYC* downregulated cell lines at two or more concentrations. These 82 compounds were considered as potential 'hits' (Figure 5.7).

The comparison of the numbers of effective compounds on the isogenic lines and those displaying a differential growth inhibitory effect according to *MYC* expression levels served to show that not all inhibitors tested targeting components of the cell cycle machinery displayed differential growth inhibition between MB cells expressing *MYC* and those with *MYC* knockdown. This confirmed the notion that the 82 compounds that presented a MYC-dependent effect according to the criteria were so due to their relationship with *MYC* expression and not solely because cell proliferation and DNA replication was impaired.

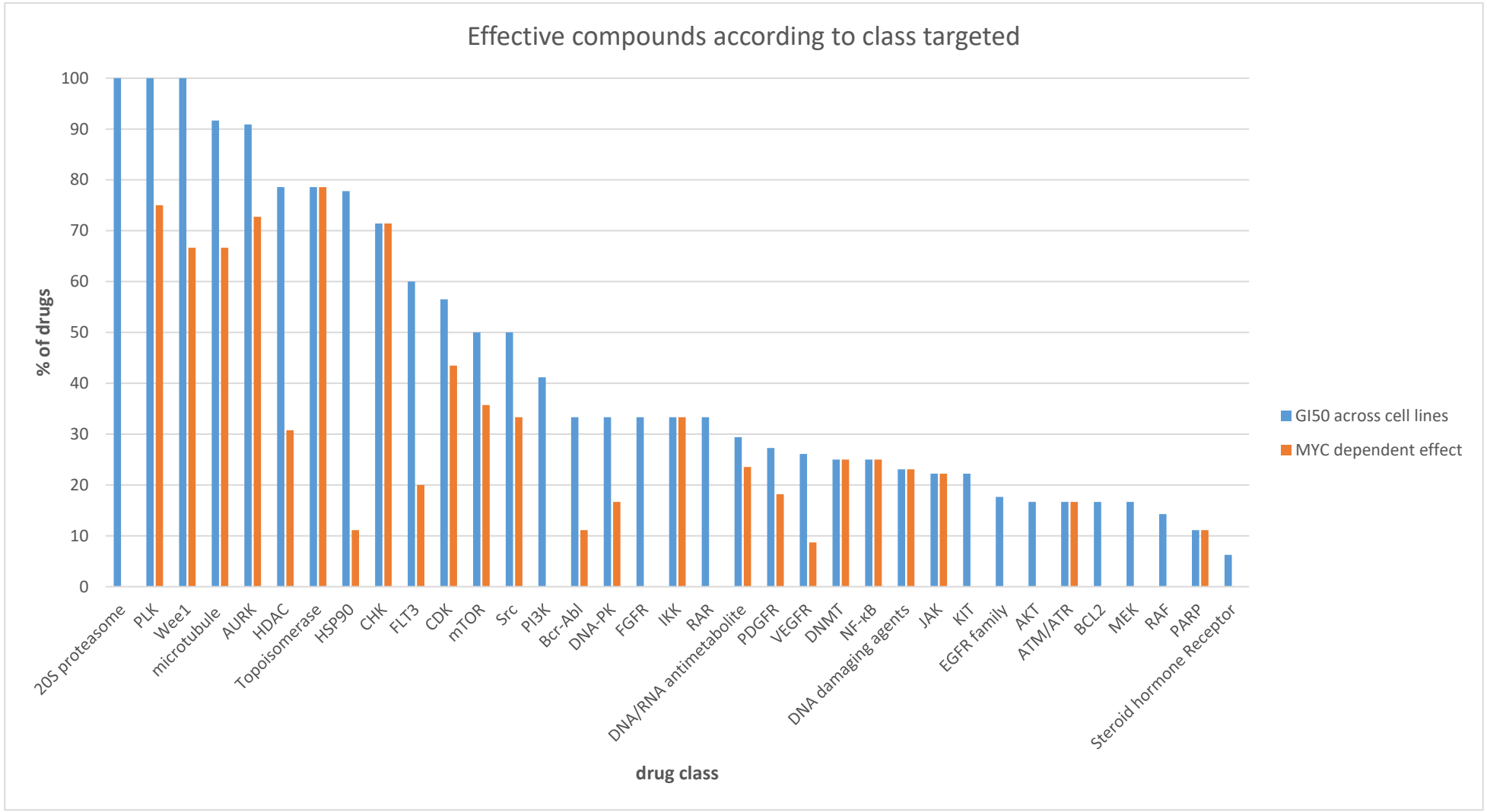

Figure 5.8. Percentage of effective inhibitors on medulloblastoma cell lines. The graph shows the percentage of compounds causing a growth-inhibitory effect of 50% (blue; GI_{50} across cell lines) and those having a differential effect between cells overexpressing *MYC* and with *MYC* knockdown (orange; *MYC*-dependent effect). Percentage of compounds displayed corresponds to the total of screen compounds targeting that specific class.

5.3.1.3.1 Mechanism of action of MYC*-dependent hits*

This approach identified 82 drugs causing significantly increased growth inhibition in *MYC* expressing cells when compared to cells with *MYC*-silenced with shRNA. No drugs showed a consistent increased growth inhibition of *MYC* silenced cells compared to *MYC* expressing cell lines. When classified according the compounds inhibitory target, a large number of the 82 drugs deemed as hits were found to act by inhibiting DNA synthesis or chromosomal replication (Figure 5.9).

Not all compounds inhibited a single class of targets. 11 compounds had multiple targets belonging to different classes. Each of the classes targeted by compounds inhibiting multiple molecules were considered for the classification of the compounds by their mechanism of action. This meant that one single compound could be classified in several classes. For example, the compound JNJ-7706621 inhibited CDK1/2 and AURKA/B, and therefore classified as targeting CDKs and AURKs. With this approach, we wanted to ensure the most accurate accountability of all the molecules inhibited by the compounds deemed as hits, and to prevent overlooking specific targets.

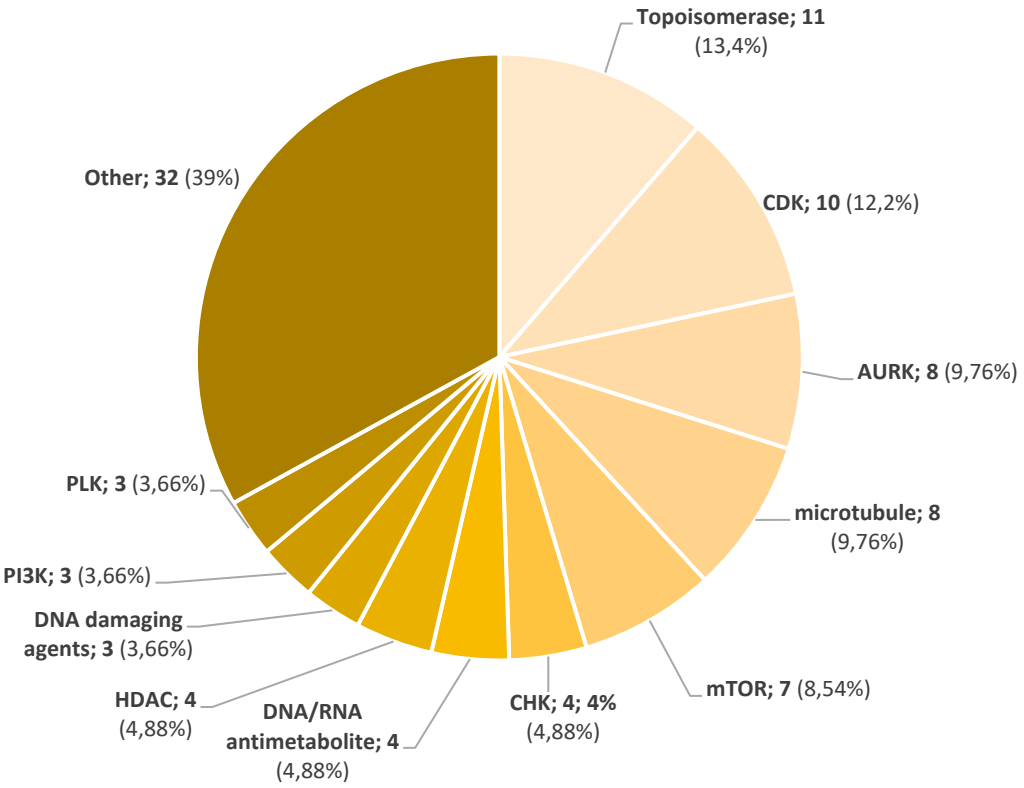

Figure 5.9. Mechanism of action/target of hits identified. Pie chart of the target/main mechanisms of action of the 82 compounds that met the established criteria and showed a *MYC*-dependent effect. Values shown corresponds to the number of compounds inhibiting that specific target and their percentage of the total of 82 drugs identified. .

When grouped according to the biological function of the mechanisms targeted, from the 82 compounds, 11 targeted topoisomerases, comprising 78.6% of all drugs screened targeting this particular enzyme (Table 5.1). Taking into consideration specific targetable molecules, 10 CDK and 8 microtubule inhibitors (comprising 43.5% and 66.7%, respectively, of total drugs targeting that particular class) had greater effect on *MYC*-overexpressing cell lines. In general, compounds targeting β-tubulin and microtubule formation had a greater effect on cells expressing high levels of *MYC* (66.7% of all microtubule inhibitors; 8/12) (Table 5.1).

8 inhibitors targeting aurora kinases caused significant cell killing on *MYC*-overexpressing cells when compared to their counterparts with *MYC* knockdown (72.7% of total of compounds targeting AURK). A similar effect was seen with inhibitors targeting checkpoint kinases, comprising 71.4% of total of compounds screened inhibiting CHK. 3 out of 4 PLK inhibitors tested on the screen were deemed as hits, composing 75% of the total. Only 7 drugs out of 16 targeting mTOR (43.8% of total) were found to have a *MYC*-dependent effect (Table 5.1).

Within all libraries, there was only 1 inhibitor targeting each of the following molecules, CNDAC, farnesyltransferase, Gli, NAE, PAK and ribonucleotide reductase, that caused greater growth inhibition on *MYC*-overexpressing cells. Due to small numbers, more compounds inhibiting these specific components should be tested to see if the effects seen were due to the inhibited target or selective toxicity of the drugs. Therefore, despite their efficacy, they were not considered for further studies.

As said previously, one of the advantages of using the compound libraries available at the ICR is the presence of conventional therapeutics in addition to targeted agents. Classification of the 82 compounds according to them being conventional or non-conventional therapeutics, gave a list of 20 compounds used in conventional cancer treatment, and 62 small molecule targeted agents. Inhibitors were then ranked by the number of statistically different concentrations between cells overexpressing *MYC* and with *MYC* knockdown ($p<0.05$). The ranked list of top 20 compounds for each category can be seen in Table 5.2.

Class	n^0 hits	TOTAL	% from total
ALK	1	2	50
ATM/ATR	1	6	17
AURK	8	11	72,7
Bcr-Abl	1	9	11
CDK	10	23	43,5
CHK	4	7	57,1
CLK	1	2	50
CNDAC	1	1	100
DNA damaging agents	3	13	23,1
DNA/RNA antimetabolite	4	17	23,5
DNA-PK	1	6	16,7
DNMT	1	4	25
farnesyl transferase	1	1	100
FLT3	1	5	20
Gli	1	1	100
HDAC	4	14	28,6
HSP90	1	9	11
IKK	1	3	33
JAK	2	9	22
kinesin spindle protein	1	2	50
MET	1	2	50
microtubule	8	12	66,7
Mps1	1	2	50
mTOR	7	16	43,8
NAE	1	1	100
NF-κB	1	4	25
PAK	1	1	100
PARP	1	9	11,1
PDGFR	2	11	18,2
PDK	1	2	50
PI3K	3	17	18
PLK	3	4	75
Ribonucleotide reductase	1	1	100
Src	2	6	33,3
Topoisomerase	11	14	78,6
Tropomyosin receptor kinase A	1	1	100
VEGFR	2	11	18
Wee1	2	3	67

Table 5.1. Summary of total number of hits grouped according to their main mechanism of action or target. Hits identified to have greater growth inhibition on D425, D283 and HDMB03 MYC2 than their counterparts with *MYC* knockdown, were classified according to their mechanism of action and the total count (n^0 hits) was compared to all compounds screened inhibiting that particular biological mechanism/target (total) to create a percentage of the total (% from total).

A)

TARGETED AGENTS		
Compound	**Target**	**Class**
BI-2536	PLK1	PLK
Dinaciclib	CDK2/5/1/9	CDK
AZD7762	CHK1/2	CHK
AZD8055	mTOR	mTOR
BMS-265246	CDK1/2	CDK
SB 743921	kinesin spindle protein	KSP
Epothilone B	β-tubulin	microtubule
MLN-4924	NEDD8-activating enzyme	NAE
VX-970	ATR	ATM/ATR
BMN-673	PARP1	PARP
GSK-2334470A	PDK1	PDK
PF-04691502	PI3K/mTOR	PI3K
PF-03814735	AURKA/B	AURK
PF-00477736	CHK	CHK
Sapacitabine	CNDAC	CNDAC
Torin	mTOR1/2	mTOR
PIK-75	p110α, DNA-PK	PI3K / DNA-PK
Flavopiridol	CDK1/2/4/6/9	CDK
PP121	PDGFR, mTOR, VEGFR2, Src, Abl	Bcr-Abl/mTOR/PDGFR/Src/VEGFR
SNS-032	CDK2/7/9	CDK

B)

CONVENTIONAL THERAPEUTICS		
Compound	**Target**	**Class**
Paclitaxel	β-tubulin	microtubule
Gemcitabine	nucleoside analog	DNA/RNA antimetabolite
SN-38	topoisomerase I	Topoisomerase
Camptothecin	topoisomerase I	Topoisomerase
Docetaxel	β-tubulin	microtubule
Vinorelbine	β-tubulin	microtubule
Mitoxantrone	topoisomerase II	Topoisomerase
Daunorubicin	topoisomerase II	Topoisomerase
Decitabine	DNA methyltransferase (DNMT)	DNMT
Epirubicin	topoisomerase II / DNA intercalation	Topoisomerase / DNA damaging agents
Doxorubicin	topoisomerase II / DNA intercalation	Topoisomerase / DNA damaging agents
Etoposide	topoisomerase II	Topoisomerase
Irinotecan	topoisomerase I	Topoisomerase
Nocodazole	β-tubulin	microtubule
Pirarubicin	topoisomerase II	Topoisomerase
Topotecan	topoisomerase I & II	Topoisomerase
Cladribine	adenosine deaminase	DNA/RNA antimetabolite
Clofarabine	ribonucleotide reductase	DNA/RNA antimetabolite
Idarubicin	topoisomerase II	Topoisomerase
Vinblastine	β-tubulin	microtubule

Table 5.2. Top 20 targeted agents and conventional therapeutics with a *MYC*-dependent growth-inhibitory effect. The tables summarise the top 20 hits identified to have greater growth inhibition on D425, D283 and HDMB03 MYC2 than their counterparts with *MYC* knockdown, when classified according to their category of conventional therapeutics (table A) or targeted agents (table B). Tables show the name of the compound, their specific targets, and the class of molecules inhibited used for their classification.

5.3.1.3.2 Class-representative hits

Data analysis from the screen identified 82 inhibitors exhibiting a *MYC*-dependent effect, causing a greater proportional reduction on cell growth when used on *MYC* overexpressing cell lines. When drugs were classified by their main mechanism of action, several representatives fitted in the same category. To narrow down the list of hits for further validation, one compound representative of each class was selected for the analysis of possible targetable molecular pathways in MB_{Group3}.

For candidate selection, initially, to focus on novel targeted therapeutic avenues, standard chemotherapeutic drugs were excluded from the list. The remaining drugs were cross-referenced with drug-sensitivity data of D283, DAOY and ONS-76 MB cell lines available from the Cancer Genome Project, which has screened thousands human cancer cell lines with hundreds of compounds, making publicly available the characterisation of their sensitivity and drug response data (https://www.cancerrxgene.org/).

On top of the drug sensitivity data available, a compilation of evidence was performed for all candidate drugs. Main criteria looked for were availability of published data of the inhibitor being tested in MB or other brain tumours, the ability of the compounds to cross the blood-brain barrier (BBB), their current testing in clinical trials, alongside information of potential mechanistic links with *MYC* oncogene already established, to ensure the most accurate and relevant choice (information summarised in Table 5.4). Some of the references used can be seen in the Appendix 5.4. The list of candidate drugs for each molecular target can be seen in Table 5.3.

Compound	Class
VX-970	ATM / ATR
MLN8237	AURK
Milciclib	CDK
AZD7762	CHK
ML167	CLK
Crizotinib	c-MET / ALK
Sapacitabine	CNDAC
Satraplatin	DNA damaging agents
Gemcitabine	DNA/RNA antimetabolite
Tipifarnib	Ftase
JK184	Gli
Vorinostat	HDAC
SNX-5422	HSP90
DMX_2320	IKK

Compound	Class
SB 743921	kinesin spindle protein
Epothilone B	microtubule
CCT271850	Mps1
MLN-4924	NAE
Triptolide	NF-κB
PF-03758309	PAK
BMN-673	PARP
GSK-2334470A	PDK
BEZ-235	PI3K / mTOR
BI-2536	PLK
Triapine	RR
KX2-391	Src
SN-38	Topoisomerase
MK-1775	Wee1

Table 5.3. List of candidate drugs. List of representative compounds of each drug class for further validation. The 82 compounds having greater cytotoxic effect on *MYC* over-expressing cell lines compared to their counterparts with *MYC* knockdown, were grouped by their main mechanism of action and a representative for each drug class was chosen considering several sources of evidence and published data.

Compound	Class	MB	Brain	BBB	clinical trials	combination	MYC	CancerRxGene
VX-970	ATM / ATR	x	✓		✓	cisplatin		
AMG-900	AURK	✓	✓		✓		✓	
Barasertib	AURK	✓	✓			ABT-737	✓	
MLN8237	AURK	✓	✓	✓	✓	WEEi / sorafenib	✓	
PF-03814735	AURK	x	x				✓	
SNS-314	AURK	✓	✓			chemo drugs		
VX-680	AURK	✓	✓		✓	vincristine / cyclophosphamine/ cisplatin	✓	✓
PP121	Bcr-Abl / mTOR / PDGFR / Src / VEGFR	x	x					
AT7519	CDK	✓	✓				✓	✓
BMS-265246	CDK	x	x					
Dinaciclib	CDK	✓	✓		✓	anti-PD1 Ab / ABT-737		
Flavopiridol	CDK	✓	✓		✓			
LY2835219	CDK	✓	✓	✓	✓	Temozolomide		
Milciclib	CDK	✓	✓	✓	✓	topotecan / cytarabine	✓	✓
P276-00	CDK	x	x		✓	bortezomib		
Roscovitine	CDK	✓	✓	✓	✓	IR	✓	
SNS-032	CDK	x	✓			Celecoxib / SU 5416 / GM 6001		
JNJ-7706621	CDK / AURK	✓	✓	✓			✓	
AZD7762	CHK	✓	✓		✓	SN-38 / gemcitabine / IR	✓	✓
LY2603618	CHK	x	x		✓	gemcitabine / pemetrexed		
PF-00477736	CHK	*discontinued by Pfizer*						
SAR-20106	CHK	x	x		x			
PD407824	CHK / Wee1	x	x			cisplatin / gemcitabine		
ML167	CLK	x	x					
PF-02341066	c-MET / ALK	x	✓	x				✓
Sapacitabine	CNDAC	x	✓			seliciclib		

Compound	Class	MB	Brain	BBB	clinical trials	combination	MYC	CancerRxGene
Satraplatin	DNA damaging agents	✓	✓		✓			
Cladribine	DNA/RNA antimetabolite	x	x				✓	
Clofarabine	DNA/RNA antimetabolite	x	✓		✓			
Gemcitabine	DNA/RNA antimetabolite	✓	✓			pemetrexed / AZD1775 /	✓	✓
Hydroxyurea	DNA/RNA antimetabolite	✓				IR		
decitabine	DNMT	✓		✓		Abacavir / Phenylbutyrate / IR		
Tipifarnib	Ftase	x	✓				✓	✓
JK184	Gli	✓	✓				✓	
Belinostat	HDAC	✓	✓		✓		✓	
JNJ-26481585	HDAC	✓	✓					
Mocetinostat	HDAC	✓			✓			
Vorinostat	HDAC	✓	✓	✓			✓	✓
SNX-5422	HSP90	x	✓		✓			
DMX_2320	IKK							
AT9283	JAK / AURK	✓	✓		✓	dasatinib	✓	
lestaurtinib	JAK / FLT3 / TrkA	✓	✓		✓			✓
SB 743921	kinesin spindle protein	x	x		✓			
Docetaxel	microtubule	✓	✓		✓			✓
Epothilone A	microtubule							
Epothilone B	microtubule	✓	✓	✓	✓	IR	✓	✓
Nocodazole	microtubule	✓	✓				✓	
Paclitaxel	microtubule	✓	✓			Bazedoxifene		✓
salinomycin	microtubule	✓	✓		✓		✓	
Vinblastine	microtubule	✓	✓			carboplatin		✓
vinorelbine	microtubule	✓			✓	cyclophosphamide / bevacizumab/ temsirolimus		✓
CCT271850	Mps1	x	✓					
AZD8055	mTOR	✓	✓		✓			✓

Compound	Class	MB	Brain	BBB	clinical trials	combination	MYC	CancerRxGene
INK	mTOR							
Torin 1	mTOR	✓	x			SAG		
Torin 2	mTOR	✓	✓					✓
MLN-4924	NAE	x	✓		✓	IR		
Triptolide	NF-κB	✓						
PF-03758309	PAK	✓	✓	✓			✓	
BMN-673	PARP	x	✓		✓	Irinotecan/temozolomide/IR		✓
GSK-2334470A	PDK							
PIK-75	PI3K / DNA-PK	✓	✓				✓	
BEZ-235	PI3K / mTOR	✓	✓			cisplatin	✓	✓
PF-04691502	PI3K / mTOR	✓	x			PF-05212384		
BI-2536	PLK	✓	✓		✓	IR	✓	✓
BI-6727	PLK	✓	✓		initial testing	vincristine	✓	
GSK461364	PLK	✓	✓				✓	
Triapine	RR	x	x		✓	IR / cisplatin/doxorubicin		
KX2-391	Src	✓			✓			
camptothecin	Topoisomerase	✓	✓					✓
Daunorubicin	Topoisomerase					idarubicin		
etoposide	Topoisomerase	✓	✓		✓	IR		✓
Idarubicin	Topoisomerase	✓			✓			
Irinotecan	Topoisomerase	✓			✓	temozolomide / Bevacizumab		
Mitoxantrone	Topoisomerase	✓				cyclophosphamide		✓
Pirarubicin	Topoisomerase	✓	✓			cyclophosphamide / 5'Fluoracil		
SN-38	Topoisomerase	✓	✓	✓			✓	✓
Topotecan	Topoisomerase	✓	✓		✓	temozolomide / cyclophosphamide		✓
Doxorubicin	topoisomerase / DNA damaging agents	✓	✓			cytoxan / adriamycin / vincristine / MS-275		✓
sunitinib	VEGFR / PDGFR	✓				FTase inhibitors		✓

Compound	Class	MB	Brain	BBB	clinical trials	combination	MYC	CancerRxGene
Epirubicin	topoisomerase / DNA damaging agents	✓						✓
MK-1775	Wee1	✓	✓	✓		Cisplatin / irinotecan / temozolomide	✓	✓

Table 5.4. Information used to select class-representative hits.A thorough research on published data of all 82 compounds having a *MYC*-dependent effect was performed in order to select a compound to represent each targeting molecular mechanism. The table summarises the information looked for each compound: evidence of its use in medulloblastoma (MB) or other brain tumours (Brain); evidence of its ability to cross the brain blood barrier (BBB); its use in clinical trials (clinical trials) or if it has been tested in combination with other agents (combinational strategies); potential mechanistic links with *MYC* oncogene (MYC), and sensitivity of MB cell lines published on the CancerRxGene (cancerRxGene) website. Data availability is denoted by ✓. Compounds selected are highlighted in yellow. IR, ionising radiation. C.D, chemotherapeutic drugs.

5.3.2 Determination of drug candidates for further validation

5.3.2.1 Integration of RNAseq and HTCS data sets

Through the analysis of *MYC*-dependent hits identified from the HTCS, a final list of 21 drugs, representative of each cellular mechanism, was created. To further reduce the list to specific candidates to validate genetically and phenotypically in our cell lines, integration of the results with further available in-house data sets was performed to decide which inhibitors would be taken forward for further validation.

From previous studies, the group had parallel RNAseq data available for all isogenic cell lines with *MYC*-modulated by shRNA, and primary MB tumour expression data from samples of known subgroups and known *MYC* status. Dr. Janet Lindsey (PBTG) performed the RNAseq analysis and compared the expression data from *MYC* isogenic cell lines to the expression data from primary tumours, using Gene Set Enrichment Analysis (GSEA) and ingenuity pathway analysis (IPA) to identify which gene sets overlapped (shared between cell lines and primary data; i.e. were upregulated in human Group 3 *MYC* amplified cells vs human Group 3 non-*MYC* amplified).

In brief, GSEA (http://software.broadinstitute.org/gsea/index.jsp) enables to distinguish statistically significant differences between predetermined gene sets of two experimental conditions. The leading-edge subset can be interpreted as the core group of genes that accounts for the gene sets' enrichment signal. For many gene sets the leading-edge genes overlap, therefore large changes in a relatively small number of genes give rise to most of the results, therefore allowing us to link changes in expression to specific regulators. In this study, this would allow the identification of those genes differentially expressed upon *MYC* knockdown.

RNAseq data collected on a cohort of 250 MB patients was used to perform the GSEA analysis. The patient cohort consisted of 83 females and 164 males, 29 of which had tumours which were MB_{WNT}, 54 MB_{SHH}, 40 MB_{Group3} and 105 MB_{Group4}. MB_{Group3} tumours from 7 male and 2 female patients showed evidence of *MYC* amplification. GSEA analysis against the Hallmark gene set database identified 8 gene sets that were positively enriched (FDR of <25%, 5 of which had a NOM (nominal) *p* value of <1%) in MB_{Group3} versus other MB subgroups (cohort of 250 primary MBs with no *MYC*-amplified status) and 24 gene sets that were negatively

enriched (FDR of <25%; 10 p<0.01). Comparing *MYC* knockdown in the cell lines to *MYC* expressing controls this analysis identified 16 gene sets that were positively enriched (11 p<0.01) and 15 gene sets that were negatively enriched (8 p<0.01)(analysis performed by Dr. Janet Lindsey; data provided by Dr. Shanel Swartz).

Genes categorised as *MYC* regulated in published datasets (where *MYC* expression is regulated or altered) were used to generate a list of '*MYC* target' genes (http://software.broadinstitute.org/gsea/msigdb/genesets.jsp?collection=H#). GSEA results showed the expected downregulation of this subgroup of genes. In contrast, the majority of *MYC* target genes were upregulated in MB_{Group3} primary samples.

Some examples of differential enrichment between gene sets, negatively enriched (downregulated) following *MYC* silencing and positively enriched (upregulated) in MB_{Group3} primary samples, were those involved in G_2-M checkpoints (important for DNA replication and cell proliferation), E2F targets (involved in the progression of the cells cycle and DNA replication) and *MTORC1* signalling (promoting cell growth and survival)(Figure 5.10).

On the other hand, *MYC* knockdown caused the upregulation in genes with a role in IL6-JAK-STAT3 signalling, hypoxia and epithelial to mesenchymal transition, where these gene sets were downregulated in MB_{Group3} primary samples and upregulated in the cell lines following *MYC* silencing (detail of results found is explained in Dr. Shanel Swartz PhD thesis).

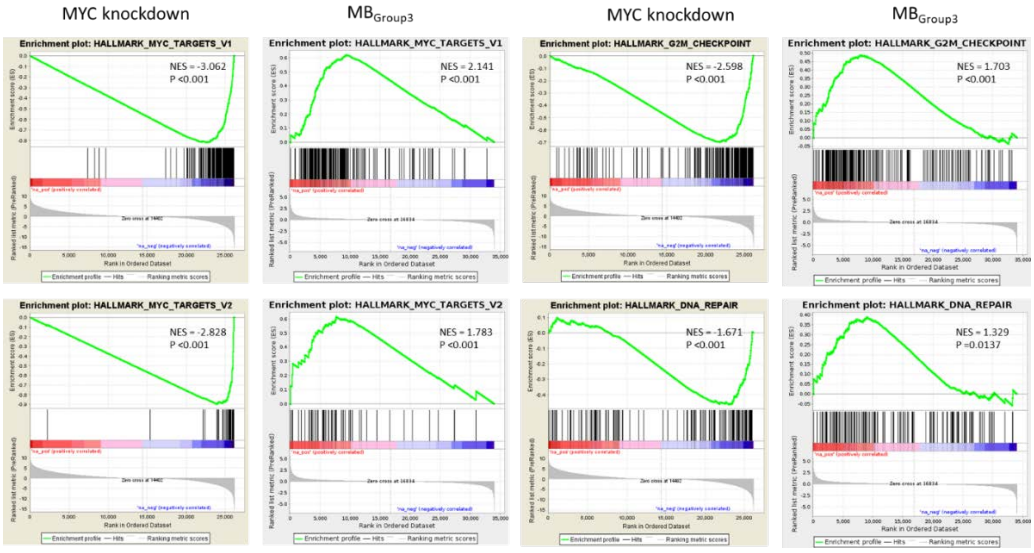

Figure 5.10. Selected hallmark GSEA enrichment plots of genetic pathways associated with MYC expression. GSEA enrichment plots of *MYC*, G_2-M checkpoint and DNA repair pathways positively or negatively enriched either in isogenic cell lines with *MYC* knockdown or in MB_{Group3} primary tumour gene sets. Data kindly provided by Dr. Janet Lindsey, PBTG, Unpublished.

Leading Edge Analysis (LEA) reveals core genes within the gene set that account for the gene set's enrichment signal, as well as genes that are overlapped among gene sets. The analysis focused on those genes shared between primary data and the *MYC*-regulable lines. LEA highlighted key genes whose expression drives the transcriptional changes seen, therefore indicating a critical role in the downstream effect of *MYC*.

Core genes highlighted in each differentially enriched gene set, between *MYC*-amplified MB_{Group3} primary samples and *MYC*-silenced with shRNA, were then overlapped with the classes of the 82 compounds identified to have a *MYC*-dependent effect. The main overlapping genes between data sets were *AURKA*, *AURKB*, *CDK4*, *PLK1*, *PLK4*, *CHK1*, *BIRC5*, *EZH2* and *ODC1* (PBTG, unpublished)(Figure 5.12).

In addition, ingenuity pathway analysis (IPA), a web-based computational software that analyses high throughput sequencing data to identify canonical pathways relevant to the gene set, was used to infer upstream regulators of the expression changes identified (www.qiagenbioinformatics.com/products/ingenuity-pathway-analysis).

GSEA gives a good indication of the downstream effects, however many drugs target upstream of *MYC*. On the other hand, IPA infers the possible upstream transcriptional regulators which can explain the observed gene expression changes. IPA was performed to identify new targets/candidate biomarkers of biological processes related to *MYC* within the context of Group 3 medulloblastoma. For the analysis, upstream regulators that had *MYC* in their network were selected. Top upstream regulators were *MYC*, β-estradiol, *CST5*, *BRD4* and *TP53* (Figure 5.11). The top networks associated with *MYC* expression were biological networks associated with cell cycle, metabolism, nervous system development and function, and processes related to cell replication (analysis performed by Dr. Janet Lindsey).

The integration of upstream regulators of the biological networks identified, with the class of compounds from the screen deemed as effective across the *MYC*-regulable cell lines, resulted in *MYC*, *EGFR*, *BRD4*, *DNMT3B* and mTOR as the set of upstream gene regulators targetable by drugs in the screen (Figure 5.11).

A)

TOP UPSTREAM REGULATORS		
Upstream regulator	***p*-value overlap**	**predicted activation**
MYC	7,98E-16	Inhibited
β-estradiol	3,36E-15	
CST5	1,34E-13	Activated
BRD4	3,08E-13	Inhibited
TP53	2,61E-12	Activated

B)

TOP NETWORKS	
ID Associated Network Functions	**score**
1. Cell Cycle, Developmental Disorder, Hereditary Disorder	36
2. Drug metabolism, Small Molecule Biochemistry, Cancer	36
3. Nervous System Development and Function, Visual System Development and Function, Nucleic Acid Metabolism	36
4. Developmental Disorder, Hereditary Disorder, Ophthalmic Disease	36
5. RNA Post-transcriptional Modification, DNA Replication, Recombination, and Repair, Dermatological Diseases and Conditions	33

Figure 5.11. Top upstream regulators from ingenuity pathway analysis. IPA analysis of expression changes following *MYC* knockdown in our 3 cell lines of interest showed several upstream regulators which overlapped with primary data (MB_{Group3} *MYC* amplified tumours compared to non-amplified MB).Table A) summarises the top 5 significant overlapping upstream regulators identified with IPA, with their *p*-value and predicted activation, whereas table B) shows the top 5 associated network functions (PBTG, Unpublished)

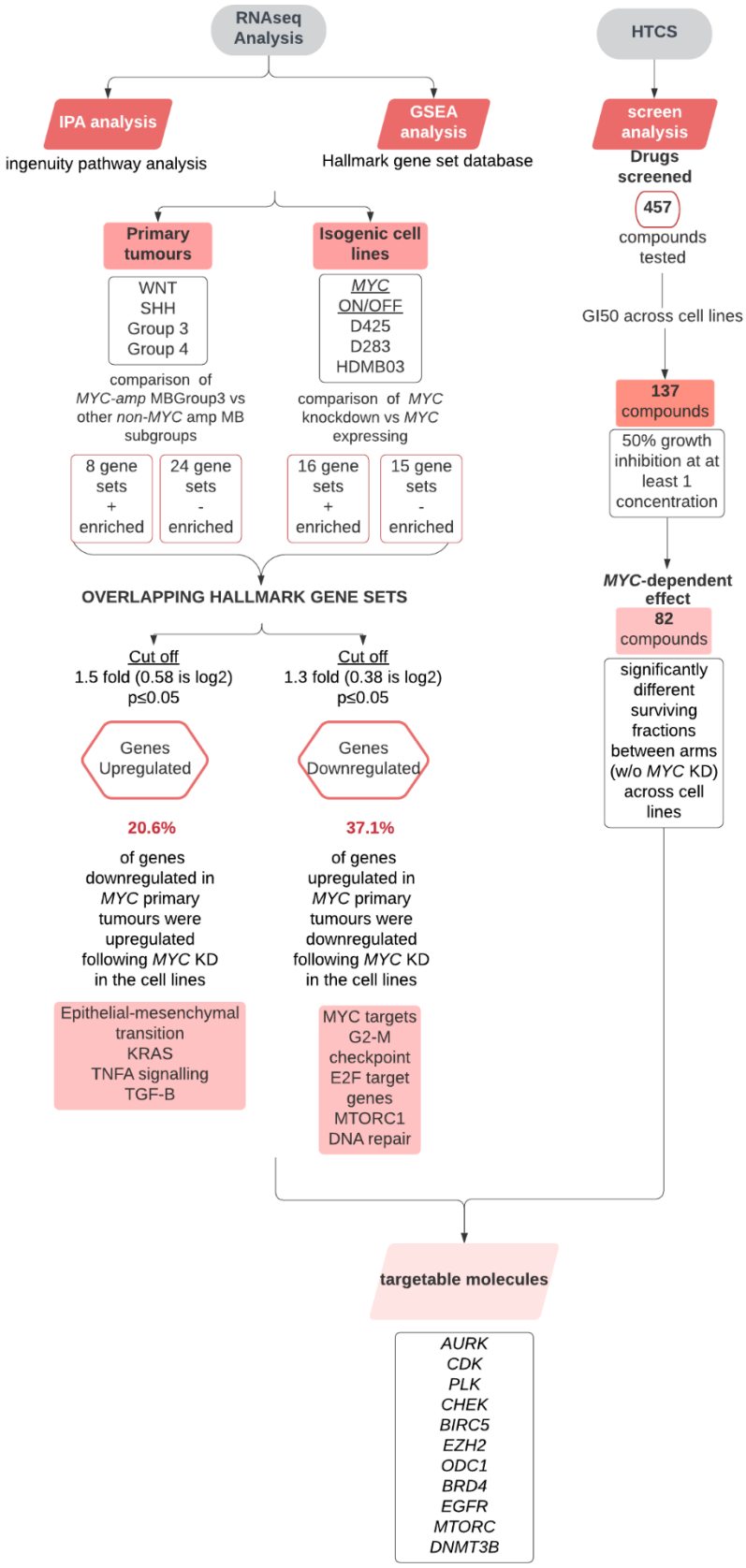

Figure 5.12. Integration of transcriptomic and high-throughput compound screen data sets. Flow diagram summarising the integrative approach of combining the transcriptomic (RNAseq) and compound screen (HTCS) data sets.

5.3.2.2 Medulloblastoma whole-genome CRISPR screen

The group also had available data from a whole-genome CRISPR screen done by Dr. Matthew Selby (PBTG, Newcastle) on a panel of MB cell lines, consisting of MB_{Group3} (D425, D283 and HDMB03) and non-MB_{Group3} (DAOY and G401) cell lines. CRISPR was performed to identify genetic dependencies associated with *MYC*, and common dependencies specific to MB_{Group3} (Selby et al., 2017).

In brief, the GeCKO screen (Shalem et al., 2014) consisted on infecting target cells with one sgRNA per cell, followed by puromycin selection and cells grown for 28 days, with genomic extractions at both 14 and 28 days (Figure 5.13). CRISPR screen causes gene knock outs (KO) rather than knockdowns, which completely removes gene expression. Gene KO was assessed by sequencing the sgRNA to see how the relative guide abundance alters compared to non-targeting controls. The output of CRISPR screening is the relative guide abundance counted by high-throughput sequencing. From these counts, the effect that a particular guide has on the cell can be inferred. If the sgRNA abundance increases compared to the non-targeting control, this implies that loss of the corresponding gene promotes growth, whereas if the sgRNA count decreases or disappears this infers the targeted gene is required for normal cell maintenance.

All CRISPR data must be compared to a baseline; the level of each sgRNA, following selection, at a point at which there has been insufficient time for a phenotypic effect. Baseline data was compared to day 14 and day 28. No-template controls (NTC) were present in the library as a control for normal growth and used to assess whether a particular sgRNA is more or less abundant than would be expected (whole-genome CRISPR screen and data analysis is described in Dr. Mathew Selby's PhD Thesis).

The GeCKO screen analysis was focused on MB_{Group3} vs non-MB_{Group3} cell lines, to identify MB_{Group3} specific genes, pathways and biological systems that are functionally important to MB_{Group3} (genes positively or negatively enriched when comparing MB_{Group3} to a non-*MYC* amplified control set of cells).

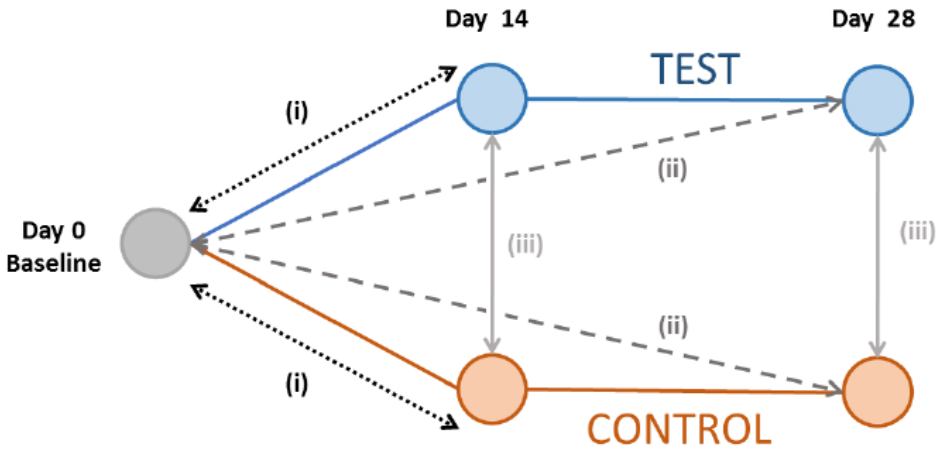

Figure 5.13. MB_{Group3} whole-genome CRISPR screen analysis overview. Schematic representation of the CRISPR screen layout. Cell lines used, MB_{Group3} (Test) and other (control), separated the data into two experimental arms. Analysis performed following the counting of data were (i-ii) the comparison of relative guide abundance to identify genes and pathways that differ between the baseline and day 14 and day 28 (MB_{Group3} and non- MB_{Group3} separately); and (iii) the comparison of relative guide abundance between MB_{Group3} and control counts on day 14 and day 28 to identify MB_{Group3}-dependent genes/pathways.) Image kindly provided by Dr. Mathew Selby (PBTG)

MAGeCK analysis (Li et al., 2014a) was used to perform pairwise tests to identify MB_{Group3}-dependent genes at days 14 and 28, by comparing positive and negative gene enrichment in MB_{Group3} lines vs the other (non-MB_{Group3}). Dr. Selby performed several comparisons, MB_{Group3} vs. baseline, other vs. baseline and MB_{Group3} vs. other (detail of the method can be found in Dr. Selby's PhD Thesis)

Analysis of results showed that at day 14, 1725 genes were enriched between MB_{Group3} and the baseline ($p \leq 0.01$), 1115 between Other and the baseline ($p \leq 0.01$) and 2812 between MB_{Group3} and the other cell lines ($p \leq 0.01$)(Figure 5.14, A). Of the genes altered, those highlighted in grey represent MB_{Group3}-dependent changes. At day 28, 1014 genes were enriched between MB_{Group3} and the baseline ($p \leq 0.05$), 1791 between other and the baseline ($p \leq 0.05$), and 1614 between MB_{Group3} and the other cell lines ($p \leq 0.01$). Of the genes that are altered those highlighted in grey represent MB_{Group3}-dependent changes (Figure 5.14, B)(data kindly provided by Dr. Selby).

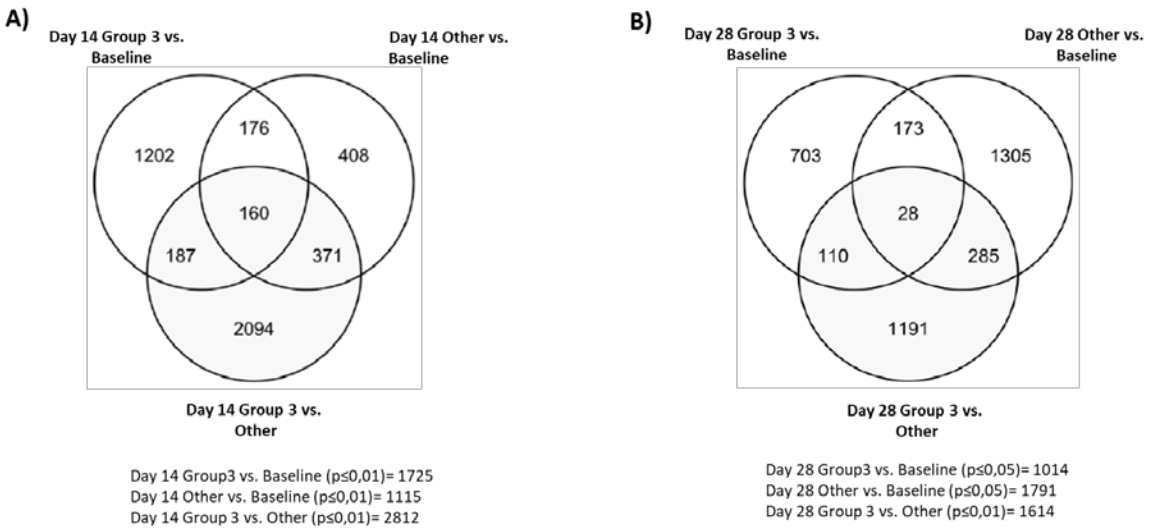

Figure 5.14. Summary of significant MB_{Group3}-dependent genes identified in the CRISPR screen. Venn diagram showing the overlap of significant genes between MB_{Group3} vs. baseline, control vs. baseline, and MB_{Group3} vs. control, at day 14 (A) and day 28 (B). Genes highlighted in grey are MB_{Group3}-dependent changes. Image and data kindly provided by Dr. Mathew Selby (PBTG)

Dr. Selby used a simple hallmark pathway library to illustrate the form of pathway results and outline some broad themes observed in the data. At day 14 and 28 the gene sets *MYC* targets, DNA repair, G_2-M checkpoint, E2F targets and MTORC signalling showed a reduction in guide abundance when compared to non-MB_{Group3} cells. Protein secretion was found to be significantly downregulated in the MB_{Group3} cell lines in a MB_{Group3}-dependent manner. Glycolysis, TGF-β signalling, IL2-STAT5 signalling and KRAS signalling were all enriched in the non- MB_{Group3} cell lines when compared to the baseline (Figure 5.15). In the hallmark analysis, the MB_{Group3}-dependent targets were only those that appeared significantly different in both arms of the screen with approximately 50% (16/35) of those pathways being identified as definitively MB_{Group3}-dependent (Dr. Mathew Selby, PhD thesis).

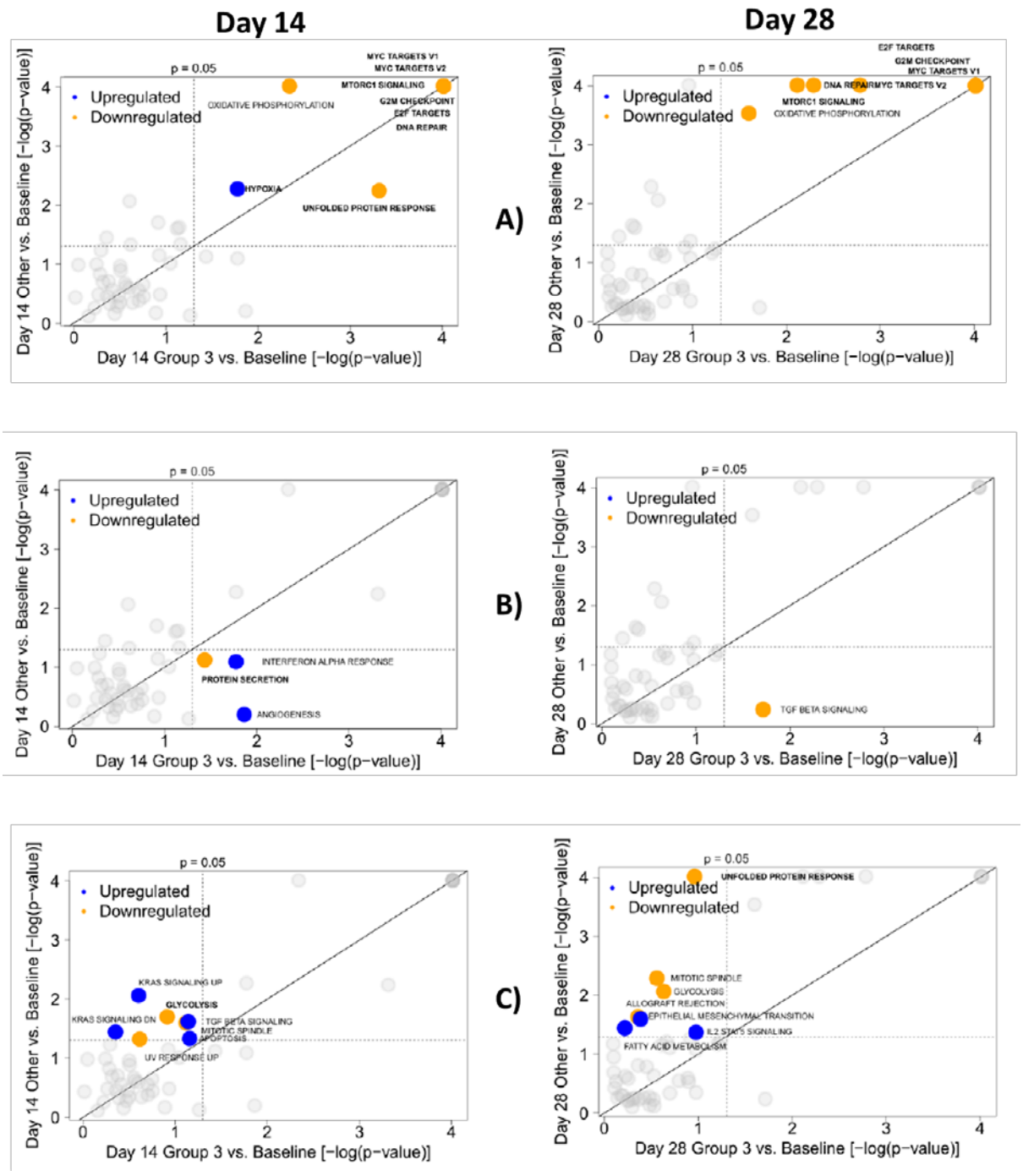

Figure 5.15. Summary of significant gene sets identified in MB_{Group3} or in non-MB_{Group3} of the CRISPR screen. Scatterplots summarising significant gene sets identified in the MB whole-genome CRISPR screen. A) Gene sets that are significant (p<0.05) in both MB_{Group3} and control. (B) Gene sets that are significant (p<0.05) in only the control. (C) Gene sets that are significant (p<0.05) in only the MB_{Group3} arm. Upregulated (blue): gene collections where knock outs cause an increase in relative guide abundance. Downregulated (orange): gene collections where knock outs cause a decrease in relative guide abundance. Pathways highlighted in bold are significant in MB_{Group3} vs. control (MB_{Group3}-dependent functionally). Data, analysis and image, done and kindly provided by Dr. Mathew Selby (PBTG).

5.3.2.3 Validation of results with whole-genome CRISPR screen

Targetable genes and signalling pathways identified through the integration of the RNAseq and HTCS data sets were cross-referenced with the MB CRISPR screen data to further validate the integrative approach taken (analysis performed with Dr. Lindsey and Dr. Selby's data).

MB_{Group3}-dependent genes identified by Dr. Selby in the CRISPR screen (genes positively or negatively enriched when comparing MB_{Group3} to non-*MYC* amplified control set of cells), showed significant overlap with those genes identified through the integration of expression and compound data which showed to vary depending on *MYC*-expression levels.

The same gene sets found to be negatively enriched in the CRISPR screen, mainly *MYC* targets, DNA repair, G_2-M checkpoint, E2F targets and MTORC signalling, were the same pathways identified through the GSEA analysis of expression data. The same overlap was seen for the IL2-STAT5 signalling pathway, which was identified in both data sets to be positively enriched and upregulated according to *MYC*-expression. A commonality found in regards of upstream regulators were genes like *BRD4*, which is widely known to play a pivotal role on *MYC* expression. Overall, the set of genes from these gene sets identified significantly overlapped with the main targetable molecules predicted to be effective in MB_{Group3}, through the integration of RNAseq and HTCS data. The significant overlap in the data provides confidence in the potential relationship these gene have with *MYC* expression and emphasises the potential targetable molecules identified to be therapeutically relevant in this subgroup of tumours.

Genes from the overlapping gene sets identified were further scrutinised by cross-referencing the results with the HTCS data. MB_{Group3}-dependent genes identified from the gene sets positively and negatively altered in the CRISPR screen at day 14 and 28, were cross-referenced with the class of compounds identified to have a *MYC*-dependent effect in the high-throughput screen. The process highlighted *EGFR*, *DNMT* and mTOR as common upstream regulators of *MYC* in MB_{Group3} cell lines, and PLK1, CHK1, AURKA/B and *BIRC5* were the top common genes with a downstream effect on MB_{Group3} cell lines.

Validation of the results from the integrative approach of combining RNAseq data with data from the high-throughput compound screen, with results from the whole-genome CRISPR screen, most strongly supported 6 molecular targets as potentially relevant in MB_{Group3} – *PLK*, *CHK, AURK*, mTOR, *CDK*, and *BIRC5* (common candidate *MYC*-dependent targets)(Figure 5.16).

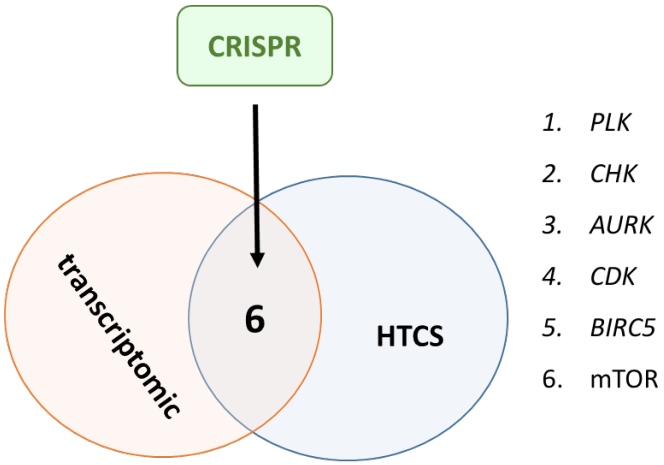

Figure 5.16. Validation of *MYC*-dependent results.Venn diagram summarising the 6 molecular targets identified through the integration of the RNAseq and HTCS data sets, that overlapped with the MB_{Group3}-dependent hits from the whole-genome MB CRISPR screen. HTCS=high-throughput compound screen; Transcriptomic=RNAseq; CRISPR=whole-genome CRISPR screen.

5.3.2.4 Revision of potential molecular targets in MB_{Group3}

Values of the surviving fractions from the list of 82 compounds identified to have a *MYC*-dependent effect on MB_{Group3} (Table 5.4) were revisited, to check the consistency of the findings from our integrative approach. The number of significant differences between treatment arms (*MYC* expressing and *MYC* silenced) of MYC2 constructs of each isogenic cell line was calculated to determine the 'hit' consistency of the inhibitors targeting the molecules identified by the integrative approach. All compounds targeting AURK, CDK, CHK and PLK showed a consistent *MYC*-dependent effect across cell lines, CHK and PLK inhibitors being the ones having greater growth-inhibitory effect on *MYC*-overexpressing cell lines compared to those with *MYC* knockdown. The total number of drug concentrations showing significant differences in the surviving fractions of D425, D283 and HDMB03 MYC2 expressing high-levels of *MYC* versus *MYC* knockdown for each compound is summarised in Table 5.5.

Compound	Target	Class	D425 M2	D283 M2	HDMB03 M2	Total
AMG	pan-AURK (A/B/C)	AURK	2	2	3	7
AT9283	JAK2/3, AURKA/B	AURK/ JAK	1	3	2	6
Barasertib	AURKB	AURK	1	3	2	6
MLN8237	AURKA	AURK	1	2	2	5
PF-03814735	AURKA/B	AURK	4	2	3	9
SNS-314	AURKA/B/C	AURK	1	2	3	6
VX-680	AURKA	AURK	2	2	2	6
AT7519	CDK1/2/4/6	CDK	2	2	2	6
BMS-265246	CDK1/2	CDK	3	4	5	12
Dinaciclib	CDK2/5/1/9	CDK	5	6	5	16
Flavopiridol	CDK1/2/4/6/9	CDK	3	2	3	8
JNJ-7706621	CDK1/2, AURKA/B	CDK/AURK	4	1	1	6
LY2835219	CDK4/6	CDK	1	2	1	4
Milciclib	CDK2	CDK	3	3	2	8
P276-00	CDK1/4/9	CDK	2	2	2	6
Roscovitine	CDK1/2/5	CDK	1	1	1	3
SNS-032	CDK2/7/9	CDK	1	3	4	8
AZD7762	CHK1/2	CHK	4	4	5	13
LY2603618	CHK1	CHK	2	2	2	6
PF-00477736	CHK	CHK	2	3	4	9
SAR-20106	CHK1	CHK	1	2	3	6
BI-2536	PLK1	PLK	7	5	6	18
BI-6727	PLK1	PLK	3	1	2	6
GSK461364	PLK1	PLK	2	2	2	6

Table 5.5. Consistency of *MYC*-dependent effect of AURK, CDK, PLK and CHK inhibitors in MYC2 MB_{Group3} cell lines.Summary table of the number of drug concentrations showing significant differences between D425, D283 and HDMB03 MYC2 expressing high-levels of *MYC* versus *MYC* knockdown for each compound. The table shows the compounds' main target and the class it belongs. The total number of significant drug concentrations between treatment arms (-/+dox) at a given concentration for each compound is summed for each cell line (D425 M2, D283 M2 and HDMB03 M2). The total number of significantly different concentrations between MYC2 cells expressing high-levels of *MYC* and with *MYC*-knockdown across cell lines is summed in the column total. Significant differences between HTCS treatment arms were calculated using the mean of triplicate data of surviving fractions (student's t-test ($p \leq 0.05$)).

Plotting of the surviving fractions of cells expressing high-levels of *MYC* and with *MYC* knockdown of the class-representative hits, revealed the *MYC*-dependent effect and showed the expected behaviour of the compounds. Some examples can be seen in Figure 5.17.

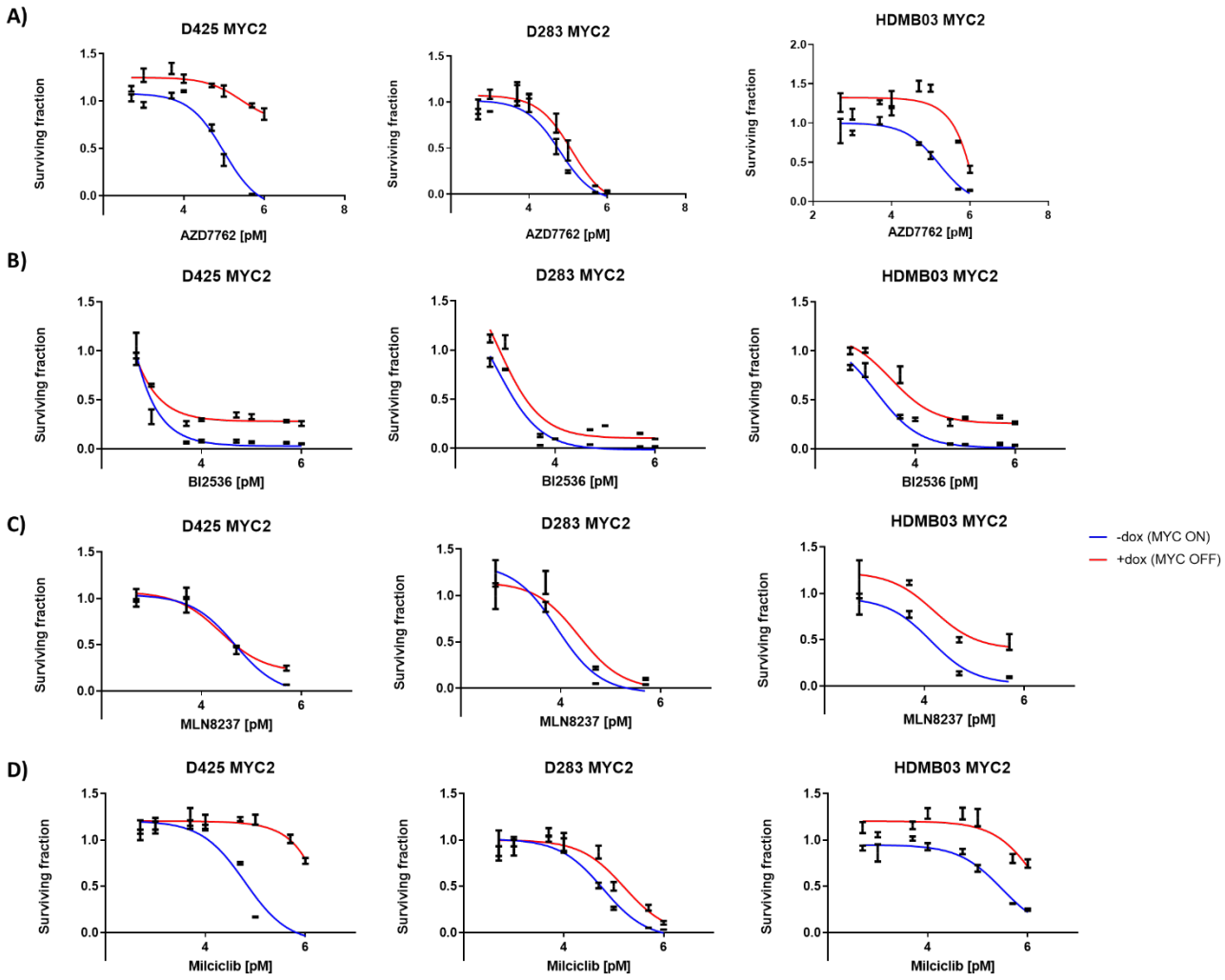

Figure 5.17. Example of growth-inhibitory curves from surviving fractions of D425, D283 and HDMB03 MYC2 cells. Dose-response curves of surviving fractions of D425, D283 and HDMB03 MYC2 cells after drug exposure to A)AZD7762 (CHK1 inhibitor), B)BI2536 (PLK1 inhibitor), C)MLN8237 (AURKA inhibitor) and D)Milciclib (CDK2 inhibitor).The graphs show the growth inhibitory effect of the inhibitors on D425, D283 and HDMB03 MYC2 overexpressing *MYC* (blue; -dox [MYC ON]) and with *MYC* silenced (red; +dox [MYC OFF]). Triplicate data of surviving fractions at each concentration from the screen was used to generate dose-inhibitory growth curves that fit a non-linear regression model. Curves are presented as log(concentration)vs response.

5.3.2.5 Candidate drug hit selection

Integration of expression data with results from the HTCS allowed the identification of several targets, such as *PLK*, *CHK, AURK*, *MTORC* and *CDK*, selectively effective in MB_{Group3}. Genes identified overlapped significantly with the main MB_{Group3}-dependent hits from the whole-genome CRISPR screen, which informed the decision to take compounds targeting these specific proteins forward for further validation.

The main goal of this project was to identify *MYC*-dependent signalling pathways to inform the design of new effective therapeutic strategies to selectively treat high-risk MB_{Group3} patients. Before the start of a clinical trial on a drug, extensive preclinical studies are needed to yield preliminary efficacy, toxicity, pharmacokinetic and safety information. These involve *in vitro* and *in vivo* experiments. Wide ranges of drug doses are tested in cell culture settings and using animal models, alongside studies of drug-target interactions and synergy studies.

To prioritise the best suitable candidates for progression to in vivo testing, and eventually taking the discoveries to clinical trial, the compounds representative of the drug classes PLK (BI2536 inhibitor), CHK (AZD7762 inhibitor), AURK (MLN8237 inhibitor) and CDK (Milciclib inhibitor) were chosen to further assess their *MYC*-dependency in vitro. Considering that the targeting of the mTOR signalling pathway with inhibitors had already been studied (Chapter 4.3), it was decided to focus further validation studies on the other molecular targets identified. The objective with this was to recapitulate the findings from the HTCS (*MYC*-dependency of compounds) in an alternative setting, to minimise false positives and further prove the validity of our results.

Through the compilation of evidence for the 82 candidate drugs, we realised that some compounds exhibiting a *MYC*-dependent effect on our cell lines, like the Wee1 inhibitor MK1775, had already been tested as means to target *MYC* in *MYC*-driven cancers (Restelli et al., 2018). Another compound exhibiting preferential sensitivity for *MYC*-overexpressing MB_{Group3} in the screen, the topoisomerase inhibitor SN-38, has been shown to synergise with the effect of CHK1 inhibitors (Xu et al., 2011), sensitising cells to chemotherapeutic agents and thus promoting apoptosis (McNeely et al., 2010, Zabludoff et al., 2008). Considering the combinatorial therapeutic potential of the drugs stated, we also considered them to further

assess their effects on a panel of MB cell lines (Figure 5.17, A and B), performed in the next chapter.

Since future work required the assessment of the *MYC*-dependent effect of the prime candidate inhibitors identified from the HTCS data analysis, a control drug (the *BIRC5* inhibitor YM155) with equal effect on both arms of the HTCS experiment was also chosen (Figure 5.18, C). In addition, integrated analysis identified *BIRC5* as a promising targetable molecule in *MYC*-driven Group 3 MB, which supports its further testing in a panel of *MYC* amplified/non-amplified MB cell lines (investigated in Chapter 6).

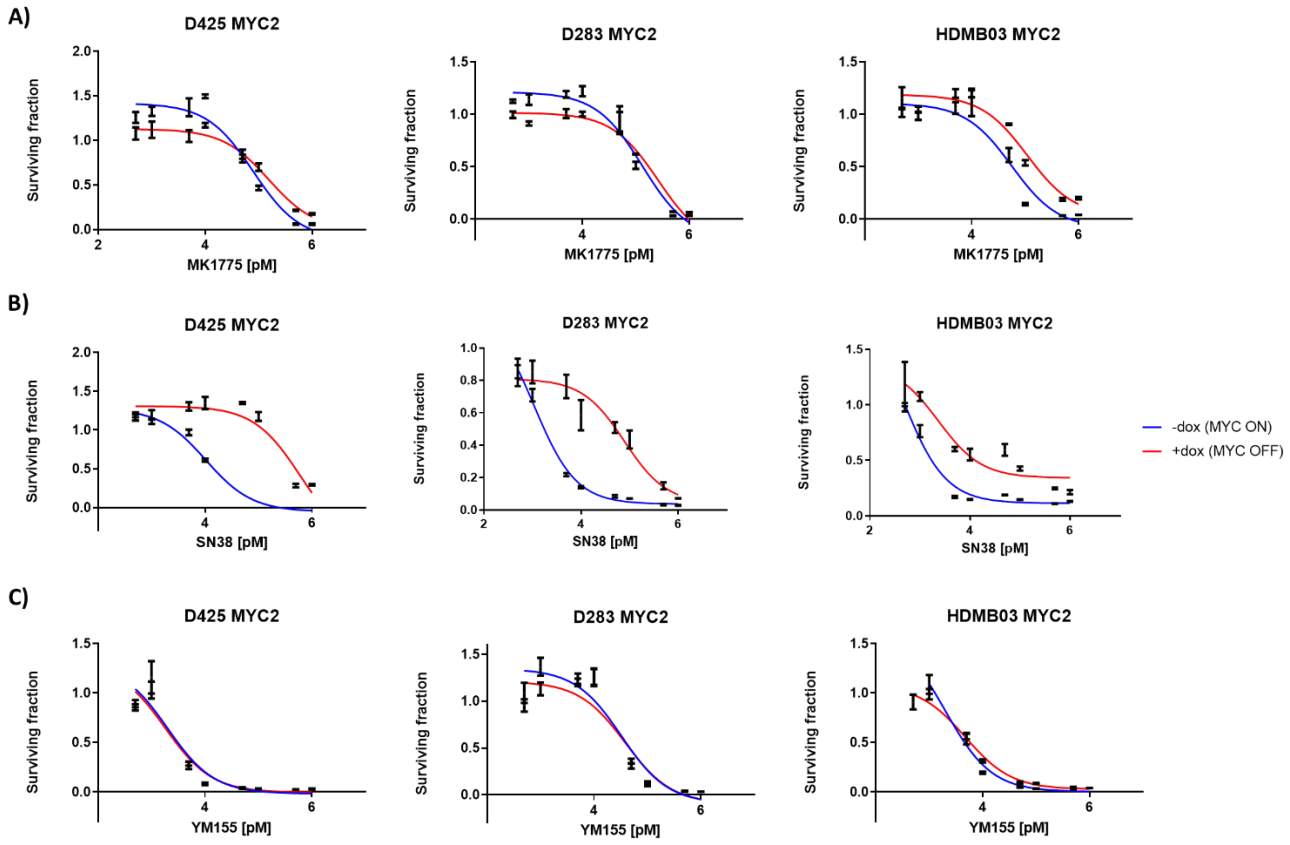

Figure 5.18. Example of growth-inhibitory curves from surviving fractions of D425, D283 and HDMB03 MYC2 cells. Dose-response curves of surviving fractions of D425, D283 and HDMB03 MYC2 cells after drug exposure to A)MK1775 (WEE1 inhibitor), B)SN38 (topoisomerase I inhibitor) and C) YM155 (BIRC5 inhibitor).The graphs show the growth inhibitory effect of the inhibitors on D425, D283 and HDMB03 MYC2 overexpressing *MYC* (blue; -dox [MYC ON]) and with *MYC* silenced (red; +dox [MYC OFF]). Triplicate data of surviving fractions at each concentration from the screen was used to generate dose-inhibitory growth curves that fit a non-linear regression model. Curves are presented as log(concentration)vs response

5.4 Discussion

Major advances in cancer therapeutics have been achieved in the last 50 years, which has led to increased survival for cancer patients. Despite increased survival, most standard therapies still come along with severe adverse effects, majorly impairing the quality of life of survivors.

The uniqueness of each type of cancer harbours the key for precision oncology. Tumours are dependent on specific genetic events that allow the acquirement of the required malignant biological capabilities to promote tumour progression. The existence of this burden has been the focus of personalised medicine to identify drugs capable to exploit these vulnerabilities as a therapeutic approach to treat the disease (Witkiewicz et al., 2016).

Identification of new anticancer drugs has improved drastically over the past decades. The availability of laboratory robots and automated machinery in combination with advances in bioinformatics platforms, has allowed the routinely use of high-throughput screenings on well-established biological models of interest to assay hundreds of potential compounds in a time- and cost-efficient manner that could be exploited in the clinic (Hajare et al., 2013).

MYC overexpression is a hallmark of MB_{Group3} tumours, and a large body of evidence indicates that MB_{Group3} tumour cells remain dependent on high levels of *MYC* expression to maintain their malignant phenotype. Several research strategies have been focusing on exploiting this *MYC* dependency for targeted therapeutic approaches (Pei et al., 2012, Weinstein and Joe, 2008). In this regard, an unbiased high-throughput drug screen on the newly established *MYC*-regulable cell models brings the unique opportunity to exploit this particular genetic vulnerability with the objective to better understand the role of *MYC* within MB_{Group3} to develop novel therapeutic strategies.

HTCS performed on D425, D283 and HDMB03 isogenic models enabled the interrogation of 489 compounds in a *MYC*-dependent manner to identify drug sensitivity effects associated with *MYC* overexpression. Our screen identified 137 small molecule inhibitors that had greater growth inhibitory effect on *MYC* overexpressing cell lines when compared to their *MYC*-knockdown counterparts. From these 137, 82 compounds were found to be consistently selectively inhibiting the growth of *MYC*-overexpressing cell lines (consistent effect across the three cell lines tested). The fact that only 16.7% (82/489) of the compounds were classified

as *MYC*-dependent candidate hits demonstrates the specific sensitivity of MB_{Group3} cells to the genes targeted.

Other drugs causing a significant growth inhibitory effect on *MYC*-overexpressing cell lines were outliers when compared to the overall of compounds inhibiting that particular target. An example was the farnesyl transferase inhibitor and the CNDAC inhibitor, which only one inhibitor targeting each molecular feature was screened (Table 5.1). Bigger number of compounds with the same mechanism of action should be tested to clarify and validate the *MYC*-dependent results seen.

Compounds identified as candidate hits showed a variety of associated mechanisms of action, with the vast majority inhibiting effectors of biological processes required for cell growth (cyclin-dependent kinases, Aurora kinases, checkpoint kinases, polo-like kinases, microtubule formation…etc.). Compounds identified, with their main molecular target/mechanism of action, is summarised in Table 5.4. *MYC*-addicted cell lines are characterised by high-proliferative rates, which could explain the profound sensitivity displayed to compounds blocking cells ability to maintain proliferation and survival. Compounds interfering directly with cell proliferation, like aurora kinases or cyclin dependent kinases, were found to be less effective on cells with *MYC* silenced by shRNA, a difference in drug sensitivity that could very likely be a direct consequence of *MYC* deficiency, indicating a possible new combinational therapeutic avenue to target *MYC*-dependent tumours.

Our results coincide with previous results from drug screens performed on MB_{Group3} models. Pei *et al.* evaluated the viability of isolated cells from a mouse model of MB_{Group3} which overexpresses *MYC* following their exposure to 3,642 compounds. 142 compounds were found to inhibit cell viability by at least 2-fold, relative to control (DMSO), and represented diverse drug classes, including inhibitors of histone deacetylases (HDAC), PI3K/mTOR and DNA topoisomerases (Pei et al., 2016). Moreover, the inhibitor BEZ-235 (dual PI3K/mTOR inhibitor) was previously identified by the same group to significantly inhibit viability of their cell models (Pei et al., 2012). Alternatively, a high-throughput screen performed by Zhang *et al*. also identified HDAC inhibitors to significantly inhibit the growth of MB_{Group3} cell lines (Zhang et al., 2019).

Another high-throughput drug screening approach performed by Endersby *et al*. identified checkpoint kinases 1 and 2 as a promising target in Group 3 medulloblastoma. Prexasertib, a dual CHK1/2 inhibitor show potency against multiple MB lines in addition to enhanced radiation-induced cytotoxicity (Endersby et al., 2018).

In summary, our results are in line with current research and results from high-throughput compound screens performed on Group 3 medulloblastoma models. The same *MYC*-driven cellular dependencies are being identified by the research community, contributing to deciphering the cellular mechanisms that cooperate with *MYC* in MB_{Group3} tumourigenesis.

5.4.1 Limitations of the work presented

It is important to describe the limitations of the results presented. It is exceptionally hard to see good responses to single doses of a particular inhibitor. Using the same broad range of concentrations for all the compounds supposes a limitation when determining differences in drug sensitivity. The largest compound library, library 13, contained 397 inhibitors that were only tested at 4 concentrations (0.5nM, 5nM, 50nM and 500nM), which could limit the ability to discern differences in sensitivity between compounds as a direct cause of *MYC*-dependencies or unselected toxicity caused by the drug, since most inhibitors will cause cell toxicity when exposed at high (i.e. >50nM) concentrations. Testing a small number of concentrations, with spread concentration range, may thus reveal non-specific toxicities masking *MYC*-dependent effects.

Chemical differences between compounds were not considered when selecting the time of exposure. Cell lines were exposed to all drugs for the same time, as a standard procedure for HTCS performance. It is possible that prolonged exposures to the compounds beyond the five days used here will elicit distinct effects on cell viability (Holme et al., 2018).

Regardless of the diversity of small molecule inhibitors contained in the compound libraries of the ICR, most drugs have been extensively studied and established for cancer treatment.

5.4.2 Prospective validation studies

Aware of the evident challenges of the experimentation performed, results from the HTCS coincide and further support the upstream and downstream regulators found through the integration of in house RNAseq and CRISPR datasets, that synergise with *MYC* causing significant growth inhibition in MB cell lines. The combination of RNAseq data on *MYC*-regulable models and the whole genome CRISPR screen on D283 and DAOY MB cell lines predicted 6 targetable molecular agents to be effective on MB_{Group3} – *PLK*, *CHK*, *AURK*, mTOR, *EGFR* and *BIRC5*. Compounds inhibiting PLK1 (75% of total PLK inhibitors), CHK (71.4% of total CHK inhibitors), CDK (43.5% of total CDK inhibitors) and AURK (72.7% of total AURK inhibitors) represented a huge number of the hits found from the HTCS, highlighting the hypersensitivity of *MYC*-overexpressing cell lines to these compounds.

Our results are in line with current published studies showing the direct relationship between PLK1, CHK1 and AURK with *MYC*, supporting the use of inhibitors against these molecules to indirectly target *MYC* in *MYC*-amplified MB. Some examples of the common understanding that we have considered in order to choose candidate drugs to take forward to assess their individual *MYC*-dependent effect in *MYC*-amplified/regulable MB cell lines, alongside non-amplified MB_{SHH} models, are the following:

5.4.2.1 Checkpoint kinase 1

MYC's ability to promote cellular proliferation is a direct cause of its control, as a transcription factor, over the expression of genes implicated in S-phase entry and progression of cells cycle, like cyclin dependent kinases (CDKs), cyclins and inhibitors of CDK. High levels of *MYC* are known to evoke replicative stress. Abnormally high cell replication rates cause the crosslink of lagging strands of DNA to arise which cells recognise as single-strand breaks, consequently triggering the DNA damage response (DDR) and holding the entry to mitosis until damage is repaired. Interference with DNA replication and suppression of replicative stress is triggered by the activation of the ATR/CHK1 signalling pathway (Figure 5.19). Activation of DNA damage repair by CHK1 ensures the efficient proliferation of cells and avoids detrimental genetic instability. Since CHK1 counteracts DNA damage, by pharmacologically inhibiting CHK1, cell replication is initiated bearing genetic abnormalities which triggers cell death mechanism and cells undergo apoptosis (Murga et al., 2011, Rohban and Campaner, 2015).

Another reason why CHK1 inhibitors are potentially a good therapeutic for MB_{Group3} is that it has been shown that high levels of *MYC* makes MB_{Group3} hypersensitive to the targeting of replicative stress responses when compared to other MB subgroups, like MB_{SHH}. This increased sensitivity of MB_{Group3} to CHK1 inhibition has been linked to its direct effect in decreasing MYC protein levels, through the decrease in GSK-3α phosphorylation. This is in line with the fact that phosphorylated GSK-3 phosphorylates c-MYC, promoting its degradation and affecting its regulated gene expression (Kruger et al., 2018).

Plotting of surviving fractions of cells from the screen revealed the same *MYC*-dependent preferential effect after treatment with the CHK1 inhibitor AZD7762, which preferentially targeted the *MYC* overexpressing arm of the experiment.

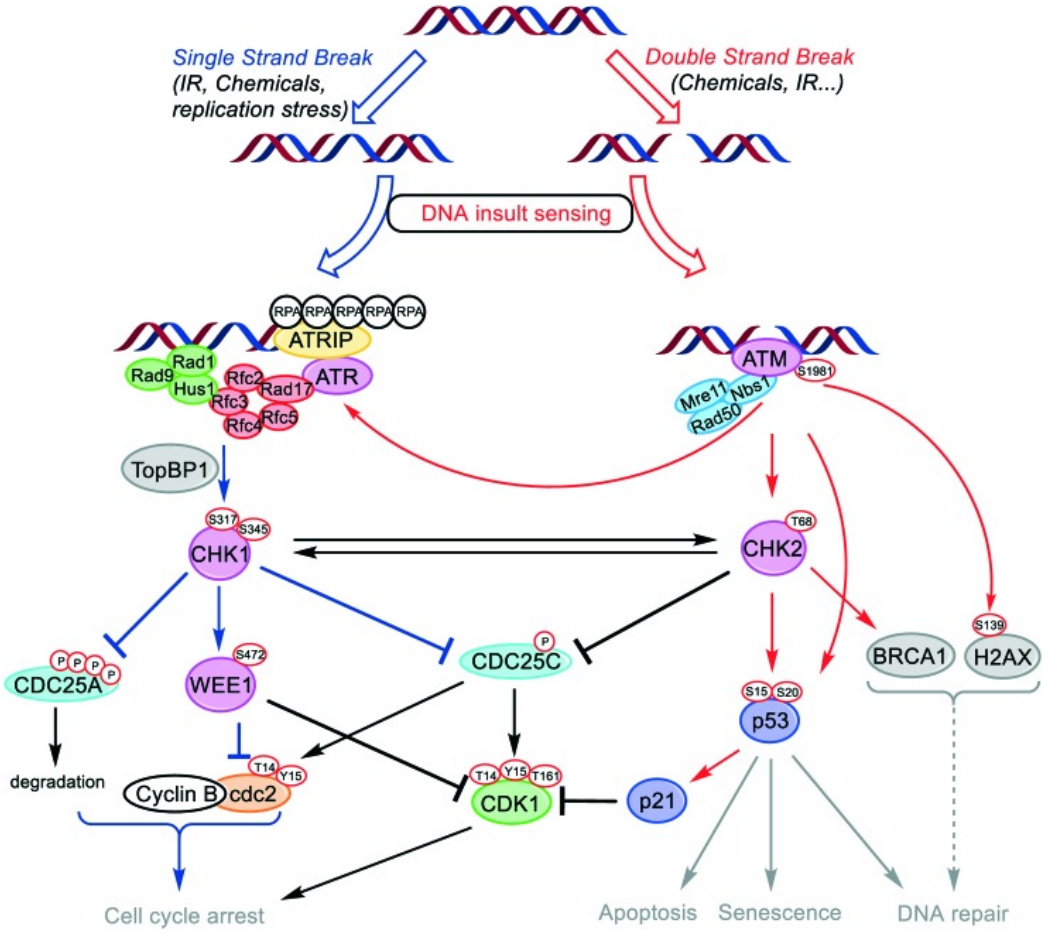

Figure 5.19. The DNA-damage response pathway. Summary of the DNA damage response pathways modulated by ATM, ATR, CHK1, CHK2 and WEE1 kinase. Chk1 is activated by phosphorylation on Ser317 and/or Ser345 by ATR after cellular DNA damage is detected by the ATM/ATR kinases. Downstream phosphorylation events result in G_2-M- and S-phase cell cycle arrest.
(Adapted from Ronco, *et al.*, 2016).

5.4.2.2 Aurora Kinases

Another downregulated target highlighted by both data sets was Aurora kinases (AURK). Part of the reason why targeting them is a promising strategy is because of their downstream effect and key role in regulating cells mitotic progression (Figure 5.20). Inhibition of Aurora Kinases inevitably slows down proliferation of cells by blocking progression of cells growth cycle.

AURK have an upstream and downstream *MYC*-dependent effect. Expression of AURKA and AURKB is directly mediated by *MYC* and at the same time, AURKA can bind onto *MYC*'s promoter and transcriptionally upregulate its expression, forming a positive regulation loop. In addition, AURK are also involved in stabilisation of MYC at the protein level. MYCN protein is stabilised through its binding with AURKA. Perturbation of this protein-protein interaction results in subsequent MYC degradation and promotion of cell death (Dauch et al., 2016, Chen et al., 2018b, Tang et al., 2017, den Hollander et al., 2010).

Some AURKA inhibitors such as MLN8237 (Alisertib) and CD532 have been shown to destabilise MYCN by promoting the disassociation of the AURKA:MYCN complex, whereas some other Aurora-A inhibitors seem to not provoke the same effect (VX-680). The current hypothesis to why these differences are seen between inhibitors is that, the destabilising inhibitors actually alter the conformation of the kinase causing an active degradation of MYCN, ultimately preventing the formation of the complex. Whereas inhibitors that compete with ATP without producing a conformational change have no effect on the complex formation and stabilisation (Li et al., 2018, Otto et al., 2009).

The potential of AURKA inhibitors as an indirect way to target *MYC*-amplified tumours has already been tested in *MYCN*-driven medulloblastoma and neuroblastoma models, which MLN8054 and MLN8237 inhibitors have been proven to be effective in promoting proteasomal degradation of MYCN and cell death in *MYCN*-amplified NB and MB (Dauch et al., 2016, Hill et al., 2015).

Based on the above studies, pharmacological inhibition of AURKA by MLN8237 supposes a good therapeutic approach to test if a similar effect in downregulating c-MYC protein levels could be seen in *MYC*-amplified MB cell lines (performed in the next Chapter).

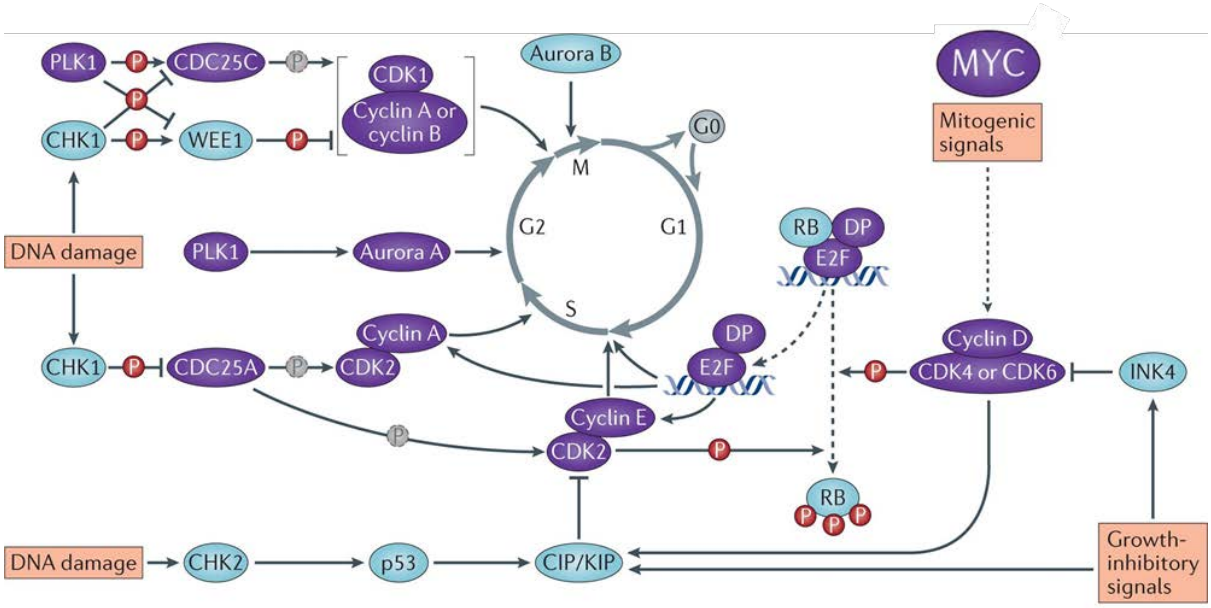

Figure 5.20. Major regulators of cells cycle progression. Schematic representation of main proteins involved in the regulation of the cell cycle. Entry into the cell cycle can be induced by the activation of transcriptional factors such as *MYC* in response to mitogenic signals, which induce the transcription of cyclins and cyclin-dependent kinases to promote cell cycle progression. Progression through the cell cycle is tightly regulated by CDKs, together with other proteins like Polo-like Kinase1 (PLK1), Aurora Kinases (Aurora A and B). upon detection of DNA damage, cell cycle arrest is triggered via checkpoint kinase 2 (CHK2) in G1 phase, or in S/G2 phase via CHK1. Correct proliferation of cells is ensured by the tight regulation of proteins involved in cells division. Purple ovals denote positive regulators of cell cycle progression and blue ovals denote negative regulators of cell cycle progression. P in dashed circle indicates dephosphorylation (adapted from Otto, et al., 2009).

5.4.2.3 Polo-like kinases

Data integration also identified polo-like kinases (PLK) as a potential *MYC*-dependent targetable molecule potentially relevant in MB_{Group3}. PLKs comprise a family of protein kinases that play key regulatory roles in several biological processes. PLK1 is the most characterised PLK family member, due to its involvement in the regulation of multiple steps of the mitotic process.

Upregulation of PLK1 expression has been reported in many cancers. Overexpression of PLK1 can lead to mitotic defects promoting survival of cells bearing chromosomal mis-arrangements and genetic damage that can cause aneuploidy, a premise for the degradation or inactivation of tumour suppressor genes like *TP53*. Loss of *TP53* causes the DDR machinery to fail to detect DNA damage, allowing the entry to mitosis of those cells with high genetic instability which favour tumour transformation (Xiao et al., 2016, Kumar and Kim, 2015).

Like AURK, apart from being downstream regulators of *MYC* expression signatures, it has been demonstrated that PLKs also affect MYC stabilisation, presenting again an upstream regulatory effect. A PLK1 and MYCN positive interconnected auto-regulatory loop has been described in *MYCN*-amplified neuroblastoma models, where PLK1 stabilises MYCN activating a feedforward circuit promoting mutual high expression. This sustained high expression leads to transcriptional amplification of *MYC* (Ren et al., 2018).

This is done through the specific binding of PLK1 to the E3 ubiquitin-protein ligase Fbw7. Fbw7 is a member of the SCF-like ubiquitin ligase complex, which targets MYC for proteasomal degradation. Phosphorylation of Fbw7 by PLK1 promotes its auto-polyubiquitination and its own proteasomal degradation, preventing the ubiquitination and subsequent degradation of MYC. Inhibition of PLK1 prevents Fbw7 degradation, causing stabilisation of MYCN that in turn directly promotes PLK1 transcription, constituting a positive feedback loop resulting in tumour proliferation (Sato et al., 2015, Xiao et al., 2016).

To evaluate if PLK1 inhibition had the same impact on c-*MYC* expression in *MYC*-amplified MB_{Group3} cell lines, the PLK1 inhibitor BI2536 tested on the screen was chosen to take forward for further validation. BI2536 is one of the most potent ATP-competitive inhibitors at low nanomolar concentrations, which has shown to downregulate expression of *MYCN*, induce apoptosis and enhance cells sensitivity to other cytotoxic agents (Chen et al., 2018b).

In summary, integrating our results with current published data, choosing PLK1, CHK1, CDK2 and AURK as the major candidate *MYC*-dependent targets to validate from our screen hold great promise for the identification of new *MYC*-regulatory mechanisms that could be therapeutically exploited against *MYC*-driven high-risk MB_{Group3}.

5.5 Appendix

Compound	Function/Target
17-AAG	HSP90
2-methoxyestradiol	HIF-1α
4-OH-tamoxifen	ER
5-FU	anti-metabolite
6-thioguanine	anti-metabolite
ABIRATERONE	CYP17A1
ABT-737	BCL2
AG-14699	PARP
AZ4547	FGFR
BEZ-235	PI3K/mTOR
BI-2536	PLK
BIBW2992	EGFR/HER2
bleomycin	DNA-damage
BMN-673	PARP
BMS-911543	JAK2
cabozantinib	MET/VEGF
camptothecin	Topoisomerase I
canertinib	pan-ErbB
carboplatin	DNA-damage
celecoxib	COX2
crizotonib	ALK
dasatinib	BCR-ABL/Src
decitabine	MTase
DMX_1783	TNKS
DMX_2320	IKKε
doxorubicin	DNA-damage
erlotinib	EGFR
etoposide	Topoisomerase II
everolimus	mTOR
flavopiridol	CDK
foretinib	MET,VEGFR2,KDR
GDC-0449	SMO
gefitinib	EGFR
gemcitabine	Thymidylate synthase
GSK1904529A	IGFR
GSK2194069A	FAS
GSK-2334470A	PDK
imatinib	BCR-ABL
KU0057788	DNA-PK
KU60019	ATM

Compound	Function/Target
lapatinib	Her2
Lenvatinib	VEGF
lestaurtinib	JAK2/FLT3/TrkA
MDV-3100	CRPC
methotrexate	DHFR
MK0752	NOTCH
MK-1175	WEE1
MK2206	AKT
MLN-4924	NEDD
MSC2358705A	DNA-PK,Merck
nilotinib	BCR-ABL
Nutlin3	MDM2
olaparib	PARP1/2
OSI-906	IGFR
Paclitaxel	microtubule
PD-0332991	CDK4/6
PD173074	FGFR
PD-184352	MEK
PF-00299804	pan-ErbB
PF-00477736	CHK1
PF-02341066	MET/ALK
PF-03758309	PAK
PF-03814735	Aurora
PF-04691502	PI3K/mTOR
PF-04929113	HSP90
PF-332991	CDK4/6
PLX-4720	BRAF
resveratrol	inflammation
RO-3306	CDK1
salinomycin	microtubule
sapacitabine	CNDAC
SAR-20106	CHK1
sorafenib	RAF,PDGF,VEGF1&2
sotrastaurin	PKC
sunitinib	VEGFR1-3,PDGFR,Kit,CSF1R
temozolomide	DNA alkylation
vinorelbine	anti-mitotic
voronostat	HDAC I&II
XAV-939	TNKS/Wnt
YM155	survivin

Appendix 5.1. Content of compound library 11-12.

Gene ID	Function/Target
(-)-Epigallocatechin	unknown
17-AAG	HSP-90
17-DMAG	HSP-90
2131TNKSi	TNKS
2-methoxyestradiol	HIF-1α
3-Methyladenine	PI3K
4-Phenylbutyrate	HDAC
877TNKSi	TNKS
A-769662	AMPK
Abiraterone	CYP17A1
Abitrexate	DHFR
ABT-263	Bcl-2
ABT-737	Bcl-2
ABT-751	microtubule
ABT-888	PARP
Adrucil	DNA/RNA Synthesis
AEE788	HER1/2, VEGFR1/2
Afatinib	EGFR
AG14361	PARP
Altretamine	DNA alkylation
AMG 900	AURK
Aminoglutethimide	Aromatase
Amuvatinib	c-kit
AnagrelideHCl	PDE
Anastrozole	Aromatase
Andarine	AR
APO866	NAMPT
AR-42	HDAC
AR-A014418	GSK-3
AS-605240	PI3K
AT-406	IAP
AT7519	CDK
AT9283	AURK
AUY922	HSP-90
Axitinib	VEGFR
AZ3146	Msp1
AZ628	Raf
Azacitidine	MTase
Azathioprine	anti-metabolite
AZD6244	MEK
AZD7762	CHK

Gene ID	Function/Target
AZD8055	mTOR
Bafetinib	Bcr-Abl
Barasertib	AURK
BAY11-7082	IKK
Bay117085	NF-κB
Belinostat	HDAC
Bendamustine	DNA alkylation
BEZ235	mTOR/PI3K
BI2536	PLK1
BI6727	PLK1
BI78D3	JNK
BIBF1120	VEGFR
BIBR1532	Telomerase
Bicalutamide	AR
BIIB021	HSP-90
BIRB796	p38 MAPK
BIX01294	HMTase
BKM120	PI3K
Bleomycin	DNA-damage
BML-277	CHK2
BMN673	PARP
BMS 777607	c-MET
BMS-599626	pan-HER
BMS794833	MET/VEGFR2
Bortezomib	proteasome
Bosutinib	Src
Brivanib	VEGFR, FGFR
BX795	TBK1/IKKε
C43TNKSi	TNKS
CAL-101	PI3K
Calpeptin	calpain
camptothecin	Topoisomerase I
Canagliflozin	SGLT
Capecitabine	anti-metabolite
Carboplatin	DNA alkylation
Carmofur	anti-metabolite
CCT18159	HSP-90
CD437	RAR-γ agonist
Cediranib	VEGFR
Celecoxib	cox-2
CEP33779	JAK

Gene ID	Function/Target
CH5132799	PI3K
Chelerythrine	PKC
CHIR-99021	GSK-3
Chrysophanicacid	EGFR
CI-1040	MEK
Cisplatin	DNA alkylation
Cladribine	DNA alkylation
Clafen	DNA alkylation
Clofarabine	anti-metabolite
CombretastatinA4	microtubule
CP-466722	ATM
Crenolanib	FLT3
Crizotinib	c-MET
CUDC-101	EGFR
CX-4945	casein kinase 2
CYC116	AURK
Cyclopamine	hedgehog
Cyclophosphamide	DNA alkylation
CyclosporinA	calcineurin
Cyt387	JAK
Dacarbazine	DNA alkylation
Dacomitinib	EGFR
Dalcetrapib	CETP
Danusertib	AURK
Dapagliflozin	SGLT
DAPT	γ-secretase
Dasatinib	Bcr-Abl
Daunorubicin	Topoisomerase II
DCC-2036	Bcr-Abl
Decitabine	MTase
Deforolimus	mTOR
Dexamethasone	IL receptor
DFMO	ornithine decarboxylase
Disulfiram	Aldehyde dehydrogenase
DMX_051_1783	TNKS
DMX_051_2384	TNKS
DMXAA	DT-diaphorase
Docetaxel	microtubule
Dovitinib	FLT3
Doxercalciferol	calcium mobilisation
Doxorubicin	DNA-damage

Gene ID	Function/Target
E7080	VEGFR
EBPC	aldose reductase
Elesclomol	HSP-90
ENMD-2076	FLT3
Entinostat	HDAC
Enzastaurin	PKC
Epirubicin	Topoisomerase II
EpothiloneA	microtubule
EpothiloneB	microtubule
Erlotinib	EGFR
Estradiol	Erα/β
Estrone	Estrogen/progestogen
Etoposide	Topoisomerase II
Everolimus	mTOR
Evista	Estrogen/progestrone
EX527	SIRT1
Exemestane	Aromatase
Ezetimibe	cholesterol absorption inhibitor
Febuxostat	Xanthine oxidase
Fenretinide	RAR
Fingolimod	S1P receptor
FK866	NAMPT
Flavopiridol	CDK
Floxuridine	anti-metabolite
Fludarabine	STAT
Fludarabine	STAT
Flutamide	AR
Fluvastatin	HMGCoA reductase
Formestane	Aromatase
FR180204	ERK1/2
Ftorafur	anti-metabolite
Fulvestrant	Estrogen receptor
Ganetespib	HSP-90
GDC-0068	AKT
GDC-0879	Raf
GDC-0941	PI3K
Gefitinib	EGFR
Geldanamycin	HSP-90
Gemcitabine	anti-metabolite
Gemcitabine	TS
Gossypol	dehydrogenase

Gene ID	Function/Target
GSK1120212	MEK
GSK1904529A	IGF-1R
GSK2126458	PI3K
GSK264220A	endothelial lipase
GSK3787	PPARδ
GSK461364	PLK1
GSK650394	SGK
GSK690693	AKT
GSK837149A	FAS
GW3965	liver x receptor
GW4064	FXR
GW9508	GPR40
Harmine	DYRK1A
Hydrocortisone	NR3C1
Hydroxyurea	ribonucleotide reductase
Ibrutinib	Btk
IC-87114	PI3K
Idarubicin	Topoisomerase II
Ifosfamide	DNA alkylation
Imatinib	PDGFR
Imatinib	PDGFR
Iniparib	PARP
INK 128	mTOR
Irinotecan	Topoisomerase I
Irinotecan	Topoisomerase I
Isotretinoin	RAR-α
Ispinesib	kinesin
Itraconazole	CYP
ITX3	TrioN RhoGEF
JK184	hedgehog
JNJ 26854165	HDM2
JNJ-26481585	c-MET
JNJ-38877605	c-MET
JNJ-7706621	AURK
JW55	TNKS
KU-0063794	mTOR
KU-55933	ATM
KU-60019	ATM/ATR
KX2-391	Src
Lapatinib	HER2
Lapatinib	HER2

Gene ID	Function/Target
LDE225	hedgehog/smoothened
LDN193189	ALK
Lenalidomide	TNFα
Letrozole	Aromatase
Linifanib	VEGFR
Linsitinib	IGFRI
L-NNA	NOS
Lomeguatrib	MGMT
Lomustine	DNA alkylation
Lonidamine	hexokinase
LY2109761	TGF-β R
LY2157299	TGF-β/Smad
LY2228820	p38 MAPK
LY2603618	CHK
LY294002	PI3K
LY320135	CB1 receptor
Maraviroc	CCR
Marimastat	MMP
Masitinib	c-Kit
MDV3100	anti-androgen
Medroxyprogesterone	Estrogen/progestogen
Megestrol	unknown
Mercaptopurine	anti-metabolite
MG149	TIP60 Histone Acetyltransferase
Mifepristone	Estrogen/progestogen
Mitoxantrone	Topoisomerase II
MK-0752	γ-secretase
MK1775	Wee1
MK-1775	Wee1
MK-2206	AKT
ML-141	Cdc42
MLN2238	proteasome
MLN8237	AURK
MLN9708	proteasome
Mocetinostat	HDAC
Motesanib	VEGFR
Mycophenolate	dehydrogenase
Mycophenolic	IMPDH
Necrostatin-1	RIPK1
Nelarabine	DNA/RNA Synthesis
Nilotinib	Bcr-Abl

Gene ID	Function/Target
Nocodazole	microtubule
NPI-2358	microtubule
NSC23766	Rac1
NSC663284	Cdc25
NU6027	ATR
NU7441	DNA-PK
Nutlin-3	Mdm2
NVP-BSK805	JAK
Obatoclax	Bcl-2
Olaparib	PARP
OSI-420	EGFR
OSI-930	c-kit
Ostarine	AR
Oxaliplatin	DNA alkylation
PAC-1	caspase
Paclitaxel	microtubule
Palbociclib	CDK4/6
Palomid529	TORC1/2
Panobinostat	HDAC
Pazopanib	RTK
PB28	TMEM97
PCI-24781	HDAC
PD0325901	MEK
PD153035	EGFR
PD173074	FGFR
PD407824	Wee1/Chk1
Pelitinib	EGFR
Pemetrexed	TS
Pentostatin	Adenosine Deaminase
Perifosine	AKT
PF 573228	FAK
PF-03758309	PAK
PF-03814735	AURK
PF-04217903	c-MET
PF-04691502	PI3K
PF-3845	FAAH
PF-4708671	S6
PF477736	CHK1
PF-562271	FAK
PF670462	CK1ε
PH-797804	p38 MAPK

Gene ID	Function/Target
PHA-665752	c-MET
PHA-793887	CDK
Phloretin	SGLT1/2
PI-103	PI3K
PIK-75	PI3K
PIK-90	PI3K
PIK-93	PI4K
PIM-1Inhibitor	PIM1
Pioglitazone	PPARγ
Pomalidomide	anti-angiogenesis
Ponatinib	Bcr-Abl
Procarbazine	DNA/RNA Synthesis
Pyroxamide	HDAC
QNZ	NF-κB
Quercetin	Sirtuin
Quizartinib	FLT3
R406	syk
R935788	syk
Raltitrexed	TS
Ranolazine	Sodium channels
Rapamycin	m-TOR
Regorafenib	VEGFR-TIE2
RG108	MTase
Rigosertib	PLK1
Roscovitine	CDK
Rosiglitazone	PPARδ
Rucaparib	PARP
Ruxolitinib	JAK
S7333	K-RAS
SANT1	SMO
Saracatinib	Src
SB 203580	p38 MAPK
SB 216763	GSK-3
SB 743921	kinesin
SB265610	CXCR2
SB42	TGF-β/Smad
SB525334	TGF-β/Smad
SB590885	Raf
SB939	HDAC
SecinH3	GDP/GTP Exchange Factor
SGI-1776	Pim

Gene ID	Function/Target
SGX-523	c-MET
SID7969543	SF-1
Sirtinol	Sirtuin
SJ172550	MDMX
SK1	Sphingosine Kinase-1
SKF91488	histamine N-methyltransferase
SKI II	Sphingosine Kinase-1
SMER3	E3 Ubiquitin Ligase (SCF)
SNS-032	CDK2,7,9
SNS-314Mesylate	AURK
Sorafenib	Raf
Sotrastaurin	PKC
SrcI1	Src
SRT1720	SIRT1 activator
S-Ruxolitinib	JAK
STAT5Inhibitor	STAT5
SU11274	c-MET
Sunitinib	PDGFR
TAE684	ALK
TAK-733	MEK
TAME	APC
Tamoxifen	Estrogen/progestogen
Tandutinib	FLT3
TCSPIM	Pim1/2 Kinase
Telatinib	VEGGFR2/3, C-KIT, PDGFR
Temozolomide	DNA alkylation
Temsirolimus	mTOR
TG101348	JAK
Tie2	Tie2
Tipifarnib	transferase
Tivozanib	VEGFR
Tofacitinib	JAK
Topotecan	Topoisomerase I
Toremifene	Estrogen/progestogen
Torin2	mTOR
Tosedostat	aminopeptidase
TPCA-1	IκB/IKK
Trichostatin	HDAC
Triciribine	AKT
Triptolide	RNA pol II
TTP22	casein kinase 2

Compound	Function/Target
TW-37	Bcl-2
UPF1035	PARP
Valproic	HDAC
Vandetanib	VEGFR
Vatalanib	VEGFR
VE-821	ATR
Vemurafenib	B-Raf
Vinblastine	microtubule
Vincristine	DNA synthesis
Vismodegib	Hedgehog/smoothened
Vorinostat	HDAC
VX-680	AURK
Vx-970	ATR
Vx-984	DNA-PK
WAY-362450	FXR
WP1130	Bcr-Abl
WYE-354	mTOR
WZ4002	EGFR
XL147	PI3K
xxx	EMPTY
Y-27632	ROCK
YM155	Survivin
YM201636	PI3K
YO-01027	γ-secretase
Zibotentan	endothelin receptor
Zileuton	5-lipooxygenase
ZSTK474	PI3K

Appendix 5.2. Content of compound library 13.

Compound	Function/Target
A-1210477	Mcl2
A-674563	PKA,CDK,Akt
ABT888/Veliparib	PARP
AG-14361	PARP
AG-14699	PARP
Amonafide	Topoisomerase II
AT7519	CDK
AT7519 HCl	CDK
AZD5438	CDK1/2/9
AZD7762	CHK
AZD8055	mTOR
BendamustineHCl	DNA alkylation
Bleomycin	DNA-damage
BML277	CHK2
BMN673	PARP
BMS-265246	CDK1/2
BS-181HCl	CDK7
Camptothecin	Topoisomerase I
Carmofur	Pyrimidine analog
CCT271850	MPS1
Cisplatin	DNA alkylation
Clofarabine	anti-metabolite
Cyclophosphamide	DNA alkylation
Dacarbazine	DNA/RNA Synthesis
Daunorubicin	Topoisomerase II
Dinaciclib	CDK1/2/5/9
DMX_1783	Tankyrase
DMX_1913	Tankyrase
DMX2131	Tankyrase
Doxorubicin	DNA-damage
E3330	APE1/Ref-1
Epirubicin	Topoisomerase II
EPZ6438	EZH2
Etoposide	Topoisomerase II
Flavopiridol	CDK
FlavopiridolHCl	CDK
FludarabinePhosphate	DNA/RNA Synthesis
Fluorouracil	DNA/RNA Synthesis
Gatifloxacin	DNA gyrase
Gimeracil	DPD
Hydroxyurea	DNA/RNA Synthesis

Compound	Function/Target
Ifosfamide	DNA alkylation
Iniparib	PARP
Irinotecan	Topoisomerase I
Irinotecan trihydrate	Topoisomerase I
JNJ-7706621	CDK, AURK
KU0057788	DNA-PK
KU-55933	ATM/ATR
KU-60019	ATM/ATR
LDC000067	CDK9
LEE011	CDK4/6
Lomustine	DNA damaging agent
LY2603618	CHK1
LY2835219	CDK4/6
Mercaptopurine	Purine analog
Methotrexate/Abitrexate	DHFR
Milciclib	CDK2
Mitoxantrone	Topoisomerase II
MK4827	PARP1/2
MK-8776	CDK, CHK
ML167	Clk4
MLN-4924	NEDD
MSC2504877A	Tankyrase
MSC4070	Tankyrase
NU6027	CDK1/2, ATR,DNA-PK
Nutlin	MDM2
NVP656	Tankyrase
Olaparib	PARP
Olaparib	PARP
OSI-027	mTOR
Oxaliplatin	DNA alkylation
P276-00	CDK1/4/9
Palbociclib	CDK4/6
Palbociclib Merck	CDK4/6
PD-407824	Wee1/CHK1
Pefloxacin	Topoisomerase II
PF3644022	MK2
PF-477736	CHK
PHA-767491	Cdc7/CDK9
PHA-793887	CDK
PIK-75	PI3K,DNA-PK
Pirarubicin	Topoisomerase II

Compound	Function/Target
PP121	DNA-PK,PDGFR,mTOR
Purvalanol A	CDK2
R547	CDK1/2/4
Raltitrexed	TS
RITA(NSC652287)	MDM2
Ro-3306	CDK
Roscovitine	CDK
Satraplatin	Platinum based
SCR7	DNA Ligase IV
SN-38	Topoisomerase I
SNS-032	CDK2/7/9
SU9516	CDK
Temozolomide	DNA alkylation
TG003	Cdc2 like kinase
Topotecan	Topoisomerase I
Torin	ATM/ATR, mTOR
Triapine	ribonuclease reductase
UPF-1035	PARP2
UPF-1069	PARP2
VE-821	ATM/ATR
VX-970	ATR
Zebularine	DNA Methyltransferase
β-Lapachone	Topoisomerase II

Appendix 5.3. Content of compound library 14.

Compound	References
VX-970 (M6620)	(Hall et al., 2014) (Kurmasheva et al., 2018) (Mittra et al., 2019); NCT02567422, NCT03896503
VX-680	(Gustafson et al., 2014) (Markant et al., 2013)
Barasertib	(Diaz et al., 2015) (Helfrich et al., 2016)
PF-03814735	(Hook et al., 2012) (Jani et al., 2010)
AT9283 (Dasatinib)	(Petersen et al., 2014) (Moreno et al., 2015) (Petersen et al., 2012) (Vitali et al., 2009) (Timeus et al., 2008) (Dong et al., 2015); NCT01467986
SNS-314	(Markant et al., 2013) (VanderPorten et al., 2009) (Arbitrario et al., 2009) (Castro-Gamero et al., 2018)
MLN8237 (Alisertib)	(Li et al., 2018) (Felgenhauer et al., 2018) (Otto et al., 2009) (Hill et al., 2015) (Dauch et al., 2016) (Levesley et al., 2018) (Kogiso et al., 2018) (Graff et al., 2016) (Nair and Schwartz, 2016) (Muscal et al., 2013) (Ahmad et al., 2015)
CYC116	(Griffiths et al., 2008) (Hajduch et al., 2008) (Park et al., 2019) (Zhou et al., 2015)
AMG-900	(Geron et al., 2015) (Ryu et al., 2018) (Paller et al., 2014)
AT7519	(Dolman et al., 2015) (Norris et al., 2016) (Aleem and Arceci, 2015)
JNJ-7706621	(Schwermer et al., 2015) (Emanuel et al., 2008) (Rødland et al., 2019)
Dinaciclib	(Bolin et al., 2018) (Kato et al., 2015) (Juric and Murphy, 2020) (Gorlick et al., 2012)
Flavopiridol	(Hanaford et al., 2015) (Shapiro et al., 1999) (Liu et al., 2019a)
BMS-265246	(Deng and Mou, 2018) (Scott et al., 2016)
LY2835219	(Raub et al., 2015) (Lang and Gershon, 2018) ; NCT04238819
R547	(Berkofsky-Fessler et al., 2009) (DePinto et al., 2006) (Soldi et al., 2013)
P276-00	(Joshi et al., 2007) (Manohar et al., 2011)

Roscovitine	(Delehouzé et al., 2014) (Federico et al., 2010) (Le Tourneau et al., 2010)
Milciclib (PHA-848125)	(Hutter et al., 2017) (Molenaar et al., 2009) (Bolin et al., 2018) (Lubanska and Porter, 2017) (Aspeslagh et al., 2017)
SNS-032	(Juric and Murphy, 2020)
Cladribine	(Morfouace et al., 2014) (Boyko and Boyko, 2018)
Gemcitabine	(Moreira et al., 2020) (Morfouace et al., 2014)
Hydroxyurea	(Levin et al., 1988) (Millard and De Braganca, 2016)
Decitabine	(Zwergel et al., 2018) (Gajjar et al., 2015) (Patties et al., 2016b); NCT02332889
AZD7762	(Yang et al., 2011) (Kruger et al., 2018) (Prince et al., 2016) (King et al., 2017) (Sausville et al., 2014) (Bartucci et al., 2012) (Gadhikar et al., 2013) (Zabludoff et al., 2008) (McNeely et al., 2010) (Xu et al., 2011)
LY2603618 (Rabusertib)	(Scagliotti et al., 2016) (Wehler et al., 2017) (King et al., 2015) (Burris, 2019) (Hong et al., 2016) (King et al., 2014)
SAR-20106 (Sutton)	(Jones et al., 2017)
PD407824	(Benada and Macurek, 2015) (Bradford et al., 2019)
PF-00477736	
Vorinostat (SAHA)	(Spiller et al., 2006) (Hummel et al., 2013) (Yuan et al., 2017) (Patties et al., 2016a) (Ecker et al., 2015) (Leary et al., 2015)
Trichostatin	(Valdora et al., 2013) (Roussel and Stripay, 2018) (Unland et al., 2014) (Horing et al., 2013)
PP121	(Che et al., 2014)
Tipifarnib	(Fouladi et al., 2007) (Kameda-Smith et al., 2018) (Haas-Kogan et al., 2011)
JK184	(Mahindroo et al., 2009)
Belinostat	(Ecker et al., 2015) (Becher, 2019) (Gimsing et al., 2008) (Zhang et al., 2019)
JNJ-26481585	(Carol et al., 2014) (Venugopal et al., 2013) (Arts et al., 2009)

Mocetinostat	(Coni et al., 2017) (Eckschlager et al., 2017) (Amarante et al., 2018)
17-DMAG	(Ayrault et al., 2009) (Mellatyar et al., 2018) (Calabrese et al., 2003)
SNX-5422	(Rajan et al., 2011) (Sun et al., 2018)
Ispinesib	(Venere et al., 2015)
PF-02341066 (Crizotinib)	(Solomon et al., 2014) (Junca et al., 2017) (Awad and Shaw, 2014)
Sapacitabine	(Lin et al., 2018) (Shapiro et al., 2013)
Satraplatin	(Akshintala et al., 2015) (Marcus et al., 2012) (Bautista et al., 2017b)
Clofarabine	(Patel et al., 2015)
Lestaurtinib	(Norris et al., 2011) (Iyer et al., 2010) (Minturn et al., 2011)
SB-743921	(Bongero et al., 2015); NCT00136513
Docetaxel	(Zwerdling et al., 2006) (Girard et al., 2015); NCT00002825
EpothiloneB	(Oehler et al., 2011) (Peereboom et al., 2014) (Oehler et al., 2012)
Paclitaxel	(Tseng et al., 1999) (Hurwitz et al., 2001) (Bautista et al., 2017a)
NPI-2358	(Heist et al., 2014) (Nicholson et al., 2006)
Nocodazole	(Antonucci et al., 2019) (Dasari et al., 2013) (Cherry et al., 2016) (Hong et al., 1999)
salinomycin	(Zhou et al., 2014) (Calzolari et al., 2014) (Dewangan et al., 2017) (Booth et al., 2014)
Vinblastine	(Jakacki et al., 2011) (Nobre et al., 2019)
Vinorelbine	(Kuttesch et al., 2009) (Vo et al., 2017) (Mascarenhas et al., 2019); NCT00180947
CCT271850	(Tannous et al., 2013) (Slee et al., 2014)
AZD8055	(Houghton et al., 2012) (Luchman et al., 2014)

Torin 1/2	(Thoreen et al., 2009) (Xie et al., 2016) (Wu et al., 2017)
MLN-4924	(Hua et al., 2015) (Vanderdys et al., 2018) (Bhatia et al., 2016)
Triptolide	(Zhang et al., 2018a)
PF-03758309	(Bondar et al., 2018) (Franovic et al., 2015) (Cosset et al., 2017)
BMN-673 (Talazoparib)	(Smith et al., 2015) (Shen et al., 2013) (Lesueur et al., 2018)
PIK-75	(Wojtalla et al., 2012) (Guerreiro et al., 2008) (Cage et al., 2015)
BEZ-235	(Shi et al., 2017) (Chaturvedi et al., 2018) (Pei et al., 2016)
PF-04691502	(Yuan et al., 2011) (Singh et al., 2016) (Aldaregia et al., 2018)
GSK461364	(Triscott et al., 2013) (Pajtler et al., 2017) (Pezuk et al., 2017)
BI6727	(Abbou et al., 2016) (Harris et al., 2012) (Gorlick et al., 2014b) (Gorlick et al., 2014a)
BI-2536	(Markant et al., 2013) (Triscott et al., 2013) (Harris et al., 2012) (Julia Alejandra et al., 2017) (Czaplinski et al., 2016) (Liu et al., 2018)
Triapine	(Kunos et al., 2017) (Kunos and Ivy, 2018) (Kunos et al., 2019)
Triptolide	(Vispé et al., 2009) (Yan and Sun, 2018) (Kim et al., 2018) (Zhang et al., 2017)
KX2-391	(Ahluwalia et al., 2010) (Puls et al., 2011) (Antonarakis et al., 2013) (Wei et al., 2019)
Camptothecin	(Stewart et al., 2005) (Li et al., 2008) (Li et al., 2009)
Daunorubcin	(Creutzig et al., 2013)
Idarubicin	(Dreyer et al., 2003b) (Pei et al., 2016)
Etoposide	(Ashley et al., 1996) (Xu et al., 2017); NCT00003573
Idarubicin	(Dreyer et al., 2003a)

Irinotecan	(Grill et al., 2013) (Bomgaars et al., 2007)
Mitoxantrone	(Boon et al., 2003) (Bacolod et al., 2008) (Lian et al., 2019)
Pirarubicin	(Dhingra et al., 1995) (Iwadate et al., 2003) (Schor, 2009)
SN-38	(Vassal et al., 1997) (Courapied et al., 2010)
Topotecan	(Blaney et al., 1996) (Wong and Berkenblit, 2004) (Shackleford et al., 2019) (Le Teuff et al., 2020)
MK-1775 (AZD1775)	(Matheson et al., 2016) (Harris et al., 2014) (Wright et al., 2017) (Sarcar et al., 2011) (Restelli et al., 2018) (Chen et al., 2018a) (Sanai et al., 2018); NCT02095132
Doxorubicin	(Chamberlain et al., 1988) (Guerreiro et al., 2008) (Häcker et al., 2011) (Tjandra et al., 2020)
Epirubicin	(Hashimoto et al., 2018)
Sunitinib	(Yang et al., 2010) (Abouantoun et al., 2011)
APO866	(Cagnetta et al., 2015) (Tateishi et al., 2016) (Olesen et al., 2010)
YM155 (Sepantronium Bromide)	(Voges et al., 2016) (Calderone et al., 2014) (Abdel-Aziz et al., 2012) (Haberler et al., 2006) (Brun et al., 2015) (Iwasa et al., 2008)

Appendix 5.4. Published information used to prioritise compounds.

Chapter 6. Validation of *MYC*-dependent sensitivity to selected chemotherapeutics in Group 3 medulloblastoma isogenic cell lines

6.1 Introduction

The integration of 'omics' techniques has been key for the identification of tumour-specific genetic changes for the design of targeted therapeutic strategies. Extensive profiling of childhood Medulloblastoma has led to its robust classification of four main subgroups and the identification of significant substructures within each group with distinct molecular features and clinicopathological outcomes (Schwalbe et al., 2017).

Despite the wealth of molecular profiling data that describe MB, the availability of MB_{Group3} biomarkers with prognostic significance is still relatively poor, with *MYC* amplification or overexpression remaining the main biological signature. Even with the identification of critical genes like *MYC*, clinical-stage small-molecules which target *MYC* directly are still unavailable due to its structural properties, leaving indirect alternative strategies the main mechanistic approach to modulate *MYC* function in *MYC*-dependent tumours.

To increase our understanding of *MYC*'s role in MB_{Group3} biology, a high-throughput compound screen (HTCS) was performed (Chapter 5) on DOX-inducible *MYC* silencing MB_{Group3} isogenic models developed in Chapter 3, to identify critical *MYC*-dependent pathways in tumour growth, which could potentially be exploited for novel therapeutic approaches to treat this specific MB subgroup.

HTCS data was specifically interrogated to find *MYC*-dependent effects, where inhibition of specific proteins resulted in differential drug sensitivity between *MYC*-overexpressing and *MYC*-knockdown cell lines. This approach identified 82 small-molecule inhibitors to which MB_{Group3} cell lines expressing *MYC* exhibited higher sensitivity (greater growth inhibition).

False-positive results often occur with HTS technologies, necessitating validation of the results. For selection of drugs for further validation, the list of candidate hits was reduced by grouping the 82 compounds according to their main inhibitory target, and a representative of each class was selected. Criteria for selection were based on current published data of the compound, which involved information on the type of cancer used for, its involvement in clinical testing and its use for MB (summary table with the information used for selection can be seen in Table 5.4, Chapter 5).

Integration of chemosensitivity data for the *MYC*-regulable isogenic D425, D283 and HDMB03 MB_{Group3} cell lines, with in-house generated *MYC*-dependent transcriptional profiles of the tumour cell lines and primary MB tumours, implicated four main targetable molecular features as being important in the growth of *MYC* expressing MB_{Group3} cell lines: PLK, CHK, CDK and AURK (Chapter 5).

To validate the findings from this integrative approach and to characterise the effect of PLK, CHK, *CDK* and AURK inhibition on MB_{Group3} and its interaction with *MYC* expression, AZD7762 (CHK1 inhibitor), BI2536 (PLK1 inhibitor), Milciclib (CDK2 inhibitor) and MLN8237 (AURKA inhibitor) inhibitors, as representatives of compound classes, were selected for further testing

Given the accumulation of data pointing to the potential of using CHK1 inhibitors in the clinical setting to target *MYC*-dependent tumours, an additional CHK1/2 inhibitor, Prexasertib (LY2606368) was also selected for testing (NCT04023669) (Campagne et al., 2020, Maharaj et al., 2018, Endersby et al., 2018). The addition of a compound that was not previously tested in our screen, would also independently validate our findings indicating the potential efficacy of CHK1/2 inhibition in MB_{Group3}, and further potential for rapid clinical translation.

Considering the future design of combinatorial therapeutic approaches for treatment of Group 3 medulloblastoma, and validate the *MYC*-dependent effect of other representative compounds of each drug class, SN-38 (topoisomerase inhibitor) and MK-1775 (WEE1 inhibitor) and YM155 (BIRC5 inhibitor) were considered for further evaluation (details of selection and information can be seen in section 5.3 of Chapter 5).

To add relevance to our findings, to better characterise the chemosensitivity effects seen in the screen, and to assess the effects of the compounds on *MYC* expression, we aimed to validate the results in a varied panel of MB cell lines. The common thread observed after exposure of the isogenic cell lines to small molecule inhibitors (Chapter 4) was a reduced sensitivity to inhibitors upon *MYC*-silencing with shRNA. It was therefore important to study further the contribution of *MYC* over-expression to drug sensitivity. For this, other available non-MB_{Group3} cell lines, DAOY (MB_{SHH}) and UW228.2 (MB_{SHH}) were used to assess whether drug sensitivity effects differed according to MB subgroup status and *MYC*-expression levels (Higdon et al., 2017).

Apart from the original isogenic models, the parental D425, D283 and HDMB03 cell lines were added to the study, in addition to an additional MB_{Group3} cell line, D458-Med (D458).

6.2 Aims

The primary aim of this chapter is to (i) validate the *MYC*-dependent effect of the prime candidate inhibitors identified from the HTCS data analysis, (ii) investigate their direct effect on *MYC* expression to validate their suitability for the development of new indirect *MYC*-targeting approaches to treat *MYC*-dependent MB tumours.

- Validate the *MYC*-dependent effect of the inhibitors on a panel of MB cell lines
- Investigate the effect of PLK1, CHK1/2, CDK2 and AURKA inhibition on *MYC* expression and downstream pathway targets

6.3 Validation of MB cell lines' sensitivity to small molecule inhibitors

To verify the sensitivity results from the HTCS and validate the hits found, AZD7762 (CHK1 inhibitor), BI2536 (PLK1 inhibitor), MLN8237 (AURKA inhibitor), Milciclib (CDK2 inhibitor), SN-38 (topoisomerase inhibitor), MK-1775 (WEE1 inhibitor) and YM155 (BIRC5 inhibitor) inhibitors were assessed on a panel of MB cell lines (Table 6.1). The effect of the compounds on cell viability of all three *MYC*-regulable cell models (D425, D283 and HDMB03) and six parental MB cell lines (D425, D283, HDMB03, D458, DAOY, UW228.2) was examined by replicating the experimental conditions of the HTCS.

INHIBITOR/TARGET	CELL LINES
BI2536 (PLK1)	D425
MK1775 (WEE1)	D425 M2
Milciclib (CDK2)	D283
MLN8237 (AURKA)	D283 M2
SN38 (TopoI)	HDMB03
YM155 (BIRC5)	HDMB03 M2
AZD7762 (CHK1)	D458
Prexasertib (CHK1/2)	DAOY
	UW228.2

Table 6.1. Inhibitors and cell lines used in this study. Summary table of inhibitors and cell lines used in this study. Molecular target of the inhibitor enclosed in brackets. Isogenic cell lines are specified with 'M2'. TopoI = topoisomerase I

The validation approach replicated the experimental conditions of the HTCS to the best of our capabilities with the available technology. MB cells plated on 384 well plates were exposed to a single dose per well of 8 different concentrations of each inhibitor (0, 0.5, 1, 5, 10, 50, 100, 500, 1000, 5000nM) for a period of five days (further details on the HTCS methodology can be found in Chapter 2). Isogenic cell lines were pre-induced with DOX 48h prior to drugging. After exposure to the drug, cell viability was assessed using CTG reagent.

Luminescence readings were normalised to the luminescent signal of the negative control (DMSO only cells), and values used to generate dose-response curves with Prism from which IC_{50} values were calculated.

6.3.1 Validation of drug-sensitivity effects on isogenic cell lines

The use of the *MYC*-regulable MB_{Goup3} models was aimed specifically to identify inhibitors with a *MYC*-dependent effect. Small molecule compounds chosen from the screen for *in vitro* validation selectively inhibited the growth of *MYC*-overexpressing cell lines over those with *MYC*-knockdown with shRNA, with the exception of YM155, which equally inhibited the growth of the cells regardless of *MYC* expression levels (Figure 6.1).

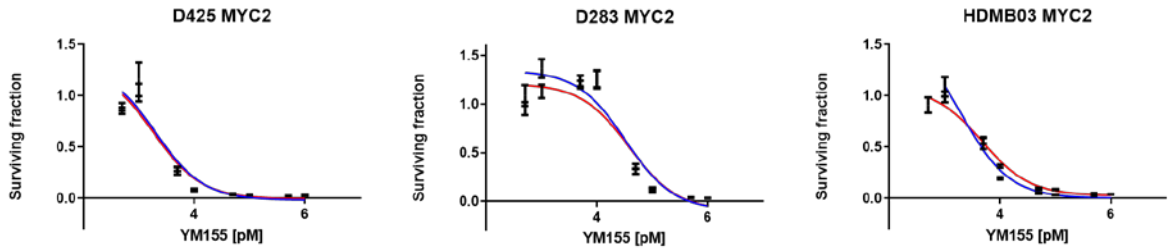

Figure 6.1. Example of growth-inhibitory curves from surviving fractions of D425, D283 and HDMB03 MYC2 to YM155. The graphs show the growth inhibitory effect of YM155 on D425, D283 and HDMB03 MYC2 overexpressing *MYC* (blue; -dox (MYC ON)) and with *MYC* silenced (red; +dox (MYC OFF)). Surviving fractions at each concentration from the screen (3 replicates) were used to generate dose-inhibitory growth curves that fit a non-linear regression model. Curves are presented as log(concentration)vs response.

Cell lines overexpressing *MYC* exhibited higher sensitivity to the inhibitors when compared to cell lines with *MYC* knockdown. Treatment with the inhibitors identified to have a *MYC*-dependent effect caused a significant (ratio paired students t-test, $p<0.05$) reduction of D425, D283 and HDMB03 (MYC2 construct) cells proliferation when compared to their counterparts expressing lower levels of *MYC* (Figure 6.2, 6.3 and 6.4). The same *MYC*-dependent growth inhibitory effect was seen across cell lines for MYC3 (Appendix 6.1, 6.2 and 6.3, for D425, D283 and HDMB03, respectively). No differences in growth inhibition were seen for the NS construct of cell lines, when grown in the presence and absence of DOX (Appendix 6.4, 6.5, 6.6 for D425, D283 and HDMB03, respectively).

In accordance with the results of the screen, treatment with the control drug YM155 (*BIRC5* inhibitor) caused greater growth inhibition of MB_{Group3} cell lines compared to the effect of the rest of compounds tested, equally for both cells with *MYC* knockdown and cells overexpressing *MYC*.

A)

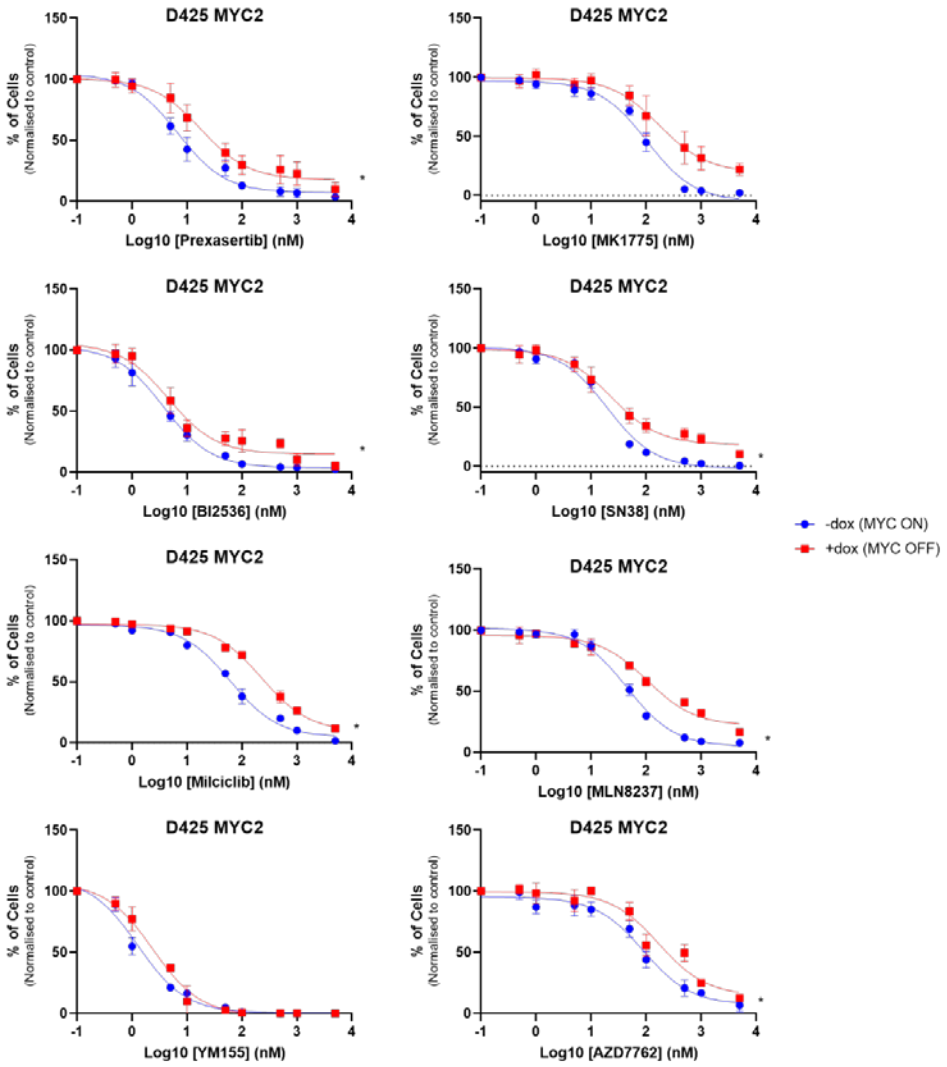

B)

D425

	BI2536		Milciclib		MLN8237		MK1775	
	MYC2 -DOX (MYC ON)	MYC2 +DOX (MYC OFF)	MYC2 -DOX (MYC ON)	MYC2 +DOX (MYC OFF)	MYC2 -DOX (MYC ON)	MYC2 +DOX (MYC OFF)	MYC2 -DOX (MYC ON)	MYC2 +DOX (MYC OFF)
IC50	3.776	4.6	61.47	227.9	44.88	104.9	103.3	171.9
P value	0.0099		0.041		0.0369		0.0456	
SD of log(ratios)	0.2587		0.2784		0.2317		0.4295	
SEM of log(ratios)	0.08179		0.08804		0.07328		0.1358	

	SN38		YM155		AZD7762		Prexasertib	
	MYC2 -DOX (MYC ON)	MYC2 +DOX (MYC OFF)	MYC2 -DOX (MYC ON)	MYC2 +DOX (MYC OFF)	MYC2 -DOX (MYC ON)	MYC2 +DOX (MYC OFF)	MYC2 -DOX (MYC ON)	MYC2 +DOX (MYC OFF)
IC50	19.63	23.09	1.274	2.39	89.66	169.2	6.819	17.85
P value	0.0284		0.5525		0.0154		0.0068	
SD of log(ratios)	0.4678		0.227		0.1219		0.2119	
SEM of log(ratios)	0.1479		0.07179		0.03855		0.0.067	

Figure 6.2. Growth-inhibitory effect of 'hit' compounds from HTCS on D425 MYC2 cells.A) Concentration-dependent inhibitory dose-curves of D425 MYC2 MB_{Group3} cells to treatment with BI2536 (PLK1 inhibitor), SN38 (topoisomerase I), Milciclib (CDK2 inhibitor), MLN8237 (AURKA inhibitor), YM155 (BIRC5 inhibitor), MK1775 (WEE1 inhibitor), AZD7762 (CHK1 inhibitor) and Prexasertib (CHK1/2 inhibitor). D425 MYC2, cultured in the absence (-dox; MYC ON) and presence (+dox; MYC OFF) of DOX for *MYC* knockdown, were exposed to a single dose of 8 different concentrations of each inhibitor (0.5, 1, 5, 10, 50, 100, 500, 1000, 5000nM) for a period of five days. After treatment, cell viability was measured with CellTiter-Glo and values obtained analysed with Prism8 to generate dose-response growth inhibition curves that fit a non-linear regression model. Curves are presented as log(concentration) vs response, and represent the percentage of cell viability of two independent experiments done in triplicate, relative to cells grown in the presence of DMSO. The growth inhibitory effect of the drug on D425 MYC2 overexpressing cell lines and with *MYC* knockdown was compared by paired student's t-test (statistical significance denoted by *; *p<0.05). B) Table summarising the half maximal inhibitory concentration (IC_{50}) calculated from the dose-response curves. Significant differences between cells expressing high (-dox: MYC ON) and low (+dox: MYC OFF) levels of *MYC* was calculated with a ratio paired student's t-test (p-value). *P*-value is shown with the SD and SEM.

A)

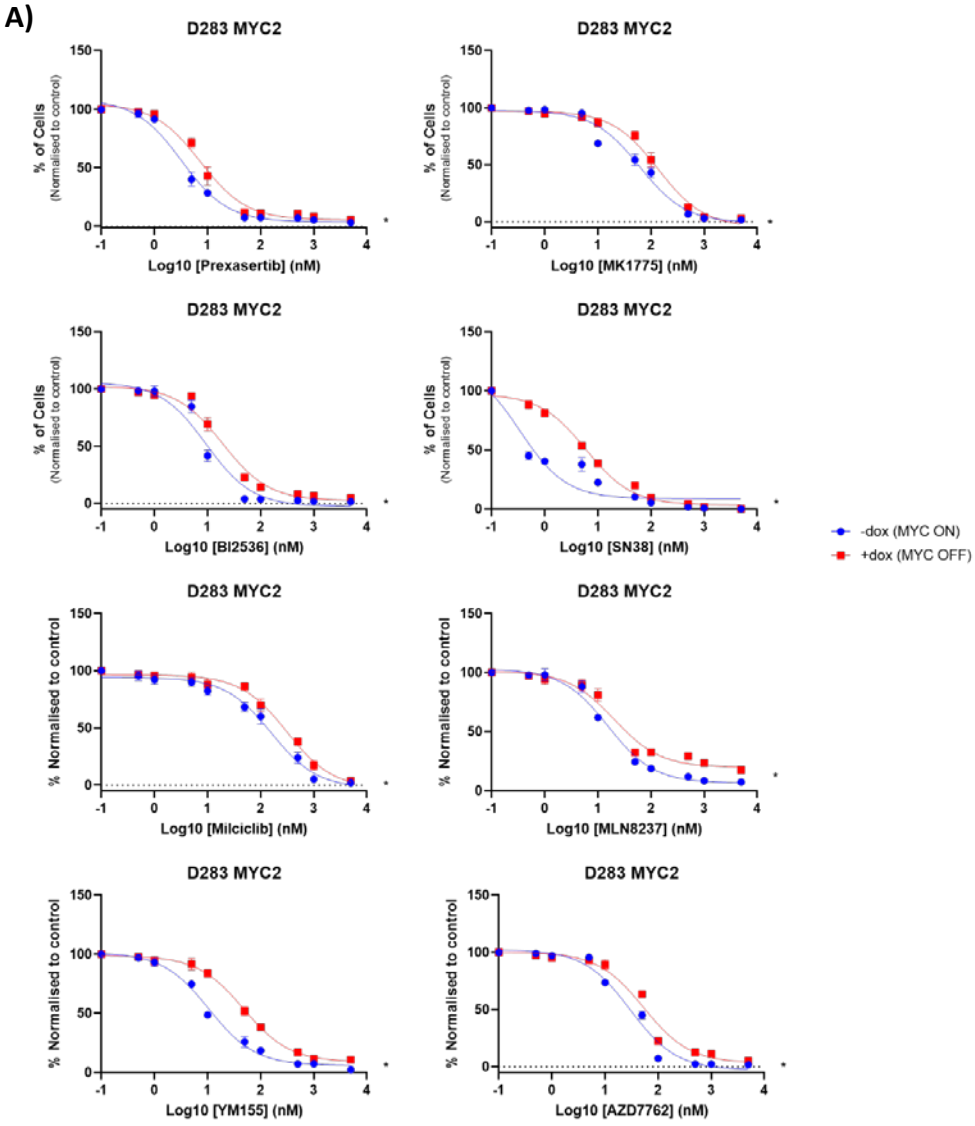

B)

D283

	BI2536		Milciclib		MLN8237		MK1775	
	MYC2 -DOX (MYC ON)	MYC2 +DOX (MYC OFF)	MYC2 -DOX (MYC ON)	MYC2 +DOX (MYC OFF)	MYC2 -DOX (MYC ON)	MYC2 +DOX (MYC OFF)	MYC2 -DOX (MYC ON)	MYC2 +DOX (MYC OFF)
IC50	9.527	19.34	157.7	309.9	15.38	20.2	61.35	136.5
P value	0.029		0.0436		0.0171		0.0198	
SD of log(ratios)	0.2029		0.1665		0.182		0.1047	
SEM of log(ratios)	0.06417		0.05266		0.05757		0.03311	

	SN38		YM155		AZD7762		Prexasertib	
	MYC2 -DOX (MYC ON)	MYC2 +DOX (MYC OFF)	MYC2 -DOX (MYC ON)	MYC2 +DOX (MYC OFF)	MYC2 -DOX (MYC ON)	MYC2 +DOX (MYC OFF)	MYC2 -DOX (MYC ON)	MYC2 +DOX (MYC OFF)
IC50	0.3466	5.999	10.64	47.88	29.86	53.51	3.259	7.367
P value	<0.0001		0.0089		0.0258		0.0011	
SD of log(ratios)	0.1086		0.2063		0.3038		0.09708	
SEM of log(ratios)	0.03435		0.06523		0.09607		0.0307	

Figure 6.3. Growth-inhibitory effect of 'hit' compounds from HTCS on D283 MYC2 cells.A)Concentration-dependent inhibitory dose-curves of D283 MYC2 MB_{Group3} cells to treatment with BI2536 (PLK1 inhibitor), SN38 (topoisomerase I), Milciclib (CDK2 inhibitor), MLN8237 (AURKA inhibitor), YM155 (BIRC5 inhibitor), MK1775 (WEE1 inhibitor), AZD7762 (CHK1 inhibitor) and Prexasertib (CHK1/2 inhibitor). D283 MYC2, cultured in the absence (-dox; MYC ON) and presence (+dox; MYC OFF) of DOX for *MYC* knockdown, were exposed to a single dose of 8 different concentrations of each inhibitor (0.5, 1, 5, 10, 50, 100, 500, 1000, 5000nM) for a period of five days. After treatment, cell viability was measured with CellTiter-Glo and values obtained analysed with Prism8 to generate dose-response growth inhibition curves that fit a non-linear regression model. Curves are presented as log(concentration) vs response, and represent the percentage of cell viability of two independent experiments done in triplicate, relative to cells grown in the presence of DMSO. The growth inhibitory effect of the drug on D283 MYC2 overexpressing cell lines and with *MYC* knockdown was compared by paired student's t-test (statistical significance denoted by *; *p<0.05). B) Table summarising the half maximal inhibitory concentration (IC_{50}) calculated from the dose response curves. Significant differences between cells expressing high (-dox: MYC ON) and low (+dox: MYC OFF) levels of *MYC* was calculated with a ratio paired student's t-test (p-value). *P*-value is shown with the SD and SEM.

A)

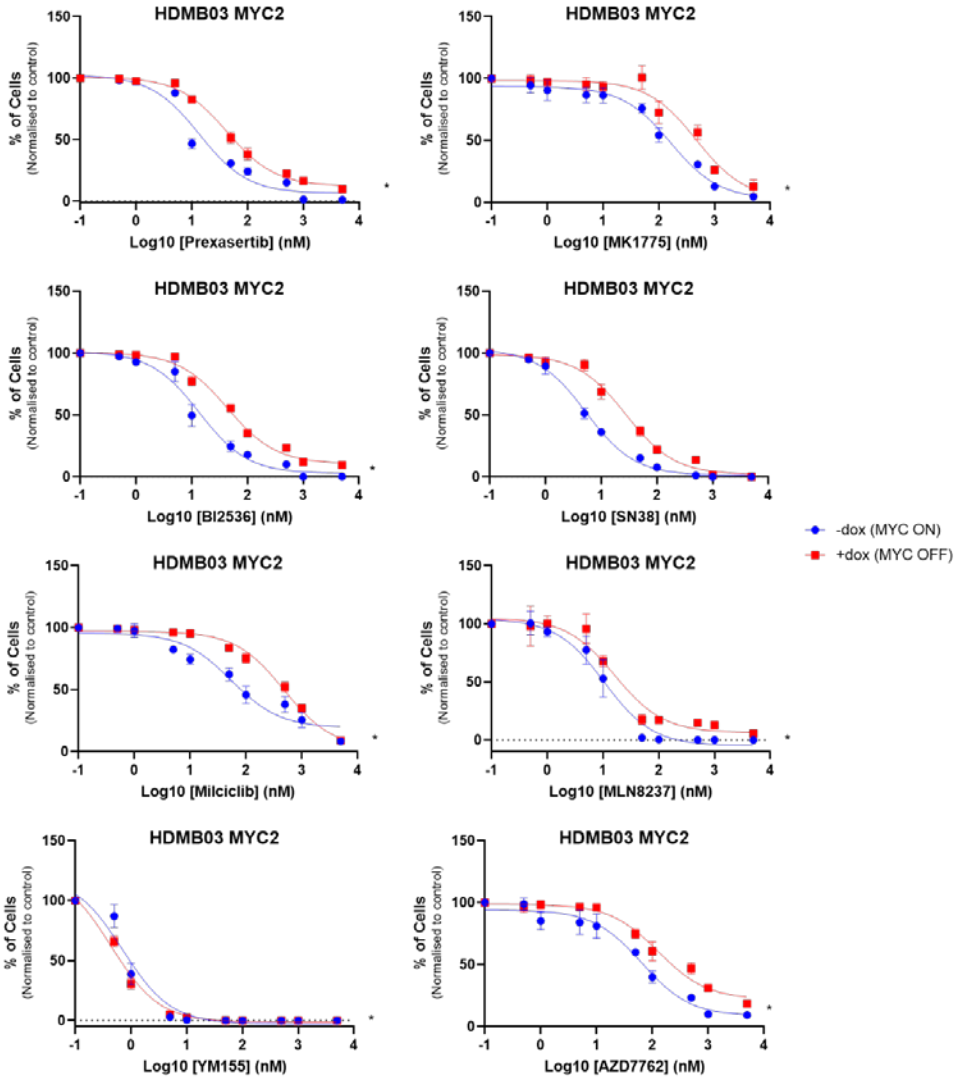

B)

HDMB03

	BI2536		Milciclib		MLN8237		MK1775	
	MYC2 -DOX (MYC ON)	MYC2 +DOX (MYC OFF)	MYC2 -DOX (MYC ON)	MYC2 +DOX (MYC OFF)	MYC2 -DOX (MYC ON)	MYC2 +DOX (MYC OFF)	MYC2 -DOX (MYC ON)	MYC2 +DOX (MYC OFF)
IC50	13.68	43.72	54.51	477.4	10.55	16.22	163.6	471.1
P value	0.049		0.0068		0.0158		0.0162	
SD of log(ratios)	0.6276		0.07484		0.9447		0.1473	
SEM of log(ratios)	0.1985		0.02367		0.2987		0.04657	

	SN38		YM155		AZD7762		Prexasertib	
	MYC2 -DOX (MYC ON)	MYC2 +DOX (MYC OFF)	MYC2 -DOX (MYC ON)	MYC2 +DOX (MYC OFF)	MYC2 -DOX (MYC ON)	MYC2 +DOX (MYC OFF)	MYC2 -DOX (MYC ON)	MYC2 +DOX (MYC OFF)
IC50	5.344	27.85	0.7099	0.4432	65.06	128.3	13.61	42.41
P value	0.096		0.0249		0.0141		0.0112	
SD of log(ratios)	0.6159		0.2924		0.1634		11.05	
SEM of log(ratios)	0.1948		0.09248		0.05168		3.495	

Figure 6.4. Growth-inhibitory effect of 'hit' compounds from HTCS on HDMB03 MYC2 cells. A)Concentration-dependent inhibitory dose-curves of HDMB03 MYC2 MB_{Group3} cells to treatment with BI2536 (PLK1 inhibitor), SN38 (topoisomerase I), Milciclib (*CDK2* inhibitor), MLN8237 (*AURKA* inhibitor), YM155 (BIRC5 inhibitor), MK1775 (WEE1 inhibitor), AZD7762 (CHK1 inhibitor) and Prexasertib (CHK1/2 inhibitor). HDMB03 MYC2, cultured in the absence (-dox; MYC ON) and presence (+dox; MYC OFF) of DOX for MYC knockdown, were exposed to a single dose of 8 different concentrations of each inhibitor (0.5, 1, 5, 10, 50, 100, 500, 1000, 5000nM) for a period of five days. After treatment, cell viability was measured with CellTiter-Glo and values obtained analysed with Prism8 to generate dose-response growth inhibition curves that fit a non-linear regression model. Curves are presented as log(concentration) vs response, and represent the percentage of cell viability of two independent experiments done in triplicate, relative to cells grown in the presence of DMSO. The growth inhibitory effect of the drug on HDMB03 MYC2 overexpressing cell lines and with *MYC* knockdown was compared by paired student's t-test (statistical significance denoted by *; *p<0.05). B)Table summarising the half maximal inhibitory concentration (IC_{50}) calculated from the dose-response curves. Significant differences between cells expressing high (-dox: MYC ON) and low (+dox: MYC OFF) levels of *MYC* was calculated with a ratio paired student's t-test (*P*-Value). *P*-value is shown with the SD and SEM.

Despite the differences in growth seen between isogenic cells expressing high and low levels of MYC, the IC_{50} calculated through the dose-response growth inhibition curves (summarised in Figure 6.2-B, 6.3-B and 6.4-B, for D425, D283 and HDMB03 respectively) did not always correlate with the effect seen on cell proliferation. For example, treatment of D425 MYC2 cells with BI2536 resulted in almost indistinguishable IC_{50} values between experimental arms. Following *MYC* knockdown, a stable population of drug-resistant cells was seen at higher concentrations of the inhibitors, therefore the IC_{50} values did not represent the true *MYC*-dependent effect on cell proliferation.

Concentrations above the IC_{50} had to be considered in order to fully appreciate the change seen in cells proliferative rate. Calculation of IC_{80} was found to better correlate with the differential *MYC*-dependent growth-inhibitory effect seen in the dose-response curves (Fallahi-Sichani et al., 2014). In fact, Milciclib (CDK2 inhibitor), despite having little growth inhibitory effect at lower doses compared to other inhibitors, showed the greatest consistent reduction in sensitivity of *MYC*-overexpressing cell lines when compared to those with *MYC* knockdown, averaging 70% reduction across cell lines (Table 6.2).

	D425		**D283**		**HDMB03**		
	IC_{50}/ IC_{50} +DOX	**%**	**IC_{50}/ IC_{50} +DOX**	**%**	**IC_{50}/ IC_{50} +DOX**	**%**	**average % reduction**
BI2536 (PLK1)	0.82	17.9	0.49	50.7	0.31	68.7	45.8
Milciclib (CDK2)	0.27	73.0	0.51	49.1	0.11	88.6	70.2
MLN8237 (AURKA)	0.43	57.2	0.76	23.9	0.65	35	38.7
MK1775 (WEE1)	0.60	39.9	0.45	55.1	0.35	65.3	53.4
SN38 (TopoI)	0.85	15	0.22	77.8	0.19	80.8	57.9
YM155 (BIRC5)	0.53	46.7	0.06	94.2	1.60	-60.2	26.9
AZD7762 (CHK1)	0.53	47.0	0.56	44.2	0.51	49.3	46.8
Prexasertib (CHK1/2)	0.38	61.8	0.44	55.9	0.32	67.9	61.9
BI2536 IC_{80}	0.62	38.2					

Table 6.2. Sensitivity of D425, D283 and HDMB03 MYC2 cells to treatment with inhibitors tested.A) Comparison of the IC_{50} values calculated from the dose-response growth inhibition curves generated on D425, D283 and HDMB03 MYC2 cultured in the absence (-dox; MYC ON) and presence (+dox; MYC OFF) of DOX for MYC knockdown. The table shows the ratio between the IC_{50} calculated from cells expressing high levels of *MYC*, and those with MYC knockdown (+dox). Table summarises the percentage reduction in sensitivity in the presence of *MYC*. For D425 MYC2 treatment with BI2536, IC_{80} concentration was used to better represent the *MYC*-dependent growth inhibitory effect. B) Consistency in the reduction of cells sensitivity across cell lines is seen in the Average % reduction table. Data is presented as the % of the average of the ratio between IC_{50} of cells expressing high levels of *MYC* and with *MYC* silenced (IC_{50}/ IC_{50} +DOX), of three independent experiments.

Through the comparison of the IC_{50} between D425, D283 and HDMB03 MYC2 expressing high and low levels of *MYC*, Prexasertib was found to have the most consistent *MYC*-dependent reduction in sensitivity (averaging 62% across cell lines)(Table 6.2).

A significant difference in sensitivity was seen when comparing the effect of CHK1 inhibitors Prexasertib and AZD7762. Prexasertib reduced viability of MB_{Group3} cell lines overexpressing *MYC* by around 62%, whereas after exposure to AZD7762 only an average of 47% was seen across D425, D283 and HDMB03. Prexasertib (LY2606368), apart from being a potent small molecule inhibitor of CHK1 protein kinase activity *in vitro*, also inhibits CHK2, with no apparent selectivity between CHK1 and CHK2 (Angius et al., 2020). On the other hand, while AZD7762 also inhibits the expression of both CHK1 and CHK2 proteins, it has selectivity for CHK1 (Matthews et al., 2013).

The CHK enzymes convey the signals received from upstream DNA-damage sensing proteins, principally ATM and ATR, to downstream effectors of cell cycle arrest and DNA repair (Smith et al., 2010). There is substantial overlap in the activation and substrates of CHK1 and CHK2. CHK2 is particularly important in the response to double strand DNA breaks (DSB) signalled through activation of ATM, and controls the p53-dependent early phase G_1-S checkpoint (Antoni et al., 2007, Garrett and Collins, 2011), although it can also contribute to S- and G_2-M-phase checkpoints. In contrast, CHK1 signalling is more important in response to single strand DNA breaks (SSB) and stalled DNA replication signalled by activation through ATR, and resulting in later S-phase and G_2-M checkpoint arrest (Dai and Grant, 2010, Matthews et al., 2013).

Although both drugs target CHK1, MB_{Group3} cell lines appeared to be extremely sensitive to Prexasertib, suggesting the importance of each of the signalling pathways associated with CHK1 and CHK2 and their effect on MB_{Group3} cell growth.

6.3.2 Validation of drug-sensitivity effects on parental cell lines

To further examine the effect on growth of the candidate inhibitors in a MB subgroup-specific context, sensitivity to the inhibitors was investigated in MB_{Group3} and MB_{SHH} parental cell lines. DAOY and UW228.2 (both MB_{SHH}) inherently express lower levels of *MYC*, compared to the MB_{Group3} that are characterised by *MYC* amplification or overexpression (Figure 6.5). Comparison of the effect the inhibitors have across subgroups will bring a better understanding of *MYC*-related drug sensitivity effects.

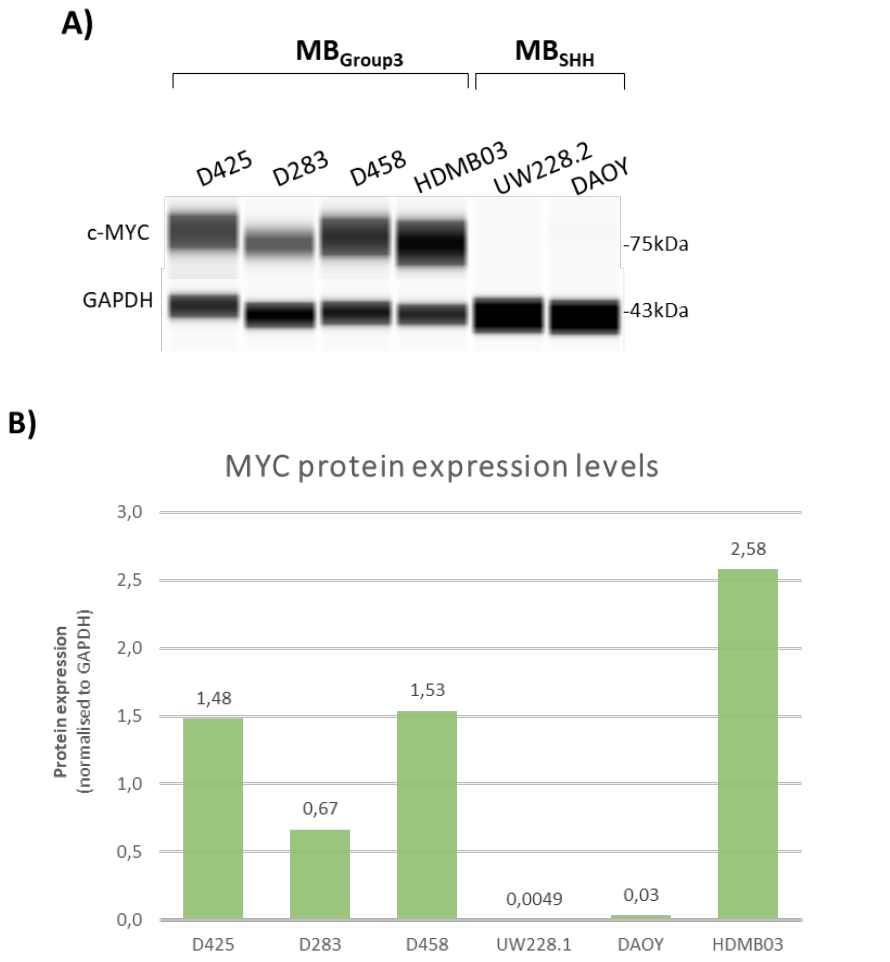

Figure 6.5. MYC protein expression levels in parental MB cell lines. A)Automated western blot (Wes) of MYC protein levels expressed by D425, D283, HDMB03, D458, DAOY and UW228.2, belonging to MB_{Group3} and MB_{SHH} subgroups. B)densitometry analysis of MYC protein expression levels. MYC expression was normalised to the loading control GAPDH.

Comparison of the concentration-dependent growth-inhibitory curves revealed that the inhibitors tested markedly inhibited the growth of MB_{Group3} cell lines at lower concentrations when compared to UW228.2 (MB_{SHH})(Figure 6.7). Similarities in drug sensitivity between DAOY and MB_{Group3} cell lines was unexpected as DAOY belongs to MB_{SHH}. However, it is dependent on *MYC* for its growth as demonstrated by our own and published CRISPR-CAS9 experiments (Selby et al., 2017), so potentially drugs that have a growth-inhibitory *MYC*-dependent effect would affect this cell line. In contrast, UW228.2 (MB_{SHH}) showed a marked difference in sensitivity, where treatment with Prexasertib (CHK1/2), BI2536 (PLK1), Milciclib (CDK2) or MLN8237 (AURKA) had little to no inhibitory effect on this cell line (Figure 6.7).

The lack of inhibitory effect on UW228.2 correlated with the IC_{50} values calculated from the growth-inhibitory curves (Table 6.3). Comparison of IC_{50}s from all parental cell lines revealed UW228.2 had reduced sensitivity to most of the compounds, changing IC_{50} from the nanomolar concentration range to the micromolar one. UW228.2 was still sensitive to BIRC5 (IC_{50}=23.53nM), but not as sensitive as the other cell lines (averaging 1.87nM). Similar IC_{50} values were seen across MB_{Group3} cell lines, corresponding well with the growth-inhibitory effect seen after treatment (see section 6.3.1 of this Chapter). DAOY showed similar sensitivities to the compounds when compared to Group 3 cell lines, with the exception of Milciclib (CDK2 inhibitor) which it was comparatively resistant to. From all the inhibitors tested, Milciclib was the only compound that had a *MYC*-dependent subgroup specific growth-inhibitory effect.

IC_{50}[nM]	**BI2536** (PLK1)	**MK1775** (WEE1)	**Milciclib** (CDK2)	**MLN8237** (AURKA)	**SN38** (topoI)	**YM155** (BIRC5)	**AZD7762** (CHK1)	**Prexasertib** (CHK1/2)
D425	3.381	134.5	110.3	20.88	26.58	0.9729	68.79	4.032
D283	7.695	144.7	105.2	36.95	2.67	6.117	33.72	2.11
HDMB03	7.97	198	132.9	20.14	3.56	0.41	50.82	5.85
D458	1.984	67.78	159.5	29.4	2.43	0.76	54.5	2.11
DAOY	2.875	94.58	2669	54.61	2.75	1.12	91.02	6.39
UW228.1	14.27	3045	6342	1664	331	23.53	2852	43.59

Table 6.3. Drug sensitivity effect of MB parental cell lines to hit compounds from high throughput screen. Cell viability assays of D425, D283, HDMB03 and D458 for MB_{Group3}, and DAOY and UW228.2 for MB_{SHH}, after 3 days of a single exposure of 8 different inhibitor concentrations were used to generate dose-response growth inhibition curves with Prism, from which IC_{50} values (nM) were calculated to determine cells sensitivity to the compounds. IC_{50} values presented are from the mean of triplicate data of least three independent experiments.

A)

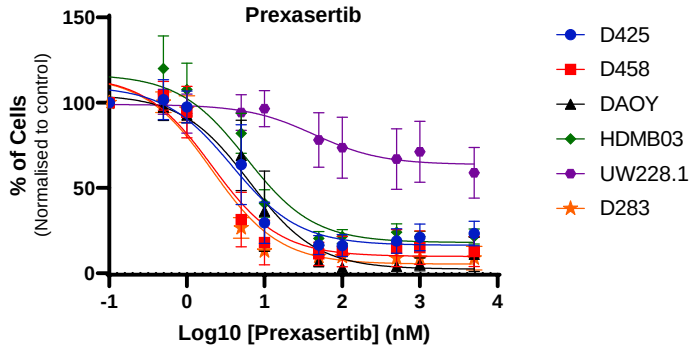

	Prexasertib					
	D425	D458	DAOY	HDMB03	UW228.1	D283
LogIC50	0.578	0.3232	0.8056	0.7668	1.639	0.3216
IC50	3.784	2.105	6.392	5.845	43.59	2.097
95% CI IC50	2.787 to 5.107	1.583 to 2.800	5.076 to 8.036	4.589 to 7.445	22.12 to 85.25	1.813 to 2.425

B)

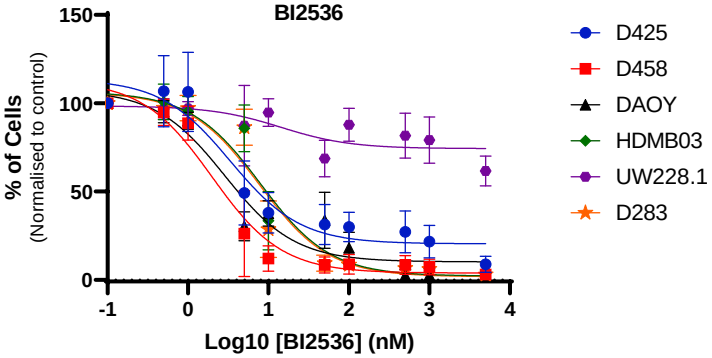

	BI2536					
	D425	D458	DAOY	HDMB03	UW228.1	D283
LogIC50	0.529	0.2974	0.4587	0.9015	1.154	0.8862
IC50	3.381	1.984	2.875	7.97	14.27	7.695
95% CI IC50	2.417 to 4.739	1.540 to 2.556	2.112 to 3.930	6.461 to 9.842	5.151 to 44.31	6.480 to 9.144

C)

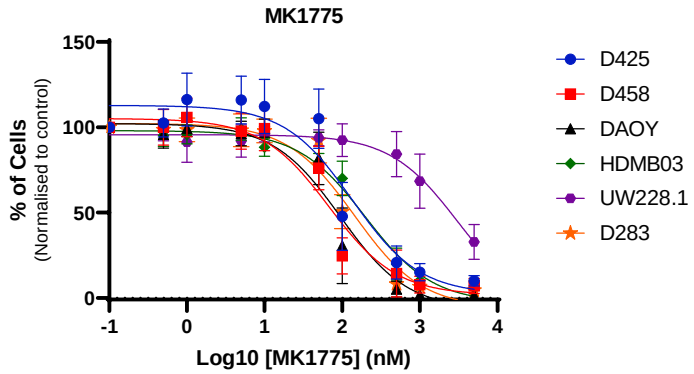

	MK1775					
	D425	D458	DAOY	HDMB03	UW228.1	D283
LogIC50	2.129	1.831	1.976	2.297	3.484	2.16
IC50	134.5	67.78	94.58	198	3045	144.7
95% CI IC50	100.2 to 182.3	51.38 to 89.37	75.71 to 118.4	169.0 to 232.0	2015 to 5142	124.0 to 169.1

D)

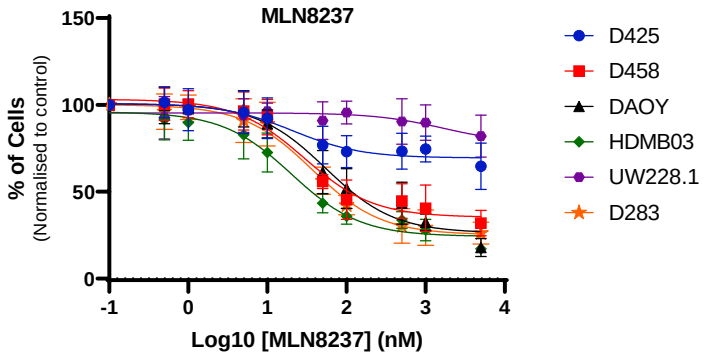

	MLN8237					
	D425	D458	DAOY	HDMB03	UW228.1	D283
LogIC50	1.32	1.468	1.737	1.304	3.221	1.568
IC50	20.88	29.4	54.61	20.14	1664	36.95
95% CI IC50	10.62 to 41.38	21.23 to 40.68	40.58 to 73.57	15.28 to 26.62	246.6 to ???	30.17 to 45.15

E)

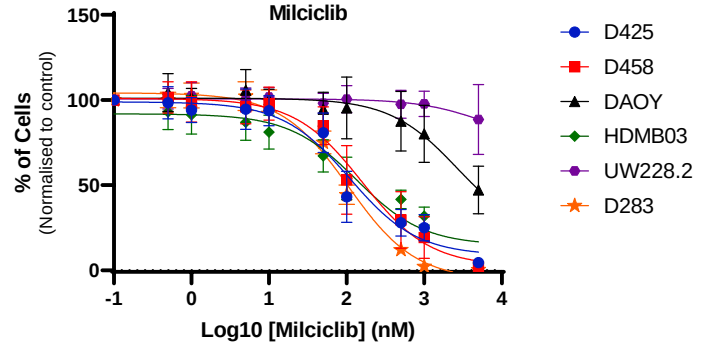

	Milciclib					
	D425	D458	DAOY	HDMB03	UW228.1	D283
LogIC50	2.043	2.203	3.426	2.124	3.802	2.022
IC50	110.3	159.5	2669	132.9	6342	105.2
95% CI IC50	84.52 to 145.3	113.6 to 227.6	1295 to 7963	87.15 to 214.6	661.7 to ???	93.07 to 118.9

F)

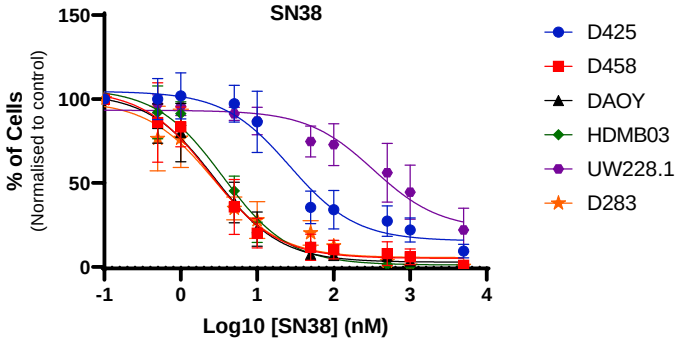

	SN38					
	D425	D458	DAOY	HDMB03	UW228.1	D283
LogIC50	1.425	0.3861	0.4385	0.551	2.52	0.4271
IC50	26.58	2.433	2.745	3.557	331	2.674
95% CI IC50	20.35 to 34.76	1.806 to 3.267	2.248 to 3.342	3.037 to 4.160	196.6 to 530.0	2.077 to 3.429

G)

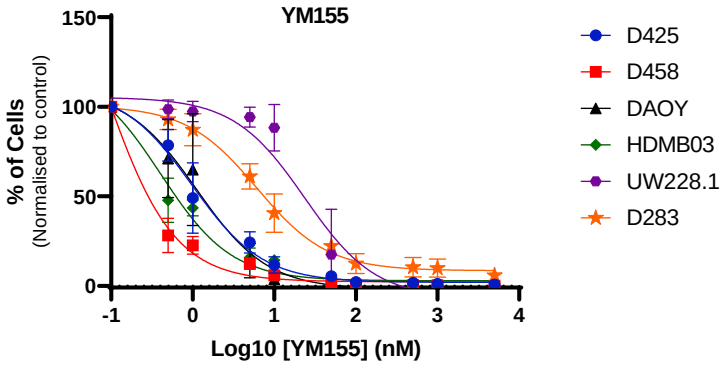

	YM155					
	D425	D458	DAOY	HDMB03	UW228.1	D283
LogIC50	-0.01194	-1.116	0.04958	-0.3902	1.372	0.7866
IC50	0.9729	0.07648	1.121	0.4072	23.53	6.117
95% CI IC50	0.8034 to 1.185	0.05095 to 0.1045	0.8408 to 1.501	0.3363 to 0.4918	19.90 to 27.82	5.416 to 6.909

H)

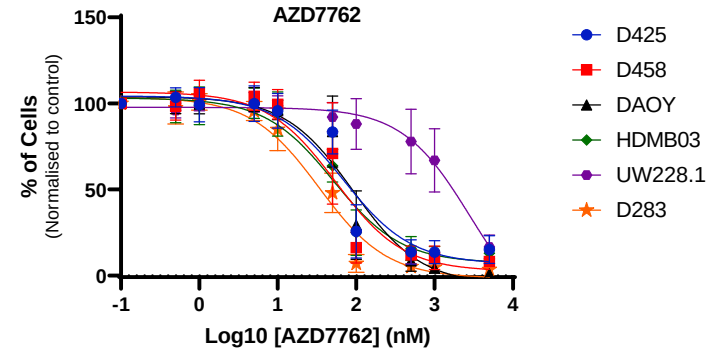

	AZD7762					
	D425	D458	DAOY	HDMB03	UW228.1	D283
LogIC50	1.838	1.736	1.959	1.706	3.455	1.528
IC50	68.79	54.5	91.02	50.82	2852	33.72
95% CI IC50	53.09 to 88.99	40.20 to 73.69	72.17 to 115.0	40.98 to 62.89	1977 to 4442	29.13 to 38.97

Figure 6.6. Growth-inhibitory effect of 'hit' compounds from the screen on parental MB cell lines. Concentration-dependent dose-response inhibition curves of MB_{Group3} and MB_{SHH} cell lines to treatment with A)Prexasertib (CHK1/2 inhibitor), B) BI2536 (PLK1 inhibitor), C)MK1775 (WEE1 inhibitor), D)MLN8237 (AURKA inhibitor), E)Milciclib (CDK2 inhibitor), F)SN38 (topoisomerase I), G)YM155 (BIRC5 inhibitor) and H)AZD7762 (CHK1 inhibitor). D425, D283, HDMB03, D458, DAOY and UW228.2 were exposed to a single dose of 8 different concentrations of each inhibitor (0.5, 1, 5, 10, 50, 100, 500, 1000, 5000nM) for a period of five days. After treatment, cell viability was measured with CellTiter-Glo and values obtained analysed with Prism8 to generate dose-response growth inhibitory curves that fit a non-linear regression model. Curves are presented as log(concentration) vs response, and represent the percentage of cell viability of two independent experiments done in triplicate, relative to cells grown in the presence of DMSO. IC_{50} values (nM) calculated for each cell line are summarised underneath each graph.

Comparison of chemosensitivity displayed by the isogenic models to the sensitivity of their parental cell lines showed no statistically significant differences (p>0.05). The lack of significant differences in cell sensitivity between the *MYC*-regulable cells and their parental corroborates the suitability of the cell lines as valid models to study MB_{Group3}.

To further validate these findings, the time of drug exposure in the assays was reduced from 5 days to 3 days. To ensure cells sensitivity to the inhibitors did not change with time of drug exposure, dose-response curves to the inhibitors were determined with drug exposures of 72h instead of 120h. Comparable *MYC*-dependent effects of the inhibitors was seen at 72h exposures using MYC2 constructs in all cell lines. Since significant differences in cell growth inhibition was still seen at 72h mark, and conscious about time constraints to finalise experimentation, remaining validation experiments were performed using MYC2 constructs and 3-day drug exposures.

6.4 Effect of pharmacological inhibition of PLK1, CHK1, CDK2 and AURKA on *MYC* expression and downstream pathway targets

From the results, it was evident that the inhibitors tested had a greater effect on cell lines expressing high levels of *MYC*, when compared to those that had *MYC* silenced with shRNA. Following the validation of the *MYC*-dependent growth-inhibitory effect, we sought to determine the impact of the inhibitors on *MYC* expression and on downstream pathway targets to assess whether the effect was specific to *MYC*-expression.

Following the rationale previously described, it was decided that in regards to the isogenic cell lines the remaining study would focus on the MYC2 shRNA constructs (MYC2). D425 MYC2, D283 MYC2 and HDMB03 MYC2, with and without pre-treatment with DOX for MYC knockdown, were exposed for 72h to a single dose of three different concentrations of each inhibitor; half the IC_{50} ($0.5xIC_{50}$), IC_{50} (IC_{50}), and twice the IC_{50} ($2xIC_{50}$), previously calculated with the dose-response growth inhibition curves and summarised in Table 6.3. IC_{50} values from *MYC*-overexpressing cell lines were used to treat their corresponding counterpart with *MYC* knockdown.

Protein analysis and quantification was done with Wes (automated western blot) (methodology explained in Chapter 2). To account for changes in protein expression as a consequence of treatment with the inhibitors, untreated cells (DMSO only) for each condition were used as a reference control.

Following the same methodology, the *MYC*-dependent effect of the inhibitors was also tested in the panel of parental MB cell lines, consisting of 4 different MB_{Group3} (D425, D283, HDMB03 and D458) and two MB_{SHH} (DAOY and UW228.2)(as described in section 6.3.2), to understand the effect *MYC* has in a specific-subgroup context.

6.4.1 PLK1 inhibition

When analysed at the protein level with Wes, BI2536 effectively reduced the total amount of PLK1, proving the effectiveness of the inhibitor on its main target. Downregulation of PLK1 was seen both in *MYC*-overexpressing and in *MYC* knockdown cell lines. PLK1 inhibition further reduced protein levels of MYC, when silenced with shRNA (Figure 6.7).

Treatment of isogenic cell lines with BI2536 caused a dose-dependent decrease in MYC protein levels across cell lines, both expressing high-levels of *MYC* and with *MYC* silenced. BI536 had the greatest effect in downregulating levels of MYC in D425, with a reduction of 70% when exposed to IC_{50} concentration when compared to its untreated control (Figure 6.7, A). To a similar degree, when exposed to the IC_{50}, MYC protein expression levels were reduced by 60% in D283 (Figure 6.7, B). PLK1 inhibition only reduced MYC protein levels by 50% in HDMB03 (Figure 6.7, C).

Inhibition of PLK1 had an additive effect with *MYC* knockdown, which further reduced MYC protein levels. D283 was the only cell line that upon *MYC* knockdown *PLK1* inhibition did not further reduce MYC protein levels between exposures of IC_{50} and $2xIC_{50}$.

Analysis of downstream effectors of PLK1 showed evidence of the effectiveness of the inhibitor on MB cell lines. Downregulation of PLK1 was greater in *MYC*-overexpressing cell lines when compared to *MYC*-knockdown.

Downregulation of MYC expression caused by PLK1 inhibition was accompanied with a reduction of levels of pCDC25 and MCL1. The regulatory effect of *PLK1* on CDC25 is represented in Figure 6.8 (Kousholt et al., 2012). Downregulation of protein levels of PLK1 and downstream effectors of its signalling pathway proved the efficacy of BI2536 in inhibiting the function of its main molecular target.

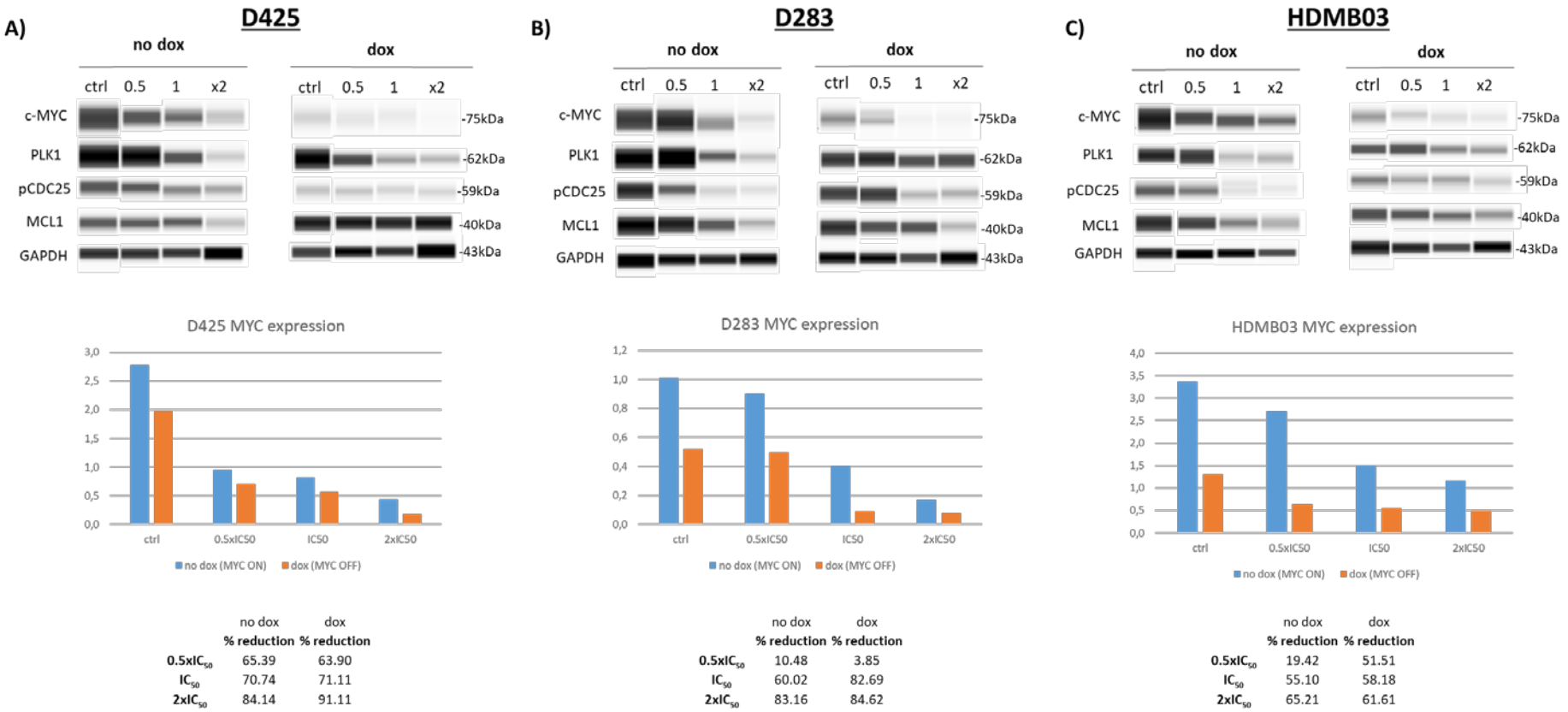

	no dox % reduction	dox % reduction
0.5xIC$_{50}$	65.39	63.90
IC$_{50}$	70.74	71.11
2xIC$_{50}$	84.14	91.11

	no dox % reduction	dox % reduction
0.5xIC$_{50}$	10.48	3.85
IC$_{50}$	60.02	82.69
2xIC$_{50}$	83.16	84.62

	no dox % reduction	dox % reduction
0.5xIC$_{50}$	19.42	51.51
IC$_{50}$	55.10	58.18
2xIC$_{50}$	65.21	61.61

Figure 6.7. Effect of PLK1 inhibition by BI2536 in isogenic D425, D283 and HDMB03 MB cell lines on MYC protein expression and downstream pathway targets. A) Automated western blot (Wes) of MYC protein levels expressed by D425, D283 and HDMB03 MYC2, cultured in the presence (dox) and absence (no dox) of doxycycline for *MYC* knockdown, after a single exposure with half the IC_{50} (0.5xIC_{50}; 0.5),, IC_{50} (IC_{50}; 1), and twice the IC_{50} (2xIC_{50}; x2) concentration calculated from the growth-inhibitory curves. Untreated cells (no drug; DMSO only) were used for each condition (+/-DOX) as controls. GAPDH was used as internal loading control. MYC protein expression was corrected to GAPDH protein expression levels and values normalised to the expression of untreated controls for each condition (no dox/dox). Graphs show the comparison of MYC protein levels between *MYC* overexpressing cell lines (blue: -dox; MYC ON) and those with *MYC* knockdown (red: +dox; MYC OFF). Percentage reduction of MYC expression after treatment is shown relative to the corresponding untreated control. Values from one experiment.

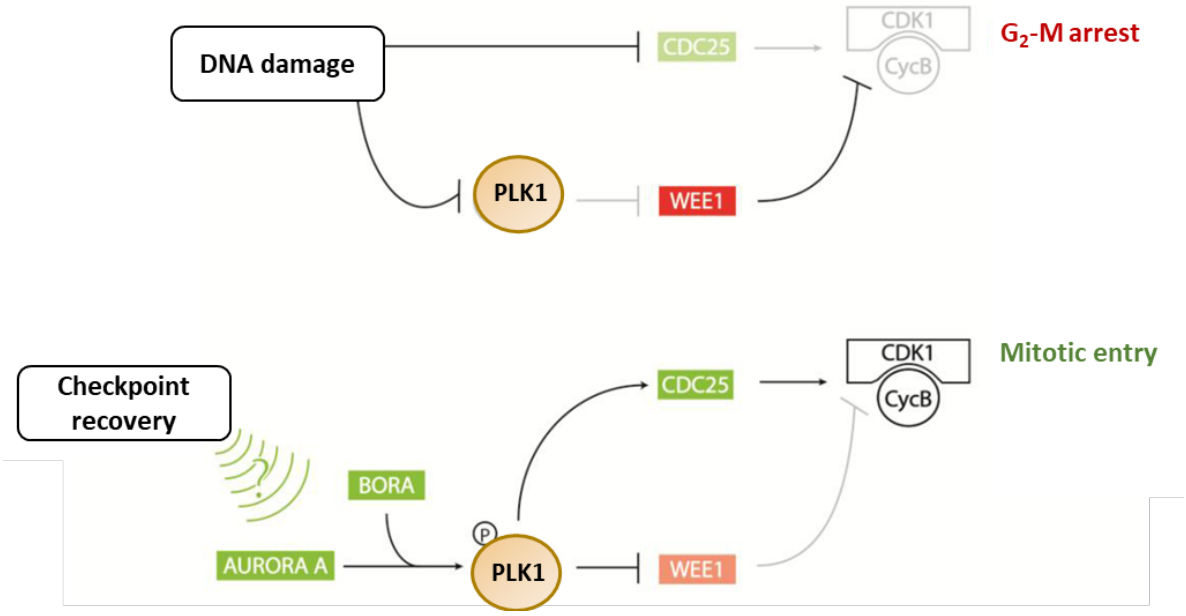

Figure 6.8. PLK1 involvement in the regulation of the cells cycle. Schematic representation of PLK1 involvement in the progression of the cells cycle after recovery of DNA damage. A)cells arrest in G_2-M phase of the cells cycle in response to DNA damage. This is caused by the direct activation of CDK1 inhibitors (like *WEE1*) and degradation of CDK1 activators (like CDC25). B)completion of DNA-damage repair, phosphorylation-dependent activation of PLK1 by AURKA and BORA in turn phosphorylates WEE1, targeting it for degradation and inducing cells entry to mitosis (Adapted from Kousholt *et* al, 2012).

Concentration-dependent downregulation of MYC was seen in all 4 parental MB_{Group3} cell lines after treatment with BI2536 (Figure 6.9). Densitometry analysis revealed that after treatment with their corresponding IC_{50} concentration, PLK1 inhibition with BI2536 reduced MYC protein levels by 50% in D425, D283 and HDMB03, when compared to untreated cells (no drug). Inhibition of PLK1 reduced MYC expression levels by 37.5% in D458. PLK1 inhibition with BI2536 reduced MYC protein levels by 26% after treatment with the highest concentration when compared to the untreated control. The opposite effect was seen in UW228.2, where MYC protein levels increased in a dose-dependent manner (Figure 6.9).

BI2536 greatly reduced PLK1 protein levels in all parental cell lines except in UW228.2, were an increase in total PLK1 protein levels were seen. PLK1 inhibition caused a reduction of the phosphorylation of CDC25. BI2536 downregulated the MCL1 protein levels in all MB_{Group3} cell lines, having no effect on DAOY and actually increasing its expression on UW228.2 (when compared to the untreated control).

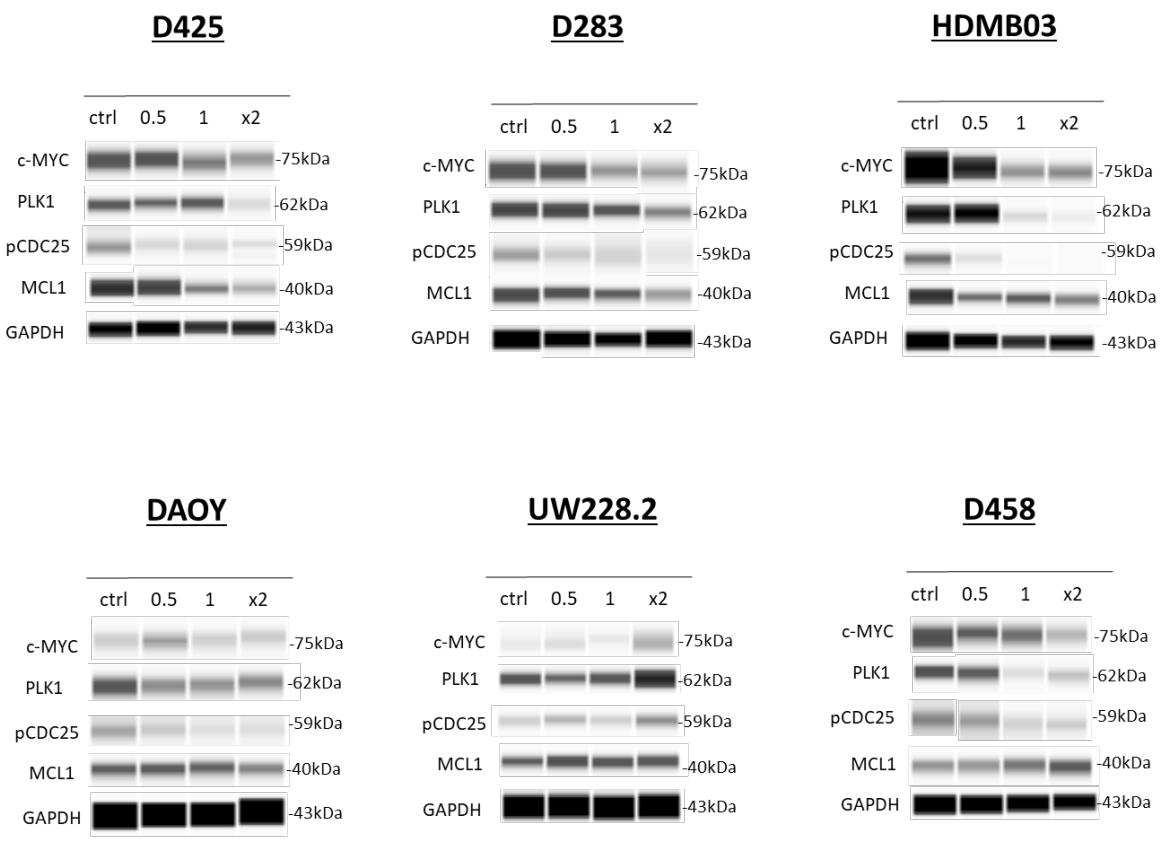

Figure 6.9. Effect of PLK1 inhibition by BI2536 in parental MB cell lines on MYC protein expression and downstream pathway targets. Automated western blot (Wes) of MYC protein levels and downstream related proteins expressed by D425, D283, HDMB03, DAOY, UW228.2 and D458, after treatment with a single exposure with half the IC_{50} (0.5), IC_{50} (1), and twice the IC_{50} (2x) concentration of BI2536 calculated from the growth-inhibitory curves. Untreated cells (ctrl; DMSO only) were used as control. GAPDH was used as internal loading control.

In summary, Wes protein quantification analysis of cells treated with BI2536 revealed a dose-dependent downregulation of MYC protein expression. Results indicate that PLK1-regulated expression of pCDC25 and MCL1 is *MYC*-dependent.

6.4.2 CDK2 inhibition

Wes protein quantification analysis of cells treated with Milciclib showed a dose-dependent downregulation of MYC expression levels (Figure 6.10), when compared to untreated cells. CDK2 inhibition caused a reduction of D425 MYC protein levels by 60% when exposed to IC_{50} (40% on cells with *MYC* knockdown). MYC expression levels of D283 and HDMB03 were only reduced by 25% and 32%, respectively (compared to around 40% with *MYC* knockdown by doxycycline in both cell lines). At the highest concentration, Milciclib reduced MYC levels by half on D425, D283 and HDMB03.

Wes protein analysis showed downregulation of CDK2 in all three lines as a direct consequence of Milciclib treatment, most prominently in D425 (Figure 6.10, A). Downregulation of protein levels of MYC and CDK2, were seen with an increase in MCL1 protein in a dose dependent manner.

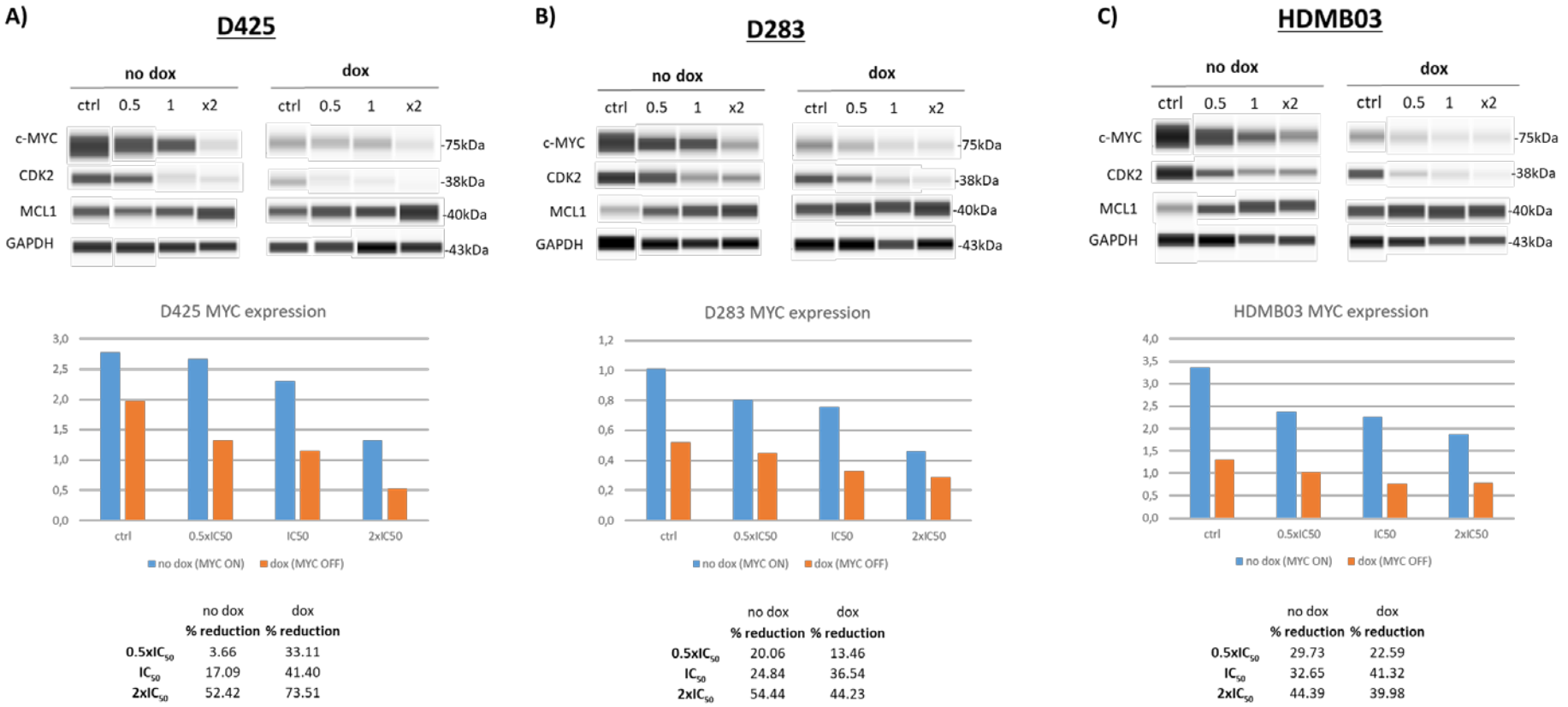

	no dox % reduction	dox % reduction
0.5xIC$_{50}$	3.66	33.11
IC$_{50}$	17.09	41.40
2xIC$_{50}$	52.42	73.51

	no dox % reduction	dox % reduction
0.5xIC$_{50}$	20.06	13.46
IC$_{50}$	24.84	36.54
2xIC$_{50}$	54.44	44.23

	no dox % reduction	dox % reduction
0.5xIC$_{50}$	29.73	22.59
IC$_{50}$	32.65	41.32
2xIC$_{50}$	44.39	39.98

Figure 6.10. Effect of CDK2 inhibition by Milciclib in isogenic D425, D283 and HDMB03 MB cell lines on MYC protein expression and downstream pathway targets. Automated western blot (Wes) of MYC protein levels expressed by D425, D283 and HDMB03 MYC, cultured in the presence (dox) and absence (no dox) of doxycycline for *MYC* knockdown, after a single exposure with half the IC_{50} ($0.5xIC_{50}$; 0.5), IC_{50} (IC_{50}; 1), and twice the IC_{50} ($2xIC_{50}$; x2) concentration calculated from the growth-inhibitory curves. Untreated cells (no drug; DMSO only) were used for each condition (+/-dox) as controls. GAPDH was used as internal loading control. MYC protein expression was corrected to GAPDH protein expression levels and values normalised to the expression of untreated controls for each condition (no dox/dox). Graphs show the comparison of MYC protein levels between *MYC* overexpressing cell lines (blue: -dox; MYC ON) and those with *MYC* knockdown (red: +dox; MYC OFF). Percentage reduction of MYC expression after treatment is shown relative to the corresponding untreated control. Values from one experiment.

When studied in subgroup context, CDK2 inhibition with Milciclib caused a dose-dependent downregulation of MYC across MB_{Group3} parental cell lines (relative to the expression of MYC of untreated cells). Milciclib reduced by 50% MYC expression in D283 and HDMB03 after drug exposure. A 25% and 28% reduction in MYC protein levels was seen in D458 and D425 respectively (Figure 6.11).

A slight reduction of MYC protein expression was seen in MB_{SHH} cell lines when treated with $2xIC_{50}$. *CDK2* inhibition reduced MYC protein levels by 15% in DAOY and was almost undetectable on UW228.2. As explained in section 6.3.2, MB_{SHH} cell lines express more than 10-fold difference in MYC expression compared to MB_{Group3} cell lines (section 6.3.2, Figure 6.5). Despite making MYC protein levels undetectable in UW228.2, it can not be said that Milcilcib had the most effective effect in downregulating MYC on the MB_{SHH} cell lines, since the starting expression levels were already extremely lower to detect a clear decrease.

Milciclib efficiently downregulated its main target, CDK2, across MB cell lines. A dose-dependent increase in MCL1 protein levels was seen following CDK2 inhibition in MB_{Group3} cell lines, whereas a reduction was seen on DAOY and UW228.2. This suggest that CDK2 inhibition has a subgroup specific effect on the expression of MYC and MCL1 proteins.

PARP, an enzyme involved in DNA repair, was used as a measurement of apoptosis after treatment with Milciclib. During apoptosis, PARP is cleaved by the active caspase-3 (Chaitanya et al., 2010), therefore, a decrease in PARP total protein can indicate induction of the apoptotic pathway after treatment with the inhibitor. A dose-dependent decrease in total levels of PARP was seen after exposures to Milciclib across cell lines and regardless of subgroup (with the exception of D283, in which a dose-dependent increase in total levels of PARP was seen).

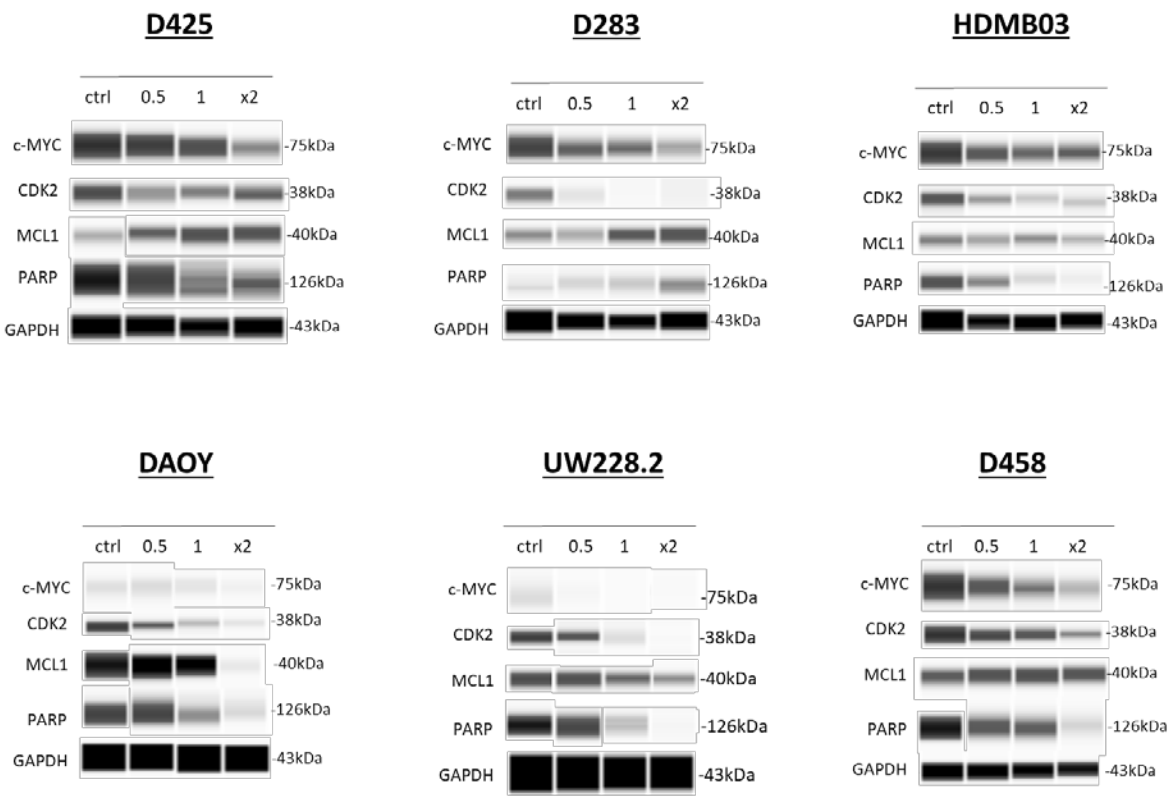

Figure 6.11. Effect of CDK2 inhibition by Milciclib in parental MB cell lines on MYC protein expression and downstream pathway targets. Automated western blot (Wes) of MYC protein levels and downstream related proteins expressed by D425, D283, HDMB03, DAOY, UW228.2 and D458, after treatment with a single exposure with half the IC_{50} (0.5), IC_{50} (1), and twice the IC_{50} (2x) concentration of Milciclib calculated from the growth-inhibitory curves. Untreated cells (ctrl; DMSO only) were used as control. GAPDH was used as internal loading control.

In conclusion, CDK2 inhibition with Milciclib caused the subgroup-specific downregulation of MYC protein expression levels and revealed the increase of MCL1 in a subgroup-specific *MYC*-dependent manner. Reduction of total levels of PARP suggests CDK9 inhibition triggers the induction of the apoptotic pathway.

6.4.3 AURKA inhibition

On Wes analysis of protein expression levels, inhibition of AURKA caused a dose-dependent downregulation of MYC protein levels in all three lines, strongest in D283 (Figure 6.12). When compared to the untreated controls, MYC protein was reduced by 30% in D425 when treated at IC_{50}, and a reduction of 25% was achieved in HDMB03. AURKA inhibition by MLN8237 caused MYC protein levels to be reduced by 70% in D283 (Figure 6.12, B). MLN8237 treatment of cells with *MYC*-silenced with shRNA had no consistent effects on MYC protein levels.

Alongside a decrease in MYC protein level, protein quantification analysis showed also a dose-dependent reduction in AURKA protein levels together with its phosphorylated form across cell lines, regardless of *MYC* expression. A dose-dependent increase in MCL1 protein levels was seen in *MYC*-overexpressing cell lines, whereas levels of MCL1 did not vary with increased dose in cells with *MYC* knockdown (results seen in all three cell lines).

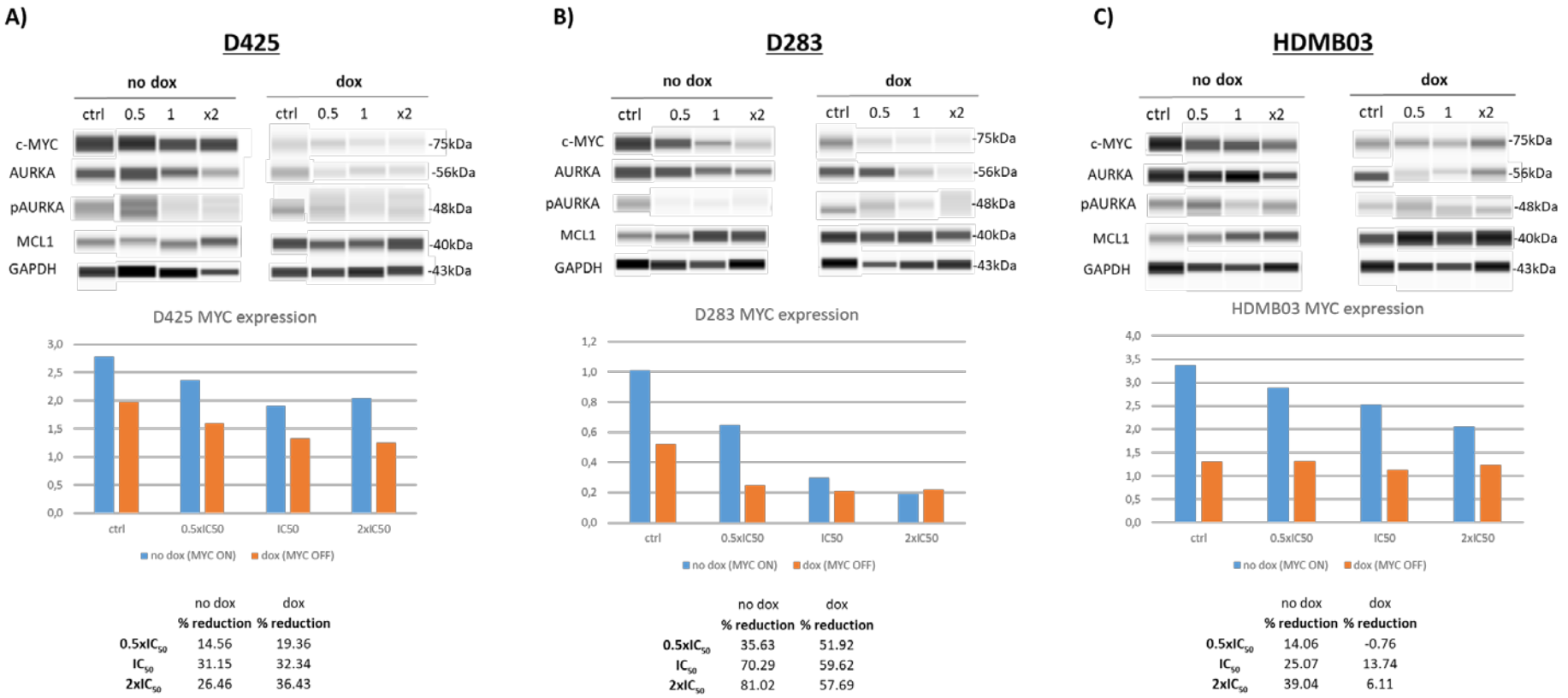

	no dox % reduction	dox % reduction
0.5xIC$_{50}$	14.56	19.36
IC$_{50}$	31.15	32.34
2xIC$_{50}$	26.46	36.43

	no dox % reduction	dox % reduction
0.5xIC$_{50}$	35.63	51.92
IC$_{50}$	70.29	59.62
2xIC$_{50}$	81.02	57.69

	no dox % reduction	dox % reduction
0.5xIC$_{50}$	14.06	-0.76
IC$_{50}$	25.07	13.74
2xIC$_{50}$	39.04	6.11

Figure 6.12. Effect of AURKA inhibition by MLN8237 in isogenic D425, D283 and HDMB03 MB cell lines on MYC protein expression and downstream pathway targets.A) Automated western blot (Wes) of MYC protein levels expressed by D425, D283 and HDMB03 MYC, cultured in the presence (dox) and absence (no dox) of doxycycline for *MYC* knockdown, after a single exposure with half the IC_{50} (0.5xIC_{50}; 0.5), IC_{50} (IC_{50}; 1), and twice the IC_{50} (2xIC_{50}; x2) concentration calculated from the growth-inhibitory curves). Untreated cells (no drug; DMSO only) were used for each condition (+/-dox) as controls. GAPDH was used as internal loading control. MYC protein expression was corrected to GAPDH protein expression levels and values normalised to the expression of untreated controls for each condition (no dox/dox). Graphs show the comparison of MYC protein levels between *MYC* overexpressing cell lines (blue: -dox; MYC ON) and those with *MYC* knockdown (red: +dox; MYC OFF). Percentage reduction of MYC expression after treatment is shown relative to the corresponding untreated control. Values from one experiment.

Automated western blot results of parental MB cell lines after treatment showed a dose-dependent decrease in MYC protein levels after inhibition of AURKA with MLN8237 across MB_{Group3} cell lines, when compared to cells unexposed to the drug (Figure 6.13). Treatment with IC_{50} concentration caused a reduction of 18% in D283, 10% in D425, 30% in D458 and 50% in HDMB03. Despite the modest reduction in MYC protein levels, the opposite effect was seen in the MB_{SHH} cells, where an increase in MYC protein levels was seen with increased concentration of the inhibitor.

As expected, MLN8237 caused a decrease in protein expression levels of its main target, AURKA, and its phosphorylated form. The effect was seen across cell lines, regardless of subgroup. MLN8237 treatment also caused an overall increase of the anti-apoptotic protein MCL1, changes in expression that were not *MYC*-dependent.

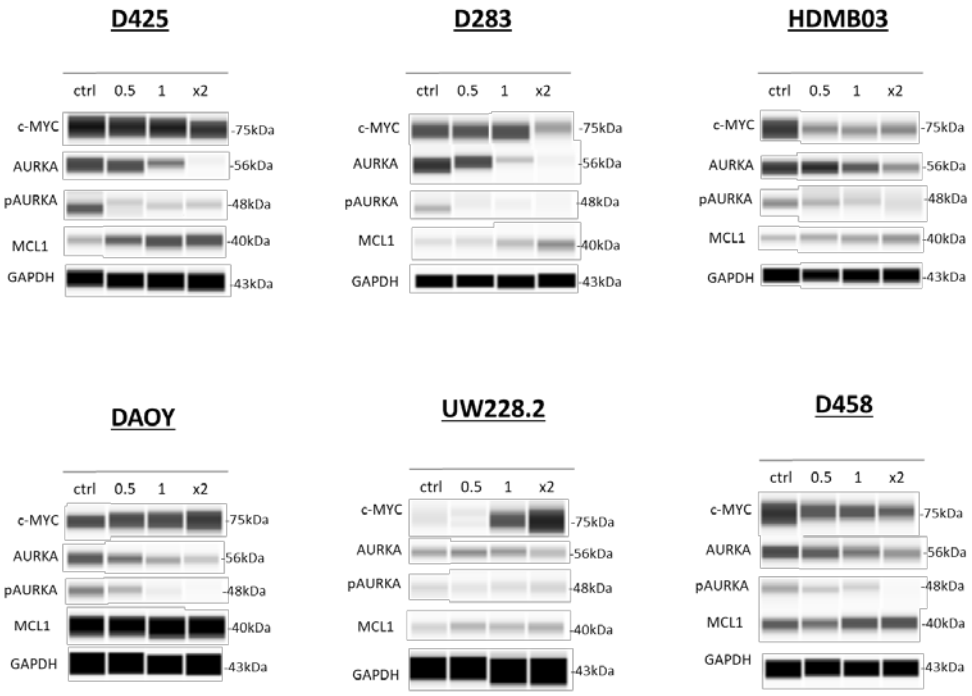

Figure 6.13. Effect of AURKA inhibition by MLN8237 in parental MB cell lines on MYC protein expression and downstream pathway targets. Automated western blot (Wes) of MYC protein levels and downstream related proteins expressed by D425, D283, HDMB03, DAOY, UW228.2 and D458, after treatment with a single exposure with half the IC_{50} (0.5), IC_{50} (1), and twice the IC_{50} (2x) concentration of MLN8237 calculated from the growth-inhibitory curves. Untreated cells (ctrl; DMSO only) were used as control. GAPDH was used as internal loading control.

In summary, *AURKA* inhibition with MLN8237 had a direct effect on *MYC*, causing a subgroup-specific reduction of MYC-protein levels. Changes in AURKA, pAURKA and MCL1 protein levels were independent of *MYC* expression levels.

6.4.4 CHK1 inhibition

6.4.4.1 AZD7762

Analysis of AZD7762's effect at the protein level revealed a dose-dependent decrease of MYC protein expression across cell lines (Figure 6.14). Treatment with IC_{50} concentration caused a 34%, 17.8% and 18.8% reduction of MYC protein in D425, D283 and HDMB03 respectively, when compared to untreated controls. A slight reduction in MYC-protein was seen after treatment with AZD7762 in cells with *MYC*-silenced with shRNA, causing a reduction by 12%, 10% and 0.8% in D425, D283 and HDMB03 respectively.

Protein analysis of downstream effectors of the signalling pathway, revealed a dose-dependent reduction of total CHK1 levels (Figure 6.14). No consistent effects were seen in levels of its phosphorylated form (pCHK1) at Ser345 across cell lines. This might be due to the lower amount of pCHK1 in the cell lines, making its chemiluminescent signal hard to detect and process with Wes, which results in more ambiguous results.

Inhibition of CHK1 resulted in a dose-dependent increase of MCL1 protein in D425, D283 and HDMB03 cells overexpressing *MYC*. In comparison, cells with *MYC* knockdown presented with higher-levels of MCL1 protein, which slightly increased throughout treatment.

PARP was used as a measurement of apoptosis after treatment with AZD7762. A dose-dependent decrease in total levels of PARP was seen after exposures to AZD7762 across cell lines and regardless of *MYC* expression, which was markedly decreased in D425 in comparison to D283 and HDMB03.

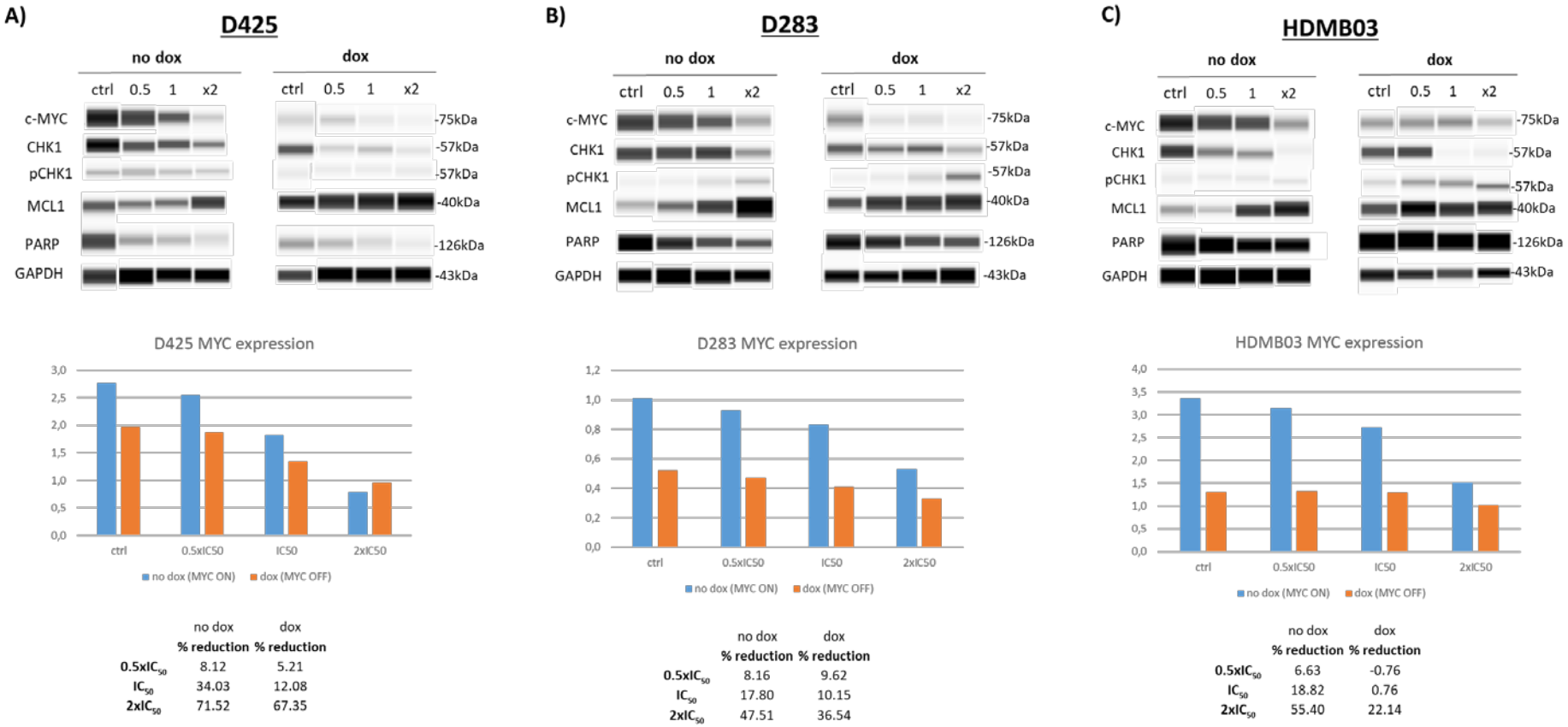

	no dox % reduction	dox % reduction
0.5xIC$_{50}$	8.12	5.21
IC$_{50}$	34.03	12.08
2xIC$_{50}$	71.52	67.35

	no dox % reduction	dox % reduction
0.5xIC$_{50}$	8.16	9.62
IC$_{50}$	17.80	10.15
2xIC$_{50}$	47.51	36.54

	no dox % reduction	dox % reduction
0.5xIC$_{50}$	6.63	-0.76
IC$_{50}$	18.82	0.76
2xIC$_{50}$	55.40	22.14

Figure 6.14. Effect of CHK1 inhibition by AZD7762 in isogenic D425, D283 and HDMB03 MB cell lines on MYC protein expression and downstream pathway targets.A) Automated western blot (Wes) of MYC protein levels expressed by D425, D283 and HDMB03 MYC, cultured in the presence (dox) and absence (no dox) of doxycycline for MYC knockdown, after a single exposure with half the IC_{50} (0.5xIC_{50}; 0.5), IC_{50} (IC_{50}; 1), and twice the IC_{50} (2xIC_{50}; x2) concentration calculated from the growth-inhibitory curves. Untreated cells (no drug; DMSO only) were used for each condition (+/-dox) as controls. GAPDH was used as internal loading control. MYC protein expression was corrected to GAPDH protein expression levels and values normalised to the expression of untreated controls for each condition (no dox/dox). Graphs show the comparison of MYC protein levels between *MYC* overexpressing cell lines (blue: -dox; MYC ON) and those with *MYC* knockdown (red: +dox; MYC OFF). Percentage reduction of MYC expression after treatment is shown relative to the corresponding untreated control. Values from one experiment.

A dose-dependent reduction of MYC protein levels was seen across parental MB_{Group3} lines after treatment with AZD7762 relative to untreated controls (Figure 6.15). Densitometry analysis of MYC protein expression following treatment with IC_{50} concentration of the inhibitor revealed a reduction of MYC protein levels by 6% in D283, 35% in D425, 34% in D458 and by 50% in HDMB03. Conversely, a dose-dependent increase in MYC expression was seen in both MB_{SHH} cell lines (Figure 6.15).

The expected reduction in total levels of CHK1 protein was seen across cell lines (Figure 6.15). Treatment with AZD7762 caused a reduction of total CHK1 protein and an increase of pCHK1 at Ser345, in all lines. Exposures to the inhibitor also increased MCL1 protein levels in a dose-dependent manner across cell lines, regardless of subgroups.

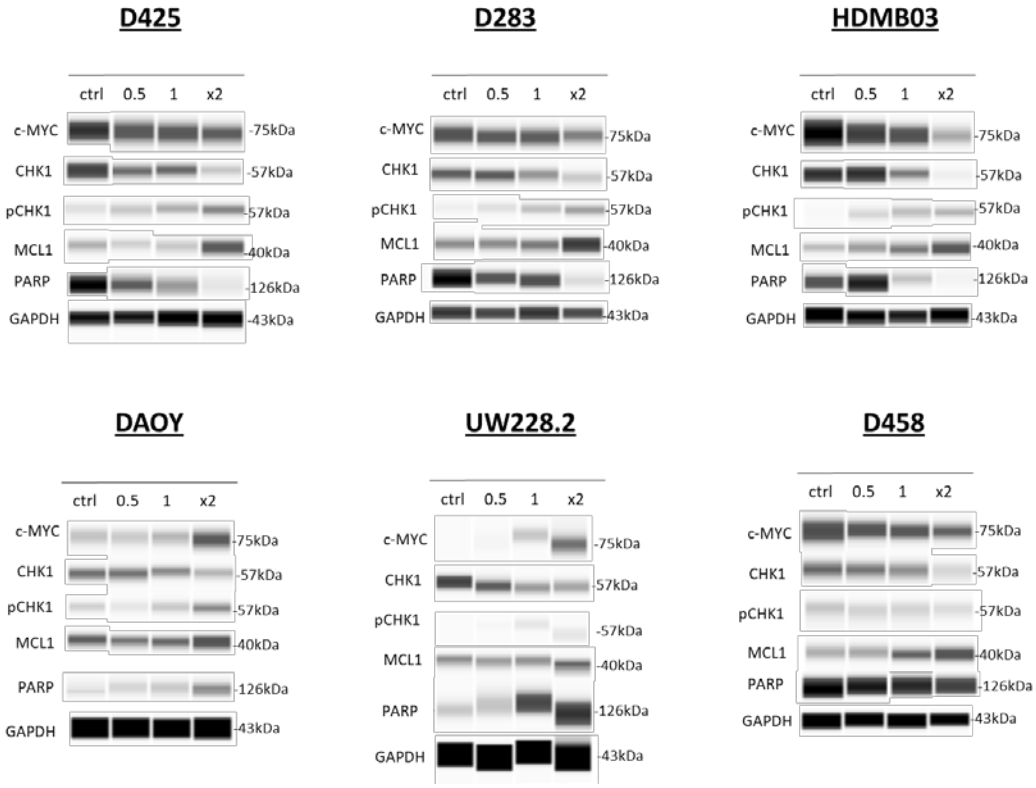

Figure 6.15. Effect of CHK1 inhibition by AZD7762 in parental MB cell lines on MYC protein expression and downstream pathway targets. Automated western blot (Wes) of MYC protein levels and downstream related proteins expressed by D425, D283, HDMB03, DAOY, UW228.2 and D458, after treatment with a single exposure with half the IC_{50} (0.5), IC_{50} (1), and twice the IC_{50} (2x) concentration of AZD7762 calculated from the growth-inhibitory curves. Untreated cells (ctrl; DMSO only) were used as control. GAPDH was used as internal loading control.

In summary, CHK1 inhibition with AZD7762 caused a decrease in MYC protein expression in a MB_{Group3} subgroup-specific dose-dependent manner. Changes in protein expression levels of downstream effectors of CHK1 signalling pathway were independent of *MYC* expression.

6.4.4.2 Prexasertib

Analysis of the effect of CHK1 inhibition by Prexasertib at the protein level revealed downregulation of MYC protein expression levels in a dose-dependent manner (Figure 6.16). MYC protein levels were reduced by more than 80% across cell lines regardless of subgroup, after exposures to the drug. *MYC* expression was almost reduced when tested with the highest concentration. D425, D283 and HDMB03 *MYC* expression levels only decreased by 15%, 4% and 1% when treated at the lowest concentration tested, with a significant reduction when exposed to their corresponding IC_{50} concentration. CHK1 inhibition with Prexasertib had an additive effect with *MYC* knockdown, where further decrease in MYC protein levels was seen after the silencing of *MYC* with DOX.

A reduction of CHK1 protein levels was seen after treatment with the inhibitor, together with a decrease in its phosphorylated form at Ser345, in both cells expressing high levels of *MYC* and in cells with *MYC* knockdown (Figure 6.16). Prexasertib also reduced levels of MCL1 in a *MYC*-dependent manner, effect seen across cell lines.

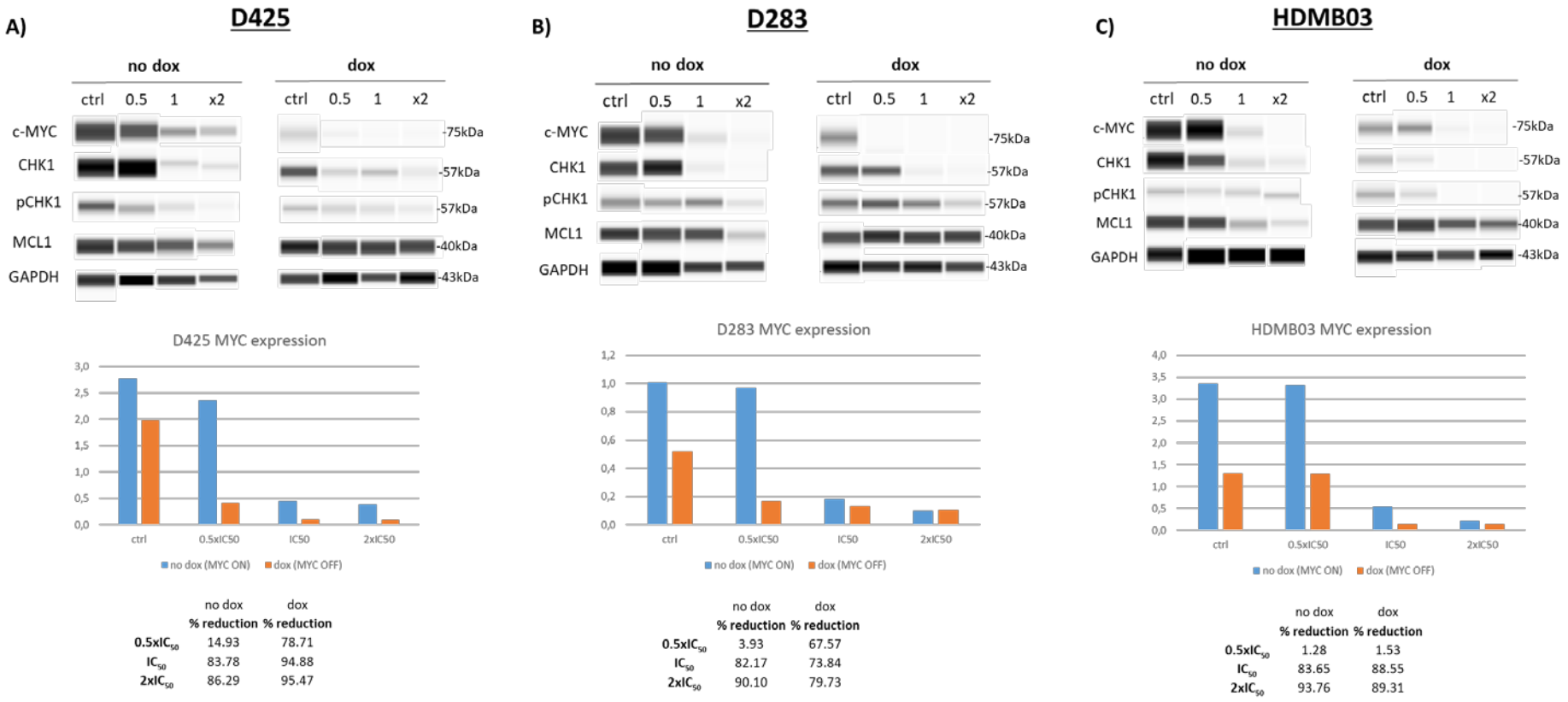

Figure 6.16. Effect of CHK1 inhibition by Prexasertib in isogenic D425, D283 and HDMB03 MB cell lines on MYC protein expression and downstream pathway targets. Automated western blot (Wes) of MYC protein levels expressed by D425, D283 and HDMB03 MYC, cultured in the presence (dox) and absence (no dox) of doxycycline for *MYC* knockdown, after a single exposure with half the IC_{50} (0.5xIC_{50}; 0.5), IC_{50} (IC_{50}; 1), and twice the IC_{50} (2xIC_{50}; x2) concentration calculated from the growth-inhibitory curves. Untreated cells (no drug; DMSO only) were used for each condition (+/-dox) as controls. GAPDH was used as internal loading control. MYC protein expression was corrected to GAPDH protein expression levels and values normalised to the expression of untreated controls for each condition (no dox/dox). Graphs show the comparison of MYC protein levels between *MYC* overexpressing cell lines (blue: -dox; MYC ON) and those with *MYC* knockdown (red: +dox; MYC OFF). Percentage reduction of MYC expression after treatment is shown relative to the corresponding untreated control. Values from one experiment.

Wes protein quantification analysis of parental MB cell lines after treatment with Prexasertib revealed a dose-dependent reduction of MYC protein levels across cell lines belonging to MB_{Group3} (Figure 6.17). Exposures to its IC_{50} concentration caused a reduction of 40%, 80%, 86% and 72% in D283, D425, D458 and HDMB03, respectively, when compared to their corresponding untreated control. The opposite effect was seen in MB_{SHH} cell lines, where CHK1 inhibition with Prexasertib resulted in a dose-dependent increase of MYC protein levels.

Prexasertib effectively downregulated CHK1 protein expression levels. CHK1 inhibition caused a decrease in the phosphorylation of CHK1 at Ser345 was seen in MB_{Group3}, whereas it increased in DAOY and UW228.2. As previously seen in the isogenic cell lines, Prexasertib downregulated MCL1 protein levels independently of *MYC* expression. The dose-dependent reduction on MCL1 was seen across cell lines regardless of subgroup.

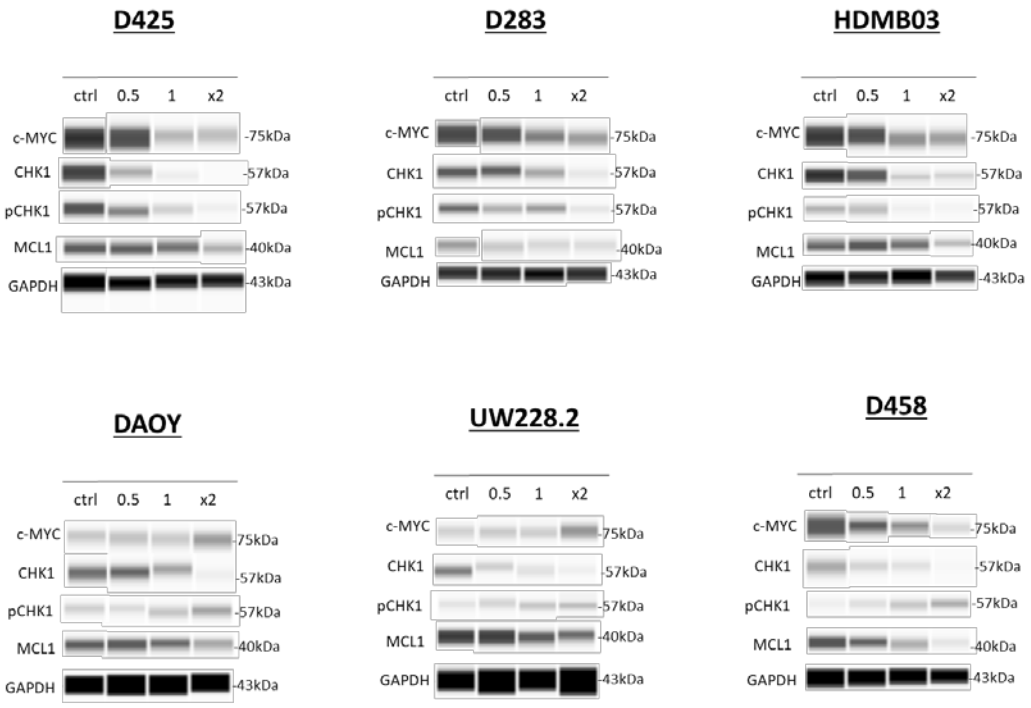

Figure 6.17. Effect of CHK1 inhibition by Prexasertib in parental MB cell lines on MYC protein expression and downstream pathway targets. Automated western blot (Wes) of MYC protein levels and downstream related proteins expressed by D425, D283, HDMB03, DAOY, UW228.2 and D458, after treatment with a single exposure with half the IC_{50} (0.5), IC_{50} (1), and twice the IC_{50} (2x) concentration of Prexasertib calculated from the growth-inhibitory curves. Untreated cells (ctrl; DMSO only) were used as control. GAPDH was used as internal loading control.

In summary, CHK1 inhibition by Prexasertib caused downregulation of MYC protein expression levels in a MB_{Group3} subgroup specific context. In addition, CHK1 inhibition caused the decrease in MCL1 protein levels in a *MYC*-independent manner.

6.4.5 Conclusion

In summary, the *MYC*-dependent sensitivities seen in the screen validated in all three cell lines in these independent experiments (Figure 6.6). When individually assessed, a *MYC*-dependent growth inhibitory effect was seen across D425, D283 and HDMB03 MYC2 cell lines after treatment with the inhibitors. Cell lines overexpressing *MYC* were more sensitive to the inhibitors when compared to those with *MYC* knockdown.

From all inhibitors tested, BI2536 (PLK1 inhibitor) and Prexasertib (CHK1/2 inhibitor) caused a significant reduction of MYC expression in a dose-dependent manner across isogenic MB_{Group3} cell lines, where MYC expression was reduced by more than 50% after IC_{50} exposure to each inhibitor.

Differences in the ability to downregulate *MYC* through CHK1 inhibition were seen depending on the inhibitors used. Exposures at IC_{50} to Prexasertib caused a greater reduction in MYC protein levels when compared to AZD7762 (averaging 82% and 24% respectively, across *MYC* overexpressing cell lines).

As explained earlier in this chapter, both CHK1 and CHK2 are essential components in the DNA-damage response (DDR). CHK1 and CHK2 respectively amplify the signals from ATR and ATM signalling, phosphorylating a variety of downstream effectors. Depending on the severity of the damage, cells will either transiently arrest cell cycle progression or undergo apoptosis (Maréchal and Zou, 2013, Ronco et al., 2016)

Analysis of the effect of CHK1 inhibition on *MYC* expression and downstream effectors of the CHK1 signalling pathway showed a significant difference between the phosphorylated levels of CHK1 at serine 345 (Ser345). Phosphorylation of CHK1 at Ser345 is a biomarker of CHK1 inhibition, and it is mainly catalysed by ATR. Inhibition of CHK1 prevents the activation of the phosphatase PP2A, which normally dephosphorylates CHK1 at Ser345. Therefore, upon CHK1 inhibition phosphorylation of at Ser345 goes up (Sancar et al., 2004, Yan et al., 2010)

Treatment with AZD7762 caused an increase of pCHK1 at Ser345 in all lines, whereas a decrease was seen after exposures to Prexasertib. Differences between inhibitors could be explained by the sort of DNA lesions caused to the cells, either SSB or DSB, which would consequently activate ATR or ATM, respectively. Depending on the DDR pathway activated, either CHK1 or CHK2 would be primarily phosphorylated (Bartek and Lukas, 2003, Ronco et

al., 2016). Our results suggest that differences in growth inhibitory potency between both inhibitors and differential levels of pCHK1 at Ser345 might be due to the type of DNA-damage caused. Prexasertib, which caused a reduction of pCHK1 (Ser345), might be inhibiting CHK2 preferentially rather than CHK1, indicating that the compound might be causing DSB and therefore that the ATM signalling pathway is activated. Increased growth-inhibitory effects displayed by Prexasertib might be indicative of a preferential dependency of *MYC*-overexpressing cell lines on the ATM over the ATR signalling pathway, and the potential of targeting *MYC*-dependent MB_{Group3} cell lines through CHK2 inhibition rather than CHK1.

An easy and practical way to further study the preferential inhibition of CHK1 and CHK2, would be to stain the cells with an antibody for pCHK2 at threonine 68 (Thr68), a marker of activation of the CHK2 pathway. In response to DNA damage, ATM phosphorylates CHK2 on Thr68, which allows its dimerisation and auto-phosphorylation in *trans* at threonines 383 and 387 resulting in full activation, and autophosphorylation in *cis* at serine 516 (Ser516). Phosphorylated Thr68 is therefore a biomarker of the upstream ATM pathway and pSer516 a marker of fully activated CHK2 kinase (Weber and Ryan, 2015, Ghelli Luserna Di Rorà et al., 2016). Staining for pCHK2 at Thr68 after treatment with Prexasertib would inform of the mechanism of action of the compound, since phosphorylated levels of CHK2 at Thr68 should go down after treatment (indicating inhibition of CHK2).

Milciclib (CDK2 inhibitor) and MLN8237 (AURKA inhibitor) had the least downregulatory effect on *MYC*, compared to the other inhibitors tested. MYC protein levels where only reduced by 50% when treated with the highest concentration of Milciclib.

Overall, analysis of the effect of the inhibitors at the protein level confirmed the *MYC*-dependent effect to treatment with the inhibitors chosen. *MYC* overexpressing cell lines had preferential sensitivity to the compounds compared to those expressing lower levels of MYC as a consequence of activation of shRNA constructs by DOX. Inhibition of PLK1, CDK2, CHK1 and AURKA caused greater reduction of MYC protein expression in *MYC* overexpressing cells than those with *MYC* knockdown, which was associated with a greater reduction of the cells' proliferation rate.

MYC-associated effects on drug sensitivity were also seen in a subgroup-specific context when parental cell lines were investigated; differential levels of *MYC* expression across subgroups

were associated with sensitivity to the inhibitors. MB_{SHH} cell lines, expressing more than 10-fold difference in MYC expression compared to MB_{Group3} cell lines used, were less sensitive to CHK1, CDK2, AURKA and PLK1 inhibition.

Treatment with the inhibitors efficiently downregulated the protein expression levels of their main molecular target, effect seen across the panel of MB cell lines. Treatment with Prexasertib (CHK1 inhibitor) and BI2536 (PLK1 inhibitor) caused the *MYC*-dependent subgroup-specific downregulation of the anti-apoptotic protein MCL1, whereas a *MYC*-dependent upregulation was seen after treatment with Milciclib (CDK2 inhibitor). Regulation of MCL1 resulted to be independent of *MYC* expression after treatment with AZD7762 (CHK1 inhibitor) and MLN8237 (AURKA inhibitor), with no subgroup specificity. The *MYC*-dependent regulation of MCL1 could explain the differences in sensitivity displayed by the inhibitors. Our results suggest that the dual effect of BI2536 and Prexasertib in reducing MYC and MCL1 protein levels caused higher growth-inhibitory effect in *MYC*-driven MB_{Group3} cell lines, sensitising them to the inhibitors.

In conclusion, inhibition of CHK1, CDK2, PLK1 and AURKA had a direct downregulatory effect on *MYC* expression in MB_{Group3} cell lines. The use of compounds inhibiting these main molecular targets could be used to specifically downregulate MYC protein expression in MB_{Group3}.

6.5 Effect of pharmacological inhibition of PLK1, CHK1, CDK2 and AURKA on cell cycle distribution

Following the identification of a *MYC*-dependent growth inhibition effect on MB cell lines after treatment with the inhibitors, it was important to better determine the mechanism by which the inhibitors were causing the decrease in cell proliferation. To this end, flow cytometry cell cycle analysis was used on the panel of MB cell lines to examine cell cycle distribution after treatment with each inhibitor.

Apoptotic cells can be detected by flow cytometry analysis by their inherent loss of DNA content in comparison to the otherwise 'healthy' population of cells. Permeabilisation of cells as a result of the induction of the apoptotic pathway can lead to loss of DNA, and cells with reduced DNA content can be detected in the sub-G_1 phase of the cell cycle when stained with an intercalating agent like propidium iodide (PI) (Riccardi and Nicoletti, 2006, Vermes et al., 2000).

As a means to better understand the underlying mechanism of the *MYC*-dependent growth-inhibitory effect caused by the inhibitors, flow cytometry cell cycle analysis considering sub-G_1 phase of the cell cycle as an indicator of apoptosis was performed to study the possible mechanism by which cells decreased their proliferative rate after treatment.

The isogenic cell lines D425, D283 and HDMB03 MYC2, overexpressing *MYC* and with *MYC* silenced with shRNA, were exposed to a single dose of three different concentrations ($0.5xIC_{50}$, IC_{50} and $2xIC_{50}$) of each inhibitor (IC_{50} determined in section 6.3 of this Chapter). NS cells were used as a negative control for the function and effect of the shRNA in response to the inhibitors. Exposures of cells to the inhibitors for cell cycle analysis were performed in three independent biological experiments.

To explore the *MYC*-dependency of the changes seen in the cells cycle distribution after treatment with the inhibitors in a MB subgroup-specific context, the inhibitors were also tested on the panel of parental MB cell lines (D425, D283, HDMB03, D458, DAOY and UW228.2). Models were exposed to the inhibitors using the IC_{50} concentrations determined with the previously generated dose-response curves (Table 6.4).

IC_{50}[nM]	**BI2536** (PLK1)	**Milciclib** (CDK2)	**MLN8237** (AURKA)	**AZD7762** (CHK1)	**Prexasertib** (CHK1/2)
D425	3.381	110.3	20.88	68.79	4.032
D283	7.695	105.2	36.95	33.72	2.11
HDMB03	7.97	132.9	20.14	50.82	5.85
D458	1.984	159.5	29.4	54.5	2.11
DAOY	3.07	2669	54.61	91.02	6.39
UW228.2	14.27	6342	1664	2852	43.59

Table 6.4. IC_{50} values of the panel of MB cell lines used for cytometry cell cycle analysis. Cell viability of D425, D283, HDMB03 and D458 for MB_{Group3}, and DAOY and UW228.2 for MB_{SHH}, after 72h of exposure to a single dose of 8 different concentrations of BI2536 (PLK1 inhibitor), Milciclib (CDK2 inhibitor), MLN8237 (AURKA inhibitor), AZD7762 (CHK1 inhibitor) and Prexasertib (CHK1/2 inhibitor), was used to generate dose-response curves with Prism8 (section 6.3.2). IC_{50} values (nM) generated from the curves were calculated to determine cells sensitivity to the compounds. Table summarises the IC_{50} of MB parental cell lines to each inhibitor. Values are presented as the mean of three independent experiments.

72h after drug exposures, cells were harvested and samples processed for the analysis of cell cycle distribution as described in Chapter 2. Untreated (no DOX and no drug; DMSO only) cells were used as control for comparison. DOX-treated cells only (DOX, no drug) were used as control for the *MYC*-knockdown arm of the experiment.

Cell cycle distribution of isogenic D425, D283 and HDMB03 MYC2 after treatment with the three different concentrations of the inhibitors can be seen in Figure 6.7 of the Appendix. Cell cycle distribution of MB parental cell lines after treatment with the three different concentrations of the inhibitors can be seen in Figure 6.8 of the Appendix.

For comparison of changes in the cell cycle distribution after treatment with the inhibitors, only differences between untreated cells (no drug, DMSO only) and those treated with half-maximal inhibitory concentration (IC_{50}) are shown.

6.5.1 PLK1 inhibition

Treatment of D425, D283 and HDMB03 with half-maximal inhibitory concentration (IC_{50}) of BI2536 significantly induced apoptosis regardless of *MYC* expression levels, seen by the accumulation of cells in the sub-G_1 phase of the cell cycle at 72h (Figure 6.19). PLK1 inhibition by BI2536 caused a significant decrease in cells at the G_1 phase of the cell cycle, regardless of *MYC* expression levels (cells overexpressing *MYC* and with *MYC* knockdown), when compared to the control. BI2536 treatment caused a significant increase in the number of cells in G_2-M phase of the cell cycle of those cells expressing high levels of *MYC* when compared to untreated cells. Increase not significant in cells with *MYC* knockdown (Figure 6.18).

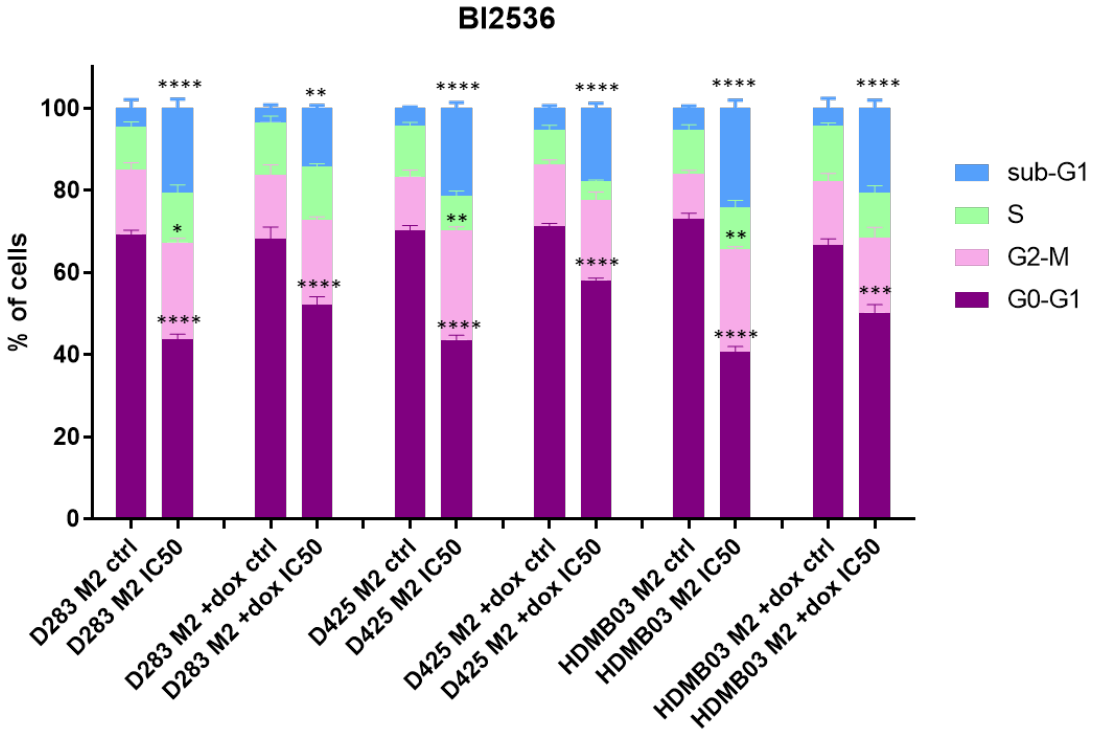

Figure 6.18. Effect of BI2536 treatment on cell cycle distribution in isogenic MB_{Group3} cell lines. Cell cycle distribution of D425, D283 and HDMB03 MYC2 cell lines after 72h of a single exposure of IC_{50} concentration of the PLK1 inhibitor BI2536. Cells were stained with propidium iodide and cell cycle distribution analysed by flow cytometry. Graph represents the percentage (%) of cells of each cell cycle phase relative to total phases, of cells expressing high levels of *MYC* and those with *MYC* knockdown (+dox). Untreated cells (ctrl - no drug; DMSO only) were used for each condition (+/- dox) as controls. Data is presented as the percentage of the mean (±SEM) of three independent experiments. Significance determined by 2-way ANOVA (*$p \leq 0.05$, **$p \leq 0.01$, ***$p \leq 0.001$, ****$p \leq 0.0001$).

The same effect was seen on parental cell lines. Compared to the untreated controls, exposure of D283, D425, HDMB03, D458, DAOY and UW228.2 to IC_{50} concentrations of BI2536 caused a significant increase in the fraction of sub-G_1 cells across cell lines (indicative of apoptotic cells). Only a slight increase in cells at sub-G_1 phase was seen in UW228.2 (the only line that did not reach statistical significance).

PLK1 inhibition by BI2536 caused a significant increase in the number of cells in G_2-M phase, together with a markedly decrease in cells at G_1 phase across MB cell lines, when compared to their corresponding controls. In D283 and D425, a significant decrease in cells in S phase was seen after treatment (Figure 6.19).

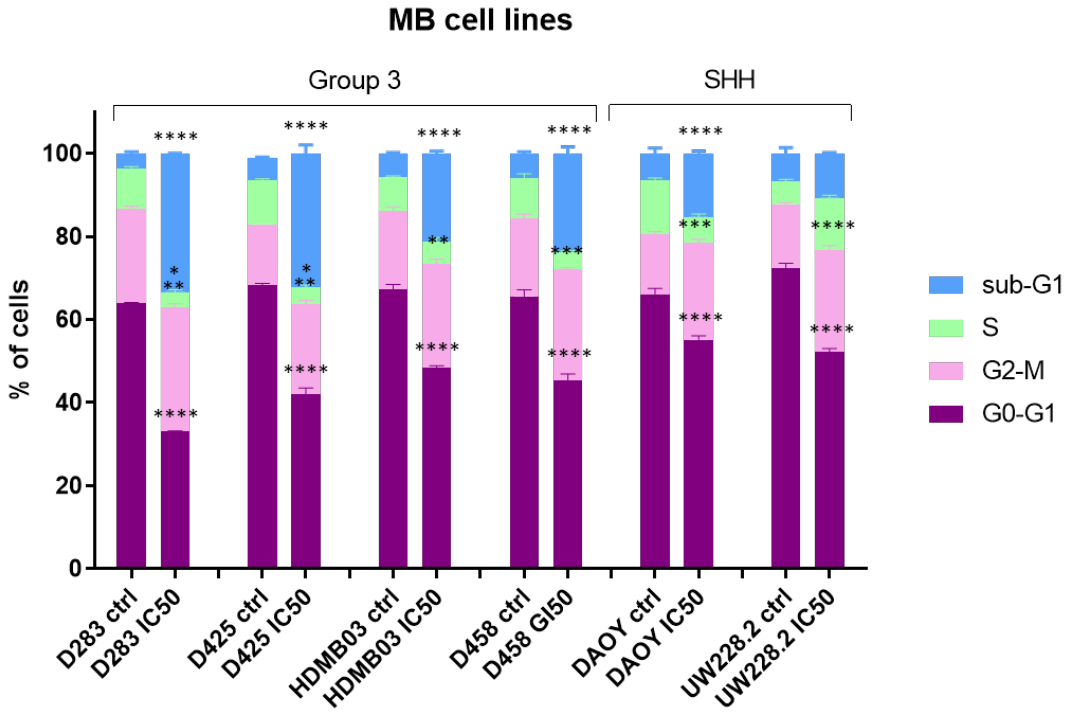

Figure 6.19. Effect of BI2536 treatment on cell cycle distribution in parental MB cell lines. Cell cycle distribution of D283, D425, HDMB03, D458, DAOY and UW228.2 after 72h of a single exposure of IC_{50} concentration of the PLK1 inhibitor BI2536. Cells were stained with propidium iodide and cell cycle distribution analysed by flow cytometry. Graph represents the percentage (%) of cells of each cell cycle phase relative to total phases. Untreated cells (ctrl - no drug; DMSO only) for each cell line were used as controls. Data is presented as the percentage of the mean (±SEM) of two independent experiments. Significance determined by 2-way ANOVA (*p≤0.05, **p≤0.01, ***p≤0.001, ****p≤0.0001).

6.5.2 CDK2 inhibition

No significant changes in the population of cells at sub-G_0 (apoptotic cells) were seen across *MYC*-regulable cell lines after exposure to Milciclib when compared to untreated controls (Figure 6.20).

Some inconsistencies in the cell cycle distribution after treatment with Milciclib were seen between D425, D283 and HDMB03 MYC2 (Figure 6.20). After treatment, all cell lines exhibited a slight decrease in cell numbers in the G_1 phase of the cell cycle. Despite the decrease observed, statistical significance was not reached in D425 with *MYC* knockdown, or in HDMB03 MYC2 cells expressing high levels of *MYC*, when compared to their corresponding controls.

Milciclib caused a significant increase in the proportion of cells in G_2-M phase in D283 overexpressing *MYC* and in HDMB03 with *MYC* knockdown. A slight decrease in the proportion of cells in S phase was seen in D425, only statistically significant when MYC was knocked down (Figure 6.20).

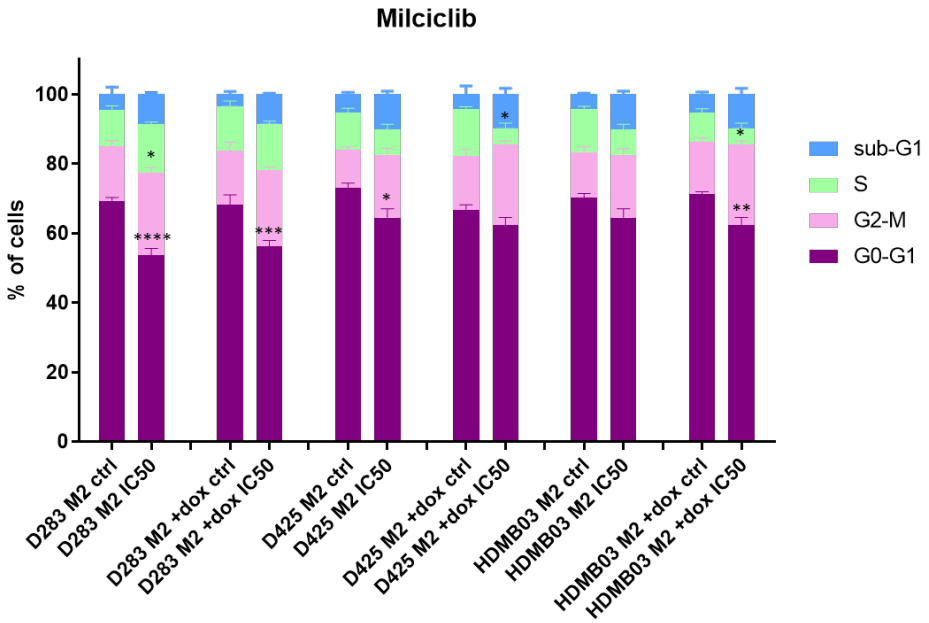

Figure 6.20. Effect of Milciclib treatment on cell cycle distribution in isogenic MB_{Group3} cell lines. Cell cycle distribution of D425, D283 and HDMB03 MYC2 cell lines after 72h of a single exposure of IC_{50} concentration of the CDK2 inhibitor Milciclib. Cells were stained with propidium iodide and cell cycle distribution analysed by flow cytometry. Graph represents the percentage (%) of cells of each cell cycle phase relative to total phases, of cells expressing high levels of *MYC* and those with *MYC* knockdown (+dox). Untreated cells (ctrl-no drug; DMSO only) were used for each condition (+/-dox) as controls. Data is presented as the percentage of the mean (±SEM) of three independent experiments. Significance determined by 2-way ANOVA (*$p \leq 0.05$, **$p \leq 0.01$, ***$p \leq 0.001$, ****$p \leq 0.0001$).

Analysis of the effect of Milciclib treatment on cell cycle distribution in parental MB cell lines showed a significant increase in the sub-G_1 population in MB_{Group3} cell lines, compared to untreated controls, most markedly seen in D458 of all MB_{Group3} lines (Figure 6.21). No significant changes in the number of cells in sub-G_1 phase were seen in MB_{SHH} cell line after treatment.

A decrease in the proportion of cells in G_1 phase of the cell cycle was seen across cell lines after treatment with the inhibitor, reaching statistical significance in D283, HDMB03, D458 and UW228.2. As an exception, after treatment, UW228.2 exhibited a significant increase in the percentage of cells in S phase (Figure 6.21).

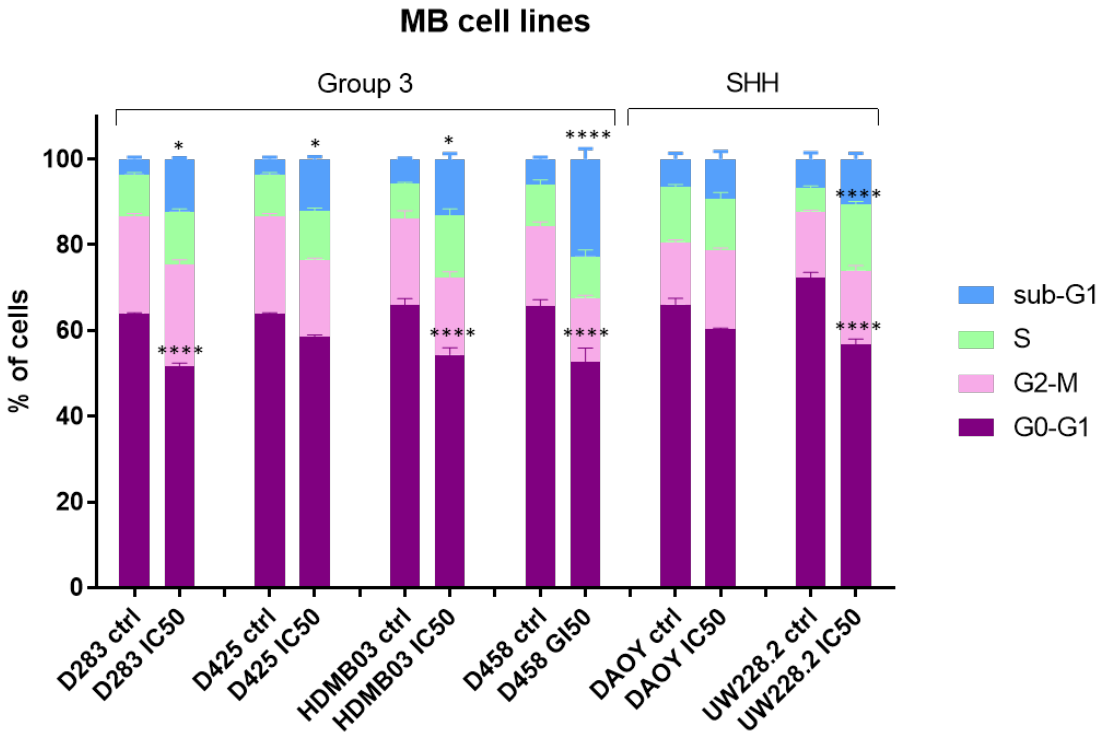

Figure 6.21. Effect of Milciclib treatment on cell cycle distribution in parental MB cell lines. Cell cycle distribution of D283, D425, HDMB03, D458, DAOY and UW228.2 after 72h of a single exposure of IC_{50} concentration of the CDK2 inhibitor Milciclib. Cells were stained with propidium iodide and cell cycle distribution analysed by flow cytometry. Graph represents the percentage (%) of cells of each cell cycle phase relative to total phases. Untreated cells (ctrl-no drug; DMSO only) for each cell line were used as controls. Data is presented as the percentage of the mean (±SEM) of two independent experiments. Significance determined by 2-way ANOVA (*p≤0.05, **p≤0.01, ***p≤0.001, ****p≤0.0001).

6.5.3 AURKA inhibition

All three isogenic cell lines tested showed a significant increase in the sub-G_1 region (dead cells) of the cell cycle after treatment with IC_{50} concentration of MLN8237 regardless of *MYC* expression levels (Figure 6.22). Although still statistically significant, the increase in cell numbers in sub-G_1 phase was less pronounced in cells with *MYC* knockdown. AURKA inhibition with MLN8237 caused a significant reduction of cells in G_1 phase of the cell cycle compared to the untreated controls, regardless of *MYC* expression levels. A significant increase in the number of cells in the G_2-M phase of the cell cycle was observed after treatment, reaching significance only in D425 with *MYC* silenced and in HDMB03 expressing high levels of *MYC* (Figure 6.22).

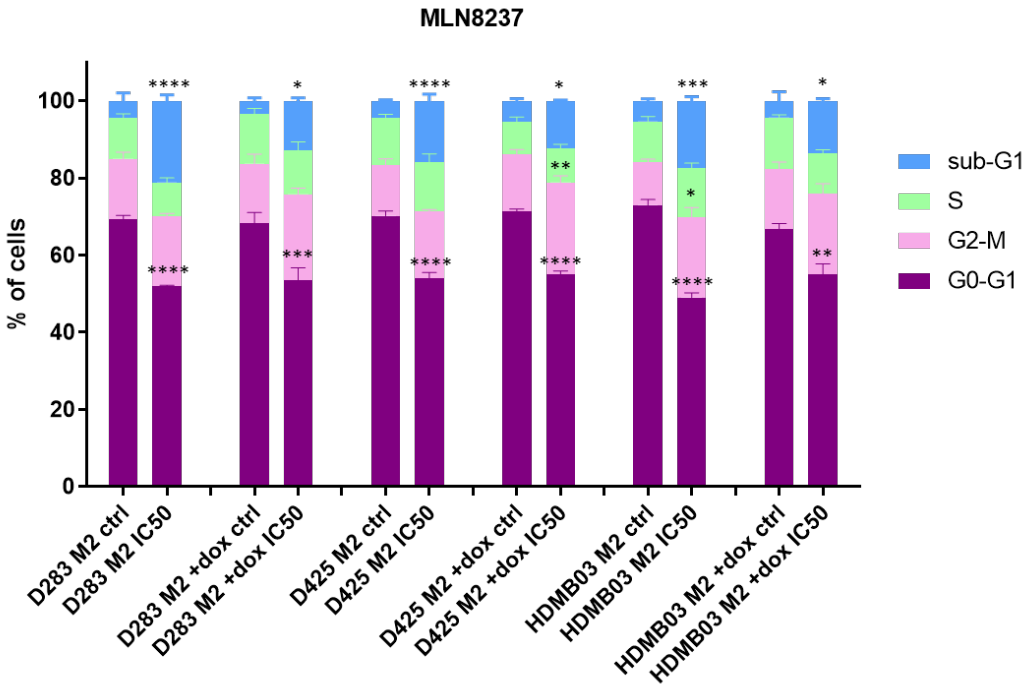

Figure 6.22. Effect of MLN8237 treatment on cell cycle distribution in isogenic MB_{Group3} cell lines. Cell cycle distribution of D425, D283 and HDMB03 MYC2 cell lines after 72h of a single exposure of IC_{50} concentration of the AURKA inhibitor MLN8237. Cells were stained with propidium iodide and cell cycle distribution analysed by flow cytometry. Graph represents the percentage (%) of cells of each cell cycle phase relative to total phases, of cells expressing high levels of *MYC* and those with *MYC* knockdown (+dox). Untreated cells (ctrl-no drug; DMSO only) were used for each condition (+/-dox) as controls. Data is presented as the percentage of the mean (±SEM) of three independent experiments. Significance determined by 2-way ANOVA (*p≤0.05, **p≤0.01, ***p≤0.001, ****p≤0.0001).

Treatment of MB_{Group3} and MB_{SHH} parental cell lines with MLN8237 also caused a significant increase in apoptotic cells, seen by the significant increase in sub-G_1 region of the cell cycle (Figure 6.23). Although still statistically significant, the increase in cell numbers in sub-G_1 phase was less pronounced in DAOY and UW228.2, compared to the increase observed in other cell lines, which suggests a subgroup specific effect.

AURKA inhibition with MLN8237 caused a significant reduction of cells in G_1 phase of the cell cycle across MB cell lines, when compared to their respective untreated controls. The decrease in the percentage of cells in G_1 phase caused by MLN8237 did not reach statistical significance in DAOY (Figure 6.23).

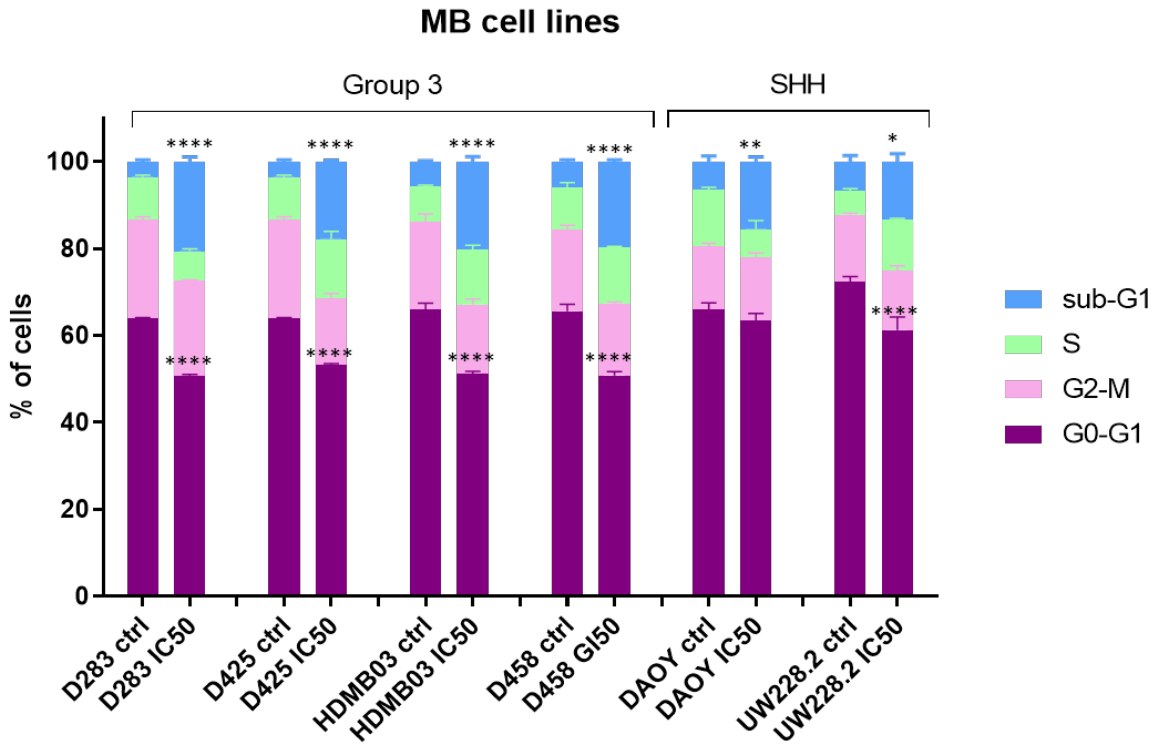

Figure 6.23. Effect of MLN8237 treatment on cell cycle distribution in parental MB cell lines. Cell cycle distribution of D283, D425, HDMB03, D458, DAOY and UW228.2 after 72h of a single exposure of IC_{50} concentration of the AURKA inhibitor MLN8237. Cells were stained with propidium iodide and cell cycle distribution analysed by flow cytometry. Graph represents the percentage (%) of cells of each cell cycle phase relative to total phases. Untreated cells (ctrl-no drug; DMSO only) for each cell line were used as controls. Data is presented as the percentage of the mean (±SEM) of two independent experiments. Significance determined by 2-way ANOVA (*p≤0.05, **p≤0.01, ***p≤0.001, ****p≤0.0001).

6.5.4 CHK1 inhibition

6.5.4.1 AZD7762

A *MYC*-dependent increase in the number of cells in sub-G_1 phase of the cell cycle was seen in D425, D283 and HDMB03 cloned with the MYC2 construct after exposure to AZD7762 (Figure 6.24). Treatment of isogenic cell lines with IC_{50} concentration of the inhibitors caused a significant increase in the number of cells in sub-G_1 phase in cells expressing high-levels of *MYC*, whereas no significant changes were seen in cells with *MYC* knockdown.

After treatment, all three *MYC*-regulable cell lines tested showed a significant decrease in the proportion of cells at G_1 phase, regardless of *MYC* expression levels. A significant accumulation of cells at G_2-M phase was seen across cell lines after treatment with AZD7762, being D425 with *MYC* knockdown the only one in which significance was not reached (Figure 6.24).

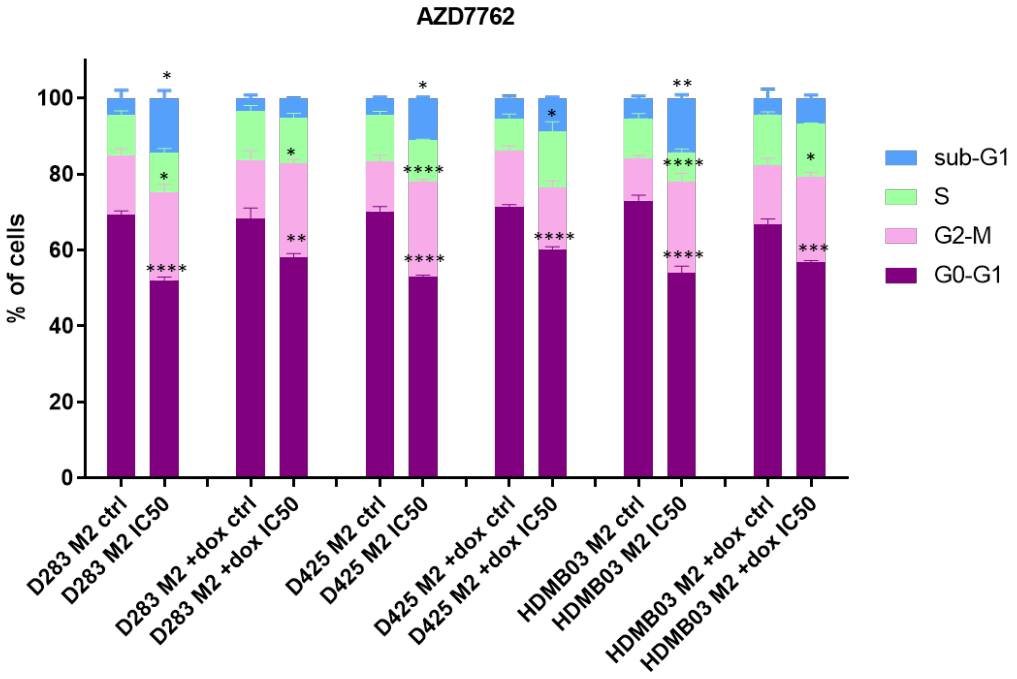

Figure 6.24. Effect of AZD7762 treatment on cell cycle distribution in isogenic MB_{Group3} cell lines. Cell cycle distribution of D425, D283 and HDMB03 MYC2 cell lines after 72h of a single exposure of IC_{50} concentration of the CHK1 inhibitor AZD7762. Cells were stained with propidium iodide and cell cycle distribution analysed by flow cytometry. Graph represents the percentage (%) of cells of each cell cycle phase relative to total phases, of cells expressing high levels of *MYC* and those with *MYC* knockdown (+dox). Untreated cells (ctrl-no drug; DMSO only) were used for each condition (+/-dox) as controls. Data is presented as the percentage of the mean (±SEM) of three independent experiments. Significance determined by 2-way ANOVA (*p≤0.05, **p≤0.01, ***p≤0.001, ****p≤0.0001).

A clear subgroup and *MYC*-dependent effect was seen in MB parental cell lines after treatment with IC_{50} concentration of AZD7762 (Figure 6.25). Exposure to the inhibitor caused a significant increase in the number of cells in sub-G_1 phase of the cell cycle only in MB_{Group3} cell lines. *CHK1* inhibition with AZD7762 slightly increased cell percentages in G_2-M phase of the cell cycle, but statistical significance was not reached. After 72h of treatment, all cell lines exhibited a decrease in the proportion of cells at G_1 phase when compared to untreated controls (non-significant in D425 and DAOY)(Figure 6.25).

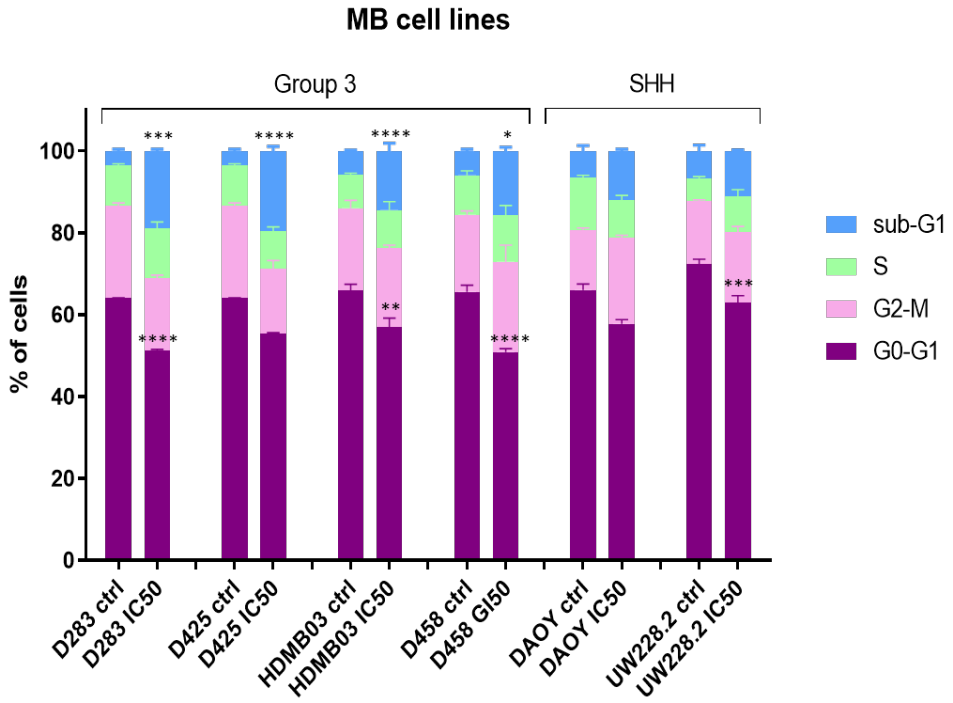

Figure 6.25. Effect of AZD7762 treatment on cell cycle distribution in parental MB cell lines. Cell cycle distribution of D283, D425, HDMB03, D458, DAOY and UW228.2 after 72h of a single exposure of IC_{50} concentration of the CHK1 inhibitor AZD7762. Cells were stained with propidium iodide and cell cycle distribution analysed by flow cytometry. Graph represents the percentage (%) of cells of each cell cycle phase relative to total phases. Untreated cells (ctrl -no drug; DMSO only) for each cell line were used as controls. Data is presented as the percentage of the mean (±SEM) of two independent experiments. Significance determined by 2-way ANOVA (*p≤0.05, **p≤0.01, ***p≤0.001, ****p≤0.0001).

6.5.4.2 Prexasertib

Exposure of *MYC*-regulable D425, D283 and HDMB03 to IC_{50} concentration of Prexasertib significantly induced apoptosis when compared to untreated cells (Figure 6.26). This increase in the number of cells in sub-G_1 phase of the cell cycle was seen across cells lines regardless of *MYC* expression levels.

CHK1 inhibition with Prexasertib caused a significant decrease in cells in G_1 phase of the cell cycle in all cell lines, when compared to untreated controls. Treatment caused a concomitant increase in the proportion of cells in G_2-M phase of the cell cycle of D425, D283 and HDMB03 expressing high levels of MYC (Figure 6.26).

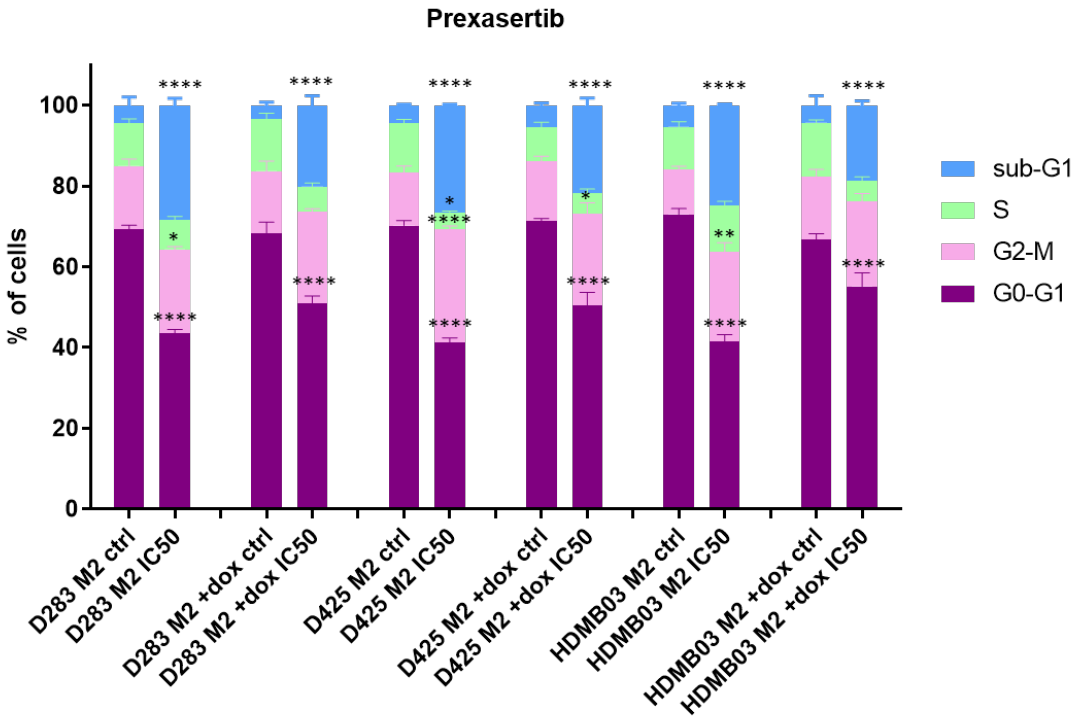

Figure 6.26. Effect of Prexasertib treatment on cell cycle distribution in isogenic MB_{Group3} cell lines. Cell cycle distribution of D425, D283 and HDMB03 MYC2 cell lines after 72h of a single exposure of IC_{50} concentration of the CHK1 inhibitor Prexasertib. Cells were stained with propidium iodide and cell cycle distribution analysed by flow cytometry. Graph represents the percentage (%) of cells of each cell cycle phase relative to total phases, of cells expressing high levels of *MYC* and those with *MYC* knockdown (+dox). Untreated cells (ctrl-no drug; DMSO only) were used for each condition (+/-dox) as controls. Data is presented as the percentage of the mean (±SEM) of three independent experiments. Significance determined by 2-way ANOVA (*$p \leq 0.05$, **$p \leq 0.01$, ***$p \leq 0.001$, ****$p \leq 0.0001$).

Exposure of parental MB cell lines to IC_{50} concentration of Prexasertib significantly induced apoptosis when compared to untreated cells (Figure 6.27). This significant increase in the number of cells in sub-G_1 phase of the cell cycle was seen across cells lines regardless of *MYC* expression levels (not *MYC*-dependent).

In general, an increase of cells in sub-G_1 phase of the cell cycle was seen together with a decrease in the proportion of cells in G_1 phase. Although it did not reach statistical significance, a slight accumulation of cells in G_2-M phase of the cell cycle was observed across cell lines after treatment (Figure 6.27).

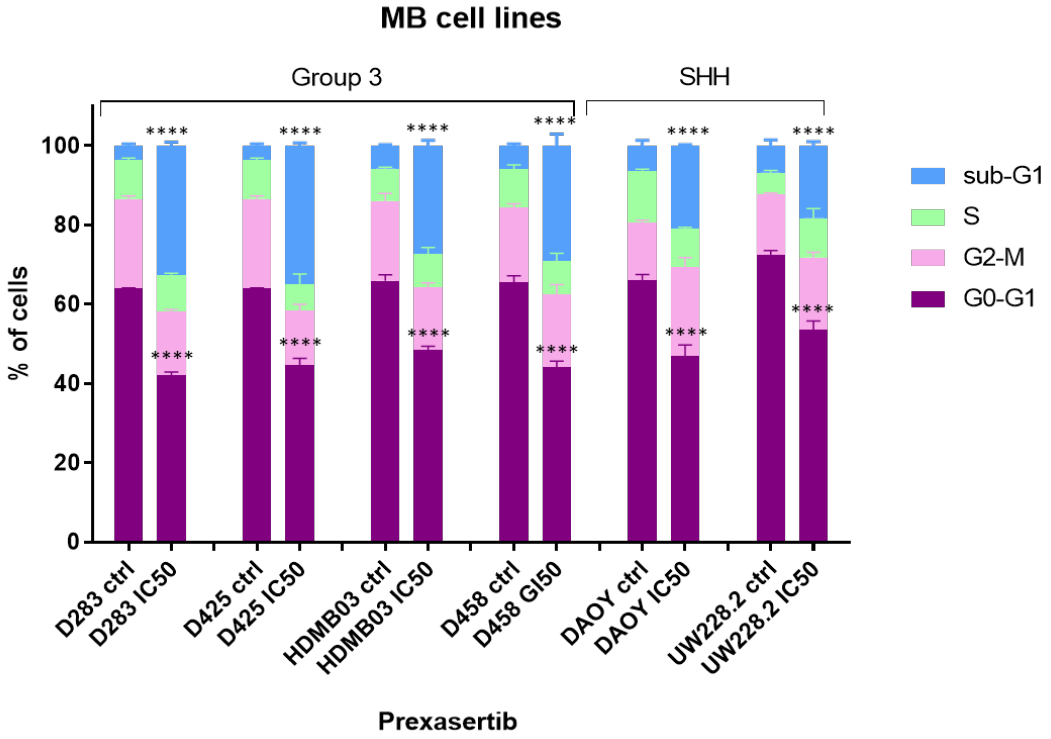

Figure 6.27. Effect of Prexasertib treatment on cell cycle distribution in parental MB cell lines. Cell cycle distribution of D283, D425, HDMB03, D458, DAOY and UW228.2 after 72h of a single exposure of IC_{50} concentration of the CHK1 inhibitor Prexasertib. Cells were stained with propidium iodide and cell cycle distribution analysed by flow cytometry. Graph represents the percentage (%) of cells of each cell cycle phase relative to total phases. Untreated cells (ctrl-no drug; DMSO only) for each cell line were used as controls. Data is presented as the percentage of the mean (±SEM) of two independent experiments. Significance determined by 2-way ANOVA (*$p \leq 0.05$, **$p \leq 0.01$, ***$p \leq 0.001$, ****$p \leq 0.0001$).

6.5.5 Conclusion

Flow cytometry analysis of MB cells' cycle distribution after treatment with the inhibitors was performed on MB_{SHH} and MB_{Group3} cell lines with the aim to better characterise the growth inhibitory effect of the compounds.

Analysis of the cell cycle distribution of D425, D283 and HDMB03 MYC2 cells overexpressing *MYC* and with *MYC* knockdown after treatment with the inhibitors, corroborated the *MYC*-dependent effect seen on cell proliferation, where higher levels of *MYC* expression sensitised cells to the effect of the inhibitors.

BI2536, Prexasertib, AZD7762 and MLN8237 caused a significant increase in the proportion of cells in sub-G_1 phase of the cell cycle after treatment, indicating an increase in apoptotic cells. The increase in apoptotic cells was seen in cells overexpressing *MYC* in comparison to those with *MYC*-knockdown. Cell cycle arrest at G_2-M phase of the cell cycle was seen in cells expressing lower levels of *MYC*. Data suggests that BI2536, Prexasertib, AZD7762 and MLN8237 preferentially kill *MYC* overexpressing cells whilst also arresting the growth of those with lower levels of *MYC*.

Treatment with Milciclib did not result in a significant increase in apoptosis in MB_{Group3} MYC2 cells expressing high levels of *MYC*. Exposures to the drug caused an increase in the proportion of cells at G_2-M phase of the cell cycle, indicating the main mechanism by which Milciclib inhibit MB_{Group3} cells proliferation is through cell cycle arrest at G_2-M phase.

The *MYC*-dependent drug-sensitivity effect was also seen in the distribution of cell cycle after treatment in a subgroup specific context. AZD7762 and Milciclib, significantly increased the proportion of dead cells after treatment in MB_{Group3} when compared to MB_{SHH} cell lines. MLN8237 treatment caused a significant increase in the proportion of dead cells regardless of subgroups. BI2536 caused cell cycle arrest at G_2-M phase across cell lines regardless of differential levels of *MYC* expression according to subgroup, and a significant increase in the proportion of cells in sub-G_1 phase of the cell cycle in all MB cell lines with the exception of UW228.2. On the other hand, Prexasertib significantly increased the number of cells in sub-G_1 phase of the cell cycle on all MB cell lines tested, showing a clear sensitivity of MB cells to the compound.

Results from the assessment of the cell cycle distribution after treatment with the inhibitors showed clear differences according to levels of *MYC* expression and subgroup, but not uniformly. This information could help prioritise inhibitors that specifically induce apoptosis in *MYC*-driven MB_{Group3} cell lines, like BI2536, AZD7762 and MLN8237. Overall, MB_{Group3} cell lines exhibited increased sensitivity to PLK1, CHK1 and AURKA inhibition with the compounds chosen, displaying a *MYC*-sensitivity subgroup-specific effect.

6.6 Cell-proliferation rescue assays

Assessment of cell cycle distribution after drug treatment revealed an increase in the number of cells in sub-G_1 phase of the cell cycle, which suggested that the inhibitors were inhibiting cells proliferation by inducing apoptosis. As preliminary experiments to assess the ability of cells to recover growth after exposures to the inhibitors, and whether this was *MYC*-dependent, a cell-proliferation rescue assay was performed on the isogenic D425, D283 and HDMB03 MYC2 cell lines (methodology described in Chapter 2). Cell proliferation was assessed with CTG at different time points after drug exposure to study if cell growth (represented by metabolically active cells) could be recovered after treatment.

D425, D283 and HDMB03 MYC2 overexpressing MYC and with MYC knockdown were exposed to a single dose of half IC_{50} ($0.5xIC_{50}$), IC_{50} (IC_{50}), and twice IC_{50} ($2xIC_{50}$) concentration of each inhibitor, and cell viability assessed after 3 and 5 days of exposure to drug. After 5 days, media-containing drug was removed and plates refreshed with new media (no drug). Cells were left to grow for additional 5 and 9 days upon removal to check cell proliferation, indicative of alive metabolically active cells. Untreated cells for both conditions (-/+ DOX) were used as controls.

Cell-proliferation rescue assay of isogenic D425, D283 and HDMB03 MYC2 after treatment with the three different concentrations of the inhibitors can be seen in figures Appendix 6.8, Appendix 6.9, Appendix 6.10, Appendix 6.11 and Appendix 6.12. For comparison of changes in metabolically active cells after exposures to the inhibitors, only differences between untreated cells (no drug) and those treated with half-maximal inhibitory concentration (IC_{50}) are shown.

6.6.1 BI2536: PLK1 inhibition

Inhibition of PLK1 by BI2536 caused a highly consistent reduction in cell proliferation in a time and dose-dependent manner across isogenic cell lines (Appendix 6.8). Treatment with the inhibitor caused a progressive decrease in cell proliferation after drug administration when compared to untreated controls, in both *MYC*-overexpressing and MYC knockdown cells across cell lines. Proliferation of cells with MYC knockdown was not as markedly reduced with treatment with BI2536 when compared to cells overexpressing *MYC*.

When treated with IC_{50} concentration, a significant decrease in metabolically active cells was seen in *MYC*-overexpressing cells and with *MYC* knockdown after drug removal, with no evidence of recovery in either (Figure 6.28). A greater reduction in cell proliferation was seen in *MYC*-overexpressing cell lines when compared to their *MYC*-silenced counterparts (D283 p=0,0156; D425 p<0.0001; HDMB03 p<0.0001). *MYC* expression sensitised the cells to the inhibitor preventing the recovery of their growth after treatment.

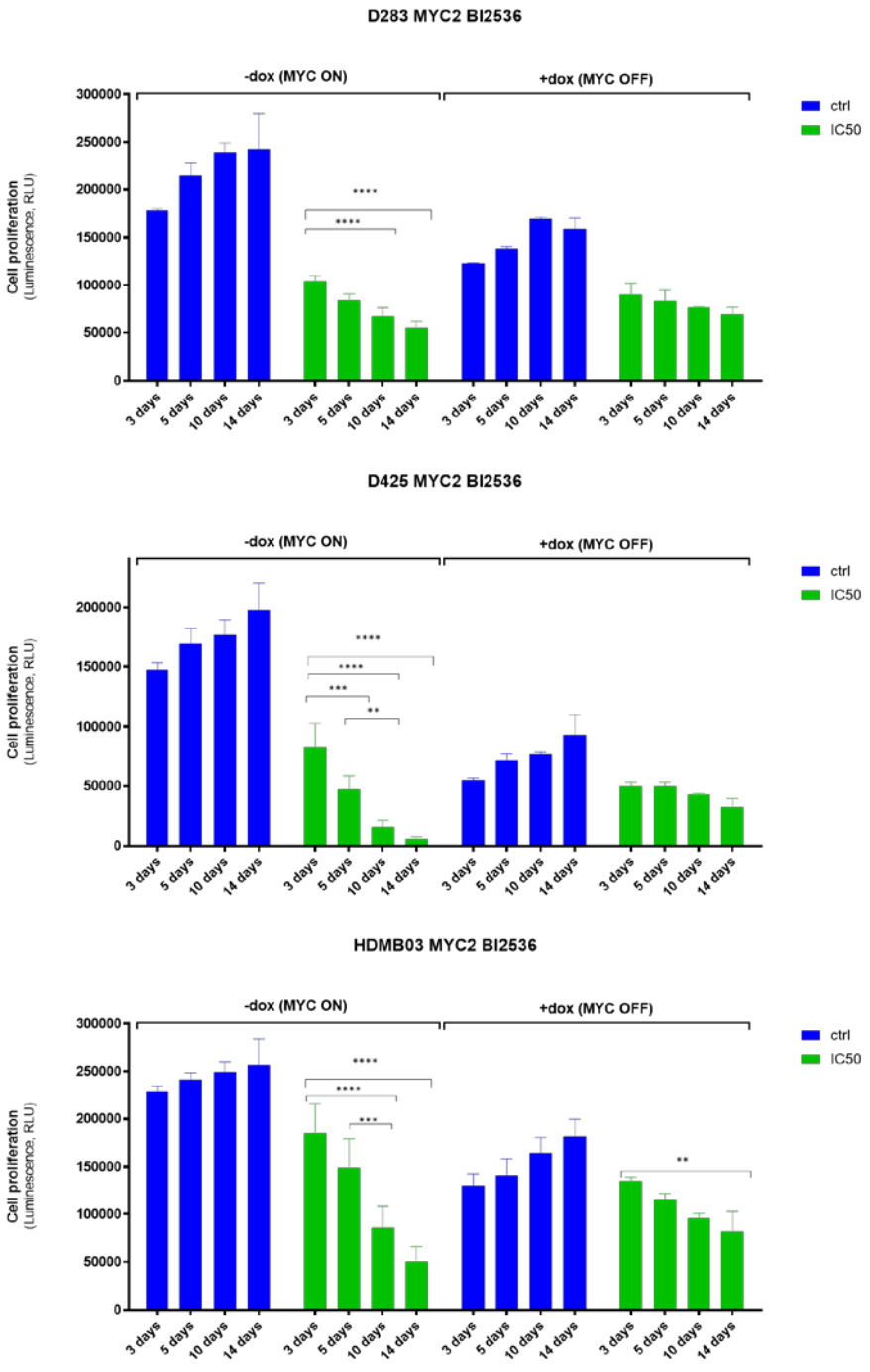

Figure 6.28. Effect of treatment with BI2536 on the proliferation of *MYC*-regulable cell lines after treatment with BI2536.Cell-proliferation rescue assay of D425, D283 and HDMB03 MYC2 during and after exposure to the *PLK1* inhibitor BI2536. Cells expressing high levels of *MYC* (-dox; MYC ON) and those with *MYC* knockdown (+dox; MYC OFF) were exposed to IC_{50} concentration (green) for 5 days. After exposure, drug was removed from the media, media changed, and cells left to grow for further 5 and 9 days. Cell proliferation was assessed with CTG 3, 5, 10 and 14 days after drugging. Untreated cells (no drug; blue) were used for each condition (+/-DOX) as controls. Data was blank-corrected to DMSO-containing wells, and normalised to day 0. Graphs show the comparison of growth between untreated cells (blue) and those treated with the inhibitor (green). Data is presented as the mean (±SEM) of two independent experiments. Significance determined by 2-way ANOVA (*$p \leq 0.05$, **$p \leq 0.01$, ***$p \leq 0.001$, ****$p \leq 0.0001$).

6.6.2 Milciclib: CDK2 inhibition

When compared to the growth of untreated cells, exposure to Milciclib (CDK2 inhibitor) caused a significant decrease in proliferation of D425, D283 and HDMB03 MYC2 cells overexpressing *MYC* and with *MYC* silenced with shRNA, in a time- and dose-dependent manner (Appendix 6.9). The decrease in cell proliferation continued after drug removal.

A sign of growth recovery was seen in cells with *MYC* knockdown after treatment with IC_{50} of Miliclib, where a significant increase in proliferation was seen after drug removal (Figure 6.29). Lower levels of *MYC* increased resistance to treatment with Milciclib when compared to counterparts expressing higher levels of *MYC*, being able to recover their growth after treatment.

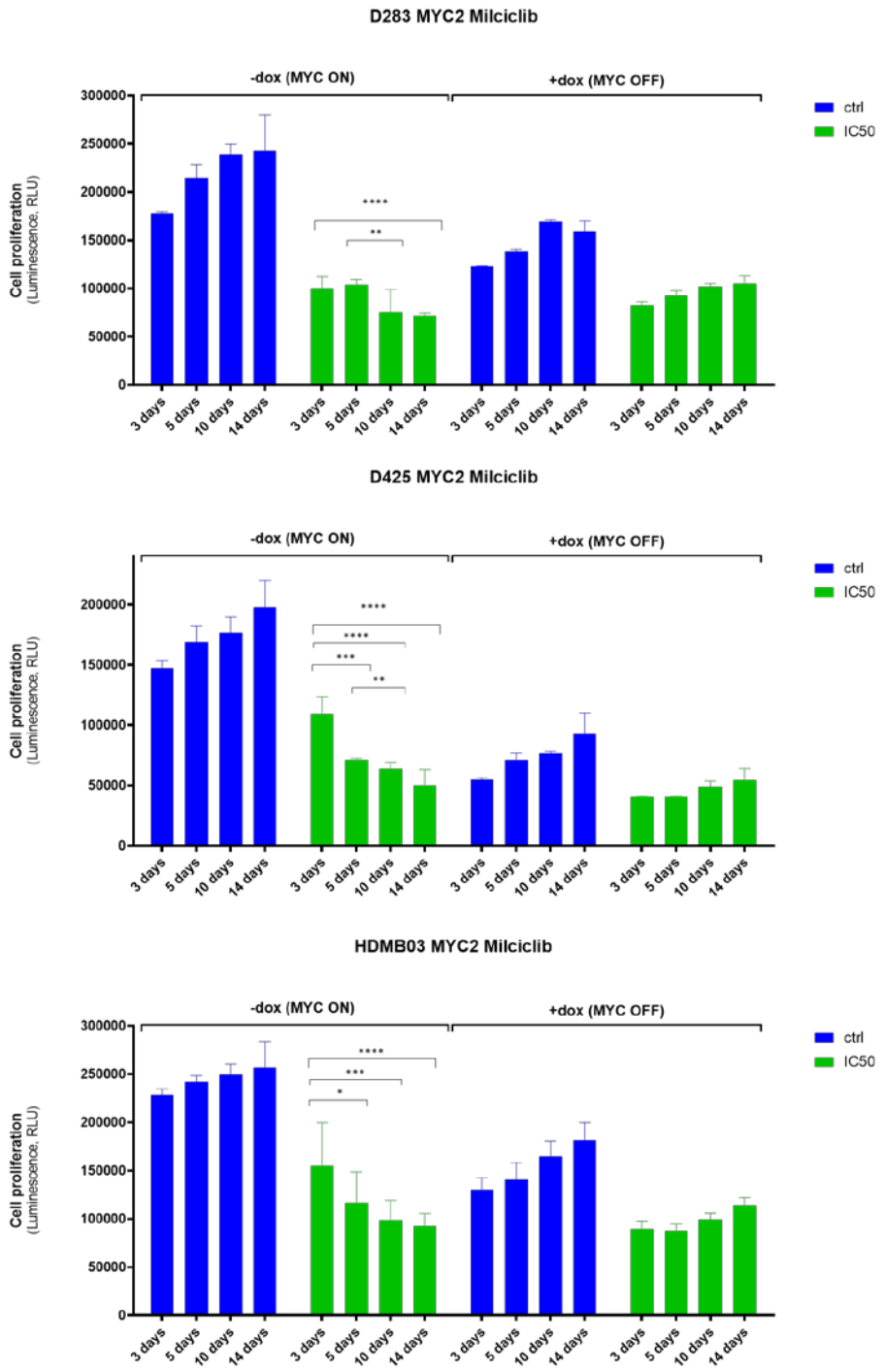

Figure 6.29. Proliferation of *MYC*-regulable cell lines after treatment with Milciclib.Cell-proliferation rescue assay of D425, D283 and HDMB03 MYC2 during and after exposure to the *CDK2* inhibitor Milciclib. Cells expressing high levels of *MYC* (-dox; MYC ON) and those with *MYC* knockdown (+dox; MYC OFF) were exposed to IC_{50} concentration (green) for 5 days. After exposure, drug was removed from the media, media changed, and cells left to grow for further 5 and 9 days. Cell proliferation was assessed with CTG 3, 5, 10 and 14 days after drugging. Untreated cells (no drug; blue) were used for each condition (+/-DOX) as controls. Data was blank-corrected to DMSO-containing wells, and normalised to day 0. Graphs show the comparison of growth between untreated cells (blue) and those treated with the inhibitor (green). Data is presented as the mean (±SEM) of two independent experiments. Significance determined by 2-way ANOVA (*p≤0.05, **p≤0.01, ***p≤0.001, ****p≤0.0001).

6.6.3 MLN8237: AURKA inhibition

Exposures to MLN8237 caused a progressive decrease in D425, D283 and HDMB03 MYC2 proliferation in a time- and dose-dependent manner when compared to untreated cells (Appendix 6.10). Assessment of cells proliferation after AURKA inhibition, revealed that treatment with MLN8237 had a higher growth-inhibitory effect in cells expressing high levels of *MYC* than in cells with *MYC* knockdown.

Upon *MYC* silencing, a slight, but non-significant, increase in the proportion of metabolically active cells was seen in D425, D283 and HDMB03, indicating a possible recovery when treated with IC_{50} concentrations of the inhibitor (Figure 6.30).

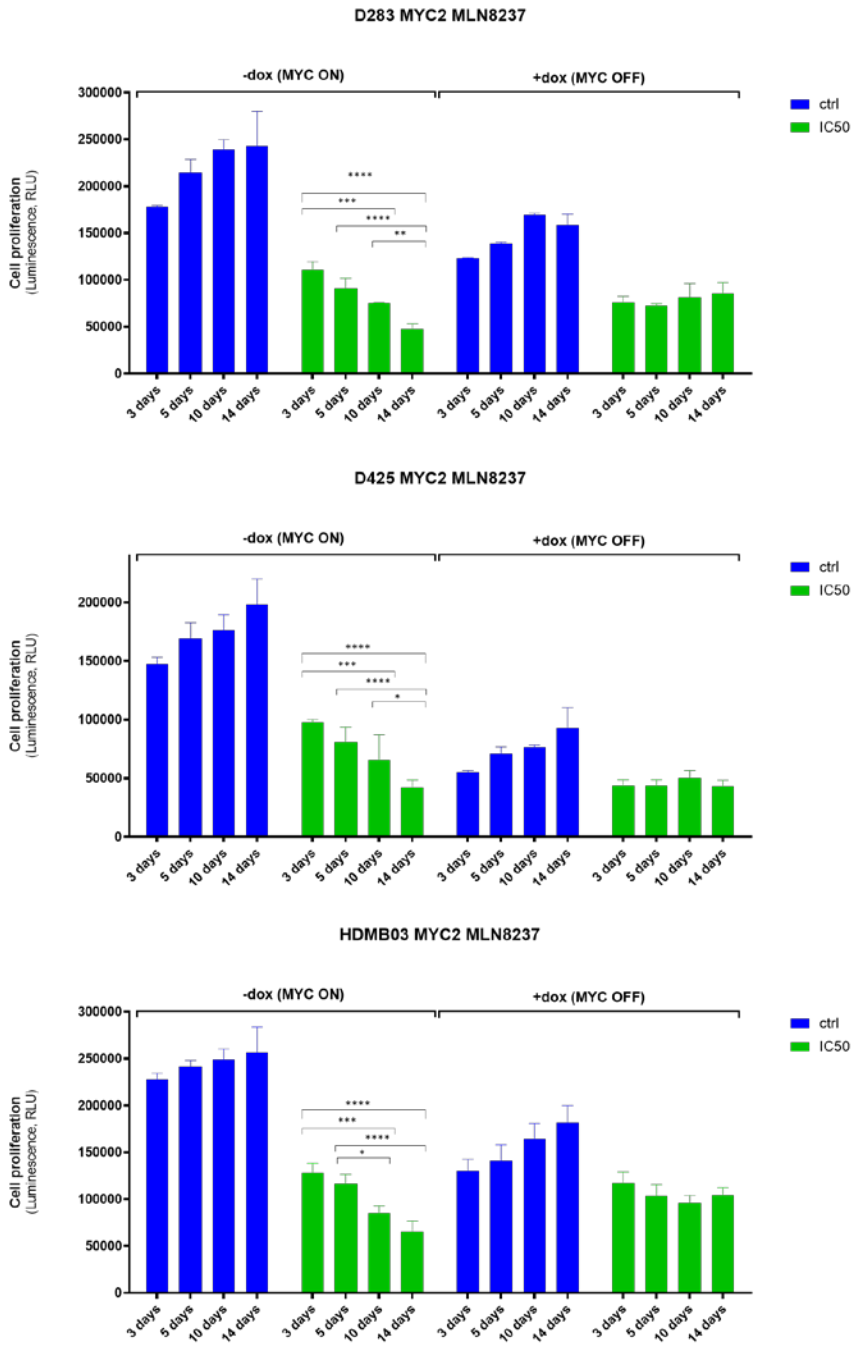

Figure 6.30. Proliferation of *MYC*-regulable cell lines after treatment with MLN8237.Cell-proliferation rescue assay of D425, D283 and HDMB03 MYC2 during and after exposure to the *AURKA* inhibitor MLN8237. Cells expressing high levels of *MYC* (-dox; MYC ON) and those with *MYC* knockdown (+dox; MYC OFF) were exposed to IC_{50} concentration (green) for 5 days. After exposure, drug was removed from the media, media changed, and cells left to grow for further 5 and 9 days. Cell proliferation was assessed with CTG 3, 5, 10 and 14 days after drugging. Untreated cells (no drug; blue) were used for each condition (+/-DOX) as controls. Data was blank-corrected to DMSO-containing wells, and normalised to day 0. Graphs show the comparison of growth between untreated cells (blue) and those treated with the inhibitor (green). Data is presented as the mean (±SEM) of two independent experiments. Significance determined by 2-way ANOVA (*p≤0.05, **p≤0.01, ***p≤0.001, ****p≤0.0001).

6.6.4 AZD7762: CHK1 inhibition

AZD7762 significantly reduced cell proliferation of D425, D283 and HDMB03 in both *MYC*-overexpressing and *MYC* knockdown cells in a time- and dose-dependent manner, when compared to their corresponding untreated counterparts (Appendix 6.11). Treatment with IC_{50} concentration of AZD7762 caused a significantly reduced proliferation of those cells expressing high-levels of *MYC*, in comparison to those treated with DOX for MYC knockdown. This effect was seen across cell lines (Figure 6.31).

A slight time-dependent increase in the proportion of metabolically active cells was seen across cell lines with *MYC* knockdown when allowed to recover after treatment with half IC_{50} concentration (Figure 6.31). Sustained time-dependent growth inhibition with no recovery was only seen in *MYC*-overexpressing cells, thus exhibiting a *MYC*-dependent effect.

The cell-proliferation rescue assay thus revealed higher sensitivity of *MYC*-overexpressing cell lines to CHK1 inhibition in comparison to those with *MYC* knockdown; effect seen through the time and dose-dependent reduction of viable cells after treatment.

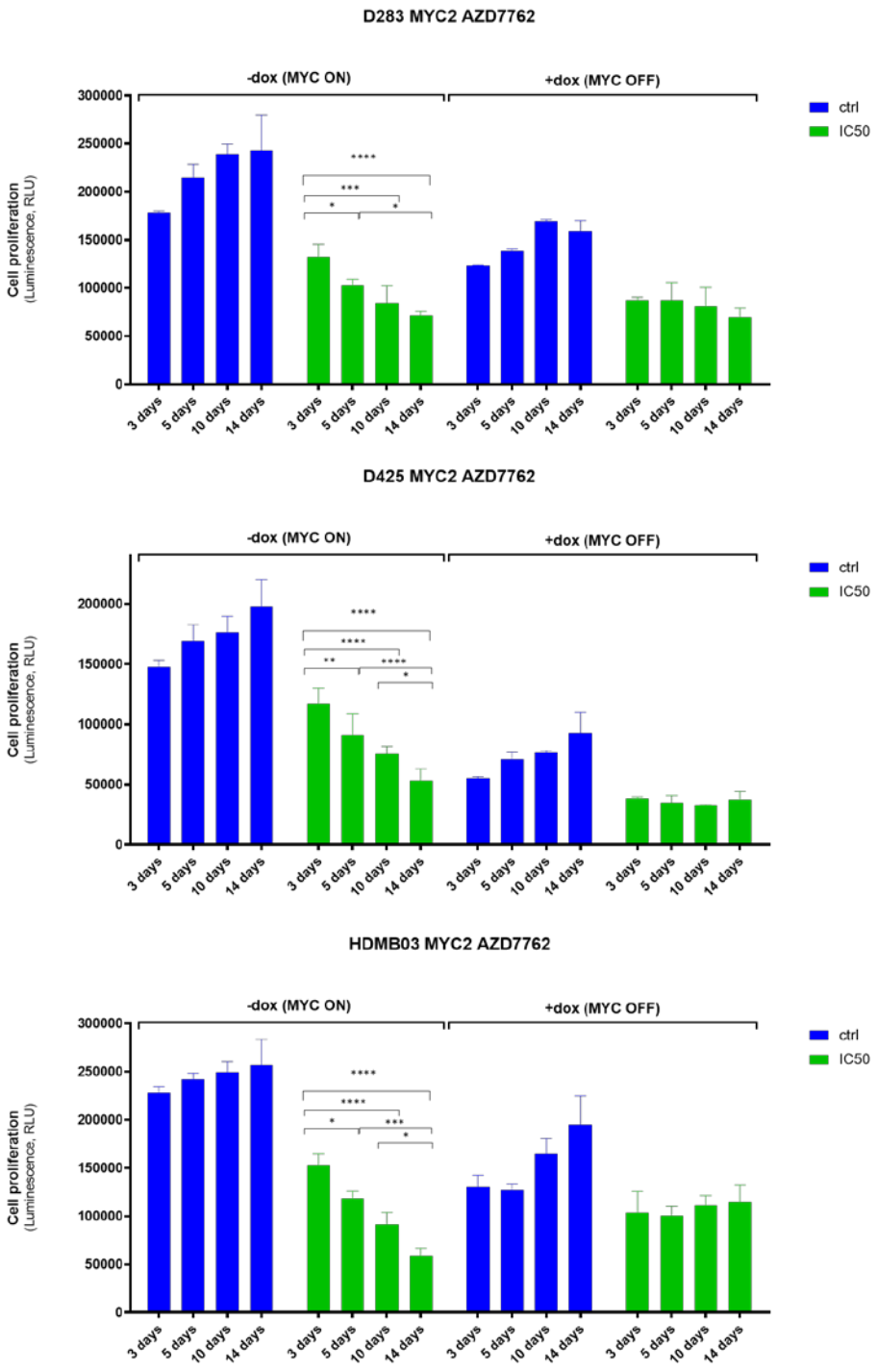

Figure 6.31. Proliferation of *MYC*-regulable cell lines after treatment with AZD7762. Cell-proliferation rescue assay of D425, D283 and HDMB03 MYC2 during and after exposure to the *CHK1* inhibitor AZD7762. Cells expressing high levels of *MYC* (-dox; MYC ON) and those with *MYC* knockdown (+dox; MYC OFF) were exposed to IC_{50} concentration (green) for 5 days. After exposure, drug was removed from the media, media changed, and cells left to grow for further 5 and 9 days. Cell proliferation was assessed with CTG 3, 5, 10 and 14 days after drugging. Untreated cells (no drug; blue) were used for each condition (+/-DOX) as controls. Data was blank-corrected to DMSO-containing wells, and normalised to day 0. Graphs show the comparison of growth between untreated cells (blue) and those treated with the inhibitor (green). Data is presented as the mean (±SEM) of two independent experiments. Significance determined by 2-way ANOVA (*p≤0.05, **p≤0.01, ***p≤0.001, ****p≤0.0001).

6.6.5 Prexasertib: CHK1 inhibition

Treatment with the CHK1/2 inhibitor Prexasertib caused, in a time and dose-dependent manner, a significant reduction in D425, D283 and HDMB03 MYC2 cell proliferation, regardless of *MYC* expression levels (Appendix 6.12).

After treatment with IC_{50} concentration of Prexasertib, cells overexpressing *MYC* exhibited a greater reduction in metabolically active cells after recovery time, when compared to their counterparts expressing lower levels of *MYC* (Figure 6.32).

Following *MYC* knockdown, a significant decrease in cell proliferation throughout time of recovery was seen in D283 and HDMB03 after exposure to IC_{50} concentration. The decrease in D425 was not statistically significant (Figure 6.32).

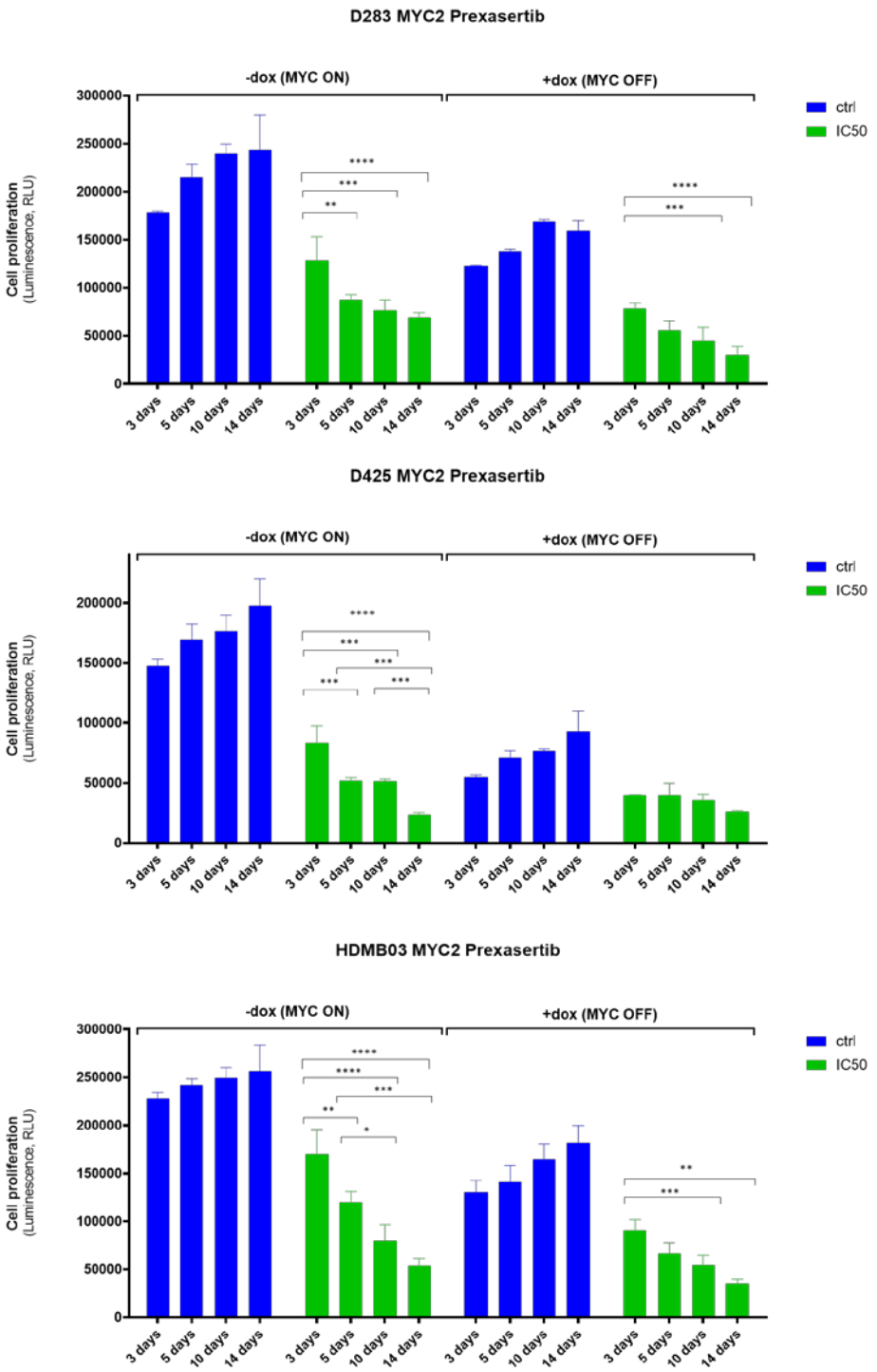

Figure 6.32. Proliferation of *MYC*-regulable cell lines after treatment with Prexasertib. Cell-proliferation rescue assay of D425, D283 and HDMB03 MYC2 during and after exposure to the *CHK1* inhibitor Prexasertib. Cells expressing high levels of *MYC* (-dox; MYC ON) and those with *MYC* knockdown (+dox; MYC OFF) were exposed to IC_{50} concentration (green) for 5 days. After exposure, drug was removed from the media, media changed, and cells left to grow for further 5 and 9 days. Cell proliferation was assessed with CTG 3, 5, 10 and 14 days after drugging. Untreated cells (no drug; blue) were used for each condition (+/-DOX) as controls. Data was blank-corrected to DMSO-containing wells, and normalised to day 0. Graphs show the comparison of growth between untreated cells (blue) and those treated with the inhibitor (green). Data is presented as the mean (±SEM) of two independent experiments. Significance determined by 2-way ANOVA (*p≤0.05, **p≤0.01, ***p≤0.001, ****p≤0.0001).

6.6.6 Conclusion

To better understand the growth-inhibitory effect of the inhibitors on MB_{Group3} cell lines and its associated *MYC*-dependency, cell-proliferation rescue assay were performed on the isogenic D425, D283 and HDMB03 MYC2 cell lines to assess the ability of cells to recover their growth after exposures to the inhibitors.

A time- and dose-dependent decrease in cells proliferation was seen across cell lines expressing high levels of MYC after treatment with BI2536 (PLK1 inhibitor), AZD7762 (CHK1 inhibitor), Milciclib (CDK2 inhibitor), MLN8237 (AURKA inhibitor) and Prexasertib (CHK1/2 inhibitor). A *MYC*-dependent drug-sensitivity effect was seen in all 3 cell lines, where greater growth inhibition was seen in MB cell lines overexpressing *MYC*, when compared to cells with *MYC* knockdown, after treatment with the inhibitors.

Cells treated with BI2536 and Prexasertib were not able to recover cell growth after drug removal, in both conditions, either expressing high levels of *MYC* or with *MYC* knockdown. In contrast, when expressing lower levels of *MYC* (*MYC* knockdown), an increase in cells proliferation was seen after treatment with Milciclib, AZD7762 and MLN8237, indicating a possible recovery.

In summary, the ability of cells to recover their growth after treatment with the inhibitors was dependent on *MYC* expression. Treatment with Milciclib, MLN8237 and AZD7762 caused a *MYC*-dependent continued cell kill after drug removal, where recovery of cells proliferation was not possible when expressing high levels of *MYC*. On the other hand, low levels of *MYC*-expression (*MYC* knockdown) allowed recovery of cells proliferation after treatment. No recovery in cell growth was seen after exposures to BI2536 and Prexasertib.

These results could help the prioritisation of inhibitors which specifically have a *MYC*-dependent effect on MB_{Group3} cells proliferation and cause a continued cell kill after drug administration.

6.7 Discussion

With the objective to better understand the role of *MYC* within MB_{Group3}, a high-throughput drug screening was performed on the *MYC*-regulable isogenic cell lines to identify targetable signalling pathways associated with *MYC* that could be exploited to treat *MYC*-driven MB_{Group3} tumours. The screen identified 82 small-molecule inhibitors which selectively inhibited the growth of *MYC*-overexpressing cell lines. As described in Chapter 5, integration of HTCS results with data on transcriptional MB dependencies predicted PLK1 (3.7% of hits), CHK (4.9% of hits), AURK (9.8% of hits) and CDK (12.2% of hits) as targetable molecules to be effective on MB_{Group3}, allowing prioritisation for further investigation.

This chapter was set out to validate the *MYC*-dependency of the compounds identified from the screen, and investigate their direct effect on MYC protein expression, cell cycle distribution and cell proliferation in *MYC*-dependent MB_{Group3} cell lines and across parental MB lines from different subgroups.

Indeed, results presented in this chapter support the fact that pharmacological inhibition of CDK2, AURKA, PLK1 and CHK1 resulted in growth inhibition, downregulation of MYC protein levels and induction of apoptosis with preferential effect in *MYC* overexpressing MB cell lines, in comparison to those expressing lower levels of *MYC*, stating the *MYC*-dependency on these proteins.

Sensitivity to AZD7762 (CHK1 inhibitor), BI2536 (PLK1 inhibitor), MLN8237 (AURKA inhibitor), Milciclib (CDK2 inhibitor), SN-38 (topoisomerase I inhibitor), MK-1775 (WEE1 inhibitor) and Prexasertib (CHK1/2 inhibitor) inhibitors was dependent on *MYC* expression levels, where exposures to the compounds had a greater growth-inhibitory effect on *MYC*-overexpressing cell lines over those with *MYC*-knockdown with shRNA. The *MYC*-dependency on these proteins was seen in a sub-group specific context, where MB_{Group3} cell lines were more sensitive to the compounds identified, in comparison to the MB_{SHH} lines DAOY and UW228.2. Drug-sensitivity effects seen are in accordance with differential levels of *MYC* expression, where MB cell lines expressing higher levels of *MYC* exhibited higher sensitivity to the compounds.

A significant difference in sensitivity was seen depending on the CHK1 inhibitor used, AZD7762 and Prexasertib. Prexasertib caused greater MB_{Group3} cell growth inhibition when compared to AZD7762. The difference in drug sensitivity could be explained by the dual inhibition of CHK1 and CHK2 by Prexasertib, indicating the potential of targeting both molecules to abrogate DDR in MB_{Group3} cell lines and force cells to undergo apoptosis. Additional experimentation studying biomarkers of CHK2 activation could shed light into the difference between inhibitors.

In addition, PLK1, CDK2, CHK1 and AURKA inhibition caused downregulation of *MYC* at the protein level in MB_{Group3} cell lines. Their inhibition resulted in a decrease in MYC protein expression in both, cells expressing high levels of *MYC* and in those cells with *MYC* knockdown. Results from the analysis of the effect of the inhibitors on parental MB cell lines at the protein level further corroborated the *MYC*-dependent effect of the inhibition of our main targets, resulting in increased levels of MYC protein in MB_{SHH} cell lines, opposite to the decrease seen in MB_{Group3} cell lines.

Analysis of expression of downstream pathway targets revealed an efficient inhibition of the main molecular target of the compounds. Downregulation of PLK1, CHK1, CDK2 and AURKA after treatment with each inhibitor was seen across cell lines regardless of *MYC* expression and subgroup. Prexasertib (CHK1/2 inhibitor) and BI2536 (PLK1 inhibitor) caused the *MYC*-dependent subgroup-specific downregulation of the anti-apoptotic protein MCL1, whereas a *MYC*-dependent upregulation was seen after treatment with Milciclib (CDK2 inhibitor). Regulation of levels of the anti-apoptotic protein MCL1 was not associated with *MYC* expression or MB subgroup after treatment with MLN8237 (AURKA inhibitor) and AZD7762 (CHK1 inhibitor). Our findings suggest that inhibitors with a downregulatory effect on both MYC and MCL1 protein expression levels, would selectively inhibit the growth of *MYC*-driven MB_{Group3} cell lines.

The regulatory effect of the inhibitors on MCL1 protein levels could reveal an extra layer of complexity to the differences in sensitivity observed. Alternatively, differences in sensitivity of MB_{Group3} to both CHK1 inhibitors could also be due to the fact that Prexasertib downregulates MCL1 protein levels. Increased levels of MCL1 trigger anti-apoptotic signalling pathways, arresting cell cycle progression to prevent cells sustaining damaged DNA from replicating (Fujise et al., 2000, Zhang et al., 2018b). Increased MCL1 levels might occur to

ensure cells bearing DNA lesions do not replicate. Downregulation of MCL1 by Prexasertib might prevent the arrest of cells cycle and promote the apoptotic pathway. Further experimentation to understand the relationship between CHK1/2 inhibition and MCL1 is required to better explain the differences in sensitivity of MB_{Group3} cell lines to the inhibitors used. Nevertheless, targeting components of the DDR has the potential to lead to novel therapeutic options for high-risk MB_{Group3} patients for whom the prognosis is still unacceptably poor.

Due to time constraints, only one experimental repeat was performed on each cell line. Despite the consistent effects seen across different MB lines, more experimental repeats should be performed in order to fully characterise the association between *MYC* and the expression of downstream pathway targets.

Our findings further provide insight into the mechanism by which the small molecule compounds repressed MB cell proliferation. A *MYC*-dependent subgroup specific increase in the proportion of cells at sub-G_1 phase of the cell cycle was seen across MB_{Group3} cell lines after treatment with BI2536, AZD7762 and MLN8237, suggesting an increase in the proportion of apoptotic cells. Increase in the population of cells at sub-G_1 phase correlated with *MYC* expression levels, where higher levels of apoptosis were seen in cells overexpressing *MYC*. The data suggests that utilisation of BI2536, AZD7762 and MLN8237 on *MYC*-driven MB_{Group3} cell lines would highly impair their viability through the induction of apoptosis.

Results from the cell-proliferation rescue assay performed on the *MYC*-regulable isogenic cell lines further supports our hypothesis that the induction of apoptosis after treatment was preferentially triggered on cells expressing high levels of *MYC* expression, in comparison to those with *MYC* knockdown. Throughout recovery time after drug treatment, a time- and dose-dependent decrease in cells proliferation was seen across cell lines. Cells expressing higher levels of *MYC* were unable to recover cell growth during recovery time, indicating cell death was induced after treatment. Increase in the proportion of metabolically active cells after treatment, following *MYC* knockdown, suggests that inhibition of PLK1, CDK2, AURKA and CHK1 did not result in such pronounced cell death, which allowed a slight recovery in cells proliferation after treatment, which was therefore *MYC*-dependent.

To further validate the *MYC*-dependency of the results presented, additional experiments using alternative backgrounds of *MYC*-expression could shed light into the relationship between *MYC* and the candidate targets selected. A direct way to study the MYC-dependency of PLK, CHK, CDK and AURK would be to engineer MB_{SHH} cell lines to over-express *MYC*. If the effect of the inhibitors were truly dependent on *MYC* expression, a change in cells sensitivity and downstream signalling effectors would be seen following exposure to the inhibitors, proving the veracity of our results and the dependency of *MYC* on these molecules.

Also, the *MYC*-dependent effect observed on MB cell lines could be studied using *MYC*-amplified or *MYC*-overexpressing cell models of other cancer types (i.e. neuroblastoma, ovarian, breast). The characterisation of the effect of the inhibitors chosen on alternative cancer models expressing high-levels of the *MYC* oncogene would selectively confirm their *MYC*-dependent effect.

Results presented strongly support the use of compounds inhibiting CHK1, PLK1 and AURKA as strategies for targeting *MYC*-amplified Group 3 medulloblastoma. Our data suggests that inhibition of CHK1, PLK1 and AURKA will result in a direct decrease of MYC protein expression, specifically impairing cell viability of *MYC*-dependent MB_{Group3}. Our data supports the evaluation of compounds inhibiting the targets identified within patient derived xenografts (PDX) and genetically engineered mouse (GEM) models to provide concluding evidence to support the development of regimens for new clinical trials to improve treatment of MB_{Group3}.

6.8 Appendix

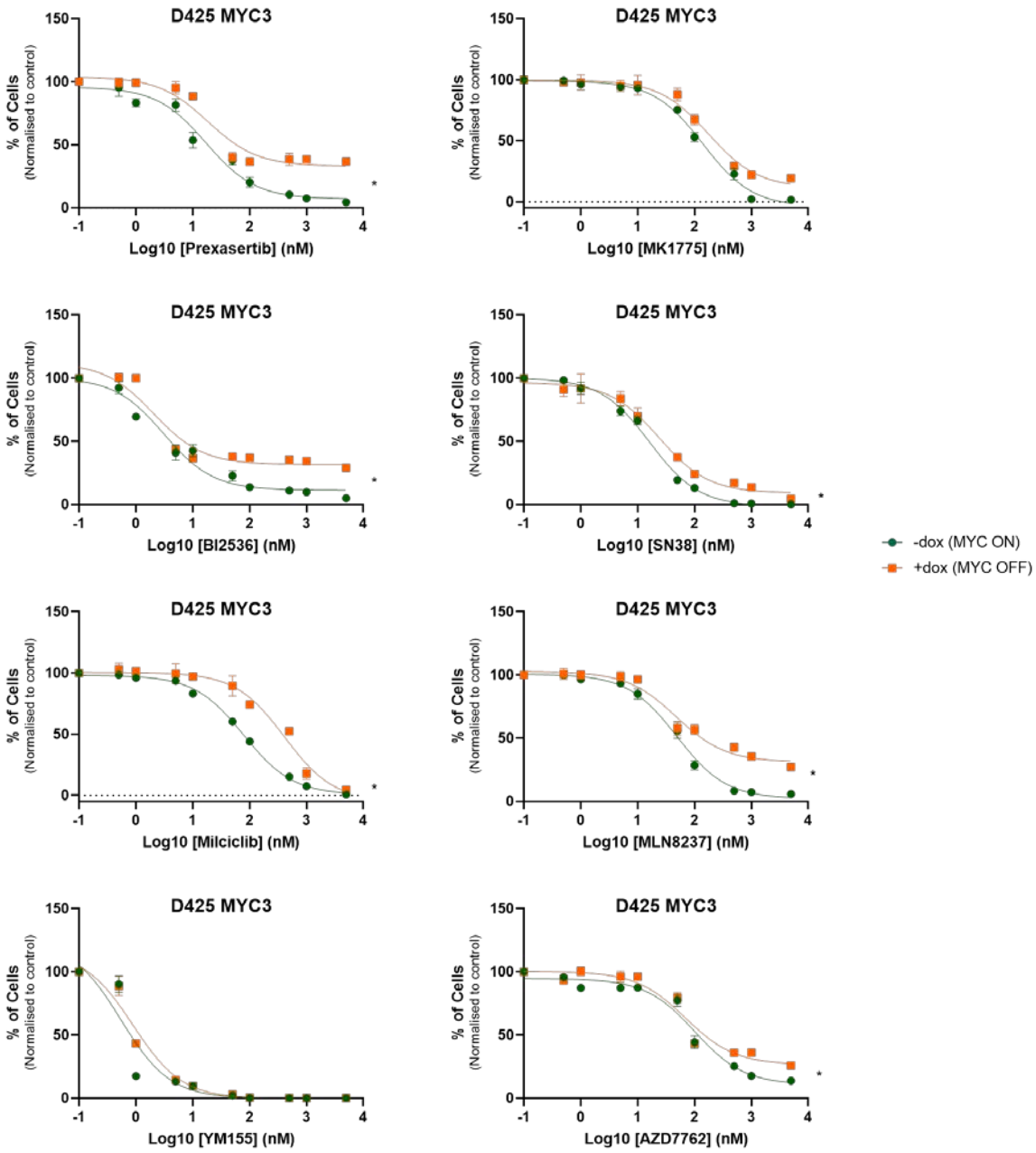

Appendix 6.1. Growth-inhibitory effect of 'hit' compounds from HTCS on D425 MYC3 cells. Concentration-dependent inhibitory dose-curves of D425 MYC3 MB_{Group3} cells to treatment with BI2536 (PLK1 inhibitor), SN38 (topoisomerase I), Milciclib (CDK2 inhibitor), MLN8237 (AURKA inhibitor), YM155 (*BIRC5* inhibitor), MK1775 (WEE1 inhibitor), AZD7762 (CHK1 inhibitor) and Prexasertib (CHK1/2 inhibitor). D425 MYC3, cultured in the absence (-dox; MYC ON) and presence (+dox; MYC OFF) of DOX for *MYC* knockdown, were exposed to a single dose of 8 different concentrations of each inhibitor (0.5, 1, 5, 10, 50, 100, 500, 1000, 5000nM) for a period of five days. After treatment, cell viability was measured with CellTiter-Glo and values obtained analysed with Prism8 to generate dose-response growth inhibition curves that fit a non-linear regression model. Curves are presented as log(concentration) vs response, and represent the percentage of cell viability of two independent experiments done in triplicate, relative to cells grown in the presence of DMSO. The growth inhibitory effect of the drug on D425 MYC3 overexpressing cell lines and with *MYC* knockdown was compared by paired student's t-test (statistical significance denoted by *; *p<0.05).

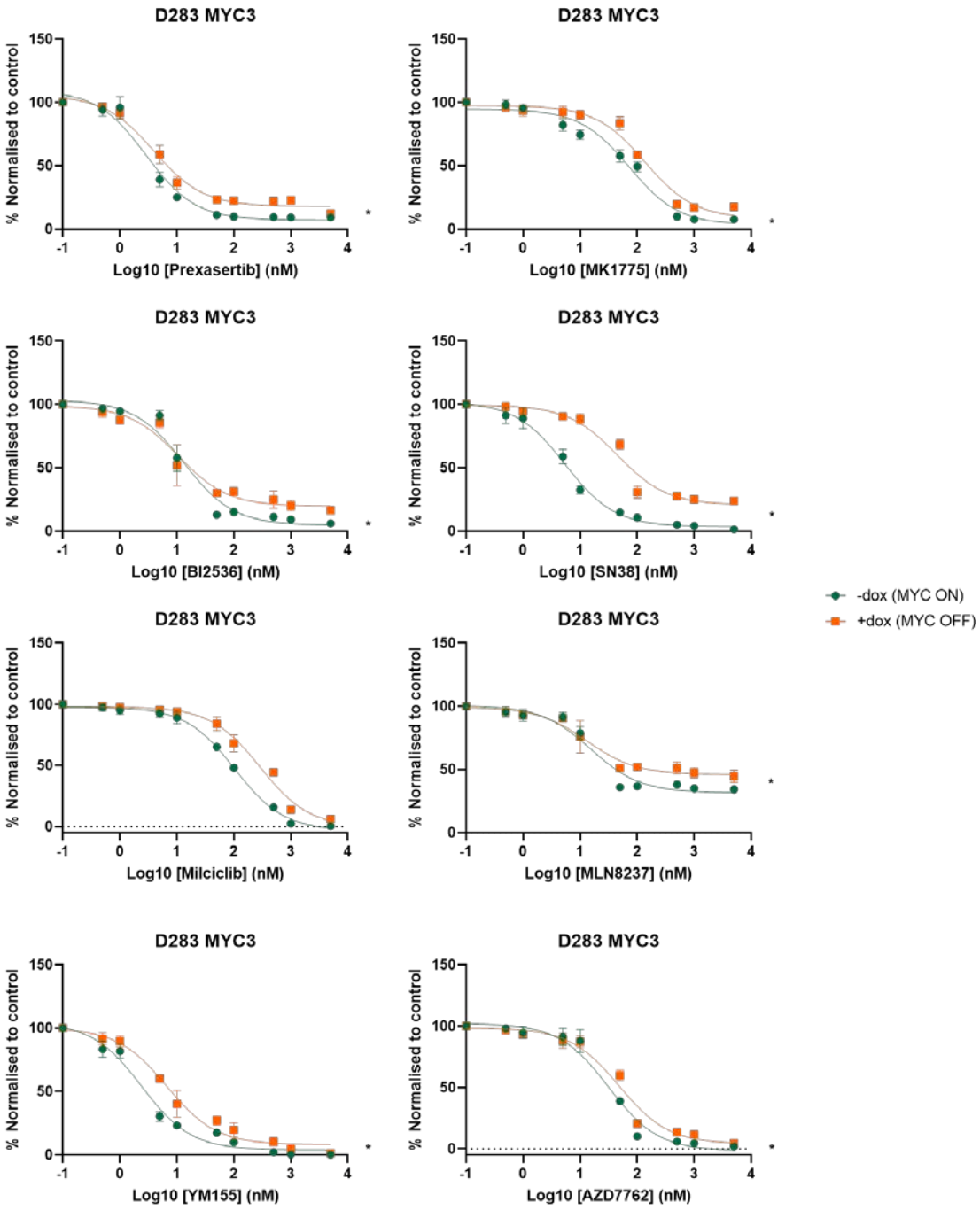

Appendix 6.2. Growth-inhibitory effect of 'hit' compounds from HTCS on D283 MYC3 cells. Concentration-dependent inhibitory dose-curves of D283 MYC3 MB_{Group3} cells to treatment with BI2536 (PLK1 inhibitor), SN38 (topoisomerase I), Milciclib (CDK2 inhibitor), MLN8237 (AURKA inhibitor), YM155 (BIRC5 inhibitor), MK1775 (WEE1 inhibitor), AZD7762 (CHK1 inhibitor) and Prexasertib (CHK1/2 inhibitor). D283 MYC3, cultured in the absence (-dox; MYC ON) and presence (+dox; MYC OFF) of DOX for *MYC* knockdown, were exposed to a single dose of 8 different concentrations of each inhibitor (0.5, 1, 5, 10, 50, 100, 500, 1000, 5000nM) for a period of five days. After treatment, cell viability was measured with CellTiter-Glo and values obtained analysed with Prism8 to generate dose-response growth inhibition curves that fit a non-linear regression model. Curves are presented as log(concentration) vs response, and represent the percentage of cell viability of two independent experiments done in triplicate, relative to cells grown in the presence of DMSO. The growth inhibitory effect of the drug on D283 MYC3 overexpressing cell lines and with *MYC* knockdown was compared by paired student's t-test (statistical significance denoted by *; *p<0.05).

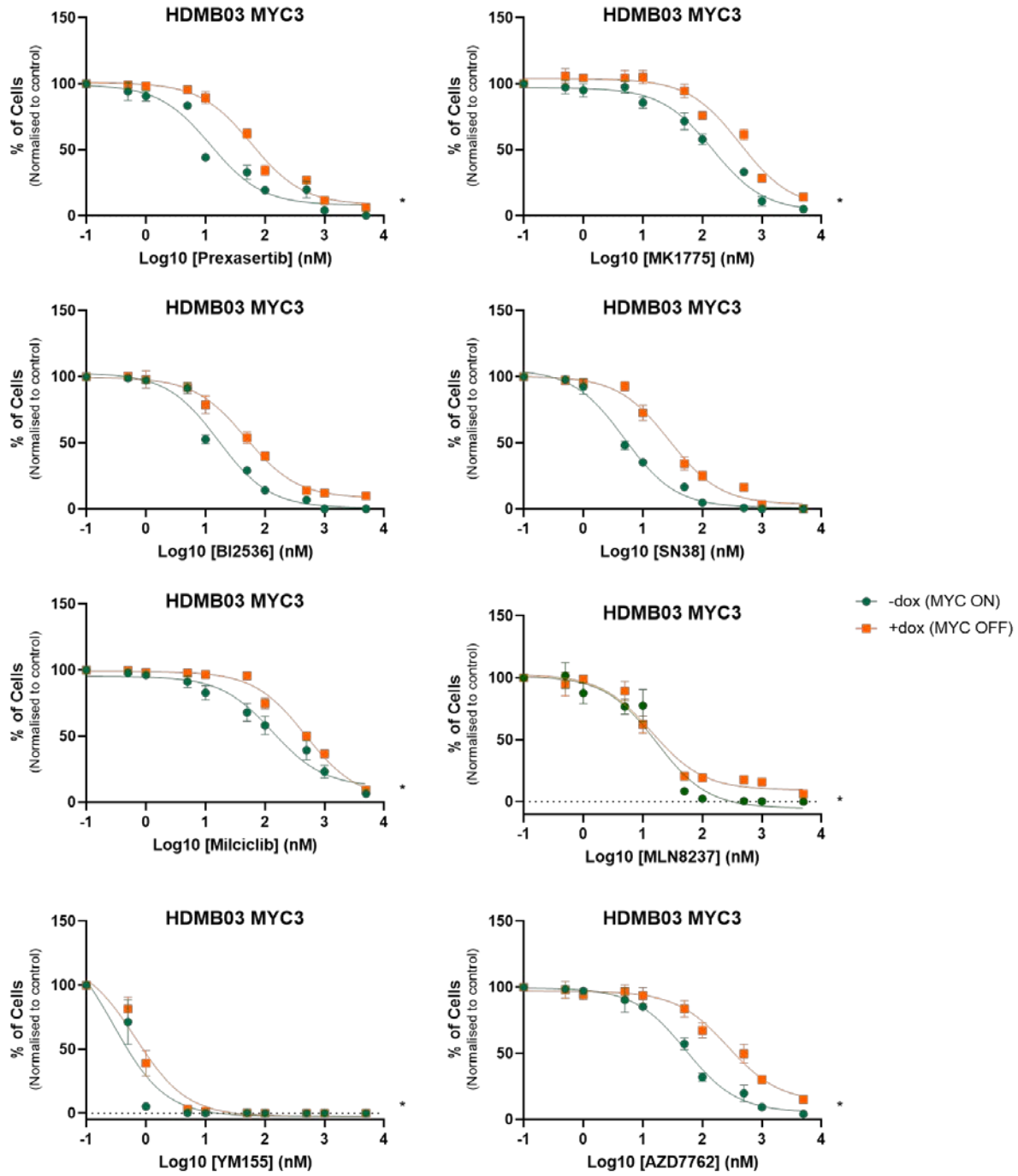

Appendix 6.3. Growth-inhibitory effect of 'hit' compounds from HTCS on HDMB03 MYC3 cells. Concentration-dependent inhibitory dose-curves of HDMB03 MYC3 MB_{Group3} cells to treatment with BI2536 (PLK1 inhibitor), SN38 (topoisomerase I), Milciclib (CDK2 inhibitor), MLN8237 (AURKA inhibitor), YM155 (BIRC5 inhibitor), MK1775 (WEE1 inhibitor), AZD7762 (CHK1 inhibitor) and Prexasertib (CHK1/2 inhibitor). HDMB03 MYC3, cultured in the absence (-dox; MYC ON) and presence (+dox; MYC OFF) of DOX for *MYC* knockdown, were exposed to a single dose of 8 different concentrations of each inhibitor (0.5, 1, 5, 10, 50, 100, 500, 1000, 5000nM) for a period of five days. After treatment, cell viability was measured with CellTiter-Glo and values obtained analysed with Prism8 to generate dose-response growth inhibition curves that fit a non-linear regression model. Curves are presented as log(concentration) vs response, and represent the percentage of cell viability of two independent experiments done in triplicate, relative to cells grown in the presence of DMSO. The growth inhibitory effect of the drug on HDMB03 MYC3 overexpressing cell lines and with *MYC* knockdown was compared by paired student's t-test (statistical significance denoted by *; *p<0.05).

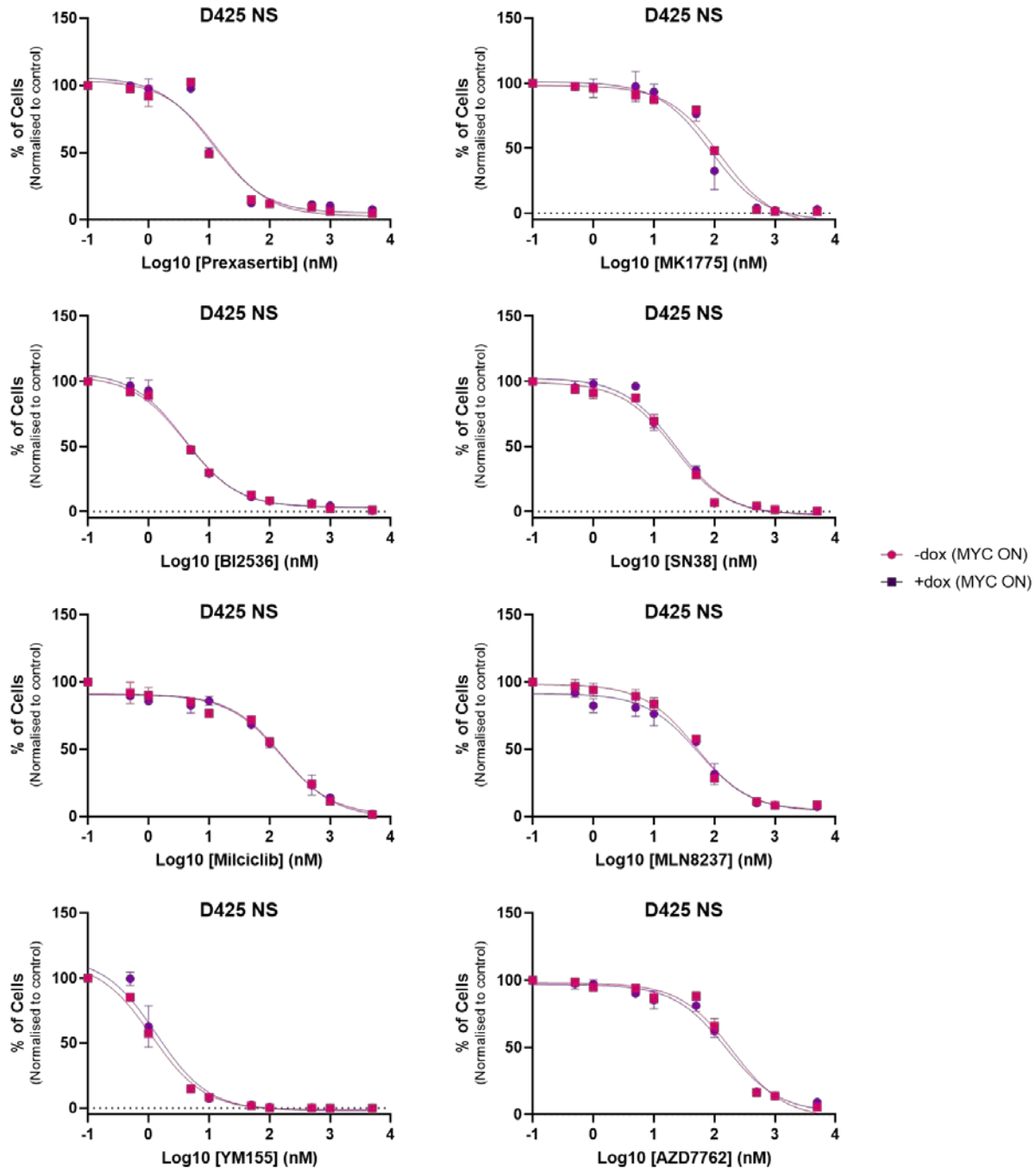

Appendix 6.4. Growth-inhibitory effect of 'hit' compounds from HTCS on D425 NS cells. Concentration-dependent inhibitory dose-curves of D425 NS MB_{Group3} cells to treatment with BI2536 (PLK1 inhibitor), SN38 (topoisomerase I), Milciclib (CDK2 inhibitor), MLN8237 (AURKA inhibitor), YM155 (BIRC5 inhibitor), MK1775 (WEE1 inhibitor), AZD7762 (CHK1 inhibitor) and Prexasertib (CHK1/2 inhibitor). D425 NS, cultured in the absence (-dox; MYC ON) and presence (+dox; MYC OFF) of DOX for *MYC* knockdown, were exposed to a single dose of 8 different concentrations of each inhibitor (0.5, 1, 5, 10, 50, 100, 500, 1000, 5000nM) for a period of five days. After treatment, cell viability was measured with CellTiter-Glo and values obtained analysed with Prism8 to generate dose-response growth inhibition curves that fit a non-linear regression model. Curves are presented as log(concentration) vs response, and represent the percentage of cell viability of two independent experiments done in triplicate, relative to cells grown in the presence of DMSO. The growth inhibitory effect of the drug on D425 NS with and without DOX was compared by paired student's t-test (statistical significance denoted by *; *p<0.05).

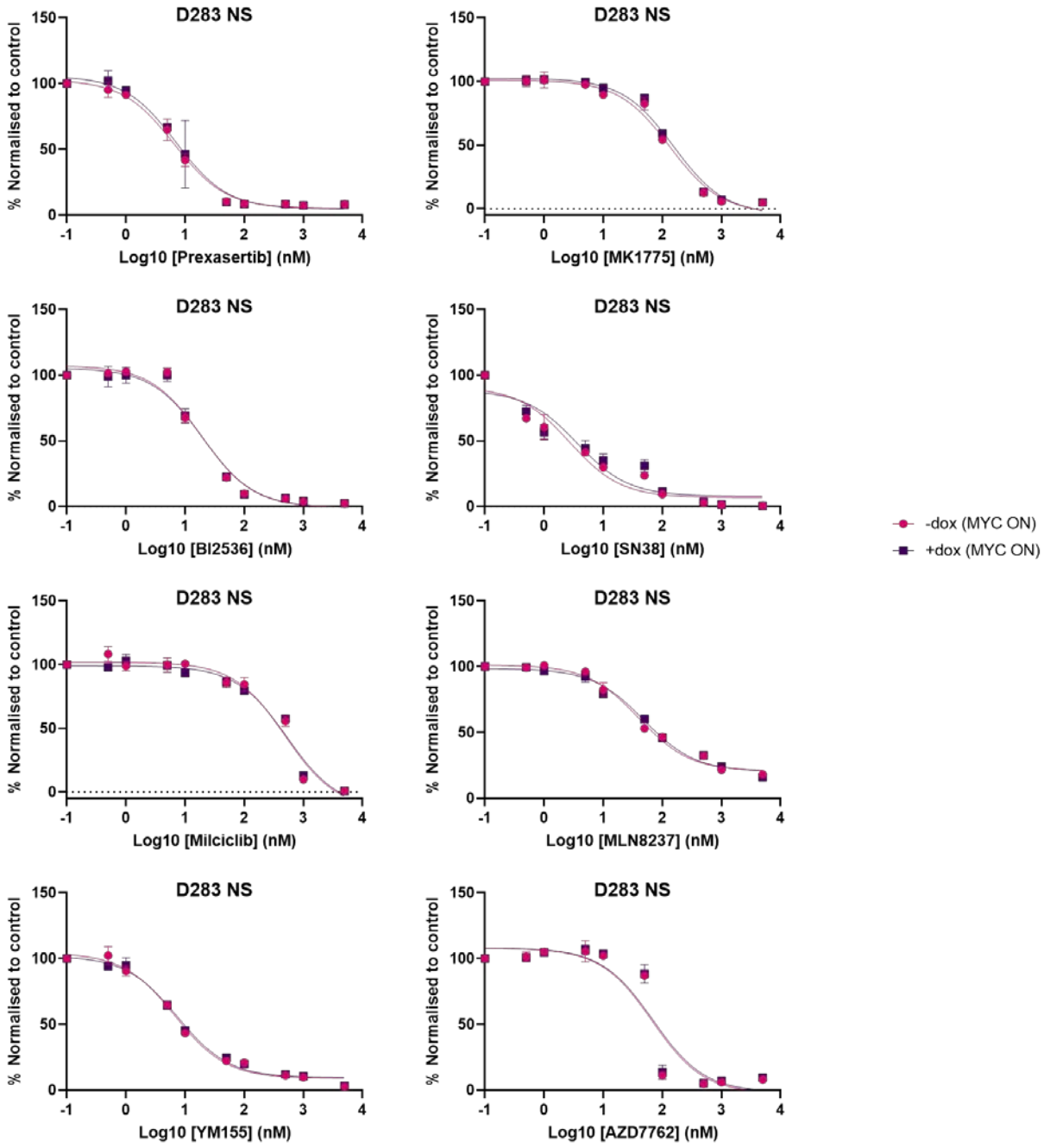

Appendix 6.5. Growth-inhibitory effect of 'hit' compounds from HTCS on D283 NS cells. Concentration-dependent inhibitory dose-curves of D283 NS MB_{Group3} cells to treatment with BI2536 (PLK1 inhibitor), SN38 (topoisomerase I), Milciclib (CDK2 inhibitor), MLN8237 (AURKA inhibitor), YM155 (BIRC5 inhibitor), MK1775 (WEE1 inhibitor), AZD7762 (CHK1 inhibitor) and Prexasertib (CHK1/2 inhibitor). D283 NS, cultured in the absence (-dox; MYC ON) and presence (+dox; MYC OFF) of DOX for *MYC* knockdown, were exposed to a single dose of 8 different concentrations of each inhibitor (0.5, 1, 5, 10, 50, 100, 500, 1000, 5000nM) for a period of five days. After treatment, cell viability was measured with CellTiter-Glo and values obtained analysed with Prism8 to generate dose-response growth inhibition curves that fit a non-linear regression model. Curves are presented as log(concentration) vs response, and represent the percentage of cell viability of two independent experiments done in triplicate, relative to cells grown in the presence of DMSO. The growth inhibitory effect of the drug on D283 NS with and without DOX was compared by paired student's t-test (statistical significance denoted by *; *p<0.05).

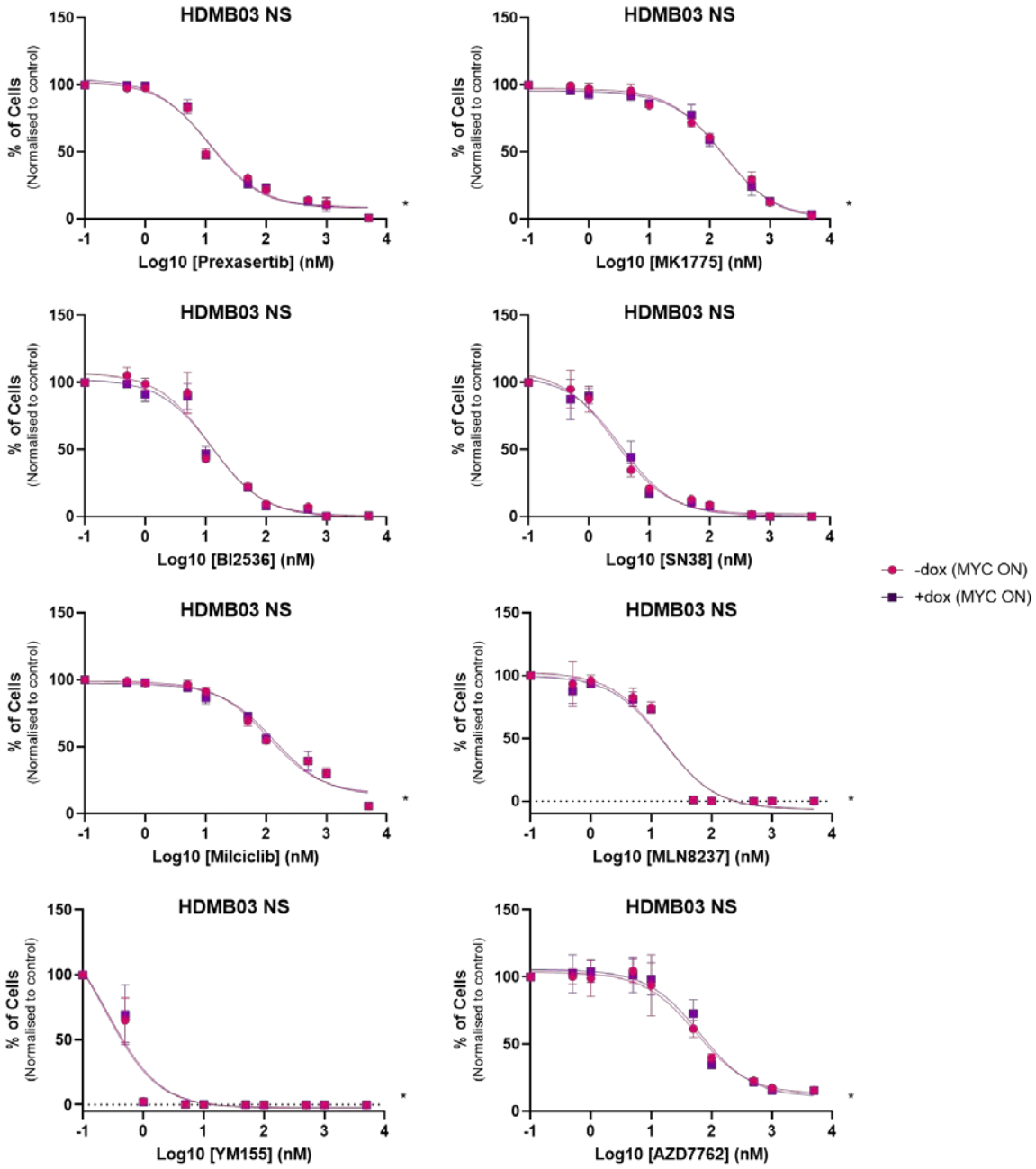

Appendix 6.6. Growth-inhibitory effect of 'hit' compounds from HTCS on HDMB03 NS cells. Concentration-dependent inhibitory dose-curves of HDMB03 NS MB_{Group3} cells to treatment with BI2536 (PLK1 inhibitor), SN38 (topoisomerase I), Milciclib (CDK2 inhibitor), MLN8237 (AURKA inhibitor), YM155 (BIRC5 inhibitor), MK1775 (WEE1 inhibitor), AZD7762 (CHK1 inhibitor) and Prexasertib (CHK1/2 inhibitor). HDMB03 NS, cultured in the absence (-dox; MYC ON) and presence (+dox; MYC OFF) of DOX for *MYC* knockdown, were exposed to a single dose of 8 different concentrations of each inhibitor (0.5, 1, 5, 10, 50, 100, 500, 1000, 5000nM) for a period of five days. After treatment, cell viability was measured with CellTiter-Glo and values obtained analysed with Prism8 to generate dose-response growth inhibition curves that fit a non-linear regression model. Curves are presented as log(concentration) vs response, and represent the percentage of cell viability of two independent experiments done in triplicate, relative to cells grown in the presence of DMSO. The growth inhibitory effect of the drug on HDMB03 NS with and without DOX was compared by paired student's t-test (statistical significance denoted by *; *p<0.05).

A)

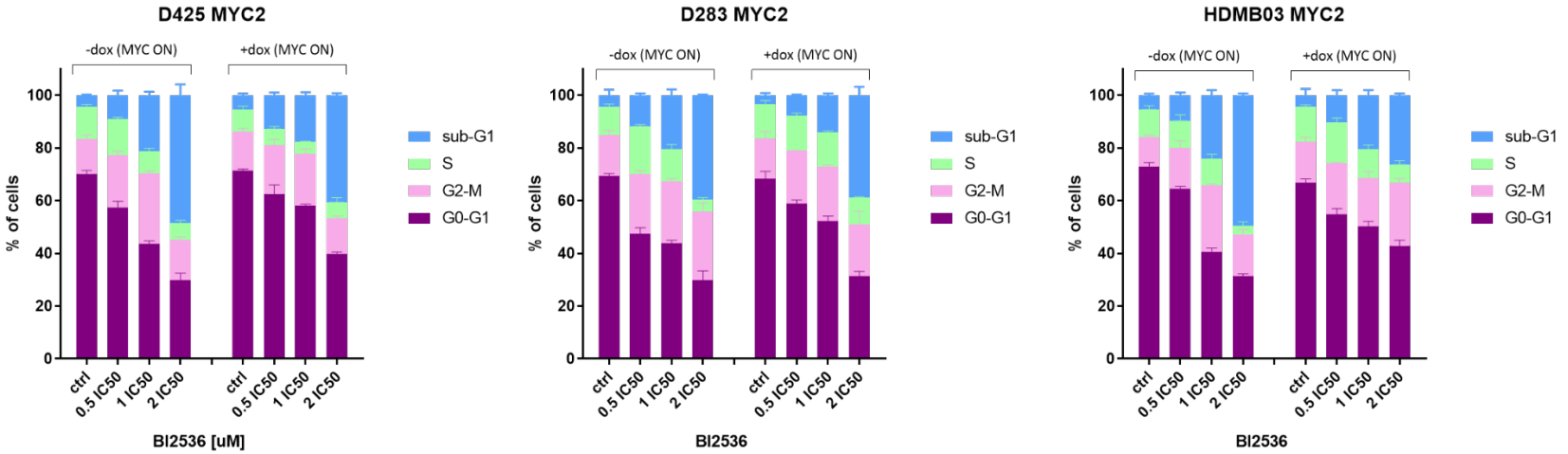
D425 MYC2
D283 MYC2
HDMB03 MYC2
-dox (MYC ON)
+dox (MYC ON)
% of cells
sub-G1
S
G2-M
G0-G1
ctrl
0.5 IC50
1 IC50
2 IC50
BI2536 [uM]
BI2536

B)

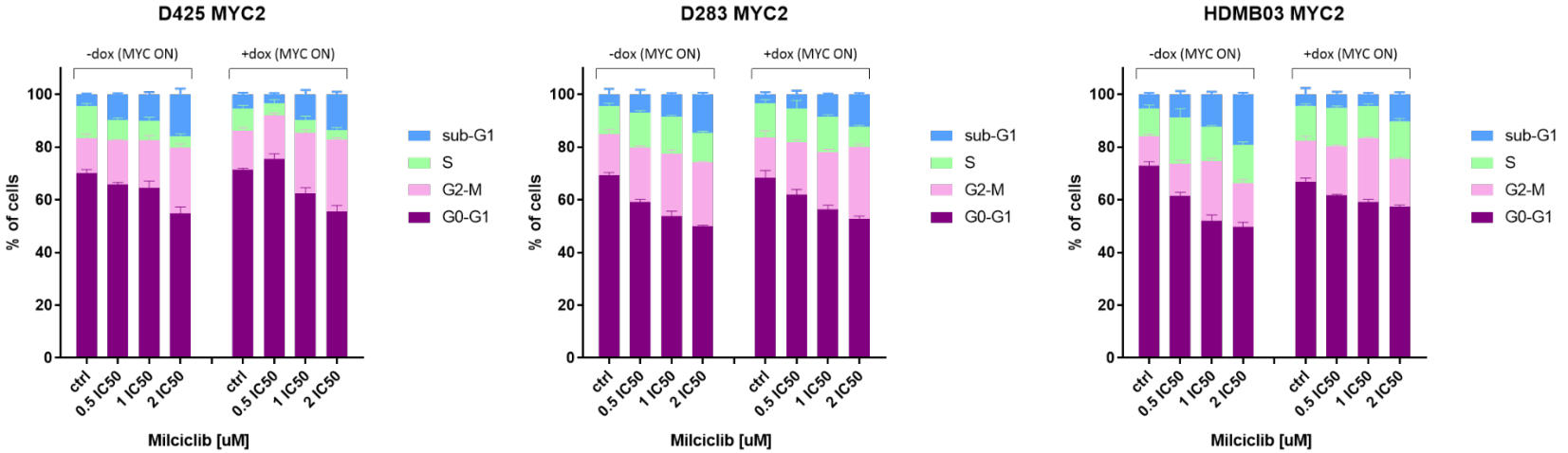
D425 MYC2
D283 MYC2
HDMB03 MYC2
-dox (MYC ON)
+dox (MYC ON)
% of cells
sub-G1
S
G2-M
G0-G1
ctrl
0.5 IC50
1 IC50
2 IC50
Milciclib [uM]

C)

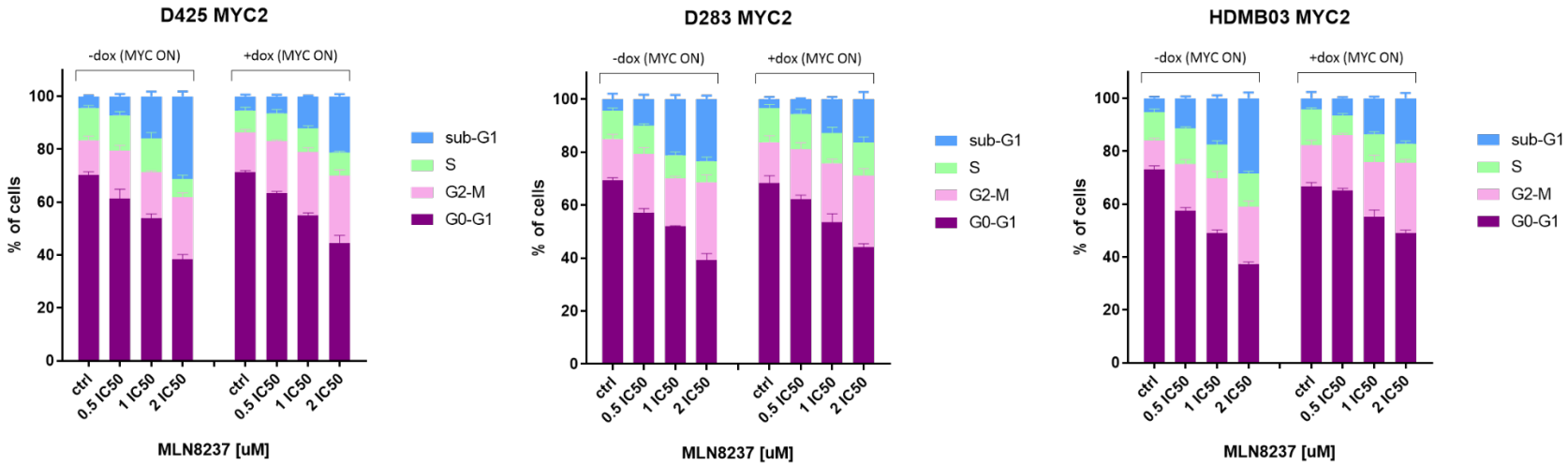
D425 MYC2
D283 MYC2
HDMB03 MYC2
-dox (MYC ON)
+dox (MYC ON)
% of cells
sub-G1
S
G2-M
G0-G1
ctrl
0.5 IC50
1 IC50
2 IC50
MLN8237 [uM]

D)

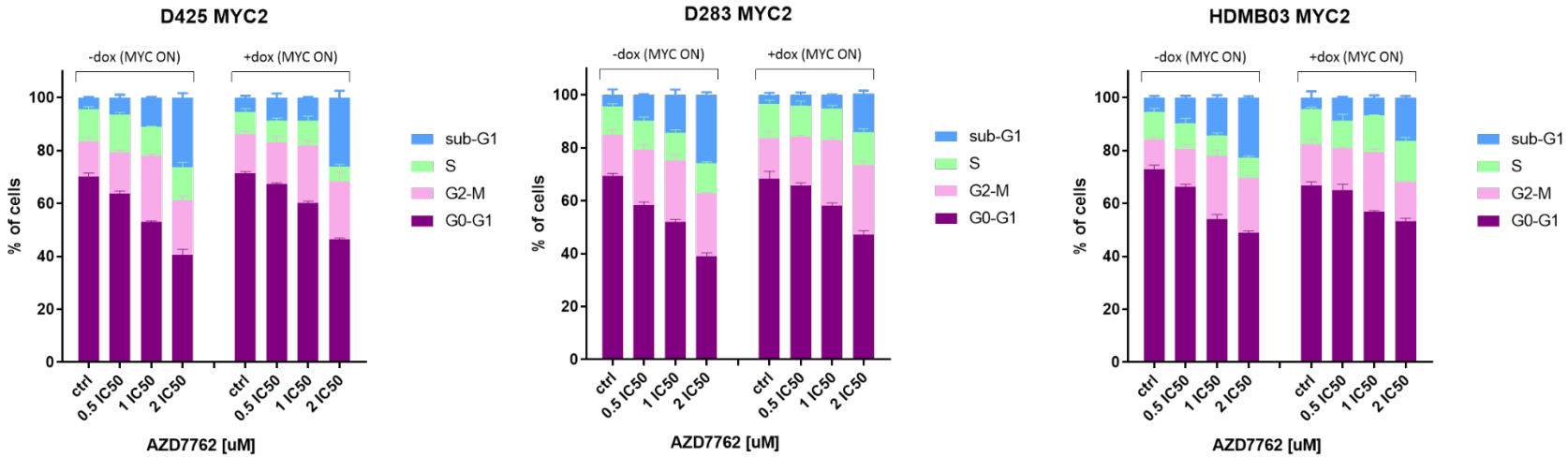
D425 MYC2
D283 MYC2
HDMB03 MYC2
-dox (MYC ON)
+dox (MYC ON)
% of cells
sub-G1
S
G2-M
G0-G1
ctrl
0.5 IC50
1 IC50
2 IC50
AZD7762 [uM]

E)

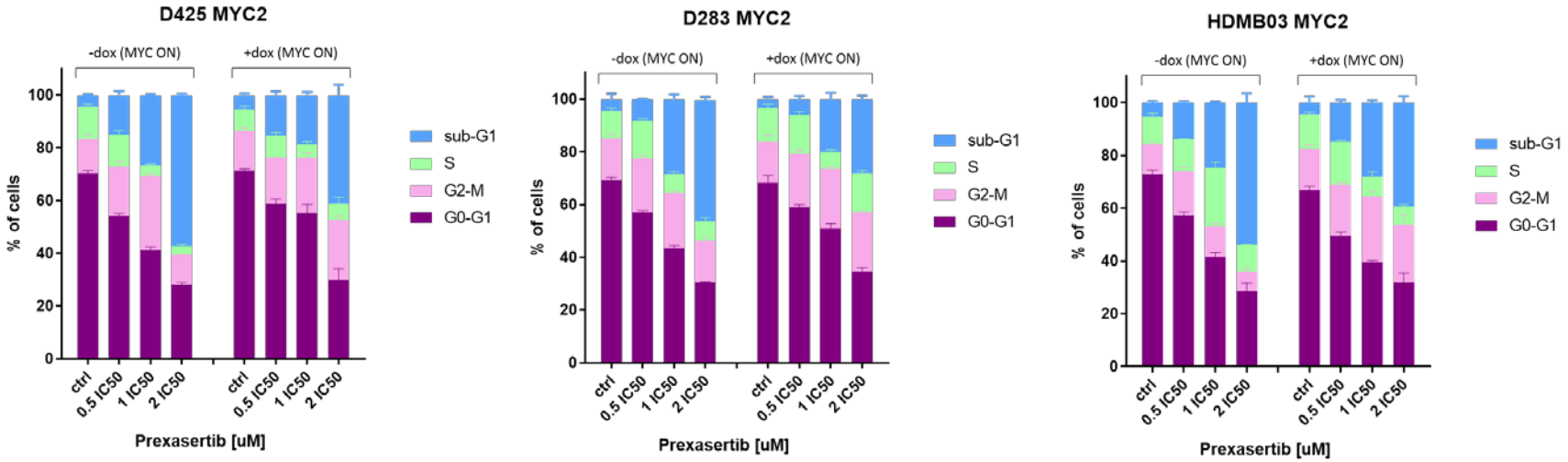

Appendix 6.7. Effect of BI2536 treatment on cell cycle distribution in isogenic MB_{Group3} cell lines. Cell cycle distribution of D425, D283 and HDMB03 MYC2 cell lines after 72h of a single exposure of half the IC_{50} ($0.5xIC_{50}$), IC_{50} ($1xIC_{50}$), and twice the IC_{50} ($2xIC_{50}$) concentration of A)BI2536, B)Milciclib, C)MLN8237, D)AZD7762 and E)Prexasertib. Cells were stained with propidium iodide and cell cycle distribution analysed by flow cytometry. Graph represents the percentage (%) of cells of each cell cycle phase relative to total phases, of cells expressing high levels of *MYC* and those with *MYC* knockdown (+DOX). Untreated cells (no drug; DMSO only) were used for each condition (+/-DOX) as controls. Data is presented as the percentage of the mean (±SEM) of three independent experiments.

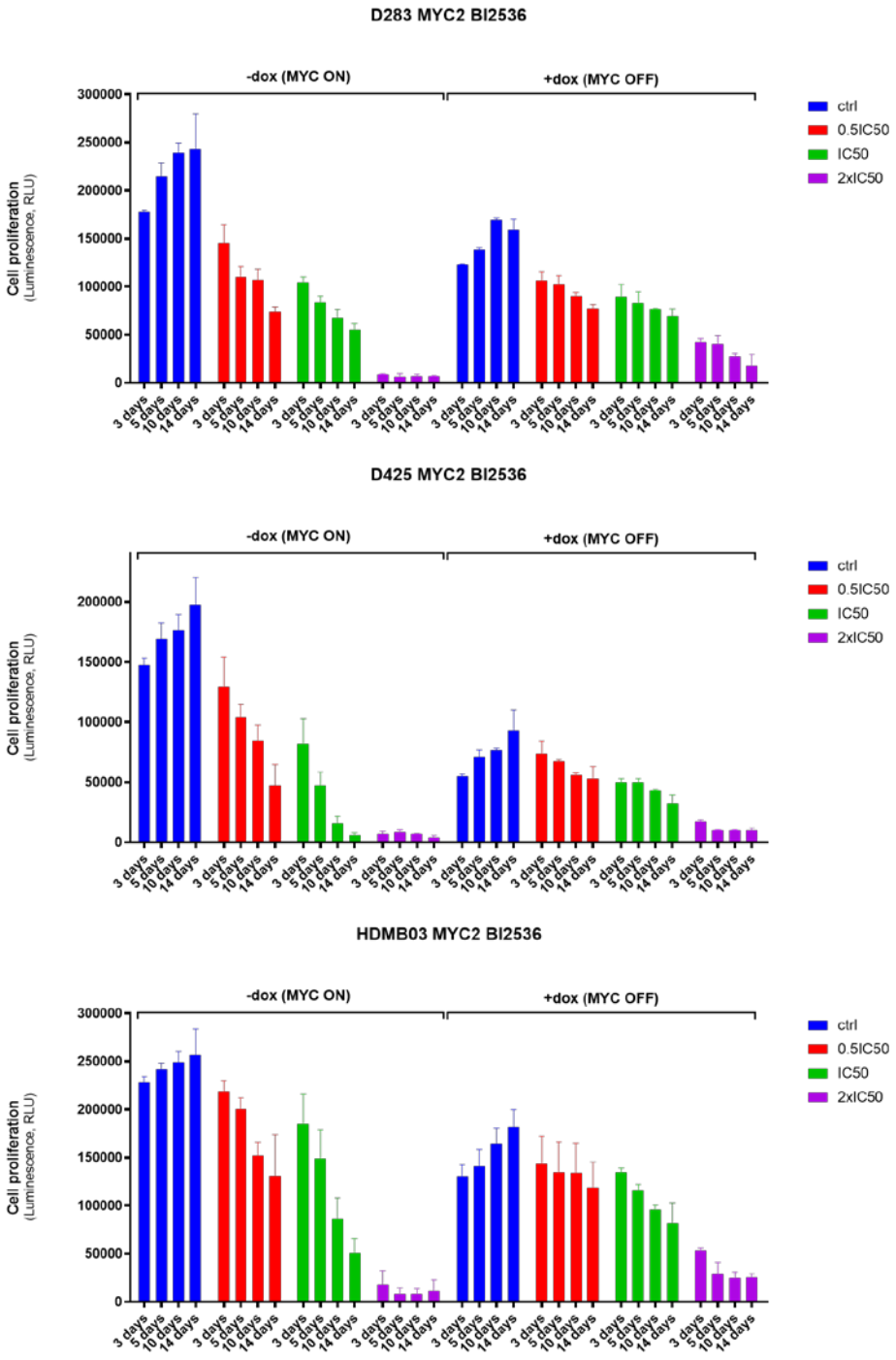

Appendix 6.8. Proliferation of isogenic MB_{Group3} cell lines after treatment with BI2536. Cell-proliferation rescue assay of D425, D283 and HDMB03 MYC2 during and after exposure to the PLK1 inhibitor BI2536. Cells expressing high levels of *MYC* (-dox; MYC ON) and those with *MYC* knockdown (+dox; MYC OFF) were exposed to 0.5xIC_{50}, IC_{50} and 2xIC_{50} concentration for 5 days. After exposure, drug was removed from the media, media changed, and cells left to grow for further 5 and 9 days. Cell proliferation was assessed with CTG at 3, 5, 10 and 14 days after drugging. Untreated cells (no drug) were used for each condition (+/-dox) as controls. Data was blank-corrected to DMSO-containing wells, and normalised to day 0. Graphs show the comparison of growth between untreated cells (blue) and those treated with the inhibitor (red, green and purple). Data is presented as the mean (±SEM) of two independent experiments.

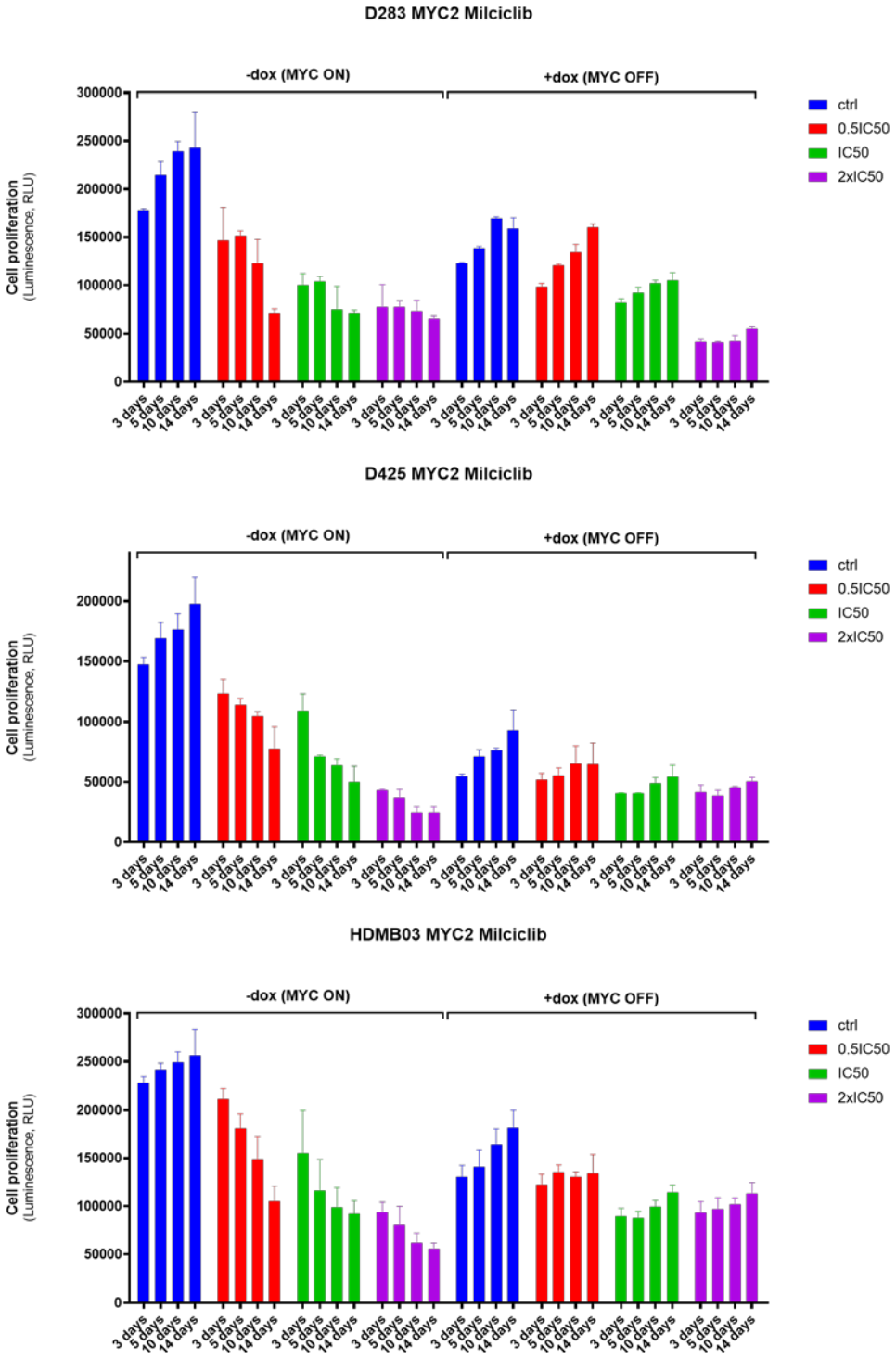

Appendix 6.9. Proliferation of isogenic MB_{Group3} cell lines after treatment with Milciclib. Cell-proliferation rescue assay of D425, D283 and HDMB03 MYC2 during and after exposure to the CDK2 inhibitor Milciclib. Cells expressing high levels of *MYC* (-dox; MYC ON) and those with *MYC* knockdown (+dox; MYC OFF) were exposed to 0.5xIC_{50}, IC_{50} and 2xIC_{50} concentration for 5 days. After exposure, drug was removed from the media, media changed, and cells left to grow for further 5 and 9 days. Cell proliferation was assessed with CTG at 3, 5, 10 and 14 days after drugging. Untreated cells (no drug) were used for each condition (+/-DOX) as controls. Data was blank-corrected to DMSO-containing wells, and normalised to day 0. Graphs show the comparison of growth between untreated cells (blue) and those treated with the inhibitor (red, green and purple). Data is presented as the mean (±SEM) of two independent experiments.

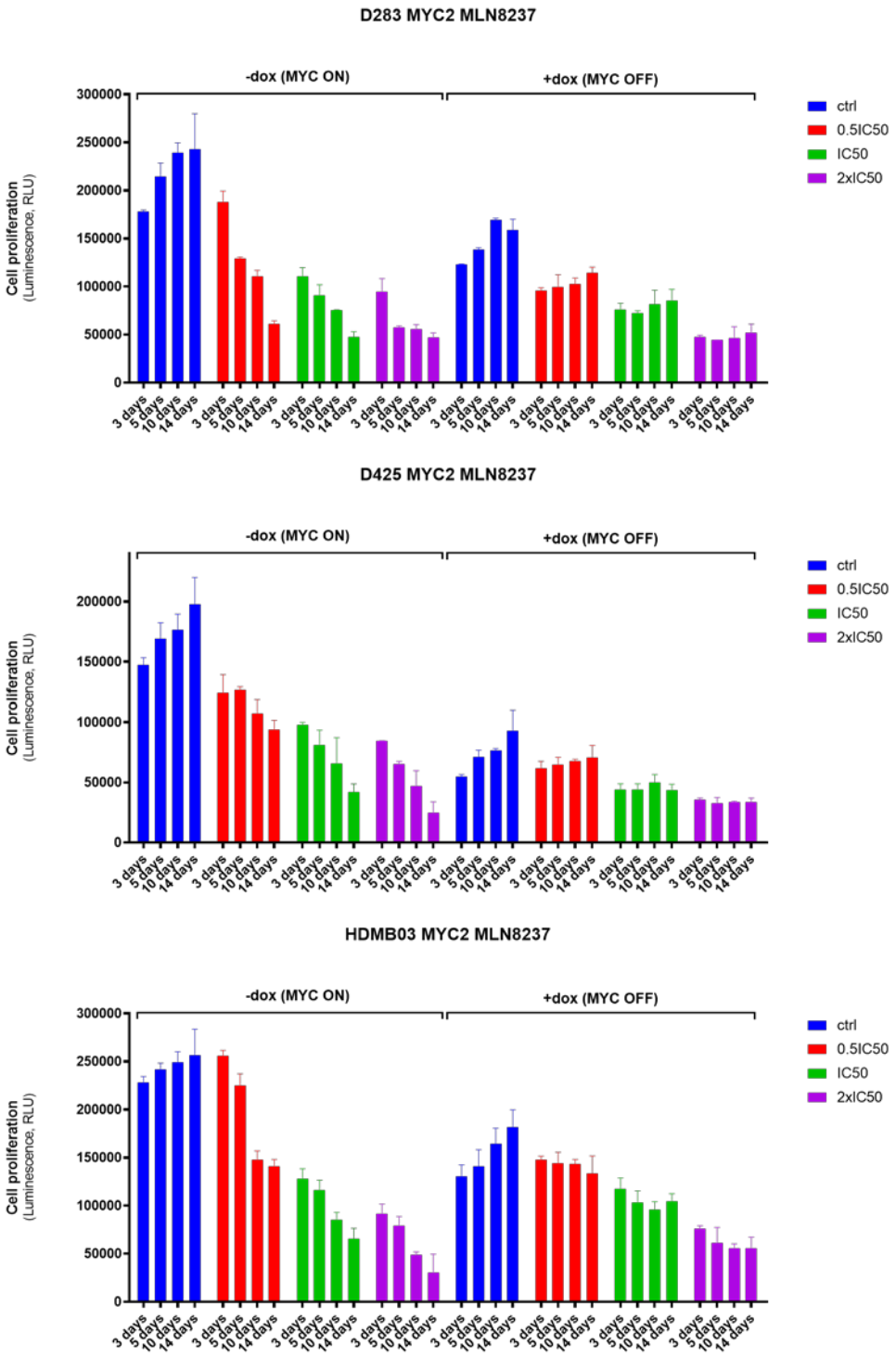

Appendix 6.10. Proliferation of isogenic MB_{Group3} cell lines after treatment with MLN8237. Cell-proliferation rescue assay of D425, D283 and HDMB03 MYC2 during and after exposure to the AURKA inhibitor MLN8237. Cells expressing high levels of *MYC* (-dox; MYC ON) and those with *MYC* knockdown (+dox; MYC OFF) were exposed to 0.5xIC_{50}, IC_{50} and 2xIC_{50} concentration for 5 days. After exposure, drug was removed from the media, media changed, and cells left to grow for further 5 and 9 days. Cell proliferation was assessed with CTG at 3, 5, 10 and 14 days after drugging. Untreated cells (no drug) were used for each condition (+/-DOX) as controls. Data was blank-corrected to DMSO-containing wells, and normalised to day 0. Graphs show the comparison of growth between untreated cells (blue) and those treated with the inhibitor (red, green and purple). Data is presented as the mean (±SEM) of two independent experiments.

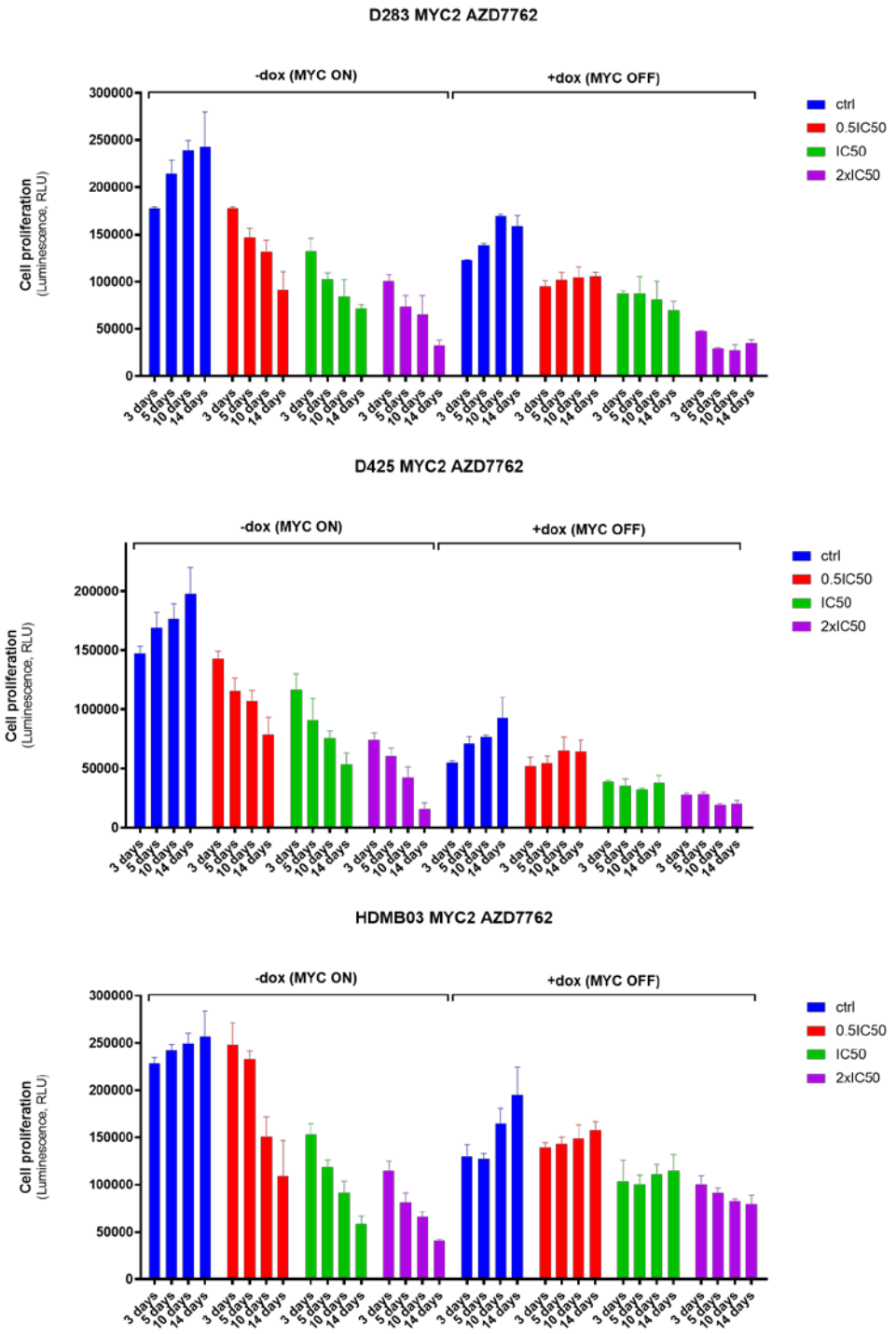

Appendix 6.11. Proliferation of isogenic MB_{Group3} cell lines after treatment with AZD7762. Cell-proliferation rescue assay of D425, D283 and HDMB03 MYC2 during and after exposure to the CHK1 inhibitor AZD7762. Cells expressing high levels of *MYC* (-dox; MYC ON) and those with *MYC* knockdown (+dox; MYC OFF) were exposed to 0.5xIC_{50}, IC_{50} and 2xIC_{50} concentration for 5 days. After exposure, drug was removed from the media, media changed, and cells left to grow for further 5 and 9 days. Cell proliferation was assessed with CTG at 3, 5, 10 and 14 days after drugging. Untreated cells (no drug) were used for each condition (+/-DOX) as controls. Data was blank-corrected to DMSO-containing wells, and normalised to day 0. Graphs show the comparison of growth between untreated cells (blue) and those treated with the inhibitor (red, green and purple). Data is presented as the mean (±SEM) of two independent experiments.

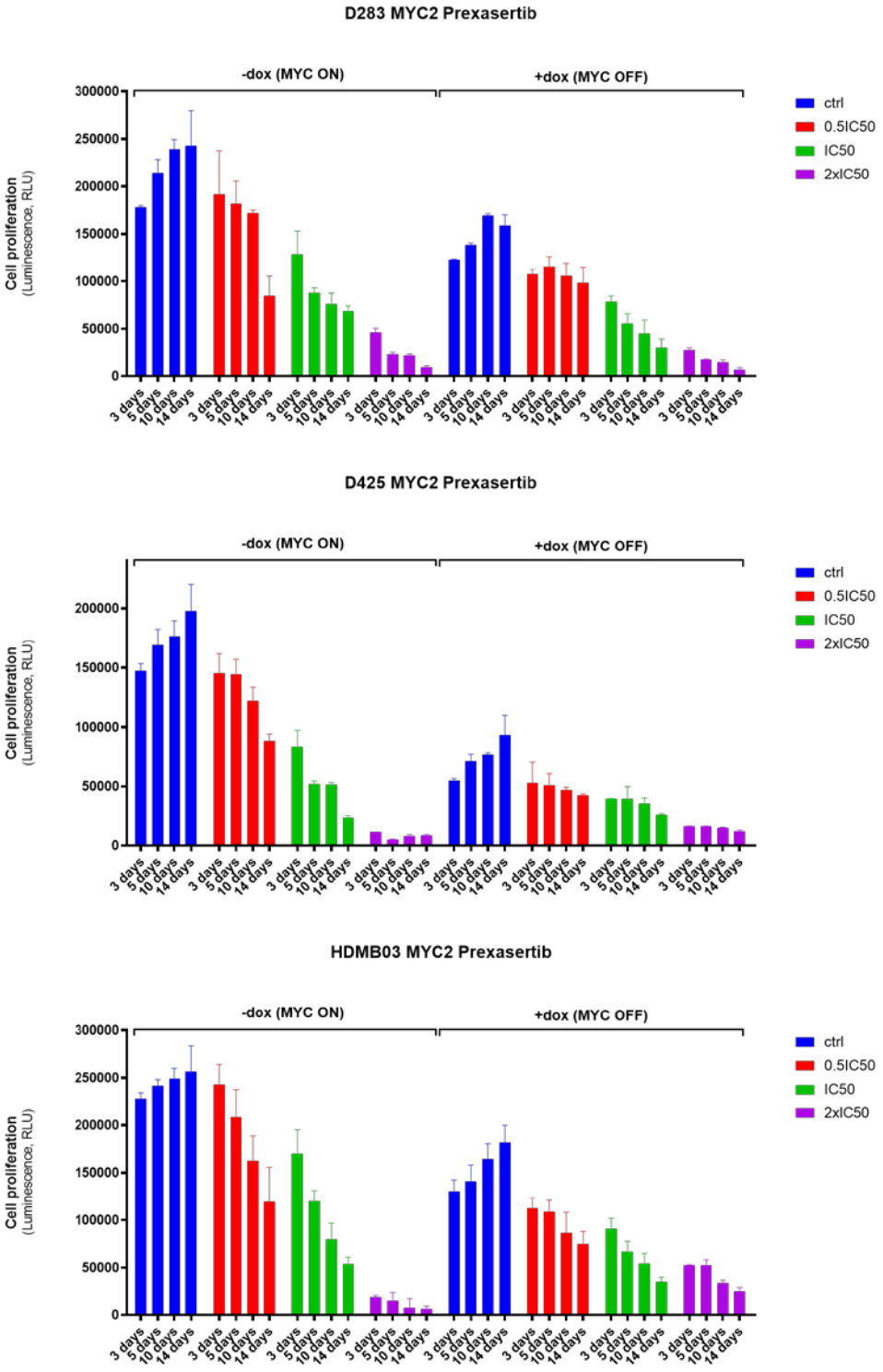

Appendix 6.12. Proliferation of isogenic MB_{Group3} cell lines after treatment with Prexasertib. Cell-proliferation rescue assay of D425, D283 and HDMB03 MYC2 during and after exposure to the CHK1 inhibitor Prexasertib. Cells expressing high levels of *MYC* (-dox; MYC ON) and those with *MYC* knockdown (+dox; MYC OFF) were exposed to 0.5xIC_{50}, IC_{50} and 2xIC_{50} concentration for 5 days. After exposure, drug was removed from the media, media changed, and cells left to grow for further 5 and 9 days. Cell proliferation was assessed with CTG at 3, 5, 10 and 14 days after drugging. Untreated cells (no drug) were used for each condition (+/-DOX) as controls. Data was blank-corrected to DMSO-containing wells, and normalised to day 0. Graphs show the comparison of growth between untreated cells (blue) and those treated with the inhibitor (red, green and purple). Data is presented as the mean (±SEM) of two independent experiments.

Chapter 7. Summary and Discussion

7.1 Introduction

Medulloblastoma is the most frequent malignant brain tumour in childhood, accounting for 10% of all paediatric deaths from cancer. Survival rates have dramatically improved over the last three decades using multimodal treatment protocol of standard care, where around 80% of standard risk patients survive over 5 years, and between 60-65% of those with high-risk features (Pizer and Clifford, 2009, Packer et al., 2006, Gajjar et al., 2006, Lannering et al., 2012). Despite reasonably high cure rates, current therapy regimes come at the expense of adverse treatment side effects that highly impair survivors´ quality of life (Edelstein et al., 2011).

Advances in molecular genomics over the past couple of decades have helped decipher the molecular underpinnings of this highly heterogeneous disease, providing some biologically and clinically relevant features. It is now recognised that MB comprises four molecular subgroups, Wnt (MB_{WNT}), Shh (MB_{SHH}), Group 3 (MB_{Group3}) and Group 4 (MB_{Group4}), characterised by distinct demographics, genetic, epigenetic and clinic-pathological features (Taylor et al., 2012, Northcott et al., 2012a). Recently, further refinement of the subgroups has recognised further substructures within each subgroup, suggesting between 7 and 12 MB subtypes (Schwalbe et al., 2017, Cavalli et al., 2017).

MB_{Group3} are highly aggressive tumours, commonly characterised by metastatic disease at diagnosis, with overall 5-year survival of less than 60%. Despite carrying the worst prognosis of all subgroups, the common driver pathway of this subgroup of tumours has not yet been identified. *MYC* oncogene amplification or overexpression is the most common recurring alteration (accounting for 17% of MB_{Group3} cases), which has become the hallmark of this subgroup of tumours (Kool et al., 2012, Northcott et al., 2012a).

The molecular characterisation of MB has already been used to guide the development of new clinical trials. Stratification of the disease incorporating pathological variants, subgroup information and molecular characteristics, has enabled adjustment of therapeutic regimes according to patients' prognosis. In this regard, SMO inhibitors have been incorporated into the treatment for MB_{SHH} patients and reduced intensity are being used for MB_{WNT} patients presenting with low-risk features (Lee et al., 2019). Unfortunately, no major changes have proceeded to enhance outcomes for MB_{Group3} patients. Despite incorporating subgroup-specific treatment stratification, substantial biological and survival differences are still

apparent within subgroups (Mack and Northcott, 2017, Schwalbe et al., 2017, Cavalli et al., 2017).

There is thus an urgent need to develop new therapeutic strategies for high-risk MB patients within Group 3. The fact that *MYC* depletion causes growth arrest and tumour regression in *MYC*-driven murine MB models, indicating the essentiality of *MYC* in MB_{Group3} tumour biology (Pei et al., 2012, Roussel and Robinson, 2013), has stimulated interest in developing strategies to disrupt *MYC* function to treat this specific subgroup of tumours.

MYC is a multifunctional transcriptional factor determining the expression of a large number of genes involved cellular processes including cell-cycle progression, metabolism, apoptosis, ribosome biogenesis and protein synthesis (Tansey, 2014). Deregulation of the *MYC* oncogene occurs in most cancers, where sustained high levels of *MYC* have a dramatic impact on a wide range of cellular processes facilitating the acquisition of the set of genetic changes required to maintain the hallmarks of malignancy (Jain et al., 2002, Hanahan and Weinberg, 2000). Upregulation of *MYC* expression alone is incapable of driving neoplastic transformation. This has led to increased interest in elucidating the biological context-specific role of *MYC* in tumorigenesis, and its complex interacting network of genes to identify those who synergise with *MYC* to promote malignant transformation and could be targeted to develop clinically relevant strategies to treat *MYC*-driven cancers (Gabay et al., 2014, Meyer and Penn, 2008, Whitfield et al., 2017)

The ever-growing knowledge regarding *MYC* biology and function from research done on all types of human cancers, an array of direct and indirect targeting strategies have been developed to abrogate *MYC* function and to manipulate *MYC*-dependent signalling pathways as a therapeutic strategy to treat *MYC*-driven cancers (Grotzer et al., 2009, Whitfield et al., 2017, Juraschka and Taylor, 2019). The feasibility of targeting *MYC* or its dependent expression programs are particularly attractive strategies to treat high-risk patients with MB_{Group3}, aiming at more biologically relevant approaches to improve standard treatment and survival rates of patients with MB_{Group3}.

7.2 Summary of findings

Deregulation of *MYC* activity in most cancers has been associated with tumour aggressiveness and poorer survival, with most of them showing a clear dependence on it. Research on *MYC* in the context of medulloblastoma has previously been conducted, with studies reporting growth arrest and tumour regression following depletion of *MYC* in *MYC*-driven cell and murine MB models. (Stearns et al., 2006, von Bueren et al., 2009, Pei et al., 2012, Roussel and Robinson, 2013, Li et al., 2014b).

MYC-dependent transcriptional signatures are cell specific, and the study of its function and biology must be done accordingly. To date, the cell-specific *MYC*-dependent expression program in MB_{Group3} has not been studied. Therefore, the current study was conceived and undertaken to provide a better understanding of *MYC´*s role in MB tumour biology by exploring it in a MB_{Group3} context-specific *MYC*-dependent manner, with the aim to provide evidence of the *MYC*-dependency of Group 3 medulloblastoma tumours and to identify *MYC*-associated pathways that could be ultimately exploited in the clinic to improve survival of MB patients with this specific subgroup.

To accomplish this, newly generated D425, D283 and HDMB03 isogenic MB_{Group3} cell lines with a DOX-inducible system for *MYC* knockdown, generated by the PBTG, were used to investigate the nature and extent of *MYC* dependency and involvement in MB_{Group3} pathogenesis.

Firstly, the effectiveness of *MYC* knockdown achieved with the inducible shRNA system was validated at the protein and mRNA level in all three sets of cell lines. Moreover, the *MYC*-dependent cancer phenotypes of the models were established and characterised, where reduction of *MYC* expression significantly decreased cells proliferation and apoptotic markers. Reduction in *MYC*-expression levels results in a G_1 cell cycle arrest, leaving cells in a metabolically activate state but without being actively growing.

Sensitisation of *MYC*-overexpressing MB_{Group3} isogenic cells to ionising radiation further exemplified the appropriateness of using the newly generated *MYC*-regulable cell lines as models to study *MYC's* dependent biology and therapeutic response within human MB_{Group3} (Chapter 3).

Following establishment of the *MYC*-dependent phenotype, the role of *MYC*-amplification/gain in drug sensitivity/resistance was investigated using the *MYC*-regulable isogenic models. The therapeutic potential of the pharmacological targeting of signalling pathways associated with *MYC* was assessed in a *MYC*-dependent manner with the newly generated models, undertaking three indirect pharmacological anti-MYC strategies (targeting *MYC* transcription through BRD4 and CDK9 inhibition, and MYC mRNA translation through mTOR inhibition), previously shown to downregulate *MYC* transcriptional signature in other *MYC*-driven cancers.

A *MYC*-dependent drug-sensitivity effect was observed following mTOR inhibition with AZD2014 (Vistusertib) and INK128 (Sapanisertib), BRD4 inhibition with JQ1 and CDK9 inhibition with CYC065; greater growth-inhibition following treatment with the inhibitors was seen in MB_{Group3} cells overexpressing *MYC* when compared to their counterparts with *MYC* knockdown, highlighting the potential interconnection of these molecular features with *MYC* expression in Group 3 medulloblastoma.

Notably, targeting MYC mRNA translation through mTOR inhibition, a downstream target of the PI3K/AKT signalling pathway, did not have a downregulatory effect on *MYC* expression. On the other hand, targeting *MYC* transcription through CDK9 and BRD4 inhibition resulted in reduced MYC protein levels, with growth arrest and apoptosis induction, highlighting the potential of BRD4 and CDK9 inhibition as a therapeutic strategy to treat *MYC* overexpressing MB_{Group3} tumours (Chapter 4).

Based on the current availability of multiple pharmacological approaches to indirectly target *MYC* at different levels, and the potential *MYC*-dependency of established chemo-therapeutics, a high-throughput compound screening (HTCS) was performed on the *MYC*-regulable isogenic cell lines to investigate the *MYC* dependency of the response of *MYC* overexpressing cells and with *MYC* knockdown to a large panel of conventional chemo-therapeutics and small molecule inhibitors. The HTCS, which covered most of the targetable molecules previously associated with a *MYC*-downregulatory effect, was used to identify drugs exhibiting a *MYC*-dependent effect (i.e. causing greater growth-inhibition of cells overexpressing *MYC*; and those with an additive effect following *MYC*-silencing with shRNA).

Scrutinisation of HTCS data identified 82 small molecule inhibitors which selectively inhibited the growth of *MYC*-overexpressing cell lines. Compounds identified showed a variety of associated mechanisms of action, with the vast majority inhibiting effectors of biological processes required for cell growth (cyclin-dependent kinases, aurora kinases, checkpoint kinases, polo-like kinases, microtubule formation…etc.). As described in Chapter 5, integration of HTCS results with data on transcriptional MB primary samples and *MYC*-regulable cell models predicted PLK1 (3.7% of hits), CHK1 (4.9% of hits), AURK (9.8% of hits) and CDK (12.2% of hits) as targetable molecular agents to be effective on MB_{Group3}. Molecules identified through the integration of data sets overlapped significantly with results from a MB whole-genome CRISPR screen, validating our experiments and approach, and allowing prioritisation for further investigation.

A compound representative of each cellular mechanism, and considering published data on its properties (i.e. previous testing in MB or brain tumours, use in clinical trials and potential mechanistic associations with *MYC* oncogene already established), was prioritised to take forward for validation of findings from Chapter 5, and to further assess their *MYC*-dependent effect in a wider varied panel of MB cell lines (*MYC*-amplified/regulable MB_{Group3} and non-amplified MB_{SHH} cell lines). Reasoning behind studying the effect of the inhibitors on other MB cell lines with different backgrounds of *MYC*-expression, was to study further the *MYC*-dependency of the molecules identified and their specific relationship with *MYC*. The use of available non-*MYC* amplified MB_{SHH} (DAOY and UW228.2) cell lines would help to study the reproducibility of the *MYC*-dependent sensitivities observed, and to demonstrate that the susceptibility observed were not a direct result of *MYC* downregulation with shRNA.

Additionally, a small molecule compound not previously tested in the screen, Prexasertib (LY2606368; CHK1 inhibitor), was taken forward to test on MB cell lines to independently confirm target-dependent results from the screen (Chapter 5).

The effect of prioritised compounds inhibiting CHK1 (AZD7762, Prexasertib), PLK1 (BI2536), CDK2 (Milciclib), AURKA (MLN8237), WEE1 (MK1775), BIRC5 (YM155), and TOP1 (SN38) was individually assessed in *MYC*-amplified/regulable MB_{Group3} and non-*MYC* amplified MB_{SHH} cell lines, broadly validating the *MYC*-dependent growth inhibitory effects seen from the HTCS after exposure to the inhibitors, with the exception of BIRC5 inhibition by YM155, a control drug which inhibited cell growth regardless of *MYC* expression levels (Chapter 6).

Further analysis of downstream pathway targets was prioritised to genes overlapping between datasets. Evaluation of changes in pharmacodynamic endpoints indicative of CHK1, PLK1, CDK2 and AURKA inhibition was performed to assess the mechanistic effects of the compounds and their effect on *MYC* expression. Inhibition of the main targetable molecules resulted in a time- and dose-dependent decrease of MYC protein levels across cell lines, with specificity of target inhibition for Group 3 compared to MB_{SHH} cell lines.

Importantly, the inhibitors exhibited a downregulatory effect of their main target protein across cell lines regardless of subgroup and *MYC* expression. In addition, analysis of expression of downstream pathway targets revealed a downregulation of the anti-apoptotic protein MCL1 in a *MYC*-dependent subgroup-specific manner after treatment with Prexasertib (CHK1/2 inhibitor) and BI2536 (PLK1 inhibitor). In comparison, Milciclib (CDK2 inhibitor) caused the MB_{Group3} subgroup-specific *MYC*-dependent upregulation of the protein, in comparison to the downregulatory effect it had on MB_{SHH} cell lines. No association with *MYC* expression or subgroup was seen after treatment with MLN8237 (AURKA inhibitor) and AZD7762 (CHK1 inhibitor), where a common observation of increased MCL1 protein levels was seen (Chapter 6).

As previously discussed in Chapter 6, differences in the growth inhibitory effect and inhibition of downstream pathway targets between both CHK1 inhibitors, AZD7762 and Prexasertib, could be a direct consequence of preferential inhibition of CHK2 over CHK1 by Prexasertib. Interference with the ATM signalling pathway through CHK2 inhibition appears to be more detrimental to MB_{Group3} cells expressing high-levels of *MYC*. Future experiments should include an extensive assessment of biomarkers of CHK1 and CHK2 inhibition, and a comprehensive study on how the inhibitors affect both DDR pathways. These studies could help understand why MB_{Group3} lines presented increased sensitivity to Prexasertib, and how this could be used to target this subgroup of tumours.

As reported in Chapter 6, the effect of PLK1, AURKA, CDK2 and CHK1 on *MYC*-overexpressing MB_{Group3} cell survival was *MYC*-dependent and linked to apoptosis, whereas at lower levels of *MYC* expression, the compounds caused G_2-M cell cycle arrest. Induction of apoptosis was confirmed by the inability of cells to recover growth after treatment with the compounds. A *MYC*-dependent time and dose-dependent decrease in cell viability after treatment further supports the notion that MB_{Group3} cells depend on the expression of PLK1, AURKA, CDK2 and

CHK1, and their inhibition causes downregulation of *MYC* with a direct impact on cell survival (Chapter 6).

In summary, this study provides the first direct and extensive investigation of therapeutic *MYC*-dependencies in Group 3 medulloblastoma, identifying CDK9, BRD4, PLK1, CDK2, AURKA and CHK1 as new *MYC*-regulatory mechanisms that could be therapeutically exploited against *MYC*-driven high-risk MB_{Group3}. The significance of our findings and how these could be advanced and translated into patient benefit are discussed below.

7.3 Relevance of results presented

For the appropriate development of tailored therapeutic approaches, a better understanding of disease biology in a subgroup specific context is essential. The lack of identified driver pathways in MB_{Group3} has placed efforts on targeting its most recurrent genetic alteration, *MYC* amplification/overexpression. So far, studies of MB_{Group3} tumour biology have utilised *MYC*-amplified cell lines and mouse models resembling *MYC*-activated MB, but elevated *MYC*-expression is a characteristic feature of only a subset of MB_{Group3} tumours (Ivanov et al., 2016) (Robinson et al., 2012, Venkataraman et al., 2014, Menyhárt et al., 2019, Kawauchi et al., 2017)

This study presented the validation of the newly generated *MYC*-regulable MB_{Group3} cell lines as new models to study MB_{Group3} biology with better resemblance to the nature of the disease, which could provide better insight into MB_{Group3} pathogenesis and *MYC*'s involvement in it. Generation of the lines was focused to enable the modulation of *MYC* to specifically study the true requirement of MB_{Group3} cell lines on *MYC* and to reveal *MYC*-associated genetic and therapeutic dependencies.

Furthermore, testing of already established indirect anti-*MYC* approaches in a *MYC*-dependent manner in MB_{Group3} highlighted the potential of BRD4 and CDK9 inhibition to specifically downregulate *MYC* expression and its oncogenic transcriptional program in *MYC*-driven MB_{Group3}. Results presented in this thesis are in accordance with current studies supporting the hypothesis of using BRD4 and CDK9 inhibitors to downregulate *MYC* transcription (Lu et al., 2015, Bolin et al., 2018, Delmore et al., 2011). These results provide new evidence of the *MYC*-dependency of these proteins in $MB_{Group3,}$ further supporting the

use of BRD4 and CDK9 inhibitors as potential new avenues against the most aggressive form of MB.

The present study provides a valuable resource of drug-sensitivity data of Group 3 MB cell lines to almost 500 cancer therapeutics and small molecule inhibitors targeting a broad range of key signalling pathways in tumour biology. Results from the high-throughput compound screen on *MYC*-regulable lines not only enabled the specific identification of differences in sensitivity according to *MYC* expression levels, but permitted the characterisation of the response to several compounds. Such compounds, with many of them already established for cancer treatment (i.e. Gemcitabine, Paclitaxel, Docetaxel, etc.) or are in late stages of clinical development (for easier and faster translation to the clinic) have never been tested in MB, which could reveal better chemotherapeutic approaches for MB_{Group3}.

Most importantly, screen data showed that current conventional therapies may be *MYC*-dependent. Classification of the 82 inhibitors with a *MYC*-dependent effect according to them being conventional or non-conventional therapeutics, identified increased sensitivity of *MYC*-overexpressing MB_{Group3} cell lines to inhibitors targeting β-tubulin for microtubule formation and topoisomerases (i.e. Paclitaxel, SN-38, Camptothecin, Docetaxel; Table 5.2 of Chapter 5). The analysis of differences in growth inhibition between *MYC*-overexpressing MB_{Group3} lines and *MYC*-silenced with shRNA revealed that current chemotherapeutic agents used in MB treatment, such as Vincristine and Cyclophosphamide, had no consistent effect on our models. Our findings can potentially explain the poor responsiveness of Group 3 medulloblastoma to current therapies, emphasising the need for alternative chemotherapeutic agents for patients with MB_{Group3}. Results from the screen suggest the use of inhibitors targeting microtubule formation and topoisomerases to be extremely effective in MB_{Group3}, identifying alternative, specific, and more potent chemotherapeutic agents that could improve current chemotherapeutic regimens for patients with Group 3 medulloblastoma.

An advantage of the approach taken with the high-throughput compound screen is the fact that it allowed us to study the response to the compounds across a range of drug concentrations, avoiding possible artefactual effects seen by other high-throughput screening methodologies, where only a single-concertation of each compound is tested, which can mask *MYC*-dependent effects (Rieken et al., 2015, Ricci* et al., 2018, Clare et al., 2019).

The key to interpreting functional screening is the ability to define 'high-confidence' hits. The opportunity to integrate data from *MYC*-dependent transcriptional profiles of the tumour cell lines and primary MB tumour with the results from the screen, and the cross-validation of results with data from genetic dependencies from CRISPR in MB lines (Selby et al., 2017), enabled a more robust and confident definition of PLK1, CHK, CDK, and AURK as relevant molecular targets in MB_{Group3}. Integrative approach allowed the specific prioritisation of compounds targeting these molecules for new effective targetable approaches for this MB subgroup.

As a master transcriptional regulator, *MYC* drives the transcription of several cell cycle proteins, including CDKs (CDK2, CDK4 and CDK6), PLK1 and AURK (Aurora A and Aurora B) to stimulate cell cycle progression (Otto and Sicinski, 2017). It is well established that *MYC* amplified tumours depend on *MYC*'s growth-regulatory signal for enhanced and uncontrolled cell proliferation, which requires a highly regulated cell cycle process to ensure genomic integrity for cell survival and consequent tumour progression (Murga et al., 2011). By dysregulating key cell cycle regulatory proteins, cells are able to enter mitosis with a greater load of genetic instability, which eventually triggers the apoptotic signalling cascade. This could explain why cells overexpressing *MYC* presented higher sensitivity to the inhibition of these molecules, with the inhibitors having a greater growth inhibitory effect on cells overexpressing *MYC*.

The importance of such proteins has led researchers to pursue their inhibition to indirectly target *MYC* activity in *MYC*-driven cancers, including medulloblastoma. (Muscal et al., 2013, Hill et al., 2015, Otto and Sicinski, 2017, Ferrao et al., 2012, Ando et al., 2019, Balakrishnan et al., 2017, Bolin et al., 2018, Campaner et al., 2010). This study presents the first-ever phenotypic and molecular characterisation of the inhibitory effect of PLK1 (BI2536), CHK1 (AZD7762; Prexasertib), CDK2 (Milciclib) and AURKA (MLN8237) on the expression of *MYC* and downstream pharmacodynamic endpoints of the signalling pathway in the specific context of MB_{Group3}, which could guide the establishment of new combinational approaches to most effectively manipulate the *MYC*-dependent expression signature in *MYC*-driven high-risk MB_{Group3} as a therapeutic avenue to treat patients with this tumours.

Data presented highlights the most effective way to target *MYC*-dependent MB_{Group3} tumours. Since lower *MYC* expression levels result in downregulation of proliferation and apoptosis, and seems to protect tumours from the effect of inhibitors, the targeting of genes and

molecular features required for *MYC*-overexpressing cell lines to survive is the most powerful approach to affect tumour cells viability.

Current literature on components of the *MYC*-interactome (Balakrishnan et al., 2017, Xiao et al., 2016, Triscott et al., 2013, Han et al., 2019b, Harris et al., 2012), in combination with the data generated from this study indicate PLK1 as the most promising target to effectively achieve growth arrest and tumour regression in *MYC*-driven MB_{Group3} tumours by compromising *MYC* expression PLK1 inhibition with BI2536 showed the most consistent *MYC* downregulatory effect, in addition to downregulating PLK1 signalling pathway, across MB_{Group3} cell lines. We provided evidence of the specific dependency of MB_{Group3} lines to PLK1, outlining the promising clinical application of PLK1 inhibitors to treat patients with Group 3 MB.

In summary, this study presents the first most extensive investigation of *MYC*-dependencies in Group 3 medulloblastoma using newly established *MYC*-regulable cell lines with the aim to provide enough evidence to develop new clinically relevant therapeutic approaches to treat patients with high-risk MB_{Group3}. This study provides a valuable resource of *MYC*-dependent drug-sensitivity data of MB_{Group3} cell lines to hundreds of small molecule compounds, providing the basis for the robust identification of molecular targets associated with *MYC* expression that could specifically be used for novel targeted therapeutic avenues to treat *MYC*-dependent MB_{Group3} tumours.

7.4 Study limitations

Some of the potential limitations of the results presented are outlined below.

This study used *MYC*-silencing isogenic models to regulate *MYC* expression to identify *MYC*-dependencies in MB_{Group3}. The use of cell models presents in itself the limitation that they fail to adequately recapitulate the heterogeneity of the disease. Despite being a useful tool to study primary tumours, they do not completely replicate primary cells and therefore might provide slightly different results. Also, cell lines may have acquired additional changes in long-term culture. Therefore, validation on patient derived xenograft (PDX) models is needed for further validation of the results.

As with any other high-throughput technology, the experimental and automated design come with some impediments that need awareness. The HTCS performed used the same broad range of concentrations for all the compounds contained in the libraries, which can limit the ability to discern differences in sensitivity between compounds as a direct result of *MYC*-dependencies or off-target toxicity caused by the drug, since most inhibitors will cause cell toxicity when exposed at high (i.e. >50nM) concentrations. Therefore, *MYC*-dependent effects identified from library 13, with the compounds only tested at four different concentrations (0.5, 5, 50 and 500nM), should be reinforced by testing the compounds at a smaller range of concentrations to better assess the *MYC*-dependency of the results.

Chemical differences between compounds were not considered when selecting the time of exposure. Cell lines were exposed to all drugs for the same time, as a standard procedure for comparison with the main HTCS database. It is possible that prolonged exposures to the compounds beyond the five days used here will elicit distinct effects on cell viability, since cell inhibitory properties of some agents are amplified over multiple cell cycles (Holme et al., 2018).

Regardless of the diversity of small molecule inhibitors contained in the compound libraries used, most drugs have been extensively studied and established for cancer treatment. One of the up-sides of the broad characterisation of the compounds is that related toxicities have already been described from clinical trials and second generations of those compounds can be further developed to amend related secondary effects (Rollins et al., 2004, Macarulla et al., 2010, Asghar et al., 2015, Canella et al., 2017). Although some inhibitors tested might not be suitable for clinical purposes, results from the screen should point us to the main signalling

pathways that synergise with *MYC*, to guide drug development for better and newer compounds targeting that specific avenue.

Selection of compounds representative of each class was performed based on current published data, rather than functional MB drug-sensitivity data, due to time constraints and expenses of experimentation. The information used for choosing compounds as class-representative of hits lacked functional relevance. It might be possible that by prioritising compounds based on published data on MB, some potent compounds against *MYC*-driven MB_{Group3} tumours might have been missed. Inhibitors to which the cells were sensitive to, but with no prior reports on them being tested on MB models were disregarded. To accurately choose the most effective compounds from the screen targeting each class, each one of the inhibitors belonging to a class should have been tested independently from the screen, and their effect in MB_{Group3} cell lines assessed. A more functional approach would have allowed a more considered selection of compounds representative of each targeted class.

The main objective of the project was to assess the *MYC*-dependency of Group 3 medulloblastoma using the newly established *MYC*-inducible isogenic cell lines. After the characterisation of the cancer phenotypes of the models, it was established that reduction of *MYC* expression significantly decreased cells proliferation and apoptotic markers. Reduction in *MYC*-expression levels results in a G_1 cell cycle arrest, leaving cells in a metabolically activated state but without being actively growing. This raises the question whether the inducible shRNA system truly reflects *MYC*-dependent sensitivities or solely identifies reduced susceptibility to the inhibitors when proliferation and cell cycle are down-regulated by *MYC* knockdown.

The common pattern observed after treatment of MB_{Group3} cells with most of the inhibitors tested in this thesis was the increased resistance of MB cells with *MYC*-silenced with shRNA. Reduction of *MYC* expression levels in *MYC*-addicted MB_{Group3} lines appears to protect them from the effects of the inhibitors, by stopping cell cycle and reducing apoptosis. Additional experiments that would expose the actual contribution of *MYC*-overexpression to the drug sensitivity are the testing of candidate inhibitors in other Group 3 cell lines without high-levels of *MYC* expression. Alternatively, performing clonogenic assays after exposure to the inhibitors would directly enable the assessment of cell viability.

Virtually, all of the Group 3 model cell lines harbour *MYC* amplifications, a characteristic of only 17% of Group 3 tumours (Roussel and Robinson, 2013). Therefore, in order to represent the full heterogeneity of patient tumours and understand *MYC*'s contribution to the high-risk aggressive Group 3 phenotype, cell line models of Group 3 tumours without *MYC* amplification should be established. As reported by Ivanov *et al.*, several MB cell lines are still poorly characterised, where over half of all available MB cell lines have not been subtyped or characterised to the standards of the molecular era of MB research (Ivanov et al., 2016). A better characterisation of their genetic features and subtyping could broaden the repertoire of models of MB_{Group3} disease, which would help in the identification of relevant cells to use to answer *MYC*-related questions in a Group 3 specific context.

Another limitation of the data presented in this study was that cell proliferation was the main parameter used to assess cells susceptibility to the inhibitors. CTG assay was used to determine the number of viable cells in culture based on quantitation of the ATP present, as an indicator of metabolically active cells (the amount of ATP is directly proportional to the number of cells present in culture). To provide evidence that the effects of *MYC*-dependency observed are not simply due to the in vitro drug sensitivity assay bias towards cell proliferation, cells capacity to divide unlimitedly could be assessed by performing alternative *in vitro* experiments, such as colony formation assays. Clonogenic assays are widely used to determine the effectiveness of treatment with cytotoxic agents by assessing cells reproductive death (Franken et al., 2006). The addition of colony formation assays to the repertoire of experiments performed on the drug candidates, would bring an extra layer of validation of the cell's susceptibility to the inhibitors.

Overall, validation of results was done in a small panel of MB cell lines. Due to the lack of Group 3 cell lines without *MYC* amplification, other MB cell lines available in the PBTG belonging to the SHH subgroup were used instead, DAOY and UW228.2.

MB_{SHH} subgroup is most frequently associated with inactivating mutations of *PTCH1* (the SHH receptor) or SUFU (a downstream signal transducer). By binding to its receptor, SHH directly upregulates *MYCN* transcription via GLI family transcription factors (Kenney et al. 2003). In addition to having uniformly high *MYCN* expression levels, *MYCN* amplification can occur in

MB_{SHH}, which is a marker of poor prognosis (Ellison et al., 2011, Northcott et al., 2012a). Overexpression of *MYCN* is sufficient to promote proliferation, and *MYCN* activity is necessary for SHH-induced proliferation.

MYCN is therefore both a marker of enhanced SHH activity; *MYCN* is a critical mediator of SHH signals in granule neuronal precursors (GNPs) (Kenney et al., 2003) and is absolutely required for normal cerebellar development. On the other hand, c-*MYC* is not normally expressed in GNPs, and its overexpression is mutually exclusive to *MYCN*. Despite the fact that *MYCN* and c-*MYC* genes are differentially expressed in the hindbrain, and that *MYCN*, but not c-*MYC*, is a target of SHH signalling, it has been reported that *MYCN* can functionally replace c-*MYC* in mouse development, proliferation and differentiation implying many interchangeable functions (Kawauchi et al., 2012)(Malynn et al., 2000)(Kenney et al., 2003)(Zindy et al., 2006).

Upregulation of *MYCN* through the SHH signalling pathway in MB_{SHH} might be affecting c-*MYC* expression and interfering with the *MYC*-dependent drug sensitivities identified. Despite probably not being the most relevant cell models to study *MYC*-dependencies, their inherent lower expression of c-*MYC* makes them an invaluable resource to compare to *MYC*-overexpressing MB_{Group3} cell lines. Although there are clear differences between the signalling pathways that define each subgroup, variation in response to the inhibitors according to *MYC* expression levels was studied to provide insight into *MYC*'s role in the pathology of MB disease, and to identify targetable pathways associated with *MYC* expression.

The use of only 2 non-*MYC* amplified MB cell lines limited the characterisation of differences in the response of non-Group 3 cell lines to the compounds (Ivanov et al., 2016). Implementation of a larger set of non-*MYC* amplified medulloblastoma cell lines would bring more genetic heterogeneity of the disease, and could help best determine the subgroup specificity of the *MYC*-dependent drug-sensitivity effects observed.

7.5 Future lines of investigation

This study validated the newly established isogenic *MYC*-regulable cell lines as new models to investigate the *MYC*-dependent biology of MB_{Group3} tumours, as a means to identify and develop novel therapeutic strategies to bring into the clinic for high-risk patients with MB_{Group3} tumours. Some future lines of investigation to exploit our findings and to establish the required evidence to support new clinical trials for patients with Group 3 MB are discussed below.

7.5.1 Combinational therapeutic approaches

Given the highly adaptative nature of *MYC*-driven MB, emergence of resistance following exposures to standard chemotherapeutic agents or small molecule compounds used as single agents it is widely established, limiting their therapeutic effectiveness (Othman et al., 2014, Bertrand et al., 2018, Dean et al., 2005). Given the complex regulation of the *MYC*-expression program, a *MYC*-inhibitory strategy should not be limited to a single agent approach, but rather a combinational strategy using different compounds targeting unique aspects of *MYC* oncogenicity to help achieve better responses.

Results presented in this study show that *MYC*-dependent Group 3 MB tumours are more susceptible to perturbation of cell cycle proteins and proteins involved in the control of the DNA-damage pathway. Therefore, we provide enough evidence to direct future strategies to include the combined use of PLK1 and BRD4 inhibitors, to efficiently downregulate *MYC*-expression signatures to sensitise cells to standard chemotherapy. Inhibition of PLK1 with BI2536 in addition to *MYC* knockdown had an additive effect on the isogenic cell lines. In principle, a decrease in *MYC* expression and destabilisation of MYC protein through the combinational inhibition of PLK1 and BRD4, can achieve a *MYC*-dependent tumour regression whilst triggering cell death for prolonged responses (Han et al., 2019b, Tontsch-Grunt et al., 2018).

An alternative potentially promising approach is the use of AURK and CHK1 inhibitors in combination with standard chemotherapy to downregulate *MYC*-expression to enhance the susceptibility of *MYC*-driven MB_{Group3} to DNA-damaging agents, promoting genomic instability and to eventually trigger the *MYC*-dependent apoptotic signalling pathway (Dammert et al., 2019). As reported in this study, inhibition of AURKA and CHK1 causes cell cycle arrest at G_2-M phase and induces apoptosis in *MYC*-overexpressing cell lines. The combined inhibition of

these key regulators of the cell cycle would preferentially kill *MYC*-overexpressing cell lines over those cells with a normal cell cycle activity and ability to repair damaged DNA caused by chemotherapeutic agents.

Treatment of GTML2 MB xenografts with a combination of CDK2 inhibitors with BRD4 has been reported to supress tumour growth *in vivo* (Bolin et al., 2018). This combination states the synergy of both proteins in efficiently downregulating *MYC*-dependent pathways in *MYC*-driven MB. A *MYC*-dependent growth inhibitory effect was seen after treatment with BRD4 and CDK2, which was linked with downregulation of MYC protein expression levels. Combined inhibition of both proteins should result in a synergistic effect in efficiently inhibiting *MYC*-dependent pathways, specifically supressing tumour growth of *MYC*-overexpressing MB_{Group3} tumours. This approach could have the potential to generate clinically relevant therapeutic effects against *MYC*-driven high-risk MB_{Group3} tumours.

Despite the increasing number of successful drug combination studies to treat *MYC*-driven cancers, discovery of such combinations are mostly based on studies on other types of cancer. As stated in this thesis, it is of crucial importance to study *MYC* in a cell-specific context. In this regard, a small-scale drug-combination high-throughput screen could be designed to study the combinational inhibitory effect of the molecular targets identified to have a *MYC*-dependent effect in our cell lines (Liu et al., 2019b).

Following the assessment of the activity of each compound as a single agent, a good way to bring drug candidates further into clinical testing would be to perform a pairwise combination screen with the inhibitors tested in this thesis. The activity of each of the compounds would be assessed against the rest of compounds to identify effective combinations. This approach would not only allow the assessment of the combinatorial effect of the dual targeting of essential molecules for Group 3 MB tumours, but also their relationship and differential effect according to *MYC* expression levels (with and without *MYC* silenced with shRNA).

However, clinical applications of combination therapy are often limited by tolerable dose ranges, and, therefore, it is desirable to identify combinations that enable dose reduction (i.e. synergistic potency)(Tallarida, 2011). Additionally, combining drugs does not necessarily translate into an increase in efficacy over the single agents, and, therefore, it is desirable to identify combinations with effects greater than what is achievable with either drug alone (i.e., synergistic efficacy)(Foucquier and Guedj, 2015, Meyer et al., 2019).

To assess a combination's performance having these two goals in mind, several drug quantitative synergy methods have been developed (Chou and Talalay, 1983, Yadav et al., 2015, Foucquier and Guedj, 2015, Twarog et al., 2016, Zimmer et al., 2016, Schindler, 2017). Current methods to quantify drug synergy are based on either Loewe additivity or Bliss independence principles. Loewe advanced the dose additivity principle (Loewe and Muischnek, 1926), and Bliss first described the multiplicative survival principle (BLISS, 1939). The goal of using synergistic drugs is to achieve more with less. Finding such combinations is vital for optimizing therapeutic windows, as there exists a fine line between clinical efficacy and tolerable doses.

One of the benefits of combination drug studies is that newly identified targeted compounds can be assessed alongside current chemotherapeutic agents used in MB treatment. It is not only important to find compounds to which cell lines are sensitive to, but to find how these new treatments could be combined with current standard of care chemotherapies, including radiation (Zhang and Yang, 2016).

An interesting approach to take with small-scale combinational studies would be, in one instance, to test inhibitors targeting PLK1, CDK2/9, CHK1, AURKA and JQ1 after exposures to IR. Assessment of cells' viability after treatment could help identify synergistic effects between targeting these molecules and radiation. Identification of inhibitors with an additive effect to radiation could be used to eradicate remaining viable cells after IR treatment, and decrease disease recurrence. On the other hand, another promising approach would be to assess the synergy of candidate inhibitors with current chemotherapeutic agents, like cisplatin, vincristine, cyclophosphamide or lomustine.

The insufficient efficacy of treatment for patients with MB_{Gorup3} highlights a pressing need for synergistically efficacious combinations in order to improve the depth and durability of response (Meyer et al., 2019). Finding effective combinational approaches of targeted compounds with chemotherapeutic agents could improve responsiveness of high-risk MB_{Gorup3} patients to therapy

7.5.2 Genetic validation of targets with siRNA

Following the identification of *MYC*-dependent targets identified from the HTCS and their pharmacological validation, the genetic validation of PLK1, CHK1, AURKA and CDK2 inhibition should be pursued as an additional approach for target validation (Perwitasari et al., 2013) .

The evaluation of *MYC* expression and changes in cell proliferation following the genetic attenuation of the expression of our genes of interest by small interfering RNA (siRNA) using the *MYC*-regulable cell lines, would further validate the interconnection of the molecules with *MYC* and establish target-dependency of this specific subgroup of tumours to these proteins, providing confidence of their therapeutic inhibitory-value and their potential use in clinical settings to target *MYC*-dependent MB tumours (von Bueren et al., 2009, Jain, 2004)

7.5.3 In vivo *assessment of candidate molecular targets*

Mouse models of MB have been instrumental in understanding the disease and the role of molecular drivers, and to establish appropriate preclinical pipelines. To date, the research community has developed accurate murine models that recapitulate all MB subgroups, each of which has been critical for the identification and development of new therapeutic approaches (Roussel and Stripay, 2020).

Mouse models have to closely resemble and recapitulate human tumours, representing disease heterogeneity and mimicking molecular, epigenetic and genetic landscapes. Conventional knock-out technology has been the pivotal approach to generate some of the most accurate genetically engineered mouse models (GEMM) of MB. One example is the widely used Patched 1 model of SHH MB, which has enabled the assessment of genes that drive MB_{SHH} tumourigenesis (Goodrich et al., 1997).

The lack of molecular drivers defining Group 3 medulloblastoma delayed the development of GEMMs for this specific subgroup. Initially, lentiviral or retroviral vectors that conditionally express or repress potential MB_{Group3} drivers, including *MYC* and *GIF1*, were used to modify purified GNPs or neural stem cells to assess the role of these potential MB_{Group3} drivers. Modified progenitors were then implanted into the cerebella of immune-compromised mice, which gave rise to tumours with histopathological and molecular characteristics consistent with Group 3. (Kawauchi et al., 2012, Pei et al., 2012, Roussel and Stripay, 2020).

MYC-overexpression is the hallmark of MB_{Group3}. While tumours in this subgroup rarely display *MYCN* amplification, the first mouse model of Group 3 developed had *MYCN* expression driven by the glutamate transporter 1 (Glt1) promoter in hindbrain progenitors (GTML) (Swartling et al., 2010). Tumours from this model resembled the phenotype and molecular profile of MB_{Group3}. Despite the histological relevance of the GTML model, *MYCN* amplification is less common than *MYC* amplification in this subgroup, which has driven the development of a derivative model, GMYC, in which *MYC* is driven by the hindbrain Glt1 promoter (Roussel and Stripay, 2020). Alternatively, other models with enforced *MYC* expression have been developed through retroviral gene transfer and the loss of Trp53 function to reprogram GNPs or NSC (Kawauchi et al., 2012, Vo et al., 2018, Huang et al., 2019).

GEMMs of MB_{Group3} are a valuable tool for *in vitro* and *in vivo* testing, but the whole heterogeneity or microenvironment of the tumour can not be fully captured. An increasingly prevalent model in MB preclinical research are patient-derived xenograft (PDX) models, which address the limitations of GEM models (Roussel and Stripay, 2020). PDXs are generated by implanting tissue from a patient's tumour into mice, amplifying tumours intracranially *in vivo* (Shu et al., 2008). The presence of stromal environmental components and the heterogeneity of the tumour cell population provide a significant advantage in regard to a more accurate interrogation of disease mechanism and therapeutic response (Hovestadt et al., 2019). Since PDXs enable a more accurate recapitulation of the disease, they are becoming the gold standard for preclinical testing (Sandén et al., 2017, Brabetz et al., 2018).

The ability of MB_{Group3} mouse models to grow as spheres *in vitro*, have become instrumental for conducting high-throughput drug screens to identify novel therapies. Using the MYC-driven, *Trp53−/−* mouse model, Pei and collaborators performed a drug screen which identified a cooperative effect between HDAC and PI3K inhibitors (Pei et al., 2016), while Morfouace and collaborators demonstrated a new combination approach of pemetrexed and gemcitabine (Morfouace et al., 2014). From these preclinical studies have emerged early stage clinical trials including SJMB12 (Pemetrexed and Gemcitabine for Newly diagnosed patients with Non-WNT, Non-SHH, MB)(NCT0187861). A more recent St. Jude clinical trial (SJDAWN) include the use of a CDK4/6 inhibitor (ribociclib) in combination with gemcitabine for recurrent MB_{Group3} (NCT03434262). Survival of mice harbouring the *MYC*-amplified MB_{Group3} patient-derived Med-311FH orthotopic xenograft, was significantly extended by the inhibition of CDK4/6 with Palbociclib (Cook Sangar et al., 2017). These studies stimulated a phase 1 study

with Palbociclib in children with recurrent, progressive or refractory CNS tumours including medulloblastoma (PBTC-042). Recently, inhibitors of CHK1 and CHK2 were found to efficiently suppress the proliferation of mouse and human MB_{Group3}, with or without *TP53* mutation, in combination with gemcitabine or cyclophosphamide (Roussel and Stripay, 2020). The clinical trial SJELiOT, designed based on this work, was recently approved by the FDA and began enrolling in July 2019 (NCT04023669).

Most of the preclinical work in MB has focused on SHH and Group 3, due in part to the need for improved therapies for the high-risk subsets of these groups (Roussel and Stripay, 2020).. Major challenges are the blood-brain and blood-tumour barriers (Fortin, 2012). These have limited the number of drugs that can be used to treat MB patients. While several drugs and small molecules have been tested in mouse models and found to be efficacious in suppressing medulloblastoma proliferation, most used established cell lines. Thus, ideally preclinical trials should be performed in multiple mouse models *in vitro* and *in vivo* and should require that all drugs be investigated for their brain and tumour penetration (Picha et al., 2012, Lee, 2014).

Based on previous work performed on *in vivo* models of Group 3 MB and considering the data presented in this thesis, there is a strong argument to further explore the role of CDK9, BRD4, PLK1, AURKA, and CHK1 inhibition in GEMM and PDX models of MB_{Group3}. Drug combinational and synergy studies would enable the prioritisation of those inhibitors with a synergistic effect with *MYC* expression for testing in relevant MB_{Group3} *in vivo* models. Experimentation *in vivo* is the key next step in the clinical development of the findings presented in this thesis, to support their use in the clinic.

Assessment of pharmacodynamic markers, dosing schedules, with special consideration to the ability of the inhibitor to penetrate the blood-brain barrier (BBB) in different GEMM and PDXs of MB_{Group3}, will provide the essential pre-clinical evidence to support the development of regimens for new clinical trials to improve treatment of this highly-aggressive and deadly MB tumours.

7.5.4 Alternative MYC-*targeting strategies*

For decades, *MYC*-mediated tumourigenesis was thought to occur mainly through tumour cell-intrinsic mechanisms, but several lines of investigation have demonstrated that manipulation of the *MYC*-signalling pathway does not only have a direct impact on tumour cells through proliferative and apoptotic mechanisms, but also through an influence on the host immune response(Casey et al., 2014b, Casey et al., 2014a, Bachireddy et al., 2012, Tran et al., 2011).

The *MYC* oncogene regulates the transcription of multiple components of the immune response, like CD47 and the programmed death-ligand 1 (PD-L1) (Majeti et al., 2009) (Atsaves et al., 2017, Casey et al., 2016). CD47 and PD-L1 are required to remodel the tumour microenvironment to recruit $CD4^+$ T cells and macrophages, associated with reduction of angiogenesis and induction of cellular senescence (Mina et al., 2015, Rakhra et al., 2010). *MYC* overexpression has been linked to upregulation of the expression of such immune checkpoints, which supresses the immune system and allow cancer cells to bypass the surveillance of the immune system (McCracken et al., 2015, Casey et al., 2016, Soucek et al., 2007, Sodir et al., 2011).

Recently, some studies have identified the requirement of a properly functioning host immune system for the effective elimination of tumour cells following inactivation of *MYC* activity (Gabay et al., 2014, Rakhra et al., 2010, Helm et al., 2013). Downregulation of *MYC* expression has been found to result in reduced expression of CD47 and PD-L1 both *in vitro* and *in vivo* studies, resulting in the recruitment of the necessary immune effectors for the complete elimination of tumours cells (Casey et al., 2016, Spranger et al., 2016).

It will be of interest to interrogate changes in expression of components of the immune response following *MYC* modulation with shRNA using the *MYC*-regulable cell models, to shed light on the mechanism by which *MYC* oncogene specifically regulates the immune response in Group 3 medulloblastoma and identify *MYC*-dependent neo-antigens which could be targeted with CAR-T (Minutolo et al., 2019).

So far, BRD4 inhibition by JQ1 inhibitor has been reported to downregulate PD-L1 and CD47 in certain *MYC*-driven tumours, which was associated with recruitment of T cells (Zhu et al., 2016, Melaiu et al., 2017, Hogg et al., 2017). Therefore, identification of the *MYC*-dependent regulatory mechanisms of the immune signalling response in *MYC*-driven MB could help direct combinational therapeutic strategies to downregulate the oncogenic activity of *MYC* and also activate the immune system *MYC*-driven MB_{Group3} tumours for most efficacious tumour eradication (Massó-Vallés et al., 2016, Casey et al., 2018).

7.6 Conclusion

In conclusion, this study was undertaken to investigate the role and involvement of *MYC* in MB_{Group3} pathogenesis, to identify biological signalling pathways associated with *MYC*-expression and essential for the maintenance of the malignant phenotype and viability of the tumour, to aid in the development of clinically relevant therapeutic strategies for patients with this highly-lethal MB subgroup.

The *MYC*-dependency of MB_{Group3} was exploited using the new *MYC*-regulable isogenic cell lines, identifying several specific Group 3 druggable dependencies (e.g. cell cycle regulators, DNA-damage response controllers, mitotic control machinery, epigenetic modifiers) with direct clinical implications for the development of personalised treatment against MB_{Group3}. Our findings provide evidence that supports *in vivo* preclinical studies using PLK1, CHK1, AURKA and CDK2 inhibitors for treating patients with *MYC*-driven MB, paving the way for improving MB treatment, through the development of targeted therapies to implement in clinical trials for MB_{Group3} tumours.

References

ABBOU, S., LANVERS-KAMINSKY, C., DAUDIGEOS-DUBUS, E., L, L. E. D., LAPLACE-BUILHE, C., MOLENAAR, J., VASSAL, G., GEOERGER, B., WITHIN THE, I. B. & PRECLINICAL EVALUATION, C. 2016. Polo-like Kinase Inhibitor Volasertib Exhibits Antitumor Activity and Synergy with Vincristine in Pediatric Malignancies. *Anticancer Res,* 36**,** 599-609.

ABDEL-AZIZ, A., MOHAMED, M., AKL, F. & TAHA, A. N. 2012. Survivin Expression in Medulloblastoma: A Possible Marker for Survival. *Pathology oncology research : POR,* 19.

ABOUANTOUN, T. J., CASTELLINO, R. C. & MACDONALD, T. J. 2011. Sunitinib induces PTEN expression and inhibits PDGFR signaling and migration of medulloblastoma cells. *Journal of Neuro-Oncology,* 101**,** 215-226.

ADHIKARY, S. & EILERS, M. 2005. Transcriptional regulation and transformation by MYC proteins. *Nature Reviews Molecular Cell Biology,* 6**,** 635-645.

AFTIMOS, P. G., BECHTER, O., AWADA, A., JUNGELS, C., DUMEZ, H., HUYVAERT, N., COSTERMANS, J., LEE, C., MEEUS, M. A., BURKARD, U., MUSA, H., ZHAO, Y. H. & SCHOFFSKI, P. 2017. Phase I first-in-man trial of a novel bromodomain and extra-terminal domain (BET) inhibitor (BI 894999) in patients (Pts) with advanced solid tumors. *Journal of Clinical Oncology,* 35.

AHLUWALIA, M. S., DE GROOT, J., LIU, W. M. & GLADSON, C. L. 2010. Targeting SRC in glioblastoma tumors and brain metastases: rationale and preclinical studies. *Cancer letters,* 298**,** 139-149.

AHMAD, Z., JASNOS, L., GIL, V., HOWELL, L., HALLSWORTH, A., PETRIE, K., SAWADO, T. & CHESLER, L. 2015. Molecular and In Vivo Characterization of Cancer-Propagating Cells Derived from MYCN-Dependent Medulloblastoma. *Plos One,* 10.

AKSHINTALA, S., MARCUS, L., WARREN, K. E., MURPHY, R. F., SISSUNG, T. M., SRIVASTAVA, A., GOODSPEED, W. J., GOODWIN, A., BREWER, C. C., ZALEWSKI, C., KING, K. A., KIM, A., FIGG, W. D. & WIDEMANN, B. C. 2015. Phase 1 trial and pharmacokinetic study of the oral platinum analog satraplatin in children and young adults with refractory solid tumors including brain tumors. *Pediatric blood & cancer,* 62**,** 603-610.

ALBRIGHT, A. L., WISOFF, J. H., ZELTZER, P. M., BOYETT, J. M., RORKE, L. B. & STANLEY, P. 1996. Effects of medulloblastoma resections on outcome in children: A report from the children's cancer group. *Neurosurgery,* 38**,** 265-270.

ALDAREGIA, J., ODRIOZOLA, A., MATHEU, A. & GARCIA, I. 2018. Targeting mTOR as a Therapeutic Approach in Medulloblastoma. *International journal of molecular sciences,* 19**,** 1838.

ALEEM, E. & ARCECI, R. J. 2015. Targeting cell cycle regulators in hematologic malignancies. *Frontiers in Cell and Developmental Biology,* 3**,** 16.

ALLEN-PETERSEN, B. L. & SEARS, R. C. 2019. Mission Possible: Advances in MYC Therapeutic Targeting in Cancer. *Biodrugs,* 33**,** 539-553.

ALQAHTANI, A., CHOUCAIR, K., ASHRAF, M., HAMMOUDA, D. M., ALLOGHBI, A., KHAN, T., SENZER, N. & NEMUNAITIS, J. 2019. Bromodomain and extra-terminal motif inhibitors: a review of preclinical and clinical advances in cancer therapy. *Future science OA,* 5**,** FSO372-FSO372.

ALSERAYE, F., PADMORE, R., WOZNIAK, M. & MCGOWAN-JORDAN, J. 2009. MYC gene amplification in double minute chromosomes in an aggressive large B-cell lymphoma with leukemic presentation: a case report. *Cancer Genet Cytogenet,* 192**,** 76-8.

AMARANTE, M. K., VITIELLO, G. A. F., ROSA, M. H., MANCILLA, I. A. & WATANABE, M. A. E. 2018. Potential use of CXCL12/CXCR4 and sonic hedgehog pathways as therapeutic targets in medulloblastoma. *Acta Oncologica,* 57**,** 1134-1142.

AMATI, B., FRANK, S. R., DONJERKOVIC, D. & TAUBERT, S. 2001. Function of the c-Myc oncoprotein in chromatin remodeling and transcription. *Biochimica Et Biophysica Acta-Reviews on Cancer,* 1471**,** M135-M145.

AMORIM, S., STATHIS, A., GLEESON, M., IYENGAR, S., MAGAROTTO, V., LELEU, X., MORSCHHAUSER, F., KARLIN, L., BROUSSAIS, F., REZAI, K., HERAIT, P., KAHATT, C., LOKIEC, F., SALLES, G., FACON, T., PALUMBO, A., CUNNINGHAM, D., ZUCCA, E. & THIEBLEMONT, C. 2016. Bromodomain inhibitor OTX015 in patients with lymphoma or multiple myeloma: a dose-escalation, open-label, pharmacokinetic, phase 1 study. *Lancet Haematology,* 3**,** E196-E204.

ANDO, K., NAKAMURA, Y., NAGASE, H., NAKAGAWARA, A., KOSHINAGA, T., WADA, S. & MAKISHIMA, M. 2019. Co-Inhibition of the DNA Damage Response and CHK1 Enhances Apoptosis of Neuroblastoma Cells. *International journal of molecular sciences,* 20**,** 3700.

ANDREWS, F. H., SINGH, A. R., JOSHI, S., SMITH, C. A., MORALES, G. A., GARLICH, J. R., DURDEN, D. L. & KUTATELADZE, T. G. 2017. Dual-activity PI3K-BRD4 inhibitor for the orthogonal inhibition of MYC to block tumor growth and metastasis. *Proc Natl Acad Sci U S A,* 114**,** E1072-E1080.

ANGIUS, G., TOMAO, S., STATI, V., VICI, P., BIANCO, V. & TOMAO, F. 2020. Prexasertib, a checkpoint kinase inhibitor: from preclinical data to clinical development. *Cancer Chemotherapy and Pharmacology,* 85**,** 9-20.

ANTONARAKIS, E. S., HEATH, E. I., POSADAS, E. M., YU, E. Y., HARRISON, M. R., BRUCE, J. Y., CHO, S. Y., WILDING, G. E., FETTERLY, G. J., HANGAUER, D. G., KWAN, M.-F. R., DYSTER, L. M. & CARDUCCI, M. A. 2013. A phase 2 study of KX2-391, an oral inhibitor of Src kinase and tubulin polymerization, in men with bone-metastatic castration-resistant prostate cancer. *Cancer Chemotherapy and Pharmacology,* 71**,** 883-892.

ANTONI, L., SODHA, N., COLLINS, I. & GARRETT, M. D. 2007. CHK2 kinase: cancer susceptibility and cancer therapy - two sides of the same coin? *Nat Rev Cancer,* 7**,** 925-36.

ANTONUCCI, L., DI MAGNO, L., D'AMICO, D., MANNI, S., SERRAO, S. M., DI PASTENA, F., BORDONE, R., YURTSEVER, Z. N., CAIMANO, M., PETRONI, M., GIORGI, A., SCHININÀ, M. E., YATES III, J. R., DI MARCOTULLIO, L., DE SMAELE, E., CHECQUOLO, S., CAPALBO, C., AGOSTINELLI, E., MARODER, M., CONI, S. & CANETTIERI, G. 2019. Mitogen-activated kinase kinase kinase 1 inhibits hedgehog signaling and medulloblastoma growth through GLI1 phosphorylation. *International journal of oncology,* 54**,** 505-514.

ARBITRARIO, J., BELMONT, B., EVANCHIK, M., FLANAGAN, M., FUCINI, R., HANSEN, S., HARRIS, S., HASHASH, A., HOCH, U., HOGAN, J., HOWLETT, A., JACOBS, J., LAM, J., RITCHIE, S., ROMANOWSKI, M., SILVERMAN, J., STOCKETT, D., TEAGUE, J., ZIMMERMAN, K. & TAVERNA, P. 2009. SNS-314, a pan-Aurora kinase inhibitor, shows potent anti-tumor activity and dosing flexibility in vivo. *Cancer chemotherapy and pharmacology,* 65**,** 707-17.

ARTS, J., KING, P., MARIËN, A., FLOREN, W., BELIËN, A., JANSSEN, L., PILATTE, I., ROUX, B., DECRANE, L., GILISSEN, R., HICKSON, I., VREYS, V., COX, E., BOL, K., TALLOEN, W., GORIS, I., ANDRIES, L., DU JARDIN, M., JANICOT, M., PAGE, M., VAN EMELEN, K. & ANGIBAUD, P. 2009. JNJ-26481585, a novel "second-generation" oral histone deacetylase inhibitor, shows broad-spectrum preclinical antitumoral activity. *Clin Cancer Res,* 15**,** 6841-51.

ASATI, V., MAHAPATRA, D. K. & BHARTI, S. K. 2016. PI3K/Akt/mTOR and Ras/Raf/MEK/ERK signaling pathways inhibitors as anticancer agents: Structural and pharmacological perspectives. *Eur J Med Chem,* 109**,** 314-41.

ASGHAR, U., WITKIEWICZ, A. K., TURNER, N. C. & KNUDSEN, E. S. 2015. The history and future of targeting cyclin-dependent kinases in cancer therapy. *Nature reviews. Drug discovery,* 14**,** 130-146.

ASHLEY, D. M., MEIER, L., KERBY, T., ZALDUONDO, F. M., FRIEDMAN, H. S., GAJJAR, A., KUN, L., DUFFNER, P. K., SMITH, S. & LONGEE, D. 1996. Response of recurrent medulloblastoma to low-dose oral etoposide. *J Clin Oncol,* 14**,** 1922-7.

ASHLEY, D. M., MERCHANT, T. E., STROTHER, D., ZHOU, T. N., DUFFNER, P., BURGER, P. C., MILLER, D. C., LYON, N., BONNER, M. J., MSALL, M., BUXTON, A., GEYER, R., KUN, L. E., COLEMAN, L. & POLLACK, I. F. 2012. Induction Chemotherapy and Conformal Radiation Therapy for Very Young Children With Nonmetastatic Medulloblastoma: Children's Oncology Group Study P9934. *Journal of Clinical Oncology,* 30**,** 3181-3186.

ASPESLAGH, S., SHAILUBHAI, K., BAHLEDA, R., GAZZAH, A., VARGA, A., HOLLEBECQUE, A., MASSARD, C., SPREAFICO, A., RENI, M. & SORIA, J.-C. 2017. Phase I dose-escalation study of milciclib in combination with gemcitabine in patients with refractory solid tumors. *Cancer Chemotherapy and Pharmacology,* 79.

ATSAVES, V., TSESMETZIS, N., CHIOUREAS, D., KIS, L., LEVENTAKI, V., DRAKOS, E., PANARETAKIS, T., GRANDER, D., MEDEIROS, L. J., YOUNG, K. H. & RASSIDAKIS, G. Z. 2017. PD-L1 is commonly expressed and transcriptionally regulated by STAT3 and MYC in ALK-negative anaplastic large-cell lymphoma. *Leukemia,* 31**,** 1633-1637.

AWAD, M. M. & SHAW, A. T. 2014. ALK inhibitors in non-small cell lung cancer: crizotinib and beyond. *Clinical advances in hematology & oncology : H&O,* 12**,** 429-439.

AYRAULT, O., GODENY, M. D., DILLON, C., ZINDY, F., FITZGERALD, P., ROUSSEL, M. F. & BEERE, H. M. 2009. Inhibition of Hsp90 via 17-DMAG induces apoptosis in a p53-dependent manner to prevent medulloblastoma. *Proceedings of the National Academy of Sciences,* 106**,** 17037-17042.

BACHIREDDY, P., RAKHRA, K. & FELSHER, D. W. 2012. Immunology in the clinic review series; focus on cancer: multiple roles for the immune system in oncogene addiction. *Clinical and experimental immunology,* 167**,** 188-194.

BACOLOD, M. D., LIN, S. M., JOHNSON, S. P., BULLOCK, N. S., COLVIN, M., BIGNER, D. D. & FRIEDMAN, H. S. 2008. The gene expression profiles of medulloblastoma cell lines resistant to preactivated cyclophosphamide. *Current cancer drug targets,* 8**,** 172-179.

BAKSHI, S., MCKEE, C., WALKER, K., BROWN, C. & CHAUDHRY, G. R. 2018. Toxicity of JQ1 in neuronal derivatives of human umbilical cord mesenchymal stem cells. *Oncotarget,* 9**,** 33853-33864.

BALAKRISHNAN, I., VENKATARAMAN, S., PIERCE, A. M., ALIMOVA, I., PRINCE, E., MOREIRA, D. C., FOSMIRE, S., MADHAVAN, K., FOREMAN, N. & VIBHAKAR, R. 2017. PLK1 inhibition in combination with standard therapies for MYC-driven medulloblastoma *Neuro-Oncology,* 19**,** iv44-iv44.

BANDOPADHAYAY, P., BERGTHOLD, G., NGUYEN, B., SCHUBERT, S., GHOLAMIN, S., TANG, Y., BOLIN, S., SCHUMACHER, S. E., ZEID, R., MASOUD, S., YU, F., VUE, N., GIBSON, W. J., PAOLELLA, B. R., MITRA, S. S., CHESHIER, S. H., QI, J., LIU, K. W., WECHSLER-REYA, R., WEISS, W. A., SWARTLING, F. J., KIERAN, M. W., BRADNER, J. E., BEROUKHIM, R. & CHO, Y. J. 2014. BET bromodomain inhibition of MYC-amplified medulloblastoma. *Clin Cancer Res,* 20**,** 912-25.

BANDOPADHAYAY, P., PICCIONI, F., O'ROURKE, R., HO, P., GONZALEZ, E. M., BUCHAN, G., QIAN, K., GIONET, G., GIRARD, E., COXON, M., REES, M. G., BRENAN, L., DUBOIS, F.,

SHAPIRA, O., GREENWALD, N. F., PAGES, M., BALBONI INIGUEZ, A., PAOLELLA, B. R., MENG, A., SINAI, C., ROTI, G., DHARIA, N. V., CREECH, A., TANENBAUM, B., KHADKA, P., TRACY, A., TIV, H. L., HONG, A. L., COY, S., RASHID, R., LIN, J. R., COWLEY, G. S., LAM, F. C., GOODALE, A., LEE, Y., SCHOOLCRAFT, K., VAZQUEZ, F., HAHN, W. C., TSHERNIAK, A., BRADNER, J. E., YAFFE, M. B., MILDE, T., PFISTER, S. M., QI, J., SCHENONE, M., CARR, S. A., LIGON, K. L., KIERAN, M. W., SANTAGATA, S., OLSON, J. M., GOKHALE, P. C., JAFFE, J. D., ROOT, D. E., STEGMAIER, K., JOHANNESSEN, C. M. & BEROUKHIM, R. 2019. Neuronal differentiation and cell-cycle programs mediate response to BET-bromodomain inhibition in MYC-driven medulloblastoma. *Nat Commun,* 10**,** 2400.

BARONE, G., ANDERSON, J., PEARSON, A. D., PETRIE, K. & CHESLER, L. 2013. New strategies in neuroblastoma: Therapeutic targeting of MYCN and ALK. *Clin Cancer Res,* 19**,** 5814-21.

BARTEK, J. & LUKAS, J. 2003. Chk1 and Chk2 kinases in checkpoint control and cancer. *Cancer Cell,* 3**,** 421-9.

BARTUCCI, M., SVENSSON, S., ROMANIA, P., DATTILO, R., PATRIZII, M., SIGNORE, M., NAVARRA, S., LOTTI, F., BIFFONI, M., PILOZZI, E., DURANTI, E., MARTINELLI, S., RINALDO, C., ZEUNER, A., MAUGERI-SACCÀ, M., ERAMO, A. & DE MARIA, R. 2012. Therapeutic targeting of Chk1 in NSCLC stem cells during chemotherapy. *Cell Death & Differentiation,* 19**,** 768-778.

BARYAWNO, N., SVEINBJORNSSON, B., EKSBORG, S., CHEN, C. S., KOGNER, P. & JOHNSEN, J. I. 2010. Small-molecule inhibitors of phosphatidylinositol 3-kinase/Akt signaling inhibit Wnt/beta-catenin pathway cross-talk and suppress medulloblastoma growth. *Cancer Res,* 70**,** 266-76.

BASU, A. & SRIDHARAN, S. 2017. Regulation of anti-apoptotic Bcl-2 family protein Mcl-1 by S6 kinase 2. *PLoS One,* 12**,** e0173854.

BAUTISTA, F., FIORAVANTTI, V., DE ROJAS, T., CARCELLER, F., MADERO, L., LASSALETTA, A. & MORENO, L. 2017a. Medulloblastoma in children and adolescents: a systematic review of contemporary phase I and II clinical trials and biology update. *Cancer medicine,* 6**,** 2606-2624.

BAUTISTA, F., FIORAVANTTI, V., DE ROJAS, T., CARCELLER, F., MADERO, L., LASSALETTA, A. & MORENO, L. 2017b. Medulloblastoma in children and adolescents: a systematic review of contemporary phase I and II clinical trials and biology update. *Cancer Medicine,* 6.

BEAULIEU, M. E., JAUSET, T., MASSO-VALLES, D., MARTINEZ-MARTIN, S., RAHL, P., MALTAIS, L., ZACARIAS-FLUCK, M. F., CASACUBERTA-SERRA, S., SERRANO DEL POZO, E., FIORE, C., FORADADA, L., CANO, V. C., SANCHEZ-HERVAS, M., GUENTHER, M., ROMERO SANZ, E., OTEO, M., TREMBLAY, C., MARTIN, G., LETOURNEAU, D., MONTAGNE, M., MORCILLO ALONSO, M. A., WHITFIELD, J. R., LAVIGNE, P. & SOUCEK, L. 2019. Intrinsic cell-penetrating activity propels Omomyc from proof of concept to viable anti-MYC therapy. *Sci Transl Med,* 11.

BECHER, O. J. 2019. HDAC inhibitors to the rescue in sonic hedgehog medulloblastoma. *Neuro-Oncology,* 21**,** 1091-1092.

BENADA, J. & MACUREK, L. 2015. Targeting the Checkpoint to Kill Cancer Cells. *Biomolecules,* 5**,** 1912-1937.

BERKOFSKY-FESSLER, W., NGUYEN, T. Q., DELMAR, P., MOLNOS, J., KANWAL, C., DEPINTO, W., ROSINSKI, J., MCLOUGHLIN, P., RITLAND, S., DEMARIO, M., TOBON, K., REIDHAAR-OLSON, J. F., RUEGER, R. & HILTON, H. 2009. Preclinical biomarkers for a cyclin-dependent kinase inhibitor translate to candidate pharmacodynamic biomarkers in phase I patients. *Molecular Cancer Therapeutics,* 8**,** 2517-2525.

BERTRAND, K. C., FARIA, C. C., SKOWRON, P., LUCK, A., GARZIA, L., WU, X., AGNIHOTRI, S., SMITH, C. A., TAYLOR, M. D., MACK, S. C. & RUTKA, J. T. 2018. A functional genomics

approach to identify pathways of drug resistance in medulloblastoma. *Acta Neuropathologica Communications,* 6**,** 146.

BHATIA, S., PAVLICK, A. C., BOASBERG, P., THOMPSON, J. A., MULLIGAN, G., PICKARD, M. D., FAESSEL, H., DEZUBE, B. J. & HAMID, O. 2016. A phase I study of the investigational NEDD8-activating enzyme inhibitor pevonedistat (TAK-924/MLN4924) in patients with metastatic melanoma. *Investigational new drugs,* 34**,** 439-449.

BLAKE, D. R., VASEVA, A. V., HODGE, R. G., KLINE, M. P., GILBERT, T. S. K., TYAGI, V., HUANG, D., WHITEN, G. C., LARSON, J. E., WANG, X., PEARCE, K. H., HERRING, L. E., GRAVES, L. M., FRYE, S. V., EMANUELE, M. J., COX, A. D. & DER, C. J. 2019. Application of a MYC degradation screen identifies sensitivity to CDK9 inhibitors in KRAS-mutant pancreatic cancer. *Sci Signal,* 12.

BLANEY, S. M., PHILLIPS, P. C., PACKER, R. J., HEIDEMAN, R. L., BERG, S. L., ADAMSON, P. C., ALLEN, J. C., SALLAN, S. E., JAKACKI, R. I., LANGE, B. J., REAMAN, G. H., HOROWITZ, M. E., POPLACK, D. G. & BALIS, F. M. 1996. Phase II evaluation of topotecan for pediatric central nervous system tumors. *Cancer,* 78**,** 527-31.

BLISS, C. I. 1939. THE TOXICITY OF POISONS APPLIED JOINTLY1. *Annals of Applied Biology,* 26**,** 585-615.

BLOM, T., ROSELLI, A., HÄYRY, V., TYNNINEN, O., WARTIOVAARA, K., KORJA, M., NORDFORS, K., HAAPASALO, H. & NUPPONEN, N. N. 2010. Amplification and overexpression of KIT, PDGFRA, and VEGFR2 in medulloblastomas and primitive neuroectodermal tumors. *Journal of Neuro-Oncology,* 97**,** 217-224.

BLOOM, H. J. G. 1982. Medulloblastoma in Children - Increasing Survival Rates and Further Prospects. *International Journal of Radiation Oncology Biology Physics,* 8**,** 2023-2027.

BLUM, K. A., ABRAMSON, J., MARIS, M., FLINN, I., GOY, A., MERTZ, J., SIMS, R., GARNER, F., SENDEROWICZ, A. & YOUNES, A. 2018. A phase I study of CPI-0610, a bromodomain and extra terminal protein (BET) inhibitor in patients with relapsed or refractory lymphoma. *Annals of Oncology,* 29.

BOLIN, S., BORGENVIK, A., PERSSON, C. U., SUNDSTROM, A., QI, J., BRADNER, J. E., WEISS, W. A., CHO, Y. J., WEISHAUPT, H. & SWARTLING, F. J. 2018. Combined BET bromodomain and CDK2 inhibition in MYC-driven medulloblastoma. *Oncogene,* 37**,** 2850-2862.

BOMGAARS, L. R., BERNSTEIN, M., KRAILO, M., KADOTA, R., DAS, S., CHEN, Z., ADAMSON, P. C. & BLANEY, S. M. 2007. Phase II trial of irinotecan in children with refractory solid tumors: a Children's Oncology Group Study. *J Clin Oncol,* 25**,** 4622-7.

BONDAR, V., ADAMSKI, C., ONUR, T., TAN, Q., WANG, L., DIAZ-GARCIA, J., PARK, J., ORR, H., BOTAS, J. & ZOGHBI, H. 2018. PAK1 regulates ATXN1 levels providing an opportunity to modify its toxicity in Spinocerebellar ataxia type 1. *Human molecular genetics,* 27.

BONGERO, D., PAOLUZZI, L., MARCHI, E., ZULLO, K. M., NEISA, R., MAO, Y., ESCANDON, R., WOOD, K. & O'CONNOR, O. A. 2015. The novel kinesin spindle protein (KSP) inhibitor SB-743921 exhibits marked activity in in vivo and in vitro models of aggressive large B-cell lymphoma. *Leuk Lymphoma,* 56**,** 2945-52.

BOON, K., EDWARDS, J. B., SIU, I. M., OLSCHNER, D., EBERHART, C. G., MARRA, M. A., STRAUSBERG, R. L. & RIGGINS, G. J. 2003. Comparison of medulloblastoma and normal neural transcriptomes identifies a restricted set of activated genes. *Oncogene,* 22**,** 7687-7694.

BOOTH, L., ROBERTS, J. L., CONLEY, A., CRUICKSHANKS, N., RIDDER, T., GRANT, S., POKLEPOVIC, A. & DENT, P. 2014. HDAC inhibitors enhance the lethality of low dose salinomycin in parental and stem-like GBM cells. *Cancer biology & therapy,* 15**,** 305-316.

BOXER, L. M. & DANG, C. V. 2001. Translocations involving c-myc and c-myc function. *Oncogene,* 20**,** 5595-610.

BOYKO, A. N. & BOYKO, O. V. 2018. Cladribine tablets' potential role as a key example of selective immune reconstitution therapy in multiple sclerosis. *Degenerative neurological and neuromuscular disease,* 8**,** 35-44.

BRABETZ, S., LEARY, S. E. S., GRÖBNER, S. N., NAKAMOTO, M. W., ŞEKER-CIN, H., GIRARD, E. J., COLE, B., STRAND, A. D., BLOOM, K. L., HOVESTADT, V., MACK, N. L., PAKIAM, F., SCHWALM, B., KORSHUNOV, A., BALASUBRAMANIAN, G. P., NORTHCOTT, P. A., PEDRO, K. D., DEY, J., HANSEN, S., DITZLER, S., LICHTER, P., CHAVEZ, L., JONES, D. T. W., KOSTER, J., PFISTER, S. M., KOOL, M. & OLSON, J. M. 2018. A biobank of patient-derived pediatric brain tumor models. *Nat Med,* 24**,** 1752-1761.

BRADFORD, S. T. J., RANGHINI, E. J., GRIMLEY, E., LEE, P. H. & DRESSLER, G. R. 2019. High-throughput screens for agonists of bone morphogenetic protein (BMP) signaling identify potent benzoxazole compounds. *The Journal of biological chemistry,* 294**,** 3125-3136.

BRISARD, D., ECKERDT, F., MARSH, L. A., BLYTH, G. T., JAIN, S., CRISTOFANILLI, M., HORIUCHI, D. & PLATANIAS, L. C. 2018. Antineoplastic effects of selective CDK9 inhibition with atuveciclib on cancer stem-like cells in triple-negative breast cancer. *Oncotarget,* 9**,** 37305-37318.

BRUGIÈRES, L., REMENIERAS, A., PIERRON, G., VARLET, P., FORGET, S., BYRDE, V., BOMBLED, J., PUGET, S., CARON, O., DUFOUR, C., DELATTRE, O., PAILLERETS, B. B.-D. & GRILL, J. 2012. High Frequency of Germline SUFU Mutations in Children With Desmoplastic/Nodular Medulloblastoma Younger Than 3 Years of Age. *Journal of Clinical Oncology,* 30**,** 2087-2093.

BRUN, S. N., MARKANT, S. L., ESPARZA, L. A., GARCIA, G., TERRY, D., HUANG, J. M., PAVLYUKOV, M. S., LI, X. N., GRANT, G. A., CRAWFORD, J. R., LEVY, M. L., CONWAY, E. M., SMITH, L. H., NAKANO, I., BEREZOV, A., GREENE, M. I., WANG, Q. & WECHSLER-REYA, R. J. 2015. Survivin as a therapeutic target in Sonic hedgehog-driven medulloblastoma. *Oncogene,* 34**,** 3770-3779.

BUCCI, B., D'AGNANO, I., AMENDOLA, D., CITTI, A., RAZA, G. H., MICELI, R., DE PAULA, U., MARCHESE, R., ALBINI, S., FELSANI, A., BRUNETTI, E. & VECCHIONE, A. 2005. Myc down-regulation sensitizes melanoma cells to radiotherapy by inhibiting MLH1 and MSH2 mismatch repair proteins. *Clin Cancer Res,* 11**,** 2756-67.

BUONAMICI, S., WILLIAMS, J., MORRISSEY, M., WANG, A., GUO, R., VATTAY, A., HSIAO, K., YUAN, J., GREEN, J., OSPINA, B., YU, Q., OSTROM, L., FORDJOUR, P., ANDERSON, D. L., MONAHAN, J. E., KELLEHER, J. F., PEUKERT, S., PAN, S., WU, X., MAIRA, S.-M., GARCÍA-ECHEVERRÍA, C., BRIGGS, K. J., WATKINS, D. N., YAO, Y.-M., LENGAUER, C., WARMUTH, M., SELLERS, W. R. & DORSCH, M. 2010. Interfering with Resistance to Smoothened Antagonists by Inhibition of the PI3K Pathway in Medulloblastoma. *Science Translational Medicine,* 2**,** 51ra70-51ra70.

BURRIS, H. A. 2019. Phase I Study of LY2606368, a Checkpoint Kinase 1 Inhibitor, in Patients With Advanced Cancer (vol 34, pg 1764, 2016). *Journal of Clinical Oncology,* 37**,** 356-356.

CAGE, T. A., CHANTHERY, Y., CHESLER, L., GRIMMER, M., KNIGHT, Z., SHOKAT, K., WEISS, W. A. & GUSTAFSON, W. C. 2015. Downregulation of MYCN through PI3K Inhibition in Mouse Models of Pediatric Neural Cancer. *Frontiers in oncology,* 5**,** 111-111.

CAGNETTA, A., SONCINI, D., CAFFA, I., ACHARYA, C., ACHARYA, P., ADAMIA, S., PIERRI, I., BERGAMASCHI, M., GARUTI, A., ORCIONI, G., PROVENZANI, A., MASTRACCI, L., ZUCAL, C., DAMONTE, G., SALIS, A., PATRONE, F., BALLESTRERO, A., GOBBI, M., MONTECUCCO,

F. & CEA, M. 2015. APO866 Increases Antitumor Activity of Cyclosporin-A by Inducing Mitochondrial and Endoplasmic Reticulum Stress in Leukemia Cells. *Clinical cancer research : an official journal of the American Association for Cancer Research,* 21.

CALABRESE, C., FRANK, A., MACLEAN, K. & GILBERTSON, R. 2003. Medulloblastoma sensitivity to 17-allylamino-17-demethoxygeldanamycin requires MEK/ERKM. *J Biol Chem,* 278**,** 24951-9.

CALABRESE, D. R., CHEN, X., LEON, E. C., GAIKWAD, S. M., PHYO, Z., HEWITT, W. M., ALDEN, S., HILIMIRE, T. A., HE, F., MICHALOWSKI, A. M., SIMMONS, J. K., SAUNDERS, L. B., ZHANG, S. L., CONNORS, D., WALTERS, K. J., MOCK, B. A. & SCHNEEKLOTH, J. S. 2018. Chemical and structural studies provide a mechanistic basis for recognition of the MYC G-quadruplex. *Nature Communications,* 9.

CALAMINUS, G., WEINSPACH, S., TESKE, C. & GOBEL, U. 2007. Quality of survival in children and adolescents after treatment for childhood cancer: the influence of reported late effects on health related quality of life. *Klin Padiatr,* 219**,** 152-7.

CALDERONE, H. M., DUTTA, A., SMITH, L., ECKARDT, A., ZHAO, P. & SHOLLER, G. S. 2014. YM155 Inhibits Neuroblastoma Cell Migration and Survival <i>in Vitro</i> and Tumor Growth and Metastatic Burden in a Pre-Clinical Model. *Journal of Cancer Therapy,* Vol.05No.13**,** 14.

CALZOLARI, A., SAULLE, E., DE ANGELIS, M. L., PASQUINI, L., BOE, A., PELACCHI, F., RICCI-VITIANI, L., BAIOCCHI, M. & TESTA, U. 2014. Salinomycin Potentiates the Cytotoxic Effects of TRAIL on Glioblastoma Cell Lines. *Plos One,* 9.

CAMARA-COSTA, H., RESCH, A., LALANDE, C., KIEFFER, V., POGGI, G., KENNEDY, C., BULL, K., CALAMINUS, G., GRILL, J., DOZ, F., RUTKOWSKI, S., MASSIMINO, M., KORTMANN, R. D., LANNERING, B., DELLATOLAS, G. & CHEVIGNARD, M. 2014. Neuropsychological Outcome of Children Treated for Standard Risk Medulloblastoma in the Hit-Siop Pnet4 European Randomised Controlled Trial of Hyperfractionated (Hfrt) Versus Standard Radiotherapy (Strt) and Maintenance Chemotherapy. *Neuro-Oncology,* 16**,** 78-79.

CAMPAGNE, O., DAVIS, A., MAHARAJ, A. R., ZHONG, B., STRIPAY, J., FARMER, D., ROUSSEL, M. F. & STEWART, C. F. 2020. CNS penetration and pharmacodynamics of the CHK1 inhibitor prexasertib in a mouse Group 3 medulloblastoma model. *European Journal of Pharmaceutical Sciences,* 142**,** 105106.

CAMPANER, S., DONI, M., HYDBRING, P., VERRECCHIA, A., BIANCHI, L., SARDELLA, D., SCHLEKER, T., PERNA, D., TRONNERSJO, S., MURGA, M., FERNANDEZ-CAPETILLO, O., BARBACID, M., LARSSON, L. G. & AMATI, B. 2010. Cdk2 suppresses cellular senescence induced by the c-myc oncogene. *Nature Cell Biology,* 12**,** 54-U132.

CAMPBELL, J., RYAN, C. J., BROUGH, R., BAJRAMI, I., PEMBERTON, H. N., CHONG, I. Y., COSTA-CABRAL, S., FRANKUM, J., GULATI, A., HOLME, H., MILLER, R., POSTEL-VINAY, S., RAFIQ, R., WEI, W., WILLIAMSON, C. T., QUIGLEY, D. A., TYM, J., AL-LAZIKANI, B., FENTON, T., NATRAJAN, R., STRAUSS, S. J., ASHWORTH, A. & LORD, C. J. 2016. Large-Scale Profiling of Kinase Dependencies in Cancer Cell Lines. *Cell reports,* 14**,** 2490-2501.

CAMPBELL, J., RYAN, C. J. & LORD, C. J. 2018. Identifying Genetic Dependencies in Cancer by Analyzing siRNA Screens in Tumor Cell Line Panels. *In:* VON STECHOW, L. (ed.) *Cancer Systems Biology: Methods and Protocols.* New York, NY: Springer New York.

CANELLA, A., WELKER, A. M., YOO, J. Y., XU, J., ABAS, F. S., KESANAKURTI, D., NAGARAJAN, P., BEATTIE, C. E., SULMAN, E. P., LIU, J., GUMIN, J., LANG, F. F., GURCAN, M. N., KAUR, B., SAMPATH, D. & PUDUVALLI, V. K. 2017. Efficacy of Onalespib, a Long-Acting Second-Generation HSP90 Inhibitor, as a Single Agent and in Combination with Temozolomide against Malignant Gliomas. *Clinical cancer research : an official journal of the American Association for Cancer Research,* 23**,** 6215-6226.

CARNEIRO, B. A., KAPLAN, J. B., ALTMAN, J. K., GILES, F. J. & PLATANIAS, L. C. 2015. Targeting mTOR signaling pathways and related negative feedback loops for the treatment of acute myeloid leukemia. *Cancer Biology & Therapy,* 16**,** 648-656.

CAROL, H., GORLICK, R., KOLB, E. A., MORTON, C. L., MANESH, D. M., KEIR, S. T., REYNOLDS, C. P., KANG, M. H., MARIS, J. M., WOZNIAK, A., HICKSON, I., LYALIN, D., KURMASHEVA, R. T., HOUGHTON, P. J., SMITH, M. A. & LOCK, R. 2014. Initial testing (stage 1) of the histone deacetylase inhibitor, quisinostat (JNJ-26481585), by the Pediatric Preclinical Testing Program. *Pediatric blood & cancer,* 61**,** 245-252.

CASEY, S. C., BAYLOT, V. & FELSHER, D. W. 2018. The MYC oncogene is a global regulator of the immune response. *Blood,* 131**,** 2007-2015.

CASEY, S. C., LI, Y., FAN, A. C. & FELSHER, D. W. 2014a. Oncogene withdrawal engages the immune system to induce sustained cancer regression. *Journal for immunotherapy of cancer,* 2**,** 24-24.

CASEY, S. C., LI, Y. & FELSHER, D. W. 2014b. An essential role for the immune system in the mechanism of tumor regression following targeted oncogene inactivation. *Immunologic research,* 58**,** 282-291.

CASEY, S. C., TONG, L., LI, Y., DO, R., WALZ, S., FITZGERALD, K. N., GOUW, A. M., BAYLOT, V., GÜTGEMANN, I., EILERS, M. & FELSHER, D. W. 2016. MYC regulates the antitumor immune response through CD47 and PD-L1. *Science (New York, N.Y.),* 352**,** 227-231.

CASTELL, A. & LARSSON, L. G. 2015. Targeting MYC Translation in Colorectal Cancer. *Cancer Discovery,* 5**,** 701-703.

CASTELL, A., YAN, Q. Z., FAWKNER, K., HYDBRING, P., ZHANG, F., VERSCHUT, V., FRANCO, M., ZAKARIA, S. M., BAZZAR, W., GOODWIN, J., ZINZALLA, G. & LARSSON, L. G. 2018. A selective high affinity MYC-binding compound inhibits MYC: MAX interaction and MYC-dependent tumor cell proliferation. *Scientific Reports,* 8.

CASTRO-GAMERO, A. M., PEZUK, J. A., BRASSESCO, M. S. & TONE, L. G. 2018. G2/M inhibitors as pharmacotherapeutic opportunities for glioblastoma: the old, the new, and the future. *Cancer biology & medicine,* 15**,** 354-374.

CAVALLI, F. M. G., REMKE, M., RAMPASEK, L., PEACOCK, J., SHIH, D. J. H., LUU, B., GARZIA, L., TORCHIA, J., NOR, C., MORRISSY, A. S., AGNIHOTRI, S., THOMPSON, Y. Y., KUZAN-FISCHER, C. M., FAROOQ, H., ISAEV, K., DANIELS, C., CHO, B. K., KIM, S. K., WANG, K. C., LEE, J. Y., GRAJKOWSKA, W. A., PEREK-POLNIK, M., VASILJEVIC, A., FAURE-CONTER, C., JOUVET, A., GIANNINI, C., RAO, A. A. N., LI, K. K. W., NG, H. K., EBERHART, C. G., POLLACK, I. F., HAMILTON, R. L., GILLESPIE, G. Y., OLSON, J. M., LEARY, S., WEISS, W. A., LACH, B., CHAMBLESS, L. B., THOMPSON, R. C., COOPER, M. K., VIBHAKAR, R., HAUSER, P., VAN VEELEN, M. L. C., KROS, J. M., FRENCH, P. J., RA, Y. S., KUMABE, T., LOPEZ-AGUILAR, E., ZITTERBART, K., STERBA, J., FINOCCHIARO, G., MASSIMINO, M., VAN MEIR, E. G., OSUKA, S., SHOFUDA, T., KLEKNER, A., ZOLLO, M., LEONARD, J. R., RUBIN, J. B., JABADO, N., ALBRECHT, S., MORA, J., VAN METER, T. E., JUNG, S., MOORE, A. S., HALLAHAN, A. R., CHAN, J. A., TIRAPELLI, D. P. C., CARLOTTI, C. G., FOULADI, M., PIMENTEL, J., FARIA, C. C., SAAD, A. G., MASSIMI, L., LIAU, L. M., WHEELER, H., NAKAMURA, H., ELBABAA, S. K., PEREZPENA-DIAZCONTI, M., DE LEON, F. C. P., ROBINSON, S., ZAPOTOCKY, M., LASSALETTA, A., HUANG, A., HAWKINS, C. E., TABORI, U., BOUFFET, E., BARTELS, U., DIRKS, P. B., RUTKA, J. T., BADER, G. D., REIMAND, J., GOLDENBERG, A., RAMASWAMY, V. & TAYLOR, M. D. 2017. Intertumoral Heterogeneity within Medulloblastoma Subgroups. *Cancer Cell,* 31**,** 737-+.

CERMELLI, S., JANG, I. S., BERNARD, B. & GRANDORI, C. 2014. Synthetic lethal screens as a means to understand and treat MYC-driven cancers. *Cold Spring Harb Perspect Med,* 4.

CHAITANYA, G. V., STEVEN, A. J. & BABU, P. P. 2010. PARP-1 cleavage fragments: signatures of cell-death proteases in neurodegeneration. *Cell communication and signaling : CCS,* 8**,** 31-31.

CHALHOUB, N. & BAKER, S. J. 2009. PTEN and the PI3-kinase pathway in cancer. *Annual review of pathology,* 4**,** 127-150.

CHAMBERLAIN, M. C., SILVER, P., EDWARDS, M. S. & LEVIN, V. A. 1988. Treatment of extraneural metastatic medulloblastoma with a combination of cyclophosphamide, adriamycin, and vincristine. *Neurosurgery,* 23**,** 476-9.

CHANG, C. H., HOUSEPIAN, E. M. & HERBERT, C., JR. 1969. An operative staging system and a megavoltage radiotherapeutic technic for cerebellar medulloblastomas. *Radiology,* 93**,** 1351-9.

CHATURVEDI, N. K., KLING, M. J., COULTER, D. W., MCGUIRE, T. R., RAY, S., KESHERWANI, V., JOSHI, S. S. & SHARP, J. G. 2018. Improved therapy for medulloblastoma: targeting hedgehog and PI3K-mTOR signaling pathways in combination with chemotherapy. *Oncotarget,* 9**,** 16619-16633.

CHE, H. Y., GUO, H. Y., SI, X. W., YOU, Q. Y. & LOU, W. Y. 2014. PP121, a dual inhibitor of tyrosine and phosphoinositide kinases, inhibits anaplastic thyroid carcinoma cell proliferation and migration. *Tumour Biol,* 35**,** 8659-64.

CHEN, B. J., WU, Y. L., TANAKA, Y. & ZHANG, W. 2014. Small Molecules Targeting c-Myc Oncogene: Promising Anti-Cancer Therapeutics. *International Journal of Biological Sciences,* 10**,** 1084-1096.

CHEN, D., LIN, X., GAO, J., SHEN, L., LI, Z., DONG, B., ZHANG, C. & ZHANG, X. 2018a. Wee1 Inhibitor AZD1775 Combined with Cisplatin Potentiates Anticancer Activity against Gastric Cancer by Increasing DNA Damage and Cell Apoptosis. *BioMed Research International,* 2018**,** 5813292.

CHEN, H., LIU, H. & QING, G. 2018b. Targeting oncogenic Myc as a strategy for cancer treatment. *Signal Transduct Target Ther,* 3**,** 5.

CHEN, R., CHEN, Y. L., FRAME, S., BLAKE, D., WIERDA, W. G., ZHELEVA, D. & PLUNKETT, W. 2018c. Strategic combination of the cyclin-dependent kinase inhibitor CYC065 with venetoclax to target anti-apoptotic proteins in chronic lymphocytic leukemia. *Cancer Research,* 78.

CHEN, Y., SUN, X.-X., SEARS, R. C. & DAI, M.-S. 2019. Writing and erasing MYC ubiquitination and SUMOylation. *Genes & diseases,* 6**,** 359-371.

CHERRY, A. E., HAAS, B. R., NAYDENOV, A. V., FUNG, S., XU, C., SWINNEY, K., WAGENBACH, M., FREELING, J., CANTON, D. A., COY, J., HORNE, E. A., RICKMAN, B., VICENTE, J. J., SCOTT, J. D., HO, R. J. Y., LIGGITT, D., WORDEMAN, L. & STELLA, N. 2016. ST-11: A New Brain-Penetrant Microtubule-Destabilizing Agent with Therapeutic Potential for Glioblastoma Multiforme. *Molecular Cancer Therapeutics,* 15**,** 2018-2029.

CHEVIGNARD, M., CAMARA-COSTA, H., DOZ, F. & DELLATOLAS, G. 2017. Core deficits and quality of survival after childhood medulloblastoma: a review. *Neuro-Oncology Practice,* 4**,** 82-97.

CHIPUMURO, E., MARCO, E., CHRISTENSEN, C. L., KWIATKOWSKI, N., ZHANG, T. H., HATHEWAY, C. M., ABRAHAM, B. J., SHARMA, B., YEUNG, C., ALTABEF, A., PEREZ-ATAYDE, A., WONG, K. K., YUAN, G. C., GRAY, N. S., YOUNG, R. A. & GEORGE, R. E. 2014. CDK7 Inhibition Suppresses Super-Enhancer-Linked Oncogenic Transcription in MYCN-Driven Cancer. *Cell,* 159**,** 1126-1139.

CHOI, S. K., HONG, S. H., KIM, H. S., SHIN, C. Y., NAM, S. W., CHOI, W. S., HAN, J. W. & YOU, J. S. 2016. JQ1, an inhibitor of the epigenetic reader BRD4, suppresses the bidirectional MYC-AP4 axis via multiple mechanisms. *Oncol Rep,* 35**,** 1186-94.

CHONG, I. Y., ARONSON, L., BRYANT, H., GULATI, A., CAMPBELL, J., ELLIOTT, R., PETTITT, S., WILKERSON, P., LAMBROS, M. B., REIS-FILHO, J. S., RAMESSUR, A., DAVIDSON, M., CHAU, I., CUNNINGHAM, D., ASHWORTH, A. & LORD, C. J. 2018. Mapping genetic vulnerabilities reveals BTK as a novel therapeutic target in oesophageal cancer. *Gut,* 67**,** 1780-1792.

CHOU, T.-C. & TALALAY, P. 1983. Analysis of combined drug effects: a new look at a very old problem. *Trends in Pharmacological Sciences,* 4**,** 450-454.

CLARE, R. H., BARDELLE, C., HARPER, P., HONG, W. D., BÖRJESSON, U., JOHNSTON, K. L., COLLIER, M., MYHILL, L., CASSIDY, A., PLANT, D., PLANT, H., CLARK, R., COOK, D. A. N., STEVEN, A., ARCHER, J., MCGILLAN, P., CHAROENSUTTHIVARAKUL, S., BIBBY, J., SHARMA, R., NIXON, G. L., SLATKO, B. E., CANTIN, L., WU, B., TURNER, J., FORD, L., RICH, K., WIGGLESWORTH, M., BERRY, N. G., O'NEILL, P. M., TAYLOR, M. J. & WARD, S. A. 2019. Industrial scale high-throughput screening delivers multiple fast acting macrofilaricides. *Nature Communications,* 10**,** 11.

CLIFFORD, S. C., LUSHER, M. E., LINDSEY, J. C., LANGDON, J. A., GILBERTSON, R. J., STRAUGHTON, D. & ELLISON, D. W. 2006. Wnt/Wingless Pathway Activation and Chromosome 6 Loss Characterise a Distinct Molecular Sub-Group of Medulloblastomas Associated with a Favourable Prognosis. *Cell Cycle,* 5**,** 2666-2670.

CONACCI-SORRELL, M., MCFERRIN, L. & EISENMAN, R. N. 2014. An Overview of MYC and Its Interactome. *Cold Spring Harbor Perspectives in Medicine,* 4.

CONI, S., MANCUSO, A. B., DI MAGNO, L., SDRUSCIA, G., MANNI, S., SERRAO, S. M., ROTILI, D., SPIOMBI, E., BUFALIERI, F., PETRONI, M., KUSIO-KOBIALKA, M., DE SMAELE, E., FERRETTI, E., CAPALBO, C., MAI, A., NIEWIADOMSKI, P., SCREPANTI, I., DI MARCOTULLIO, L. & CANETTIERI, G. 2017. Selective targeting of HDAC1/2 elicits anticancer effects through Gli1 acetylation in preclinical models of SHH Medulloblastoma. *Scientific reports,* 7**,** 44079-44079.

COOK SANGAR, M. L., GENOVESI, L. A., NAKAMOTO, M. W., DAVIS, M. J., KNOBLUAGH, S. E., JI, P., MILLAR, A., WAINWRIGHT, B. J. & OLSON, J. M. 2017. Inhibition of CDK4/6 by Palbociclib Significantly Extends Survival in Medulloblastoma Patient-Derived Xenograft Mouse Models. *Clin Cancer Res,* 23**,** 5802-5813.

COSSET, É., ILMJÄRV, S., DUTOIT, V., ELLIOTT, K., VON SCHALSCHA, T., CAMARGO, M. F., REISS, A., MOROISHI, T., SEGUIN, L., GOMEZ, G., MOO, J.-S., PREYNAT-SEAUVE, O., KRAUSE, K.-H., CHNEIWEISS, H., SARKARIA, J. N., GUAN, K.-L., DIETRICH, P.-Y., WEIS, S. M., MISCHEL, P. S. & CHERESH, D. A. 2017. Glut3 Addiction Is a Druggable Vulnerability for a Molecularly Defined Subpopulation of Glioblastoma. *Cancer cell,* 32**,** 856-868.e5.

COURAPIED, S., CHERIER, J., VIGNERON, A., TROADEC, M.-B., GIRAUD, S., VALO, I., PRIGENT, C., GAMELIN, E., COQUERET, O. & BARRÉ, B. 2010. Regulation of the Aurora-A gene following topoisomerase I inhibition: implication of the Myc transcription factor. *Molecular cancer,* 9**,** 205-205.

COWLEY, G. S., WEIR, B. A., VAZQUEZ, F., TAMAYO, P., SCOTT, J. A., RUSIN, S., EAST-SELETSKY, A., ALI, L. D., GERATH, W. F. J., PANTEL, S. E., LIZOTTE, P. H., JIANG, G., HSIAO, J., TSHERNIAK, A., DWINELL, E., AOYAMA, S., OKAMOTO, M., HARRINGTON, W., GELFAND, E., GREEN, T. M., TOMKO, M. J., GOPAL, S., WONG, T. C., LI, H., HOWELL, S., STRANSKY, N., LIEFELD, T., JANG, D., BISTLINE, J., HILL MEYERS, B., ARMSTRONG, S. A., ANDERSON, K. C., STEGMAIER, K., REICH, M., PELLMAN, D., BOEHM, J. S., MESIROV, J. P., GOLUB, T. R., ROOT, D. E. & HAHN, W. C. 2014. Parallel genome-scale loss of function screens in 216 cancer cell lines for the identification of context-specific genetic dependencies. *Scientific Data,* 1**,** 140035.

CREUTZIG, U., ZIMMERMANN, M., BOURQUIN, J. P., DWORZAK, M. N., FLEISCHHACK, G., GRAF, N., KLINGEBIEL, T., KREMENS, B., LEHRNBECHER, T., VON NEUHOFF, C., RITTER, J., SANDER, A., SCHRAUDER, A., VON STACKELBERG, A., STARÝ, J. & REINHARDT, D. 2013. Randomized trial comparing liposomal daunorubicin with idarubicin as induction for pediatric acute myeloid leukemia: results from Study AML-BFM 2004. *Blood,* 122**,** 37-43.

CROWTHER, A. J., OCASIO, J. K., FANG, F., MEIDINGER, J., WU, J., DEAL, A. M., CHANG, S. X., YUAN, H., SCHMID, R., DAVIS, I. & GERSHON, T. R. 2016. Radiation Sensitivity in a Preclinical Mouse Model of Medulloblastoma Relies on the Function of the Intrinsic Apoptotic Pathway. *Cancer research,* 76**,** 3211-3223.

CRUK 2016.

ĆWIEK, P., LENI, Z., SALM, F., DIMITROVA, V., STYP-REKOWSKA, B., CHIRIANO, G., CARROLL, M., HÖLAND, K., DJONOV, V., SCAPOZZA, L., GUIRY, P. & ARCARO, A. 2015. RNA interference screening identifies a novel role for PCTK1/CDK16 in medulloblastoma with c-Myc amplification. *Oncotarget,* 6**,** 116-129.

CZAPLINSKI, S., HUGLE, M., STIEHL, V. & FULDA, S. 2016. Polo-like kinase 1 inhibition sensitizes neuroblastoma cells for vinca alkaloid-induced apoptosis. *Oncotarget,* 7**,** 8700-8711.

DAI, Y. & GRANT, S. 2010. New insights into checkpoint kinase 1 in the DNA damage response signaling network. *Clin Cancer Res,* 16**,** 376-83.

DAMMERT, M. A., BRÄGELMANN, J., OLSEN, R. R., BÖHM, S., MONHASERY, N., WHITNEY, C. P., CHALISHAZAR, M. D., TUMBRINK, H. L., GUTHRIE, M. R., KLEIN, S., IRELAND, A. S., RYAN, J., SCHMITT, A., MARX, A., OZRETIĆ, L., CASTIGLIONE, R., LORENZ, C., JACHIMOWICZ, R. D., WOLF, E., THOMAS, R. K., POIRIER, J. T., BÜTTNER, R., SEN, T., BYERS, L. A., REINHARDT, H. C., LETAI, A., OLIVER, T. G. & SOS, M. L. 2019. MYC paralog-dependent apoptotic priming orchestrates a spectrum of vulnerabilities in small cell lung cancer. *Nature Communications,* 10**,** 3485.

DANG, C. V. 1999. c-Myc target genes involved in cell growth, apoptosis, and metabolism. *Mol Cell Biol,* 19**,** 1-11.

DANG, C. V. 2012. MYC on the path to cancer. *Cell,* 149**,** 22-35.

DANG, C. V., O'DONNELL, K. A., ZELLER, K. I., NGUYEN, T., OSTHUS, R. C. & LI, F. 2006. The c-Myc target gene network. *Semin Cancer Biol,* 16**,** 253-64.

DAS, T., PANDA, D., SAHA, P. & DASH, J. 2018. Small Molecule Driven Stabilization of Promoter G-Quadruplexes and Transcriptional Regulation of c-MYC. *Bioconjugate Chemistry,* 29**,** 2636-2645.

DASARI, V. R., ASUTHKAR, S., NALLA, A. K. & RAO, J. S. 2013. Abstract 1731: Decreased cyclin B1 expression contributes to mitochondrial apoptosis in medulloblastoma. *Cancer Research,* 73**,** 1731-1731.

DAUCH, D., RUDALSKA, R., COSSA, G., NAULT, J.-C., KANG, T.-W., WUESTEFELD, T., HOHMEYER, A., IMBEAUD, S., YEVSA, T., HOENICKE, L., PANTSAR, T., BOZKO, P., MALEK, N. P., LONGERICH, T., LAUFER, S., POSO, A., ZUCMAN-ROSSI, J., EILERS, M. & ZENDER, L. 2016. A MYC–aurora kinase A protein complex represents an actionable drug target in p53-altered liver cancer. *Nature Medicine,* 22**,** 744-753.

DEAN, M., FOJO, T. & BATES, S. 2005. Tumour stem cells and drug resistance. *Nature Reviews Cancer,* 5**,** 275-284.

DELEHOUZÉ, C., GODL, K., LOAËC, N., BRUYÈRE, C., DESBAN, N., OUMATA, N., GALONS, H., ROUMELIOTIS, T. I., GIANNOPOULOU, E. G., GRENET, J., TWITCHELL, D., LAHTI, J., MOUCHET, N., GALIBERT, M. D., GARBIS, S. D. & MEIJER, L. 2014. CDK/CK1 inhibitors roscovitine and CR8 downregulate amplified MYCN in neuroblastoma cells. *Oncogene,* 33**,** 5675-5687.

DELMORE, J. E., ISSA, G. C., LEMIEUX, M. E., RAHL, P. B., SHI, J., JACOBS, H. M., KASTRITIS, E., GILPATRICK, T., PARANAL, R. M., QI, J., CHESI, M., SCHINZEL, A. C., MCKEOWN, M. R., HEFFERNAN, T. P., VAKOC, C. R., BERGSAGEL, P. L., GHOBRIAL, I. M., RICHARDSON, P. G., YOUNG, R. A., HAHN, W. C., ANDERSON, K. C., KUNG, A. L., BRADNER, J. E. & MITSIADES, C. S. 2011. BET bromodomain inhibition as a therapeutic strategy to target c-Myc. *Cell,* 146**,** 904-17.

DEN HOLLANDER, J., RIMPI, S., DOHERTY, J. R., RUDELIUS, M., BUCK, A., HOELLEIN, A., KREMER, M., GRAF, N., SCHEERER, M., HALL, M. A., GOGA, A., VON BUBNOFF, N., DUYSTER, J., PESCHEL, C., CLEVELAND, J. L., NILSSON, J. A. & KELLER, U. 2010. Aurora kinases A and B are up-regulated by Myc and are essential for maintenance of the malignant state. *Blood,* 116**,** 1498-505.

DENG, J. & MOU, F. 2018. CDK inhibitor BMS-265246 induces cell cycle arrest and apoptosis of liver cancer cells in vitro. *Tumor,* 38**,** 189-195 and 214.

DEPINTO, W., CHU, X.-J., YIN, X., SMITH, M., PACKMAN, K., GOELZER, P., LOVEY, A., CHEN, Y., QIAN, H., HAMID, R., XIANG, Q., TOVAR, C., BLAIN, R., NEVINS, T., HIGGINS, B., LUISTRO, L., KOLINSKY, K., FELIX, B., HUSSAIN, S. & HEIMBROOK, D. 2006. In vitro and in vivo activity of R547: a potent and selective cyclin-dependent kinase inhibitor currently in phase I clinical trials. *Molecular Cancer Therapeutics,* 5**,** 2644-2658.

DEUTSCH, M., THOMAS, P. R. M., KRISCHER, J., BOYETT, J. M., ALBRIGHT, L., ARONIN, P., LANGSTON, J., ALLEN, J. C., PACKER, R. J., LINGGOOD, R., MULHERN, R., STANLEY, P., STEHBENS, J. A., DUFFNER, P., KUN, L., RORKE, L., CHERLOW, J., FREIDMAN, H., FINLAY, J. L. & VIETTI, T. 1996. Results of a prospective randomized trial comparing standard dose neuraxis irradiation (3,600cGy/2O) with reduced neuraxis irradiation (2,340cGy/13) in patients with low-stage medulloblastoma - A combined Children's Cancer Group Pediatric Oncology Group Study. *Pediatric Neurosurgery,* 24**,** 167-176.

DEWANGAN, J., SRIVASTAVA, S. & RATH, S. K. 2017. Salinomycin: A new paradigm in cancer therapy. *Tumour Biol,* 39**,** 1010428317695035.

DEY, N., LEYLAND-JONES, B. & DE, P. 2015. MYC-xing it up with PIK3CA mutation and resistance to PI3K inhibitors: summit of two giants in breast cancers. *Am J Cancer Res,* 5**,** 1-19.

DHALL, G., GRODMAN, H., JI, L. Y., SANDS, S., GARDNER, S., DUNKEL, I. J., MCCOWAGE, G. B., DIEZ, B., ALLEN, J. C., GOPALAN, A., CORNELIUS, A. S., TERMUHLEN, A., ABROMOWITCH, M., SPOSTO, R. & FINLAY, J. L. 2008. Outcome of children less than three years old at diagnosis with non-metastatic medulloblastoma treated with chemotherapy on the "Head Start" I and II protocols. *Pediatric Blood & Cancer,* 50**,** 1169-1175.

DHINGRA, K., FRYE, D., NEWMAN, R. A., WALTERS, R., THERIAULT, R., FRASCHINI, G., SMITH, T., BUZDAR, A. & HORTOBAGYI, G. N. 1995. Phase II clinical and pharmacological study of pirarubicin in combination with 5-fluorouracil and cyclophosphamide in metastatic breast cancer. *Clin Cancer Res,* 1**,** 691-7.

DIAZ, R. J., GOLBOURN, B., FARIA, C., PICARD, D., SHIH, D., RAYNAUD, D., LEADLY, M., MACKENZIE, D., BRYANT, M., BEBENEK, M., SMITH, C. A., TAYLOR, M. D., HUANG, A. & RUTKA, J. T. 2015. Mechanism of action and therapeutic efficacy of Aurora kinase B inhibition in MYC overexpressing medulloblastoma. *Oncotarget,* 6**,** 3359-74.

DOBBELSTEIN, M. & SORENSEN, C. S. 2015. Exploiting replicative stress to treat cancer. *Nat Rev Drug Discov,* 14**,** 405-23.

DOLMAN, M. E. M., POON, E., EBUS, M. E., DEN HARTOG, I. J. M., VAN NOESEL, C. J. M., JAMIN, Y., HALLSWORTH, A., ROBINSON, S. P., PETRIE, K., SPARIDANS, R. W., KOK, R. J., VERSTEEG, R., CARON, H. N., CHESLER, L. & MOLENAAR, J. J. 2015. Cyclin-Dependent

Kinase Inhibitor AT7519 as a Potential Drug for MYCN-Dependent Neuroblastoma. *Clinical Cancer Research,* 21**,** 5100-5109.

DOMINGUEZ-SOLA, D. & GAUTIER, J. 2014. MYC and the Control of DNA Replication. *Cold Spring Harbor Perspectives in Medicine,* 4.

DONATI, B., LORENZINI, E. & CIARROCCHI, A. 2018. BRD4 and Cancer: going beyond transcriptional regulation. *Molecular Cancer,* 17**,** 164.

DONG, J., EZHILARASAN, R., WU, S., SULMAN, E. & DE GROOT, J. 2015. Aurora kinase B inhibitor AT9283 enhanced radiation therapy in Glioblastoma. *Neuro-Oncology,* 17**,** v22-v22.

DONG, X., HU, X., CHEN, J., HU, D. & CHEN, L. F. 2018. BRD4 regulates cellular senescence in gastric cancer cells via E2F/miR-106b/p21 axis. *Cell Death Dis,* 9**,** 203.

DOUSSOUKI, M., GAJJAR, A. & CHAMDINE, O. 2019. Molecular genetics of medulloblastoma in children: Diagnostic, therapeutic and prognostic implications. *Future Neurology,* 14.

DREYER, Z. E., KADOTA, R. P., STEWART, C. F., FRIEDMAN, H. S., MAHONEY, D. H., KUN, L. E., MCCLUGGAGE, C. W., BURGER, P. C., KEPNER, J. & HEIDEMAN, R. L. 2003a. Phase 2 study of idarubicin in pediatric brain tumors: Pediatric Oncology Group study POG 9237. *Neuro-Oncology,* 5**,** 261-267.

DREYER, Z. E., KADOTA, R. P., STEWART, C. F., FRIEDMAN, H. S., MAHONEY, D. H., KUN, L. E., MCCLUGGAGE, C. W., BURGER, P. C., KEPNER, J., HEIDEMAN, R. L. & PEDIATRIC ONCOLOGY, G. 2003b. Phase 2 study of idarubicin in pediatric brain tumors: Pediatric Oncology Group study POG 9237. *Neuro-oncology,* 5**,** 261-267.

ECKER, J., OEHME, I., MAZITSCHEK, R., KORSHUNOV, A., KOOL, M., HIELSCHER, T., KISS, J., SELT, F., KONRAD, C., LODRINI, M., DEUBZER, H. E., VON DEIMLING, A., KULOZIK, A. E., PFISTER, S. M., WITT, O. & MILDE, T. 2015. Targeting class I histone deacetylase 2 in MYC amplified group 3 medulloblastoma. *Acta neuropathologica communications,* 3**,** 22-22.

ECKERDT, F., CLYMER, J., BELL, J. B., BEAUCHAMP, E. M., BLYTH, G. T., GOLDMAN, S. & PLATANIAS, L. C. 2019. Pharmacological mTOR targeting enhances the antineoplastic effects of selective PI3Kalpha inhibition in medulloblastoma. *Sci Rep,* 9**,** 12822.

ECKSCHLAGER, T., PLCH, J., STIBOROVA, M. & HRABETA, J. 2017. Histone Deacetylase Inhibitors as Anticancer Drugs. *International journal of molecular sciences,* 18**,** 1414.

EDELSTEIN, K., SPIEGLER, B. J., FUNG, S., PANZARELLA, T., MABBOTT, D. J., JEWITT, N., D'AGOSTINO, N. M., MASON, W. P., BOUFFET, E., TABORI, U., LAPERRIERE, N. & HODGSON, D. C. 2011. Early aging in adult survivors of childhood medulloblastoma: long-term neurocognitive, functional, and physical outcomes. *Neuro Oncol,* 13**,** 536-45.

EISCHEN, C. M., WOO, D., ROUSSEL, M. F. & CLEVELAND, J. L. 2001. Apoptosis triggered by Myc-induced suppression of Bcl-X(L) or Bcl-2 is bypassed during lymphomagenesis. *Mol Cell Biol,* 21**,** 5063-70.

ELLISON, D. W. 2010. Childhood medulloblastoma: novel approaches to the classification of a heterogeneous disease. *Acta Neuropathologica,* 120**,** 305-316.

ELLISON, D. W., DALTON, J., KOCAK, M., NICHOLSON, S. L., FRAGA, C., NEALE, G., KENNEY, A. M., BRAT, D. J., PERRY, A., YONG, W. H., TAYLOR, R. E., BAILEY, S., CLIFFORD, S. C. & GILBERTSON, R. J. 2011. Medulloblastoma: clinicopathological correlates of SHH, WNT, and non-SHH/WNT molecular subgroups. *Acta neuropathologica,* 121**,** 381-396.

EMANUEL, S. L., HUGHES, T. V., ADAMS, M., RUGG, C. A., FUENTES-PESQUERA, A., CONNOLLY, P. J., PANDEY, N., MORENO-MAZZA, S., BUTLER, J., BOROWSKI, V., MIDDLETON, S. A., GRUNINGER, R. H., STORY, J. R., NAPIER, C., HOLLISTER, B. & GREENBERGER, L. M. 2008. Cellular and in Vivo Activity of JNJ-28871063, A Nonquinazoline Pan-ErbB Kinase

Inhibitor That Crosses the Blood-Brain Barrier and Displays Efficacy against Intracranial Tumors. *Molecular Pharmacology,* 73**,** 338-348.

ENDERSBY, R., HII, H., STROWGER, B., DYER, P., HOWLETT, M., KUCHIBHOTLA, M. & GOTTARDO, N. 2018. MBRS-35. COMBINING Chk1/2 INHIBITION WITH RADIATION ENHANCES IN VITRO AND IN VIVO CYTOTOXICITY IN MEDULLOBLASTOMA. *Neuro-Oncology,* 20**,** i135-i136.

ENTZEROTH, M., FLOTOW, H. & CONDRON, P. 2009. Overview of high-throughput screening. *Curr Protoc Pharmacol,* Chapter 9**,** Unit 9 4.

EVANS, A. E., JENKIN, R. D. T., SPOSTO, R., ORTEGA, J. A., WILSON, C. B., WARA, W., ERTEL, I. J., KRAMER, S., CHANG, C. H., LEIKIN, S. L. & HAMMOND, G. D. 1990. The Treatment of Medulloblastoma - Results of a Prospective Randomized Trial of Radiation-Therapy with and without Ccnu, Vincristine, and Prednisone. *Journal of Neurosurgery,* 72**,** 572-582.

FALLAHI-SICHANI, M., HONARNEJAD, S., HEISER, L. M., GRAY, J. W. & SORGER, P. K. 2014. Metrics other than potency reveal systematic variation in responses to cancer drugs. *Cancer Research,* 74.

FAN, Y. H., CHENG, J., VASUDEVAN, S. A., DOU, J., ZHANG, H., PATEL, R. H., MA, I. T., ROJAS, Y., ZHAO, Y., YU, Y., ZHANG, H., SHOHET, J. M., NUCHTERN, J. G., KIM, E. S. & YANG, J. 2013. USP7 inhibitor P22077 inhibits neuroblastoma growth via inducing p53-mediated apoptosis. *Cell death & disease,* 4**,** e867-e867.

FARIA, C. C., AGNIHOTRI, S., MACK, S. C., GOLBOURN, B. J., DIAZ, R. J., OLSEN, S., BRYANT, M., BEBENEK, M., WANG, X., BERTRAND, K. C., KUSHIDA, M., HEAD, R., CLARK, I., DIRKS, P., SMITH, C. A., TAYLOR, M. D. & RUTKA, J. T. 2015. Identification of alsterpaullone as a novel small molecule inhibitor to target group 3 medulloblastoma. *Oncotarget,* 6**,** 21718-21729.

FEDERICO, M., SYMONDS, C. E., BAGELLA, L., RIZZOLIO, F., FANALE, D., RUSSO, A. & GIORDANO, A. 2010. R-Roscovitine (Seliciclib) prevents DNA damage-induced cyclin A1 upregulation and hinders non-homologous end-joining (NHEJ) DNA repair. *Molecular Cancer,* 9**,** 208.

FELGENHAUER, J., TOMINO, L., SELICH-ANDERSON, J., BOPP, E. & SHAH, N. 2018. Dual BRD4 and AURKA Inhibition Is Synergistic against MYCN-Amplified and Nonamplified Neuroblastoma. *Neoplasia (New York, N.Y.),* 20**,** 965-974.

FELSHER, D. W. 2010. MYC Inactivation Elicits Oncogene Addiction through Both Tumor Cell-Intrinsic and Host-Dependent Mechanisms. *Genes & cancer,* 1**,** 597-604.

FELSHER, D. W. & BISHOP, J. M. 1999. Transient excess of MYC activity can elicit genomic instability and tumorigenesis. *Proceedings of the National Academy of Sciences of the United States of America,* 96**,** 3940-3944.

FERNANDEZ, P. C., FRANK, S. R., WANG, L. Q., SCHROEDER, M., LIU, S. X., GREENE, J., COCITO, A. & AMATI, B. 2003. Genomic targets of the human c-Myc protein. *Genes & Development,* 17**,** 1115-1129.

FERRAO, P. T., BUKCZYNSKA, E. P., JOHNSTONE, R. W. & MCARTHUR, G. A. 2012. Efficacy of CHK inhibitors as single agents in MYC-driven lymphoma cells. *Oncogene,* 31**,** 1661-1672.

FLOREA, V., BHAGAVATULA, N., SIMOVIC, G., MACEDO, F. Y., FOCK, R. A. & RODRIGUES, C. O. 2013. c-Myc is essential to prevent endothelial pro-inflammatory senescent phenotype. *PLoS One,* 8**,** e73146.

FLORENCE, B. & FALLER, D. V. 2001. You bet-cha: a novel family of transcriptional regulators. *Front Biosci,* 6**,** D1008-18.

FORTIN, D. 2012. The blood-brain barrier: its influence in the treatment of brain tumors metastases. *Curr Cancer Drug Targets,* 12**,** 247-59.

FOUCQUIER, J. & GUEDJ, M. 2015. Analysis of drug combinations: current methodological landscape. *Pharmacology Research & Perspectives,* 3**,** e00149.

FOULADI, M., NICHOLSON, H. S., ZHOU, T., LANINGHAM, F., HELTON, K. J., HOLMES, E., COHEN, K., SPEIGHTS, R. A., WRIGHT, J. & POLLACK, I. F. 2007. A phase II study of the farnesyl transferase inhibitor, tipifarnib, in children with recurrent or progressive high-grade glioma, medulloblastoma/primitive neuroectodermal tumor, or brainstem glioma: A children's oncology group study. *Cancer,* 110**,** 2535-2541.

FOWLER, T., SEN, R. & ROY, A. L. 2011. Regulation of primary response genes. *Mol Cell,* 44**,** 348-60.

FRANGE, P., ALAPETITE, C., GABORIAUD, G., BOURS, D., ZUCKER, J. M., ZERAH, M., BRISSE, H., CHEVIGNARD, M., MOSSERI, V., BOUFFET, E. & DOZ, F. 2009. From childhood to adulthood: long-term outcome of medulloblastoma patients. The Institut Curie experience (1980-2000). *Journal of Neuro-Oncology,* 95**,** 271-279.

FRANK, S. B., SCHULZ, V. V. & MIRANTI, C. K. 2017. A streamlined method for the design and cloning of shRNAs into an optimized Dox-inducible lentiviral vector. *Bmc Biotechnology,* 17.

FRANKEN, N. A., RODERMOND, H. M., STAP, J., HAVEMAN, J. & VAN BREE, C. 2006. Clonogenic assay of cells in vitro. *Nat Protoc,* 1**,** 2315-9.

FRANOVIC, A., ELLIOTT, K. C., SEGUIN, L., CAMARGO, M. F., WEIS, S. M. & CHERESH, D. A. 2015. Glioblastomas require integrin αvβ3/PAK4 signaling to escape senescence. *Cancer research,* 75**,** 4466-4473.

FRASSON, C., RAMPAZZO, E., ACCORDI, B., BEGGIO, G., PISTOLLATO, F., BASSO, G. & PERSANO, L. 2015. Inhibition of PI3K Signalling Selectively Affects Medulloblastoma Cancer Stem Cells. *Biomed Res Int,* 2015**,** 973912.

FUJISE, K., ZHANG, D., LIU, J. & YEH, E. T. 2000. Regulation of apoptosis and cell cycle progression by MCL1. Differential role of proliferating cell nuclear antigen. *J Biol Chem,* 275**,** 39458-65.

GABAY, M., LI, Y. L. & FELSHER, D. W. 2014. MYC Activation Is a Hallmark of Cancer Initiation and Maintenance. *Cold Spring Harbor Perspectives in Medicine,* 4.

GADHIKAR, M. A., SCIUTO, M. R., ALVES, M. V. O., PICKERING, C. R., OSMAN, A. A., NESKEY, D. M., ZHAO, M., FITZGERALD, A. L., MYERS, J. N. & FREDERICK, M. J. 2013. Chk1/2 inhibition overcomes the cisplatin resistance of head and neck cancer cells secondary to the loss of functional p53. *Molecular cancer therapeutics,* 12**,** 1860-1873.

GAJJAR, A., BOWERS, D. C., KARAJANNIS, M. A., LEARY, S., WITT, H. & GOTTARDO, N. G. 2015. Pediatric Brain Tumors: Innovative Genomic Information Is Transforming the Diagnostic and Clinical Landscape. *J Clin Oncol,* 33**,** 2986-98.

GAJJAR, A., CHINTAGUMPALA, M., ASHLEY, D., KELLIE, S., KUN, L. E., MERCHANT, T. E., WOO, S., WHEELER, G., AHERN, V., KRASIN, M. J., FOULADI, M., BRONISCER, A., KRANCE, R., HALE, G. A., STEWART, C. F., DAUSER, R., SANFORD, R. A., FULLER, C., LAU, C., BOYETT, J. M., WALLACE, D. & GILBERTSON, R. J. 2006. Risk-adapted craniospinal radiotherapy followed by high-dose chemotherapy and stem-cell rescue in children with newly diagnosed medulloblastoma (St Jude Medulloblastoma-96): long-term results from a prospective, multicentre trial. *Lancet Oncology,* 7**,** 813-820.

GAJJAR, A., SANFORD, R. A., BHARGAVA, R., HEIDEMAN, R., WALTER, A., LI, Y. L., LANGSTON, J. W., JENKINS, J. J., MUHLBAUER, M., BOYETT, J. & KUN, L. E. 1996. Medulloblastoma with brain stem involvement: The impact of gross total resection on outcome. *Pediatric Neurosurgery,* 25**,** 182-187.

GAJJAR, A., STEWART, C. F., ELLISON, D. W., KASTE, S., KUN, L. E., PACKER, R. J., GOLDMAN, S., CHINTAGUMPALA, M., WALLACE, D., TAKEBE, N., BOYETT, J. M., GILBERTSON, R. J. & CURRAN, T. 2013. Phase I study of vismodegib in children with recurrent or refractory medulloblastoma: a pediatric brain tumor consortium study. *Clinical cancer research : an official journal of the American Association for Cancer Research,* 19**,** 6305-6312.

GAJJAR, A. J. & ROBINSON, G. W. 2014. Medulloblastoma—translating discoveries from the bench to the bedside. *Nature Reviews Clinical Oncology,* 11**,** 714-722.

GANDOLA, L., MASSIMINO, M., CEFALO, G., SOLERO, C., SPREAFICO, F., PECORI, E., RIVA, D., COLLINI, P., PIGNOLI, E., GIANGASPERO, F., LUKSCH, R., BERRETTA, S., POGGI, G., BIASSONI, V., FERRARI, A., POLLO, B., FAVRE, C., SARDI, I., TERENZIANI, M. & FOSSATI-BELLANI, F. 2009. Hyperfractionated Accelerated Radiotherapy in the Milan Strategy for Metastatic Medulloblastoma. *Journal of Clinical Oncology,* 27**,** 566-571.

GANUZA, M., SAIZ-LADERA, C., CANAMERO, M., GOMEZ, G., SCHNEIDER, R., BLASCO, M. A., PISANO, D., PARAMIO, J. M., SANTAMARIA, D. & BARBACID, M. 2012. Genetic inactivation of Cdk7 leads to cell cycle arrest and induces premature aging due to adult stem cell exhaustion. *Embo Journal,* 31**,** 2498-2510.

GARCIA-CUELLAR, M. P., FULLER, E., MATHNER, E., BREITINGER, C., HETZNER, K., ZEITLMANN, L., BORKHARDT, A. & SLANY, R. K. 2014. Efficacy of cyclin-dependent-kinase 9 inhibitors in a murine model of mixed-lineage leukemia. *Leukemia,* 28**,** 1427-1435.

GARCIA-GUTIERREZ, L., DELGADO, M. D. & LEON, J. 2019. MYC Oncogene Contributions to Release of Cell Cycle Brakes. *Genes (Basel),* 10.

GARRETT, M. D. & COLLINS, I. 2011. Anticancer therapy with checkpoint inhibitors: what, where and when? *Trends Pharmacol Sci,* 32**,** 308-16.

GARRIGA, J., BHATTACHARYA, S., CALBÓ, J., MARSHALL, R. M., TRUONGCAO, M., HAINES, D. S. & GRAÑA, X. 2003. CDK9 is constitutively expressed throughout the cell cycle, and its steady-state expression is independent of SKP2. *Molecular and cellular biology,* 23**,** 5165-5173.

GERBER, N. U., MYNAREK, M., VON HOFF, K., FRIEDRICH, C., RESCH, A. & RUTKOWSKI, S. 2014. Recent developments and current concepts in medulloblastoma. *Cancer Treatment Reviews,* 40**,** 356-365.

GERLACH, D., TONTSCH-GRUNT, U., BAUM, A., POPOW, J., SCHARN, D., HOFMANN, M. H., ENGELHARDT, H., KAYA, O., BECK, J., SCHWEIFER, N., GERSTBERGER, T., ZUBER, J., SAVARESE, F. & KRAUT, N. 2018. The novel BET bromodomain inhibitor BI 894999 represses super-enhancer-associated transcription and synergizes with CDK9 inhibition in AML. *Oncogene,* 37**,** 2687-2701.

GERON, L., BORGES, K. S., ANDRADE, A. F., SUAZO, V. K., SCRIDELI, C. A. & TONE, L. G. 2015. Antitumour activity of AMG 900 alone or in combination with histone deacetylase inhibitor SaHa on medulloblastoma cell lines. *Neurol Res,* 37**,** 703-11.

GHELLI LUSERNA DI RORÀ, A., IACOBUCCI, I., IMBROGNO, E., PAPAYANNIDIS, C., DERENZINI, E., FERRARI, A., GUADAGNUOLO, V., ROBUSTELLI, V., PARISI, S., SARTOR, C., ABBENANTE, M. C., PAOLINI, S. & MARTINELLI, G. 2016. Prexasertib, a Chk1/Chk2 inhibitor, increases the effectiveness of conventional therapy in B-/T- cell progenitor acute lymphoblastic leukemia. *Oncotarget,* 7**,** 53377-53391.

GILBERTSON, R. J. & ELLISON, D. W. 2008. The origins of medulloblastoma subtypes. *Annual Review of Pathology-Mechanisms of Disease,* 3**,** 341-365.

GIMSING, P., HANSEN, M., KNUDSEN, L., KNOBLAUCH, P., CHRISTENSEN, I., OOI, C. & JENSEN, P. 2008. A phase I clinical trial of the histone deacetylase inhibitor belinostat in patients with advanced hematological neoplasia. *European journal of haematology,* 81**,** 170-6.

GIRARD, E., DITZLER, S., LEE, D., RICHARDS, A., YAGLE, K., PARK, J., ESLAMY, H., BOBILEV, D., VRIGNAUD, P. & OLSON, J. 2015. Efficacy of cabazitaxel in mouse models of pediatric brain tumors. *Neuro Oncol,* 17**,** 107-15.

GOODRICH, L. V., MILENKOVIĆ, L., HIGGINS, K. M. & SCOTT, M. P. 1997. Altered neural cell fates and medulloblastoma in mouse patched mutants. *Science,* 277**,** 1109-13.

GORLICK, R., KOLB, E., KEIR, S., MARIS, J., REYNOLDS, C., KANG, M., CAROL, H., LOCK, R., BILLUPS, C., KURMASHEVA, R., HOUGHTON, P. & SMITH, M. 2014a. Initial Testing (Stage 1) of the Polo-Like Kinase Inhibitor Volasertib (BI 6727), by the Pediatric Preclinical Testing Program. *Pediatric blood & cancer,* 61.

GORLICK, R., KOLB, E. A., HOUGHTON, P. J., MORTON, C. L., NEALE, G., KEIR, S. T., CAROL, H., LOCK, R., PHELPS, D., KANG, M. H., REYNOLDS, C. P., MARIS, J. M., BILLUPS, C. & SMITH, M. A. 2012. Initial testing (stage 1) of the cyclin dependent kinase inhibitor SCH 727965 (dinaciclib) by the pediatric preclinical testing program. *Pediatric blood & cancer,* 59**,** 1266-1274.

GORLICK, R., KOLB, E. A., KEIR, S. T., MARIS, J. M., REYNOLDS, C. P., KANG, M. H., CAROL, H., LOCK, R., BILLUPS, C. A., KURMASHEVA, R. T., HOUGHTON, P. J. & SMITH, M. A. 2014b. Initial testing (stage 1) of the Polo-like kinase inhibitor volasertib (BI 6727), by the Pediatric Preclinical Testing Program. *Pediatric blood & cancer,* 61**,** 158-164.

GOTTARDO, N. G. & GAJJAR, A. 2006. Current therapy for medulloblastoma. *Curr Treat Options Neurol,* 8**,** 319-34.

GOTTARDO, N. G., HANSFORD, J. R., MCGLADE, J. P., ALVARO, F., ASHLEY, D. M., BAILEY, S., BAKER, D. L., BOURDEAUT, F., CHO, Y. J., CLAY, M., CLIFFORD, S. C., COHN, R. J., COLE, C. H., DALLAS, P. B., DOWNIE, P., DOZ, F., ELLISON, D. W., ENDERSBY, R., FISHER, P. G., HASSALL, T., HEATH, J. A., HII, H. L., JONES, D. T., JUNCKERSTORFF, R., KELLIE, S., KOOL, M., KOTECHA, R. S., LICHTER, P., LAUGHTON, S. J., LEE, S., MCCOWAGE, G., NORTHCOTT, P. A., OLSON, J. M., PACKER, R. J., PFISTER, S. M., PIETSCH, T., PIZER, B., POMEROY, S. L., REMKE, M., ROBINSON, G. W., RUTKOWSKI, S., SCHOEP, T., SHELAT, A. A., STEWART, C. F., SULLIVAN, M., TAYLOR, M. D., WAINWRIGHT, B., WALWYN, T., WEISS, W. A., WILLIAMSON, D. & GAJJAR, A. 2014. Medulloblastoma Down Under 2013: a report from the third annual meeting of the International Medulloblastoma Working Group. *Acta Neuropathol,* 127**,** 189-201.

GRAFF, J. N., HIGANO, C. S., HAHN, N. M., TAYLOR, M. H., ZHANG, B., ZHOU, X., VENKATAKRISHNAN, K., LEONARD, E. J. & SARANTOPOULOS, J. 2016. Open-label, multicenter, phase 1 study of alisertib (MLN8237), an aurora A kinase inhibitor, with docetaxel in patients with solid tumors. *Cancer,* 122**,** 2524-2533.

GRANDORI, C., COWLEY, S. M., JAMES, L. P. & EISENMAN, R. N. 2000. The Myc/Max/Mad network and the transcriptional control of cell behavior. *Annu Rev Cell Dev Biol,* 16**,** 653-99.

GRIFFITHS, G., SCAEROU, F., MIDGLEY, C., MCCLUE, S., TOSH, C., JACKSON, W., MACCALLUM, D., WANG, S., FISCHER, P., GLOVER, D. & ZHELEVA, D. 2008. Anti-tumor activity of CYC116, a novel small molecule inhibitor of Aurora kinases and VEGFR2. *Cancer Research,* 68**,** 5644-5644.

GRILL, J., GEOERGER, B., GESNER, L., PEREK, D., LEBLOND, P., CAÑETE, A., AERTS, I., MADERO, L., DE TOLEDO CODINA, J. S., VERLOOY, J., ESTLIN, E., CISAR, L., BREAZNA, A., DORMAN, A., BAILEY, S., NICOLIN, G., GRUNDY, R. G. & HARGRAVE, D. 2013. Phase II study of irinotecan in combination with temozolomide (TEMIRI) in children with recurrent or refractory medulloblastoma: a joint ITCC and SIOPE brain tumor study. *Neuro Oncol,* 15**,** 1236-43.

GRINDE, M. T., HILMARSDOTTIR, B., TUNSET, H. M., HENRIKSEN, I. M., KIM, J., HAUGEN, M. H., RYE, M. B., MAELANDSMO, G. M. & MOESTUE, S. A. 2019. Glutamine to proline conversion is associated with response to glutaminase inhibition in breast cancer. *Breast Cancer Research,* 21.

GROTZER, M. A., CASTELLETTI, D., FIASCHETTI, G., SHALABY, T. & ARCARO, A. 2009. Targeting Myc in Pediatric Malignancies of the Central and Peripheral Nervous System. *Current Cancer Drug Targets,* 9**,** 176-188.

GUERREIRO, A. S., FATTET, S., FISCHER, B., SHALABY, T., JACKSON, S. P., SCHOENWAELDER, S. M., GROTZER, M. A., DELATTRE, O. & ARCARO, A. 2008. Targeting the PI3K p110α Isoform Inhibits Medulloblastoma Proliferation, Chemoresistance, and Migration. *Clinical Cancer Research,* 14**,** 6761-6769.

GURI, Y. & HALL, M. N. 2016. mTOR Signaling Confers Resistance to Targeted Cancer Drugs. *Trends Cancer,* 2**,** 688-697.

GUSTAFSON, WILLIAM C., MEYEROWITZ, JUSTIN G., NEKRITZ, ERIN A., CHEN, J., BENES, C., CHARRON, E., SIMONDS, ERIN F., SEEGER, R., MATTHAY, KATHERINE K., HERTZ, NICHOLAS T., EILERS, M., SHOKAT, KEVAN M. & WEISS, WILLIAM A. 2014. Drugging MYCN through an Allosteric Transition in Aurora Kinase A. *Cancer Cell,* 26**,** 414-427.

HAAS-KOGAN, D. A., BANERJEE, A., POUSSAINT, T. Y., KOCAK, M., PRADOS, M. D., GEYER, J. R., FOULADI, M., BRONISCER, A., MINTURN, J. E., POLLACK, I. F., PACKER, R. J., BOYETT, J. M. & KUN, L. E. 2011. Phase II trial of tipifarnib and radiation in children with newly diagnosed diffuse intrinsic pontine gliomas. *Neuro-oncology,* 13**,** 298-306.

HABERLER, C., SLAVC, I., CZECH, T., GELPI, E., HEINZL, H., BUDKA, H., URBAN, C., SCARPATETTI, M., EBETSBERGER-DACHS, G., SCHINDLER, C., JONES, N., KLEIN-FRANKE, A., MAIER, H., JAUK, B., KIEFER, A. & HAINFELLNER, J. A. 2006. Histopathological prognostic factors in medulloblastoma: High expression of survivin is related to unfavourable outcome. *European Journal of Cancer,* 42**,** 2996-3003.

HÄCKER, S., KARL, S., MADER, I., CRISTOFANON, S., SCHWEITZER, T., KRAUSS, J., RUTKOWSKI, S., DEBATIN, K. M. & FULDA, S. 2011. Histone deacetylase inhibitors prime medulloblastoma cells for chemotherapy-induced apoptosis by enhancing p53-dependent Bax activation. *Oncogene,* 30**,** 2275-81.

HAJARE, A., SALUNKHE, S., MALI, S., GORDE, S., NADAF, S. & PISHAWIKAR, S. 2013. Review on: High-throughput screening is an approach to drug discovery. *American Journal of PharmTech Research,* 4**,** 112-129.

HAJDUCH, M., VYDRA, D., DZUBAK, P., DZIECHCIARKOVA, M., STUART, I. & ZHELEVA, D. 2008. In vivo mode of action of CYC116, a novel small molecule inhibitor of Aurora kinases and VEGFR2. *Cancer Research,* 68**,** 5645-5645.

HALL, A. B., NEWSOME, D., WANG, Y., BOUCHER, D. M., EUSTACE, B., GU, Y., HARE, B., JOHNSON, M. A., MILTON, S., MURPHY, C. E., TAKEMOTO, D., TOLMAN, C., WOOD, M., CHARLTON, P., CHARRIER, J.-D., FUREY, B., GOLEC, J., REAPER, P. M. & POLLARD, J. R. 2014. Potentiation of tumor responses to DNA damaging therapy by the selective ATR inhibitor VX-970. *Oncotarget,* 5**,** 5674-5685.

HAN, H. Y., JAIN, A. D., TRUICA, M. I., IZQUIERDO-FERRER, J., ANKER, J. F., LYSY, B., SAGAR, V., LUAN, Y., CHALMERS, Z. R., UNNO, K., MOK, H., VATAPALLI, R., YOO, Y. A., RODRIGUEZ, Y., KANDELA, I., PARKER, J. B., CHAKRAVARTI, D., MISHRA, R. K., SCHILTZ, G. E. & ABDULKADIR, S. A. 2019a. Small-Molecule MYC Inhibitors Suppress Tumor Growth and Enhance Immunotherapy. *Cancer Cell,* 36**,** 483-+.

HAN, Y., LINDNER, S., BEI, Y., GARCIA, H. D., TIMME, N., ALTHOFF, K., ODERSKY, A., SCHRAMM, A., LISSAT, A., KUNKELE, A., DEUBZER, H. E., EGGERT, A., SCHULTE, J. H. & HENSSEN, A.

G. 2019b. Synergistic activity of BET inhibitor MK-8628 and PLK inhibitor Volasertib in preclinical models of medulloblastoma. *Cancer Lett,* 445**,** 24-33.

HANAFORD, A., ARCHER, T., TAMAYO, P., POMEROY, S., EBERHART, C. & RAABE, E. 2015. MB-27: PATHWAY ANALYSIS OF A HUMAN NEURAL STEM CELL MODEL OF AGGRESSIVE MEDULLOBLASTOMA REVEALS CKD INBHIBITION AS A POTENTIAL THERAPEUTIC MODALITY. *Neuro-Oncology,* 17**,** iii25-iii26.

HANAHAN, D. & WEINBERG, R. A. 2000. The hallmarks of cancer. *Cell,* 100**,** 57-70.

HANAHAN, D. & WEINBERG, R. A. 2011. Hallmarks of Cancer: The Next Generation. *Cell,* 144**,** 646-674.

HANN, S. R., DIXIT, M., SEARS, R. C. & SEALY, L. 1994. The Alternatively Initiated C-Myc Proteins Differentially Regulate Transcription through a Noncanonical DNA-Binding Site. *Genes & Development,* 8**,** 2441-2452.

HARRIS, P. S., VENKATARAMAN, S., ALIMOVA, I., BIRKS, D. K., BALAKRISHNAN, I., CRISTIANO, B., DONSON, A. M., DUBUC, A. M., TAYLOR, M. D., FOREMAN, N. K., REIGAN, P. & VIBHAKAR, R. 2014. Integrated genomic analysis identifies the mitotic checkpoint kinase WEE1 as a novel therapeutic target in medulloblastoma. *Molecular cancer,* 13**,** 72-72.

HARRIS, P. S., VENKATARAMAN, S., ALIMOVA, I., BIRKS, D. K., DONSON, A. M., KNIPSTEIN, J., DUBUC, A., TAYLOR, M. D., HANDLER, M. H., FOREMAN, N. K. & VIBHAKAR, R. 2012. Polo-like kinase 1 (PLK1) inhibition suppresses cell growth and enhances radiation sensitivity in medulloblastoma cells. *BMC Cancer,* 12**,** 80.

HARTMANN, W., DIGON-SONTGERATH, B., KOCH, A., WAHA, A., ENDL, E., DANI, I., DENKHAUS, D., GOODYER, C. G., SORENSEN, N., WIESTLER, O. D. & PIETSCH, T. 2006. Phosphatidylinositol 3'-kinase/AKT signaling is activated in medulloblastoma cell proliferation and is associated with reduced expression of PTEN. *Clin Cancer Res,* 12**,** 3019-27.

HASHIGUCHI, T., BRUSS, N., BEST, S., LAM, V., DANILOVA, O., PAIVA, C. J., WOLF, J., GILBERT, E. W., OKADA, C. Y., KAUR, P., DREW, L., CIDADO, J., HURLIN, P. & DANILOV, A. V. 2019. Cyclin-Dependent Kinase-9 Is a Therapeutic Target in MYC-Expressing Diffuse Large B-Cell Lymphoma. *Mol Cancer Ther,* 18**,** 1520-1532.

HASHIMOTO, Y., PENAS-PRADO, M., ZHOU, S., WEI, J., KHATUA, S., HODGES, T. R., SANAI, N., XIU, J., GATALICA, Z., KIM, L., KESARI, S., RAO, G., SPETZLER, D. & HEIMBERGER, A. 2018. Rethinking medulloblastoma from a targeted therapeutics perspective. *Journal of neuro-oncology,* 139**,** 713-720.

HEIST, R. S., AREN, O. R., MITA, A. C., POLIKOFF, J., BAZHENOVA, L., LLOYD, G. K., MIKRUT, W., REICH, S. D., SPEAR, M. A. & HUANG, L. 2014. Randomized phase 2 trial of plinabulin (NPI-2358) plus docetaxel in patients with advanced non-small cell lung cancer (NSCLC). *Journal of Clinical Oncology,* 32.

HELFRICH, B. A., KIM, J., GAO, D., CHAN, D. C., ZHANG, Z., TAN, A.-C. & BUNN, P. A., JR. 2016. Barasertib (AZD1152), a Small Molecule Aurora B Inhibitor, Inhibits the Growth of SCLC Cell Lines In Vitro and In Vivo. *Molecular cancer therapeutics,* 15**,** 2314-2322.

HELLVARD, A., ZEITLMANN, L., HEISER, U., KEHLEN, A., NIESTROJ, A., DEMUTH, H.-U., KOZIEL, J., DELALEU, N., JAN, P. & MYDEL, P. 2016. Inhibition of CDK9 as a therapeutic strategy for inflammatory arthritis. *Scientific Reports,* 6**,** 31441.

HELM, F., KAMMERTOENS, T., LEHMANN, F. M., WILKE, A., BRUNS, H., MAUTNER, J., BORNKAMM, G. W. & GERBITZ, A. 2013. Targeting c-MYC with T-Cells. *PLOS ONE,* 8**,** e77375.

HENSSEN, A., THOR, T., ODERSKY, A., HEUKAMP, L., EL-HINDY, N., BECKERS, A., SPELEMAN, F., ALTHOFF, K., SCHAFERS, S., SCHRAMM, A., SURE, U., FLEISCHHACK, G., EGGERT, A. &

SCHULTE, J. H. 2013. BET bromodomain protein inhibition is a therapeutic option for medulloblastoma. *Oncotarget,* 4**,** 2080-95.

HIGDON, R., KALA, J., WILKINS, D., YAN, J. F., SETHI, M. K., LIN, L., LIU, S., MONTAGUE, E., JANKO, I., CHOINIERE, J., KOLKER, N., HANCOCK, W. S., KOLKER, E. & FANAYAN, S. 2017. Integrated Proteomic and Transcriptomic-Based Approaches to Identifying Signature Biomarkers and Pathways for Elucidation of Daoy and UW228 Subtypes. *Proteomes,* 5**,** 5.

HILL, R. M., KUIJPER, S., LINDSEY, J. C., PETRIE, K., SCHWALBE, E. C., BARKER, K., BOULT, J. K. R., WILLIAMSON, D., AHMAD, Z., HALLSWORTH, A., RYAN, S. L., POON, E., ROBINSON, S. P., RUDDLE, R., RAYNAUD, F. I., HOWELL, L., KWOK, C., JOSHI, A., NICHOLSON, S. L., CROSIER, S., ELLISON, D. W., WHARTON, S. B., ROBSON, K., MICHALSKI, A., HARGRAVE, D., JACQUES, T. S., PIZER, B., BAILEY, S., SWARTLING, F. J., WEISS, W. A., CHESLER, L. & CLIFFORD, S. C. 2015. Combined MYC and P53 defects emerge at medulloblastoma relapse and define rapidly progressive, therapeutically targetable disease. *Cancer cell,* 27**,** 72-84.

HO, J. S. L., MA, W., MAO, D. Y. L. & BENCHIMOL, S. 2005. p53-Dependent transcriptional repression of c-myc is required for G1 cell cycle arrest. *Molecular and cellular biology,* 25**,** 7423-7431.

HOGG, S. J., WELLINGER, L., RUEFLIBRASSE, A. & JOHNSTONE, R. W. 2017. Clinical BET Inhibitor RG6146 Induces Intrinsic Apoptosis and Down-Regulates PD-L1 Expression and Induces Potent Anti-Tumor Activity in Models of Hematological Malignancy. *Blood,* 130**,** 2537-2537.

HOLLAND, A. J. & CLEVELAND, D. W. 2012. Chromoanagenesis and cancer: mechanisms and consequences of localized, complex chromosomal rearrangements. *Nat Med,* 18**,** 1630-8.

HOLME, H., GULATI, A., BROUGH, R., FLEUREN, E. D. G., BAJRAMI, I., CAMPBELL, J., CHONG, I. Y., COSTA-CABRAL, S., ELLIOTT, R., FENTON, T., FRANKUM, J., JONES, S. E., MENON, M., MILLER, R., PEMBERTON, H. N., POSTEL-VINAY, S., RAFIQ, R., SELFE, J. L., VON KRIEGSHEIM, A., MUNOZ, A. G., RODRIGUEZ, J., SHIPLEY, J., VAN DER GRAAF, W. T. A., WILLIAMSON, C. T., RYAN, C. J., PETTITT, S., ASHWORTH, A., STRAUSS, S. J. & LORD, C. J. 2018. Chemosensitivity profiling of osteosarcoma tumour cell lines identifies a model of BRCAness. *Sci Rep,* 8**,** 10614.

HONG, D., INFANTE, J., JANKU, F., JONES, S., NGUYEN, L. M., BURRIS, H., NAING, A., BAUER, T. M., PIHA-PAUL, S., JOHNSON, F. M., KURZROCK, R., GOLDEN, L., HYNES, S., LIN, J., LIN, A. B. & BENDELL, J. 2016. Phase I Study of LY2606368, a Checkpoint Kinase 1 Inhibitor, in Patients With Advanced Cancer. *Journal of Clinical Oncology,* 34**,** 1764-+.

HONG, F. D., CHEN, J., DONOVAN, S., SCHNEIDER, N. & NISEN, P. D. 1999. Taxol, vincristine or nocodazole induces lethality in G1-checkpoint-defective human astrocytoma U373MG cells by triggering hyperploid progression. *Carcinogenesis,* 20**,** 1161-1168.

HOOK, K. E., GARZA, S. J., LIRA, M. E., CHING, K. A., LEE, N. V., CAO, J., YUAN, J., YE, J., OZECK, M., SHI, S. T., ZHENG, X., REJTO, P. A., KAN, J. L. C., CHRISTENSEN, J. G. & PAVLICEK, A. 2012. An Integrated Genomic Approach to Identify Predictive Biomarkers of Response to the Aurora Kinase Inhibitor PF-03814735. *Molecular Cancer Therapeutics,* 11**,** 710-719.

HORING, E., PODLECH, O., SILKENSTEDT, B., ROTA, I. A., ADAMOPOULOU, E. & NAUMANN, U. 2013. The histone deacetylase inhibitor trichostatin a promotes apoptosis and antitumor immunity in glioblastoma cells. *Anticancer Res,* 33**,** 1351-60.

HOTTINGER, A. F., SANSON, M., MOYAL, E., DELORD, J., REZAI, K., LEUNG, A., PEREZ, S., BEKRADDA, M., LACHAUX, N. & CHINOT, O. 2016. Dose Optimization of Mk-8628

(Otx015), a Small Molecule Inhibitor of Bromodomain and Extra-Terminal (Bet) Proteins, in Patients with Recurrent Glioblastoma. *Neuro-Oncology,* 18**,** 56-56.

HOUGHTON, P. J., GORLICK, R., KOLB, E. A., LOCK, R., CAROL, H., MORTON, C. L., KEIR, S. T., REYNOLDS, C. P., KANG, M. H., PHELPS, D., MARIS, J. M., BILLUPS, C. & SMITH, M. A. 2012. Initial testing (stage 1) of the mTOR kinase inhibitor AZD8055 by the pediatric preclinical testing program. *Pediatric blood & cancer,* 58**,** 191-199.

HOVESTADT, V., SMITH, K. S., BIHANNIC, L., FILBIN, M. G., SHAW, M. L., BAUMGARTNER, A., DEWITT, J. C., GROVES, A., MAYR, L., WEISMAN, H. R., RICHMAN, A. R., SHORE, M. E., GOUMNEROVA, L., ROSENCRANCE, C., CARTER, R. A., PHOENIX, T. N., HADLEY, J. L., TONG, Y., HOUSTON, J., ASHMUN, R. A., DECUYPERE, M., SHARMA, T., FLASCH, D., SILKOV, A., LIGON, K. L., POMEROY, S. L., RIVERA, M. N., ROZENBLATT-ROSEN, O., RUSERT, J. M., WECHSLER-REYA, R. J., LI, X. N., PEYRL, A., GOJO, J., KIRCHHOFER, D., LÖTSCH, D., CZECH, T., DORFER, C., HABERLER, C., GEYEREGGER, R., HALFMANN, A., GAWAD, C., EASTON, J., PFISTER, S. M., REGEV, A., GAJJAR, A., ORR, B. A., SLAVC, I., ROBINSON, G. W., BERNSTEIN, B. E., SUVÀ, M. L. & NORTHCOTT, P. A. 2019. Resolving medulloblastoma cellular architecture by single-cell genomics. *Nature,* 572**,** 74-79.

HSIEH, A. L. & DANG, C. V. 2016. MYC, Metabolic Synthetic Lethality, and Cancer. *Recent Results Cancer Res,* 207**,** 73-91.

HUA, W., LI, C., YANG, Z., LI, L., JIANG, Y., YU, G., ZHU, W., LIU, Z., DUAN, S., CHU, Y., YANG, M., ZHANG, Y., MAO, Y. & JIA, L. 2015. Suppression of glioblastoma by targeting the overactivated protein neddylation pathway. *Neuro-oncology,* 17**,** 1333-1343.

HUANG, M., TAILOR, J., ZHEN, Q., GILLMOR, A. H., MILLER, M. L., WEISHAUPT, H., CHEN, J., ZHENG, T., NASH, E. K., MCHENRY, L. K., AN, Z., YE, F., TAKASHIMA, Y., CLARKE, J., AYETEY, H., CAVALLI, F. M. G., LUU, B., MORIARITY, B. S., ILKHANIZADEH, S., CHAVEZ, L., YU, C., KURIAN, K. M., MAGNALDO, T., SEVENET, N., KOCH, P., POLLARD, S. M., DIRKS, P., SNYDER, M. P., LARGAESPADA, D. A., CHO, Y. J., PHILLIPS, J. J., SWARTLING, F. J., MORRISSY, A. S., KOOL, M., PFISTER, S. M., TAYLOR, M. D., SMITH, A. & WEISS, W. A. 2019. Engineering Genetic Predisposition in Human Neuroepithelial Stem Cells Recapitulates Medulloblastoma Tumorigenesis. *Cell Stem Cell,* 25**,** 433-446.e7.

HUGHES, J. P., REES, S., KALINDJIAN, S. B. & PHILPOTT, K. L. 2011. Principles of early drug discovery. *British journal of pharmacology,* 162**,** 1239-1249.

HUMMEL, T. R., WAGNER, L., AHERN, C., FOULADI, M., REID, J. M., MCGOVERN, R. M., AMES, M. M., GILBERTSON, R. J., HORTON, T., INGLE, A. M., WEIGEL, B. & BLANEY, S. M. 2013. A pediatric phase 1 trial of vorinostat and temozolomide in relapsed or refractory primary brain or spinal cord tumors: a Children's Oncology Group phase 1 consortium study. *Pediatric blood & cancer,* 60**,** 1452-1457.

HURWITZ, C. A., STRAUSS, L. C., KEPNER, J., KRETSCHMAR, C., HARRIS, M. B., FRIEDMAN, H., KUN, L. & KADOTA, R. 2001. Paclitaxel for the treatment of progressive or recurrent childhood brain tumors: a pediatric oncology phase II study. *J Pediatr Hematol Oncol,* 23**,** 277-81.

HUTTER, S., BOLIN, S., WEISHAUPT, H. & SWARTLING, F. J. 2017. Modeling and Targeting MYC Genes in Childhood Brain Tumors. *Genes,* 8.

IVANOV, D. P., COYLE, B., WALKER, D. A. & GRABOWSKA, A. M. 2016. In vitro models of medulloblastoma: Choosing the right tool for the job. *Journal of Biotechnology,* 236**,** 10-25.

IWADATE, Y., FUJIMOTO, S., NAMBA, H. & YAMAURA, A. 2003. Promising survival for patients with glioblastoma multiforme treated with individualised chemotherapy based on in vitro drug sensitivity testing. *Br J Cancer,* 89**,** 1896-900.

IWASA, T., OKAMOTO, I., SUZUKI, M., NAKAHARA, T., YAMANAKA, K., HATASHITA, E., YAMADA, Y., FUKUOKA, M., ONO, K. & NAKAGAWA, K. 2008. Radiosensitizing Effect of YM155, a Novel Small-Molecule Survivin Suppressant, in Non–Small Cell Lung Cancer Cell Lines. *Clinical Cancer Research,* 14**,** 6496-6504.

IYER, R., EVANS, A. E., QI, X., HO, R., MINTURN, J. E., ZHAO, H., BALAMUTH, N., MARIS, J. M. & BRODEUR, G. M. 2010. Lestaurtinib enhances the antitumor efficacy of chemotherapy in murine xenograft models of neuroblastoma. *Clinical cancer research : an official journal of the American Association for Cancer Research,* 16**,** 1478-1485.

JAIN, K. K. 2004. RNAi and siRNA in target validation. *Drug Discov Today,* 9**,** 307-9.

JAIN, M., ARVANITIS, C., CHU, K., DEWEY, W., LEONHARDT, E., TRINH, M., SUNDBERG, C. D., BISHOP, J. M. & FELSHER, D. W. 2002. Sustained loss of a neoplastic phenotype by brief inactivation of MYC. *Science,* 297**,** 102-4.

JAKACKI, R. I., BOUFFET, E., ADAMSON, P. C., POLLACK, I. F., INGLE, A. M., VOSS, S. D. & BLANEY, S. M. 2011. A phase 1 study of vinblastine in combination with carboplatin for children with low-grade gliomas: a Children's Oncology Group phase 1 consortium study. *Neuro Oncol,* 13**,** 910-5.

JANI, J. P., ARCARI, J., BERNARDO, V., BHATTACHARYA, S. K., BRIERE, D., COHEN, B. D., COLEMAN, K., CHRISTENSEN, J. G., EMERSON, E. O., JAKOWSKI, A., HOOK, K., LOS, G., MOYER, J. D., PRUIMBOOM-BREES, I., PUSTILNIK, L., ROSSI, A. M., STEYN, S. J., SU, C., TSAPARIKOS, K., WISHKA, D., YOON, K. & JAKUBCZAK, J. L. 2010. PF-03814735, an Orally Bioavailable Small Molecule Aurora Kinase Inhibitor for Cancer Therapy. *Molecular Cancer Therapeutics,* 9**,** 883-894.

JONES, D. T., JAGER, N., KOOL, M., ZICHNER, T., HUTTER, B., SULTAN, M., CHO, Y. J., PUGH, T. J., HOVESTADT, V., STUTZ, A. M., RAUSCH, T., WARNATZ, H. J., RYZHOVA, M., BENDER, S., STURM, D., PLEIER, S., CIN, H., PFAFF, E., SIEBER, L., WITTMANN, A., REMKE, M., WITT, H., HUTTER, S., TZARIDIS, T., WEISCHENFELDT, J., RAEDER, B., AVCI, M., AMSTISLAVSKIY, V., ZAPATKA, M., WEBER, U. D., WANG, Q., LASITSCHKA, B., BARTHOLOMAE, C. C., SCHMIDT, M., VON KALLE, C., AST, V., LAWERENZ, C., EILS, J., KABBE, R., BENES, V., VAN SLUIS, P., KOSTER, J., VOLCKMANN, R., SHIH, D., BETTS, M. J., RUSSELL, R. B., COCO, S., TONINI, G. P., SCHULLER, U., HANS, V., GRAF, N., KIM, Y. J., MONORANU, C., ROGGENDORF, W., UNTERBERG, A., HEROLD-MENDE, C., MILDE, T., KULOZIK, A. E., VON DEIMLING, A., WITT, O., MAASS, E., ROSSLER, J., EBINGER, M., SCHUHMANN, M. U., FRUHWALD, M. C., HASSELBLATT, M., JABADO, N., RUTKOWSKI, S., VON BUEREN, A. O., WILLIAMSON, D., CLIFFORD, S. C., MCCABE, M. G., COLLINS, V. P., WOLF, S., WIEMANN, S., LEHRACH, H., BRORS, B., SCHEURLEN, W., FELSBERG, J., REIFENBERGER, G., NORTHCOTT, P. A., TAYLOR, M. D., MEYERSON, M., POMEROY, S. L., YASPO, M. L., KORBEL, J. O., KORSHUNOV, A., EILS, R., PFISTER, S. M. & LICHTER, P. 2012. Dissecting the genomic complexity underlying medulloblastoma. *Nature,* 488**,** 100-5.

JONES, S., FLEUREN, E., FRANKUM, J., KONDE, A., WILLIAMSON, C., KRASTEV, D., PEMBERTON, H., CAMPBELL, J., GULATI, A., ELLIOTT, R., MENON, M., SELFE, J., BROUGH, R., PETTITT, S., NIEDZWIEDZ, W., VAN DER GRAAF, W., SHIPLEY, J., ASHWORTH, A. & LORD, C. 2017. ATR Is a Therapeutic Target in Synovial Sarcoma. *Cancer Research,* 77**,** canres.2056.2017.

JOSHI, K. S., RATHOS, M. J., JOSHI, R. D., SIVAKUMAR, M., MASCARENHAS, M., KAMBLE, S., LAL, B. & SHARMA, S. 2007. In vitro antitumor properties of a novel cyclin-dependent kinase inhibitor, P276-00. *Molecular Cancer Therapeutics,* 6**,** 918-925.

JULIA ALEJANDRA, P., MARIA SOL, B., PRISCILA MARIA MANZINI, R., CARLOS ALBERTO, S. & LUIZ GONZAGA, T. 2017. Polo-Like Kinase 1 Pharmacological Inhibition as

Monotherapy or in Combination: Comparative Effects of Polo-Like Kinase 1 Inhibition in Medulloblastoma Cells. *Anti-Cancer Agents in Medicinal Chemistry,* 17**,** 1278-1291.

JUNCA, A., VILLALVA, C., TACHON, G., RIVET, P., CORTES, U., GUILLOTEAU, K., BALBOUS, A., GODET, J., WAGER, M. & KARAYAN-TAPON, L. 2017. Crizotinib targets in glioblastoma stem cells. *Cancer medicine,* 6**,** 2625-2634.

JUNG, L. A., GEBHARDT, A., KOELMEL, W., ADE, C. P., WALZ, S., KUPER, J., VON EYSS, B., LETSCHERT, S., REDEL, C., D'ARTISTA, L., BIANKIN, A., ZENDER, L., SAUER, M., WOLF, E., EVAN, G., KISKER, C. & EILERS, M. 2017. OmoMYC blunts promoter invasion by oncogenic MYC to inhibit gene expression characteristic of MYC-dependent tumors. *Oncogene,* 36**,** 1911-1924.

JURASCHKA, K. & TAYLOR, M. D. 2019. Medulloblastoma in the age of molecular subgroups: a review. *Journal of Neurosurgery-Pediatrics,* 24**,** 353-363.

JURIC, V. & MURPHY, B. 2020. Cyclin-dependent kinase inhibitors in brain cancer: current state and future directions. *Cancer Drug Resistance,* 3**,** 48-62.

KAMEDA-SMITH, M., WANG, A., ABDULHADI, N., ADILE, A., AJANI, O., YARASCAVITCH, B., FARROKHYAR, F., TINA, P., SAMAAN, C., ALYMAN, C., SINGH, S. & FLEMING, A. 2018. MBCL-09. SALVAGE THERAPY FOR CHILDHOOD MEDULLOBLASTOMA: A SINGLE CENTER EXPERIENCE. *Neuro-Oncology,* 20**,** i119-i119.

KANG, J., SERGIO, C. M., SUTHERLAND, R. L. & MUSGROVE, E. A. 2014. Targeting cyclin-dependent kinase 1 (CDK1) but not CDK4/6 or CDK2 is selectively lethal to MYC-dependent human breast cancer cells. *Bmc Cancer,* 14.

KATO, S., SCHWAEDERLE, M., DANIELS, G. A., PICCIONI, D., KESARI, S., BAZHENOVA, L., SHIMABUKURO, K., PARKER, B. A., FANTA, P. & KURZROCK, R. 2015. Cyclin-dependent kinase pathway aberrations in diverse malignancies: clinical and molecular characteristics. *Cell Cycle,* 14**,** 1252-1259.

KAWAUCHI, D., OGG, R. J., LIU, L., SHIH, D. J. H., FINKELSTEIN, D., MURPHY, B. L., REHG, J. E., KORSHUNOV, A., CALABRESE, C., ZINDY, F., PHOENIX, T., KAWAGUCHI, Y., GRONYCH, J., GILBERTSON, R. J., LICHTER, P., GAJJAR, A., KOOL, M., NORTHCOTT, P. A., PFISTER, S. M. & ROUSSEL, M. F. 2017. Novel MYC-driven medulloblastoma models from multiple embryonic cerebellar cells. *Oncogene,* 36**,** 5231-5242.

KAWAUCHI, D., ROBINSON, G., UZIEL, T., GIBSON, P., REHG, J., GAO, C., FINKELSTEIN, D., QU, C., POUNDS, S., ELLISON, D. W., GILBERTSON, R. J. & ROUSSEL, M. F. 2012. A mouse model of the most aggressive subgroup of human medulloblastoma. *Cancer cell,* 21**,** 168-180.

KENNEDY, C., BULL, K., CHEVIGNARD, M., CULLIFORD, D., DORR, H. G., DOZ, F., KORTMANN, R. D., LANNERING, B., MASSIMINO, M., GUTIERREZ, A. N., RUTKOWSKI, S., SPOUDEAS, H. A., CALAMINUS, G. & SIOP-E, I. S. P. O. 2014. Quality of Survival and Growth in Children and Young Adults in the PNET4 European Controlled Trial of Hyperfractionated Versus Conventional Radiation Therapy for Standard-Risk Medulloblastoma. *International Journal of Radiation Oncology Biology Physics,* 88**,** 292-300.

KIESSLING, A., SPERL, B., HOLLIS, A., EICK, D. & BERG, T. 2006. Selective inhibition of c-Myc/Max dimerization and DNA binding by small molecules. *Chemistry & Biology,* 13**,** 745-751.

KIM, S. T., KIM, S. Y., LEE, J., KIM, K., PARK, S. H., PARK, Y. S., LIM, H. Y., KANG, W. K. & PARK, J. O. 2018. Triptolide as a novel agent in pancreatic cancer: the validation using patient derived pancreatic tumor cell line. *BMC Cancer,* 18**,** 1103.

KING, A. R., CORSO, C. D., CHEN, E. M., SONG, E., BONGIORNI, P., CHEN, Z., SUNDARAM, R. K., BINDRA, R. S. & SALTZMAN, W. M. 2017. Local DNA Repair Inhibition for Sustained Radiosensitization of High-Grade Gliomas. *Mol Cancer Ther,* 16**,** 1456-1469.

KING, C., DIAZ, H., BARNARD, D., BARDA, D., CLAWSON, D., BLOSSER, W., COX, K., GUO, S. & MARSHALL, M. 2014. Characterization and preclinical development of LY2603618: a selective and potent Chk1 inhibitor. *Investigational New Drugs,* 32**,** 213-226.

KING, C., DIAZ, H. B., MCNEELY, S., BARNARD, D., DEMPSEY, J., BLOSSER, W., BECKMANN, R., BARDA, D. & MARSHALL, M. S. 2015. LY2606368 Causes Replication Catastrophe and Antitumor Effects through CHK1-Dependent Mechanisms. *Mol Cancer Ther,* 14**,** 2004-13.

KINOSHITA, S., ISHIDA, T., ITO, A., NARITA, T., MASAKI, A., SUZUKI, S., YOSHIDA, T., RI, M., KUSUMOTO, S., KOMATSU, H., SHIMIZU, N., INAGAKI, H., KURODA, T., SCHOLZ, A., UEDA, R., SANDA, T. & IIDA, S. 2018. Cyclin-dependent kinase 9 as a potential specific molecular target in NK-cell leukemia/lymphoma. *Haematologica,* 103**,** 2059-2068.

KOGISO, M., QI, L., BRAUN, F. K., INJAC, S. G., ZHANG, L., DU, Y. C., ZHANG, H. Y., LIN, F. Y., ZHAO, S. B., LINDSAY, H., SU, J. M., BAXTER, P. A., ADESINA, A. M., LIAO, D., QIAN, M. G., BERG, S., MUSCAL, J. A. & LI, X. N. 2018. Concurrent Inhibition of Neurosphere and Monolayer Cells of Pediatric Glioblastoma by Aurora A Inhibitor MLN8237 Predicted Survival Extension in PDOX Models. *Clinical Cancer Research,* 24**,** 2159-2170.

KOLTSOVA, A. S., PENDINA, A. A., EFIMOVA, O. A., CHIRYAEVA, O. G., KUZNETZOVA, T. V. & BARANOV, V. S. 2019. On the Complexity of Mechanisms and Consequences of Chromothripsis: An Update. *Front Genet,* 10**,** 393.

KOOL, M., JONES, D. T., JÄGER, N., NORTHCOTT, P. A., PUGH, T. J., HOVESTADT, V., PIRO, R. M., ESPARZA, L. A., MARKANT, S. L., REMKE, M., MILDE, T., BOURDEAUT, F., RYZHOVA, M., STURM, D., PFAFF, E., STARK, S., HUTTER, S., SEKER-CIN, H., JOHANN, P., BENDER, S., SCHMIDT, C., RAUSCH, T., SHIH, D., REIMAND, J., SIEBER, L., WITTMANN, A., LINKE, L., WITT, H., WEBER, U. D., ZAPATKA, M., KÖNIG, R., BEROUKHIM, R., BERGTHOLD, G., VAN SLUIS, P., VOLCKMANN, R., KOSTER, J., VERSTEEG, R., SCHMIDT, S., WOLF, S., LAWERENZ, C., BARTHOLOMAE, C. C., VON KALLE, C., UNTERBERG, A., HEROLD-MENDE, C., HOFER, S., KULOZIK, A. E., VON DEIMLING, A., SCHEURLEN, W., FELSBERG, J., REIFENBERGER, G., HASSELBLATT, M., CRAWFORD, J. R., GRANT, G. A., JABADO, N., PERRY, A., COWDREY, C., CROUL, S., ZADEH, G., KORBEL, J. O., DOZ, F., DELATTRE, O., BADER, G. D., MCCABE, M. G., COLLINS, V. P., KIERAN, M. W., CHO, Y. J., POMEROY, S. L., WITT, O., BRORS, B., TAYLOR, M. D., SCHÜLLER, U., KORSHUNOV, A., EILS, R., WECHSLER-REYA, R. J., LICHTER, P. & PFISTER, S. M. 2014. Genome sequencing of SHH medulloblastoma predicts genotype-related response to smoothened inhibition. *Cancer Cell,* 25**,** 393-405.

KOOL, M., KORSHUNOV, A., REMKE, M., JONES, D. T. W., SCHLANSTEIN, M., NORTHCOTT, P. A., CHO, Y. J., KOSTER, J., SCHOUTEN-VAN MEETEREN, A., VAN VUURDEN, D., CLIFFORD, S. C., PIETSCH, T., VON BUEREN, A. O., RUTKOWSKI, S., MCCABE, M., COLLINS, V. P., BACKLUND, M. L., HABERLER, C., BOURDEAUT, F., DELATTRE, O., DOZ, F., ELLISON, D. W., GILBERTSON, R. J., POMEROY, S. L., TAYLOR, M. D., LICHTER, P. & PFISTER, S. M. 2012. Molecular subgroups of medulloblastoma: an international meta-analysis of transcriptome, genetic aberrations, and clinical data of WNT, SHH, Group 3, and Group 4 medulloblastomas. *Acta Neuropathologica,* 123**,** 473-484.

KOUSHOLT, A. N., MENZEL, T. & SØRENSEN, C. S. 2012. Pathways for genome integrity in G2 phase of the cell cycle. *Biomolecules,* 2**,** 579-607.

KRUGER, K., GEIST, K., STUHLDREIER, F., SCHUMACHER, L., BLUMEL, L., REMKE, M., WESSELBORG, S., STORK, B., KLOCKER, N., BORMANN, S., ROOS, W. P., HONNEN, S. &

FRITZ, G. 2018. Multiple DNA damage-dependent and DNA damage-independent stress responses define the outcome of ATR/Chk1 targeting in medulloblastoma cells. *Cancer Lett,* 430**,** 34-46.

KUMAR, S. & KIM, J. 2015. PLK-1 Targeted Inhibitors and Their Potential against Tumorigenesis. *Biomed Research International*.

KUMARI, A., FOLK, W. P. & SAKAMURO, D. 2017. The Dual Roles of MYC in Genomic Instability and Cancer Chemoresistance. *Genes (Basel),* 8.

KUNOS, C. A., ANDREWS, S. J., MOORE, K. N., CHON, H. S. & IVY, S. P. 2019. Randomized Phase II Trial of Triapine-Cisplatin-Radiotherapy for Locally Advanced Stage Uterine Cervix or Vaginal Cancers. *Frontiers in Oncology,* 9.

KUNOS, C. A., CHU, E., BEUMER, J. H., SZNOL, M. & IVY, S. P. 2017. Phase I trial of daily triapine in combination with cisplatin chemotherapy for advanced-stage malignancies. *Cancer chemotherapy and pharmacology,* 79**,** 201-207.

KUNOS, C. A. & IVY, S. P. 2018. Triapine Radiochemotherapy in Advanced Stage Cervical Cancer. *Frontiers in oncology,* 8**,** 149-149.

KURMASHEVA, R. T., KURMASHEV, D., REYNOLDS, C. P., KANG, M., WU, J., HOUGHTON, P. J. & SMITH, M. A. 2018. Initial testing (stage 1) of M6620 (formerly VX-970), a novel ATR inhibitor, alone and combined with cisplatin and melphalan, by the Pediatric Preclinical Testing Program. *Pediatric blood & cancer,* 65**,** 10.1002/pbc.26825.

KUTTESCH, J. F., JR., KRAILO, M. D., MADDEN, T., JOHANSEN, M. & BLEYER, A. 2009. Phase II evaluation of intravenous vinorelbine (Navelbine) in recurrent or refractory pediatric malignancies: a Children's Oncology Group study. *Pediatr Blood Cancer,* 53**,** 590-3.

LANDIER, W., ARMENIAN, S. & BHATIA, S. 2015. Late effects of childhood cancer and its treatment. *Pediatr Clin North Am,* 62**,** 275-300.

LANG, P. Y. & GERSHON, T. R. 2018. A New Way to Treat Brain Tumors: Targeting Proteins Coded by Microcephaly Genes?: Brain tumors and microcephaly arise from opposing derangements regulating progenitor growth. Drivers of microcephaly could be attractive brain tumor targets. *BioEssays : news and reviews in molecular, cellular and developmental biology,* 40**,** e1700243.

LANNERING, B., RUTKOWSKI, S., DOZ, F., PIZER, B., GUSTAFSSON, G., NAVAJAS, A., MASSIMINO, M., REDDINGIUS, R., BENESCH, M., CARRIE, C., TAYLOR, R., GANDOLA, L., BJORK-ERIKSSON, T., GIRALT, J., OLDENBURGER, F., PIETSCH, T., FIGARELLA-BRANGER, D., ROBSON, K., FORNI, M., CLIFFORD, S. C., WARMUTH-METZ, M., VON HOFF, K., FALDUM, A., MOSSERI, V. & KORTMANN, R. 2012. Hyperfractionated Versus Conventional Radiotherapy Followed by Chemotherapy in Standard-Risk Medulloblastoma: Results From the Randomized Multicenter HIT-SIOP PNET 4 Trial. *Journal of Clinical Oncology,* 30**,** 3187-3193.

LAW, N., GREENBERG, M., BOUFFET, E., TAYLOR, M. D., LAUGHLIN, S., STROTHER, D., FRYER, C., MCCONNELL, D., HUKIN, J., KAISE, C., WANG, F. & MABBOTT, D. J. 2012. Clinical and neuroanatomical predictors of cerebellar mutism syndrome. *Neuro-Oncology,* 14**,** 1294-1303.

LE TEUFF, G., CASTANEDA-HEREDIA, A., DUFOUR, C., JASPAN, T., CALMON, R., DEVOS, A., MCHUGH, K., LEBLOND, P., FRAPPAZ, D., AERTS, I., ZWAAN, C. M., DUCASSOU, S., CHASTAGNER, P., VERSCHUUR, A., CORRADINI, N., CASANOVA, M., RUBIE, H., RICCARDI, R., LE DELEY, M.-C., VASSAL, G., GEOERGER, B. & CANCER, E. C. I. T. F. C. W. 2020. Phase II study of temozolomide and topotecan (TOTEM) in children with relapsed or refractory extracranial and central nervous system tumors including medulloblastoma with post hoc Bayesian analysis: A European ITCC study. *Pediatric Blood & Cancer,* 67**,** e28032.

LE TOURNEAU, C., FAIVRE, S., LAURENCE, V., DELBALDO, C., VERA, K., GIRRE, V., CHIAO, J., ARMOUR, S., FRAME, S., GREEN, S. R., GIANELLA-BORRADORI, A., DIÉRAS, V. & RAYMOND, E. 2010. Phase I evaluation of seliciclib (R-roscovitine), a novel oral cyclin-dependent kinase inhibitor, in patients with advanced malignancies. *Eur J Cancer,* 46**,** 3243-50.

LEARY, S., KILBURN, L., GEYER, J. R., OLSON, J. M., MACDONALD, T., ELLISON, D., KOCAK, M., ONAR, A., ERMOIAN, R., POUSSAINT, T. Y., BOYETT, J. M., KUN, L. & FOULADI, M. 2015. MB-32FEASIBILITY OF VORINOSTAT COMBINED WITH ISOTRETINOIN AND CHEMOTHERAPY FOR YOUNG CHILDREN WITH NEWLY DIAGNOSED EMBRYONAL BRAIN TUMORS: A PEDIATRIC BRAIN TUMOR CONSORTIUM STUDY. *Neuro-Oncology,* 17**,** iii27-iii27.

LEE, C., RUDNEVA, V. A., ERKEK, S., ZAPATKA, M., CHAU, L. Q., TACHEVA-GRIGOROVA, S. K., GARANCHER, A., RUSERT, J. M., AKSOY, O., LEA, R., MOHAMMAD, H. P., WANG, J. X., WEISS, W. A., GRIMES, H. L., PFISTER, S. M., NORTHCOTT, P. A. & WECHSLER-REYA, R. J. 2019. Lsd1 as a therapeutic target in Gfi1-activated medulloblastoma. *Nature Communications,* 10.

LEE, H. 2014. Genetically engineered mouse models for drug development and preclinical trials. *Biomolecules & therapeutics,* 22**,** 267-274.

LEON, J., FERRANDIZ, N., ACOSTA, J. C. & DELGADO, M. D. 2009. Inhibition of cell differentiation A critical mechanism for MYC-mediated carcinogenesis? *Cell Cycle,* 8**,** 1148-1157.

LESUEUR, P., CHEVALIER, F., EL-HABR, E. A., JUNIER, M.-P., CHNEIWEISS, H., CASTERA, L., MÜLLER, E., STEFAN, D. & SAINTIGNY, Y. 2018. Radiosensitization Effect of Talazoparib, a Parp Inhibitor, on Glioblastoma Stem Cells Exposed to Low and High Linear Energy Transfer Radiation. *Scientific Reports,* 8**,** 3664.

LEVENS, D. 2008. How the c-myc promoter works and why it sometimes does not. *J Natl Cancer Inst Monogr***,** 41-3.

LEVESLEY, J., STEELE, L., BRUNING-RICHARDSON, A., DAVISON, A., ZHOU, J., DING, C. Y., LAWLER, S. & SHORT, S. C. 2018. Selective BCL-X-L inhibition promotes apoptosis in combination with MLN8237 in medulloblastoma and pediatric glioblastoma cells. *Neuro-Oncology,* 20**,** 203-214.

LEVIN, V. A., RODRIGUEZ, L. A., EDWARDS, M. S., WARA, W., LIU, H. C., FULTON, D., DAVIS, R. L., WILSON, C. B. & SILVER, P. 1988. Treatment of medulloblastoma with procarbazine, hydroxyurea, and reduced radiation doses to whole brain and spine. *J Neurosurg,* 68**,** 383-7.

LI, W., XU, H., XIAO, T., CONG, L., LOVE, M. I., ZHANG, F., IRIZARRY, R. A., LIU, J. S., BROWN, M. & LIU, X. S. 2014a. MAGeCK enables robust identification of essential genes from genome-scale CRISPR/Cas9 knockout screens. *Genome Biol,* 15**,** 554.

LI, X., SEEBACHER, N. A., XIAO, T., HORNICEK, F. J. & DUAN, Z. 2019. Targeting regulation of cyclin dependent kinase 9 as a novel therapeutic strategy in synovial sarcoma. *J Orthop Res,* 37**,** 510-521.

LI, Y., CASEY, S. C. & FELSHER, D. W. 2014b. Inactivation of MYC reverses tumorigenesis. *Journal of Internal Medicine,* 276**,** 52-60.

LI, Y., GOODWIN, C. R., SANG, Y., ROSEN, E. M., LATERRA, J. & XIA, S. 2009. Camptothecin and Fas receptor agonists synergistically induce medulloblastoma cell death: ROS-dependent mechanisms. *Anticancer Drugs,* 20**,** 770-8.

LI, Y., GUESSOUS, F., JOHNSON, E. B., EBERHART, C. G., LI, X.-N., SHU, Q., FAN, S., LAL, B., LATERRA, J., SCHIFF, D. & ABOUNADER, R. 2008. Functional and molecular interactions

between the HGF/c-Met pathway and c-Myc in large-cell medulloblastoma. *Laboratory Investigation,* 88**,** 98-111.

LI, Y., LI, X., PU, J., YANG, Q., GUAN, H., JI, M., SHI, B., CHEN, M. & HOU, P. 2018. c-Myc Is a Major Determinant for Antitumor Activity of Aurora A Kinase Inhibitor MLN8237 in Thyroid Cancer. *Thyroid,* 28**,** 1642-1654.

LIAN, H., HAN, Y.-P., ZHANG, Y.-C., ZHAO, Y., YAN, S., LI, Q.-F., WANG, B.-C., WANG, J.-J., MENG, W., YANG, J., WANG, Q.-H., MAO, W.-W. & MA, J. 2019. Integrative analysis of gene expression and DNA methylation through one-class logistic regression machine learning identifies stemness features in medulloblastoma. *Molecular Oncology,* 13**,** 2227-2245.

LIN, Z. P., ZHU, Y.-L. & RATNER, E. S. 2018. Targeting Cyclin-Dependent Kinases for Treatment of Gynecologic Cancers. *Frontiers in Oncology,* 8.

LINDSEY, J. C., HILL, R. M., MEGAHED, H., LUSHER, M. E., SCHWALBE, E. C., COLE, M., HOGG, T. L., GILBERTSON, R. J., ELLISON, D. W., BAILEY, S. & CLIFFORD, S. C. 2011. TP53 mutations in favorable-risk Wnt/Wingless-subtype medulloblastomas. *J Clin Oncol,* 29**,** e344-6; author reply e347-8.

LINDSEY, J. C., SCHWALBE, E. C., POTLURI, S., BAILEY, S., WILLIAMSON, D. & CLIFFORD, S. C. 2014. TERT promoter mutation and aberrant hypermethylation are associated with elevated expression in medulloblastoma and characterise the majority of non-infant SHH subgroup tumours. *Acta Neuropathol,* 127**,** 307-9.

LIU, F., JIANG, W., SUI, Y., MENG, W., HOU, L., LI, T., LI, M., ZHANG, L., MO, J., WANG, J., ZHAO, Y., ZHANG, L., MA, J. & TANG, Y. 2019a. CDK7 inhibition suppresses aberrant hedgehog pathway and overcomes resistance to smoothened antagonists. *Proceedings of the National Academy of Sciences,* 116**,** 12986-12995.

LIU, H., ZHANG, W., ZOU, B., WANG, J., DENG, Y. & DENG, L. 2019b. DrugCombDB: a comprehensive database of drug combinations toward the discovery of combinatorial therapy. *Nucleic Acids Res*.

LIU, N., HU, G., WANG, H., LI, Z. & GUO, Z. 2018. PLK1 inhibitor facilitates the suppressing effect of temozolomide on human brain glioma stem cells. *Journal of cellular and molecular medicine,* 22**,** 5300-5310.

LOEWE, S. & MUISCHNEK, H. 1926. Über Kombinationswirkungen. *Naunyn-Schmiedebergs Archiv für experimentelle Pathologie und Pharmakologie,* 114**,** 313-326.

LU, H., XUE, Y., YU, G. K., ARIAS, C., LIN, J., FONG, S., FAURE, M., WEISBURD, B., JI, X., MERCIER, A., SUTTON, J., LUO, K., GAO, Z. & ZHOU, Q. 2015. Compensatory induction of MYC expression by sustained CDK9 inhibition via a BRD4-dependent mechanism. *Elife,* 4**,** e06535.

LUBANSKA, D. & PORTER, L. 2017. Revisiting CDK Inhibitors for Treatment of Glioblastoma Multiforme. *Drugs in R&D,* 17**,** 255-263.

LUCHMAN, H. A., STECHISHIN, O. D. M., NGUYEN, S. A., LUN, X. Q., CAIRNCROSS, J. G. & WEISS, S. 2014. Dual mTORC1/2 Blockade Inhibits Glioblastoma Brain Tumor Initiating Cells In Vitro and In Vivo and Synergizes with Temozolomide to Increase Orthotopic Xenograft Survival. *Clinical Cancer Research,* 20**,** 5756-5767.

LUOTO, K. R., MENG, A. X., WASYLISHEN, A. R., ZHAO, H., COACKLEY, C. L., PENN, L. Z. & BRISTOW, R. G. 2010. Tumor cell kill by c-MYC depletion: role of MYC-regulated genes that control DNA double-strand break repair. *Cancer Res,* 70**,** 8748-59.

MA, H., SEEBACHER, N. A., HORNICEK, F. J. & DUAN, Z. 2019. Cyclin-dependent kinase 9 (CDK9) is a novel prognostic marker and therapeutic target in osteosarcoma. *EBioMedicine,* 39**,** 182-193.

MACARULLA, T., CERVANTES, A., ELEZ, E., RODRIGUEZ-BRAUN, E., BASELGA, J., ROSELLO, S., SALA, G., BLASCO, I., DANAEE, H., LEE, Y., ECSEDY, J., SHINDE, V., CHAKRAVARTY, A., BOWMAN, D., LIU, H., ETON, O., FINGERT, H. & TABERNERO, J. 2010. Phase I study of the selective Aurora A kinase inhibitor MLN8054 in patients with advanced solid tumors: safety, pharmacokinetics, and pharmacodynamics. *Mol Cancer Ther,* 9**,** 2844-52.

MACK, S. C. & NORTHCOTT, P. A. 2017. Genomic Analysis of Childhood Brain Tumors: Methods for Genome-Wide Discovery and Precision Medicine Become Mainstream. *Journal of Clinical Oncology,* 35**,** 2346-+.

MAHARAJ, A., DAVIS, A., ZHONG, B., ROUSSEL, M. F. & STEWART, C. F. 2018. Abstract 4927: Plasma and CNS pharmacokinetics of the CHK-1 inhibitor prexasertib (LY-2606368) in mice bearing orthotopic group 3 medulloblastoma. *Cancer Research,* 78**,** 4927-4927.

MAHINDROO, N., PUNCHIHEWA, C. & FUJII, N. 2009. Hedgehog-Gli signaling pathway inhibitors as anticancer agents. *Journal of medicinal chemistry,* 52**,** 3829-3845.

MAJETI, R., CHAO, M. P., ALIZADEH, A. A., PANG, W. W., JAISWAL, S., GIBBS, K. D., JR., VAN ROOIJEN, N. & WEISSMAN, I. L. 2009. CD47 is an adverse prognostic factor and therapeutic antibody target on human acute myeloid leukemia stem cells. *Cell,* 138**,** 286-299.

MANOHAR, S., RATHOS, M., SONAWANE, V., RAO, S. & JOSHI, K. 2011. Cyclin-dependent kinase inhibitor, P276-00 induces apoptosis in multiple myeloma cells by inhibition of Cdk9-T1 and RNA polymerase II-dependent transcription. *Leukemia research,* 35**,** 821-30.

MARCUS, L., MURPHY, R., FOX, E., MCCULLY, C., CRUZ, R., WARREN, K. E., MEYER, T., MCNIFF, E., BALIS, F. M. & WIDEMANN, B. C. 2012. The plasma and cerebrospinal fluid pharmacokinetics of the platinum analog satraplatin after intravenous administration in non-human primates. *Cancer chemotherapy and pharmacology,* 69**,** 247-252.

MARÉCHAL, A. & ZOU, L. 2013. DNA damage sensing by the ATM and ATR kinases. *Cold Spring Harbor perspectives in biology,* 5**,** a012716.

MARKANT, S. L., ESPARZA, L. A., SUN, J., BARTON, K. L., MCCOIG, L. M., GRANT, G. A., CRAWFORD, J. R., LEVY, M. L., NORTHCOTT, P. A., SHIH, D., REMKE, M., TAYLOR, M. D. & WECHSLER-REYA, R. J. 2013. Targeting sonic hedgehog-associated medulloblastoma through inhibition of Aurora and Polo-like kinases. *Cancer research,* 73**,** 6310-6322.

MARTIROSIAN, V. & NEMAN, J. 2019. Medulloblastoma: Challenges and advances in treatment and research. *CANCER REPORTS,* 2**,** e1146.

MASCARENHAS, L., CHI, Y.-Y., HINGORANI, P., ANDERSON, J. R., LYDEN, E. R., RODEBERG, D. A., INDELICATO, D. J., KAO, S. C., DASGUPTA, R., SPUNT, S. L., MEYER, W. H. & HAWKINS, D. S. 2019. Randomized Phase II Trial of Bevacizumab or Temsirolimus in Combination With Chemotherapy for First Relapse Rhabdomyosarcoma: A Report From the Children's Oncology Group. *Journal of Clinical Oncology,* 37**,** 2866-2874.

MASSÓ-VALLÉS, D., JAUSET, T. & SOUCEK, L. 2016. Ibrutinib repurposing: from B-cell malignancies to solid tumors. *Oncoscience,* 3**,** 147-148.

MATHESON, C. J., VENKATARAMAN, S., AMANI, V., HARRIS, P. S., BACKOS, D. S., DONSON, A. M., WEMPE, M. F., FOREMAN, N. K., VIBHAKAR, R. & REIGAN, P. 2016. A WEE1 Inhibitor Analog of AZD1775 Maintains Synergy with Cisplatin and Demonstrates Reduced Single-Agent Cytotoxicity in Medulloblastoma Cells. *ACS Chemical Biology,* 11**,** 921-930.

MATTHEWS, T. P., JONES, A. M. & COLLINS, I. 2013. Structure-based design, discovery and development of checkpoint kinase inhibitors as potential anticancer therapies. *Expert opinion on drug discovery,* 8**,** 621-640.

MAZOUZI, A., VELIMEZI, G. & LOIZOU, J. I. 2014. DNA replication stress: causes, resolution and disease. *Exp Cell Res,* 329**,** 85-93.

MBONYE, U., WANG, B. L., GOKULRANGAN, G., SHI, W. X., YANG, S. C. & KARN, J. 2018. Cyclin-dependent kinase 7 (CDK7)-mediated phosphorylation of the CDK9 activation loop promotes P-TEFb assembly with Tat and proviral HIV reactivation. *Journal of Biological Chemistry,* 293**,** 10009-10025.

MCCRACKEN, M. N., CHA, A. C. & WEISSMAN, I. L. 2015. Molecular Pathways: Activating T Cells after Cancer Cell Phagocytosis from Blockade of CD47 "Don't Eat Me" Signals. *Clinical cancer research : an official journal of the American Association for Cancer Research,* 21**,** 3597-3601.

MCKEOWN, M. R. & BRADNER, J. E. 2014. Therapeutic Strategies to Inhibit MYC. *Cold Spring Harbor Perspectives in Medicine,* 4.

MCMAHON, S. B. 2014. MYC and the Control of Apoptosis. *Cold Spring Harbor Perspectives in Medicine,* 4.

MCNEELY, S., CONTI, C., SHEIKH, T., PATEL, H., ZABLUDOFF, S., POMMIER, Y., SCHWARTZ, G. & TSE, A. 2010. Chk1 inhibition after replicative stress activates a double strand break response mediated by ATM and DNA-dependent protein kinase. *Cell Cycle,* 9**,** 995-1004.

MELAIU, O., MINA, M., CHIERICI, M., BOLDRINI, R., JURMAN, G., ROMANIA, P., D'ALICANDRO, V., BENEDETTI, M. C., CASTELLANO, A., LIU, T., FURLANELLO, C., LOCATELLI, F. & FRUCI, D. 2017. PD-L1 Is a Therapeutic Target of the Bromodomain Inhibitor JQ1 and, Combined with HLA Class I, a Promising Prognostic Biomarker in Neuroblastoma. *Clin Cancer Res,* 23**,** 4462-4472.

MELLATYAR, H., TALAEI, S., PILEHVAR-SOLTANAHMADI, Y., BARZEGAR, A., AKBARZADEH, A., SHAHABI, A., BAREKATI-MOWAHED, M. & ZARGHAMI, N. 2018. Targeted cancer therapy through 17-DMAG as an Hsp90 inhibitor: Overview and current state of the art. *Biomedicine & Pharmacotherapy,* 102**,** 608-617.

MENDOZA, M. C., ER, E. E. & BLENIS, J. 2011. The Ras-ERK and PI3K-mTOR pathways: cross-talk and compensation. *Trends Biochem Sci,* 36**,** 320-8.

MENON, M., ELLIOTT, R., BOWERS, L., BALAN, N., RAFIQ, R., COSTA-CABRAL, S., MUNKONGE, F., TRINIDADE, I., PORTER, R., CAMPBELL, A. D., JOHNSON, E. R., ESDAR, C., BUCHSTALLER, H. P., LEUTHNER, B., ROHDICH, F., SCHNEIDER, R., SANSOM, O., WIENKE, D., ASHWORTH, A. & LORD, C. J. 2019. A novel tankyrase inhibitor, MSC2504877, enhances the effects of clinical CDK4/6 inhibitors. *Sci Rep,* 9**,** 201.

MENYHÁRT, O., GIANGASPERO, F. & GYŐRFFY, B. 2019. Molecular markers and potential therapeutic targets in non-WNT/non-SHH (group 3 and group 4) medulloblastomas. *Journal of Hematology & Oncology,* 12**,** 29.

MEYER, C. T., WOOTEN, D. J., PAUDEL, B. B., BAUER, J., HARDEMAN, K. N., WESTOVER, D., LOVLY, C. M., HARRIS, L. A., TYSON, D. R. & QUARANTA, V. 2019. Quantifying Drug Combination Synergy along Potency and Efficacy Axes. *Cell Syst,* 8**,** 97-108.e16.

MEYER, N. & PENN, L. Z. 2008. MYC - TIMELINE Reflecting on 25 years with MYC. *Nature Reviews Cancer,* 8**,** 976-990.

MICHALSKI, J., VEZINA, G., BURGER, P., GAJJAR, A., POLLACK, I., MERCHANT, T., FITZGERALD, T. J., BOOTH, T., TARBELL, N., SHIEH, I., WILLIAMS-HUGHES, C., LI, Y., BILLUPS, C., PACKER, R. & JANSS, A. 2016. MB-109: PRELIMINARY RESULTS OF COG ACNS0331: A PHASE III TRIAL OF INVOLVED FIELD RADIOTHERAPY (IFRT) AND LOW DOSE CRANIOSPINAL IRRADIATION (LD-CSI) WITH CHEMOTHERAPY IN AVERAGE RISK MEDULLOBLASTOMA: A REPORT FROM THE CHILDREN'S ONCOLOGY GROUP. *Neuro-Oncology,* 18**,** iii122-iii122.

MILLARD, N. E. & DE BRAGANCA, K. C. 2016. Medulloblastoma. *Journal of child neurology,* 31**,** 1341-1353.

MILLER, A. L., FEHLING, S. C., GARCIA, P. L., GAMBLIN, T. L., COUNCIL, L. N., VAN WAARDENBURG, R., YANG, E. S., BRADNER, J. E. & YOON, K. J. 2019. The BET inhibitor JQ1 attenuates double-strand break repair and sensitizes models of pancreatic ductal adenocarcinoma to PARP inhibitors. *EBioMedicine,* 44**,** 419-430.

MINA, M., BOLDRINI, R., CITTI, A., ROMANIA, P., D'ALICANDRO, V., DE IORIS, M., CASTELLANO, A., FURLANELLO, C., LOCATELLI, F. & FRUCI, D. 2015. Tumor-infiltrating T lymphocytes improve clinical outcome of therapy-resistant neuroblastoma. *Oncoimmunology,* 4**,** e1019981.

MINTURN, J. E., EVANS, A. E., VILLABLANCA, J. G., YANIK, G. A., PARK, J. R., SHUSTERMAN, S., GROSHEN, S., HELLRIEGEL, E. T., BENSEN-KENNEDY, D., MATTHAY, K. K., BRODEUR, G. M. & MARIS, J. M. 2011. Phase I trial of lestaurtinib for children with refractory neuroblastoma: a new approaches to neuroblastoma therapy consortium study. *Cancer chemotherapy and pharmacology,* 68**,** 1057-1065.

MINUTOLO, N. G., HOLLANDER, E. E. & POWELL, D. J., JR. 2019. The Emergence of Universal Immune Receptor T Cell Therapy for Cancer. *Frontiers in oncology,* 9**,** 176-176.

MITTRA, A., O'SULLIVAN COYNE, G. H., DO, K. T., PIHA-PAUL, S. A., KUMMAR, S., TAKEBE, N., BRUNS, A., JUWARA, L., RUBINSTEIN, L., HOGU, M., KINDERS, R. J., PARCHMENT, R. E., MILLER, B., WILSKER, D., MONGE B, M. C., KHAN, S. S., DOYLE, L. A., DOROSHOW, J. H. & CHEN, A. P. 2019. Safety and tolerability of veliparib, an oral PARP inhibitor, and M6620 (VX-970), an ATR inhibitor, in combination with cisplatin in patients with refractory solid tumors. *Journal of Clinical Oncology,* 37**,** 3067-3067.

MO, H. & HENRIKSSON, M. 2006. Identification of small molecules that induce apoptosis in a Myc-dependent manner and inhibit Myc-driven transformation. *Proceedings of the National Academy of Sciences of the United States of America,* 103**,** 6344-6349.

MOLENAAR, J. J., EBUS, M. E., GEERTS, D., KOSTER, J., LAMERS, F., VALENTIJN, L. J., WESTERHOUT, E. M., VERSTEEG, R. & CARON, H. N. 2009. Inactivation of CDK2 is synthetically lethal to MYCN over-expressing cancer cells. *Proceedings of the National Academy of Sciences,* 106**,** 12968-12973.

MOREIRA, D. C., VENKATARAMAN, S., SUBRAMANIAN, A., DESISTO, J., BALAKRISHNAN, I., PRINCE, E., PIERCE, A., GRIESINGER, A., GREEN, A., EBERHARDT, C. G., FOREMAN, N. K. & VIBHAKAR, R. 2020. Targeting MYC-driven replication stress in medulloblastoma with AZD1775 and gemcitabine. *Journal of Neuro-Oncology,* 147**,** 531-545.

MORENO, L., MARSHALL, L. V., PEARSON, A. D. J., MORLAND, B., ELLIOTT, M., CAMPBELL-HEWSON, Q., MAKIN, G., HALFORD, S. E. R., ACTON, G., ROSS, P., KAZMI-STOKES, S., LOCK, V., RODRIGUEZ, A., LYONS, J. F., BODDY, A. V., GRIFFIN, M. J., YULE, M. & HARGRAVE, D. 2015. A Phase I Trial of AT9283 (a Selective Inhibitor of Aurora Kinases) in Children and Adolescents with Solid Tumors: A Cancer Research UK Study. *Clinical Cancer Research,* 21**,** 267-273.

MORFOUACE, M., SHELAT, A., JACUS, M., FREEMAN, B. B., 3RD, TURNER, D., ROBINSON, S., ZINDY, F., WANG, Y.-D., FINKELSTEIN, D., AYRAULT, O., BIHANNIC, L., PUGET, S., LI, X.-N., OLSON, J. M., ROBINSON, G. W., GUY, R. K., STEWART, C. F., GAJJAR, A. & ROUSSEL, M. F. 2014. Pemetrexed and gemcitabine as combination therapy for the treatment of Group3 medulloblastoma. *Cancer cell,* 25**,** 516-529.

MUELLNER, M. K., URAS, I. Z., GAPP, B. V., KERZENDORFER, C., SMIDA, M., LECHTERMANN, H., CRAIG-MUELLER, N., COLINGE, J., DUERNBERGER, G. & NIJMAN, S. M. 2011. A chemical-genetic screen reveals a mechanism of resistance to PI3K inhibitors in cancer. *Nat Chem Biol,* 7**,** 787-93.

MULHERN, R. K., PALMER, S. L., MERCHANT, T. E., WALLACE, D., KOCAK, M., BROUWERS, P., KRULL, K., CHINTAGUMPALA, M., STARGATT, R., ASHLEY, D. M., TYC, V. L., KUN, L., BOYETT, J. & GAJJAR, A. 2005. Neurocognitive consequences of risk-adapted therapy for childhood medulloblastoma. *J Clin Oncol,* 23**,** 5511-9.

MURGA, M., CAMPANER, S., LOPEZ-CONTRERAS, A. J., TOLEDO, L. I., SORIA, R., MONTANA, M. F., D'ARTISTA, L., SCHLEKER, T., GUERRA, C., GARCIA, E., BARBACID, M., HIDALGO, M., AMATI, B. & FERNANDEZ-CAPETILLO, O. 2011. Exploiting oncogene-induced replicative stress for the selective killing of Myc-driven tumors. *Nature Structural & Molecular Biology,* 18**,** 1331-U38.

MUSCAL, J. A., SCORSONE, K. A., ZHANG, L., ECSEDY, J. A. & BERG, S. L. 2013. Additive effects of vorinostat and MLN8237 in pediatric leukemia, medulloblastoma, and neuroblastoma cell lines. *Investigational new drugs,* 31**,** 39-45.

NAIR, J. S. & SCHWARTZ, G. K. 2016. MLN-8237: A dual inhibitor of aurora A and B in soft tissue sarcomas. *Oncotarget,* 7**,** 12893-12903.

NESBIT, C. E., TERSAK, J. M. & PROCHOWNIK, E. V. 1999. MYC oncogenes and human neoplastic disease. *Oncogene,* 18**,** 3004-3016.

NICHOLSON, B., LLOYD, G. K., MILLER, B. R., PALLADINO, M. A., KISO, Y., HAYASHI, Y. & NEUTEBOOM, S. T. C. 2006. NPI-2358 is a tubulin-depolymerizing agent: in-vitro evidence for activity as a tumor vascular-disrupting agent. *Anti-Cancer Drugs,* 17**,** 25-31.

NOBRE, L., PAUCK, D., GOLBOURN, B., MAUE, M., BOUFFET, E., REMKE, M. & RAMASWAMY, V. 2019. Effective and safe tumor inhibition using vinblastine in medulloblastoma. *Pediatr Blood Cancer,* 66**,** e27694.

NORRIS, R., MINTURN, J., BRODEUR, G., MARIS, J. & ADAMSON, P. 2011. Preclinical evaluation of lestaurtinib (CEP701) in combination with retinoids for neuroblastoma. *Cancer Chemotherapy and Pharmacology - CANCER CHEMOTHER PHARMACOL,* 68.

NORRIS, R. E., PINK, J. J., PAREEK, T. & LETTERIO, J. L. 2016. Abstract 2816: Evaluation of Cdk5 inhibitors in neural crest tumors. *Cancer Research,* 76**,** 2816-2816.

NORTHCOTT, P. A., BUCHHALTER, I., MORRISSY, A. S., HOVESTADT, V., WEISCHENFELDT, J., EHRENBERGER, T., GROBNER, S., SEGURA-WANG, M., ZICHNER, T., RUDNEVA, V. A., WARNATZ, H. J., SIDIROPOULOS, N., PHILLIPS, A. H., SCHUMACHER, S., KLEINHEINZ, K., WASZAK, S. M., ERKEK, S., JONES, D. T. W., WORST, B. C., KOOL, M., ZAPATKA, M., JAGER, N., CHAVEZ, L., HUTTER, B., BIEG, M., PARAMASIVAM, N., HEINOLD, M., GU, Z. G., ISHAQUE, N., JAGER-SCHMIDT, C., IMBUSCH, C. D., JUGOLD, A., HUBSCHMANN, D., RISCH, T., AMSTISLAVSKIY, V., GONZALEZ, F. G. R., WEBER, U. D., WOLF, S., ROBINSON, G. W., ZHOU, X., WU, G., FINKELSTEIN, D., LIU, Y. L., CAVALLI, F. M. G., LUU, B., RAMASWAMY, V., WU, X. C., KOSTER, J., RYZHOVA, M., CHO, Y. J., POMEROY, S. L., HEROLD-MENDE, C., SCHUHMANN, M., EBINGER, M., LIAU, L. M., MORA, J., MCLENDON, E., JABADO, N., KUMABE, T., CHUAH, E., MA, Y., MOORE, R. A., MUNGALL, A. J., MUNGALL, K. L., THIESSEN, N., TSE, K., WONG, T., JONES, S. J. M., WITT, O., MILDE, T., VON DEIMLING, A., CAPPER, D., KORSHUNOV, A., YASPO, M. L., KRIWACKI, R., GAJJAR, A., ZHANG, J. H., BEROUKHIM, R., FRAENKEL, E., KORBEL, J. O., BRORS, B., SCHLESNER, M., EILS, R., MARRA, M. A., PFISTER, S. M., TAYLOR, M. D. & LICHTER, P. 2017. The whole-genome landscape of medulloblastoma subtypes. *Nature,* 547**,** 311-+.

NORTHCOTT, P. A., KORSHUNOV, A., PFISTER, S. M. & TAYLOR, M. D. 2012a. The clinical implications of medulloblastoma subgroups. *Nature Reviews Neurology,* 8**,** 340-351.

NORTHCOTT, P. A., LEE, C., ZICHNER, T., STUTZ, A. M., ERKEK, S., KAWAUCHI, D., SHIH, D. J. H., HOVESTADT, V., ZAPATKA, M., STURM, D., JONES, D. T. W., KOOL, M., REMKE, M.,

CAVALLI, F. M. G., ZUYDERDUYN, S., BADER, G. D., VANDENBERG, S., ESPARZA, L. A., RYZHOVA, M., WANG, W., WITTMANN, A., STARK, S., SIEBER, L., SEKER-CIN, H., LINKE, L., KRATOCHWIL, F., JAGER, N., BUCHHALTER, I., IMBUSCH, C. D., ZIPPRICH, G., RAEDER, B., SCHMIDT, S., DIESSL, N., WOLF, S., WIEMANN, S., BRORS, B., LAWERENZ, C., EILS, J., WARNATZ, H. J., RISCH, T., YASPO, M. L., WEBER, U. D., BARTHOLOMAE, C. C., VON KALLE, C., TURANYI, E., HAUSER, P., SANDEN, E., DARABI, A., SIESJO, P., STERBA, J., ZITTERBART, K., SUMERAUER, D., VAN SLUIS, P., VERSTEEG, R., VOLCKMANN, R., KOSTER, J., SCHUHMANN, M. U., EBINGER, M., GRIMES, H. L., ROBINSON, G. W., GAJJAR, A., MYNAREK, M., VON HOFF, K., RUTKOWSKI, S., PIETSCH, T., SCHEURLEN, W., FELSBERG, J., REIFENBERGER, G., KULOZIK, A. E., VON DEIMLING, A., WITT, O., EILS, R., GILBERTSON, R. J., KORSHUNOV, A., TAYLOR, M. D., LICHTER, P., KORBEL, J. O., WECHSLER-REYA, R. J. & PFISTER, S. M. 2014. Enhancer hijacking activates GFI1 family oncogenes in medulloblastoma. *Nature,* 511**,** 428-+.

NORTHCOTT, P. A., ROBINSON, G. W., KRATZ, C. P., MABBOTT, D. J., POMEROY, S. L., CLIFFORD, S. C., RUTKOWSKI, S., ELLISON, D. W., MALKIN, D., TAYLOR, M. D., GAJJAR, A. & PFISTER, S. M. 2019. Medulloblastoma. *Nature Reviews Disease Primers,* 5.

NORTHCOTT, P. A., SHIH, D. J. H., PEACOCK, J., GARZIA, L., MORRISSY, A. S., ZICHNER, T., STUTZ, A. M., KORSHUNOV, A., REIMAND, J., SCHUMACHER, S. E., BEROUKHIM, R., ELLISON, D. W., MARSHALL, C. R., LIONEL, A. C., MACK, S., DUBUC, A., YAO, Y., RAMASWAMY, V., LUU, B., ROLIDER, A., CAVALLI, F. M. G., WANG, X., REMKE, M., WU, X. C., CHIU, R. Y. B., CHU, A., CHUAH, E., CORBETT, R. D., HOAD, G. R., JACKMAN, S. D., LI, Y. S., LO, A., MUNGALL, K. L., NIP, K. M., QIAN, J. Q., RAYMOND, A. G. J., THIESSEN, N., VARHOL, R. J., BIROL, I., MOORE, R. A., MUNGALL, A. J., HOLT, R., KAWAUCHI, D., ROUSSEL, M. F., KOOL, M., JONES, D. T. W., WITT, H., FERNANDEZ-L, A., KENNEY, A. M., WECHSLER-REYA, R. J., DIRKS, P., AVIV, T., GRAJKOWSKA, W. A., PEREK-POLNIK, M., HABERLER, C. C., DELATTRE, O., REYNAUD, S. S., DOZ, F. F., PERNET-FATTET, S. S., CHO, B. K., KIM, S. K., WANG, K. C., SCHEURLEN, W., EBERHART, C. G., FEVRE-MONTANGE, M., JOUVET, A., POLLACK, I. F., FAN, X., MURASZKO, K. M., GILLESPIE, G. Y., DI ROCCO, C., MASSIMI, L., MICHIELS, E. M. C., KLOOSTERHOF, N. K., FRENCH, P. J., KROS, J. M., OLSON, J. M., ELLENBOGEN, R. G., ZITTERBART, K., KREN, L., THOMPSON, R. C., COOPER, M. K., LACH, B., MCLENDON, R. E., BIGNER, D. D., FONTEBASSO, A., ALBRECHT, S., JABADO, N., LINDSEY, J. C., BAILEY, S., GUPTA, N., WEISS, W. A., BOGNAR, L., KLEKNER, A., VAN METER, T. E., KUMABE, T., TOMINAGA, T., ELBABAA, S. K., LEONARD, J. R., RUBIN, J. B., et al. 2012b. Subgroup-specific structural variation across 1,000 medulloblastoma genomes. *Nature,* 488**,** 49-56.

OEHLER, C., FREI, K., RUSHING, E. J., MCSHEEHY, P. M., WEBER, D., ALLEGRINI, P. R., WENIGER, D., LUTOLF, U. M., KNUTH, A., YONEKAWA, Y., BARATH, K., BROGGINI-TENZER, A., PRUSCHY, M. & HOFER, S. 2012. Patupilone (epothilone B) for recurrent glioblastoma: clinical outcome and translational analysis of a single-institution phase I/II trial. *Oncology,* 83**,** 1-9.

OEHLER, C., VON BUEREN, A. O., FURMANOVA, P., BROGGINI-TENZER, A., ORLOWSKI, K., RUTKOWSKI, S., FREI, K., GROTZER, M. A. & PRUSCHY, M. 2011. The microtubule stabilizer patupilone (epothilone B) is a potent radiosensitizer in medulloblastoma cells. *Neuro-oncology,* 13**,** 1000-1010.

OLESEN, U., THOUGAARD, A., JENSEN, P. & SEHESTED, M. 2010. A Preclinical Study on the Rescue of Normal Tissue by Nicotinic Acid in High-Dose Treatment with APO866, a Specific Nicotinamide Phosphoribosyltransferase Inhibitor. *Molecular cancer therapeutics,* 9**,** 1609-17.

OSTER, S. K., HO, C. S. W., SOUCIE, E. L. & PENN, L. Z. 2002. The myc oncogene: MarvelouslY Complex. *Advances in Cancer Research, Vol 84,* 84**,** 81-154.

OTHMAN, R. T., KIMISHI, I., BRADSHAW, T. D., STORER, L. C. D., KORSHUNOV, A., PFISTER, S. M., GRUNDY, R. G., KERR, I. D. & COYLE, B. 2014. Overcoming multiple drug resistance mechanisms in medulloblastoma. *Acta neuropathologica communications,* 2**,** 57-57.

OTTO, T., HORN, S., BROCKMANN, M., EILERS, U., SCHUTTRUMPF, L., POPOV, N., KENNEY, A. M., SCHULTE, J. H., BEIJERSBERGEN, R., CHRISTIANSEN, H., BERWANGER, B. & EILERS, M. 2009. Stabilization of N-Myc Is a Critical Function of Aurora A in Human Neuroblastoma. *Cancer Cell,* 15**,** 67-78.

OTTO, T. & SICINSKI, P. 2017. Cell cycle proteins as promising targets in cancer therapy. *Nature Reviews Cancer,* 17**,** 93-115.

OYHARCABAL-BOURDEN, V., KALIFA, C., GENTET, J. C., FRAPPAZ, D., EDAN, C., CHASTAGNER, P., SARIBAN, E., PAGNIER, A., BABIN, A., PICHON, F., NEUENSCHWANDER, S., VINCHON, M., BOURS, D., MOSSERI, V., LE GALES, C., RUCHOUX, M., CARRIE, C. & DOZ, F. 2005. Standard-risk medulloblastoma treated by adjuvant chemotherapy followed by reduced-dose craniospinal radiation therapy: a French Society of Pediatric Oncology Study. *J Clin Oncol,* 23**,** 4726-34.

PACKER, R. J., GAJJAR, A., VEZINA, G., RORKE-ADAMS, L., BURGER, P. C., ROBERTSON, P. L., BAYER, L., LAFOND, D., DONAHUE, B. R., MARYMONT, M. H., MURASZKO, K., LANGSTON, J. & SPOSTO, R. 2006. Phase III study of craniospinal radiation therapy followed by adjuvant chemotherapy for newly diagnosed average-risk medulloblastoma. *Journal of Clinical Oncology,* 24**,** 4202-4208.

PACKER, R. J., ZHOU, T. N., HOLMES, E., VEZINA, G. & GAJJAR, A. 2013. Survival and secondary tumors in children with medulloblastoma receiving radiotherapy and adjuvant chemotherapy: results of Children's Oncology Group trial A9961. *Neuro-Oncology,* 15**,** 97-103.

PAJTLER, K. W., SADOWSKI, N., ACKERMANN, S., ALTHOFF, K., SCHÖNBECK, K., BATZKE, K., SCHÄFERS, S., ODERSKY, A., HEUKAMP, L., ASTRAHANTSEFF, K., KÜNKELE, A., DEUBZER, H. E., SCHRAMM, A., SPRÜSSEL, A., THOR, T., LINDNER, S., EGGERT, A., FISCHER, M. & SCHULTE, J. H. 2017. The GSK461364 PLK1 inhibitor exhibits strong antitumoral activity in preclinical neuroblastoma models. *Oncotarget,* 8**,** 6730-6741.

PALLER, C. J., WISSING, M. D., MENDONCA, J., SHARMA, A., KIM, E., KIM, H.-S., KORTENHORST, M. S. Q., GERBER, S., ROSEN, M., SHAIKH, F., ZAHURAK, M. L., RUDEK, M. A., HAMMERS, H., RUDIN, C. M., CARDUCCI, M. A. & KACHHAP, S. K. 2014. Combining the pan-aurora kinase inhibitor AMG 900 with histone deacetylase inhibitors enhances antitumor activity in prostate cancer. *Cancer Medicine,* 3**,** 1322-1335.

PALMER, S. L., GAJJAR, A., REDDICK, W. E., GLASS, J. O., KUN, L. E., WU, S., XIONG, X. & MULHERN, R. K. 2003. Predicting intellectual outcome among children treated with 35-40 Gy craniospinal irradiation for medulloblastoma. *Neuropsychology,* 17**,** 548-55.

PALMER, S. L., REDDICK, W. E. & GAJJAR, A. 2007. Understanding the cognitive impact on children who are treated for medulloblastoma. *J Pediatr Psychol,* 32**,** 1040-9.

PARK, Y. H., KIM, H. W., KIM, H. S., NAM, S. T., LEE, D., LEE, M. B., MIN, K. Y., KOO, J., KIM, S. J., KIM, Y. M., KIM, H. S. & CHOI, W. S. 2019. An Anti-Cancer Drug Candidate CYC116 Suppresses Type I Hypersensitive Immune Responses through the Inhibition of Fyn Kinase in Mast Cells. *Biomolecules & therapeutics,* 27**,** 311-317.

PATEL, Y. T., JACUS, M. O., BOULOS, N., DAPPER, J. D., DAVIS, A. D., VUPPALA, P. K., FREEMAN, B. B., 3RD, MOHANKUMAR, K. M., THROM, S. L., GILBERTSON, R. J. & STEWART, C. F. 2015. Preclinical examination of clofarabine in pediatric ependymoma: intratumoral

concentrations insufficient to warrant further study. *Cancer chemotherapy and pharmacology,* 75**,** 897-906.

PATNAIK, A., CARVAJAL, R. D., KOMATSUBARA, K. M., BRITTEN, C. D., WESOLOWSKI, R. & MICHELSON, G. 2018. Phase ib/2a study of PLX51107, a small molecule BET inhibitor, in subjects with advanced hematological malignancies and solid tumors. *Journal of Clinical Oncology,* 36.

PATTIES, I., KORTMANN, R.-D., MENZEL, F. & GLASOW, A. 2016a. Enhanced inhibition of clonogenic survival of human medulloblastoma cells by multimodal treatment with ionizing irradiation, epigenetic modifiers, and differentiation-inducing drugs. *Journal of experimental & clinical cancer research : CR,* 35**,** 94-94.

PATTIES, I., KORTMANN, R. D., MENZEL, F. & GLASOW, A. 2016b. Enhanced inhibition of clonogenic survival of human medulloblastoma cells by multimodal treatment with ionizing irradiation, epigenetic modifiers, and differentiation-inducing drugs. *J Exp Clin Cancer Res,* 35**,** 94.

PEEREBOOM, D. M., MURPHY, C., AHLUWALIA, M. S., CONLIN, A., EICHLER, A., VAN POZNAK, C., BAAR, J., ELSON, P. & SEIDMAN, A. D. 2014. Phase II trial of patupilone in patients with brain metastases from breast cancer. *Neuro-oncology,* 16**,** 579-583.

PEI, Y., LIU, K.-W., WANG, J., GARANCHER, A., TAO, R., ESPARZA, L. A., MAIER, D. L., UDAKA, Y. T., MURAD, N., MORRISSY, S., SEKER-CIN, H., BRABETZ, S., QI, L., KOGISO, M., SCHUBERT, S., OLSON, J. M., CHO, Y.-J., LI, X.-N., CRAWFORD, J. R., LEVY, M. L., KOOL, M., PFISTER, S. M., TAYLOR, M. D. & WECHSLER-REYA, R. J. 2016. HDAC and PI3K Antagonists Cooperate to Inhibit Growth of MYC-Driven Medulloblastoma. *Cancer cell,* 29**,** 311-323.

PEI, Y., MOORE, C. E., WANG, J., TEWARI, A. K., EROSHKIN, A., CHO, Y. J., WITT, H., KORSHUNOV, A., READ, T. A., SUN, J. L., SCHMITT, E. M., MILLER, C. R., BUCKLEY, A. F., MCLENDON, R. E., WESTBROOK, T. F., NORTHCOTT, P. A., TAYLOR, M. D., PFISTER, S. M., FEBBO, P. G. & WECHSLER-REYA, R. J. 2012. An animal model of MYC-driven medulloblastoma. *Cancer Cell,* 21**,** 155-67.

PELENGARIS, S., KHAN, M. & EVAN, G. 2002. c-MYC: More than just a matter of life and death. *Nature Reviews Cancer,* 2**,** 764-776.

PERWITASARI, O., BAKRE, A., TOMPKINS, S. M. & TRIPP, R. A. 2013. siRNA Genome Screening Approaches to Therapeutic Drug Repositioning. *Pharmaceuticals (Basel),* 6**,** 124-60.

PETERSEN, W., LIU, J., YUAN, L., ZHANG, H., SCHNEIDERJAN, M., CHO, Y.-J. & MACDONALD, T. J. 2014. Dasatinib suppression of medulloblastoma survival and migration is markedly enhanced by combining treatment with the aurora kinase inhibitor AT9283. *Cancer letters,* 354**,** 68-76.

PETERSEN, W. C., LIU, J. & MACDONALD, T. J. 2012. Abstract 2485: Combined Src and aurora kinase inhibition in medulloblastoma. *Cancer Research,* 72**,** 2485-2485.

PEZUK, J. A., BRASSESCO, M. S., RAMOS, P. M. M., SCRIDELI, C. A. & TONE, L. G. 2017. Polo-Like Kinase 1 Pharmacological Inhibition as Monotherapy or in Combination: Comparative Effects of Polo-Like Kinase 1 Inhibition in Medulloblastoma Cells. *Anti-Cancer Agents in Medicinal Chemistry,* 17**,** 1278-1291.

PEZZOLO, A., COCO, S., RASO, A., PARODI, F., PISTORIO, A., VALDORA, F., CAPRA, V., ZOLLO, M., ASCHERO, S., BASSO, E., CAMA, A., NOZZA, P., GAMBINI, C., CINALLI, G., GARRE, M. L., IOLASCON, A., PISTOIA, V. & TONINI, G. P. 2011. Loss of 10q26.1-q26.3 in association with 7q34-q36.3 gain or 17q24.3-q25.3 gain predict poor outcome in pediatric medulloblastoma. *Cancer Letters,* 308**,** 215-224.

PHESSE, T. J., MYANT, K. B., COLE, A. M., RIDGWAY, R. A., PEARSON, H., MUNCAN, V., VAN DEN BRINK, G. R., VOUSDEN, K. H., SEARS, R., VASSILEV, L. T., CLARKE, A. R. & SANSOM,

O. J. 2014. Endogenous c-Myc is essential for p53-induced apoptosis in response to DNA damage in vivo. *Cell Death and Differentiation,* 21**,** 956-966.

PICHA, B., THOMPSON, M. & VONDRISKA, T. M. 2012. Preclinical trials: Keep 'reproducibility' in context. *Nature,* 485**,** 41.

PIETSCH, T. & HABERLER, C. 2016. Update on the integrated histopathological and genetic classification of medulloblastoma - a practical diagnostic guideline. *Clinical neuropathology,* 35**,** 344-352.

PIHA-PAUL, S. A., SACHDEV, J. C., BARVE, M., LORUSSO, P., SZMULEWITZ, R., PATEL, S. P., LARA, P. N., JR., CHEN, X., HU, B., FREISE, K. J., MODI, D., SOOD, A., HUTTI, J. E., WOLFF, J. & O'NEIL, B. H. 2019. First-in-Human Study of Mivebresib (ABBV-075), an Oral Pan-Inhibitor of Bromodomain and Extra Terminal Proteins, in Patients with Relapsed/Refractory Solid Tumors. *Clin Cancer Res*.

PIZER, B. & CLIFFORD, S. 2008. Medulloblastoma: new insights into biology and treatment. *Archives of Disease in Childhood-Education and Practice Edition,* 93**,** 137-144.

PIZER, B. L. & CLIFFORD, S. C. 2009. The potential impact of tumour biology on improved clinical practice for medulloblastoma: progress towards biologically driven clinical trials. *British Journal of Neurosurgery,* 23**,** 364-375.

PORTA, C., PAGLINO, C. & MOSCA, A. 2014. Targeting PI3K/Akt/mTOR Signaling in Cancer. *Frontiers in Oncology,* 4.

POSTEL-VINAY, S., BAJRAMI, I., FRIBOULET, L., ELLIOTT, R., FONTEBASSO, Y., DORVAULT, N., OLAUSSEN, K. A., ANDRE, F., SORIA, J. C., LORD, C. J. & ASHWORTH, A. 2013. A high-throughput screen identifies PARP1/2 inhibitors as a potential therapy for ERCC1-deficient non-small cell lung cancer. *Oncogene,* 32**,** 5377-87.

POSTERNAK, V. & COLE, M. D. 2016. Strategically targeting MYC in cancer. *F1000Res,* 5.

PRINCE, E. W., BALAKRISHNAN, I., SHAH, M., LEVY, J. M. M., GRIESINGER, A. M., ALIMOVA, I., HARRIS, P. S., BIRKS, D. K., DONSON, A. M., DAVIDSON, N., REMKE, M., TAYLOR, M. D., HANDLER, M. H., FOREMAN, N. K., VENKATARAMAN, S. & VIBHAKAR, R. 2016. Checkpoint kinase 1 expression is an adverse prognostic marker and therapeutic target in MYC-driven medulloblastoma. *Oncotarget,* 7**,** 53881-53894.

PUGH, T. J., WEERARATNE, S. D., ARCHER, T. C., POMERANZ KRUMMEL, D. A., AUCLAIR, D., BOCHICCHIO, J., CARNEIRO, M. O., CARTER, S. L., CIBULSKIS, K., ERLICH, R. L., GREULICH, H., LAWRENCE, M. S., LENNON, N. J., MCKENNA, A., MELDRIM, J., RAMOS, A. H., ROSS, M. G., RUSS, C., SHEFLER, E., SIVACHENKO, A., SOGOLOFF, B., STOJANOV, P., TAMAYO, P., MESIROV, J. P., AMANI, V., TEIDER, N., SENGUPTA, S., FRANCOIS, J. P., NORTHCOTT, P. A., TAYLOR, M. D., YU, F., CRABTREE, G. R., KAUTZMAN, A. G., GABRIEL, S. B., GETZ, G., JAGER, N., JONES, D. T., LICHTER, P., PFISTER, S. M., ROBERTS, T. M., MEYERSON, M., POMEROY, S. L. & CHO, Y. J. 2012. Medulloblastoma exome sequencing uncovers subtype-specific somatic mutations. *Nature,* 488**,** 106-10.

PUISSANT, A., FRUMM, S. M., ALEXE, G., BASSIL, C. F., QI, J., CHANTHERY, Y. H., NEKRITZ, E. A., ZEID, R., GUSTAFSON, W. C., GRENINGER, P., GARNETT, M. J., MCDERMOTT, U., BENES, C. H., KUNG, A. L., WEISS, W. A., BRADNER, J. E. & STEGMAIER, K. 2013. Targeting MYCN in neuroblastoma by BET bromodomain inhibition. *Cancer Discov,* 3**,** 308-23.

PULS, L. N., EADENS, M. & MESSERSMITH, W. 2011. Current status of SRC inhibitors in solid tumor malignancies. *The oncologist,* 16**,** 566-578.

PURZNER, T., PURZNER, J., BUCKSTAFF, T., COZZA, G., GHOLAMIN, S., RUSERT, J. M., HARTL, T. A., SANDERS, J., CONLEY, N., GE, X. C., LANGAN, M., RAMASWAMY, V., ELLIS, L., LITZENBURGER, U., BOLIN, S., THERUVATH, J., NITTA, R., QI, L., LI, X. N., LI, G., TAYLOR, M. D., WECHSLER-REYA, R. J., PINNA, L. A., CHO, Y. J., FULLER, M. T., ELIAS, J. E. & SCOTT, M. P. 2018. Developmental phosphoproteomics identifies the kinase CK2 as a

driver of Hedgehog signaling and a therapeutic target in medulloblastoma. *Science Signaling,* 11.

RAHL, P. B. & YOUNG, R. A. 2014. MYC and transcription elongation. *Cold Spring Harb Perspect Med,* 4**,** a020990.

RAJAN, A., KELLY, R. J., TREPEL, J. B., KIM, Y. S., ALARCON, S. V., KUMMAR, S., GUTIERREZ, M., CRANDON, S., ZEIN, W. M., JAIN, L., MANNARGUDI, B., FIGG, W. D., HOUK, B. E., SHNAIDMAN, M., BREGA, N. & GIACCONE, G. 2011. A phase I study of PF-04929113 (SNX-5422), an orally bioavailable heat shock protein 90 inhibitor, in patients with refractory solid tumor malignancies and lymphomas. *Clinical cancer research : an official journal of the American Association for Cancer Research,* 17**,** 6831-6839.

RAKHRA, K., BACHIREDDY, P., ZABUAWALA, T., ZEISER, R., XU, L., KOPELMAN, A., FAN, A. C., YANG, Q., BRAUNSTEIN, L., CROSBY, E., RYEOM, S. & FELSHER, D. W. 2010. CD4(+) T cells contribute to the remodeling of the microenvironment required for sustained tumor regression upon oncogene inactivation. *Cancer cell,* 18**,** 485-498.

RAMASWAMY, V., REMKE, M., BOUFFET, E., BAILEY, S., CLIFFORD, S. C., DOZ, F., KOOL, M., DUFOUR, C., VASSAL, G., MILDE, T., WITT, O., VON HOFF, K., PIETSCH, T., NORTHCOTT, P. A., GAJJAR, A., ROBINSON, G. W., PADOVANI, L., ANDRE, N., MASSIMINO, M., PIZER, B., PACKER, R., RUTKOWSKI, S., PFISTER, S. M., TAYLOR, M. D. & POMEROY, S. L. 2016. Risk stratification of childhood medulloblastoma in the molecular era: the current consensus. *Acta Neuropathol,* 131**,** 821-31.

RAUB, T. J., GELBERT, L. M., WISHART, G. N., SANCHEZ-MARTINEZ, C., KULANTHAIVEL, P., STATON, B. A., AJAMIE, R. T., SAWADA, G. A., SHANNON, H. E. & DE DIOS, A. 2015. Abemaciclib (LY2835219) is an Oral Inhibitor of the Cyclin-Dependent Kinases 4/6 that Crosses the Blood-Brain Barrier and Demonstrates In Vivo Activity Against Intracranial Human Brain Tumor Xenografts. *Drug Metabolism and Disposition***,** dmd.114.062745.

RAUSCH, T., JONES, D. T., ZAPATKA, M., STÜTZ, A. M., ZICHNER, T., WEISCHENFELDT, J., JÄGER, N., REMKE, M., SHIH, D., NORTHCOTT, P. A., PFAFF, E., TICA, J., WANG, Q., MASSIMI, L., WITT, H., BENDER, S., PLEIER, S., CIN, H., HAWKINS, C., BECK, C., VON DEIMLING, A., HANS, V., BRORS, B., EILS, R., SCHEURLEN, W., BLAKE, J., BENES, V., KULOZIK, A. E., WITT, O., MARTIN, D., ZHANG, C., PORAT, R., MERINO, D. M., WASSERMAN, J., JABADO, N., FONTEBASSO, A., BULLINGER, L., RÜCKER, F. G., DÖHNER, K., DÖHNER, H., KOSTER, J., MOLENAAR, J. J., VERSTEEG, R., KOOL, M., TABORI, U., MALKIN, D., KORSHUNOV, A., TAYLOR, M. D., LICHTER, P., PFISTER, S. M. & KORBEL, J. O. 2012. Genome sequencing of pediatric medulloblastoma links catastrophic DNA rearrangements with TP53 mutations. *Cell,* 148**,** 59-71.

REN, Y., BI, C., ZHAO, X., LWIN, T., WANG, C., YUAN, J., SILVA, A. S., SHAH, B. D., FANG, B., LI, T., KOOMEN, J. M., JIANG, H., CHAVEZ, J. C., PHAM, L. V., SUDALAGUNTA, P. R., WAN, L., WANG, X., DALTON, W. S., MOSCINSKI, L. C., SHAIN, K. H., VOSE, J., CLEVELAND, J. L., SOTOMAYOR, E. M., FU, K. & TAO, J. 2018. PLK1 stabilizes a MYC-dependent kinase network in aggressive B cell lymphomas. *J Clin Invest,* 128**,** 5517-5530.

RESTELLI, V., VAGNI, M., ARRIBAS, A. J., BERTONI, F., DAMIA, G. & CARRASSA, L. 2018. Inhibition of CHK1 and WEE1 as a new therapeutic approach in diffuse large B cell lymphomas with MYC deregulation. *British Journal of Haematology,* 181**,** 129-133.

RIBI, K., RELLY, C., LANDOLT, M. A., ALBER, F. D., BOLTSHAUSER, E. & GROTZER, M. A. 2005. Outcome of medulloblastoma in children: long-term complications and quality of life. *Neuropediatrics,* 36**,** 357-65.

RICCARDI, C. & NICOLETTI, I. 2006. Analysis of apoptosis by propidium iodide staining and flow cytometry. *Nature Protocols,* 1**,** 1458-1461.

RICCI*, F., CARRASSA, L., CHRISTODOULOU, M. S., PASSARELLA, D., MICHEL, B., BENHIDA, R., MARTINET, N., HUNYADI, A., IOANNOU, E., ROUSSIS, V., MUSSO, L., DALLAVALLE, S., SILVESTRI, R., WESTWOOD, N., MORI, M., INGALLINA, C., BOTTA, B., KAVETSOU, E., DETSI, A., MAJER, Z., HUDECZ, F., BOSZE, S., KAMINSKA, B., HANSEN, T. V., BERTRAND, P., ATHANASSOPOULOS, C. M. & DAMIA*, G. 2018. A High-throughput Screening of a Chemical Compound Library in Ovarian Cancer Stem Cells. *Combinatorial Chemistry & High Throughput Screening,* 21**,** 50-56.

RICHARDS, M. W., BURGESS, S. G., POON, E., CARSTENSEN, A., EILERS, M., CHESLER, L. & BAYLISS, R. 2016. Structural basis of N-Myc binding by Aurora-A and its destabilization by kinase inhibitors. *Proceedings of the National Academy of Sciences of the United States of America,* 113**,** 13726-13731.

RIEKEN, S., RIEBER, J., BRONS, S., HABERMEHL, D., RIEF, H., ORSCHIEDT, L., LINDEL, K., WEBER, K. J., DEBUS, J. & COMBS, S. E. 2015. Radiation-induced motility alterations in medulloblastoma cells. *J Radiat Res,* 56**,** 430-6.

RILEY, T., SONTAG, E., CHEN, P. & LEVINE, A. 2008. Transcriptional control of human p53-regulated genes. *Nat Rev Mol Cell Biol,* 9**,** 402-12.

ROBINSON, G., PARKER, M., KRANENBURG, T. A., LU, C., CHEN, X., DING, L., PHOENIX, T. N., HEDLUND, E., WEI, L., ZHU, X., CHALHOUB, N., BAKER, S. J., HUETHER, R., KRIWACKI, R., CURLEY, N., THIRUVENKATAM, R., WANG, J., WU, G., RUSCH, M., HONG, X., BECKSFORT, J., GUPTA, P., MA, J., EASTON, J., VADODARIA, B., ONAR-THOMAS, A., LIN, T., LI, S., POUNDS, S., PAUGH, S., ZHAO, D., KAWAUCHI, D., ROUSSEL, M. F., FINKELSTEIN, D., ELLISON, D. W., LAU, C. C., BOUFFET, E., HASSALL, T., GURURANGAN, S., COHN, R., FULTON, R. S., FULTON, L. L., DOOLING, D. J., OCHOA, K., GAJJAR, A., MARDIS, E. R., WILSON, R. K., DOWNING, J. R., ZHANG, J. & GILBERTSON, R. J. 2012. Novel mutations target distinct subgroups of medulloblastoma. *Nature,* 488**,** 43-8.

RODE, A., MAASS, K. K., WILLMUND, K. V., LICHTER, P. & ERNST, A. 2016. Chromothripsis in cancer cells: An update. *Int J Cancer,* 138**,** 2322-33.

RØDLAND, G. E., MELHUS, K., GENERALOV, R., GILANI, S., BERTONI, F., DAHLE, J., SYLJUÅSEN, R. & PATZKE, S. 2019. The Dual Cell Cycle Kinase Inhibitor JNJ-7706621 Reverses Resistance to CD37 Targeted Radioimmunotherapy in Activated B Cell like Diffuse Large B Cell Lymphoma Cell Lines. *Blood,* 134**,** 2574-2574.

ROGERS, H. A., ESTRANERO, J., GUDKA, K. & GRUNDY, R. G. 2017. The therapeutic potential of targeting the PI3K pathway in pediatric brain tumors. *Oncotarget,* 8**,** 2083-2095.

ROHBAN, S. & CAMPANER, S. 2015. Myc induced replicative stress response: How to cope with it and exploit it. *Biochimica Et Biophysica Acta-Gene Regulatory Mechanisms,* 1849**,** 517-524.

ROLLINS, N., WINICK, N., BASH, R. & BOOTH, T. 2004. Acute methotrexate neurotoxicity: findings on diffusion-weighted imaging and correlation with clinical outcome. *AJNR Am J Neuroradiol,* 25**,** 1688-95.

ROMER, J. & CURRAN, T. 2005. Targeting Medulloblastoma: Small-Molecule Inhibitors of the Sonic Hedgehog Pathway as Potential Cancer Therapeutics. *Cancer Research,* 65**,** 4975-4978.

RONCO, C., MARTIN, A. R., DEMANGE, L. & BENHIDA, R. 2016. ATM, ATR, CHK1, CHK2 and WEE1 inhibitors in cancer and cancer stem cells. *MedChemComm,* 8**,** 295-319.

ROUSSEL, M. F. & ROBINSON, G. W. 2013. Role of MYC in Medulloblastoma. *Cold Spring Harbor Perspectives in Medicine,* 3.

ROUSSEL, M. F. & STRIPAY, J. L. 2018. Epigenetic Drivers in Pediatric Medulloblastoma. *Cerebellum (London, England),* 17**,** 28-36.

ROUSSEL, M. F. & STRIPAY, J. L. 2020. Modeling pediatric medulloblastoma. *Brain pathology (Zurich, Switzerland),* 30**,** 703-712.

ROUX, P. P. & TOPISIROVIC, I. 2018. Signaling Pathways Involved in the Regulation of mRNA Translation. *Molecular and Cellular Biology,* 38.

ROZENGURT, E., SOARES, H. P. & SINNET-SMITH, J. 2014. Suppression of feedback loops mediated by PI3K/mTOR induces multiple overactivation of compensatory pathways: an unintended consequence leading to drug resistance. *Mol Cancer Ther,* 13**,** 2477-88.

RUTKOWSKI, S., MODENA, P., WILLIAMSON, D., KERL, K., NYSOM, K., PIZER, B., BARTELS, U., PUGET, S., DOZ, F., MICHALSKI, A., VON HOFF, K., CHEVIGNARD, M., AVULA, S., MURRAY, M. J., SCHONBERGER, S., CZECH, T., SCHOUTEN-VAN MEETEREN, A. Y. N., KORDES, U., KRAMM, C. M., VAN VUURDEN, D. G., HULLEMAN, E., JANSSENS, G. O., SOLANKI, G. A., VAN VEELEN, M. L. C., THOMALE, U., SCHUHMANN, M. U., JONES, C., GIANGASPERO, F., FIGARELLA-BRANGER, D., PIETSCH, T., CLIFFORD, S. C., PFISTER, S. M. & VAN GOOL, S. W. 2018. Biological material collection to advance translational research and treatment of children with CNS tumours: position paper from the SIOPE Brain Tumour Group. *Lancet Oncology,* 19**,** E419-E428.

RYAN, K. M. & BIRNIE, G. D. 1996. Myc oncogenes: The enigmatic family. *Biochemical Journal,* 314**,** 713-721.

RYAN, S. L., SCHWALBE, E. C., COLE, M., LU, Y., LUSHER, M. E., MEGAHED, H., O'TOOLE, K., NICHOLSON, S. L., BOGNAR, L., GARAMI, M., HAUSER, P., KORSHUNOV, A., PFISTER, S. M., WILLIAMSON, D., TAYLOR, R. E., ELLISON, D. W., BAILEY, S. & CLIFFORD, S. C. 2012. MYC family amplification and clinical risk-factors interact to predict an extremely poor prognosis in childhood medulloblastoma. *Acta Neuropathologica,* 123**,** 501-513.

RYL, T., KUCHEN, E. E., BELL, E., SHAO, C., FLOREZ, A. F., MONKE, G., GOGOLIN, S., FRIEDRICH, M., LAMPRECHT, F., WESTERMANN, F. & HOFER, T. 2017. Cell-Cycle Position of Single MYC-Driven Cancer Cells Dictates Their Susceptibility to a Chemotherapeutic Drug. *Cell Syst,* 5**,** 237-250 e8.

RYU, J., PYO, J., LEE, C. W. & KIM, J. E. 2018. An Aurora kinase inhibitor, AMG900, inhibits glioblastoma cell proliferation by disrupting mitotic progression. *Cancer Medicine,* 7**,** 5589-5603.

SAKAGUCHI, T., YOSHINO, H., SUGITA, S., MIYAMOTO, K., YONEMORI, M., OSAKO, Y., MEGURO-HORIKE, M., HORIKE, S. I., NAKAGAWA, M. & ENOKIDA, H. 2018. Bromodomain protein BRD4 inhibitor JQ1 regulates potential prognostic molecules in advanced renal cell carcinoma. *Oncotarget,* 9**,** 23003-23017.

SALADINO, C., FRAME, S., DAVIS, S., BLAKE, D. & ZHELEVA, D. 2015. CYC065, a novel CDK2/5/9 inhibitor: detailed mechanistic studies, determinants of sensitivity and synergistic combinations. *Cancer Research,* 75.

SANAI, N., LI, J., BOERNER, J., STARK, K., WU, J., KIM, S., DEROGATIS, A., MEHTA, S., DHRUV, H. D., HEILBRUN, L. K., BERENS, M. E. & LORUSSO, P. M. 2018. Phase 0 Trial of AZD1775 in First-Recurrence Glioblastoma Patients. *Clinical Cancer Research,* 24**,** 3820-3828.

SANCAR, A., LINDSEY-BOLTZ, L. A., UNSAL-KAÇMAZ, K. & LINN, S. 2004. Molecular mechanisms of mammalian DNA repair and the DNA damage checkpoints. *Annu Rev Biochem,* 73**,** 39-85.

SANDÉN, E., DYBERG, C., KRONA, C., GALLO-OLLER, G., OLSEN, T. K., ENRÍQUEZ PÉREZ, J., WICKSTRÖM, M., ESTEKIZADEH, A., KOOL, M., VISSE, E., EKSTRÖM, T. J., SIESJÖ, P., JOHNSEN, J. I. & DARABI, A. 2017. Establishment and characterization of an orthotopic patient-derived Group 3 medulloblastoma model for preclinical drug evaluation. *Sci Rep,* 7**,** 46366.

SARCAR, B., KAHALI, S., PRABHU, A. H., SHUMWAY, S. D., XU, Y., DEMUTH, T. & CHINNAIYAN, P. 2011. Targeting Radiation-Induced G₂ Checkpoint Activation with the Wee-1 Inhibitor MK-1775 in Glioblastoma Cell Lines. *Molecular Cancer Therapeutics,* 10**,** 2405-2414.

SATO, M., RODRIGUEZ-BARRUECO, R., YU, J. Y., DO, C., SILVA, J. M. & GAUTIER, J. 2015. MYC is a critical target of FBXW7. *Oncotarget,* 6**,** 3292-3305.

SAUSVILLE, E., LORUSSO, P., CARDUCCI, M., CARTER, J., QUINN, M., MALBURG, L., AZAD, N., COSGROVE, D., KNIGHT, R., BARKER, P., ZABLUDOFF, S., AGBO, F., OAKES, P. & SENDEROWICZ, A. 2014. Phase I dose-escalation study of AZD7762, a checkpoint kinase inhibitor, in combination with gemcitabine in US patients with advanced solid tumors. *Cancer chemotherapy and pharmacology,* 73.

SAVINO, M., ANNIBALI, D., CARUCCI, N., FAVUZZI, E., COLE, M. D., EVAN, G. I., SOUCEK, L. & NASI, S. 2011. The Action Mechanism of the Myc Inhibitor Termed Omomyc May Give Clues on How to Target Myc for Cancer Therapy. *Plos One,* 6.

SCAGLIOTTI, G., KANG, J. H., SMITH, D., ROSENBERG, R., PARK, K., KIM, S.-W., SU, W.-C., BOYD, T. E., RICHARDS, D. A., NOVELLO, S., HYNES, S. M., MYRAND, S. P., LIN, J., SMYTH, E. N., WIJAYAWARDANA, S., LIN, A. B. & PINDER-SCHENCK, M. 2016. Phase II evaluation of LY2603618, a first-generation CHK1 inhibitor, in combination with pemetrexed in patients with advanced or metastatic non-small cell lung cancer. *Investigational New Drugs,* 34**,** 625-635.

SCHINDLER, M. 2017. Theory of synergistic effects: Hill-type response surfaces as 'null-interaction' models for mixtures. *Theoretical Biology and Medical Modelling,* 14**,** 15.

SCHMITZ, R., CERIBELLI, M., PITTALUGA, S., WRIGHT, G. & STAUDT, L. M. 2014. Oncogenic mechanisms in Burkitt lymphoma. *Cold Spring Harb Perspect Med,* 4.

SCHOR, N. F. 2009. Pharmacotherapy for adults with tumors of the central nervous system. *Pharmacology & therapeutics,* 121**,** 253-264.

SCHORL, C. & SEDIVY, J. M. 2003. Loss of protooncogene c-Myc function impedes G1 phase progression both before and after the restriction point. *Mol Biol Cell,* 14**,** 823-35.

SCHREIBER, J. E., PALMER, S. L., CONKLIN, H. M., MABBOTT, D. J., SWAIN, M. A., BONNER, M. J., CHAPIESKI, M. L., HUANG, L., ZHANG, H. & GAJJAR, A. 2017. Posterior fossa syndrome and long-term neuropsychological outcomes among children treated for medulloblastoma on a multi-institutional, prospective study. *Neuro-Oncology,* 19**,** 1673-1682.

SCHWALBE, E. C., LINDSEY, J. C., NAKJANG, S., CROSIER, S., SMITH, A. J., HICKS, D., RAFIEE, G., HILL, R. M., ILIASOVA, A., STONE, T., PIZER, B., MICHALSKI, A., JOSHI, A., WHARTON, S. B., JACQUES, T. S., BAILEY, S., WILLIAMSON, D. & CLIFFORD, S. C. 2017. Novel molecular subgroups for clinical classification and outcome prediction in childhood medulloblastoma: a cohort study. *Lancet Oncology,* 18**,** 958-971.

SCHWALBE, E. C., WILLIAMSON, D., LINDSEY, J. C., HAMILTON, D., RYAN, S. L., MEGAHED, H., GARAMI, M., HAUSER, P., DEMBOWSKA-BAGINSKA, B., PEREK, D., NORTHCOTT, P. A., TAYLOR, M. D., TAYLOR, R. E., ELLISON, D. W., BAILEY, S. & CLIFFORD, S. C. 2013. DNA methylation profiling of medulloblastoma allows robust subclassification and improved outcome prediction using formalin-fixed biopsies. *Acta Neuropathologica,* 125**,** 359-371.

SCHWERMER, M., LEE, S., KOSTER, J., VAN MAERKEN, T., STEPHAN, H., EGGERT, A., MORIK, K., SCHULTE, J. H. & SCHRAMM, A. 2015. Sensitivity to cdk1-inhibition is modulated by p53 status in preclinical models of embryonal tumors. *Oncotarget,* 6**,** 15425-15435.

SCOTT, G. K., CHU, D., KAUR, R., MALATO, J., ROTHSCHILD, D. E., FRAZIER, K., EPPENBERGER-CASTORI, S., HANN, B., PARK, B. H. & BENZ, C. C. 2016. ERpS294 is a biomarker of ligand

or mutational ERα activation and a breast cancer target for CDK2 inhibition. *Oncotarget,* 8**,** 83432-83445.

SEARS, R. C. 2004. The life cycle of C-myc - From synthesis to degradation. *Cell Cycle,* 3**,** 1133-1137.

SELBY, M. P., FINETTI, M. A., BASHTON, M., CRANSTON, R. E., GRABOVSKA, Y., DEL-CARPIO-PONS, A., SMITH, A., BAILEY, S., CLIFFORD, S. C. & WILLIAMSON, D. 2017. Investigating the biology of atypical teratoid/rhabdoid tumors by whole genome CRISPR/Cas9 screening. *Cancer Research,* 77.

SHACKLEFORD, G. M., MAHDI, M. Y., MOATS, R. A., HAWES, D., TRAN, H. C., FINLAY, J. L., HOANG, T. Q., MENG, E. F. & ERDREICH-EPSTEIN, A. 2019. Continuous and bolus intraventricular topotecan prolong survival in a mouse model of leptomeningeal medulloblastoma. *PLoS One,* 14**,** e0206394.

SHALABY, T. & GROTZER, M. A. 2016. MYC as Therapeutic Target for Embryonal Tumors: Potential and Challenges. *Curr Cancer Drug Targets,* 16**,** 2-21.

SHALEM, O., SANJANA, N. E., HARTENIAN, E., SHI, X., SCOTT, D. A., MIKKELSON, T., HECKL, D., EBERT, B. L., ROOT, D. E., DOENCH, J. G. & ZHANG, F. 2014. Genome-scale CRISPR-Cas9 knockout screening in human cells. *Science (New York, N.Y.),* 343**,** 84-87.

SHAPIRO, G. I., HILTON, J., CLEARY, J. M., TOLANEY, S. M., GHANDI, L., KWAK, E. L., CLARK, J. W., WOLANSKI, A., BELL, T., SCHULZ, J., FRAME, S., SALADINO, C., HOGBEN, M., RODIG, S. J., CHIAO, J. H. & BLAKE, D. 2013. Abstract LB-202: Responses to sequential sapacitabine and seliciclib in patients with BRCA-deficient solid tumors. *Cancer Research,* 73**,** LB-202-LB-202.

SHAPIRO, G. I., KOESTNER, D. A., MATRANGA, C. B. & ROLLINS, B. J. 1999. Flavopiridol Induces Cell Cycle Arrest and p53-independent Apoptosis in Non-Small Cell Lung Cancer Cell Lines. *Clinical Cancer Research,* 5**,** 2925-2938.

SHEN, Y., REHMAN, F. L., FENG, Y., BOSHUIZEN, J., BAJRAMI, I., ELLIOTT, R., WANG, B., LORD, C. J., POST, L. E. & ASHWORTH, A. 2013. BMN 673, a novel and highly potent PARP1/2 inhibitor for the treatment of human cancers with DNA repair deficiency. *Clinical cancer research : an official journal of the American Association for Cancer Research,* 19**,** 5003-5015.

SHEPHERD, C., BANERJEE, L., CHEUNG, C. W., MANSOUR, M. R., JENKINSON, S., GALE, R. E. & KHWAJA, A. 2013. PI3K/mTOR inhibition upregulates NOTCH-MYC signalling leading to an impaired cytotoxic response. *Leukemia,* 27**,** 650-60.

SHI, F., ZHANG, J., LIU, H., WU, L., JIANG, H., WU, Q., LIU, T., LOU, M. & WU, H. 2017. The dual PI3K/mTOR inhibitor dactolisib elicits anti-tumor activity in vitro and in vivo. *Oncotarget,* 9**,** 706-717.

SHU, Q., WONG, K. K., SU, J. M., ADESINA, A. M., YU, L. T., TSANG, Y. T., ANTALFFY, B. C., BAXTER, P., PERLAKY, L., YANG, J., DAUSER, R. C., CHINTAGUMPALA, M., BLANEY, S. M., LAU, C. C. & LI, X. N. 2008. Direct orthotopic transplantation of fresh surgical specimen preserves CD133+ tumor cells in clinically relevant mouse models of medulloblastoma and glioma. *Stem Cells,* 26**,** 1414-24.

SHUKLA, A. 2016. High Throughput Screening of Small Molecule Library: Procedure, Challenges and Future. *Journal of Cancer Prevention & Current Research,* 5**,** 154.

SIMS, R. J., 3RD, BELOTSERKOVSKAYA, R. & REINBERG, D. 2004. Elongation by RNA polymerase II: the short and long of it. *Genes Dev,* 18**,** 2437-68.

SINGH, A. R., JOSHI, S., ZULCIC, M., ALCARAZ, M., GARLICH, J. R., MORALES, G. A., CHO, Y. J., BAO, L., LEVY, M. L., NEWBURY, R., MALICKI, D., MESSER, K., CRAWFORD, J. & DURDEN, D. L. 2016. PI-3K Inhibitors Preferentially Target CD15+ Cancer Stem Cell Population in SHH Driven Medulloblastoma. *PLOS ONE,* 11**,** e0150836.

SIRACHAINAN, N., NUCHPRAYOON, I., THANARATTANAKORN, P., PAKAKASAMA, S., LUSAWAT, A., VISUDIBHAN, A., DHANACHAI, M., LARBCHAROENSUB, N., AMORNFA, J., SHOTELERSUK, K., KATANYUWONG, K., TANGKARATT, S. & HONGENG, S. 2011. Outcome of medulloblastoma in children treated with reduced-dose radiation therapy plus adjuvant chemotherapy. *Journal of Clinical Neuroscience,* 18**,** 515-519.

SLEE, R. B., GRIMES, B. R., BANSAL, R., GORE, J., BLACKBURN, C., BROWN, L., GASAWAY, R., JEONG, J., VICTORINO, J., MARCH, K. L., COLOMBO, R., HERBERT, B. S. & KORC, M. 2014. Selective inhibition of pancreatic ductal adenocarcinoma cell growth by the mitotic MPS1 kinase inhibitor NMS-P715. *Mol Cancer Ther,* 13**,** 307-315.

SMITH, J., THO, L. M., XU, N. & GILLESPIE, D. A. 2010. The ATM-Chk2 and ATR-Chk1 pathways in DNA damage signaling and cancer. *Adv Cancer Res,* 108**,** 73-112.

SMITH, M. A., REYNOLDS, C. P., KANG, M. H., KOLB, E. A., GORLICK, R., CAROL, H., LOCK, R. B., KEIR, S. T., MARIS, J. M., BILLUPS, C. A., LYALIN, D., KURMASHEVA, R. T. & HOUGHTON, P. J. 2015. Synergistic activity of PARP inhibition by talazoparib (BMN 673) with temozolomide in pediatric cancer models in the pediatric preclinical testing program. *Clinical cancer research : an official journal of the American Association for Cancer Research,* 21**,** 819-832.

SMITH, M. J., BEETZ, C., WILLIAMS, S. G., BHASKAR, S. S., O'SULLIVAN, J., ANDERSON, B., DALY, S. B., URQUHART, J. E., BHOLAH, Z., OUDIT, D., CHEESMAN, E., KELSEY, A., MCCABE, M. G., NEWMAN, W. G. & EVANS, D. G. 2014. Germline mutations in SUFU cause Gorlin syndrome-associated childhood medulloblastoma and redefine the risk associated with PTCH1 mutations. *J Clin Oncol,* 32**,** 4155-61.

SMOLL, N. R. & DRUMMOND, K. J. 2012. The incidence of medulloblastomas and primitive neurectodermal tumours in adults and children. *Journal of Clinical Neuroscience,* 19**,** 1541-1544.

SODIR, N. M., SWIGART, L. B., KARNEZIS, A. N., HANAHAN, D., EVAN, G. I. & SOUCEK, L. 2011. Endogenous Myc maintains the tumor microenvironment. *Genes & development,* 25**,** 907-916.

SOLDI, R., COHEN, A. L., CHENG, L., SUN, Y., MOOS, P. J. & BILD, A. H. 2013. A genomic approach to predict synergistic combinations for breast cancer treatment. *The Pharmacogenomics Journal,* 13**,** 94-104.

SOLOMON, B. J., MOK, T., KIM, D. W., WU, Y. L., NAKAGAWA, K., MEKHAIL, T., FELIP, E., CAPPUZZO, F., PAOLINI, J., USARI, T., IYER, S., REISMAN, A., WILNER, K. D., TURSI, J., BLACKHALL, F. & INVESTIGATORS, P. 2014. First-line crizotinib versus chemotherapy in ALK-positive lung cancer. *N Engl J Med,* 371**,** 2167-77.

SONG, H., BHAKAT, R., KLING, M. J., COULTER, D. W., CHATURVEDI, N. K., RAY, S. & JOSHI, S. S. 2019. Targeting cyclin-dependent kinase 9 sensitizes medulloblastoma cells to chemotherapy. *Biochem Biophys Res Commun*.

SOUCEK, L., JUCKER, R., PANACCHIA, L., RICORDY, R., TATO, F. & NASI, S. 2002. Omomyc, a potential Myc dominant negative, enhances Myc-induced apoptosis. *Cancer Research,* 62**,** 3507-3510.

SOUCEK, L., LAWLOR, E. R., SOTO, D., SHCHORS, K., SWIGART, L. B. & EVAN, G. I. 2007. Mast cells are required for angiogenesis and macroscopic expansion of Myc-induced pancreatic islet tumors. *Nat Med,* 13**,** 1211-8.

SOUCEK, L., NASI, S. & EVAN, G. I. 2004. Omomyc expression in skin prevents Myc-induced papillomatosis. *Cell Death and Differentiation,* 11**,** 1038-1045.

SOUCIE, E. L., ANNIS, M. G., SEDIVY, J., FILMUS, J., LEBER, B., ANDREWS, D. W. & PENN, L. Z. 2001. Myc potentiates apoptosis by stimulating Bax activity at the mitochondria. *Molecular and Cellular Biology,* 21**,** 4725-4736.

SPILLER, S. E., RAVANPAY, A. C., HAHN, A. W. & OLSON, J. M. 2006. Suberoylanilide hydroxamic acid is effective in preclinical studies of medulloblastoma. *Journal of Neuro-Oncology,* 79**,** 259-270.

SPRANGER, S., GAJEWSKI, T. F. & KLINE, J. 2016. MYC - a thorn in the side of cancer immunity. *Cell Res,* 26**,** 639-40.

ST CLAIR, W. H., ADAMS, J. A., BUES, M., FULLERTON, B. C., LA SHELL, S., KOOY, H. M., LOEFFLER, J. S. & TARBELL, N. J. 2004. Advantage of protons compared to conventional X-ray or IMRT in the treatment of a pediatric patient with medulloblastoma. *Int J Radiat Oncol Biol Phys,* 58**,** 727-34.

STATHIS, A. & BERTONI, F. 2018. BET Proteins as Targets for Anticancer Treatment. *Cancer Discov,* 8**,** 24-36.

STEARNS, D., CHAUDHRY, A., ABEL, T. W., BURGER, P. C., DANG, C. V. & EBERHART, C. G. 2006. c-myc overexpression causes anaplasia in medulloblastoma. *Cancer Res,* 66**,** 673-81.

STEWART, C. F., LEGGAS, M. & FRIEDMAN, H. S. 2005. Camptothecins in the Treatment of Primary Brain Tumors. *In:* ADAMS, V. R. & BURKE, T. G. (eds.) *Camptothecins in Cancer Therapy.* Totowa, NJ: Humana Press.

STIEWE, T. 2007. The p53 family in differentiation and tumorigenesis. *Nat Rev Cancer,* 7**,** 165-8.

STREBHARDT, K. 2010. Multifaceted polo-like kinases: drug targets and antitargets for cancer therapy. *Nature Reviews Drug Discovery,* 9**,** 643-U24.

STRUNTZ, N. B., CHEN, A., DEUTZMANN, A., WILSON, R. M., STEFAN, E., EVANS, H. L., RAMIREZ, M. A., LIANG, T., CABALLERO, F., WILDSCHUT, M. H. E., NEEL, D. V., FREEMAN, D. B., POP, M. S., MCCONKEY, M., MULLER, S., CURTIN, B. H., TSENG, H., FROMBACH, K. R., BUTTY, V. L., LEVINE, S. S., FEAU, C., ELMILIGY, S., HONG, J. A., LEWIS, T. A., VETERE, A., CLEMONS, P. A., MALSTROM, S. E., EBERT, B. L., LIN, C. Y., FELSHER, D. W. & KOEHLER, A. N. 2019. Stabilization of the Max Homodimer with a Small Molecule Attenuates Myc-Driven Transcription. *Cell Chemical Biology,* 26**,** 711-+.

SUN, K. M., ATOYAN, R., BOREK, M. A., DELLAROCCA, S., SAMSON, M. E. S., MA, A. W., XU, G. X., PATTERSON, T., TUCK, D. P., VINER, J. L., FATTAEY, A. & WANG, J. 2017. Dual HDAC and PI3K Inhibitor CUDC-907 Downregulates MYC and Suppresses Growth of MYC-dependent Cancers. *Molecular Cancer Therapeutics,* 16**,** 285-299.

SUN, Y., HU, X. & ORLEMANS, E. 2018. Abstract B139: Promising antitumor effects of SNX-5422 in combination with checkpoint inhibitors in an MC38 murine model. *Molecular Cancer Therapeutics,* 17**,** B139-B139.

SWARTLING, F. J., GRIMMER, M. R., HACKETT, C. S., NORTHCOTT, P. A., FAN, Q.-W., GOLDENBERG, D. D., LAU, J., MASIC, S., NGUYEN, K., YAKOVENKO, S., ZHE, X.-N., GILMER, H. C. F., COLLINS, R., NAGAOKA, M., PHILLIPS, J. J., JENKINS, R. B., TIHAN, T., VANDENBERG, S. R., JAMES, C. D., TANAKA, K., TAYLOR, M. D., WEISS, W. A. & CHESLER, L. 2010. Pleiotropic role for MYCN in medulloblastoma. *Genes & development,* 24**,** 1059-1072.

SZYMANSKI, P., MARKOWICZ, M. & MIKICIUK-OLASIK, E. 2012. Adaptation of high-throughput screening in drug discovery-toxicological screening tests. *Int J Mol Sci,* 13**,** 427-52.

TALLARIDA, R. J. 2011. Quantitative Methods for Assessing Drug Synergism. *Genes & Cancer,* 2**,** 1003-1008.

TANG, A. Q., GAO, K. Y., CHU, L. L., ZHANG, R., YANG, J. & ZHENG, J. N. 2017. Aurora kinases: novel therapy targets in cancers. *Oncotarget,* 8**,** 23937-23954.

TANNOUS, B. A., KERAMI, M., VAN DER STOOP, P. M., KWIATKOWSKI, N., WANG, J., ZHOU, W., KESSLER, A. F., LEWANDROWSKI, G., HIDDINGH, L., SOL, N., LAGERWEIJ, T., WEDEKIND, L., NIERS, J. M., BARAZAS, M., NILSSON, R. J., GEERTS, D., DE WITT HAMER, P. C.,

HAGEMANN, C., VANDERTOP, W. P., VAN TELLINGEN, O., NOSKE, D. P., GRAY, N. S. & WÜRDINGER, T. 2013. Effects of the selective MPS1 inhibitor MPS1-IN-3 on glioblastoma sensitivity to antimitotic drugs. *J Natl Cancer Inst,* 105**,** 1322-31.

TANSEY, W. 2014. Mammalian MYC Proteins and Cancer. *New Journal of Science,* 2014**,** 1-27.

TATEISHI, K., IAFRATE, A. J., HO, Q., CURRY, W. T., BATCHELOR, T. T., FLAHERTY, K. T., ONOZATO, M. L., LELIC, N., SUNDARAM, S., CAHILL, D. P., CHI, A. S. & WAKIMOTO, H. 2016. Myc-Driven Glycolysis Is a Therapeutic Target in Glioblastoma. *Clinical cancer research : an official journal of the American Association for Cancer Research,* 22**,** 4452-4465.

TAVANA, O., LI, D., DAI, C., LOPEZ, G., BANERJEE, D., KON, N., CHEN, C., CALIFANO, A., YAMASHIRO, D. J., SUN, H. & GU, W. 2016. HAUSP deubiquitinates and stabilizes N-Myc in neuroblastoma. *Nature medicine,* 22**,** 1180-1186.

TAYLOR, C., JALAVA, A. & MAI, S. 1997. c-Myc dependent initiation of genomic instability during neoplastic transformation. *Curr Top Microbiol Immunol,* 224**,** 201-7.

TAYLOR, M. D., LIU, L., RAFFEL, C., HUI, C. C., MAINPRIZE, T. G., ZHANG, X., AGATEP, R., CHIAPPA, S., GAO, L., LOWRANCE, A., HAO, A., GOLDSTEIN, A. M., STAVROU, T., SCHERER, S. W., DURA, W. T., WAINWRIGHT, B., SQUIRE, J. A., RUTKA, J. T. & HOGG, D. 2002. Mutations in SUFU predispose to medulloblastoma. *Nat Genet,* 31**,** 306-10.

TAYLOR, M. D., NORTHCOTT, P. A., KORSHUNOV, A., REMKE, M., CHO, Y. J., CLIFFORD, S. C., EBERHART, C. G., PARSONS, D. W., RUTKOWSKI, S., GAJJAR, A., ELLISON, D. W., LICHTER, P., GILBERTSON, R. J., POMEROY, S. L., KOOL, M. & PFISTER, S. M. 2012. Molecular subgroups of medulloblastoma: the current consensus. *Acta Neuropathologica,* 123**,** 465-472.

TAYLOR, R. E., BAILEY, C. C., ROBINSON, K., WESTON, C. L., ELLISON, D., IRONSIDE, J., LUCRAFT, H., GILBERTSON, R., TAIT, D. M., WALKER, D. A., PIZER, B. L., IMESON, J. & LASHFORD, L. S. 2003. Results of a randomized study of preradiation chemotherapy versus radiotherapy alone for nonmetastatic medulloblastoma: The International Society of Paediatric Oncology United Kingdom Children's Cancer Study Group PNET-3 study. *Journal of Clinical Oncology,* 21**,** 1581-1591.

THOMAS, A. & NOËL, G. 2019. Medulloblastoma: optimizing care with a multidisciplinary approach. *Journal of multidisciplinary healthcare,* 12**,** 335-347.

THOMPSON, E. M., BRAMALL, A., HERNDON, J. E., TAYLOR, M. D. & RAMASWAMY, V. 2018. The clinical importance of medulloblastoma extent of resection: a systematic review. *Journal of Neuro-Oncology,* 139**,** 523-539.

THOMPSON, E. M., HIELSCHER, T., BOUFFET, E., REMKE, M., LUU, B., GURURANGAN, S., MCLENDON, R. E., BIGNER, D. D., LIPP, E. S., PERREAULT, S., CHO, Y. J., GRANT, G., KIM, S. K., LEE, J. Y., RAO, A. A. N., GIANNINI, C., LI, K. K. W., NG, H. K., YAO, Y., KUMABE, T., TOMINAGA, T., GRAJKOWSKA, W. A., PEREK-POLNIK, M., LOW, D. C. Y., SEOW, W. T., CHANG, K. T. E., MORA, J., POLLACK, I. F., HAMILTON, R. L., LEARY, S., MOORE, A. S., INGRAM, W. J., HALLAHAN, A. R., JOUVET, A., FEVRE-MONTANGE, M., VASILJEVIC, A., FAURE-CONTER, C., SHOFUDA, T., KAGAWA, N., HASHIMOTO, N., JABADO, N., WEIL, A. G., GAYDEN, T., WATAYA, T., SHALABY, T., GROTZER, M., ZITTERBART, K., STERBA, J., KREN, L., HORTOBAGYI, T., KLEKNER, A., LASZLO, B., POCZA, T., HAUSER, P., SCHULLER, U., JUNG, S., JANG, W. Y., FRENCH, P. J., KROS, J. M., VAN VEELEN, M. C., MASSIMI, L., LEONARD, J. R., RUBIN, J. B., VIBHAKAR, R., CHAMBLESS, L. B., COOPER, M. K., THOMPSON, R. C., FARIA, C. C., CARVALHO, A., NUNES, S., PIMENTEL, J., FAN, X., MURASZKO, K. M., LOPEZ-AGUILAR, E., LYDEN, D., GARZIA, L., SHIH, D. J. H., KIJIMA, N., SCHNEIDER, C., ADAMSKI, J., NORTHCOTT, P. A., KOOL, M., JONES, D. T. W., CHAN, J. A., NIKOLIC, A., GARRE, M. L., VAN MEIR, E. G., OSUKA, S., OLSON, J. J., JAHANGIRI, A.,

CASTRO, B. A., GUPTA, N., WEISS, W. A., MOXON-EMRE, I., MABBOTT, D. J., LASSALETTA, A., HAWKINS, C. E., TABORI, U., DRAKE, J., KULKARNI, A., et al. 2016. Prognostic value of medulloblastoma extent of resection after accounting for molecular subgroup: a retrospective integrated clinical and molecular analysis. *Lancet Oncol,* 17**,** 484-495.

THOREEN, C. C., KANG, S. A., CHANG, J. W., LIU, Q., ZHANG, J., GAO, Y., REICHLING, L. J., SIM, T., SABATINI, D. M. & GRAY, N. S. 2009. An ATP-competitive mammalian target of rapamycin inhibitor reveals rapamycin-resistant functions of mTORC1. *J Biol Chem,* 284**,** 8023-32.

TIMEUS, F., CRESCENZIO, N., FANDI, A., DORIA, A., FOGLIA, L. & CORDERO DI MONTEZEMOLO, L. 2008. In vitro antiproliferative and antimigratory activity of dasatinib in neuroblastoma and Ewing sarcoma cell lines. *Oncol Rep,* 19**,** 353-9.

TJANDRA, K. C., MCCARTHY, N., YANG, L., LAOS, A. J., SHARBEEN, G., PHILLIPS, P. A., FORGHAM, H., SAGNELLA, S. M., WHAN, R. M., KAVALLARIS, M., THORDARSON, P. & MCCARROLL, J. A. 2020. Identification of Novel Medulloblastoma Cell-Targeting Peptides for Use in Selective Chemotherapy Drug Delivery. *Journal of Medicinal Chemistry,* 63**,** 2181-2193.

TONTSCH-GRUNT, U., RUDOLPH, D., WAIZENEGGER, I., BAUM, A., GERLACH, D., ENGELHARDT, H., WURM, M., SAVARESE, F., SCHWEIFER, N. & KRAUT, N. 2018. Synergistic activity of BET inhibitor BI 894999 with PLK inhibitor volasertib in AML in vitro and in vivo. *Cancer Lett,* 421**,** 112-120.

TOPHAM, C. H. & TAYLOR, S. S. 2013. Mitosis and apoptosis: how is the balance set? *Curr Opin Cell Biol,* 25**,** 780-5.

TRAN, P. T., BENDAPUDI, P. K., LIN, H. J., CHOI, P., KOH, S., CHEN, J., HORNG, G., HUGHES, N. P., SCHWARTZ, L. H., MILLER, V. A., KAWASHIMA, T., KITAMURA, T., PAIK, D. & FELSHER, D. W. 2011. Survival and death signals can predict tumor response to therapy after oncogene inactivation. *Science translational medicine,* 3**,** 103ra99-103ra99.

TRISCOTT, J., LEE, C., FOSTER, C., MANORANJAN, B., PAMBID, M. R., BERNS, R., FOTOVATI, A., VENUGOPAL, C., O'HALLORAN, K., NARENDRAN, A., HAWKINS, C., RAMASWAMY, V., BOUFFET, E., TAYLOR, M. D., SINGHAL, A., HUKIN, J., RASSEKH, R., YIP, S., NORTHCOTT, P., SINGH, S. K., DUNHAM, C. & DUNN, S. E. 2013. Personalizing the Treatment of Pediatric Medulloblastoma: Polo-like Kinase 1 as a Molecular Target in High-Risk Children. *Cancer Research,* 73**,** 6734-6744.

TSENG, S. H., BOBOLA, M. S., BERGER, M. S. & SILBER, J. R. 1999. Characterization of paclitaxel (Taxol) sensitivity in human glioma- and medulloblastoma-derived cell lines. *Neuro Oncol,* 1**,** 101-8.

TWAROG, N. R., STEWART, E., HAMMILL, C. V. & SHELAT, A. A. 2016. BRAID: A Unifying Paradigm for the Analysis of Combined Drug Action. *Scientific Reports,* 6**,** 25523.

TWIGG, S. R. F., HUFNAGEL, R. B., MILLER, K. A., ZHOU, Y., MCGOWAN, S. J., TAYLOR, J., CRAFT, J., TAYLOR, J. C., SANTORO, S. L., HUANG, T. S., HOPKIN, R. J., BRADY, A. F., CLAYTON-SMITH, J., CLERICUZIO, C. L., GRANGE, D. K., GROESSER, L., HAFNER, C., HORN, D., TEMPLE, I. K., DOBYNS, W. B., CURRY, C. J., JONES, M. C. & WILKIE, A. O. M. 2016. A Recurrent Mosaic Mutation in SMO, Encoding the Hedgehog Signal Transducer Smoothened, Is the Major Cause of Curry-Jones Syndrome. *American Journal of Human Genetics,* 98**,** 1256-1265.

UNLAND, R., KERL, K., SCHLOSSER, S., FARWICK, N., PLAGEMANN, T., LECHTAPE, B., CLIFFORD, S. C., KRETH, J. H., GERSS, J., MUHLISCH, J., RICHTER, G. H. S., HASSELBLATT, M. & FRUHWALD, M. C. 2014. Epigenetic repression of the dopamine receptor D4 in

pediatric tumors of the central nervous system. *Journal of Neuro-Oncology,* 116**,** 237-249.

VAFA, O., WADE, M., KERN, S., BEECHE, M., PANDITA, T. K., HAMPTON, G. M. & WAHL, G. M. 2002. c-Myc can induce DNA damage, increase reactive oxygen species, and mitigate p53 function: A mechanism for oncogene-induced genetic instability. *Molecular Cell,* 9**,** 1031-1044.

VALDORA, F., BANELLI, B., STIGLIANI, S., PFISTER, S. M., MORETTI, S., KOOL, M., REMKE, M., BAI, A. H., BRIGATI, C., HIELSCHER, T., ROMANI, M., SERVIDEI, T., ZOLLO, M., CINALLI, G., OBERTHUER, A., TONINI, G. P. & COCO, S. 2013. Epigenetic Silencing of DKK3 in medulloblastoma. *Int J Mol Sci,* 14**,** 7492-505.

VANDERDYS, V., ALLAK, A., GUESSOUS, F., BENAMAR, M., READ, P. W., JAMESON, M. J. & ABBAS, T. 2018. The Neddylation Inhibitor Pevonedistat (MLN4924) Suppresses and Radiosensitizes Head and Neck Squamous Carcinoma Cells and Tumors. *Molecular Cancer Therapeutics,* 17**,** 368-380.

VANDERPORTEN, E. C., TAVERNA, P., HOGAN, J. N., BALLINGER, M. D., FLANAGAN, W. M. & FUCINI, R. V. 2009. The Aurora kinase inhibitor SNS-314 shows broad therapeutic potential with chemotherapeutics and synergy with microtubule-targeted agents in a colon carcinoma model. *Molecular Cancer Therapeutics,* 8**,** 930-939.

VANNINI, A. & CRAMER, P. 2012. Conservation between the RNA Polymerase I, II, and III Transcription Initiation Machineries. *Molecular Cell,* 45**,** 439-446.

VASSAL, G., BOLAND, I., SANTOS, A., BISSERY, M.-C., TERRIER-LACOMBE, M.-J., MORIZET, J., SAINTE-ROSE, C., LELLOUCH-TUBIANA, A., KALIFA, C. & GOUYETTE, A. 1997. Potent therapeutic activity of irinotecan (CPT-11) and its schedule dependency in medulloblastoma xenografts in nude mice. *International Journal of Cancer,* 73**,** 156-163.

VATNER, R. E., NIEMIERKO, A., MISRA, M., WEYMAN, E. A., GOEBEL, C. P., EBB, D. H., JONES, R. M., HUANG, M. S., MAHAJAN, A., GROSSHANS, D. R., PAULINO, A. C., STANLEY, T., MACDONALD, S. M., TARBELL, N. J. & YOCK, T. I. 2018. Endocrine Deficiency As a Function of Radiation Dose to the Hypothalamus and Pituitary in Pediatric and Young Adult Patients With Brain Tumors. *Journal of Clinical Oncology,* 36**,** 2854-+.

VENERE, M., HORBINSKI, C., CRISH, J. F., JIN, X., VASANJI, A., MAJOR, J., BURROWS, A. C., CHANG, C., PROKOP, J., WU, Q., SIMS, P. A., CANOLL, P., SUMMERS, M. K., ROSENFELD, S. S. & RICH, J. N. 2015. The mitotic kinesin KIF11 is a driver of invasion, proliferation, and self-renewal in glioblastoma. *Science translational medicine,* 7**,** 304ra143-304ra143.

VENKATARAMAN, S., ALIMOVA, I., BALAKRISHNAN, I., HARRIS, P., BIRKS, D. K., GRIESINGER, A., AMANI, V., CRISTIANO, B., REMKE, M., TAYLOR, M. D., HANDLER, M., FOREMAN, N. K. & VIBHAKAR, R. 2014. Inhibition of BRD4 attenuates tumor cell self-renewal and suppresses stem cell signaling in MYC driven medulloblastoma. *Oncotarget,* 5**,** 2355-71.

VENUGOPAL, B., BAIRD, R., KRISTELEIT, R. S., PLUMMER, R., COWAN, R., STEWART, A., FOURNEAU, N., HELLEMANS, P., ELSAYED, Y., MCCLUE, S., SMIT, J. W., FORSLUND, A., PHELPS, C., CAMM, J., EVANS, T. R., DE BONO, J. S. & BANERJI, U. 2013. A phase I study of quisinostat (JNJ-26481585), an oral hydroxamate histone deacetylase inhibitor with evidence of target modulation and antitumor activity, in patients with advanced solid tumors. *Clin Cancer Res,* 19**,** 4262-72.

VERMES, I., HAANEN, C. & REUTELINGSPERGER, C. 2000. Flow cytometry of apoptotic cell death. *Journal of Immunological Methods,* 243**,** 167-190.

VERVOORTS, J., LUSCHER-FIRZLAFF, J. & LUSCHER, B. 2006. The ins and outs of MYC regulation by posttranslational mechanisms. *J Biol Chem,* 281**,** 34725-9.

VILLA, C., MIQUEL, C., MOSSES, D., BERNIER, M. & DI STEFANO, A. L. 2018. The 2016 World Health Organization classification of tumours of the central nervous system. *La Presse Médicale,* 47**,** e187-e200.

VISPÉ, S., DEVRIES, L., CRÉANCIER, L., BESSE, J., BRÉAND, S., HOBSON, D. J., SVEJSTRUP, J. Q., ANNEREAU, J.-P., CUSSAC, D., DUMONTET, C., GUILBAUD, N., BARRET, J.-M. & BAILLY, C. 2009. Triptolide is an inhibitor of RNA polymerase I and II–dependent transcription leading predominantly to down-regulation of short-lived mRNA. *Molecular Cancer Therapeutics,* 8**,** 2780-2790.

VITA, M. & HENRIKSSON, M. 2006. The Myc oncoprotein as a therapeutic target for human cancer. *Seminars in Cancer Biology,* 16**,** 318-330.

VITALI, R., MANCINI, C., CESI, V., TANNO, B., PISCITELLI, M., MANCUSO, M., SESTI, F., PASQUALI, E., CALABRETTA, B., DOMINICI, C. & RASCHELLÀ, G. 2009. Activity of tyrosine kinase inhibitor Dasatinib in neuroblastoma cells in vitro and in orthotopic mouse model. *International Journal of Cancer,* 125**,** 2547-2555.

VLADOIU, M. C., EL-HAMAMY, I., DONOVAN, L. K., FAROOQ, H., HOLGADO, B. L., SUNDARAVADANAM, Y., RAMASWAMY, V., HENDRIKSE, L. D., KUMAR, S., MACK, S. C., LEE, J. J. Y., FONG, V., JURASCHKA, K., PRZELICKI, D., MICHEALRAJ, A., SKOWRON, P., LUU, B., SUZUKI, H., MORRISSY, A. S., CAVALLI, F. M. G., GARZIA, L., DANIELS, C., WU, X. C., QAZI, M. A., SINGH, S. K., CHAN, J. A., MARRA, M. A., MALKIN, D., DIRKS, P., HEISLER, L., PUGH, T., NG, K., NOTTA, F., THOMPSON, E. M., KLEINMAN, C. L., JOYNER, A. L., JABADO, N., STEIN, L. & TAYLOR, M. D. 2019. Childhood cerebellar tumours mirror conserved fetal transcriptional programs. *Nature,* 572**,** 67-+.

VO, B. T., KWON, J. A., LI, C., FINKELSTEIN, D., XU, B., ORR, B. A., SHERR, C. J. & ROUSSEL, M. F. 2018. Mouse medulloblastoma driven by CRISPR activation of cellular Myc. *Scientific reports,* 8**,** 8733-8733.

VO, B. T., WOLF, E., KAWAUCHI, D., GEBHARDT, A., REHG, J. E., FINKELSTEIN, D., WALZ, S., MURPHY, B. L., YOUN, Y. H., HAN, Y. G., EILERS, M. & ROUSSEL, M. F. 2016. The Interaction of Myc with Miz1 Defines Medulloblastoma Subgroup Identity. *Cancer Cell,* 29**,** 5-16.

VO, K. T., KARSKI, E. E., NASHOLM, N. M., ALLEN, S., HOLLINGER, F., GUSTAFSON, W. C., LONG-BOYLE, J. R., SHIBOSKI, S., MATTHAY, K. K. & DUBOIS, S. G. 2017. Phase 1 study of sirolimus in combination with oral cyclophosphamide and topotecan in children and young adults with relapsed and refractory solid tumors. *Oncotarget,* 8**,** 23851-23861.

VOGES, Y., MICHAELIS, M., ROTHWEILER, F., SCHALLER, T., SCHNEIDER, C., POLITT, K., MERNBERGER, M., NIST, A., STIEWE, T., WASS, M. N., RÖDEL, F. & CINATL, J. 2016. Effects of YM155 on survivin levels and viability in neuroblastoma cells with acquired drug resistance. *Cell Death & Disease,* 7**,** e2410-e2410.

VON BUEREN, A. O., KORTMANN, R. D., VON HOFF, K., FRIEDRICH, C., MYNAREK, M., MULLER, K., GOSCHZIK, T., ZUR MUHLEN, A., GERBER, N., WARMUTH-METZ, M., SOERENSEN, N., DEINLEIN, F., BENESCH, M., ZWIENER, I., KWIECIEN, R., FALDUM, A., BODE, U., FLEISCHHACK, G., HOVESTADT, V., KOOL, M., JONES, D., NORTHCOTT, P., KUEHL, J., PFISTER, S., PIETSCH, T. & RUTKOWSKI, S. 2016. Treatment of Children and Adolescents With Metastatic Medulloblastoma and Prognostic Relevance of Clinical and Biologic Parameters. *J Clin Oncol,* 34**,** 4151-4160.

VON BUEREN, A. O., OEHLER, C., SHALABY, T., VON HOFF, K., PRUSCHY, M., SEIFERT, B., GERBER, N. U., WARMUTH-METZ, M., STEARNS, D., EBERHART, C. G., KORTMANN, R. D., RUTKOWSKI, S. & GROTZER, M. A. 2011. c-MYC expression sensitizes

medulloblastoma cells to radio- and chemotherapy and has no impact on response in medulloblastoma patients. *BMC Cancer,* 11**,** 74.

VON BUEREN, A. O., SHALABY, T., OEHLER-JANNE, C., ARNOLD, L., STEARNS, D., EBERHART, C. G., ARCARO, A., PRUSCHY, M. & GROTZER, M. A. 2009. RNA interference-mediated c-MYC inhibition prevents cell growth and decreases sensitivity to radio- and chemotherapy in childhood medulloblastoma cells. *BMC Cancer,* 9**,** 10.

VORA, S. R., JURIC, D., KIM, N., MINO-KENUDSON, M., HUYNH, T., COSTA, C., LOCKERMAN, E. L., POLLACK, S. F., LIU, M., LI, X., LEHAR, J., WIESMANN, M., WARTMANN, M., CHEN, Y., CAO, Z. A., PINZON-ORTIZ, M., KIM, S., SCHLEGEL, R., HUANG, A. & ENGELMAN, J. A. 2014. CDK 4/6 inhibitors sensitize PIK3CA mutant breast cancer to PI3K inhibitors. *Cancer Cell,* 26**,** 136-49.

VOUSDEN, K. H. & LANE, D. P. 2007. p53 in health and disease. *Nat Rev Mol Cell Biol,* 8**,** 275-83.

WANG, E., SOROLLA, A., CUNNINGHAM, P. T., BOGDAWA, H. M., BECK, S., GOLDEN, E., DEWHURST, R. E., FLOREZ, L., CRUICKSHANK, M. N., HOFFMANN, K., HOPKINS, R. M., KIM, J., WOO, A. J., WATT, P. M. & BLANCAFORT, P. 2019a. Tumor penetrating peptides inhibiting MYC as a potent targeted therapeutic strategy for triple-negative breast cancers. *Oncogene,* 38**,** 140-150.

WANG, H., MANNAVA, S., GRACHTCHOUK, V., ZHUANG, D., SOENGAS, M. S., GUDKOV, A. V., PROCHOWNIK, E. V. & NIKIFOROV, M. A. 2008. c-Myc depletion inhibits proliferation of human tumor cells at various stages of the cell cycle. *Oncogene,* 27**,** 1905-1915.

WANG, J., DEAN, D. C., HORNICEK, F. J., SHI, H. & DUAN, Z. 2019b. Cyclin-dependent kinase 9 (CDK9) is a novel prognostic marker and therapeutic target in ovarian cancer. *FASEB J,* 33**,** 5990-6000.

WANG, S. & FISCHER, P. M. 2008. Cyclin-dependent kinase 9: a key transcriptional regulator and potential drug target in oncology, virology and cardiology. *Trends Pharmacol Sci,* 29**,** 302-13.

WANG, X., YU, C., WANG, C., MA, Y., WANG, T., LI, Y., HUANG, Z., ZHOU, M., SUN, P., ZHENG, J., YANG, S., FAN, Y. & XIANG, R. 2019c. Novel cyclin-dependent kinase 9 (CDK9) inhibitor with suppression of cancer stemness activity against non-small-cell lung cancer. *Eur J Med Chem,* 181**,** 111535.

WANG, X. F., LIU, Z. Y., ZHANG, L., YANG, Z. Z., CHEN, X. X., LUO, J. R., ZHOU, Z. R., MEI, X., YU, X. L., SHAO, Z. M., FENG, Y., FU, S., ZHANG, Z., WEI, D. P., JIA, L. J., MA, J. L. & GUO, X. M. 2018. Targeting deubiquitinase USP28 for cancer therapy. *Cell Death & Disease,* 9.

WARD, E., DESANTIS, C., ROBBINS, A., KOHLER, B. & JEMAL, A. 2014. Childhood and adolescent cancer statistics, 2014. *CA: A Cancer Journal for Clinicians,* 64**,** 83-103.

WASZAK, S. M., NORTHCOTT, P. A., BUCHHALTER, I., ROBINSON, G. W., SUTTER, C., GROEBNER, S., GRUND, K. B., BRUGIERES, L., JONES, D. T. W., PAJTLER, K. W., MORRISSY, A. S., KOOL, M., STURM, D., CHAVEZ, L., ERNST, A., BRABETZ, S., HAIN, M., ZICHNER, T., SEGURA-WANG, M., WEISCHENFELDT, J., RAUSCH, T., MARDIN, B. R., ZHOU, X., BACIU, C., LAWERENZ, C., CHAN, J. A., VARLET, P., GUERRINI-ROUSSEAU, L., FULTS, D. W., GRAJKOWSKA, W., HAUSER, P., JABADO, N., RA, Y. S., ZITTERBART, K., SHRINGARPURE, S. S., DE LA VEGA, F. M., BUSTAMANTE, C. D., NG, H. K., PERRY, A., MACDONALD, T. J., HERNAIZ DRIEVER, P., BENDEL, A. E., BOWERS, D. C., MCCOWAGE, G., CHINTAGUMPALA, M. M., COHN, R., HASSALL, T., FLEISCHHACK, G., EGGEN, T., WESENBERG, F., FEYCHTING, M., LANNERING, B., SCHUZ, J., JOHANSEN, C., ANDERSEN, T. V., ROOSLI, M., KUEHNI, C. E., GROTZER, M., KJAERHEIM, K., MONORANU, C. M., ARCHER, T. C., DUKE, E., POMEROY, S. L., SHELAGH, R., FRANK, S., SUMERAUER, D., SCHEURLEN, W., RYZHOVA, M. V., MILDE, T., KRATZ, C. P., SAMUEL, D., ZHANG, J.,

SOLOMON, D. A., MARRA, M., EILS, R., BARTRAM, C. R., VON HOFF, K., RUTKOWSKI, S., RAMASWAMY, V., GILBERTSON, R. J., KORSHUNOV, A., TAYLOR, M. D., LICHTER, P., MALKIN, D., GAJJAR, A., KORBEL, J. O. & PFISTER, S. M. 2018. Spectrum and prevalence of genetic predisposition in medulloblastoma: a retrospective genetic study and prospective validation in a clinical trial cohort. *Lancet Oncol,* 19**,** 785-798.

WEBER, A. M. & RYAN, A. J. 2015. ATM and ATR as therapeutic targets in cancer. *Pharmacology & Therapeutics,* 149**,** 124-138.

WEHLER, T., THOMAS, M., SCHUMANN, C., BOSCH-BARRERA, J., SEGARRA, N. V., DICKGREBER, N. J., DALHOFF, K., SEBASTIAN, M., JAIME, J. C., ALONSO, M., HYNES, S. M., LIN, J., HURT, K., LIN, A. B., CALVO, E. & PAZ-ARES, L. 2017. A randomized, phase 2 evaluation of the CHK1 inhibitor, LY2603618, administered in combination with pemetrexed and cisplatin in patients with advanced nonsquamous non-small cell lung cancer. *Lung Cancer,* 108**,** 212-216.

WEI, J., MA, L., LI, C., PIERSON, C. R., FINLAY, J. L. & LIN, J. 2019. Targeting Upstream Kinases of STAT3 in Human Medulloblastoma Cells. *Current cancer drug targets,* 19**,** 571-582.

WEINSTEIN, I. B. & JOE, A. 2008. Oncogene Addiction. *Cancer Research,* 68**,** 3077-3080.

WELCKER, M., ORIAN, A., JIN, J. P., GRIM, J. A., HARPER, J. W., EISENMAN, R. N. & CLURMAN, B. E. 2004. The Fbw7 tumor suppressor regulates glycogen synthase kinase 3 phosphorylation-dependent c-Myc protein degradation. *Proceedings of the National Academy of Sciences of the United States of America,* 101**,** 9085-9090.

WESTERMANN, F., MUTH, D., BENNER, A., BAUER, T., HENRICH, K. O., OBERTHUER, A., BRORS, B., BEISSBARTH, T., VANDESOMPELE, J., PATTYN, F., HERO, B., KONIG, R., FISCHER, M. & SCHWAB, M. 2008. Distinct transcriptional MYCN/c-MYC activities are associated with spontaneous regression or malignant progression in neuroblastomas. *Genome Biol,* 9**,** R150.

WHITFIELD, J. R., BEAULIEU, M. E. & SOUCEK, L. 2017. Strategies to Inhibit Myc and Their Clinical Applicability. *Frontiers in Cell and Developmental Biology,* 5.

WHITTAKER, S. R., MALLINGER, A., WORKMAN, P. & CLARKE, P. A. 2017. Inhibitors of cyclin-dependent kinases as cancer therapeutics. *Pharmacol Ther,* 173**,** 83-105.

WIEDERSCHAIN, D., WEE, S., CHEN, L., LOO, A., YANG, G. Z., HUANG, A., CHEN, Y., CAPONIGRO, G., YAO, Y. M., LENGAUER, C., SELLERS, W. R. & BENSON, J. D. 2009. Single-vector inducible lentiviral RNAi system for oncology target validation. *Cell Cycle,* 8**,** 498-504.

WILLIAMS, M. M. & COOK, R. S. 2015. Bcl-2 family proteins in breast development and cancer: could Mcl-1 targeting overcome therapeutic resistance? *Oncotarget,* 6**,** 3519-30.

WITKIEWICZ, A. K., BALAJI, U., ESLINGER, C., MCMILLAN, E., CONWAY, W., POSNER, B., MILLS, G. B., O'REILLY, E. M. & KNUDSEN, E. S. 2016. Integrated Patient-Derived Models Delineate Individualized Therapeutic Vulnerabilities of Pancreatic Cancer. *Cell Rep,* 16**,** 2017-31.

WOJTALLA, A., SALM, F., CHRISTIANSEN, D. G., CREMONA, T., CWIEK, P., SHALABY, T., GROSS, N., GROTZER, M. A. & ARCARO, A. 2012. Novel agents targeting the IGF-1R/PI3K pathway impair cell proliferation and survival in subsets of medulloblastoma and neuroblastoma. *PloS one,* 7**,** e47109-e47109.

WONG, E. T. & BERKENBLIT, A. 2004. The Role of Topotecan in the Treatment of Brain Metastases. *The Oncologist,* 9**,** 68-79.

WRIGHT, G., GOLUBEVA, V., REMSING RIX, L. L., BERNDT, N., LUO, Y., WARD, G. A., GRAY, J. E., SCHONBRUNN, E., LAWRENCE, H. R., MONTEIRO, A. N. A. & RIX, U. 2017. Dual Targeting of WEE1 and PLK1 by AZD1775 Elicits Single Agent Cellular Anticancer Activity. *ACS Chemical Biology,* 12**,** 1883-1892.

WU, C.-C., HOU, S., ORR, B. A., KUO, B. R., YOUN, Y. H., ONG, T., ROTH, F., EBERHART, C. G., ROBINSON, G. W., SOLECKI, D. J., TAKETO, M. M., GILBERTSON, R. J., ROUSSEL, M. F. & HAN, Y.-G. 2017. mTORC1-Mediated Inhibition of 4EBP1 Is Essential for Hedgehog Signaling-Driven Translation and Medulloblastoma. *Developmental cell,* 43**,** 673-688.e5.

XIA, X. & WONG, S. T. 2012. Concise review: a high-content screening approach to stem cell research and drug discovery. *Stem Cells,* 30**,** 1800-7.

XIAO, D., YUE, M., SU, H., REN, P., JIANG, J., LI, F., HU, Y., DU, H., LIU, H. & QING, G. 2016. Polo-like Kinase-1 Regulates Myc Stabilization and Activates a Feedforward Circuit Promoting Tumor Cell Survival. *Mol Cell,* 64**,** 493-506.

XIAO, D. B., REN, P., SU, H. X., YUE, M., XIU, R. J., HU, Y. F., LIU, H. D. & QING, G. L. 2015. Myc promotes glutaminolysis in human neuroblastoma through direct activation of glutaminase 2. *Oncotarget,* 6**,** 40655-40666.

XIE, J., WANG, X. & PROUD, C. G. 2016. mTOR inhibitors in cancer therapy. *F1000Research,* 5**,** F1000 Faculty Rev-2078.

XU, H., CHEUNG, I. Y., WEI, X. X., TRAN, H., GAO, X. & CHEUNG, N. K. 2011. Checkpoint kinase inhibitor synergizes with DNA-damaging agents in G1 checkpoint-defective neuroblastoma. *Int J Cancer,* 129**,** 1953-62.

XU, J., REN, X., PATHANIA, A. S., FERNANDEZ, G. E., TRAN, A., ZHANG, Y., MOATS, R. A., SHACKLEFORD, G. M. & ERDREICH-EPSTEIN, A. 2017. PID1 increases chemotherapy-induced apoptosis in medulloblastoma and glioblastoma cells in a manner that involves NFκB. *Scientific Reports,* 7**,** 835.

XU, J. Y., MARGOL, A., ASGHARZADEH, S. & ERDREICH-EPSTEIN, A. 2015. Pediatric Brain Tumor Cell Lines. *Journal of Cellular Biochemistry,* 116**,** 218-224.

YADAV, B., WENNERBERG, K., AITTOKALLIO, T. & TANG, J. 2015. Searching for Drug Synergy in Complex Dose–Response Landscapes Using an Interaction Potency Model. *Computational and Structural Biotechnology Journal,* 13**,** 504-513.

YAN, P. & SUN, X. 2018. Triptolide: A new star for treating human malignancies. *Journal of Cancer Research and Therapeutics,* 14**,** 271-275.

YAN, Y., CAO, P. T., GREER, P. M., NAGENGAST, E. S., KOLB, R. H., MUMBY, M. C. & COWAN, K. H. 2010. Protein phosphatase 2A has an essential role in the activation of γ-irradiation-induced G2/M checkpoint response. *Oncogene,* 29**,** 4317-4329.

YANG, F., JOVE, V., XIN, H., HEDVAT, M., VAN METER, T. E. & YU, H. 2010. Sunitinib induces apoptosis and growth arrest of medulloblastoma tumor cells by inhibiting STAT3 and AKT signaling pathways. *Molecular cancer research : MCR,* 8**,** 35-45.

YANG, H., YOON, S. J., JIN, J., CHOI, S. H., SEOL, H. J., LEE, J. I., NAM, D. H. & YOO, H. Y. 2011. Inhibition of checkpoint kinase 1 sensitizes lung cancer brain metastases to radiotherapy. *Biochemical and Biophysical Research Communications,* 406**,** 53-58.

YANG, J., NIE, J., MA, X., WEI, Y., PENG, Y. & WEI, X. 2019. Targeting PI3K in cancer: mechanisms and advances in clinical trials. *Mol Cancer,* 18**,** 26.

YANG, Z., YIK, J. H., CHEN, R., HE, N., JANG, M. K., OZATO, K. & ZHOU, Q. 2005. Recruitment of P-TEFb for stimulation of transcriptional elongation by the bromodomain protein Brd4. *Mol Cell,* 19**,** 535-45.

YOCK, T. I., YEAP, B. Y., EBB, D. H., WEYMAN, E., EATON, B. R., SHERRY, N. A., JONES, R. M., MACDONALD, S. M., PULSIFER, M. B., LAVALLY, B., ABRAMS, A. N., HUANG, M. S., MARCUS, K. J. & TARBELL, N. J. 2016. Long-term toxic effects of proton radiotherapy for paediatric medulloblastoma: a phase 2 single-arm study. *Lancet Oncol,* 17**,** 287-98.

YOU, J. S. & HAN, J. H. 2014. Targeting components of epigenome by small molecules. *Arch Pharm Res,* 37**,** 1367-74.

YU, L., YU, T.-T. & YOUNG, K. H. 2019. Cross-talk between Myc and p53 in B-cell lymphomas. *Chronic diseases and translational medicine,* 5**,** 139-154.

YUAN, J., LLAMAS LUCEÑO, N., SANDER, B. & GOLAS, M. M. 2017. Synergistic anti-cancer effects of epigenetic drugs on medulloblastoma cells. *Cellular Oncology,* 40**,** 263-279.

YUAN, J., MEHTA, P. P., YIN, M. J., SUN, S., ZOU, A., CHEN, J., RAFIDI, K., FENG, Z., NICKEL, J., ENGEBRETSEN, J., HALLIN, J., BLASINA, A., ZHANG, E., NGUYEN, L., SUN, M., VOGT, P. K., MCHARG, A., CHENG, H., CHRISTENSEN, J. G., KAN, J. L. & BAGRODIA, S. 2011. PF-04691502, a potent and selective oral inhibitor of PI3K and mTOR kinases with antitumor activity. *Mol Cancer Ther,* 10**,** 2189-99.

ZABLUDOFF, S. D., DENG, C., GRONDINE, M. R., SHEEHY, A. M., ASHWELL, S., CALEB, B. L., GREEN, S., HAYE, H. R., HORN, C. L., JANETKA, J. W., LIU, D., MOUCHET, E., READY, S., ROSENTHAL, J. L., QUEVA, C., SCHWARTZ, G. K., TAYLOR, K. J., TSE, A. N., WALKER, G. E. & WHITE, A. M. 2008. AZD7762, a novel checkpoint kinase inhibitor, drives checkpoint abrogation and potentiates DNA-targeted therapies. *Molecular Cancer Therapeutics,* 7**,** 2955-2966.

ZHANG, C., HE, X.-J., LI, L., LU, C. & LU, A.-P. 2017. Effect of the Natural Product Triptolide on Pancreatic Cancer: A Systematic Review of Preclinical Studies. *Frontiers in pharmacology,* 8**,** 490-490.

ZHANG, H., LI, H., LIU, Z., GE, A., GUO, E., LIU, S. & CHEN, Z. 2018a. Triptolide inhibits the proliferation and migration of medulloblastoma Daoy cells by upregulation of microRNA-138. *J Cell Biochem,* 119**,** 9866-9877.

ZHANG, H. P., LI, G. Q., ZHANG, Y., GUO, W. Z., ZHANG, J. K., LI, J., LV, J. F. & ZHANG, S. J. 2018b. Upregulation of Mcl-1 inhibits JQ1-triggered anticancer activity in hepatocellular carcinoma cells. *Biochem Biophys Res Commun,* 495**,** 2456-2461.

ZHANG, L. & YANG, H. 2016. Design and Evaluation of Drug Combination Studies.

ZHANG, S., GONG, Z., OLADIMEJI, P. O., CURRIER, D. G., DENG, Q., LIU, M., CHEN, T. & LI, Y. 2019. A high-throughput screening identifies histone deacetylase inhibitors as therapeutic agents against medulloblastoma. *Experimental Hematology & Oncology,* 8**,** 30.

ZHOU, S., WANG, F., ZHANG, Y., JOHNSON, M. R., QIAN, S., WU, M. & WU, E. 2014. Salinomycin Suppresses PDGFRβ, MYC, and Notch Signaling in Human Medulloblastoma. *Austin journal of pharmacology and therapeutics,* 2**,** 1020-1020.

ZHOU, Y., FENG, J., YOU, L., MENG, H. & QIAN, W. 2015. Matrine and CYC116 synergistically inhibit growth and induce apoptosis in multiple myeloma cells. *Chinese Journal of Integrative Medicine,* 21**,** 635-639.

ZHU, H., BENGSCH, F., SVORONOS, N., RUTKOWSKI, M. R., BITLER, B. G., ALLEGREZZA, M. J., YOKOYAMA, Y., KOSSENKOV, A. V., BRADNER, J. E., CONEJO-GARCIA, J. R. & ZHANG, R. 2016. BET Bromodomain Inhibition Promotes Anti-tumor Immunity by Suppressing PD-L1 Expression. *Cell reports,* 16**,** 2829-2837.

ZHUKOVA, N., RAMASWAMY, V., REMKE, M., MARTIN, D. C., CASTELO-BRANCO, P., ZHANG, C. H., FRASER, M., TSE, K., POON, R., SHIH, D. J. H., BASKIN, B., RAY, P. N., BOUFFET, E., DIRKS, P., VON BUEREN, A. O., PFAFF, E., KORSHUNOV, A., JONES, D. T. W., NORTHCOTT, P. A., KOOL, M., PUGH, T. J., POMEROY, S. L., CHO, Y. J., PIETSCH, T., GESSI, M., RUTKOWSKI, S., BOGNAR, L., CHO, B. K., EBERHART, C. G., CONTER, C. F., FOULADI, M., FRENCH, P. J., GRAJKOWSKA, W. A., GUPTA, N., HAUSER, P., JABADO, N., VASILJEVIC, A., JUNG, S., KIM, S. K., KLEKNER, A., KUMABE, T., LACH, B., LEONARD, J. R., LIAU, L. M., MASSIMI, L., POLLACK, I. F., RA, Y. S., RUBIN, J. B., VAN MEIR, E. G., WANG, K. C., WEISS, W. A., ZITTERBART, K., BRISTOW, R. G., ALMAN, B., HAWKINS, C. E., MALKIN, D., CLIFFORD, S. C., PFISTER, S. M., TAYLOR, M. D. & TABORI, U. 2014. WNT

activation by lithium abrogates TP53 mutation associated radiation resistance in medulloblastoma. *Acta Neuropathologica Communications,* 2.

ZHUKOVA, N., RAMASWAMY, V., REMKE, M., PFAFF, E., SHIH, D. J., MARTIN, D. C., CASTELO-BRANCO, P., BASKIN, B., RAY, P. N., BOUFFET, E., VON BUEREN, A. O., JONES, D. T., NORTHCOTT, P. A., KOOL, M., STURM, D., PUGH, T. J., POMEROY, S. L., CHO, Y. J., PIETSCH, T., GESSI, M., RUTKOWSKI, S., BOGNAR, L., KLEKNER, A., CHO, B. K., KIM, S. K., WANG, K. C., EBERHART, C. G., FEVRE-MONTANGE, M., FOULADI, M., FRENCH, P. J., KROS, M., GRAJKOWSKA, W. A., GUPTA, N., WEISS, W. A., HAUSER, P., JABADO, N., JOUVET, A., JUNG, S., KUMABE, T., LACH, B., LEONARD, J. R., RUBIN, J. B., LIAU, L. M., MASSIMI, L., POLLACK, I. F., SHIN RA, Y., VAN MEIR, E. G., ZITTERBART, K., SCHÜLLER, U., HILL, R. M., LINDSEY, J. C., SCHWALBE, E. C., BAILEY, S., ELLISON, D. W., HAWKINS, C., MALKIN, D., CLIFFORD, S. C., KORSHUNOV, A., PFISTER, S., TAYLOR, M. D. & TABORI, U. 2013. Subgroup-specific prognostic implications of TP53 mutation in medulloblastoma. *J Clin Oncol,* 31**,** 2927-35.

ZIMMER, A., KATZIR, I., DEKEL, E., MAYO, A. E. & ALON, U. 2016. Prediction of multidimensional drug dose responses based on measurements of drug pairs. *Proceedings of the National Academy of Sciences,* 113**,** 10442-10447.

ZWERDLING, T., KRAILO, M., MONTELEONE, P., BYRD, R., SATO, J., DUNAWAY, R., SEIBEL, N., CHEN, Z., STRAIN, J. & REAMAN, G. 2006. Phase II investigation of docetaxel in pediatric patients with recurrent solid tumors: a report from the Children's Oncology Group. *Cancer,* 106**,** 1821-8.

ZWERGEL, C., ROMANELLI, A., STAZI, G., BESHARAT, Z. M., CATANZARO, G., TAFANI, M., VALENTE, S. & MAI, A. 2018. Application of Small Epigenetic Modulators in Pediatric Medulloblastoma. *Frontiers in pediatrics,* 6**,** 370-370.